Characterizing the Roles of APC2 Protein in Ovarian Homeostasis and Tumourigenesis

Thesis submitted for the award of Ph.D. by

Noha-Ehssan Mohamed

The European Cancer Stem Cell Research Institute
Division of Biomedicine
School of Biosciences
College of Biomedical and Life Sciences
Cardiff University
2013-2017

Declaration

This work has not been submitted in substance for any other degree or award at this or any other university or place of learning, nor is being submitted concurrently in candidature for any degree or other award.

Signed…… (candidate) Date …….

STATEMENT 1

This thesis is being submitted in partial fulfillment of the requirements for the degree of Ph.D.

Signed…… (candidate) Date …….

STATEMENT 2

This thesis is the result of my own independent work/investigation, except where otherwise stated, and the thesis has not been edited by a third party beyond what is permitted by Cardiff University's Policy on the Use of Third Party Editors by Research Degree Students. Other sources are acknowledged by explicit references. The views expressed are my own.

Signed…… (candidate) Date …….

STATEMENT 3

I hereby give consent for my thesis, if accepted, to be available online in the University's Open Access repository and for inter-library loan, and for the title and summary to be made available to outside organisations.

Signed…… (candidate) Date …….

Acknowledgments

I praise and thank **Allah** SWT for His greatness, blessings and for giving me the strength and patience to complete this thesis. I would like to thank all my supervisors for giving me support, trust, encouragement as well as independence. I am very grateful to the late Professor **Alan Clarke** for giving me the opportunity to join his lab and start this unique exciting project. I am very thankful to Professor **Matt Smalley** whose supervision was an important turning point for my Ph.D. I value very much his input to the project, and his effort especially during the last month reading my thesis to help me submit on time. Special thanks to Dr. **Trevor Hay** for being a supportive supervisor as well as a good friend.

I would also want to thank all members of ARC and MJS groups. Special thanks to DR. **Valerie Meniel** for her kindness, friendship and help offering whenever needed, DR. **Karen Reed** for critically-reading part of this thesis and for our scientific discussions, DR. **Giusy Tornillo** for her valuable suggestions and help with Western blotting, Mr. **Howard Kendrick** for teaching me genomic analysis, and my Ph.D. journey partner **Maria Konstantinou** for her friendship, support and humour. I would also like to thank Professor **Owen Sansom** for his scientific support and suggestions, Professor **Geraint Williams** for his time teaching me ovarian histology, and DR. **Andrea Flesken-Nikitin** for kindly replying my e-mails regarding the ovarian intrabursal injection technique.

I would like to acknowledge the **Missions Sector of Egyptian Ministry of Higher Education**, represented by the Egyptian cultural and educational Bureau in London, for funding my Ph.D.. Special thanks to **National Organization for Drug Control And Research** NODCAR, where I work in Egypt, for supporting my grant application and facilitating my mission, and to my colleagues in **Hormones Evaluation Department** in NODCAR for encouragement, support and finishing any paperwork required while I was away. I am grateful

for **Cancer Research UK** CRUK for partially funding the project through Professor Alan Clarke program grant. I would like to acknowledge the **Banfill Grant** for financially supporting my participation in the 16th biennial meeting of the international gynaecological cancer society in 2016.

I am grateful to the technical team who helped me with this project. Special thanks for Mrs. **Bridget Allen** for performing intrabursal injections, Mr. **Matt Zverev** and Mr. **Mark Bishop** for performing mouse genotyping, Miss **Elaine Taylor** for assisting with mice weaning and ear tipping, and Mr. **Derek Scarborough** for processing all tissues for histology, especially for his patience while serially-sectioning and re-dipping my fixed tissues.

I would not have finished this Ph.D. without the support of my family, to whom I dedicate this thesis. I am very grateful to my loving husband DR. **Mohamed Gebely** for considering my Ph.D. our priority, and helping me a lot especially during the last year to give me time to focus on my work. I have to thank my wonderful kids **Ganna**, **Ali** and **Ammar** for their unconditional love, patience, understanding, and happiness they radiate into my life. I would not have started this Ph.D. without the love and passion to scientific research, which my Dad, Eng. **Ahmed Ehssan Aly**, dedicated his life to teach me, among other valuable core knowledge and ethics. I am very grateful to him, and I hope that by now I achieved his dreams, and that my success partially rewards his sacrifices. I am very grateful to my **Mum** whose love, supportive words and care for me and my kids helped me a lot especially during Ammar's early days. I am blessed to have my sister and life-journey partner DR. **Soha Mohamed** here in Cardiff to share our Ph.D. journeys together, although I missed her presence at the very end of the journey. I am grateful to Ammar's childminder and her family, without their ultimate love and care for my son, I would have never been able to focus on my studies, and finish my Ph.D. on time. Words are not enough to express how I am blessed to have all of you in my life.

Table of contents

List of figures

List of tables

List of Abbreviations

A

Ad: adenovirus

AMH: anti-müllerian hormone

Amhr2: anti-Müllerian hormone receptor 2

ANOVA: analysis of variance

APC: Adenomatous polyposis coli

APC2/APCL: adenomatous polyposis coli 2/like

ARID1A: AT-Rich Interaction Domain 1A

B

BSA : bovine serum albumin

C

CA125: cancer antigen 125

CAFs: cancer-associated fibroblasts

CaMKII: calcium/calmodulin-dependent protein kinase II

CCC: clear cell carcinoma

cGMP: cyclic guanosine monophosphate

CK1: casein kinase-1

COC: cumulus oocyte/oophorous complex

CSCs: cancer stem cells

D

DAB: diaminobenzidine

DKK: Dickkopf

DMBA: dimethylbenz[a]antrhracene

Dvl: dishevelled

E

EGF: epidermal growth factor

EMT: epithelial to mesenchymal transition

EOC: epithelial ovarian cancer

ERα: estrogen receptor alpha

F

FDR: false discovery rate

FGFR: fibroblast growth factor receptor

FIGO: International Federation of Gynaecologists and Obstetricians

FOX: forkhead box family of transcription factors

FSH: follicle-stimulating hormone

FZD: frizzled

G

GCT: granulosa cell tumour

GEMMs: genetically-engineered mouse models

GnRH: gonadotrophin-releasing hormone

GSK-3: Glycogen synthase kinase-3

H

H&E: Haematoxylin and eosin

HCG: human chorionic gonadotrophin

HE4: human epididymis protein 4

HGSOC: high-grade serous ovarian carcinoma

HRP: horseradish peroxidase

I

IGF: insulin-like growth factor

IHC: immunohistochemistry

IL: interleukin

IP3: inositol triphosphate

J

JNK: Jun N-terminal kinase

K

KRAS: Kirsten rat sarcoma viral oncogene homolog

L

LGSOC: low-grade serous ovarian carcinoma

LH: luteinizing hormone

LHCGR: luteinizing hormone chorionic gonadotrophin receptor

LRP: low density lipoprotein-related protein

LSD: least significant difference

M

MEK: mitogen-activated protein (MAP) extracellular signal-related kinase (ERK) kinase

Misr2: Müllerian inhibitory substance type II receptor

MRI: magnetic resonance imaging

mTOR: mammalian target of rapamycin

N

NICE: National Institute for Health and Care Excellence

O

OC: ovarian cancer

OEA: ovarian endometrioid adenocarcinoma

OSE: ovarian surface epithelium

Ovgp1: oviductal glycoprotein 1

P

PCOS: polycystic ovary syndrome

PCP: planar cell polarity

PFU: plaque-forming units

PI3K: phosphatodylinositol-3-kinase

PIP2: phosphatidylinositol-4,5-biphosphate

PIP3: phosphatidylinositol-3,4,5-triphosphate

PKC: protein kinase C

PLC: phospholipase C

PMSG: pregnant mare's serum gonadotropin

PTEN: phosphatase and tensin homolog

Q

qRT-PCR: quantitative reverse transcription polymerase chain reaction

R

Rb: retinoblastoma protein

ROCK: Rho-associated protein kinase

RPKM: reads per kilo base million

Rspo1: Rspondin1

RTK: receptor tyrosine kinase

S

SF1: steroidogenic factor 1

T

TBST : Tris-buffered saline, 1% Tween 20

TGF-β: transforming growth factor β superfamily of transcription factors

TNF: tumour necrosis factor

V

VEGF: vascular endothelial growth factor

W

WT: wild type

Abstract

Canonical WNT signalling plays a critical role in the regulation of ovarian development during embryogenesis; dysregulation of this pathway in adult ovary is associated with subfertility and tumourigenesis. The aim of the current study was to elucidate the previously unexplored roles of Adenomatous polyposis coli 2 (APC2), a WNT signalling pathway regulator, in the ovary using an *Apc2* constitutive knockout mouse. For the first time, the current work demonstrated essential roles of APC2 in regulating ovarian WNT signalling and ovarian homeostasis. In early adulthood, APC2-deficiency resulted in WNT signalling activation and sub-fertility driven by intra-ovarian defects. Follicular growth was perturbed, resulting in a reduced rate of ovulation and corpora lutea formation, which was not rescued by administration of gonadotrophins.

The current study provides fundamental new knowledge on the role of APC2 in ovarian tumourigenesis. APC2-deficiency (on the background of a hypomorph Apc^{-} allele) resulted in a predisposition to granulosa cell tumour (GCT) formation, accompanied by acute tumour-associated WNT-signalling activation and expression of a histologic pattern and molecular signature seen in human adult GCTs. Hence, APC2 has an important tumour-suppressor activity within ovarian granulosa cells.

However, APC2 is dispensable for ovarian surface epithelium (OSE) homeostasis. APC2 loss on its own, or combined with PTEN or APC loss in the OSE, failed to cause tumour development. Introducing APC2-deficiency to an ovarian endometrioid adenocarcinoma (OEA) mouse model, driven by loss of PTEN and APC in the OSE, resulted in early initiation of tumourigenesis, but attenuated tumour growth. This attenuation was accompanied by squamous metaplasia, decreased mitosis, decreased p-ERK1/2 expression and disrupted immune/inflammatory signalling. Thus, for the first time, an APC2 functional dualism in initiation and progression of WNT-driven OEA in mice is reported. RNA sequence analysis unraveled 2 transcripts (HAL and HUNK) associated with OEA progression and should be considered for future research.

1. Introduction

1.1. The ovary

1.1.1. Ovarian biology

The ovary is the female reproductive organ responsible for the production and release of oocytes during ovulation. It also acts as an endocrine gland, secreting the steroidal hormones estradiol and progesterone. Histologically, the ovary is formed of an outer cortex and an inner medulla. The cortex is composed of ovarian follicles embedded in connective tissue stroma. The medulla is formed of loose connective tissue stroma containing blood vessels, lymphatic vessels and nerves. The ovarian surface is lined with a single layer of epithelium, the ovarian surface epithelium (OSE), formerly known as the germinal epithelium, which is weakly attached to a basement membrane. Immediately under the OSE is a layer of fibrous connective tissue, the tunica albuginea, which separates the OSE from the ovarian stroma (Figure 1.1) (Orsi *et al.* 2014).

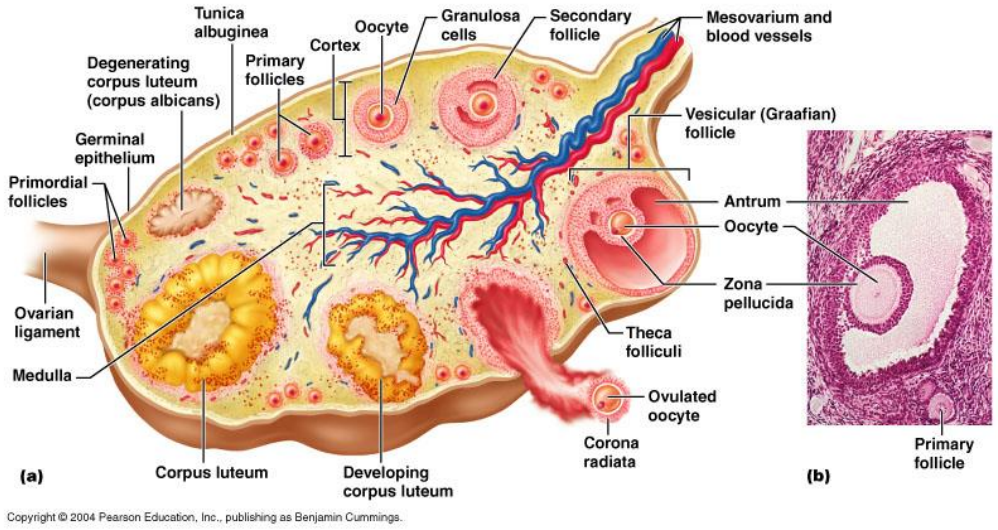

Figure 1.1: The structure of the ovary. (a) Schematic diagram of the ovary showing the different functional compartments and follicular developmental stages. (b) Structure of Graafian (pre-ovulatory) follicle. Copyright © 2004 Pearson education, Inc. publishing.

During embryogenesis, the ‘bipotential gonad’ is formed of the gonadal ridge and migrating primordial germ cells. The gonadal ridge is formed of a projection from the mesothelium, while primordial germ cells are derived from the epiblast, and migrate to the gonadal ridge forming ‘oogonia’. Differentiation into an ovary is governed by sex chromosomes (absence of Y chromosome), and activation of β-catenin signalling by Rspondin1 and Wnt4. Oogonia proliferate by mitosis and then undergo meiosis at embryonic day E12.5, when they become oocytes and are arrested at the diploid prophase of meiosis I. These oocytes are found in nests, which break down during foetal development, when most of them degrade by apoptosis. Surviving oocytes are surrounded by single layer of squamous pre-granulosa cells, in the second half of foetal development and in early post-natal days, giving rise to a ‘finite pool’ of primordial follicles, which are recruited in ‘groups’ throughout life until they become completely depleted at menopause (Edson *et al.* 2009).

Primordial follicles start to be recruited to grow into primary follicles as early as their formation. This ‘initial recruitment’ causes follicles to grow up to the antral stage and then undergo atresia. However, after puberty another recruitment, the ‘cyclic recruitment’, happens every cycle where a number of primordial follicles are recruited to grow, reaching the antral stage but acquiring a different fate (McGee and Hsueh 2000). Puberty-onset happens when pulses of gonadotrophin-releasing hormone (GnRH) from the hypothalamus induce the rise of follicle-stimulating hormone (FSH) and luteinizing hormone (LH) produced by the pituitary gland (Chamberlain *et al.* 2013). Rising levels of FSH rescues some antral follicles from atresia, allowing them to grow further. In humans, one follicle grows faster than the remaining follicles, producing high levels of estradiol and inhibin, which by negative feedback inhibits FSH production by the pituitary gland, causing the remaining follicles to degenerate (McGee and Hsueh 2000). With LH surge before ovulation, the oocyte completes meiosis I, giving 2 haploid daughter cells (secondary oocyte and polar body). Following this, the secondary oocyte

enters meiosis II when it is arrested at metaphase until fertilization occurs (Rodriguez and Pangas 2016).

1.1.1.1. Mouse vs. Human ovary

Anatomical and physiologic differences exist between mouse and human ovary. For instance, while the human ovarian surface is exposed to the surrounding tissue in the peritoneal cavity, the mouse ovary is enclosed in a membrane-like balloon, the bursa (Treuting and Dintzis 2011). Physiologically, the ovary is an active organ with cyclic changes happening every 28 days in human, and every 4-5 days in the mouse (Byers *et al.* 2012). Starting from puberty, a certain number of primordial follicles are recruited for follicular growth into primary, secondary and one fully mature pre-ovulatory (Graafian) follicle. During maturation, both the oocytes and the follicles enlarge, and the follicular cells become small cuboidal basophilic granulosa cells, which are surrounded by theca cells. The main function of theca cells is the production of androgens; the precursors of estradiol produced by the granulosa cells of follicles. On ovulation, the mature Graafian follicle is ruptured along with the adjacent part of the OSE, and the oocyte is released from the ovary. In the mouse, several follicles are fully mature at the time of ovulation, all of which rupture during ovulation (Treuting and Dintzis 2011).

Following ovulation, the remaining somatic granulosa cells of the ovulated follicle form the corpus luteum, which is responsible for progesterone secretion and maintenance of pregnancy after fertilization of the oocyte. In the absence of fertilization, the corpus luteum degenerates and is converted to the non-functional corpus albicans in human. In contrast, the corpora lutea from previous cycles do not degenerate in the mouse, with the ovary containing both mature corpora lutea from previous ovulations and immature corpora lutea from the most recent ovulation. The mature corpora lutea are characterized by large eosinophilic cells and are mostly located deeper in the ovarian medulla. The immature recently-developed corpora lutea

are characterized by smaller basophilic cells, similar to granulosa cells, and are embedded in the ovarian cortex (Dixon *et al.* 2014).

1.1.1.2. The ovarian surface epithelium

The biology and functions of OSE are not as well characterized as the remaining structures of the ovary. OSE functions in transporting molecules to and from the peritoneal cavity. It plays important roles in ovulation and post-ovulatory wound repair (Murdoch and McDonnel 2002). Histologically, the OSE is formed of squamous to cuboidal epithelial cells which tend to assume columnar shapes upon metaplastic transformation (Okamoto *et al.* 2009). With age, OSE irregularities form leading to OSE-lined surface invaginations (clefts) and epithelial inclusion cysts within the ovarian cortex. These clefts and inclusion cysts have historically been thought to be the preferred sites of neoplastic progression (Auersperg *et al.* 2001). OSE is a modified pelvic mesothelium, which is less differentiated than other pelvic epithelia. OSE displays both epithelial and mesenchymal features but retains the ability of other coelomic epithelium to differentiate under pathologic condition (Auersperg *et al.* 2001). OSE shifts to the differentiated epithelial phenotype during neoplastic transformation via mesenchymal to epithelial transition (Ahmed *et al.* 2007). On the other hand, OSE acquires mesenchymal phenotype during metastasis by epithelial to mesenchymal transition (Lili *et al.* 2013).

1.1.2. Regulation of ovarian functions

The complicated biological processes taking place during folliculogenesis and ovulation are tightly regulated by endocrine, autocrine and paracrine signals (Orsi *et al.* 2014). The extra-ovarian regulation of ovarian functions is controlled by the hypothalamus and the pituitary gland via the hypothalamic-pituitary-ovarian axis. The autocrine and paracrine regulation of ovarian functions is controlled mainly by members of TGF-β transcription superfamily (Knight and Glister 2006).

1.1.2.1. Hypothalamic-pituitary-ovarian axis

The pulsatile release of GnRH from the hypothalamus triggers the production and secretion of FSH and LH from the pituitary gland. The cyclic changes in levels of these hormones control follicular growth and ovulation as well as secretion of estradiol and progesterone from the ovary (Figure 1.2a). The hypothalamic and pituitary hormonal secretion is tightly regulated by feedback loops governed by ovarian hormones (Figure 1.2b). As their names imply, FSH controls follicular growth and maturation, while the main function of LH is the luteinisation of ovarian follicles after ovulation. A surge in both LH and FSH is needed for ovulation. During folliculogenesis, LH stimulates theca cells to produce androgens, while FSH stimulates granulosa cells to produce estradiol. After ovulation, LH controls the development and functional activities of the corpus luteum, most critically progesterone secretion (Orsi *et al.* 2014).

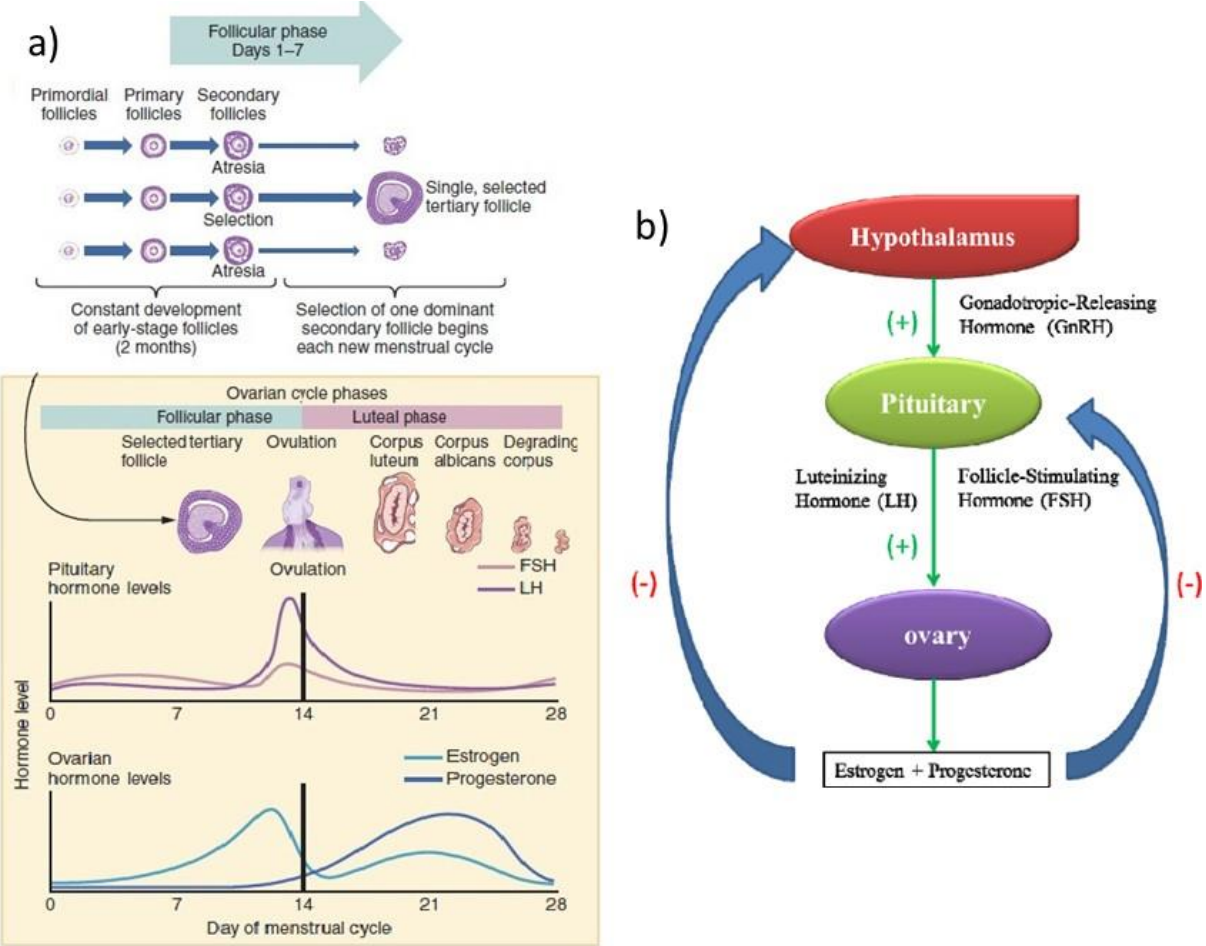

Figure 1.2: Schematic representation of (a) Hormonal cyclic changes (Gray 2013), and (b) Feedback mechanisms regulating the hypothalamic-pituitary-ovarian axis (Sun *et al.* 2013). (+) represents positive feedback. (-) represents negative feedback.

1.1.2.2. Biosynthesis of ovarian hormones

Progesterone is considered the precursor of all other hormones synthesized in the ovary. Progesterone biosynthesis requires only 2 enzymes, cholesterol side chain cleavage enzyme and 3 beta-hydroxysteroid dehydrogenase, both present in granulosa cells, theca cells and luteal cells of growing follicles and corpora lutea, respectively. Estradiol, the key female sex hormone responsible for follicle growth and maturation, is secreted from granulosa cells in response to FSH. According to the two-cell theory of estradiol biosynthesis, the enzymatic machinery needed to synthesize progesterone from cholesterol is present in both theca cells and granulosa cells. However, the enzymes responsible for the synthesis of androstenedione and testosterone,

namely 17α-hydroxylase and C17,20-lyase, are only present in theca cells. On the other hand, the aromatase enzyme, which is responsible for the synthesis of estradiol from these 2 androgens, is only present in the granulosa cells. This necessitates the transport of androgens to granulosa cells prior to their conversion to estradiol (Figure 1.3) (Orsi *et al.* 2014).

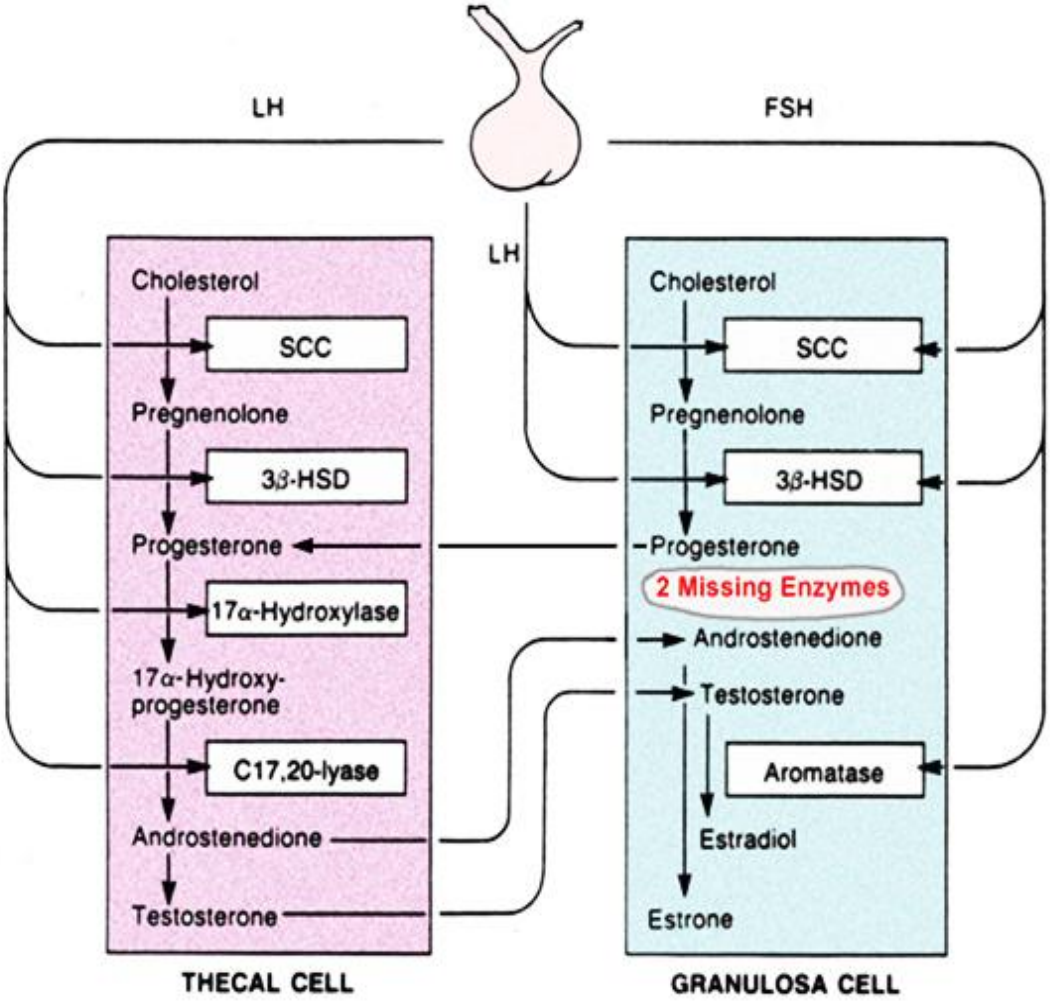

Figure 1.3: Biosynthesis of steroid hormones in the ovary. SCC: cholesterol side chain cleavage enzyme, 3β-HSD: 3β-hydroxysteroid dehydrogenase (Griffin and Ojeda 1992)

1.1.2.3. Autocrine and paracrine regulators

Due to the complexity of folliculogenesis, hormonal regulation is not considered enough to explain processes such as follicle recruitment and selection of dominant follicles. Autocrine and paracrine regulators, proteins which are endogenously secreted by ovarian cells

and act locally on the producer cell or on nearby cells, are believed to modulate and interact with gonadotrophins during folliculogenesis (Canipari *et al.* 2012). The most studied ovarian autocrine and paracrine regulators are the transforming growth factor β superfamily of transcription factors (TGF-β)(Knight and Glister 2006), the forkhead box family of transcription factors (FOX) (Uhlenhaut and Treier 2011), the insulin-like growth factor system (IGF) (Silva *et al.* 2009), and interleukins (Smolikova *et al.* 2012).

1.1.2.3.1. TGF-β superfamily

Activin, inhibin and anti-müllerian hormone (AMH) are members of the TGF-β transcription superfamily that are secreted by granulosa cells of growing follicles. Activin is secreted from granulosa cells of pre-antral follicles, and functions to increase FSH secretion from the pituitary gland via a positive feedback loop. In addition, it has been shown to increase the responsiveness of growing follicles to FSH by inducing the expression of FSH receptors (Katayama *et al.* 2000). Induction of aromatase expression by activin augments the FSH-induced estradiol secretion, resulting in the stimulation of granulosa cell proliferation and follicular growth (Nomura *et al.* 2013).

Inhibin is produced by granulosa cells of antral and pre-ovulatory follicles, and is believed to have opposite biological functions to those of activin. Inhibin decreases the synthesis and secretion of FSH from the pituitary gland in a negative feedback fashion (Childs *et al.* 1997). In this manner, inhibin prevents the proliferation of granulosa cells of antral follicles, hampering their further growth apart from the dominant 'selected' follicle (Geng *et al.* 2008).

AMH, the third member of TGF-β transcription superfamily, is produced by granulosa cells of pre-antral follicles. Its main function is to limit the recruitment of primordial follicles for folliculogenesis, stimulated by FSH. In this manner, AMH spares the primordial follicle

pool throughout the female fertile/reproductive period by preventing their early depletion (Durlinger *et al.* 1999).

1.1.2.3.2. FOX family

FOXL2, one of the FOX transcription factor proteins, gained a lot of interest recently after the discovery of a somatic missense mutation in 97% of adult granulosa cell tumour (GCT) patients (Kalfa *et al.* 2009). It plays an important role in maintaining the identity of granulosa cells (Schmidt *et al.* 2004), as well as regulating expression of the steroidogenic enzyme machinery (Caburet *et al.* 2012).

The FOXO family members FOXO1, FOXO3 and FOXO4 are all expressed in the ovary (Uhlenhaut and Treier 2011). FOXO3 is expressed in granulosa cells as well as oocytes (Liu *et al.* 2013), and has been shown to reserve the primordial follicle pool from early depletion in mice (Pelosi *et al.* 2013). Activation of FOXO3 causes granulosa cell apoptosis, and has been linked to polycystic ovary syndrome (PCOS) in humans (Mikaeili *et al.* 2016). FOXO1 protein is primarily expressed in ovarian granulosa cells of activin-high growing follicles, as well as in atretic follicles (Liu *et al.* 2013). FOXO1 has been shown to downregulate follicular steroidogenesis (Liu *et al.* 2009), repress LH receptor expression in the ovary (Law *et al.* 2013), and activate apoptosis of granulosa cells (Zhang *et al.* 2016). FOXO1 expression is controlled by FSH, causing downregulation of FOXO1 and inhibition of FOXO1-dependent apoptosis of ovarian granulosa cells (Shen *et al.* 2014). Although FOXO4 is expressed in granulosa cells of ovarian follicles, its deletion does not affect viability or fertility, leaving its ovarian function unidentified (Hosaka *et al.* 2004).

1.1.2.3.3. IGF

The IGF system consists of IGF binding proteins (IGFBP1-6), IGF and insulin receptors, in addition to the ligands insulin, IGF-1 and IGF-2 (Silva *et al.* 2009). IGF-1 and

gonadotrophins mutually regulate each other, and IGF-1 has been shown to potentiate the response to gonadotrophins by ovarian follicles (Mani *et al.* 2010). IGF-1 induces follicular growth, and its intra-ovarian levels are regulated by gonadotrophins (Checura *et al.* 2010).

IGF-2 is thought to function in the selection and maintenance of the dominant follicle, by increasing the proliferation of granulosa cells (Livingstone and Borai 2014). In addition, it has been reported that it increases the production of androgens from theca cells, and estradiol from granulosa cells of follicles (Livingstone and Borai 2014).

1.1.2.3.4. Interleukins

Interleukins are a subset of cytokines, which are preferentially produced in reproduction-related fluids and all types of follicular cells (Smolikova *et al.* 2012). They are believed to play an autocrine role in the regulation of follicular growth and ovulation; a process which is mediated by and results in an inflammatory response (Gerard *et al.* 2004). Most research has been directed towards elucidating the regulatory effects of interleukin-1 (IL-1) on ovarian functions. It has been shown to increase the growth of the dominant follicle and the maturation of the oocyte (Caillaud *et al.* 2005). In addition, it is believed to stimulate ovulation by inducing the secretion of inflammatory mediators such as prostaglandins, nitric oxides as well as proteolytic enzymes (Gerard *et al.* 2004), as well as regulating steroidogenesis in pre-ovulatory follicles by inducing progesterone synthesis and inhibiting estradiol synthesis (Caillaud and Gerard 2009).

1.1.3. Ovarian stem cells

Stem cells are rare undifferentiated somatic cells which have the ability to indefinitely self-renew and differentiate (Mayani 2003). Much effort has been recently directed towards characterizing this population in the ovary, following the identification of cellular markers for this population. However, no stem cells have been identified in granulosa cells or theca cells

(Ng and Barker 2015). Controversy exists about the presence of ovarian germ stem cells (Pan *et al.* 2016). However, success has been achieved in identifying the stem cell pool in the OSE (Flesken-Nikitin *et al.* 2013; Ng *et al.* 2014).

The hypothesis for the presence of stem cells in the OSE stems from the efficient regeneration and repair of OSE after the rupture caused by ovulation. These stem cells were recently characterized in the adult mouse by two groups. Nikitin and colleagues proposed the presence of a stem cell niche at the ovarian hilum; the site of entry of blood vessels and nerves to the ovary and the junctional area between OSE, mesothelium and oviductal epithelium (Flesken-Nikitin *et al.* 2013). Ng and colleagues showed that, in addition to the hilum, the stem cells are also present at the cleft regions between growing follicles or corpora lutea, and are abundant at the ovulatory rupture sites (Ng *et al.* 2014).

1.2. Ovarian cancer

1.2.1. Ovarian cancer statistics

Ovarian cancer (OC) is a term used to describe a heterogeneous group of malignancies, which arise from or involve the ovaries. OC is the second most common gynaecological malignancy and the deadliest of them (Marcus *et al.* 2014). The prevalence of OC is continuously rising, with nearly 239 000 new cases diagnosed worldwide in 2012 (Ferlay *et al.* 2015). In the UK, OC is the fifth most prevalent cancer in women, with 7378 new cases diagnosed in 2014 (4% of all female cancer cases)(CancerResearchUK 2017).

OC survival rates have changed a little over the last 20 years despite advances in treatment. In particular, poor patient survival is related to a lack of specific symptoms, leading to late diagnosis, the risk of relapse and development of chemoresistance (Bonome *et al.* 2008). Although one-year survival rates for OC are greater than 70%, 5-year survival rates are less than 45% (Siegel *et al.* 2015). It is the fifth highest cause of cancer deaths in women in the UK, accounting for 4128 deaths in 2014 (5% of cancer deaths in women) (CancerResearchUK 2017).

OC is considered a disease of the elderly, with 53% of cases diagnosed at the age of 65 and over. Incidence rates start to rise after the age of 30, and peak in women aged 65-69 (CancerResearchUK 2017).

1.2.2. Risk factors

Some factors might increase the risk of developing OC. It is believed that women who ovulate more tend to have higher risk of developing OC. It is well established that increasing parity, breast-feeding or oral contraceptive use reduces the risk of OC. On the other hand, infertility or hormone replacement therapy use increases OC risk (Doufekas and Olaitan 2014).

Lifestyle is considered a potentially controllable risk factor for OC, estimated to relate to 21% of OC cases in UK. Smoking tobacco causes OC, with 3% of cases diagnosed in UK believed to be linked to smoking (CancerResearchUK 2017). Obesity, talcum powder used in the genital area, occupational exposure to asbestos and radiation exposure have been linked to OC, although stronger evidence is still needed to confirm these links (Huncharek and Muscat 2011; Bounin *et al.* 2014; Usset *et al.* 2016).

About 10% of OC cases are caused by familial genetic mutations. *BRCA1* and *BRCA2* gene mutations account for 90% of inherited predispositions to OC (Randall and Pothuri 2016). Women with endometriosis or a history of breast cancer also have increased risk of OC (Munksgaard and Blaakaer 2011). Other medical conditions which have been linked to OC include diabetes and Lynch syndrome (Hereditary non-polyposis colorectal cancer) (CancerResearchUK 2017).

1.2.3. Types and origins of OC

According to the historic histologic classification of OC based on the cell of origin, OCs are classified into epithelial, sex-cord stromal and germ cell tumours (Figure 1.4). The most prevalent OCs are epithelial tumours, accounting for 90% of cases, followed by sex-cord stromal tumours (7%) and germ cell tumours (3%) (Bidus *et al.* 2012).

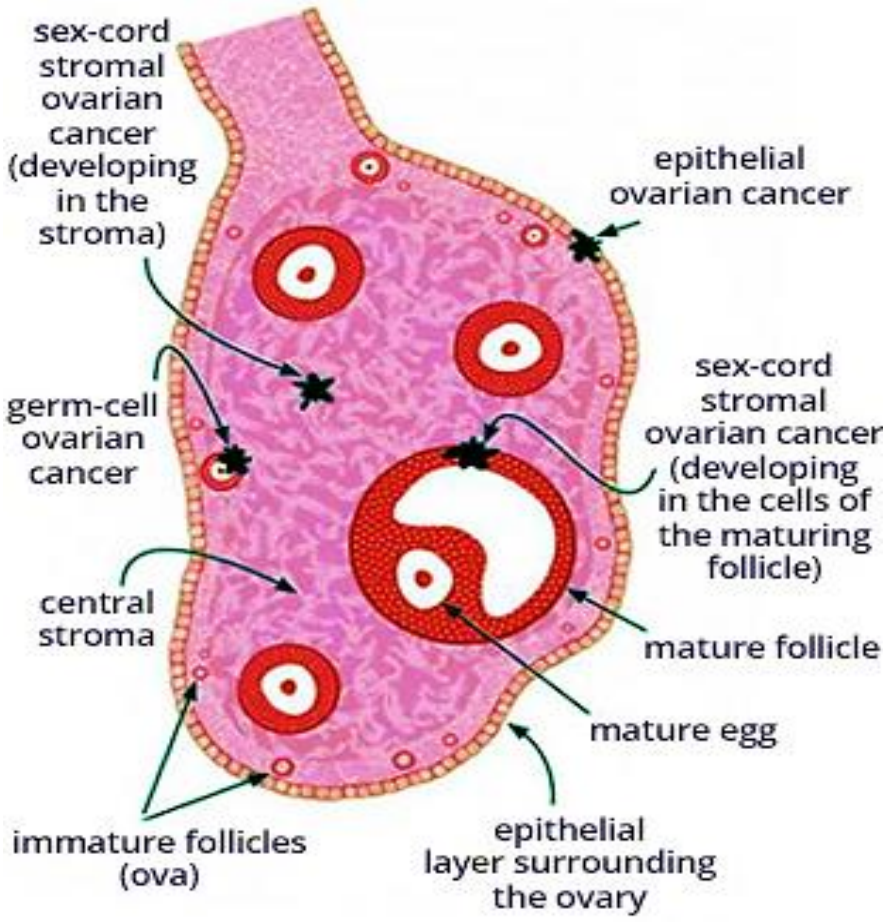

Figure 1.4: Schematic representation showing the cell of origin of the major types of ovarian cancer. Diagram © Commenwealth of Australia 2016

1.2.3.1. Epithelial ovarian cancer (EOC)

EOC includes histologic subtypes, which differ in their proposed origin, pathogenesis and molecular alterations. Histologically, EOCs are classified as serous (30-70%), endometrioid (10-20%), mucinous (5-20%) and clear cell (3-10%) and undifferentiated carcinomas (1%) (Rosen *et al.* 2009).

Serous carcinomas show a broad range of histologic features, in contrast to other ovarian carcinomas, which have less morphological variations. Serous carcinomas resemble cells of the tubal epithelium and display papillary architecture with focal slit-like spaces and irregular luminal contours. Ovarian endometrioid adenocarcinomas (OEA) resemble

endometrial glands with tubular sheet-like growth and papillae (Przybycin and Soslow 2011). Mucinous OC cells resemble gastrointestinal or endocervical epithelial cells, with intracytoplasmic mucin, and composed of closely packed glands and cysts (Lee and Nucci 2003). Clear cell carcinomas (CCC) demonstrate a limited architecture composed of 'hobnail cells' with clear cytoplasm, which resemble cells found in nests in the vagina (Przybycin and Soslow 2011). Undifferentiated carcinomas lack histological differentiating features.

Different theories have been proposed to define the cell of origin of EOC (Figure 1.5). Different histologic types of EOC have historically been thought to be derived from the OSE following metaplastic changes, leading to the development of different histotypes whose epithelium resembles müllerian duct-derived epithelium. These metaplastic changes are believed to be associated with ovulation, which contributes to increased risk for genetic aberrations to the OSE in response to repeated rupture and repair (Fleming *et al.* 2006). In this model, OSE clefts and inclusion cysts are the preferred sites for neoplastic progression of OSE. This may be attributed to the fact that the epithelial cells in the cleft and cysts are not separated from the underlying stroma, enhancing their access to stromal-derived cytokines and hormones, which promote neoplastic progression (Deligdisch *et al.* 1995).

With the recent advances in the identification and isolation of stem cells from the OSE, it could be suggested that OSE stem cells, when trapped inside the ovary, can initiate EOC and differentiate into any of the müllerian tumour lineages (Ng and Barker 2015).

An alternative theory proposes that tumours with a müllerian phenotype (serous, endometrioid or clear cell) are derived from müllerian-type tissue not the OSE mesothelium. These tumours can be derived from para-ovarian and para-tubal microscopic structures, collectively known as 'secondary müllerian system' (Dubeau 1999). Another hypothesis is that these cells are derived from epithelial cells of the uterine endometrium (endometrioid and clear

cell histotypes) or fallopian tube (serous histotype) by retrograde menstruation, following their travel up to the ovary and shedding from the distal part of the fallopian tube (fimbria) into the ovary at the site of rupture post ovulation (Kurman and Shih 2016).

More recently a third theory has been advanced which argues that the majority of ovarian carcinomas, the high grade serous carcinomas, arise primarily in the fallopian tube as serous tubal intraepithelial carcinomas, which then spread to the ovary (Seidman *et al.* 2011).

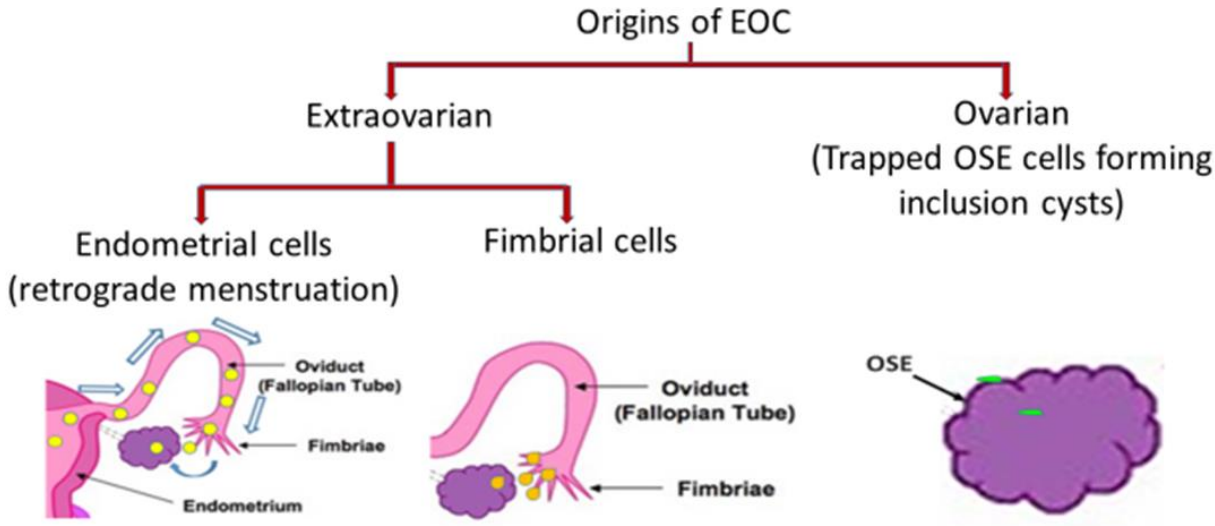

Figure 1.5: Schematic outline of different theories proposed to define epithelial ovarian cancer EOC cell of origin.

1.2.3.1.1. Ovarian cancer stem cells

Cancer stem cells (CSCs) represent a very small subgroup of tumour cells characterized by their capacity of self-renewal, differentiation and tumour initiation (Wicha *et al.* 2006). Unlike rapidly dividing cancerous cells, CSCs are quiescent, thus escaping the effects of current cytotoxic therapies designed to destroy rapidly dividing cells. CSCs may have upregulated DNA repair capacity, be resistant to apoptosis and over-express ATP-binding cassette (ABC) drug efflux transporters. They are thus believed to play a crucial role in tumour development, chemo-resistance and relapse after initial treatment (Tomao *et al.* 2014).

CSCs from OC were first isolated from malignant ascites (Bapat *et al.* 2005), and thereafter from primary human ovarian tumours and OC cell lines (Lin *et al.* 2011; Wang *et al.* 2012). Ovarian CSCs are regulated by a variety of genes, micro RNAs and the surrounding tumour microenvironment (termed 'CSC niche'). Developmental signalling pathways, including Notch, WNT, Hedgehog and TGF-β have been implicated in the regulation of CSCs including ovarian CSCs (Kwon and Shin 2013).

1.2.3.2. Non- epithelial ovarian tumours

Sex-cord stromal tumours originate from the stromal cells or somatic cells of the growing follicles. Granulosa cell tumours are the most prevalent histotype in this group, representing about 5% of all OC cases. Other types in this group are thecoma (from theca cells), fibroma (from fibroblasts), luteoma (from luteal cells) and androblastoma (Sertoli-Leydig cell phenotype) (Horta and Cunha 2015).

Germ cell tumours, arising from the germinal cells (which give rise to the oocyte), are the least prevalent. These tumours are further classified into dysgerminoma, teratoma and yolk sac tumours (Shaaban *et al.* 2014).

1.2.4. Molecular pathogenesis of OC

The molecular pathogenesis of OC differs from one histotype to another. In high-grade serous ovarian carcinoma (HGSOC), mutations in *TP53* and genomic instability predominate in 95% of cases, with frequent germline (9%) and somatic (3%) mutations in *BRCA1* and *BRCA2* (CGARN 2011). Low-grade serous ovarian carcinoma (LGSOC) often harbours activating mutations in *KRAS* and its downstream mediator *BRAF* (Singer *et al.* 2003).

Aberrant activation of Wnt/β-catenin signalling, mainly via activating mutations of catenin β1 (*CTNBB1*) gene and microsatellite instability, are characteristic of ovarian endometrioid adenocarcinoma (OEA) (Wu *et al.* 2001; Tanwar *et al.* 2013). Somatic

inactivating mutations in the chromatin remodelling gene *ARID1A*, together with inactivating mutations of *PTEN* or activating mutations in *PIK3CA*, are common in both OEA and clear cell carcinoma (CCC) (Fujiwara *et al.* 2016). Recently, increased promoter methylation of genes involved in the estrogen receptor α (ERα) pathway have also been identified in CCC, in addition to loss of promoter methylation in genes of the hepatocyte nuclear factor 1 pathway (Yamaguchi *et al.* 2014).

In the remaining histologic subtypes, *KRAS* activating mutations along with amplification of its signalling activator *HER2* and the downstream target *BRAF*, are present in 90% of mucinous carcinomas (Anglesio *et al.* 2013). Frequent mutations in *TP53* are present in mucinous carcinomas and recently another inactivating mutation, the *RNF43* mutation, has also been identified (Ryland *et al.* 2013). In adult granulosa cell tumours, *FOXL2* somatic missense mutation has been identified in 97% of tumours (Shah *et al.* 2009). *DICER1* mutations are present in 60% of Sertoli-Leydig cell tumours of the ovary (Wang *et al.* 2015b).

1.2.5. Grading EOC

Kurman and Shih have proposed a dualistic model that categorizes EOC into low grade Type I and high grade Type II (Figure 1.6) (Kurman and Shih Ie 2010; Kurman and Shih 2016). Type I tumours make up 10-20% of EOC, are diagnosed in an early stage and have better prognosis. They include mucinous, clear cell, and low-grade serous and endometrioid histotypes. These tumours are genetically more stable and are characterized by the presence of somatic mutations in one or more of *KRAS*, *BRAF*, *ERBB2 (HER2)* , *CTNNB1*, *PTEN*, *PIK3CA* and *ARID1A* genes. Type II tumours are more aggressive, always diagnosed at an advanced stage and with poor prognosis. They include HGSOC, high-grade OEA, and undifferentiated cancers. They are characterized by marked chromosomal instability with a very high frequency of *TP53* mutations.

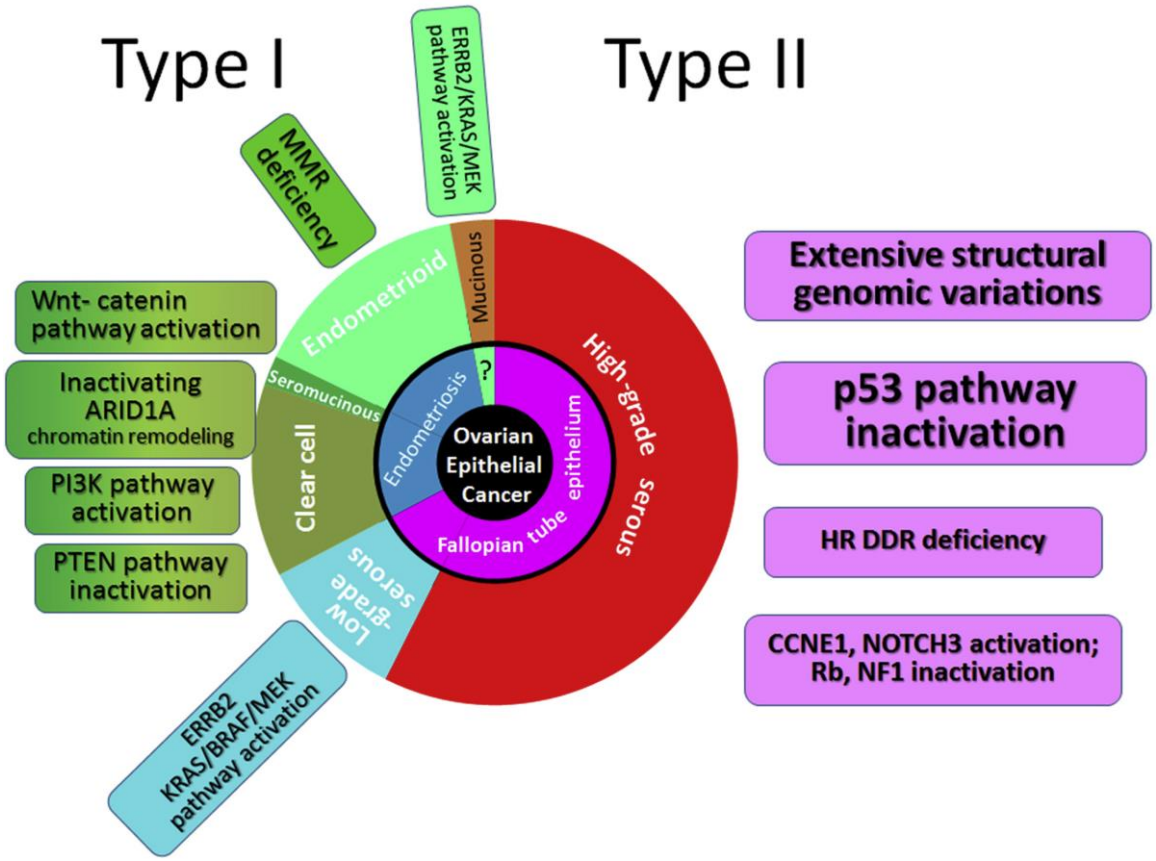

Figure 1.6: Dualistic model of grading EOC as proposed by Kurman and Shih (Kurman and Shih 2016). ARID1A: AT-rich interaction domain 1A; BRAF: B-Raf proto-oncogene; CCNE1: cyclin E1; ERRB2: estrogen-related receptor β2; HR DDR: homologous recombination-mediated DNA damage repair; KRAS: Kirsten rat sarcoma viral oncogene homologue; MEK: mitogen-activated protein (MAP) extracellular signal-related kinase (ERK) kinase; MMR: DNA mismatch repair; NF1: nuclear factor 1; PI3K: phosphatidylinositol 3-kinase; PTEN: phosphatase and tensin homologue; Rb: retinoblastoma protein.

1.2.6. Staging OC

Staging of gynaecological cancers, including OC, has been standardized by The International Federation of Gynaecologists and Obstetricians (FIGO) (Prat 2013). OC, together with primary fallopian tube and primary peritoneal cancer, are staged surgically and pathologically into 4 stages (Prat 2013).

Stage I: Tumour confined to ovaries or fallopian tube(s). Most OC patients are diagnosed beyond this stage, apart from GCT patients, who are mostly diagnosed at this stage (Mangili *et al.* 2013), with overall 15% OC patients being diagnosed at this stage (Jelovac and Armstrong 2011)

Stage II: Tumour involves one or both ovaries or fallopian tubes spreading to the fallopian tube or uterus (IIA) or is associated with primary pelvic intraperitoneal cancer (IIB). 17% of cases are diagnosed at this stage (Jelovac and Armstrong 2011)

Stage III: Tumour involves one or both ovaries or fallopian tubes, or primary pelvic intraperitoneal cancer, with confirmed cytological or histological spread to the peritoneum outside the pelvis, and/or metastasis to the retroperitoneal lymph nodes. The majority of OC patients (62%) are presented at this stage (Jelovac and Armstrong 2011)

Stage IV: Ovarian tumours with distant metastasis excluding peritoneal metastases. This includes pleural effusion with positive cytology (IVA) or liver, spleen and extra-abdominal metastases (IVB). Less than 10% of patients are diagnosed at this stage (Cormio *et al.* 2003)

1.2.7. EOC screening

One of the major problems with EOC is being asymptomatic in early stages of the disease. The most common symptoms of EOC are related to abdominal discomfort, back pain and urgency to urinate, which could easily be mistaken for irritable bowel syndrome or pre-menstrual syndrome. Given that EOC is located deep within the pelvis, and a lack of effective diagnostic methods, more than 60% of patients are diagnosed at advanced stages. Therefore, it is important to develop early detection markers to be used for screening and following up patients with EOC.

There is currently no screening test reliable enough to detect early stage EOC patients. Cancer antigen 125 (CA125) is the most widely studied biomarker for EOC, as it tends to be higher in women with EOC. However, it can be increased in many other conditions unrelated to OC (e.g. abdominal disorders, lung diseases and non-malignant gynaecological diseases) as well as in other cancers, decreasing its specificity (Buamah 2000). Its sensitivity as a screening tool to identify early stage disease is limited, with only 50% of patients with stage I ovarian cancer showing elevated levels (Nossov *et al.* 2008).

Another useful biomarker is the human epididymis protein 4 (HE4), which shows better sensitivity compared to CA125 (mainly for early-stage EOC), and the ability to differentiate between benign and malignant tumours (Simmons *et al.* 2013). Multiplex screening using a panel of serum biomarkers, including CA125 and HE4, has proved to have better sensitivity, specificity and reliability compared to any individual biomarker (Moore *et al.* 2009).

It is therefore vital to identify and validate new diagnostic biomarkers for early diagnosis of EOC. Various gene- and microRNA-based OC biomarkers have been recently identified and might be promising in early detection of the different histotypes of EOC, but their clinical utility is still under investigation (Zhang *et al.* 2011a; Pal *et al.* 2015).

1.2.8. EOC diagnosis

According to the National Institute for Health and Care Excellence (NICE) guidelines, any female patient (especially older than 50) suffering from abdominal bloating, pelvic pain or increased frequency to urinate should have a CA125 serum measurement test. If CA125 levels are higher than 35 IU/ml, an ultrasound scan of the abdomen and pelvis should be arranged. The same applies for any woman with ascites, pelvic or abdominal mass during physical examination (NICE 2011).

If the ultrasound, together with physical examination and elevated CA125 levels suggest EOC, a computerized tomography (CT) scan for pelvis and abdomen should be performed. If confirmed, the disease should be identified and staged histologically by examining a tumour specimen either after surgical resection or on a biopsy obtained via percutaneous image-guided biopsy (NICE 2011).

1.2.9. EOC treatment

1.2.9.1.Management of EOC patients

The current gold standard treatment strategy for EOC is surgical resection, followed by platinum or taxane therapy (Fujiwara *et al.* 2013), which reduces tumour burden and causes cancer cell death via DNA and cytoskeletal damage responses (Abubaker *et al.* 2014). In patients with early disease (FIGO stage I-II), surgery is able to cure the disease without adjuvant chemotherapy and the 5-year survival rate is around 90%. However, only 30% of OC cases are diagnosed at this early stage. In patients diagnosed with FIGO (III-IV) OC, maximal surgical cytoreduction (total abdominal hysterectomy, bilateral salpingo-oophorectomy, pelvic and para-aortic lymphadenectomy and omentectomy) followed by systemic platinum-based chemotherapy, is the standard treatment strategy, with a 5-year survival of 10-30% (Kim *et al.* 2012). This low survival is due to the fact that approximately 80% of women with advanced OC (stage III and IV) will have tumour recurrence. This is usually eventually fatal due to the emergence of drug resistance in the microscopic residual disease persisting after the first line chemotherapy (Luvero *et al.* 2014).

1.2.9.2. Chemoresistance to cytotoxic agents

The development of chemoresistance in EOC is poorly understood, although many different theories have been proposed to explain the origin of chemoresistant cells. One theory proposes cytotoxicity-induced mutations occurring within the tumour population, that lead to chemoresistance (Fraser *et al.* 2003). Another suggests that genetically heterogeneous clones

exist in the tumour that differentially respond to the cytotoxic therapy, with the chemosensitive clones eradicated post-treatment, thus leaving the resistant clones to survive after therapy (Cunnea and Stronach 2014). Those chemoresistant tumour cells express high levels of multidrug resistance transporters, proliferate slowly and can repair damaged DNA, a phenotype that is commonly displayed by CSCs (Ahmed *et al.* 2013). A recent theory relates chemoresistance to the metabolic interaction between tumour cells and their microenvironment, which can cause tumour cells to become quiescent, thereby escaping cytotoxic effects (Suh *et al.* 2014). Targeting molecular pathways and mechanisms responsible for chemoresistance could lead to better prognosis.

1.2.9.3. Targeting OC microenvironment

It is now widely accepted that cells (tumour, stromal and inflammatory cells) and molecules present in the tumour microenvironment affect tumourigenesis, mainly through promoting angiogenesis and modulating stromal invasion and metastasis. Antiangiogenic agents, targeting endothelial cells, are currently undergoing clinical trials for use as single agents or in combination therapy with platinum or taxanes, and the results published so far are promising, as reflected by improved progression-free survival and objective response rate (Luvero *et al.* 2014). Bevacizumab, a recombinant antibody targeting vascular endothelial growth factor (VEGF), is approved by the European Medicines Agency for use in treating primary OC patients with tumour stage beyond FIGO stage IIIA, and in recurrent OC cases (Lokadasan *et al.* 2016).

Cancer-associated fibroblasts (CAFs) have been shown to play important roles in EOC progression and metastasis. Targeting fibroblast growth factor receptor (FGFR) appears to be an attractive intervention, and several clinical trials are testing the efficacy of non-specific targeting of FGFR using receptor tyrosine kinase inhibitors in solid tumours (Hansen *et al.* 2016). Of interest are the clinical trials on nintedanib, a non-specific receptor tyrosine kinase

inhibitor, which targets FGFR in addition to VEGFR and platelet-derived growth factor receptors. It is now undergoing phase III clinical trials as a single agent or in combination with platinum/taxane treatment in primary or recurrent EOC patients, and the results published so far are promising, showing an increase in progression-free survival (du Bois *et al.* 2016).

Inflammation has historically been hypothesized as an initiator of EOC. Inflammatory mediators have been shown to promote tumour progression and metastasis (Knutson *et al.* 2015), and targeting such molecules in the microenvironment is an attractive alternative. Some success was reported by targeting the pro-inflammatory tumour necrosis factor-α (TNF-α) and interleukin-6 (IL-6). Targeting TNF-α prolonged disease stabilization in 20% of patients undergoing phase II clinical trial, and targeting interleukin-6 (IL-6) in a phase II clinical trial (in combination therapy) resulted in 1/18 patient with a partial response and 7/18 with periods of disease stabilization. TNF-α antagonists etanercept and infliximab are currently undergoing clinical trials for their use in OC patients (Coward *et al.* 2015).

1.2.9.4. Targeting signalling pathways in EOC

Targeting PTEN/PI3K/AKT could be useful in many type I EOC patients, where inactivating mutations of *PTEN* or activating mutations in *PIK3CA*, are common (Fujiwara *et al.* 2016). Clinical trials have been conducted for a range of mTOR inhibitors, either as a single agent or in combination with other agents, but the results were disappointing because of low response rates (Cheaib *et al.* 2015). More promising results were encountered with AKT inhibitors and PI3K inhibitors, showing higher response rates in combination therapy with cytotoxic agents, and are undergoing phase II clinical trials (Cheaib *et al.* 2015).

WNT signalling has been previously shown to play important roles in EOC tumourigenesis, chemoresistance and activation of ovarian CSCs (Nagaraj *et al.* 2015). Early-stage clinical trials for targeting WNT signalling in many solid tumours, including OC, are

currently ongoing (Masuda *et al.* 2015). Several approaches are under investigation, including targeting extracellular secretion of Wnt proteins using porcupine inhibitor, targeting Frizzled (FZD) receptors using monoclonal antibodies (e.g. vanituctumab) and targeting β-catenin co-activators (e.g. PRI-724) (Zhang and Hao 2015).

WNT signalling activation contributes to the tumorigenicity of CSCs. A new Wnt antagonist, OMP-54F28, was recently developed. Preclinical studies showed reduced tumour growth and decreased CSC frequency when OMP-54F28 was used as a single agent or in combination with other chemotherapeutic agents. A phase 1B trial is ongoing to study OMP-54F28 in combination with paclitaxel and carboplatin in OC patients (Le *et al.* 2014).

Targeting KRAS/BRAF could be an effective strategy for treating patients with low-grade serous or mucinous OC. Some success was achieved using MEK inhibitors for treating low-grade serous carcinoma (Coward *et al.* 2015). A phase II/III clinical trial is currently ongoing in the UK for assessing the efficacy of the MEK inhibitor trametinib (GSK 1120212) in patients with recurrent or progressive low-grade serous OC or peritoneal cancer (Coward *et al.* 2015).

HGSOC patients with *BRCA1* or *BRCA2* mutations could benefit from poly adenosine diphosphate (ADP)-ribose polymerase (PARP) inhibitors. Food and Drug Administration (FDA) has recently approved the use of olaparib, the leading PARP inhibitor, as a fourth-line therapy in recurrent HGSOC *BRCA*-mutated patients (Meehan and Chen 2016).

1.2.9.5.Targeting CSCs

Targeting CSCs, the cell population thought to be responsible for chemoresistance and relapse, appears attractive (Walters Haygood *et al.* 2014), and several approaches are currently being developed. One is to target regulatory signalling pathways of CSCs e.g. WNT signalling. Another approach is to use immunologic therapy, with antibodies to CSC-surface markers.

Hyaluronic acid-cisplatin and hyaluronic acid-paclitaxel conjugates were both tested to target CD44-positive cancer cells in a xenograft EOC model (Li and Howell 2010; Lee *et al.* 2012). Both interventions reduced tumour growth when compared to free unconjugated cytotoxic treatment. A third approach is to target the metabolic interaction between CSCs and their microenvironment; modulating the energy metabolism in ovarian CSCs using metformin was shown to restrict the growth and proliferation of ovarian cancer stem cells *in vitro* and *in vivo* (Kim *et al.* 2014b).

1.3. Signalling pathways dysregulated in OEAs

1.3.1. WNT signalling

WNT signalling is a highly conserved developmental signalling pathway that is known to play several roles during embryogenesis, adulthood and tumourigenesis, through the regulation of cell fate, proliferation, migration and stem cell activity (Smalley and Dale 1999). Wnt is a family of secreted glycoproteins with 19 identified members, which bind mainly with the FZD receptor to transduce the signal intracellularly via Dishevelled (Dvl) and initiate the response via activating downstream signalling cascades (Anastas and Moon 2013). These signalling cascades are classified into canonical (Wnt/B-catenin) and non-canonical WNT signalling cascades, the latter of which includes planar cell polarity (PCP) and Wnt/calcium signalling pathways (Figure 1.7)(Inestrosa and Varela-Nallar 2015).

1.3.1.1. Non-canonical WNT signalling

Calcium-dependent WNT signalling transduces the signal via increasing the intracellular concentration of calcium. This subsequently leads to the repression of cyclic guanosine monophosphate (cGMP) and activation of NEAT transcription factor, and protein kinases including protein kinase C (PKC) and calcium/calmodulin-dependent protein kinase II (CaMKII) (Inestrosa and Varela-Nallar 2015).

Unlike calcium-dependent and canonical WNT signalling cascades, the PCP pathway does not activate gene transcription. Instead, Wnt glycoproteins bind to FZD receptors (and/or RYC, ROR receptors) to phosphorylate Dvl, causing activation of small GTPases RHO and RAC, which subsequently activate JNK proteins, known regulators of cytoskeletal arrangement, cell migration and cell polarity (Inestrosa and Varela-Nallar 2015).

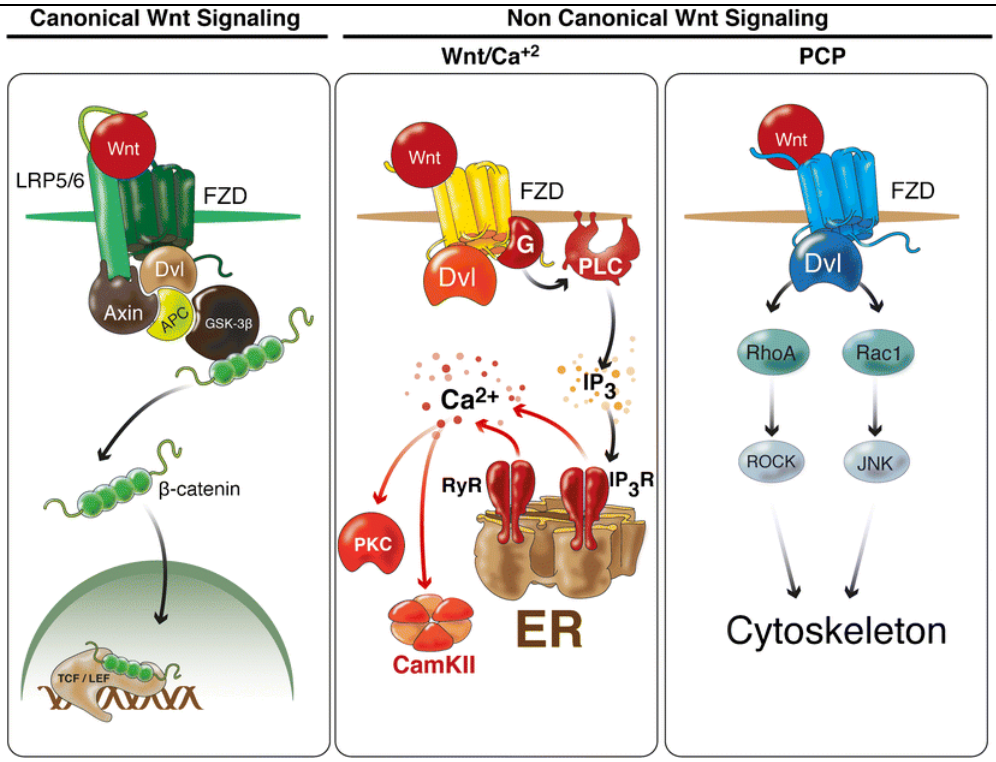

Figure 1.7: Schematic illustration of WNT signalling pathway: Canonical WNT signalling, calcium-dependent pathway (Wnt/Ca^{+2}), and planar cell polarity (PCP) pathway. Frizzled (*FZD*). Low density lipoprotein-related protein 5 or 6 (LRP5/*6*). Dishevelled (Dvl). Glycogen synthase kinase-3β (GSK-*3β*). Adenomatous polyposis coli (*APC*). Phospholipase C (PLC). Inositol triphosphate (IP3). Endoplasmic reticulum (ER). Calcium/calmodulin-dependent protein kinase II (CamKII). Protein kinase C (PKC). Rho-associated protein kinase (ROCK). Jun N-terminal kinase (JNK). (Inestrosa and Varela-Nallar 2015)

Historically, Wnt glycoproteins were classified as canonical or non-canonical (Du *et al.* 1995). However, it has been shown that some Wnt glycoproteins can interact with both cascades in different manners, and their interaction is context-specific. For example, Wnt11 has been shown to activate both canonical and non-canonical WNT signalling (Cha *et al.* 2008). Conversely, Wnt5a which activates non-canonical WNT signalling, has been shown to both activate and repress canonical WNT signalling (van Amerongen *et al.* 2012).

1.3.1.2. Canonical WNT signalling

This signalling cascade regulates the transcription of genes controlling cell proliferation, differentiation and fate. In the absence of Wnt glycoprotein, a β-catenin destruction complex is formed of the scaffolding protein AXIN1, adenomatous polyposis coli (APC), glycogen synthase kinase-3 (GSK3) and casein kinase-1 (CK1) proteins, resulting in phosphorylation of β-catenin, marking it for ubiquitination and degradation. This keeps the cytoplasmic β-catenin concentration low, thus preventing its translocation to the nucleus. Conversely, after the binding of Wnt glycoproteins to FZD receptors and LRP co-receptors, Dvl is phosphorylated and recruited to interact with AXIN1, causing the destruction complex to fall apart. This prevents phosphorylation of β-catenin, leading to its accumulation in the cytoplasm and subsequent translocation to the nucleus, where β-catenin initiates the transcription of Wnt target genes upon binding with TCF (Figure 1.8)(Clevers 2006).

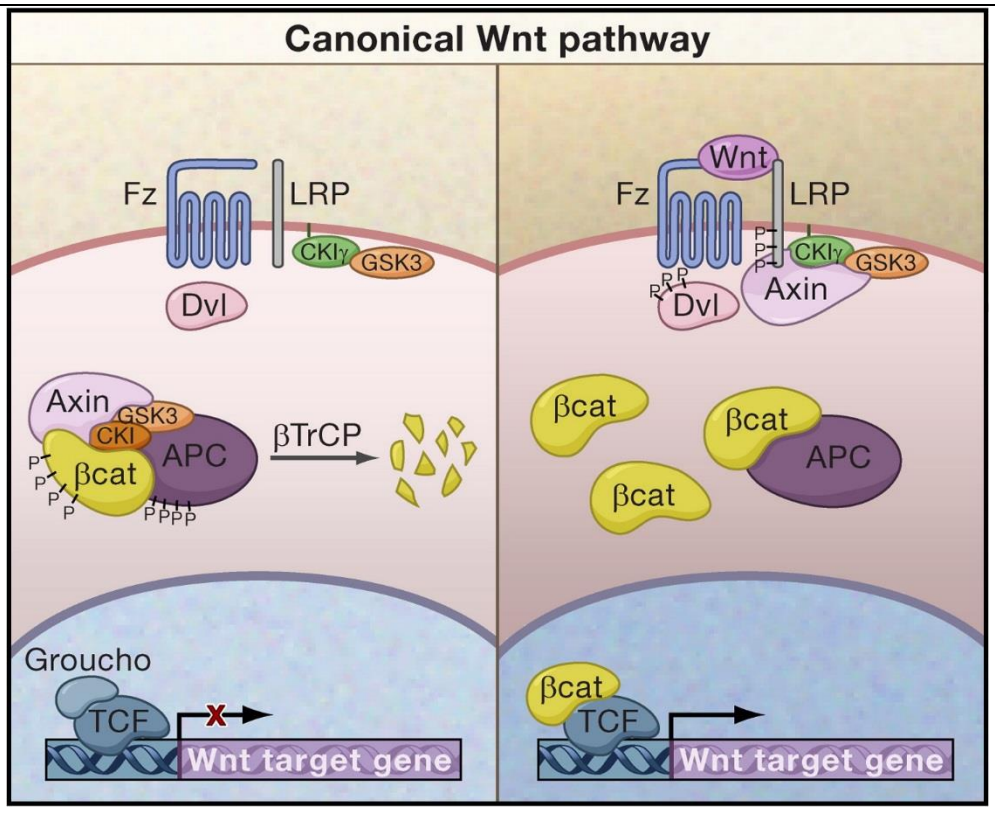

Figure 1.8: Schematic representation of canonical WNT signalling pathway (Clevers 2006).

Canonical WNT signalling was previously reported to regulate female gonadal differentiation and development during embryogenesis (Pellegrino *et al.* 2010). In addition, WNT signalling functions in regulating follicular development, corpus luteum maturation and ovarian steroidogenesis (Richards and Pangas 2010; Lapointe and Boerboom 2011; Pan *et al.* 2014). It has been suggested that WNT signalling is important for the differentiation of OSE, and that WNT signalling deregulation in the OSE plays a functional role in tumourigenesis. However, the exact mechanisms are not yet defined (Usongo 2013).

Aberrant WNT signalling is involved in tumour initiation and progression in many epithelial tumours, including EOC (Arend *et al.* 2013; Voloshanenko *et al.* 2013; Jiang *et al.* 2014). WNT signalling is considered to play an important role in epithelial to mesenchymal transition (EMT) in EOC, a process implicated in chemoresistance and metastasis (Ford *et al.* 2014). WNT signalling is one of the important signalling pathways deregulated in cancer stem cells, driving their self-renewal and differentiation (Holland *et al.* 2013). With the exception of OEA, mutations in WNT signalling genes are considered rare in EOC. It was believed that WNT signalling is implicated in the pathogenesis of OEA subtype only. However, emerging data shows that WNT signalling is involved in the tumorigenesis of other histotypes of EOC (Maria and Rebecca 2011).

1.3.1.3. Adenomatous polyposis coli APC

Adenomatous polyposis coli (APC) is a tumour suppressor protein which negatively regulates canonical WNT signalling, being a part of the β-catenin destruction complex (Benchabane and Ahmed 2009). APC protein function is attenuated by mutations of one or both *APC* alleles or by promoter methylation, leading to tumourigenesis, mainly in colorectal cancer (TCGA 2012), but also in hepatocellular carcinoma (Xu *et al.* 2014) and ovarian cancer (Shen *et al.* 2016).

APC is a large multifactorial protein widely expressed in all body tissues, formed of 2843 amino acids encoded by 16 exons (Crist *et al.* 2010). APC is formed of different domains which function in the control of cell migration, adhesion, proliferation, differentiation, chromosomal segregation and stabilization of microtubules (Figure 1.9) (Aoki and Taketo 2007). Point mutations mostly occur in the mutational cluster region, causing truncation of the protein C-terminal (including β-catenin binding domains) and subsequently causing canonical WNT signalling activation leading to upregulation of downstream oncoproteins such as MYC and Cyclin D1 (Aoki and Taketo 2007).

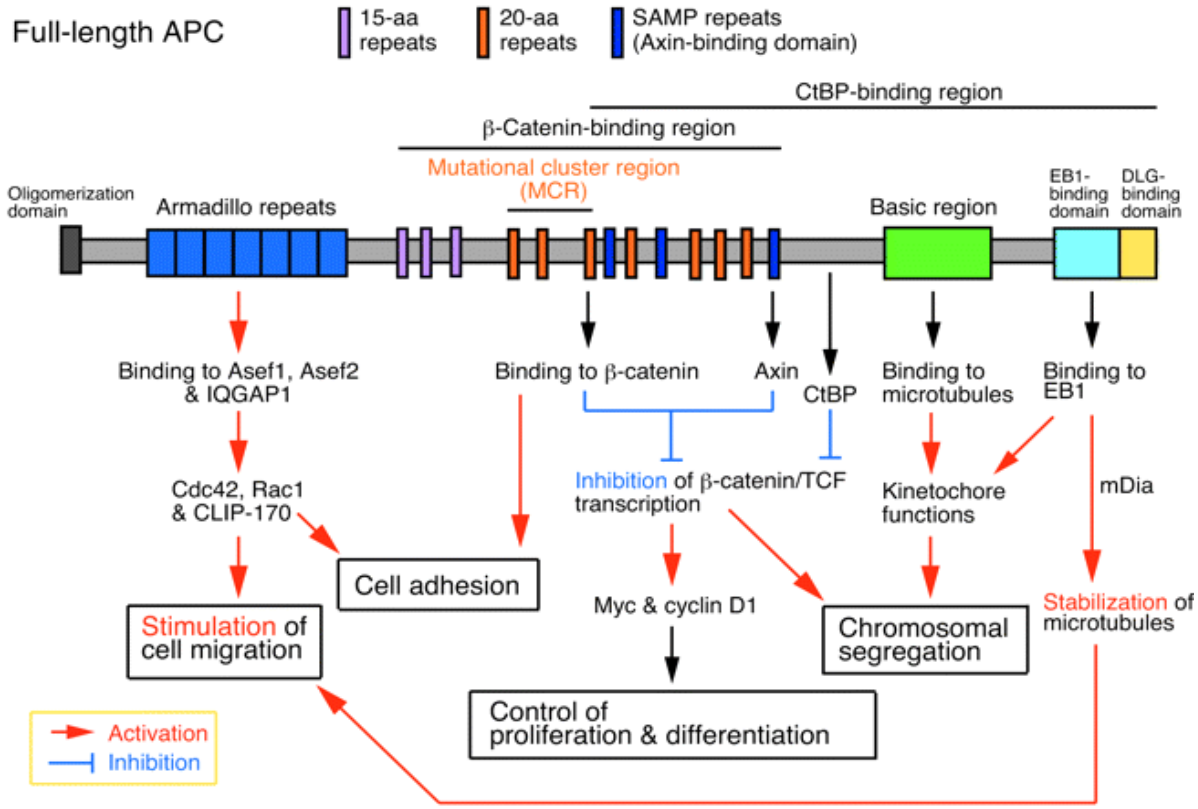

Figure 1.9: Schematic representation of APC protein domains and their functions. APC armadillo repeats bind to Asef1 and Asef2 to stimulate cell migration. APC controls cell adhesion via controlling β-catenin membranous and cytoplasmic distribution. APC inhibits transcription of β-catenin target genes. APC controls chromosomal segregation via kinetochore binding and suppression of canonical WNT signalling. (Aoki and Taketo 2007)

1.3.1.4. Adenomatous polyposis coli 2 APC2

Adenomatous polyposis coli 2 (APC2), formerly known as APC-like (APCL), is a tumour suppressor protein homologous to APC. In humans, the protein is encoded by the *APC2* gene, present on chromosome 19 and formed of 17 exons (Van Es *et al.* 1999). The Mouse *Apc2* gene is homologous to the human APC2 gene, is located on chromosome 10, spans 14 kb and is formed of 14 exons (Figure 1.10)(Bell *et al.* 1999). The highest expression of APC2 has been detected in the foetal and adult brain respectively (Van Es *et al.* 1999). Low levels of APC2 are expressed in a wide range of tissues, including the ovary (Jarrett *et al.* 2001).

Most of the studies carried out to functionally characterize APC2 have been performed in *Drosophila* or mammalian cell lines. Using a mammalian carcinoma cell line, it was shown that APC2 downregulates β-catenin and regulates the formation of β-catenin-TCF complexes, suggesting that it plays a role in the Wnt/β-catenin signalling pathway (Van Es *et al.* 1999). This role was confirmed in a study with cell lines and *Drosophila* embryos, showing that APC2's regulation of WNT signalling is independent of its cytoplasmic localization or ability to enter the nucleus (Roberts *et al.* 2012).

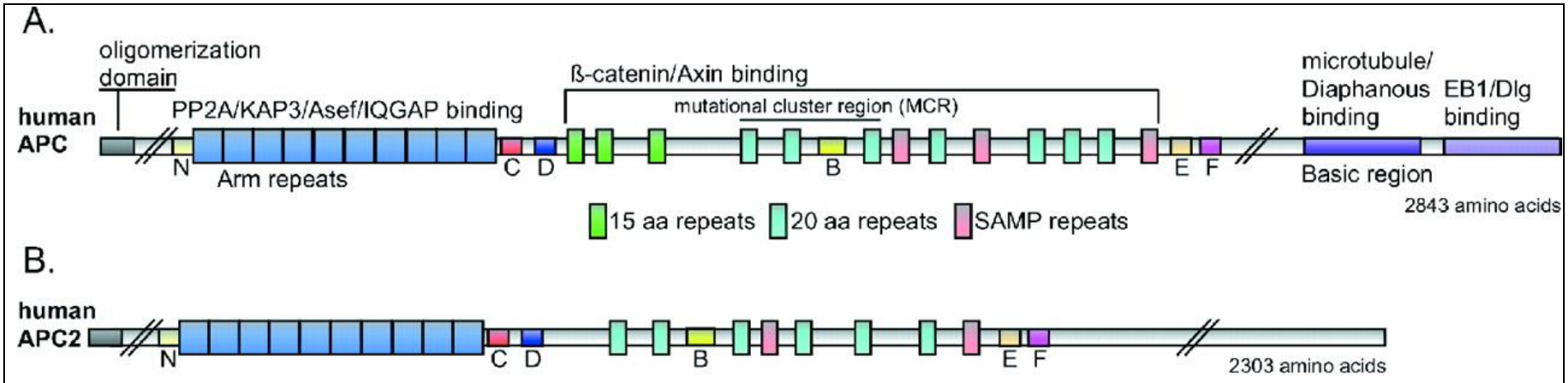

Figure 1.10: Schematic representation showing similarities between human (A) APC and (B) APC2 proteins.(McCartney *et al.* 2006)

Biochemical and localization studies in *Drosophila* suggested that APC2 has a role in cytoskeleton regulation and microtubule association (McCartney *et al.* 1999). APC2 plays a role in spindle anchoring during mitosis in the *Drosophila* embryo, and participates with armadillo and β-catenin in linking mitotic spindles to cortical actin (McCartney *et al.* 2001). These findings were confirmed in work using ovarian cancer cell lines, showing that APC2 colocalizes with the Golgi apparatus and actin filaments (Jarrett *et al.* 2001). These findings suggest that the APC2 interaction with actin filaments could influence cell motility and adhesion. Using a chick retinotectal topographic projection system, APC2 was shown to induce the stabilization of microtubules, affecting axonal projections and influencing nervous system development (Shintani *et al.* 2009). Using mammalian cell lines, APC2 was shown to colocalize with p53 binding protein 2 in the perinuclear region, and it was suggested that APC2 might regulate the p53/Bcl2-linked pathway of cell-cycle progression and apoptosis (Nakagawa *et al.* 2000a).

Little is known about how APC2 functions in adult ovaries, but APC2 loss has been reported in EOC. *APC2* allelic imbalance was reported in 19 of 20 human ovarian cancers screened (Jarrett *et al.* 2001). *APC2* genomic copy number alterations (deletions) have also been reported in human high grade serous carcinoma (Perets *et al.* 2013). A study in the *Drosophila* ovary has shown that APC2 controls stem cell niche size, architecture and stem cell numbers through negative regulation of WNT signalling, and regulation of cortical actin (Oliver and McCartney 2014). A recent study supported this hypothesis, showing that miR-939, which functions via downregulation of *APC2* and subsequently deregulates Wnt/β-catenin signalling, is a potential tumour promotor in the ovaries (Ying *et al.* 2015). However, it is still unknown whether APC2 loss contributes to tumourigenesis or occurs passively during tumour progression.

1.3.2. PTEN/PI3K/AKT signalling

PTEN is the first tumour suppressor protein discovered to have phosphatase activity. Because of its homology to tensin protein, its phosphatase activity towards protein substrates and lipids, and the frequent mutations of *PTEN* gene (located on chromosome 10 in humans) in cancers, it gained its name PTEN (Phosphatase and tensin homologue, mutated on chromosome 10; also known as MMAC1 and TEP1) (Li *et al.* 1997).

PTEN directly antagonizes phosphatodylinositol-3-kinase (PI3K) function. While PI3K catalyses the conversion of phosphatidylinositol-4,5-biphosphate (PIP2) to phosphatidylinositol-3,4,5-triphosphate (PIP3), PTEN dephosphorylates PIP3 converting it back to PIP2 (Maehama and Dixon 1998).

PI3K is normally present in a catalytically inactive state in the cytoplasm. However, activation of receptor tyrosine kinase (RTK) by growth factors or activated RAS signalling activates the catalytic subunit of PI3K; the p110 subunit (Vivanco and Sawyers 2002). Subsequently, PIP2 is converted to PIP3, which activates AKT by phosphorylation at threonine 308 and serine 473 residues. Phosphorylated AKT (p-AKT) phosphorylates a range of downstream target proteins, causing the deactivation of apoptosis-effector proteins (e.g. BAD-FOXO proteins) and evasion of cell death, one of the hallmarks of cancer (Kandel and Hay 1999). In addition, p-AKT activates the mammalian target of rapamycin (mTOR) signalling pathway, causing activation of ribosomal biogenesis, increased cellular growth, upregulation of anabolic processes and downregulation of autophagy and catabolic processes (Figure 1.11)(Wullschleger *et al.* 2006).

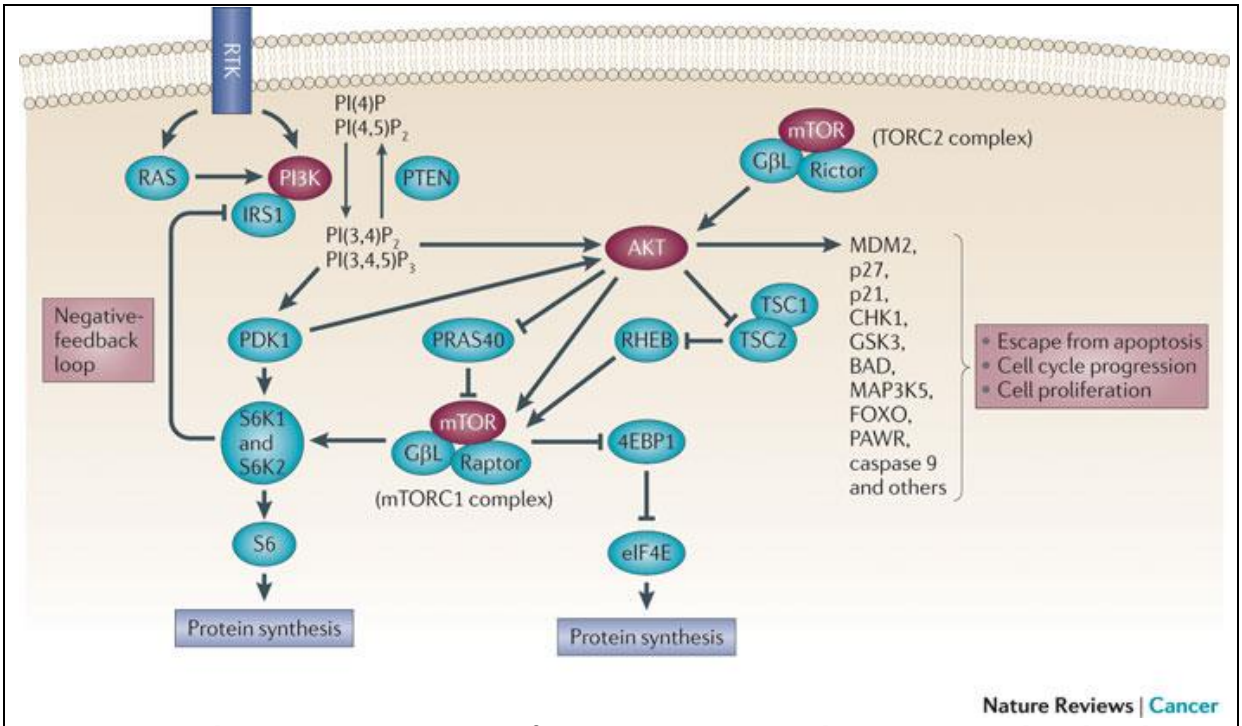

Figure 1.11: Schematic representation of PTEN/PI3K/AKT pathway. p-AKT phosphorylates a group of proteins including p21 ,p27, GSK3 and FOXO, which causes evasion of apoptosis, cell cycle progression and cell proliferation. In addition, p-AKT activates mTOR signalling. (Hollander *et al.* 2011)

In the ovary, PTEN functions mainly to regulate recruitment of primordial follicles during folliculogenesis (Reddy *et al.* 2008). In addition, it has been shown to regulate steroidogenesis in theca cells (Lan *et al.* 2017), OSE hyperplasia and papillary growth (Bajwa *et al.* 2016), and terminal differentiation of granulosa cells into luteal cells (Goto *et al.* 2009). Stemming from these functions, PTEN has been shown to play a role in polycystic ovary syndrome (Ouyang *et al.* 2013), premature ovarian failure (Kuang *et al.* 2009), ovarian endometriosis (King *et al.* 2016), and ovarian tumours. Deletion of PTEN or activation of PI3K has been shown to contribute to the progression of ovarian GCTs (Richards *et al.* 2012; Liu *et al.* 2013), and ovarian epithelial tumours including serous (Mullany *et al.* 2011; Kinross *et al.* 2012; Perets *et al.* 2013), endometrioid (Obata *et al.* 1998; Dinulescu *et al.* 2005; Castiblanco *et al.* 2006; Wu *et al.* 2007; Tanwar *et al.* 2013), and clear cell carcinomas (Castiblanco *et al.* 2006; Hashiguchi *et al.* 2006; Chandler *et al.* 2015).

1.4. Mouse models of EOC

Modelling EOC is a challenge due to the complexity of the disease and the limited understanding of OSE biology. However, mouse models can provide better understanding of tumour biology in terms of progression, regression and relapse. In addition, they can be used for identifying new biomarkers and investigating the efficacy of new treatments.

1.4.1. Carcinogen-induced models

The first trial to model ovarian cancer was done as early as 1954 by applying dimethylbenz[a]antrhracene (DMBA) oil solution externally on the ventral surface of female mice fortnightly. However, this only resulted in the development of ovarian GCTs (Howell *et al.* 1954). Changing the route of administration, by implanting a sterile silk immersed in melted DMBA on the ovary, induced the development of adenocarcinomas in 50% of the experimental animals investigated (Wang *et al.* 2008). Carcinogen-induced ovarian mouse models, although efficient in developing different histotypes of ovarian tumours, had an important drawback; those carcinogens used are not known to be associated with OC etiology.

1.4.2. Xenografts

Attempting a different technique, xenografting tumour cells from human OC cell lines or fresh tumour fragments from individual patients, proved to be successful and was previously reviewed (Connolly and Hensley 2009; House *et al.* 2014). Tumour cells were transplanted subcutaneously, intraperitoneally or orthotopically into the ovaries of immune compromised mice. This resulted in the formation of tumour grafts, which were able to recapitulate the histopathology, heterogeneity, genetic alterations and biological behaviour of the original tumour. These characteristics rendered tumour grafts a suitable model for testing the efficacy of promising new therapies. They can also be used to study the implications of altered gene expression on tumour behaviour and pathogenesis, by genetically manipulating the cells *in vitro* before transplantation.

Comparing and contrasting the different techniques used in xenografting, it is obvious that subcutaneous xenografts are very useful in accurately measuring tumour volume, and subsequently in assessing the efficacy of treatments in reducing tumour burden (Abubaker *et al.* 2014). However, tumours grow away from their natural anatomical site, and thus the effect of interaction between the tumour and its microenvironment cannot be achieved. Implanting tumour cells intraperitoneally or orthotopically allows the study of tumour growth in a more relevant microenvironment. *In vitro* manipulation of tumour cells, by introducing luminescent or fluorescent reporter genes before transplantation, allows the quantitative assessment of tumour growth. Although grafting fresh patient-isolated tumour cells are more promising than cell lines in predicting therapeutic responses, it is challenging to access the patients' samples and to efficiently process them (Connolly and Hensley 2009).

Although xenografts are generally valuable, especially for evaluating tumourigenesis in a timely fashion, they have some limitations. The main one is the use of immune-compromised mice, rendering the model unsuitable to study the inherent immune responses or to test immunotherapies. Results taken from these models should be dealt with cautiously, as they may not accurately represent disease progression and therapeutic responses in immune-competent cases. It would thus be more useful to use immune-competent mice to model EOC.

1.4.3. Syngeneic models

Syngeneic models were developed to generate EOC mouse models by combining *in vitro* and *in vivo* techniques. In these models, mouse OSE cells are transformed *in vitro* before being transplanted into immune-competent mice (Testa *et al.* 1994). Roby et *al.* established the technique, using multiple passaging of mouse OSE cells *in vitro* to induce their transformation before injecting them intraperitoneally or subcutaneously into female mice (Roby *et al.* 2000). Subcutaneous injection resulted in localized tumour formation over a period of 4 months, while intraperitoneal injection caused ascites accumulation and multiple tumour

formation 30 days post-injection. These tumours were histologically characterized by the presence of anaplastic malignant carcinomatous and sarcomatous cells (Roby *et al.* 2000).

Although syngeneic mice provide a model where immune interactions in the establishment, progression and treatment of OC could be studied, they have the drawback of requiring *ex vivo* manipulations, which is different from the pathogenesis of OC. In addition, they cannot be used as a pure model for EOC, due to the mixed phenotype of the malignant cells observed.

1.4.4. Genetically-engineered mouse models

Genetically-engineered mouse models (GEMMs), are the most efficient way to study the function of a gene and characterize its associated phenotypes. GEMMs are immune-competent mice with one or more genetic defects that are introduced via inducible gene expression or viruses. These genetic defects can be expressed in all the cells of the mouse using germ-line mutations (constitutive models), or can be limited to a specific tissue via the use of tissue-specific promoters (conditional models) (Sharpless and Depinho 2006).

In EOC, a complex disease whose etiology is not fully understood, GEMMs can be useful in elucidating the site of origin, pathogenesis, early events and biological behaviour of tumours. They can be equally valuable in identifying biomarkers for early diagnosis and testing pathway-targeted therapy, thus accelerating the most promising therapies from preclinical laboratory investigations into clinical trials. Many GEMMs are available for low and high grade serous histotype (Hasan *et al.* 2015), but only one model was developed for clear cell carcinoma (Chandler *et al.* 2015), and one model for the mucinous EOC (Ren *et al.* 2016). In the following sections, GEMMs available for the ovarian endometrioid adenocarcinoma (OEA) histotype will be reviewed, being the histotype where WNT signalling dysregulation is believed to play a role in tumourigenesis, rendering it a suitable histotype to study roles of APC2 protein

in epithelial ovarian tumourigenesis. A review of published models was performed to choose the most suitable OEA model to be used for molecular and phenotypic characterization of APC2 (Chapter 6).

1.4.4.1.Methods used for inducing recombination of targeted genes

In this section, different methods used for inducing recombination of targeted genes while developing OEA models will be reviewed. Most of methods used in this section were successfully used in generating other EOC models, meaning that they are not specific to OEA. Whenever a method was used successfully to generate EOC models representing different histotypes, it will be mentioned as a method of developing an 'EOC' model rather than an 'OEA' model.

The development of GEMMs for EOC has been hampered due to the lack of transcriptional promoters specifically expressing in the OSE, the historically proposed cell of origin of EOC, to drive the expression of the *cre*. The *cre* recombinase enzyme induces excision of the DNA sequence flanked by loxP sites inserted in the gene of interest, causing DNA rearrangements resulting in 'turning off 'of the required gene or activation of a quiescent transgene (activated post-excision of polyadenylation-silencing sequences) (Sauer 1998; Bouabe and Okkenhaug 2013). The first trial to develop an EOC transgenic mouse model was attempted by Connolly *et al.* using the Müllerian inhibitory substance type II receptor *cre* (*Misr2-cre*, also known as the anti-Müllerian hormone receptor 2-cre, *Amhr2-cre*) to target the expression of simian virus SV40 TAg specifically to the OSE (Connolly *et al.* 2003). This *cre* is expressed in the OSE in addition to granulosa cells of pre-antral follicles, and in the stroma of Müllerian duct-derived organs, such as the oviducts and uterus. In the SV40 TAg model, 50% of the female mice developed bilateral ovarian carcinomas, which were either poorly differentiated or resembling serous carcinomas. 3% of the female mice developed uterine leiomyoma, and 3% developed polycystic kidney with neoplastic component (Connolly *et al.*

2003). In 28% of the male mice, testicular cancers were observed. As can be seen from these results, the Amhr2-*cre* expression was not limited to the OSE and its recombination site was unpredictable, causing the formation of tumours in other Müllerian duct-derived organs. Even the tumours formed in the ovaries were not purely epithelial. The timing of recombination of floxed genes is unpredictable, but is thought to be anytime during development and early life, in contrast to EOC where the genetic alterations happen during adulthood.

Because of the complexity in finding a specific promoter for OSE, a different technique was developed for targeting the OSE, by making use of its anatomical location (Flesken-Nikitin *et al.* 2003). OSE is a single layer of epithelial cells covering the whole surface of the ovary. The mouse ovary differs from the human ovary by being enclosed within a balloon-like membrane, the bursa. The proposed technique delivered adenoviral vector-expressing *cre* recombinase (Ad-*cre*) to the exposed OSE cells via trans-infundibular intrabursal injection, thus inducing the recombination of floxed genes exclusively in the OSE. This technique was successful and induced the formation of epithelial tumours in the ovary, and has since been chosen by many researchers working on developing EOC GEMMs.

The main advantages of this technique are the ability to control the site of recombination, and performing the inductions in adult mice. Some drawbacks are related to the technical difficulty of correctly targeting the intra-bursal space and the need to perform a surgery, which makes it not a preferred choice for large-scale application. In addition, some reviewers questioned the exposure of other cell types to the viral injection, such as the bursal membrane and the oviductal epithelium. To avoid later issues, intrabursal injection was attempted directly into the bursa and compared to oviductal injection (Tirodkar *et al.* 2014). Both the intrabursal and intraoviductal injection induced recombination of floxed genes in ovaries and oviducts respectively, with the formation of tumours. Another concern is whether the adenovirus leaks away from its site of injection to outside. Preliminary studies showed that

no leakage was observed with an injection volume up to 10 µl (Flesken-Nikitin *et al.* 2003). Most published experiments working with this technique used an injection volume ranging from 2-10 µl.

Recent emerging evidence suggests that the fallopian tube could be an alternative origin of EOC. To test this hypothesis in OEA development, progesterone (*Pgr*) promoter was used to drive recombination of floxed *Apc* in the mouse oviduct (van der Horst *et al.* 2014). *Pgr* is expressed in Müllerian duct-derived organs, granulosa cells of growing follicles in the ovary, but not in the OSE (van der Horst *et al.* 2014). Driving recombination of floxed *Apc* in the mouse oviduct resulted in OEAs in 28% of the mice, and granulosa cell tumours in 2% of the mice. Although successful in testing the hypothesis, this promoter suffers from the limitation of being expressed in more than one cell type (stromal and epithelial cells in oviducts, and granulosa cells in the ovary), and unpredictable recombination time.

Another promoter was recently used to initiate OEA from oviducts, the oviductal glycoprotein 1 (*Ovgp1*) promoter (Wu *et al.* 2016). *Ovgp1* is exclusively expressed in the oviductal epithelium, but not in the OSE (Wu *et al*. 2016). Driving recombination of floxed *Apc* and *Pten* in the mouse oviductal epithelium post-tamoxifen induction of the *cre* recombinase in adult mice resulted in oviductal endometrioid adenocarcinoma-like tumour of 100 % penetrance, which metastasized to the ovary in 66% of mice 16-33 weeks post-induction (Wu *et al.* 2016).

Advances made in the last few years in the isolation of OSE could help in identifying genes preferentially expressed within it. This question was addressed by comparing the gene expression profile of mouse OSE to the remaining ovarian cells, as well as its expression profile during different stages of the oestrous cycle (Gava *et al.* 2008). The results showed that 30% of 3075 transcripts studied were more highly expressed in OSE than in the remaining ovary,

with only 25% of the identified transcripts corresponding to genes with known functions (Gava *et al.* 2008). However, genes identified with known functions are common genes involved in many cellular processes in different organs, and thus could not be used as an OSE-specific promoter. Hopefully, with advances in characterizing genes of unknown functions, one or more genes might be identified in the future to be exclusively expressed in the OSE, and thus useful as an OSE-specific promoter.

1.4.4.2. Can a single genetic alteration drive OEAs?

Over the last decade, massive advances were achieved in defining the molecular pathogenesis of EOC, including OEA histotype. With many genes being identified as potential oncogenes or tumour suppressor genes, attempts were made to elucidate their functions using GEMMs. Whether a single genetic alteration is sufficient to initiate OEA formation was investigated by many research groups. Discrepancies in their findings are evident and will be discussed shortly in this section.

1.4.4.2.1. WNT signalling

WNT signalling dysregulation is believed to play a role in the initiation of OEA. In human OEA cases, *CTNNB1*, the gene encoding for the β-catenin protein, is the most frequently-reported mutated gene in the pathway, followed by mutations in the *APC* gene (Palacios and Gamallo 1998). A conditional gain-of-function *Ctnnb1* mutation mouse model was designed such that Amhr2-*cre* was used to drive the recombination of *Ctnnb1* in the OSE, resulting in the formation of degradation-resistant functionally active β- catenin (Tanwar *et al.* 2011a). Tumour development was observed in 50% of mice aged 8-12 months, and most of the tumours were classified as OEAs (Tanwar *et al.* 2011a). Tanwar *et al.* proposed that activation of WNT signalling is required for OEA development. However, they proposed that the slow progression of tumours was caused by an increase in PTEN expression which antagonized the Wnt-induced tumour progression (Tanwar *et al.* 2011a). They proved their hypothesis by

combining *Pten* deletion with *Ctnnb1* activation, which resulted in rapid development of more aggressive OEAs (Figure 1.12).

The *APC* gene, a negative regulator of canonical WNT signalling, was previously shown to be mutated in many human cancers, including EOCs (Wu *et al.* 2001). Loss-of-function mutation in the *Apc* gene, induced by the conditional deletion of exon 14 in the mouse OSE, has been studied by two different groups. Wu *et al*. induced recombination in the OSE using the adenovirus-*cre* and did not observe tumours in mice 12-13 months old; however, they reported the development of endometriosis in 18% of these mice (Wu *et al.* 2011). On the other hand, the use of Amhr2-*cre* to induce recombination of floxed *Apc* in the OSE resulted the development of OEAs in 35% of mice by 11 months of age (Tanwar *et al.* 2013). Tanwar group has also shown that *Hoxa10* expression was increased following *Apc* deletion, and proposed this as a mechanism driving differentiation into OEA histotype (Figure 1.12)(Tanwar *et al.* 2013).

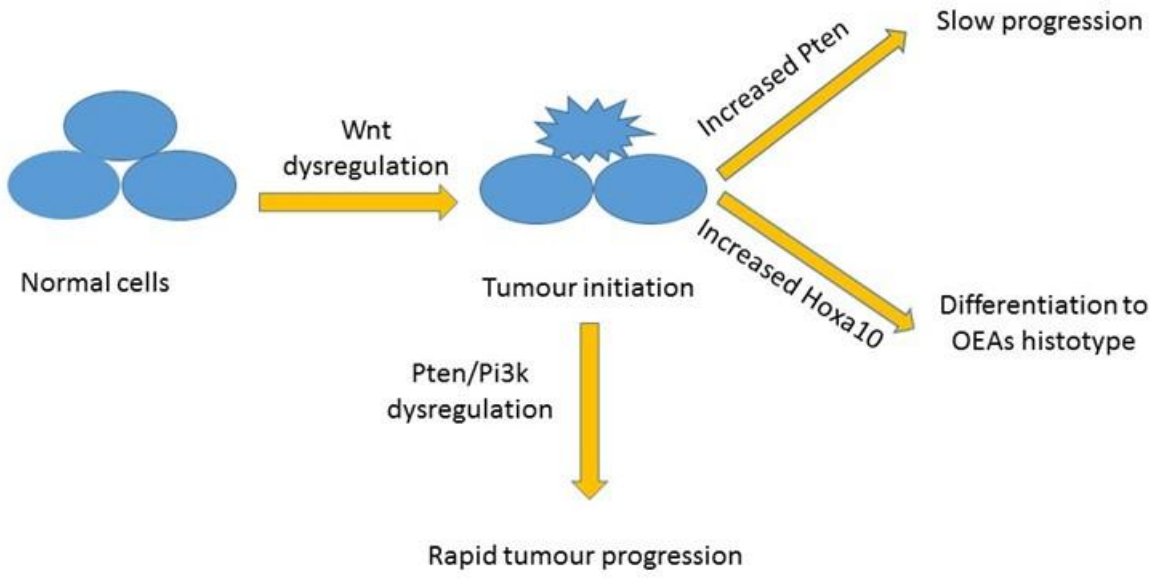

Figure 1.12: Schematic representation of ovarian endometrioid adenocarcinoma initiation and progression in WNT/PI3K dysregulated murine model, as proposed by Tanwar *et al.* (Tanwar *et al.* 2011a; Tanwar *et al.* 2013).

It is noteworthy that Tanwar group had previously reported that *Amhr2*-driven *Apc* deletion caused endometrial adenocarcinomas in the uterus (Tanwar *et al.* 2011b). Whether these cancers are contributing to the phenotype observed in the ovary is not clear. Performing hysterectomy in mice early before uterine tumour progression would have helped to clarify this ambiguity.

Another model was developed using a different mutation in the *Apc* gene; deletion of exon 15 (van der Horst *et al.* 2014). A different promoter was used to drive this mutation; the Pgr-*cre* recombining in the oviductal epithelium. Tubal and ovarian endometrioid tumours were observed in 28% of the mice between 20-40 weeks of age. Thus far, this is the only reported GEMM for OEAs where endometrioid adenocarcinoma originates from outside the ovary (van der Horst *et al.* 2014).

1.4.4.2.2. *PTEN/PI3K/AKT* signalling

Frequent genetic alterations in *PTEN*, which codes for PTEN protein, the negative regulator of PI3K, have been found in many types of human cancers, including EOCs (Saito *et al.* 2000). Conditional deletion of *Pten* in the OSE, using Amhr2-*cre* or adenovirus-*cre*, did not result in any ovarian lesions or tumours in 2 separate studies (Tanwar *et al.* 2011a; Wu *et al.* 2011). However, a third study reported the development of ovarian surface papillary hyperplasia and OEAs in 62% and 7.5% (respectively) of 26-week-old *Pten*-conditionally deleted (exon 5) mice using adenovirus-*cre* (Dinulescu *et al.* 2005). This could be partly explained by differences in the genetic manipulation and location of loxP sites within the *Pten* gene in these different models.

1.4.4.3.Multi-mutational tumour models and their application in cancer research

1.4.4.3.1. Activated KRAS/PTEN-deficient model

The first OEA transgenic mouse model, developed by conditional expression of oncogenic *Kras* concomitantly with deletion of *Pten* in the OSE using intrabursal injection of adenovirus-*cre*, resulted in invasive OEAs in all the mice as early as 7 weeks post-induction (Dinulescu *et al.* 2005). Although *Kras* is not frequently mutated in human OEAs, the tumours in this model recapitulated their histological and biological behaviour.

This model was successfully used to define the PI3K isoform dependency of this subset of OEAs (Schmit *et al.* 2014). Results showed that the developed OEAs depend on p110α isoform of PI3K, and that its loss prevents tumour formation. These results suggest the usefulness of PI3K (specifically p110α isoform) inhibitors in OEA patients with these genetic alterations. This hypothesis was tested using supramolecular nanoparticles to deliver the PI3K inhibitor PI103 (Kulkarni *et al.* 2013). Mice treated following tumour development showed significant tumour regression, as assessed by a bioluminescence signal. This was associated with a significant decrease of downstream PI3K target genes, such as phospho-mTOR, phospho-AKT and phospho-S6 (Kulkarni *et al.* 2013). Another preclinical study was performed using this model, to test a dual PI3K/mTOR inhibitor PF-04691502 (Kinross *et al.* 2011). Treatments for 2 or 7 days with PF-04691502 following tumour development caused a decrease in p-AKT and p-S6 protein levels post-treatment. However, Kinross group was not able to use the model for a larger preclinical testing of the compound, due to inability to follow tumour growth by palpation, long latency of tumour development (compared to transplants) and difficulty identifying tumours and following their response to therapy, even with ultrasound, due to the development of ascites and peritoneal metastases (Kinross *et al.* 2011).

An attractive research question emerging from epidemiological studies is the role of combined oral contraceptives in decreasing the risk of developing EOC, and the KRAS/PTEN

model has been used to research this question (Romero *et al.* 2009). Treatment with norethindrone alone or in combination with ethinyl estadiol was started 3 weeks prior to tumour induction and continued thereafter for 8 weeks, which caused a trend of decrease in tumour weight with both treatments. The study findings pointed to a decrease in matrix metalloproteinase 2 (MMP2) activity, which is known to play important roles in cancer initiation and/or progression through remodelling of the extracellular matrix of the tumour, and controlling important cellular process such as proliferation, apoptosis and differentiation (Romero *et al.* 2009). However, because treatments were started before tumour formation and continued thereafter, it is hard to conclude whether the reduction in tumour weight observed happened due to delaying tumour initiation or by slowing tumour progression.

The model was further developed by conditionally expressing a human *MUC1* allele in the OSE using the adenovirus-*cre* injection (Budiu *et al.* 2013). The new triple (*MUC1/Kras/Pten*) mouse model developed OEAs similar to those previously described in the *Kras/Pten* model, but also developed ascites and loco-regional metastases more frequently. This model closely mimics human EOCs, which were previously reported to highly express *MUC1* regardless of the tumour histotype, and has proven to be useful in preclinical studies of EOC using immunotherapeutics targeting MUC1. Administration of MUC1 vaccine loaded onto type 1 polarized dendritic cells significantly prolonged survival via downregulation of regulatory T cells and upregulation of multiple immune effector genes such as CD80, CD40 and CD45 (Budiu *et al.* 2013) .

1.4.4.3.2. APC/PTEN double knockout model

Wu *et al.* were the first to describe an OEA mouse model developed by dysregulation of both canonical WNT signalling and PTEN/PI3K signalling (Wu *et al.* 2007). In their model, intrabursal injection of adenovirus-*cre* was used to induce the recombination of floxed *Apc* and *Pten* in the OSE cells, causing loss of functional APC and PTEN proteins. This model

genetically and histologically resembled a subset of human OEAs with the same genetic mutations. However, tumours showed some glandular formation mixed with less differentiated mesenchymal cells, unlike the human OEAs, which show more epithelial differentiation. Wu group proposed an epithelial to mesenchymal transition (EMT) in these less differentiated areas due to dysregulation in WNT signalling, but they did not fully characterize the proposed EMT. They concluded that this model could successfully be used to study the biology of low grade Type I OEAs (Wu *et al.* 2007). After a decade, Wu group were able to use an Ovgp1-*cre* to drive recombination of the same genes in the oviducts, and reported the development of oviductal endometrioid adenocarcinoma-like tumours which histologically and molecularly more closely resembled human OEA compared to the OEAs originating from OSE post-adenovirus *cre* induction (Wu *et al.* 2016).

Wu *et al.* continued working with their model to explore OEA biology and in translational studies for drug testing and *in vivo* imaging. They reported that either *Pik3ca* mutation or *Trp53* mutation/deletion in the *Apc/Pten* double knockout mouse caused the tumour to be more aggressive, resulting in metastasis even to distant organs, coupled with reduced survival (Wu *et al.* 2013). They concluded that progression from type I to type II OEAs requires additional mutations in other genes such as *Trp53* or *Pik3ca* and introduced this as a model, which could be used for preclinical testing of therapeutics targeting type II OEAs patients (Wu *et al.* 2013).

Another study adapted this model to elucidate the effect of additionally deleting *Arid1a*, the gene encoding for the chromatin remodelling complex protein AT-Rich Interaction Domain 1A, which is frequently mutated in OEAs (Takeda *et al.* 2016). Deleting *Arid1a* in the *Apc/Pten* double knockout model resulted in the formation of larger and more epithelial-differentiated OEA, which more closely resembled human OEA, but surprisingly prolonged mice survival

(Zhai *et al.* 2016). These findings suggest that ARID1A may contribute to the EMT proposed by Wu and colleagues when they first introduced the *Apc/Pten* double knock out OEA model.

Two different interventions were carried out using the *Apc*/*Pten* double knockout model to enable *in vivo* imaging of tumour progression. The first was performed by incorporating a luciferase reporter allele, which is activated after the adenovirus-*cre* intrabursal injection (Wu *et al.* 2011). The usefulness of this mouse to follow tumour burden and metastasis using bioluminescence imaging was proven in mice treated by AKT/mTOR inhibitors (rapamycin, perifosine or API-2)(Wu *et al.* 2011). The second intervention was performed by crossing a conditional bioluminescent apoptosis reporter mouse with the *Apc/Pten* mouse to generate *Apc/Pten*/*Apoptosis reporter* mouse (Wang *et al.* 2013). The efficacy of using this mouse to follow response to treatment was tested using cisplatin and/or perifosine (AKT pathway inhibitor), once tumours of 50 mm^3 were formed and detected by magnetic resonance imaging (MRI). Mice treated with the combination therapy showed the highest bioluminescence, indicating the highest level of apoptosis, which in turn resulted in the greatest reduction in tumour burden, as measured by MRI (Wang *et al.* 2013).

1.4.4.3.3. Activated β-catenin/PTEN deficient model

One more model with dysregulation of canonical WNT and PTEN/PI3K signalling pathways was developed by combining PTEN deletion with conditional expression of degradation-resistant β-catenin mutant protein, which resulted in the formation of aggressive OEAs in all experimental mice as early as 6 weeks of age (Tanwar *et al.* 2011a).

1.4.4.3.4. ARID1A/PTEN double knockout model

ARID1A mutations are often present with mutations in the *PTEN/PI3K* signalling pathway in human endometrioid and clear cell ovarian histotypes (Guan *et al.* 2014). A double knock out *Arid1a/Pten* ovarian mouse model was generated by driving recombination of floxed

Arid1a and *Pten* in the OSE using adenovirus-*cre* (Guan *et al.* 2014). Loss of ARID1A and PTEN proteins resulted in the development of either OEAs or undifferentiated carcinomas with metastaic potential 6-9 months post-induction (Guan *et al.* 2014). Shortly after this, another mouse model was developed based on the knockout of *Arid1a* accompanied by *Pik3ca* activating mutation in the OSE (Chandler *et al.* 2015), where recombination of the floxed genes was performed in a similar way. This lead to the development of the first ovarian clear cell carcinoma (CCC) GEMM, which was genetically and histopathologically similar to human CCC. An autocrine IL-6 signalling was identified to contribute to the pathogenesis of CCC in this model by promoting tumour cell growth (Chandler *et al.* 2015). Chandler *et al.* proposed a model where PI3K acts as an inflammatory 'insult' driving the cells to produce IL-6, which remains highly sustained due to the absence of its negative regulator, ARID1A (Chandler *et al.* 2015).

1.4.4.4.Limitations of GEMM in OEA modelling

1.4.4.4.1. Human *vs.* mouse ovarian anatomy and physiology

There are some anatomical and functional differences between mouse and human ovaries, which should be taken into consideration when interpreting results related to tumour initiation, progression, metastasis and response to therapy. Firstly, the mouse ovary is surrounded by the ovarian bursa, which potentially could be protecting other organs in the peritoneal cavity from invasion and metastasis. In humans, ovarian tumour cells are directly shed into the peritoneal cavity, whereas in the mouse case, they are shed into the intrabursal space.

Other major differences between mouse and human ovaries are related to ovulation. Human are mono-ovulatory while mice are poly-ovulatory, meaning that more damage is potentially caused to the OSE in mice during ovulation as compared to humans. Mice tend to retain corpora lutea from previous ovulations, as well as those from the most recent ovulation,

inside their ovaries while in humans, only one corpus luteum is formed per ovulation and deteriorates by the end of the cycle. The presence of these multiple corpora lutea could influence the hormonal status between the 2 species. There is also a great difference in the length of the menstruation cycle, with mice showing a very short cycle of 4-5 days, in contrast to humans whose cycles are 28 days in length.

1.4.4.4.2. Phenotypic differences

Discrepancies in the literature describing phenotypes of mice carrying the same genetic modifications, could be attributed to a number of reasons. These may include, first, differences in the experimental design, especially for the follow-up period after induction, which could account for the failure of some groups to describe phenotypes which have been reported by others. A second reason could be differences in the genetic background of the mouse strains used by the different groups in their experiments. Differences in the site of the genetic modification of the gene itself (loxP sites) could also attribute to the different phenotypes observed.

Another significant variable is the use of different types of *cre*, especially the use of a *cre* exclusively recombining in the OSE (adenovirus-*cre*) in contrast to a *cre* driving recombination in OSE cells as well as other cells in the ovary (Amhr2-*cre*). The effect of crosstalk between stromal and epithelial cells has been reported in other cancers, and driving recombination in stromal cells as well as OSE/oviductal epithelial cells using the Amhr2-*cre* or Pgr-*cre*, respectively, could affect ovarian cancer pathogenesis and/or progression. With the ability of these *cre* to induce tumour formation in other organs (e.g. oviducts and uterus), it is hard to tell whether tumours formed originate from the ovary or extra-ovarian tumours are contributing to the observed phenotypes. Of note is that Amhr2-*cre* was successful to drive tumour formation from a single genetic alteration while the adenovirus-*cre* failed to do so. Thus, comparative studies using these 2 *cre* types would be useful to show whether stromal

interactions are required for the early initiation and/or progression of ovarian tumours arising from the OSE.

1.5. Modelling ovarian granulosa cell tumour

As mentioned previously, the prevalence of ovarian GCT is low and its prognosis is favourable. However, the main concern about GCT is the risk of relapse years after removal of the primary tumour, which requires long term follow up of patients. Unfortunately, GCT biology is less well defined compared to epithelial ones. This necessitates the development of mouse models, which can be used to study tumour biology and act as preclinical models for testing therapeutics.

1.5.1. GCT transplantation models

As early as 1946, transplantation models were developed for GCTs (Furth 1946). These models were mainly used to define gross pathologies associated with tumour progression, such as hypervolemia (Furth and Sobel 1947; Cliffton and Wolstenholme 1949; Furth and Moshman 1951), hormone production (Van Nie 1957) and vascularity (Waters and Green 1959). Later on, they were used to explore the interaction between steroidal hormones and tumour progression (Hatanaka *et al.* 1981). However, the main drawback of these models was the transplantation of tumours to sites away from their organ of origin, such as into the spleen, under the kidney capsule or into the liver (Lipschutz *et al.* 1964). Another important drawback was the development and progression pattern of GCT, whereby a luteoma is converted to GCT (Lipschutz *et al.* 1967), which is not similar to the natural progression of the disease.

1.5.2. Chemically-induced GCT

Carcinogens such as 7,12-DMBA (Jull *et al.* 1966), 7,8,12-trimethylbenz-[a]anthracene (Uematsu and Huggins 1968), and 9,10-DMBA (Krarup 1969) were successfully used to induce ovarian GCTs. However, these chemicals are not known to play a role in the etiology of the tumour.

The first trial to induce ovarian GCT by hormonal administration was conducted using prolonged and continuous administration of progesterone, which led to successful development of ovarian GCTs, starting from the periphery of the ovary (Lipschutz *et al.* 1967). Although administration of pregnant mare's serum gonadotrophin (PMSG) failed to induce ovarian GCT in Balb/C mice (Menczer *et al.* 1977), priming ovaries by PMSG followed by mutagen or carcinogen administration, increased the incidence of GCT (Rao 1981).

1.5.3. Spontaneous ovarian GCT models

Some mouse strains (e.g. SWXJ-9 and SWR) are known to spontaneously develop GCT around puberty (Beamer *et al.* 1985). SWXJ-9 mice were used to explore the effect of hormonal treatment with dehydroepiandrosterone, which appeared to increase the incidence of ovarian GCT (Beamer *et al.* 1988). Using a SWR spontaneous model, it was shown that EGFR is upregulated in GCT cells, causing increased proliferation in response to EGF (Tennent *et al.* 1989). Xenografting ovaries from these mouse strains under the kidney capsule of immune-deficient and immune-intact mice revealed comparable tumour incidence, and showed that the immune system does not contribute to tumourigenesis (Beamer *et al.* 1993). However, xenografting under the kidney capsule of gonadotrophin-producing or gonadotrophin-deficient mice revealed that tumourigenesis is dependent on gonadotrophins, primarily due to gonadotrophin-dependent production of androgens (Beamer *et al.* 1993).

1.5.4. GEMMs of adult GCT

Because GCTs are believed to originate from granulosa cells of growing follicles, early efforts of modelling were designed to disrupt regulatory pathways known to control granulosa cell proliferation and/or differentiation. Later on, oncogenes and tumour suppressors known to play a role in tumourigenesis in other tissues were conditionally targeted in the ovarian granulosa cells to explore their ability to initiate ovarian GCTs.

1.5.4.1. Targeting female hormones or hormone receptors

The first mouse model developed to test the effect of gonadotrophins on GCT formation was a mouse hypersecreting LH from the pituitary gland, leading to infertility, polycystic ovaries and ovarian GCT formation in 4-9 months old female mice (Risma *et al.* 1995).

Another mouse expressing a constitutively-active mutant luteinizing hormone chorionic gonadotrophin receptor (LHCGR) was developed (McGee and Narayan 2013), wherein 50% of the female mice developed GCTs by 6 months of age (Hai *et al.* 2015).

The ovaries are known to express both estrogen receptors α and β (ERα and ERβ), with ERβ being predominantly expressed in granulosa cells (Sar and Welsch 1999). In addition, ERβ is exclusively expressed in gonadotrophin-releasing neurons (Hrabovszky *et al.* 2007). ERα, ERβ and double knockout models were developed (Emmen and Korach 2003). Of the 3 models studied, only ERβ knockout female mice developed ovarian GCTs as early as 15 months of age, secondary to hormonally-active pituitary tumours (Fan *et al.* 2010b)

1.5.4.2. Targeting TGFβ signalling pathway

Inhibin-α was the first member of the TGFβ family of transcription factors to be targeted by constitutive deletion in all the mouse cells of the whole body, which resulted in the development of ovarian sex-cord stromal tumours including GCTs (Matzuk *et al.* 1992). Co-deletion of the cell cycle inhibitor p27 enhanced tumour progression, leading to earlier mortality (Cipriano *et al.* 2001). With the hypothesis that SMAD3 is required for activin signalling, and thus for tumour development and progression in inhibin-α null mice, a double knockout model of SMAD3 and inhibin-α was developed (Looyenga and Hammer 2007). SMAD3 deletion attenuated GCT formation in 2 months-old ovaries (Looyenga and Hammer 2007). Later, a similar model was developed, in which inhibin-α and SMAD2 were both targeted (Rajanahally *et al.* 2010). Unlike the SMAD3/inhibin-α double knockout model, these

mice developed ovarian GCTs which were comparable to inhibin-α null mice, indicating that SMAD2 is not required for ovarian activin-mediated tumourigenesis (Rajanahally *et al.* 2010). With activin-A being the main driver of tumourigenesis in inhibin-α-null mice, counteracting activin-A signalling was predicted to decrease tumour development (Gold *et al.* 2013). To test this hypothesis, a mouse overexpressing activin-β C, which antagonizes activin-A, was crossed with inhibin-α-null mouse, resulting in at least 50% decrease in GCT development and a 50% increase in survival (Gold *et al.* 2013).

Single constitutive or conditional deletion of the BMP-signalling SMADs (SMAD1, SMAD5 or SMAD8), using Amhr2-*cre* failed to drive GCT formation in the ovary (Pangas *et al.* 2008). However, conditional deletion of both SMAD1 and SMAD5, or triple deletion of SMAD1, SMAD5 and SMAD8 caused the formation of metastatic GCTs with 100% penetrance as early as 3 months of age (Pangas *et al.* 2008). A similar effect was seen with conditional deletion of BMP receptors; where a single deletion of either BMPR1A or BMPR1B did not cause GCT formation, while knockout of both together resulted in the development of ovarian GCTs as early as 8 months of age (Edson *et al.* 2010).

A recent ovarian GCT model was developed by conditionally-expressing activated transforming growth factor β receptor TGFBR1 in granulosa cells of growing follicles using Amhr2-*cre* or Cyp19-*cre* (Gao *et al.* 2016). Activation of TGFBR1 led to the development of adult GCTs with 100% penetrance as early as 2 months of age, with tumours phenocopying the human adult ovarian GCTs and eventually causing mortality with tumour progression (Gao *et al.* 2016).

1.5.4.3. Targeting FOX transcription proteins

As mentioned previously, members of the FOX family of transcription proteins, such as FOXO1, FOXO3 and FOXO4, are expressed in the ovary and have been shown to control

granulosa cell proliferation and follicular activity (Uhlenhaut and Treier 2011). Conditional deletion of FOXO1 and FOXO3 in granulosa cells of pre-antral follicles (using Amhr2-*cre*) or antral follicles (using Cyp19-*cre*) lead to the development of GCTs in 20% of mice aged to 6-8 months (Liu *et al.* 2015). A single-dose treatment with superovulatory gonadotrophins increased the incidence of tumour formation, with 62.5% of mice now developing GCTs by 2.5 months (Liu *et al.* 2015). The same happened when a triple knockout mouse was developed by deleting PTEN, FOXO1 and FOXO3 in granulosa cells of antral follicles, with 60% of mice developing GCTs by 2-3 months (Liu *et al.* 2015)

1.5.4.4. Targeting paracrine regulators of granulosa cells

As mentioned previously, ovarian functions are tightly regulated by hormonal, paracrine and autocrine signals. PI3K signalling has been identified as a paracrine regulator of follicular growth, where the high levels of PI3K in oocytes control growth of somatic follicular cells through a bidirectional communication between oocytes and surrounding granulosa cells (Liu *et al.* 2006). A proof-of-concept mouse model was recently published, in which conditional activation of PI3K in oocytes using Gdf9-*cre*, which recombines exclusively in germ cells, resulted in GCT development in 100% of mice by 65 days (Kim *et al.* 2016).

1.5.4.5. Targeting oncogenes and tumour suppressor genes

1.5.4.5.1. Simian virus 40 T-antigen

Simian Virus 40 T-antigen (TAg) is a well-known viral oncogene, and was used in the early days to develop an *in vivo* model of ovarian GCT, although it is not a known clinical cause of GCT. This was achieved by directing expression of the oncogene to the ovarian granulosa cells using the inhibin-α promoter (Kananen *et al.* 1995). This mouse model was successfully used to test the contribution of gonadotrophins to tumourigenesis, by giving the mice a gonadotrophin-releasing hormone antagonist, which resulted in complete or partial inhibition of tumour development in 2 different mouse lines (Kananen *et al.* 1997). When this

mouse was crossed with a hypogonadotrophic mouse, double mutant mice did not develop GCTs, even after long-term treatment with testosterone (Rilianawati *et al.* 2000). Mice of the original model were treated with a lytic peptide (Hecate) conjugated to chorionic gonadotrophin-beta subunit, to target LHCGR-expressing GCT cells (Bodek *et al.* 2005). This treatment resulted in a 36% reduction in ovarian tumour volume due to increased tumour cell death (Bodek *et al.* 2005). Attempting immunotherapy was successful as well, by immunizing inhibin α-TAg mice with anti-zona pellucida-3 protein, a protein highly expressed in GCT, which stopped tumour formation or delayed tumour progression, depending on the time of immunization (Rahman *et al.* 2012). The results were reproducible when mice were immunized with the mouse inhibin-α peptide 215-234 (Altuntas *et al.* 2012).

Another promoter was used to drive the expression of TAg to the ovaries, the ovarian-specific promoter OSP1, which is exclusively expressed in different ovarian lineages (Garson *et al.* 2003). Although 2/3 of the female mice developed ovarian GCTs, the promoter was leaky in cells of other tissues, leading to tumour development in many tissues other than the ovary (Garson *et al.* 2003).

1.5.4.5.2. WNT signalling

Ovarian GCTs have been shown to express nuclear β-catenin in granulosa cells, suggesting that WNT signalling dysregulation may be contributing to tumourigenesis (Boerboom *et al.* 2005). Amhr2-*cre* was used to develop an ovarian GCT model with 57% penetrance, by expressing a mutant gene coding for degradation-resistant β-catenin protein (Boerboom *et al.* 2005). When PTEN loss was combined with degradation-resistant β-catenin expression, 100% of mice developed metastatic GCT as early as 6 weeks (Lague *et al.* 2008), similar to the accelerated GCT development seen when degradation-resistant β-catenin expression was combined with activated KRAS (Richards *et al.* 2012). The combined PTEN loss/activated β-catenin model was successfully used as a preclinical model in 2 studies, where

either treatment with mTOR inhibitor everolimus (Rico *et al.* 2012), or with the anti-VEGFA antibody (Tsoi *et al.* 2013) resulted in reduced tumour growth and prolonged survival.

A novel mouse model was developed by expressing activated Rspondin1 (RSPO1), a known WNT signalling regulator protein, using steroidogenic factor 1-*cre* (SF1-*cre*) (De Cian *et al.* 2016). This *cre* recombines in the ovaries as well as in the hypothalamus, pituitary glands and adrenal glands (Bingham *et al.* 2006). Conditional activation of RSPO1 caused ovarian GCT development in 10% of mice, starting at 12 months of age (De Cian *et al.* 2016).

1.5.4.5.3. Fanconi anaemia

Loss of Fanconi anaemia genes, including *Fancf*, predisposes to leukaemia and solid tumours, including gynaecological tumours, both in anaemic and non-anaemic carriers (Bakker *et al.* 2012). To directly elucidate whether FANCF protein loss contributes to ovarian tumourigenesis, a constitutive knockout mouse for *Fancf* was developed (Bakker *et al.* 2012). In this model, more than 50% of female mice homozygous for *Fancf*-null allele developed ovarian GCTs as early as 390 days of age (Bakker *et al.* 2012).

1.5.5. Future directions

Similar to epithelial ovarian cancer, the last decade has witnessed the development of multiple GEMMs for GCTs, which could serve as valuable tools for studying cancer biology and as preclinical models. However, one important model which still needs to be developed is a mouse which bears a mutation of *Foxl2* gene. With recent advances in defining the molecular pathology of adult GCT pointing to the *FOXL2* mutation as a major contributor in 97% of human GCTs (Shah *et al.* 2009), the pathogenesis of this mutation and its consequences need to be studied. With the accumulating evidence from mouse models that FOXL2 protein expression is elevated in GCTs (Liu *et al.* 2015; Gao *et al*. 2016), it seems crucial to develop a

degradation-resistant FOXL2 conditional mutation targeted to the granulosa cells, to see whether it contributes to tumourigenesis.

Acknowledging the efforts done by the Boerboom lab and apart from the efforts done using the Simian virus TAg model, GEMMs of ovarian GCT have been rarely used in translational medicine; a limitation which needs to be addressed in the near future. With further insights being revealed about GCT biology from both human studies and GEMMs, more studies should be directed towards testing the efficacy of targeted therapy in tumour eradication and prevention of relapse.

2. Aims

APC2 has been shown to negatively regulate WNT signalling in *Drosophila* and in cancer cell lines. However, little is known about APC2 role in regulating WNT signalling in an *in vivo* setting. It is noteworthy that because the highest levels of expression of APC2 protein are found in the brain, most *in vivo* research has been directed towards the brain.

Shortly after the discovery of APC2, Van Es *et al.* constructed a constitutive knockout *Apc2* mouse to study whether APC2 loss contributes to colon cancer, similar to its homologous *Apc* tumour suppressor (Van Es *et al.* 1999). However, they did not fully publish their results, and only reported that mice did not develop colon cancer. This mouse was gifted to the Clarke lab, which started to explore roles of APC2 protein on WNT signalling and tumour formation in different mammalian tissues. It has been shown that APC2 regulation of WNT signalling is tissue-specific, with APC2 regulating WNT signalling in the liver and intestines but not in mammary glands (Daly 2013). APC2 roles in homeostasis were tissue-specific as well, with only intestinal homeostasis shown to be disrupted following APC2 loss, unlike the mammary gland or the liver (Daly 2013). APC2 loss on its own failed to induce tumourigenesis in any of these tissues. However, combining both APC2 and APC loss initiated tumour formation in the mammary gland (Daly *et al.* 2016), attenuated APC-driven tumour formation in the liver and did not alter APC-driven tumourigenesis in the intestine (Daly 2013).

It has been observed in the Clarke lab that a subset of aging *Apc2*$^{-/-}$ mice developed ovarian cysts, which were not observed in their control littermates. However, this phenotype has not been further characterized. With the accumulating evidence that APC2 is lost in EOC, and stemming from the previous characterization performed for APC2 protein in different mouse tissues in the Clarke lab, the aims of the work outlined in this thesis were:

- To investigate whether APC2 loss activates WNT signalling in the ovaries

- To characterize the consequences of APC2 loss on ovarian homeostasis and female fertility in early adulthood.
- To follow ovarian tumour formation in aging APC2-deficient mice.
- To elucidate whether APC2 loss in combination with APC or PTEN loss can initiate epithelial tumourigenesis in the ovaries
- To unravel contributions of APC2 in epithelial ovarian tumourigenesis using an OEA GEMM.

3. Material and methods

3.1. Breeding and maintenance of experimental animals

3.1.1. Animal husbandry

All mice were bred and maintained according to UK Home Office Regulations. They were housed in plastic cages with free access to Harlan standard diet (Special Diets Service, UK) and water.

3.1.2. Breeding

All mice were maintained on a mixed background. Adult mice over 6 weeks of age with known genotypes were bred in trios (one male and 2 females in the same cage). The pups were left in the breeding cages with their mothers until they were able to feed independently. Pups were weaned when they were 3-4 weeks old (no more than this to avoid female mice getting pregnant). At weaning, pups were sexed, ear-tipped for identification and placed in separate cages (maximum 5 mice/cage). The ear tips were then processed for genotyping (Section 3.3.1).

3.2. Transgenic mice

In this study, 3 different genetic alleles were utilized. Mice with an allele of the constitutive knockout of *Apc2* (*Apc2*$^{-}$) were a kind gift from Prof. Hans Clevers lab (Daly *et al.* 2016). This allele was genetically-engineered to produce a truncated APC2 protein lacking the important functional β-catenin and Axin binding domains (Daly 2013). The alleles for conditional deletion of *Apc* (*Apc*^{fl}) and *Pten* (*Pten*^{fl}) were previously described (Shibata *et al.* 1997; Suzuki *et al.* 2001). They were developed by flanking the desired exons (exons 4 and 5 in *Pten*, and exon 14 in *Apc*) with loxP sites, allowing for the conditional deletion (floxing) of the genes using the *Cre*-recombinase enzyme. Conditional deletion of the floxed genes in the OSE was performed by injecting a replication-incompetent adenovirus-expressing *cre*-

recombinase under the control of the CMV promoter (Ad-*cre*) into the ovarian bursa (Section 3.3.4,(Flesken-Nikitin *et al.* 2013)).

3.3. Experimental procedures on mice

All experimental procedures performed were approved by the UK Home Office under project licences 30/2737 and 30/3279 and were performed by UK Home Office personal licence holders.

3.3.1. Ear notching for genotyping

Mice were genotyped for *Apc*, *Apc2* and *Pten* alleles using gDNA extracted from ear notches used for mouse identification purposes, collected at the time of weaning. A regenotyping was performed for all mice at the end of experiments (at time of culling). Primers used in genotyping were either provided by collaborators (*Apc2* primer sequences from the Clevers lab) or established and used in the Clarke lab (*Apc* and *Pten* primer sequences, (Daly 2013). All the primers were synthesised by Sigma (Table 3.1). All the ear notching and genotyping were kindly performed by Elaine Taylor and Matthew Zverev.

3.3.1.1. DNA extraction and purification (Puregene® method)

The Gentra Puregene® tissue kit (Qiagen) was used for DNA extraction. An ear biopsy was placed in a 1.5 ml microcentrifuge tube, containing 250 µl cell lysis buffer (Puregene®, USA) and 1.5 µl of Proteinase K (20 mg/ml, Roche, Switzerland), and incubated overnight in a shaking incubator at 55ºC. Following this, the protein was precipitated by adding 100 µl of protein precipitation solution (Puregene®, USA) and contents mixed by vortexing followed by 1 hour incubation at 4ºC. The samples were centrifuged at 10 000 rpm for 10 minutes. The supernatant was carefully removed, mixed with 100 µl isopropanol, incubated for 1 hour at 4ºC and centrifuged at 10 000 rpm for 15 minutes. The supernatant was carefully discarded and the

formed pellet containing gDNA was air dried for 1 hour before dissolving in 250 µl of ultrapure water (Sigma, USA). The gDNA was stored at 4ºC until further processing.

Table 3.1: Primer sequences and reaction conditions used in genotyping

Gene	Primer sequence	Taq polymerase	Buffer	PCR cycle
Apc	Forward primer (5'-3') GTTCTGTATCATGGAAAGATAGGTGGTC Reverse primer (5'-3') CACTCAAAACGCTTTTGAGGGTTGATTC	Dream Taq® (Thermo Fisher Scientific, USA)	Green	Initial denaturation: 95ºC X 3 minutes followed by 30 cycles (95ºC X 30 seconds, 60ºC X 30 seconds, 72ºC X 1 minute) and a final extension at 72ºC X 5 minutes.
Apc2	Forward primer (5'-3') • Wild type primer: CTCCAAACACAAGATGATCG • Knockout primer: AGGTCTGAAGAGGAGTTTAC Reverse primer (5'-3') AGCTGTGTCTGATGAGGTG	Go Taq® (Promega, USA)	Clear	Initial denaturation: 95ºC X 3 minutes followed by 30 cycles (95ºC X 30 seconds, 60ºC X 30 seconds, 72ºC X 1 minute) and a final extension at 72ºC X 5 minutes.
Pten	Forward primer (5'-3') CTCCTCTACTCCATTCTTCCC Reverse primer (5'-3') ACTCCCACCAATGAACAAAC	Dream Taq® (Thermo Fisher Scientific)	Green	Initial denaturation at 95ºC X 2.5 minutes followed by 30 cycles (94ºC X 1 minute, 54ºC X 1 minute and 72ºC X 1 minute) and a final extension at 72ºC X 5 minutes.

3.3.1.2. PCR amplification

The PCR reaction was performed in strip-tubes (Grenier Bio-one, Austria) using 2.5 µl of the prepared gDNA added to 47.5 µl of master mix consisting of Taq polymerase (Promega, USA), polymerase buffer (Promega, USA), specific gene primer mix (Sigma, USA Table 3.1), ultrapure water (Sigma, USA), magnesium chloride (Promega, USA) and dNTPs (Bioline, UK) (Table 3.2). For each PCR reaction, one sample was prepared with 2.5 µl of ultrapure water (Sigma, USA) instead of gDNA to serve as control (negative) reaction. All the strip-tube components were mixed, centrifuged for 10 seconds and placed in a thermal cycler according to the specific reaction conditions (Table 2.1).

Table 3.2: Composition of PCR master mix

Constituent	Volume required
Buffer	10 µl
Mg (25 mM)	5 µl
dNTPs	0.4 µl
Primers (10 µm)	1 µl
Taq polymerase	0.2 µl
Ultrapure water	30.9 µl

3.3.1.3. PCR product visualization

PCR products were visualized by agarose gel electrophoresis. A 1% w/v agarose gel was prepared in a conical flask by dissolving 1 gram agarose (Sigma) in 100 ml 1 X Tris Borate EDTA (TBE) buffer [Appendix 1] using a microwave. The dissolved agarose was cooled by swirling the bottom of the conical flask under running water. 5 µl of SafeView® nucleic acid stain (NBS Biologicals, UK) were added to the gel and mixed well before pouring into the gel mould and inserting the comb to create the wells. After the gel was set, the combs were

carefully removed and the gel placed in an electrophoresis tank filled with TBE buffer containing 5 µl of SafeView®/100 ml TBE. 5 µl of the PCR products were mixed with 5 µl of loading dye [50% glycerol + 50% ultrapure water + 0.1% bromophenol blue (all from Sigma, USA)] and loaded into wells alongside 100 bp and 1Kbp DNA ladders (Promega, USA). The gel was run at 100V for 40 minutes and DNA bands visualized by UV light using GelDoc XR (Bio-Rad, USA).

3.3.2. Synchronization of oestrous cycle

Female mice aged 10 weeks, 6, 12 or 18 months, were synchronized for oestrous cycle by manually staging the mice using the vaginal cytology method (Byers *et al.* 2012). Briefly, the vagina was flushed with 50 µl of sterile 1X phosphate buffered saline (PBS) solution, pH 7.4 (Gibco®, Life Technologies, USA) by inserting the plastic tip of micropipette, filled with PBS, into the vagina and repipetting for 3-5 times. The vaginal flush contained in the pipette tip was placed on a glass slide, air-dried and stained with Haemalum (RA Lamb, ThermoFisher, USA) for 1 min. The slide was washed with running water, air-dried and examined under a light microscope using 10X objective (Section 3.5.4.1). Mice were manually staged for 5 consecutive days, and culled when present at the diestrus stage of the oestrous cycle, at which point ovaries were dissected and processed.

3.3.3. Superovulation

Randomly-cycling female mice aged 10 weeks were superovulated by giving the mice a single intraperitoneal injection (using a 1 ml insulin syringe) of 5 I.U. pregnant mare's serum gonadotropin (PMSG) [Folligon®, MSD animal health, UK] to induce follicular growth, followed by a single intraperitoneal injection of 5 I.U. human chorionic gonadotrophin (HCG) [Chorulon®, MSD animal health, UK] 47 hours later to induce ovulation (Luo *et al.* 2011). Mice were either culled 16-17 hours post-HCG injection (for oocyte retrieval, (Zudova *et al.* 2004)) or 24 hours post-HCG injection (for collecting ovaries at diestrus stage).

3.3.4. Induction of genetic recombination in the OSE

To induce recombination of floxed genes exclusively in the OSE, virgin female mice at 9-13 weeks of age were anaesthetized and $2.4x10^8$ plaque forming units (PFU) of Ad-*cre* were injected directly into the ovarian bursa. Both right and left ovaries were injected to reduce the number of mice used in the study.

3.3.4.1. Induction of anaesthesia

All of the injectable solutions used in this section were prepared aseptically in sterile bijou tubes and stored at 4ºC for up to 7 days. The mice were anaesthetised using a ketamine and medetomidine combination, as recommended by the named veterinary surgeon for our animal facility. Briefly, 150 µl of ketamine hydrochloride (Ketamidor ® 100 mg/ml solution for injection, Chanelle, Ireland) and 200 µl of medetomidine (Domitor® solution for injection, 1 mg/ml, Orion pharma, Finland) were added to 3.65 ml of sterile saline solution [Appendix 1]. Intraperitoneal injection of 0.2 ml/10 g body weight was used to induce anaesthesia. Following the onset of anaesthesia, a single dose of meloxicam was given as an analgesic. This was prepared by diluting 100 µl of meloxicam (Metacam® solution for injection, 2 mg/ml, Boehringer Ingelheim, Germany) to a final volume of 2 ml using sterile saline as a diluent. 0.1 ml/10 g body weight was injected subcutaneously (SC). Before performing the surgery, deep anaesthesia was confirmed by checking the loss of pedal reflexes (approximately 20 minutes post-anaesthesia).

3.3.4.2. Intrabursal injection of adenovirus-cre

All pieces of the surgical equipment were autoclaved prior to surgery, and all solutions used were aseptically prepared. The surgery was performed in a class 2 biological safety cabinet.

3.3.4.2.1. Preparation of Adenovirus-*cre*

The Adenovirus-*cre* (a replication-incompetent adenovirus expressing *cre* recombinase under the control of the CMV promoter, Ad5-CMV-*cre*) was purchased from Vector Development Lab (Houston, USA) with an infectious titre of 2.4×10^{11} PFU/ml. Once received, the virus was divided into 25 µl aliquots in sterile small microcentrifuge tubes in a class 2 biological safety cabinet, and stored at -80ºC. On the day of the surgery, a 25 µl aliquot of the adenovirus-*cre* was thawed on ice and diluted with 74 µl of sterile 1X PBS (Gibco® Life technologies, USA) and 1 µl of sterile Trypan blue dye (Life technologies, USA) to a final infectious titre of 2.4×10^{8} PFU/4 µl.

3.3.4.2.2. Injection of Adenovirus-*cre*

After the complete loss of pedal reflexes, the mouse was placed on its ventral surface on a piece of paper towel and the fur on its dorsal surface was sprayed with 70% ethanol. Using a pair of scissors, a 1 cm transverse incision was made in the skin slightly below the mid-back of the mouse (towards the tail) and a small piece of paper towel sprayed with 70% ethanol was used to remove any hair surrounding the incision (Figure 3.1). The incision was placed over the left ovary and a pair of springbow scissors was used first to cut the fine membrane covering the muscles followed by cutting the muscle (a small vertical incision of 3 mm just enough to pull the ovary out). The ovary was carefully pulled out of the body cavity by holding the fat pad surrounding the ovary with a pair of forceps. The exposed ovary was placed over a small piece of paper towel (placed on the right side of the incision) and was kept in position either by using a surgical clamp attached to the fat pad or by using a small piece of paper towel over the fat pad. A 25 µl Hamilton syringe with a 32 gauge bevelled needle was used to inject 4 µl of the diluted virus slowly into the ovarian bursa, by going through the bursal membrane in the small space next to the entrance of the oviduct into the bursa. Following injection, the ovary was returned back to inside the body cavity, and the skin incision was placed over the right

ovary, for which the same procedure was performed. After both ovaries were injected and returned back to their position in the body cavity, the skin incision was closed by wound clips using a clip applicator. These clips were removed 7-10 days post-surgery using a clip remover. The intrabursal injections were kindly performed by Bridget Allen.

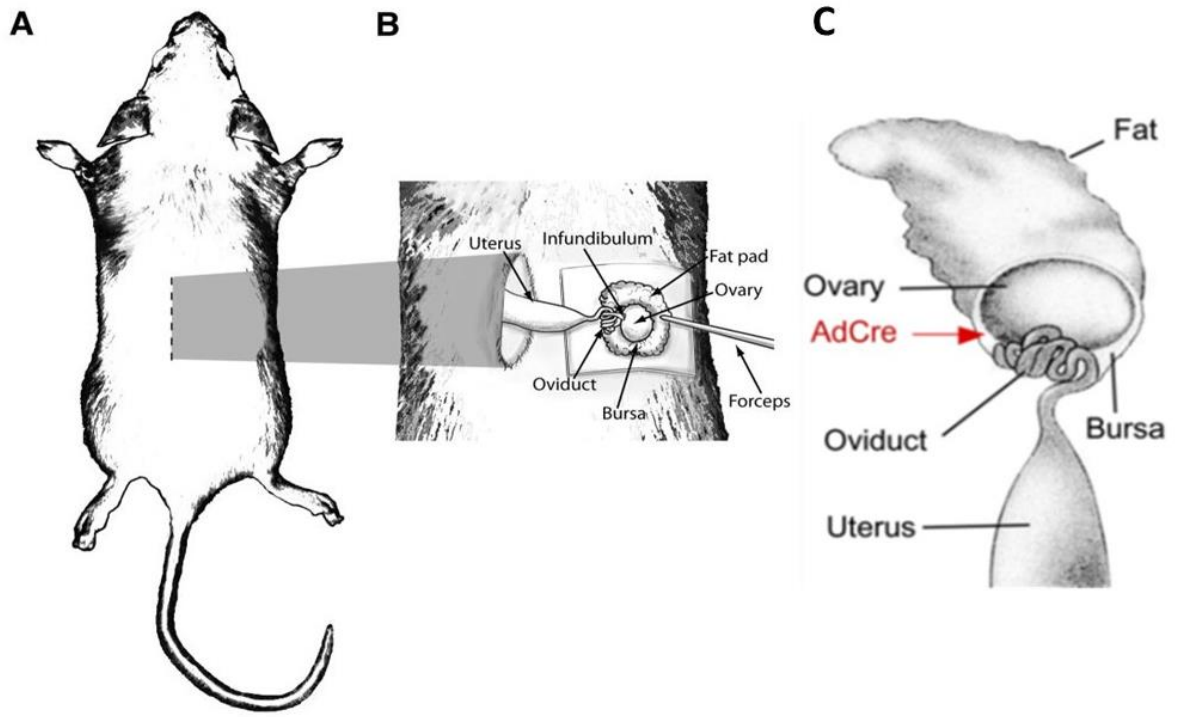

Figure 3.1: An outline of the intrabursal injection used for adenovirus-cre delivery. (A) Positioning the mouse and the place of incision. (B) Pulling the ovary outside the body from the fat pad and placing it on a piece of paper towel prior to injection. (C) Site of adenovirus-*cre* (AdCre) injection into the bursa. Adapted from (Wu *et al.* 2007; Cordero *et al.* 2010).

3.3.4.3. Reversing anaesthesia

Reversal of anaesthesia was performed at the completion of surgery by SC injection of 0.1 ml/10 g body weight of atipamezole hydrochloride, prepared by diluting 0.05 ml of atipamezole hydrochloride (Antisedan® solution for injection, 5 mg/ml, Orion pharma, Finland) in 2.45 ml of sterile saline. During recovery, mice were housed up to 3/cage and placed

on a paper towel without bedding (to prevent inhalation of bedding which can cause asphyxia). Mice were covered by a paper towel until fully recovered to provide warmth and avoid dryness of eyes. The cages were placed on a fluffy wool mat to avoid loss of heat during recovery. Animals were closely monitored until fully recovered (at least 2 hours) and kept in the class 2 biological safety cabinet for 24-48 hours, with free access to food and water. After this period, the paper towels were removed and the animals provided with normal bedding, before being moved to a negative pressure isolator. Mice were housed in the negative pressure isolator for 2 weeks before being transferred to conventional housing.

3.4. Tissue preparation

3.4.1. Tissue dissection

Mice were culled by cervical dislocation Schedule 1 method. The mouse ventral surface was sprayed with ethanol and an incision made throughout the skin and the abdominal wall to open the abdominal cavity. A pair of fine scissors were used to cut through the heart and a 1 ml syringe shaft was used to collect blood before placing it into a clean microcentrifuge tube. A second pair of fine scissors and forceps were used to pull the ovaries out by holding them from the fat pad, and both sets of ovary, oviduct and uterine horn were dissected as an individual unit. On a piece of paper towel, the extra adipose was removed. One set was kept attached together and fixed in 10% neutral buffered formalin (Sigma, USA). For the other set, the organs (ovary, oviduct and uterine horn) were seperated, placed individually in clean microcentrifuge tube and snap frozen on dry ice (Section 3.4.7). For oocyte retrieval, the oviducts were dissected and placed in sterile 1X PBS (Gibco®, Life technologies, USA) until further processing (Section 3.4.3).

For brain dissections, the head was sprayed with 70% ethanol and the skin covering the skull completely removed. A pair of scissors was used to cut and remove the parietal and frontal parts of the skull without damaging the soft brain tissue. Using a dissecting section lifter, the

brain was removed and a small piece placed in a clean microcentrifuge tube and snap frozen (Section 3.4.7).

Other tissues, such as the lungs, liver, kidney, spleen and lymph nodes were all placed in one flat-bottomed tube filled with 10% neutral buffered formalin solution (Sigma, USA) to fix the tissue before embedding in paraffin. A small piece from the ear was collected and used for re-genotyping as mentioned previously (Section 3.3.1).

3.4.2. Estimating ovarian volume

A set of calipers was used to measure the length (L), width (W) and height (H) of the ovaries, just after dissection and before fixing or snap-freezing. The following ellipsoid volume equation was used to estimate the normal ovarian or ovarian tumour volume (Pavlik *et al.* 2000):

$$Ovarian\ volume = \frac{4}{3}\ \pi\ (\frac{L}{2})(\frac{W}{2})(\frac{H}{2})$$

3.4.3. Oocyte retrieval

Each oviduct was placed on a microscope slide and bathed in 40 µl 1X PBS (Gibco®, Life technologies, USA). It was held in position by a pair of forceps and a small hole was made in the ampulla using a blunt needle. Using forceps or a needle, the oviduct was squeezed in the direction of the opening to force the cumulus oophorous complexes (COCs) to move out of the oviduct and into the PBS droplet (Figure 3.2). Oocyte retrieval was kindly performed by Elaine Taylor.

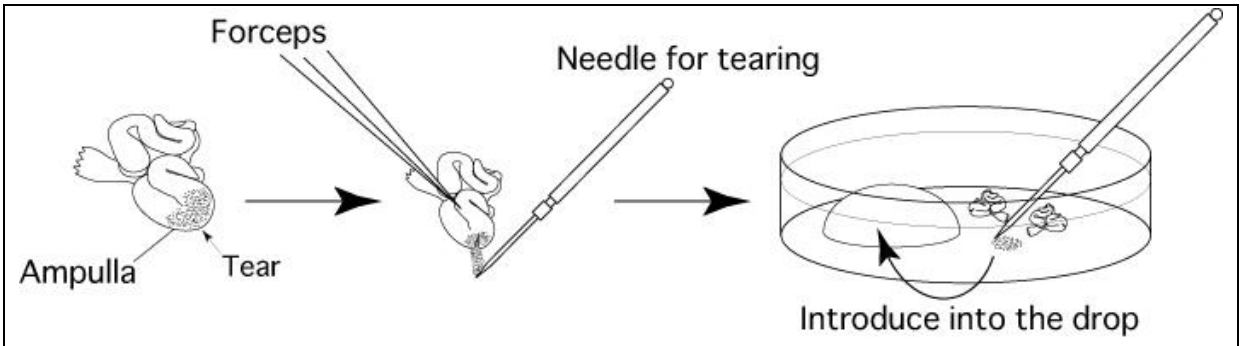

Figure 3.2: Schematic diagram for oocyte retrieval from the oviducts (Center for Animal Resources and Development 2016).

3.4.4. Tissue fixation using formalin

Tissues were fixed by placing them in flat-bottomed tubes filled with ice-cold 10% neutral buffered formalin (Sigma, USA), and incubating overnight at 4ºC. Subsequently, the formalin was discarded and the tissue stored in 70% ethanol at 4ºC until paraffin embedding.

3.4.5. Paraffin embedding of fixed tissue

Fixed tissues were removed from the 70% ethanol and placed into cassettes (Fisher, USA). They were processed using the automatic processor (Leica TP1050, Germany). The tissues were dehydrated by placing in increasing concentrations of ethanol [1 hour 70% ethanol, 1 hour 95 % ethanol, 2 X 1.5 hours 100% ethanol, 2 hours 100% ethanol]. This was followed by 2 X xylene incubation each lasting for 2 hour. The tissues were then transferred to liquid paraffin and incubated initially for 1 hour followed by 2 incubations each 2 hours long. Following this, the tissues were taken out of the liquid paraffin, placed in paraffin wax and left until complete solidification.

3.4.6. Sectioning of fixed tissue

The fixed tissues were cut into 5 µm sections using a microtome (Leica RM2135, Germany). The sections were placed on poly L-lysine (PLL)-coated glass slides and baked at 58ºC for 24 hours.

When serial sectioning was required, the tissue was cut into 100 sections, each 5 µm thick, with 2 sections placed per slide. Every 10th section (5th slide) was stained with H&E and used for histologic assessment. Because this resulted in most of the paraffin-embedded tissue being sectioned, all the PLL slides were redipped in paraffin wax to preserve antigens from being lost during storage (mainly the membranous antigens).

Paraffin embedding and sectioning of fixed tissue was kindly performed by Derek Scarborough.

3.4.7. Snap-freezing

Ovaries, oviducts and uterine horns were dissected separately and placed in clean microcentrifuge tubes. For brain and spleen, small pieces of the tissue were dissected and placed in clean microcentrifuge tubes. Immediately after this, the tubes were either placed on dry ice or immersed in liquid nitrogen and transferred to a -80ºC freezer until required.

3.4.8. Isolation of ovarian surface epithelium (OSE)

When OSE was needed for *in vitro* experiments, it was separated from the rest of the ovary according to the method of Nikitin *et al.* with slight modifications (Flesken-Nikitin *et al.* 2013). Individual ovaries were dissected from 10-12 weeks old virgin mice and washed twice with ice cold sterile 1X PBS (Gibco®, Life technologies). Each individual ovary was then transferred to a capped microcentrifuge tube filled with 200 µl digestion-buffer [prepared as shown in Table 3.3 and sterilized by filtration using 40 µl cell strainer (Falcon®, Fisher, USA)], and incubated for 60-75 minutes at 37°C in a 5% CO2 incubator with intermittent shaking. The complete peeling-off of the epithelial cells was checked under the microscope before removing the ovary from the tube. Following this, 1 ml of OSE complete medium (Table 3.3, prepared aseptically) was added to the tube and samples centrifuged at 1000 rpm for 5 minutes. The supernatant was discarded and the pellet washed with 1 ml of ice-cold sterile 1X PBS. The tube

was centrifuged and the pellet was resuspended in 500 µl of OSE complete medium for OSE 2D cultures (Section 3.9.1).

Table 3.3: Preparations used in OSE isolation from ovaries

Preparation name	**Ingredients**	**Amount required**
Digestion buffer	DMEM/F12 medium (Mediatech)	1 ml
	Collagenase-dispase (Roche)	4 mg
	Bovine serum albumin (Sigma)	30 mg
	Dnase I (Sigma)	1 µl
OSE complete medium	DMEM/F12 medium (Mediatech)	450 ml
	Fetal bovine serum (Sigma)	25 ml
	L-glutamine 200 mM (Mediatech)	10 ml
	ITS liquid media supplement 100X (Sigma)	5 ml
	Sodium pyruvate 100 mM (Mediatech)	5 ml
	MEM non-essential amino acids 100X (Mediatech)	5 ml
	Hydrocortisone (Sigma)	250 mg
	Epidermal growth factor EGF (Sigma)	10 mg

3.4.9. Serum collection

Blood collected at diestrus stage from 10-week-old *Apc2*$^{+/+}$ and *Apc2*$^{-/-}$ mice was placed in microcentrifuge tubes and allowed to clot for 90 minutes at room temperatures. Following this, samples were centrifuged for 10 minutes at 2000 rpm. Serum was collected and stored in microcentrifuge tubes at -80ºC until used for hormone assays.

3.5. Histological analysis

3.5.1. Dewaxing and hydrating PLLs

Prior to IHC staining, PLLs were placed in a plastic slide staining rack. Dewaxing of paraffin-embedded 5 µm tissue sections was performed by dipping the PLLs 2 X 5 minutes in

xylene solution, until complete removal of the paraffin wax. Slides which had been redipped in paraffin wax were incubated overnight in Histoclear (National Diagnostics, USA) bath for complete removal of the thick paraffin layer before performing the dewaxing steps described above. Following this, hydration was performed by dipping the sections in decreasing concentration of ethanol (2 X 100% ethanol, 1 X 95% ethanol, 1 X 70% ethanol, for 3 minutes each). The hydrated PLLs were then transferred to distilled water until further processing.

3.5.2. Haematoxylin and eosin (H&E) staining

Fully hydrated PLLs were stained with H&E to enable the histologic assessment of tissues. The hydrated PLLs were immersed in Mayer's Haemalum (RA Lamb, ThermoFisher, USA) stain for 1 minute, washed in running water for 5 minutes and dipped in Eosin (RA Lamb, ThermoFisher, USA) stain for 1 minute. Following a further wash under running tap water for 5 minutes, sections were dehydrated and mounted (Section 3.5.3.8). H&E staining was kindly performed by Derek Scarborough.

3.5.3. Immunohistochemistry

Immunohistochemistry was used to assess the expression and localization of proteins of interest in the ovarian sections (Table 3.4). PLLs were first dewaxed and hydrated (Section 3.5.1) before processing as described below. A negative control (lacking primary antibody) was included each time an immunostain was performed, to support the validity of the staining. Oviducts and uteri present on slides served as positive controls for most of the proteins assessed.

3.5.3.1. Antigen retrieval

Antigen retrieval was performed by boiling hydrated PLLs in citrate buffer [Appendix 1] to unmask the antigens from protein crosslinking that occurs during fixation. Briefly, 800 ml of citrate buffer was placed in a pressure cooker and preheated in a microwave oven for 5

minutes at 900 W. The slides were placed in the preheated citrate buffer in the pressure cooker and heated at 900 W for 5 minutes (until the pressure valve rises). This was followed by heating for a further 15 minutes at 300 W. After the pressure was released from the pressure cooker, the lid was removed and the slides left to cool down to room temperature in the solution. Following this, the slides were removed and washed twice with distilled water for 5 minutes with continuous agitation.

3.5.3.2. Blocking endogenous peroxidase activity

As horseradish peroxidase (HRP) enzyme catalyses the final reaction required for antibody visualization later in the procedure (Section 3.5.3.7), endogenous peroxidase activity was blocked to avoid interference and prevent false positive results. This was performed by incubating the slides for 30 minutes in 1.5% hydrogen peroxide (Sigma, USA) with shaking on a rocker. The slides were then washed 2 X 5 minutes with distilled water, followed by 1 X 5 minutes TBST buffer [Appendix 1] with continuous shaking.

3.5.3.3. Blocking of non-specific antibody binding

Blocking of non-specific antibody binding was performed by incubating the slides in 10% serum (in TBST) from the species that the secondary antibody was raised in, for 60 minutes at room temperature in a humidified chamber (Table 3.4). When using a mouse primary antibody, the mouse on mouse (M.O.M) Ig blocking reagent of the M.O.M kit (Vector Labs, USA) was used instead (prepared by diluting 9 µl of the reagent with 250 µl TBST). A wax pen (ImmEdge hydrophobic barrier pen, Vectorlabs, USA) was used to draw wells surrounding the tissue to be stained and 70 µl of the diluted blocking reagent or serum was applied to each section.

3.5.3.4. Application of primary antibody

Antibodies against proteins of interest were diluted in 10% blocking serum (in TBST) to an appropriate concentration (Table 3.4). The blocking serum was tipped off slides and 80 µl of the primary antibody solution applied to each tissue section and incubated in a humidified chamber for 1 hour at room temperature or overnight at 4ºC. A piece of parafilm was placed on each slide to minimize evaporation.

3.5.3.5. Application of secondary antibody

Slides were washed 3 X 5 minutes with TBST. Before incubation with a secondary antibody against the host species in which the primary antibody was raised. Either 1:200 [in 10% blocking serum] biotinylated secondary antibody (Vector labs, USA) or undiluted HRP-conjugated (Dako Envision plus kit, Agilent, USA) secondary antibody was utilized (Table 2.4). When using M.O.M kit, 1:250 MOM biotinylated anti-mouse Ig reagent [in M.O.M diluent prepared by adding 600 µl of protein concentrate stock solution to 7.5 ml of TBST] 80 µl was applied to each tissue section and incubated for 60 minutes at room temperature in a humidified chamber.

3.5.3.6. Signal amplification

A signal amplification step was required when a biotinylated secondary antibody was used. This was carried out using the VECTASTAIN ABC kit (Vector labs, USA), which enables the binding of HRP to the biotin of the secondary antibody. The ABC working solution was prepared 30 minutes prior to use (1 drop of reagent A added to 2.5 ml of TBST, followed by 1 drop of reagent B) and incubated at room temperature. Following the secondary antibody incubation, the slides were washed 3 X 5 minutes with TBST with agitation. 80 µl of ABC working solution was applied to the sections and incubated in the humidified chamber for 30 minutes at room temperature.

3.5.3.7. Visualization of antibody binding

Diaminobenzidine (DAB) reagent (Dako, Agilent, USA) is utilized as a substrate for the HRP enzyme conjugated to the secondary antibody. DAB is oxidized by HRP to give a brown colour at the site of the antibody binding. Following the secondary antibody step (and signal amplification step if required), the slides were washed 3 X 5 minutes with TBST solution. 80 µl of DAB working solution (prepared by adding 1 drop of the DAB chromogen to 1 ml of DAB substrate buffer) were applied for 5-10 minutes. After the development of brown colour, the DAB reagent was tipped off. Slides were washed 2 X 5 minutes in TBST before performing a final wash for 5 minutes in distilled water. Slides were then placed in a bath of Mayer's Haemalum (RA Lamb, USA) stain for 1 minute and subsequently washed under running water until complete removal of excess Haemalum (5 minutes).

3.5.3.8. Dehydration and mounting of slides

The slides were removed from water and placed in increasing concentration of ethanol to dehydrate the slides (1 x 3 minutes in 70% ethanol, 1 x 3 minutes in 95% ethanol, 3 x 3 minutes in 100% ethanol). This was followed by 2 x 5 minutes incubation in xylene. Slides were then mounted using DPX mounting medium (RA Lamb, USA) and 40 mm coverslip were applied, avoiding air bubble formation. Slides were left to dry in the fume hood overnight.

Table 3.4: Antibodies and conditions required for immunohistochemistry staining

Primary antibody	**IgG source**	**Dilution used**	**Blocking serum**	**Secondary antibody and dilution used**
APC2 Abcam 113370	Rabbit polyclonal	1/400	10% goat serum	Biotinylated Goat Anti-Rabbit Immunoglobulins
APC2 Santa cruz 12425	Goat polyclonal	1/400	10% rabbit serum	Biotinylated rabbit anti-goat immunoglobulin
Ki67 Abcam Ab1667	Rabbit polyclonal	1/75	10% goat serum	Biotinylated goat anti-rabbit immunoglobulins

Active caspase-3 Cell signalling 9661	Rabbit polyclonal	1/200	10% goat serum	Biotinylated Goat Anti-Rabbit Immunoglobulins
CD34 Abcam Ab81289	Rabbit polyclonal	1/150	10% goat serum	Biotinylated Goat Anti-Rabbit Immunoglobulins
E-cadherin BD Transduction 610182	Mouse monoclonal	1/200	MOM blocking reagent	EnVision+ System-HRP Labelled anti-mouse
Vimentin Santa cruz SC-7557	Goat polyclonal	1/300	10% rabbit serum	Biotinylated rabbit anti-goat immunoglobulin
Cytokeratin 18 multiepitope cocktail Progen 651134	Mouse monoclonal	1/5	MOM blocking reagent	MOM biotinylated anti-mouse Ig reagent
B-catenin Pharmingen 562505	Mouse	1/200	10% rabbit serum	EnVision+ System-HRP Labelled Polymer Anti-mouse
PTEN Cell signalling 9559	Rabbit monoclonal	1/200	10% goat serum	Biotinylated Goat Anti-Rabbit Immunoglobulin (1/200)
p-AKT (Ser 473 D9E) Cell signalling 4060S	Rabbit Monoclonal	1/75	10% goat serum	Biotinylated Goat Anti-Rabbit Immunoglobulin (1/200)
p-FOXO1/3/4 Cell signalling 2599	Rabbit monoclonal	1/40	10% goat serum	Biotinylated Goat Anti-Rabbit Immunoglobulin (1/200)
FOXL2 Abcam Ab5096	Goat polyclonal	1/750	10% rabbit serum	Biotinylated rabbit anti-goat immunoglobulin (1/200)
ERα	Mouse	1/500	MOM blocking reagent	MOM biotinylated anti-mouse Ig reagent (1/250)
FOXO1 Cell signalling 14952	Mouse	1/500	10% goat serum	EnVision+ System-HRP Labelled anti-mouse
Inhibin α (T-17) Santa cruz 22048	Goat polyclonal	1/20	10% rabbit serum	Biotinylated rabbit anti-goat immunoglobulin (1/200)
p44/42 MAPK (Erk1/2) (137F5) Cell signalling 4695S	Rabbit	1/100	10% goat serum	Biotinylated Goat Anti-Rabbit Immunoglobulin (1/200)

3.5.4. Image acquisition and analysis

Stained sections were examined with an Olympus BX43 light microscope Photomicrographs were taken by 5 Megapixel HD Microscope Camera (Leica MC170 HD, Germany) or using the ZEISS Axio Scan Z1 (Zeiss, Germany). The 4X magnification lens was used for counting ovarian follicles, corpora lutea and cysts. The 10X magnification was used for the vaginal smear examination for oestrous cycle staging. The 20X and 40X magnification was used for detailed H&E or immunohistochemistry ovarian tissue/tumour examination.

3.5.4.1. Cytological assessment of vaginal smear

The cytological evaluation of oestrous cycle stage was performed as previously described by McLean *et al.* (McLean *et al.* 2012). The three cell types identified in vaginal smears and used for staging are nucleated epithelium (NE), cornified epithelium (CE) and leucocytes (L). In the proestrus stage, the NE predominates. In the estrus stage, the CE predominates, with cells often aggregated in clusters. In the metestrus stage, the CE are still present but with less clustering and leucocytes are also observed. In the diestrus stage, leucocytes predominate, and occasional NE and CE are present (Figure 3.3).

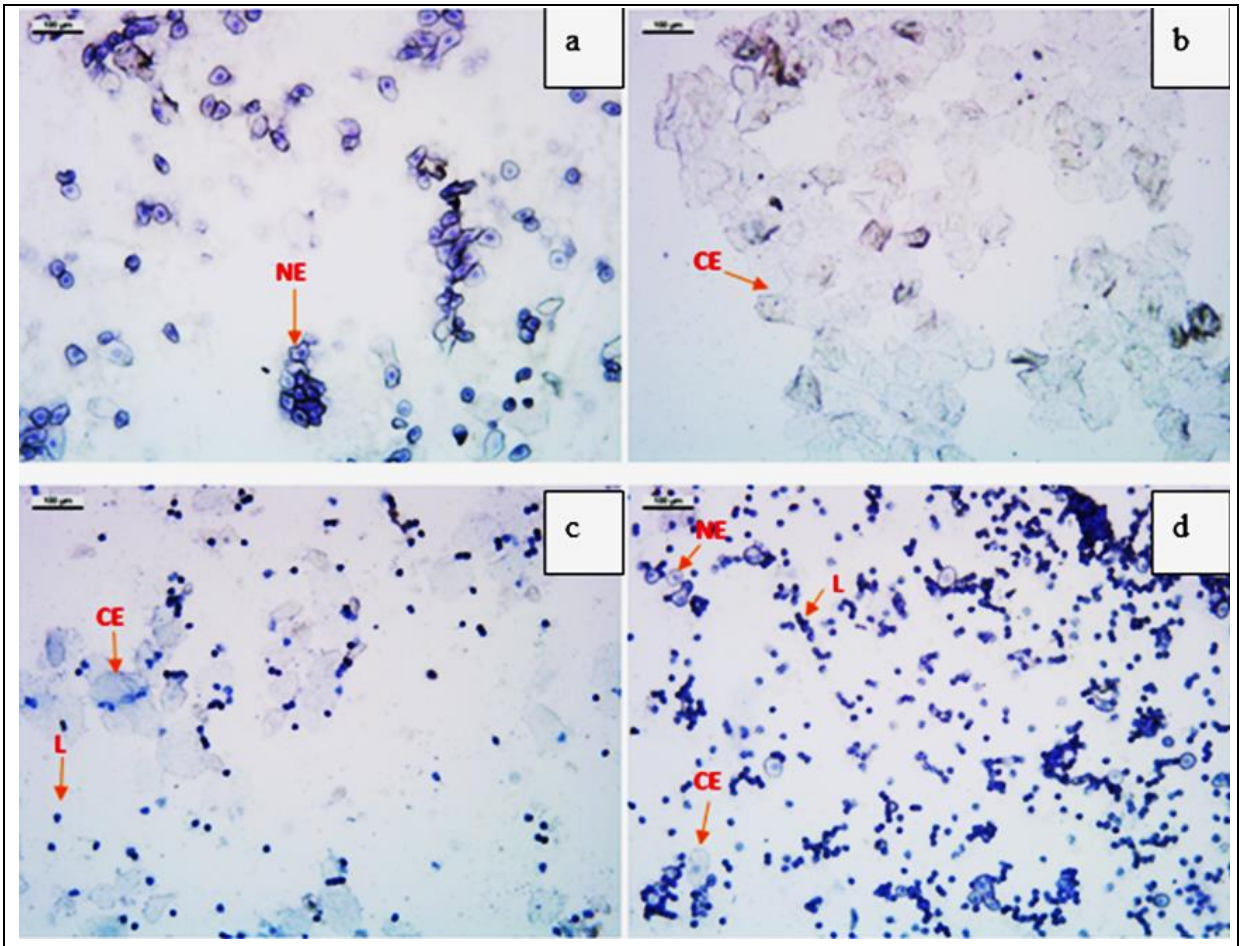

Figure 3.3: Cytological assessment of vaginal smears to identify oestrous stage. Red arrowheads indicates the three main cell types detected in vaginal smear samples: nucleated epithelial cells (NE), cornified squamous epithelial cells (CE), and leukocytes (L). Vaginal smear of mouse at (a) Proestrus stage showing the dominance of nucleated epithelial cells, (b) Estrus stage when the cornified epithelial cells predominate, (c) Metestrus stage showing cornified epithelial cells and leucocytes, and (d) Diestrus stage showing the presence of all three cell types. Scale bar 100 µm.

3.5.4.2. Characterization of cumulus oophorous complexes retrieved from oviducts

After releasing COCs from the oviducts (Section 3.4.3) under a dissection microscope using 2X magnification, the number of COCs released from each oviduct was counted. They were examined under a bright field microscope to assess their morphology, by counting the number of layers of cumulus cells surrounding the oocyte. Following this, 40 µl of 4 mg/ml

collagenase/dispase (Roche, Switzerland) dissolved in DMEM/F12 medium (Mediatech, USA) were applied to the PBS drop to free oocytes from surrounding cumulus cells. Gentle pipetting was performed and the solution left for 10 minutes to complete the digestion. Oocytes were examined under the microscope to determine their integrity, by recording cytoplasmic fragmentation, surface granulation and/or blebbing and smoothness of oocyte edge (Kiyosu *et al.* 2012) and to measure oocyte diameter (Brown *et al.* 2010). A minimum of 8 diameters were measured in order to determine the mean oocyte diameter.

3.5.4.3. Histological characterization of the ovary

Formalin-fixed paraffin-embedded ovaries were serially sectioned into 100 sections, each of 5 µm thickness, with each 10th section stained with H&E. Growing follicles were counted every 10th section when the nucleus of the oocyte was present. Decisions about basophilic intra-ovarian structures without a clear oocyte in the section (i.e. whether growing follicle or cyst) were made by examining the previous and following 10th stained sections. The total number of structures throughout the 10 counted sections was used as an estimate for the number in the whole ovary. The identification of the range of structures and abnormalities listed below was done according to the published INHAND project (International Harmonization of Nomenclature and Diagnostic Criteria for Lesions in Rats and Mice) (Dixon *et al.* 2014).

3.5.4.3.1. Quantifying follicles

All growing follicles with intact oocytes were counted and classified into primary follicles (oocyte surrounded by one layer of cuboidal granulosa cells); secondary follicles (oocyte surrounded by two or more layers of cuboidal granulosa cells and devoid of antral space), antral follicles (oocyte surrounded by multiple layers of cuboidal granulosa cells, with the presence of an antral space) and **pre-ovulatory follicles** (oocyte surrounded by multiple

layers of cuboidal granulosa cells, with the presence of an antral space and cumulus oophorous that forms a stalk into the antral cavity) (Figure 3.4; (Balla *et al.* 2003)). **Atretic follicles** were identified by the presence of pyknotic bodies in the granulosa cells and/or oocyte degeneration, and counted separately (Visser *et al.* 2007).

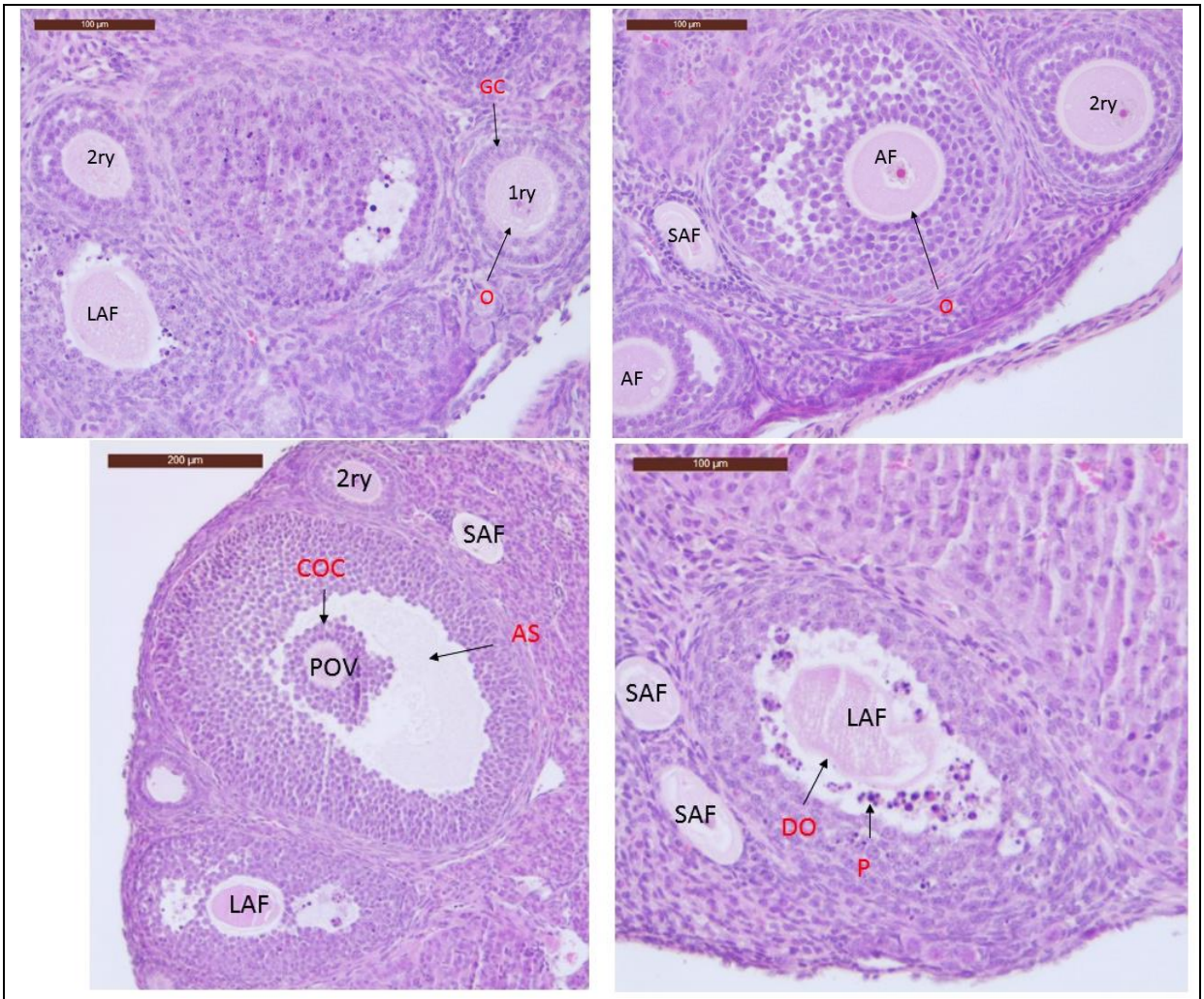

Figure 3.4: Photomicrographs of the follicles (black letters) quantified in serial sections. Primary follicles (1ry), secondary follicles (2ry), antral follicles (AF), pre-ovulatory follicle (POV). Atretic follicles were classified as small atretic follicles (SAF) and large atretic follicles (LAF). Different elements of the follicles are labelled using red letters. O:oocyte. GC: granulosa cells. COC: cumulus oophorus comples. AS: antral space/antrum. DO: degenerating oocytes. P: pyknotic body (Pyknosis). Scale bars all 100 µm except lower left panel (scale bar 200 µm).

3.5.4.3.2. Quantifying corpora lutea

All corpora lutea (CL) were counted, whether they were an eosinophilic CL (mature, present near to the surface or towards the centre, representing newly formed, recent or old CL) or a basophilic CL (recent, present close to the ovarian surface, resulting from the most recent ovulation, Figure 3.5).

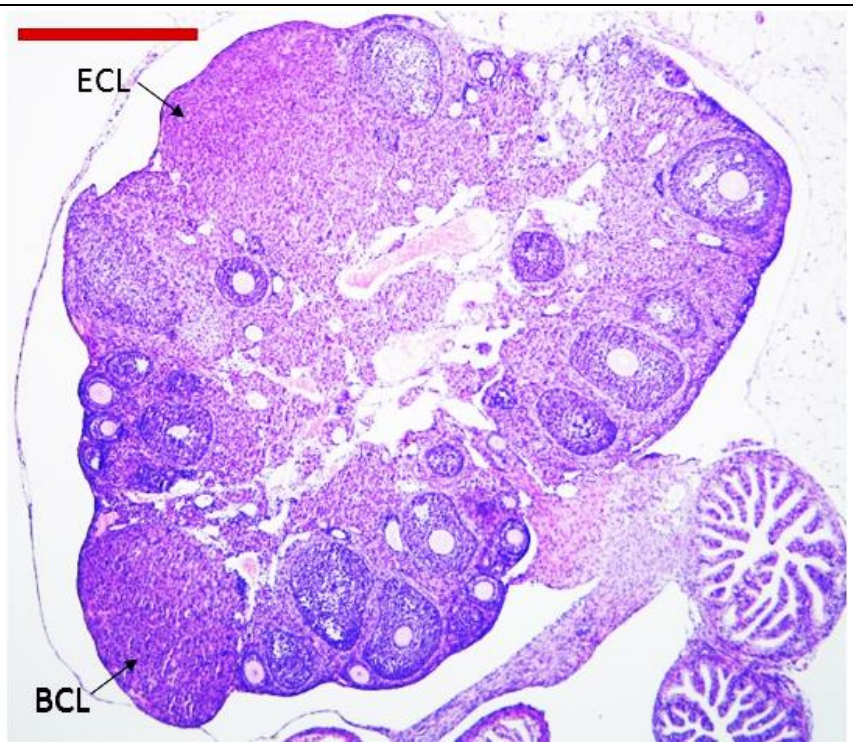

Figure 3.5: Corpora lutea in ovarian sections. ECL: eosinophilic corpus luteum. BCL: basophilic corpus luteum. Scale bar 500 µm.

3.5.4.3.3. OSE irregularities

A range of OSE irregularities was observed in induced ovaries and counted whenever identified. The presence of papillary-like epithelial structures projecting to the outside were identified as 'papillary epithelium'. Presence of more than one layer of epithelial cells was identified as 'multi-layering'. A deep groove inside the ovarian tissue formed of epithelial cells was identified as 'OSE invagination'. Bulging of the normal contour of the ovary was identified as 'ovarian outgrowth' (Figure 2.6).

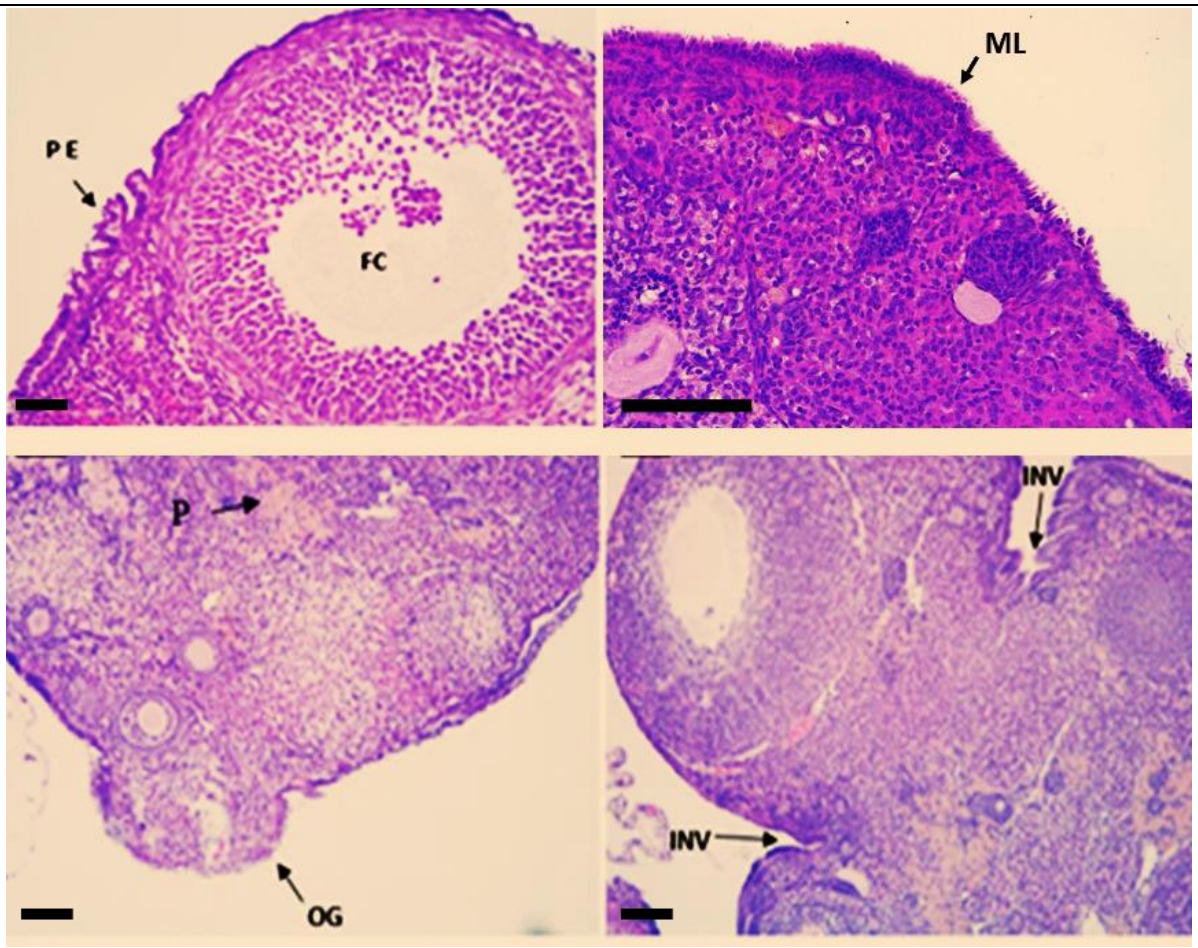

Figure 3.6: Photomicrographs of OSE irregularities analysed, representing papillary epithelium (PE), multi-layering (ML), ovarian outgrowth (OG) and invaginations in the OSE (INV). Other abnormalities inside the ovaries include follicular cysts (FC) and pigmentation (P). Scale bar 100 µm.

3.5.4.3.4. Abnormal structures inside the ovary

Decisions about cysts were only made after examining the serial sections to ensure that none of them contained an oocyte in another section (Figure 3.7). Any structure present inside the ovary, of the same size or bigger than a normal corpus luteum, having one or more granulosa cell layers without an oocyte and with a large empty space was identified as a 'follicular cyst'. Any cystic structure filled with blood was identified as 'blood cyst'. When the cyst was lined with epithelial cells (confirmed by E-cadherin immunostaining), it was identified as an 'epithelial cyst'.

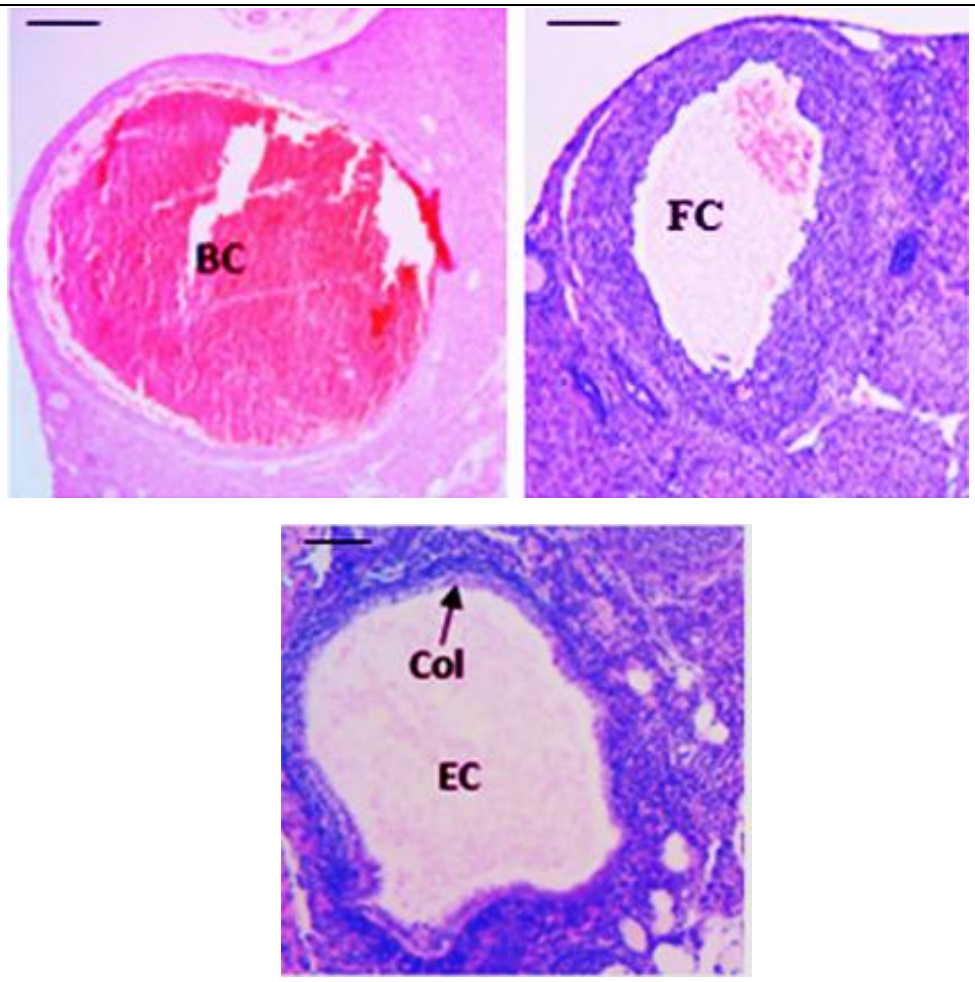

Figure 3.7: Photomicrographs of cysts or abnormal follicles found inside the ovary, representing blood cysts (BC), folliclular cysts (FC), and epithelial cysts (EC) lined with columnar epithelium (Col). Scale bar 100 µm.

3.6. Quantitative Reverse-Transcription Polymerase Chain Reaction (qRT-PCR)

qRT-PCR was used to analyze the relative expression levels of genes present in ovarian tissue or ovarian tumours. RNA was extracted from the whole ovaries or a piece of the tumour. A reverse transcription step was performed to synthesize cDNA from the isolated RNA prior to performing the PCR amplification. A minimum of three mice per cohort was assessed, unless it was only one tumour per cohort when 2 different samples of the same tumour were processed separately.

3.6.1. RNA extraction

Total RNA was extracted from individual ovaries or tumours using RNeasy plus mini extraction kit (Qiagen, Germany) in accordance with the manufacturer's instructions. Briefly, the whole ovary or a tumour piece weighing 10 mg, was homogenized in 350 µl RLT buffer using a hand-held tissue grinder and disposable plastic pestles (FisherBrand® disposable pestle system, ThermoFisher, USA). A series of columns and reagents were used to extract the RNA according to the manufacturer instructions (Figure 3.8). The total RNA extracted from one whole ovary was dissolved in 50 µl of ultrapure water (Sigma, USA). The RNA quantity and quality were measured using a NanoDrop 2000® (Thermo Scientific, USA). The extracted RNA was kept at -80ºC until further processing for cDNA synthesis.

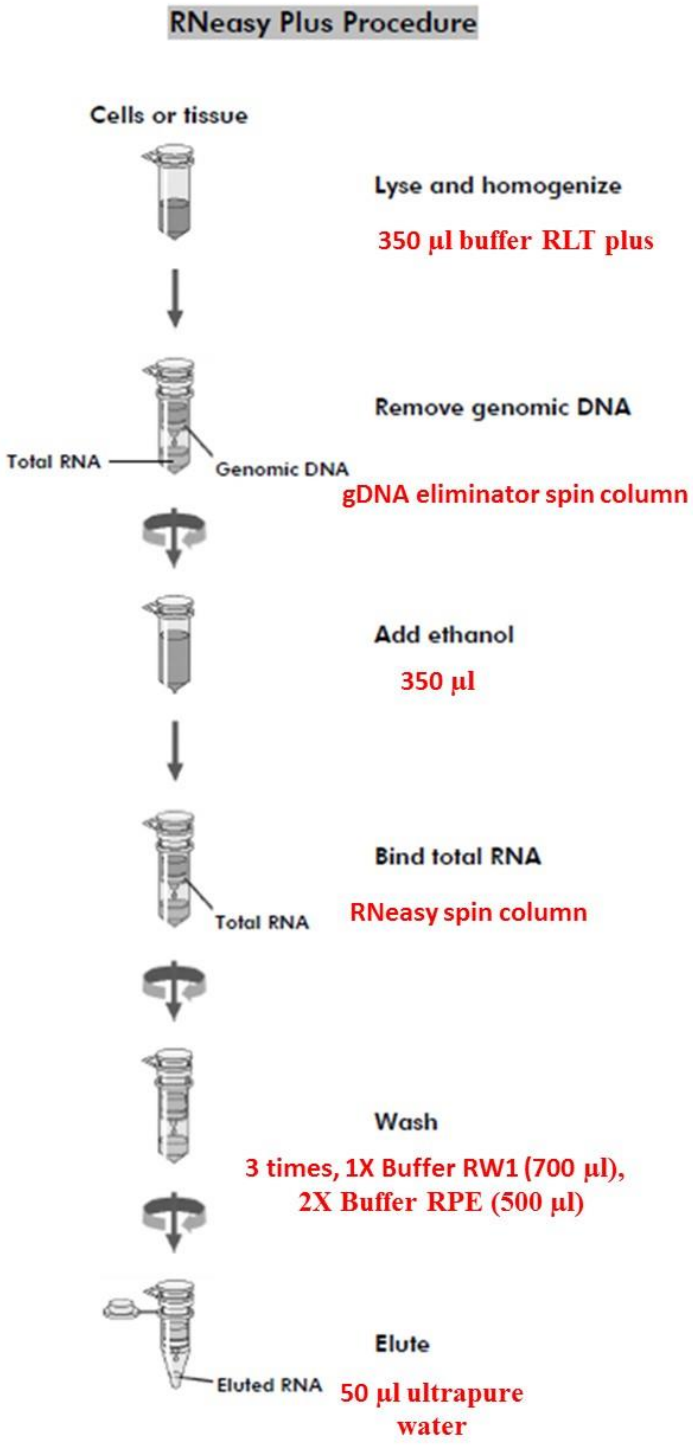

Figure 3.8: Workflow of RNeasy plus mini extraction kit. Picture adapted from RNeasy plus mini handbook available at https://www.qiagen.com/kr/resources/resourcedetail?id=c8cdc6bf-5bbf-4e3b-a0f4-476da9215012&lang=en

3.6.2. Reverse transcription

A volume equivalent to 1 µg of RNA was used for genomic DNA (gDNA) removal followed by cDNA synthesis by reverse transcription, using QuantiTect reverse transcription kit (Qiagen, Germany). Briefly, template RNA was placed in one well of a strip tube, 2 µl of 7X gDNA wipeout buffer were subsequently added and the volume adjusted to 14 µl using ultrapure water (Sigma, USA). The strip tube was then incubated at 42ºC for 2 minutes to remove gDNA. Following this, reverse transcription was performed by adding 6 µl of reverse transcription master mix [consisting of 1 µl reverse transcriptase, 4 µl 5X RT buffer and 1 µl RT primer mix] to each well and incubated at 42ºC for 15 minutes, followed by a 3 minutes incubation at 95ºC to inactivate the transcriptase. The synthesized cDNA (20 µL) was stored at -20ºC or directly used as a template for polymerase chain reaction (PCR).

3.6.3. Quantitative polymerase chain reaction (qPCR)

qPCR reactions were performed in triplicates in 384-well reaction plates (Applied Biosystems). To normalize the expression of genes of interest, β-actin was used as an endogenous housekeeping control gene. In order to compare mRNA expression levels, each cDNA sample was amplified using primer pairs (SYBR® Green analysis) or predesigned probes (TaqMan® analysis) of genes of interest as well as β-actin. A "no template control" that contained water was included in each plate.

3.6.3.1. SYBR Green gene expression analysis preparation

All primers used were designed using Primer BLAST (available at http://www.ncbi.nlm.nih.gov/tools/primer-blast) and synthesized by Sigma (Table 3.5). Each reaction mixture contained 0.5 µl cDNA, 0.25 µl forward primer (10mM), 0.25 µl reverse primer (10mM), 5 µl PowerUp™ SYBR™ green master mix (Applied Biosystems, USA) and 4 µl ultrapure water (Sigma, USA) to a final volume of 10 µl. The plate was sealed and

centrifuged for 1 minute at 10 000 rpm. The plates were either amplified on the PCR machine on the same day of preparation or stored at 4ºC and amplified the following day.

Real-time RT-PCR was performed using QuantStudio™ 7 Flex Real-Time PCR System (ThermoFisher, USA) according to the manufacturer's instructions. After an initial hold stage (2 minutes at 20ºC), followed by an initial denaturation at 95ºC for 10 minutes, amplification was performed for 40 cycles, each of 15 seconds denaturation at 95ºC followed by 60 seconds of annealing and extension at 60ºC. A final melt curve stage was performed (15 seconds at 95ºC followed by 1 minute at 60ºC and 15 seconds at 95ºC).

Table 3.5: List of genes and primers used in SYBR Green gene expression analysis

Gene	Forward primer sequence (5'-3')	Reverse primer sequence (5'-3')
Actb (actin b)	GCT ACA GCT TCA CCA CCA CA	TCT CCA GGG AGG AAG AGG
Apc2 exon 13 beginning	CTC TGT GGA ACC TGT CAG CA	AAC CCA GTG CAC CAT CTA CC
Apc2 exon 13 end	GGA ACT CCC TGG CAG TCA TC	TAG TCC TCC CGT GTG GCA AT
Apc2 exon 14	GGA GGA TGC AAC ACC ATC CA	ACG GAA CTA CAA CGG CTC AG

Results of *Apc2* expression analysis using SYBR Green gene expression are presented in Appendix 2.

3.6.3.2. TaqMan gene expression analysis

All primer/probe sets used were pre-designed and purchased from ThermoFisher Scientific, USA. They were selected using Taqman® gene expression assay search tool by searching for mouse gene expression assay and choosing the primer/probe set with the best coverage (Table 3.6). Each reaction mixture contained 0.5 µl cDNA, 0.5 µl TaqMan® assay (primer/probe set), 5 µl TaqMan® universal master mix II with UNG (Applied Biosystems, USA) and 4 µl ultrapure water (Sigma, USA) to a final volume of 10 µl. The plate was sealed

and centrifuged for 1 minute at 10 000 rpm. The reactions were either amplified on the PCR machine on the same day of preparation or stored at 4ºC and amplified the following day.

Table 3.6: List of TaqMan® assays used in gene expression analysis.

Taqman® Gene Expression Assay	Assay ID	Taqman® Gene Expression Assay	Assay ID
Actb	Mm00607939_s1	***Esr1***	Mm00433149_m1
Apc	Mm00545877_m1	***Esr2***	Mm00599819_m1
Apc2	Mm00478649_m1	***Fasl***	Mm00438864_m1
Ar	Mm00442688_m1	***Fgf1***	Mm00438906_m1
Areg	Mm00437583_m1	***Foxl2***	Mm00843544_s1
Axin2	Mm00443610_m1	***Foxo1***	Mm00490671_m1
Bcl2l11	Mm00437796_m1	***Foxo3***	Mm01185722_m1
Bcl6	Mm00477633_m1	***Fshr***	Mm00442819_m1
Cd44	Mm01277163_m1	***Gdf9***	Mm00433565_m1
Cdh1	Mm01247357_m1	***Kitlg***	Mm00442972_m1
Cdkn1b	Mm00438168_m1	***Lef1***	Mm00550265_m1
Ctnnb1	Mm00483039_m1	***Lgr5***	Mm00438890_m1
Cyp11a1	Mm00490735_m1	***Lhcgr***	Mm00442931_m1
Cyp17a1	Mm00484040_m1	***Pgr***	Mm00435625_m1
Cyp19a1	Mm00484049_m1	***Pten***	Mm00477210_m1
Egf	Mm00438696_m1	***Tnfsf10***	Mm01283606_m1
Egfr	Mm00433023_m1	***Vegfa***	Mm01281448_g1
Ereg	Mm00514794_m1	***Wif1***	Mm00442355_m1

Real-time RT-PCR was performed using QuantStudio™ 7 Flex Real-Time PCR System (ThermoFisher, USA) according to the manufacturer's instructions. After an initial hold stage (2 minutes at 20ºC followed by an initial denaturation at 95ºC for 10 minutes),

amplification was performed (PCR stage) for 40 cycles of 15 seconds denaturation at 95ºC followed by 60 seconds of annealing and extension at 60ºC.

3.6.4. Gene expression analysis

Gene expression analysis was performed using QuantStudio™ Real-Time PCR software version 1.3 (available at https://www.thermofisher.com/uk/en/home/technical-resources/software-downloads/quantstudio-flex-real-time-pcr-system.html), utilizing the 2(-Delta Delta C(T)) method to calculate relative gene expression levels (Livak and Schmittgen 2001). Melt curves for each reaction were checked to confirm the presence of one peak only and to avoid potential interference due to primer-dimer formation (for SYBR gene expression). A threshold was set in the exponential linear range on the amplification curve. A cycle threshold (C_T) was defined as the number of thermocycles required by each well reaction to reach the threshold. The 3 readings of the triplicates were used in the analysis, provided that they did not differ by more than 1 C_T value. Any reaction with more than one peak on the melting curve or differing by more than 1 C_T value was excluded from the analysis. The sample C_T value was calculated as the average value of the triplicates (or valid results) for each gene of interest. The readings of each sample were normalized by subtracting the average C_T value of β-actin from the average C_T value of the gene of interest to calculate ΔC_T value. The $\Delta\Delta C_T$ values were calculated using the control cohort (*Apc2*$^{+/+}$ group) as the calibrator, by subtracting the average ΔC_T value of the control cohort from the average ΔC_T value of the test cohort. The relative mRNA expression level was calculated using the formula:

$$Relative\ mRNA\ expression\ level = 2^{-\Delta\Delta CT}$$

Relative expression levels (RQ), minimum (RQ Min) and maximum (RQ Max) values were extracted from the QuantStudio™ software output after performing the analysis. These

values were used to plot the graphs, and statistical significance was estimated using the overlap rule for 95% confidence interval bars (Cumming *et al.* 2007) for small biological groups (n=3).

3.7. Western blotting

3.7.1. Preparation of protein extract

Cryogenic grinding was used to mechanically disrupt tissue and produce the desired lysate. Frozen whole ovaries or small pieces of brain (up to 20 mg) were ground under liquid nitrogen using a mortar and pestle until the tissue was fully powdered. It was collected in a 1.5 ml microcentrifuge tube and 100 µl of lysis buffer [preheated at 95ºC for 2 minutes on a heat block, supplemented with protease inhibitors] were added to the tube (Table 3.7). The contents were mixed by vortexing for 1 minute and placed on a heat block for 3 minutes at 95ºC. This vortex-heat cycle was repeated 3 times and cell lysate centrifuged at 13 000 rpm for 5 minutes at room temperature. The supernatant was aliquoted in clean microcentrifuge tubes and stored at -80ºC until further processing.

Table 3.7: Lysis buffer supplemented with protease inhibitors

Constituent	**Preparation**	**Amount used in lysis buffer**
50 mM Tris buffer pH 7.4+2% SDS	0.71 g of Tris (Fisher Bioreagents, USA) dissolved in 100 ml of ultrapure water (Sigma, USA), pH adjusted to 7.4 using concentrated hydrochloric acid (Sigma, USA). 2.35 g of sodium dodecyl sulphate SDS (Sigma, USA) were then added to the solution (stored at room temperature)	850 µl (kept at room temperature to avoid SDS precipitation)
Protease inhibitor (complete mini EDTA-free protease inhibitor cocktail tablet, Roche, Switzerland)	One tablet was dissolved in 1.5 ml of ultrapure water (Sigma, USA) and stored in aliquots of 150 µl at -20ºC	150 µl (added just before use of lysis buffer)

3.7.2. Protein quantification

Protein quantification was determined colorimetrically using the bicinchoninic acid (BCA) reaction (Smith *et al.* 1985). This method combines the Biuret reaction (reduction of divalent copper ions to monovalent copper ions by protein in alkaline medium) with the colorimetric determination of the monovalent copper ions produced, using BCA. One copper monovalent ion chelates with 2 BCA molecules forming a purple complex with a strong absorbance at 562 nm. The number of copper ions present is directly proportional to the protein concentration of the samples, thus allowing it to be determined colorimetrically (Figure 3.9).

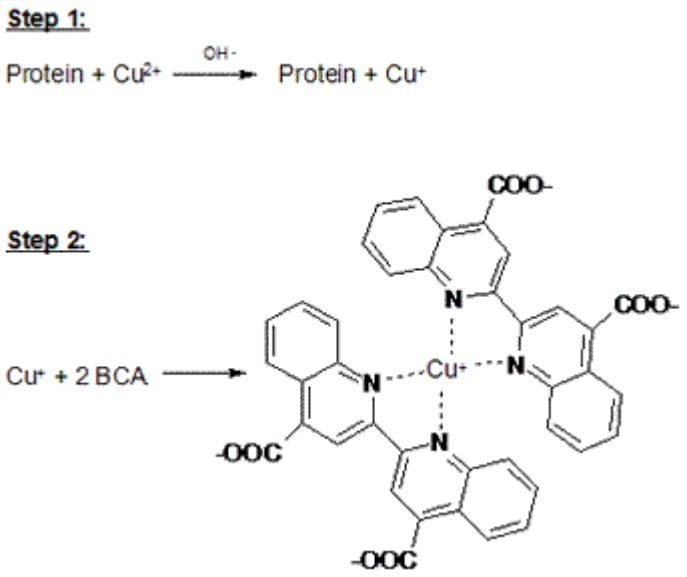

Figure 3.9: Schematic representation of chemical reactions in the BCA assay of protein determination. Figure taken from Biotek website and available at http://www.biotek.com/resources/articles/in-situ-micro-volume-bicinchoninic-acid-protein-assay.html

The concentration of protein in the lysate was determined using the Pierce BCA protein assay kit (ThermoFisher Scientific, USA). The working reagent (WR) was prepared by adding 5 ml of reagent A to 0.1 ml of reagent B. Protein standards were prepared by dissolving stock bovine serum albumin (BSA) in the lysis buffer used and diluting to yield 8 different

concentrations (25, 125, 250, 500, 750, 1000, 1500 and 2000 µg/ml). In a microplate well, 10 µl of the prepared protein lysate or standard dilution were added to 200 µl of WR (assayed in duplicates). The contents were mixed on a plate shaker for 30 seconds after which the plate was covered and incubated at 37ºC for 30 minutes. The plate was left to cool to room temperature and the absorbance of the colour formed was measured colorimetrically using a CLARIOstar® monochromator microplate reader (BMG Labtech, Germany) set at 562 nm. Absorbances of the different concentrations of BSA were used to construct a calibration curve, and the protein concentration of samples calculated using this calibration curve.

3.7.3. PAGE gel preparation

Gels used were hand-cast in house. Gel cassettes were set up in Mini-PROTEAN® tetra hand casting system (BioRad, USA) with a 10 well comb. The short plate and spacer plate of the cast were cleaned thoroughly with detergents, rinsed with ultrapure water (Sigma, USA) followed by 70% ethanol and dried with paper towel. The assembled plate was then placed in the frame of the casting stand (on a rubber gasket) and clamps closed. Leakage was tested after the assembly by using ultrapure water (Sigma, USA), which was subsequently poured off. The running gel (6% acrylamide) and the stacking gel (3% acrylamide) were both prepared in sterile falcon tubes (recipes in Table 3.8), but without adding TEMED (ThermoFisher Scientific, USA). Once ready, TEMED was added to the running gel and mixed by inversion. Quickly, a micropipette set at 1000 µl was used to pour the gel between the plates to 2 cm below the top of the short plate. 2 ml of ultrapure water (Sigma, USA) were then added on top of the gel to avoid formation of air bubble and to ensure the gel surface is flat. Once the gel was set (after 15 or 20 minutes), the water was poured off, TEMED was added to the stacking gel which was mixed and poured on top the running gel. A 1.5mm 10 well comb was inserted into the stacking gel and left to set. Once set, the plates were removed from the casting apparatus. The gel was either used on the same day or stored in the fridge for up to 4 days, after wrapping the plates in

paper towels and generously spraying them with ultrapure water (Sigma, USA) to avoid dryness. For use, the gel was placed in a Mini-PROTEAN® tetra vertical electrophoresis cell (BioRad, USA) and the tank filled with 1X running buffer (Table 3.8). The comb was removed and the wells washed with the running buffer using a 100 µl micropipette (to remove any debris from the wells). The wells were then thoroughly checked and any air bubbles removed.

Table 3.8: Recipes of gels and running buffer used for protein separation

Preparation name	**Ingredients**	**Amount required (added in the same order written)**
Running/separating gel (6% acrylamide)	Ultrapure water (Sigma, USA) Tris (Fisher Bioreagent, USA) 1.5M pH 8.8 30% Acrylamide (Sigma, USA) 10% SDS (Sigma, USA) 25% Ammonium persulfate (Sigma, USA) Temed (Sigma, USA)	4 ml 1.875 ml 1.5 ml (toxic) 75 µl 50 µl 10 µl
Stacking gel (3% acrylamide)	Ultrapure water (Sigma) Tris (Fisher Bioreagent, USA) 0.625M pH 6.8 30% Acrylamide (Sigma, USA) 10% SDS (Sigma, USA) 25% Ammonium persulfate (Sigma, USA) Temed (Sigma, USA)	2.525 ml 0.625 ml 0.525 ml 37.5 µl 75 µl 7.5 µl
Running buffer (1X)	Tris base (Fisher Bioreagent, USA) Glycine (Sigma, USA) 10% SDS (Sigma, USA) Ultrapure water (Sigma, USA)	3.02 grams 18.8 grams 10 ml Up to 1000 ml

3.7.4. Loading protein samples and running the gel (SDS-Page)

Prior to loading onto the gel, frozen protein aliquots were defrosted on ice. A volume equivalent to 50 µg protein was pipetted into a clean microcentrifuge tube, 5 µl of 4X Laemmli buffer (Sigma, USA) was added and ultrapure water (Sigma, USA) used to adjust the final volume to 20 µl. The protein sample was then denatured by placing on a heat block at 95ºC for 10 minutes. After heating, the samples were quenched on ice, briefly centrifuged and loaded into the wells of the gel. The PageRuler™ Plus pre-stained protein ladder (ThermoFisher Scientific, USA), with proteins ranging from 10 to 250 kDa was used as a protein marker. This was performed by mixing 5 µl of the PageRuler™ with 15 µl of 1X Leammli buffer (Sigma, USA) and loading in one well of the gel. The gel was then run at 125V for 75 minutes. The gel was removed from the electrophoresis cell, the plates were separated and the stacking gel was cut away and discarded. The gel was then carefully peeled off the plate and soaked in a box filled with transfer buffer (Table 3.9) until ready to be transferred.

Table 3.9: Recipe of transfer buffer

Ingredients	Amount required
Tris base (Fisher BioReagent, USA)	2.9 grams
Glycine (Sigma, USA)	14.5 grams
Methanol (Sigma, USA)	200 ml
Ultrapure water (Sigma, USA)	Up to 1000 ml

3.7.5. Protein transfer (Electrophoretic blotting)

The wet transfer method was used for protein transfer. Mini Trans-Blot® cell (BioRad, USA) and polyvinylidene difluoride membrane PVDF (BioRad, USA) were used. Because PVDF is highly hydrophobic, it was activated by soaking in methanol (Sigma, USA) for 2 minutes. It was then rinsed with ultrapure water (Sigma, USA) at least 3 times until it could be submerged into water and then soaked in the transfer buffer until used. The transfer stack was

then built in a mini gel holder cassette, where the gel and the PVDF membrane were sandwiched between sponges and filter papers (Whatman, UK) which had been pre-soaked in transfer buffer (Figure 3.10). The Mini Trans-Blot® cell was then filled with a pre-chilled transfer buffer and the transfer stack was placed in the central core. The cooling unit was placed in the cell and the transfer performed at 120V for 75 minutes at 4ºC (cold room). After transfer, the PVDF membrane was carefully removed and washed with ultrapure water (Sigma, USA) for 5 minutes. Ponceau S® (Sigma, USA) was applied to the membrane for 1 minute for rapid visualization of separated protein bands. The membrane was washed with ultrapure water (Sigma, USA) for 5 minutes on a lab rocker to remove the red Ponceau stain. A final wash with 1X TBST buffer was performed before further processing.

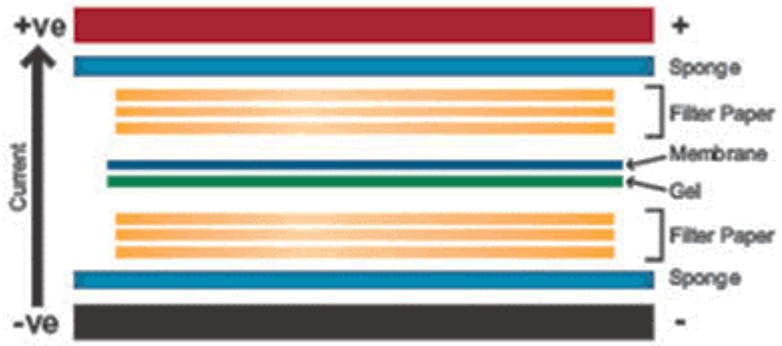

Figure 3.10: Assembly of the transfer stack used in electrophoretic blotting (Taken from Abcam Western blot protocol, http://www.abcam.com/protocols/general-western-blot-protocol)

3.7.6. Antibody probing of the PVDF membrane

To prevent non-specific background protein binding, the PVDF was blocked with 5% bovine serum albumin (BSA) solution [prepared by dissolving 0.5 g of BSA (Sigma) in 10 ml of TBST buffer] for 1 hour with shaking on a rocker at room temperature. The membrane was washed with 1X TBST for 5 minutes. The diluted APC2 primary antibody [Abcam ab113370, 1:1300, using 1% BSA/TBST as diluent] was applied and incubated overnight at 4ºC with

continuous agitation, such that the membrane was fully immersed all the time. This was followed by washing the PVDF membrane 1X15 minutes, 2X5 minutes with TBST at room temperature with continuous shaking. The horseradish peroxidase (HRP)-conjugated goat anti-rabbit secondary antibody [1:5000 in TBST, Vector Labs, UK] was applied to the PVDF membrane for 1 hour at room temperature with continuous shaking, followed by washing 1X15 minutes, 2X5 minutes with TBST prior to signal detection.

3.7.7. Signal detection

Luminata Forte Western HRP substrate (Merck Millipore, USA) was used as the chemiluminescent HRP detection reagent. The membrane was incubated with 1 ml of the Luminata reagent for 1 minute at room temperature and excess reagent discarded. The membrane was placed inside the GelDoc XR (Bio Rad, USA) chamber and Image Lab software was used for image acquisition using signal accumulation mode, to allow for a cumulative sequence of exposures. The settings were adjusted to get the first image after 5 seconds, followed by one image every 20 seconds up to 5 minutes.

3.7.8. Confirming equal protein loading (GAPDH re-probing)

In order to ensure that differences in APC2 protein expression were not due to unequal loading of protein samples, membranes were re-probed with an antibody to the house-keeping protein GAPDH. Following APC2 protein signal detection, the membrane was washed 3X5 minutes with TBST to remove residual Luminata reagent. The diluted GAPDH primary antibody (Millipore MAB374, 1:2000) was applied overnight at 4ºC. This was followed by washing the membrane 3X5 minutes with TBST, applying the diluted secondary antibody (anti mouse IgG, Sigma A4416, 1:5000) for 1 hour at room temperature and performing signal detection as described above (Section 3.7.7).

Results of Western blotting for APC2 protein are presented in Appendix 2.

3.8. *Apc2* mutant allele (*Apc2*$^{-}$) DNA sequencing

3.8.1. PCR amplification

DNA extraction and PCR product visualization were done by methods described in Section 3.3.1. PCR reaction was performed using 170 ng of prepared DNA. An equivalent volume of DNA template was added to a strip-tube well containing 25 µl GoTaq long PCR master mix (Promega, USA), 5µl of the forward primer (10 µmol), 5µl of the reverse primer (10 µmol) and ultrapure water (Sigma, USA) up to a final volume of 50 µl. The components were mixed, centrifuged for 10 seconds and placed in a thermal cycler. Samples were subjected to 2 minutes initial denaturation at 95ºC followed by 34 cycles of 30 seconds denaturation at 94ºC and 6 minutes annealing and extension at 65ºC. A final extension was done at 72ºC for 10 minutes. The primers used for amplification were either the previously described *Apc2* primers used in genotyping (primer pair 1, Table 3.10), or a forward primer designed using Primer BLAST (available at http://www.ncbi.nlm.nih.gov/tools/primer-blast) to amplify DNA starting from exon 13, with the same reverse primer of primer pair 1 (primer pair 2, Table 3.10). All primers were synthesized by Sigma

Table 3.10: Primers used for genomic DNA amplification and sequencing of Apc2^{-} *allele*

	Forward primer sequence (5'-3')	Reverse primer sequence (5'-3')
Primer pair 1 (Clevers' primers)	*Apc2*$^{+}$ primer: CTCCAAACACAAGATGATCG	AGCTGTGTCTGATGAGGTG
	Apc2^{-} primer: AGGTCTGAAGAGGAGTTTAC	
Primer pair 2	CTCTGTGGAACCTGTCAGCA	AGCTGTGTCTGATGAGGTG

3.8.2. PCR product cleaning

PCR products (amplified by primer pair 1, Table 3.10) were cleaned prior to sending for sequencing. Briefly, 40 µl of PCR products were added to 4 µl of 3M sodium acetate (Sigma, USA) and 80 µl of 100% ethanol (Sigma, USA) in a 1.5ml microcentrifuge tube. The tube was placed at -20ºC for 1 hour to precipitate DNA, and centrifuged at 13 000 rpm for 10 minutes. The supernatant was discarded and the pellet washed with 70% ethanol and centrifuged again. After discarding the ethanol, the DNA was left to air-dry for 1 hour. It was dissolved in 20 µl ultrapure water (Sigma, USA) and incubated on a hot plate at 55ºC for 1 hour with occasional vortexing. The concentration of DNA was measured using the NanoDrop® and the DNA stored at 4ºC until further processing. PCR product, amplified using primer pair 2 (Table 3.10) was sent for a walking primer sequencing project without performing this cleaning step.

3.8.3. Sequencing

The amplified PCR product (using primer pair 1, Table 3.10) together with the primers used for DNA amplification were sent to and sequenced by Eurofins Genomics DNA automated Sanger sequencing service. Following this, a walking primer sequencing project was performed on DNA amplified using primer pair 2 (Table 3.10) by Eurofins Genomics to unravel the full sequence of *Apc2*$^{-}$ allele.

Results of *Apc2*$^{-}$ walking primer sequencing project are presented in Appendix 3.

3.9. In vitro characterization of OSE

3.9.1. OSE 2D culturing

Wells were gelatinized by incubating 500 µl of 0.1% sterile gelatine solution [Appendix 1] per well for 30 minutes. Following this, gelatine solution was aspirated and wells washed with 500 µl sterile 1X PBS (Gibco, Life technologies, USA). A second aliquot of PBS was

placed in individual wells (to prevent gelatine cracking) and discarded just before seeding the cells.

Isolated OSE cells from a single ovary were resuspended in 500 µl OSE complete medium (Section 3.4.7), seeded onto one gelatinized well of a 24 well plate and incubated at 37ºC and 5% CO2 (Flesken-Nikitin *et al.* 2013).

3.9.2. Passaging OSE cells

When cultured cells reached 80-90% confluency (3-5 days post-seeding), the media was aspirated, each well washed twice with 500 µl of PBS, and 400 µl of 0.25% trypsin (Mediatech, Germany) was added to each well and incubated for 10 minutes with occasional tapping. At the end of the incubation, the trypsin digestion was stopped by adding an equivalent amount of OSE complete medium, and cells were collected by centrifugation. Cells were washed by resuspending in 1000 µl of sterile 1X PBS (Gibco, Life Technologies, USA) and re-centrifuged. Following this, they were resuspended in 1500 µl OSE complete medium and seeded onto three gelatinized wells of a 24 well plate at 37ºC and 5% CO2.

3.9.3. Quantifying viable cells

Viable cells were quantified based on the amount of ATP present using the Cell Titer-Glo 2 assay (Promega, USA) according to the manufacturer instructions. Briefly, passaged cells were resuspended in 1000 µl OSE complete medium and cell counts were determined using a haemocytometer. Subsequently, cells were diluted to a final concentration of 50 cells/µl using OSE complete medium and 100 µl of the diluted cell suspension were seeded on to one gelatinized well of a 96 opaque-walled well plate and incubated at 37ºC and 5% CO2 for 72 hours. The plate was equilibrated to room temperature for 30 minutes before adding 100 µl of the Cell Titer-Glo 2 reagent. The cells were then shaken for 2 minutes on an orbital shaker and incubated for 10 minutes to stabilize the luminescent signal before measuring the luminescence

formed using CLARIOStar monochromator microplate reader (BMG LabTech, Germany) with an integration time of 1 second/well.

3.9.4. Sphere formation assay

The sphere-forming ability of OSE cells in suspension was assessed based on a previously-published method (Flesken-Nikitin *et al.* 2013). Briefly, 1000 OSE cells were suspended in 200 µl OSE sphere formation medium **[**DMEM/F12 (Ham's) medium (Mediatech, Germany) supplemented with 2.4% methyl cellulose (Sigma, USA), 0.4% Bovine serum albumin (Sigma, USA), 4 mM L-glutamine (Mediatech, Germany), 1 mM sodium pyruvate (Mediatech, Germany), 10 ng/ml epidermal growth factor (Sigma, USA), 500 ng/ml hydrocortisone (Sigma, USA), 5 µg/ml insulin (Sigma, USA), 5 µg/ml transferrin (Sigma, USA), 5 ng/ml sodium selenite (Sigma, USA), 0.1 mM MEM non-essential amino acids (Mediatech, Germanay), 10 ng/ml fibroblast growth factor basic (Sigma, USA), 10 ng/ml leukaemia inhibitory factor (Millipore, USA)**]** per well of a 96-well ultra-low attachment plate (Corning NY, USA) for 14 days. 100 µl of OSE formation medium were added to the well 7 days post-seeding. The number of spheres formed whose diameter was greater than 50 µm were counted under the microscope every 3 days.

3.9.5. Migration assay

Migration of OSE cells was evaluated using the scratch assay developed by Liang *et al.* (Liang *et al.* 2007). Briefly, OSE cells were grown on one gelatinized well of a 24-well plate supplemented with 500 µl OSE complete medium (Section 3.9.1) until 80% confluency and then a scratch was done using a sterile 200 µl micropipette tip. Subsequently, cells were washed with sterile 1X PBS (Gibco, Life Technologies, USA) to remove any debris, supplemented with 500 µl OSE complete medium and incubated at 37ºC and 5% CO2 for 24 hours. Images were captured at 0 and 24 hours following the scratch for the same field, identified by a marker

reference point drawn close to the scratch but not within it. Quantitative analysis of the captured images was performed by measuring the distance in µm between the 2 sides of the scratch using ImageJ software. At least 10 distances were measured for each image. Distance migrated was calculated using the following formula

Distance migrated = (Average scratch width at zero time) – (Average scratch width 24 hours post scratch)

3.10. RNA sequencing analysis

RNA sequencing was performed for the ovarian tumours formed 8-weeks post adenovirus-*cre* injection from the 2 experimental cohorts *Pten*$^{-/-}$*Apc*$^{-/-}$*Apc*$^{+/+}$ and *Pten*$^{-/-}$*Apc*$^{-/-}$ *Apc2*$^{-/-}$. RNA was extracted from whole tumour-bearing ovaries and sent to Wales Gene Park, where the analysis was performed.

3.10.1. RNA-Seq sample preparation and sequencing

Total RNA quality and quantity was assessed using Agilent 2100 Bioanalyser and a RNA Nano 6000 kit (Agilent Technologies, USA). 100-900 ng of Total RNA with a RNA integrity number (RIN) >8 was depleted of ribosomal RNA and the sequencing libraries were prepared using the Illumina® TruSeq® Stranded Total RNA with Ribo-Zero Gold™ kit (Illumina Inc., USA). The steps included rRNA depletion and clean up, RNA fragmentation, 1st strand cDNA synthesis, 2nd strand cDNA synthesis, adenylation of 3' ends, adapter ligation, PCR amplification (12-cycles) and validation. The manufacturer's instructions were followed except for the clean up after the ribozero depletion step where Ampure® XP beads (Beckman Coulter, USA) and 80% Ethanol were used. The libraries were validated using the Agilent 2100 Bioanalyser and a high-sensitivity kit (Agilent Technologies, USA) to ascertain the insert size, and the Qubit® (Life Technologies, USA) was used to perform the fluorometric quantitation. Following validation, the libraries were normalized to 4 nM, pooled together and clustered on

the cBot™2 following the manufacturer's recommendations. The pool was then sequenced using a 75-base paired-end (2x75bp PE) dual index read format on the Illumina® HiSeq2500 in high-output mode according to the manufacturer's instructions. Each sample was run in one sequencing lane. This work was kindly performed by Sarah Edkins and her team in Wales Gene Park.

3.10.2. Data quality control

All the quality control for the RNA seq data was kindly performed by Dr. Anna Evans, Wales Gene Park. Each sequencing lane was represented by two fastq files, which represented the paired-end reads generated within that lane. The fastq files were labelled R1 and R2 and represented the forward and reverse tags within the paired-end read, respectively. Trimming to remove adapter sequences and poor quality ends of reads was performed by Trim Galore (a wrapper to cutadapt). Trimming was performed using default parameters in paired-end mode. Trimmed reads were aligned to the mouse Mm10 genome using TopHat, a fast splice junction mapper for RNA-Seq reads. Tophat aligned reading using the Bowtie mapper before analyzing the results to identify splice junctions between exons. The RPKM (reads per kilobase million) scores for both (i) exons and (ii) transcripts were calculated using a Wales Gene Park in-house software for all six samples.

To define the exon and transcript locations used in the analysis, the RefSeq gene model RefGene, as provided by the UCSC mouse reference Mm10 website (http://hgdownload.cse.ucsc.edu/goldenPath/mm10/database/) was used.

In counting reads, at least 20 bases of a read had to map to the exon for that read to be counted. In addition, reads had to have the same orientation. Mapping quality and read duplication were ignored due to limited data.

3.10.3. Differential gene expression testing

Differentially-expressed genes were identified using an DEseq2 analysis (Love, 2014) on normalized count data. The analysis was modelled using the null hypothesis that no transcript is affected by *Apc2* deletion. The resultant p-values were corrected for multiple testing and false discovery issues using the FDR method (Benjamini & Hochberg, 1995). Outputs generated were matrix of normalized counts for each transcript, p-values, corrected p-values and fold-change calculations. All these data were kindly produced by Dr. Anna Evans.

3.10.4. Generating heatmaps

The Wales Gene Park in house software was used to generate heatmaps for the genes with FDR values<0.05. Data were log2 transformed and median centered before hierarchical clustering (using average linkage and Pearson's correlation as the similarity metric) to group similar data together and reveal any patterns within the dataset.

3.10.5. Generating protein-protein interaction networks

Protein symbols for upregulated or downregulated genes with FDR values<0.05 were pasted in the multiple protein search box of STRING v.10.5 online tool (available at https://string-db.org/cgi) and *Mus musculus* was selected as the organism of choice (Szklarczyk *et al.* 2015). The settings were adjusted to select for interactions extracted from curated experiments or databases only, and protein interaction networks were generated. Following this, protein interactions of both upregulated and downregulated lists were exported in a tabular form, a SIF file was generated (4 columns representing node1, interaction, node2, combined score), and imported as a network in Cytoscape 3.4.0. software (available to download at http://www.cytoscape.org/download.php)(Su *et al.* 2014). A protein interaction network for all interacting protein of differentially-expressed genes with FDR<0.05 was generated, and the

style was adjusted so that yellow circles denote upregulated genes, blue circles denote downregulated genes and edges in the form of arrows pointing from source to target.

3.10.6. Pathway analysis

Pathway analysis for upregulated or downregulated genes with FDR<0.01 was performed using DAVID bioinformatics resources 6.8 (available at https://david.ncifcrf.gov/) (Huang da *et al.* 2009). Briefly, gene accession codes were pasted to generate a gene list and and genebank accession was selected as the identifier. Following this, pathway analysis was performed by selecting functional annotation chart option using Goterm BP Direct gene ontology database. Biological functions of most differentially regulated genes were performed using DAVID bioinformatics resources 6.8, by selecting functional annotation table option using SP Comment Type functional category database.

3.11. Data processing and statistical analysis

A minimum of 3 animals were analysed per experimental cohort. All statistical analyses were performed by using IBM SPSS version 20 (SPSS Inc, Chicago, IL, USA). Descriptive statistics were calculated. Values are presented as mean ± standard error, except for qRT-PCR data which are presented as mean±95% confidence interval.

When 2 experimental cohorts were compared, significance testing was performed using unpaired 2-tailed Student's t-test, along with Levene's test for equality of variance. When more than 2 experimental cohorts were compared, ANOVA (analysis of variance) test was used to test whether their means were significantly different. When the F-statistic value was significant, a post-hoc analysis was done to test for significant differences between every 2 cohorts within the cohorts tested in the ANOVA. Levene's test for equality of variances was run first. When variances of groups were homogeneous, post-hoc analysis was performed using least significant difference (LSD) test. When variances of tested groups were not

homogeneous, post-hoc analysis was performed using Games-Howell test. A p-value < 0.05 was considered statistically significant.

Means and standard errors calculated by SPSS were imported to Excel. All the graphs presented were prepared by Excel 2013 software package.

4. Roles of APC2 protein in ovarian homeostasis

4.1. Introduction

The role of APC2 protein in ovarian WNT signalling was not studied before. For the first time, this question is addressed here. In addition, roles of APC2 protein in ovarian homeostasis and female fertility are being characterized, using a constitutive *Apc2*$^{-/-}$ genetically-engineered mouse model (GEMM).

4.1.1. Regulation of ovarian homeostasis

The ovary is the female reproductive organ responsible for production of oocytes through the processes of folliculogenesis and ovulation. In addition, it is an endocrine organ producing the female hormones estradiol and progesterone (Adhikari and Liu 2013).

In adult mammals, the ovarian cycle starts with recruitment of a subset of quiescent primordial follicles to undergo folliculogenesis (Diagram 4.1). First, primary follicles are formed. This non-gonadotrophin dependent recruitment is primarily activated by oocyte PI3K/AKT signalling while being inhibited by estradiol, AMH, PTEN and FOXO3 (McLaughlin and McIver 2009). Follicles continue to grow to form secondary or pre-antral follicles. Although the growth at this stage is gonadotrophin-independent, it is responsive to FSH, activated by insulin-like growth factor 1 (IGF1) (Shiomi-Sugaya *et al.* 2015) and members of TGFβ superfamily secreted by either the oocyte or granulosa cells (such as activin and BMP), and inhibited by AMH (Dunlop and Anderson 2014). The continued growth of follicles beyond this stage, from antral stage onwards, is gonadotrophin-dependent and relies on estradiol. Selection of dominant follicles, which reach the pre-ovulatory stage, happens when FSH levels drop as a result of increased estradiol concentration. Only the follicles that can continue to grow under low FSH/increasing LH levels are able to survive, and grow to pre-

ovulatory follicles. However, the majority of antral follicles cannot thrive under these conditions and undergo atresia via apoptosis (Ginther *et al.* 2001).

Ovulation of the oocyte from the pre-ovulatory follicle is under the control of LH. An LH surge happens before ovulation, and binding of LH to its receptor initiates a cascade of signalling events, mediated by EGF family members, to cause terminal differentiation of granulosa cells, release of the oocyte and conversion of the remaining follicle cells to the corpus luteum (Stocco *et al.* 2007). The corpora lutea are the sites of synthesis of progesterone, which is required to maintain pregnancy in the first few days post-fertilization.

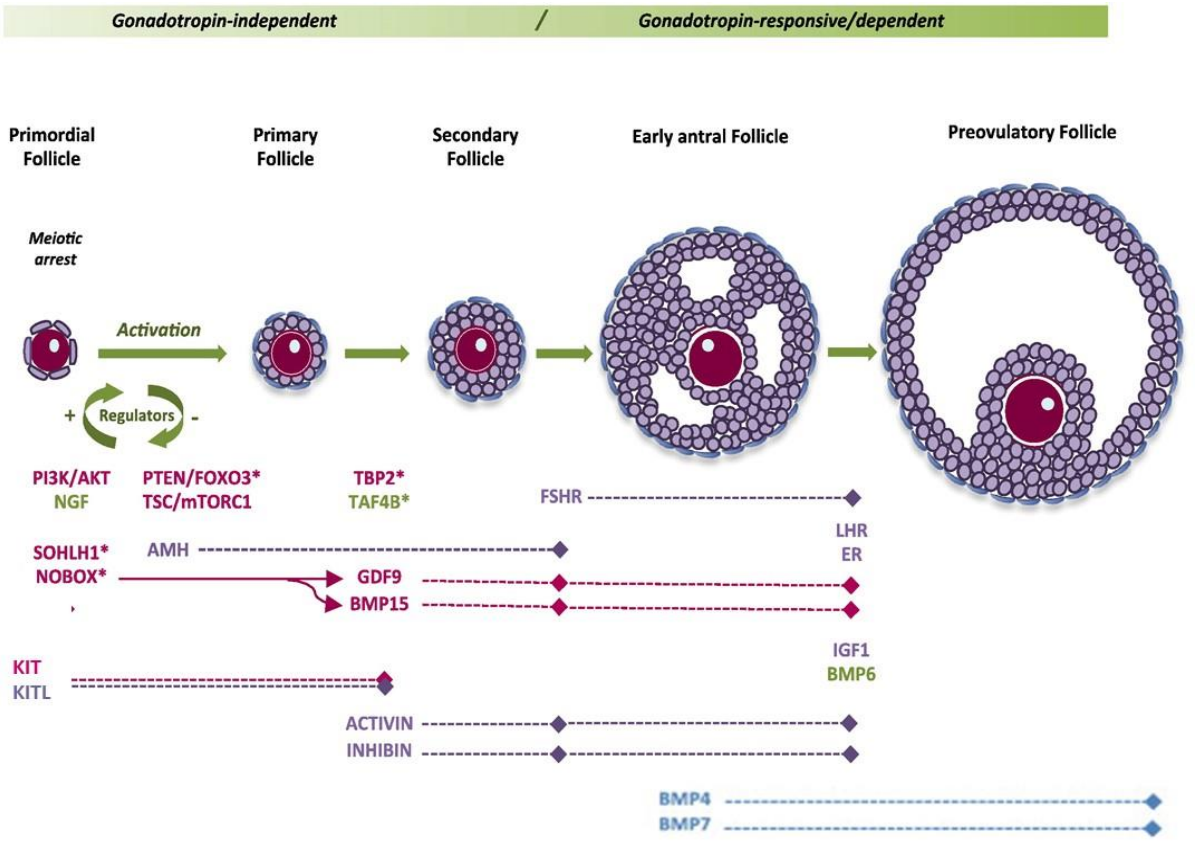

Diagram 4.1 Factors controlling folliculogenesis, adapted from Sanchez and Smitz (Sánchez and Smitz 2012; Chang *et al.* 2017). The blue lines indicate factors secreted by theca cells, purple lines indicate factors secreted by granulosa cells, magenta lines indicate factors secreted by oocytes, and green colours are factors secreted by both oocyte and granulosa cells. * denotes transcription factors.

4.1.2. Roles of canonical WNT signalling in ovarian homeostasis

Canonical WNT signalling has been shown to be detrimental for female sex differentiation during embryogenesis (Biason-Lauber and Chaboissier 2015). *Wnt4* levels increase in the mouse ovary as early as 11.5 days post conception, followed by upregulation of the canonical WNT activator *Rspo1* (Rspondin1), and downstream targets *Axin2* and *Lef1* one day later (Chassot *et al.* 2008). GEMMs studying roles of *Rspo1*, *Wnt4* and *Ctnnb1* (gene encoding for β-catenin) in sex determination have illustrated a female-to-male sex reversal after deletion of these factors in XX gonadal cells (Ottolenghi *et al.* 2007; Tomizuka *et al.* 2008). The reverse was also true; a male-to-female sex reversal was observed after expressing these factors in XY gonadal cells (Maatouk *et al.* 2008; Jameson *et al.* 2012). Advances in molecular diagnosis of sex reversal in humans pointed to these WNTt members as main players of female sex determination. *WNT4* (Domenice *et al.* 2004) or *RSPO1* (Tomaselli *et al.* 2008) inactivating mutations have been reported in XX hermaphrodite cases. Thus, data from human and mouse models support the importance of canonical WNT signalling in female sex determination.

Roles of canonical WNT signalling in adult ovarian homeostasis are not as well characterized. It was first thought that active canonical WNT signalling was important for ovarian folliculogenesis, ovulation and corpus luteum formation. This hypothesis relied on the presence of different Wnt members and Frizzled receptors in the cells of different ovarian compartments (Hernandez Gifford 2015). *In vitro* studies, using granulosa cell cultures, reflected an increase in β-catenin levels post-gonadotrophin treatment (Law *et al.* 2013), and pointed to β-catenin roles in inducing aromatase activity and estradiol production in response to FSH (Parakh *et al.* 2006). However, studies utilizing GEMMs did not confirm this hypothesis. When *Ctnnb1* was conditionally deleted in murine granulosa cells of pre-antral follicles, using the Amhr2-*cre*, folliculogenesis and ovulation were normal (Hernandez Gifford *et al.* 2009). However, due to the nature of Amhr2-*cre*, the recombination of *Ctnnb1* in oviducts

and uteri resulted in abnormalities in their formation, causing lack of implantation sites and rendering these mice infertile (Hernandez Gifford *et al.* 2009). Despite these abnormalities, ovaries were completely functional. This finding was reproduced when *Ctnnb1* was conditionally-deleted in granulosa cells of antral follicles (Fan *et al.* 2010a), using an aromatase-*cre* which drives recombination exclusively in these cells. These mice were completely fertile and delivered comparable number of pups to their control (Fan *et al.* 2010a). Conditional deletion of *Wnt4* (Boyer *et al.* 2010), or constitutive deletion of *Fzd4* (Hsieh *et al.* 2005) in mice caused subfertility and complete infertility, respectively. However, in these models, WNT signalling activity was not measured and it is unclear whether the reported phenotypes are caused by impaired canonical WNT signalling or by other mechanisms. This was evident when FZD1 was constitutively deleted in mice. The female mice were fertile apart from 17.6% of mice which were completely infertile due to early follicle depletion (Lapointe *et al.* 2012). In these mice, despite FZD1 deletion, total activated catenin levels in ovaries were not changed when compared to the control (Lapointe *et al.* 2012). Collectively, data from GEMMs indicate that active canonical WNT signalling is not essential for adult ovarian folliculogenesis and fertility.

However, GEMMs provided some evidence that over-activation of canonical WNT signalling has deleterious effects on ovarian homeostasis. Over-expression of *Rspo1* (De Cian *et al.* 2016), deletion of *Wnt5a* (antagonist of canonical WNT signalling; (Abedini *et al.* 2016)), or expression of dominant stable β-catenin (Boerboom *et al.* 2005; Fan *et al.* 2010a) all upregulated ovarian WNT signalling and caused ovarian subfertility of different phenotypes. Inhibitory effects of over-activated WNT signalling on follicular growth were also tested *in vitro*. Follicle cultures were used to test this hypothesis by characterizing the effects of canonical WNT signalling activators (Lithium chloride or WNT3a) and WNT inhibitor (IWR1) on the growth of mouse secondary follicles (Li *et al.* 2014). Treatments with WNT activators

impaired follicular growth, estradiol synthesis and increased apoptosis while the WNT inhibitor caused the reverse and increased follicular growth (Li *et al.* 2014). These findings were reproduced when cultured rat granulosa cells were treated with WNT3a; inhibition of steroidogenesis was reported (Stapp *et al.* 2014). Taken together, these findings indicate the importance of repressing canonical WNT signalling in growing follicles as early as the pre-antral stage.

4.1.3. Roles of APC2 in canonical WNT signalling

When APC2 (APCL or E-APC) was first discovered, it was described as a homologue of the tumour suppressor protein APC (Hamada *et al.* 1999; Van Es *et al.* 1999). Structurally, APC2 possesses Axin1 and β-catenin binding sites, which enables it to destabilize β-catenin targeting it for degradation and thus suppressing its transcriptional activity (Hamada *et al.* 1999; Van Es *et al.* 1999). This finding was true both in *Drosophila* and in cell lines of intestinal tumours (Hamada *et al.* 1999; Van Es *et al.* 1999). However, in an *in vivo* mammalian setting, the situation is different. The Clarke lab using a constitutive *Apc2*$^{-/-}$ mouse, kindly gifted by Prof. Hans Clevers, reported that the extent and effects of WNT signalling activation caused by APC2 loss are tissue specific. APC2 loss caused WNT signalling activation in the small intestine and liver, but not in the mammary glands (Daly 2013). Phenotypic changes post-APC2 loss were only observed in the small intestine (Daly 2013).

4.1.4. Aims, hypothesis and highlights

It had been previously observed in the Clarke group that a subset of ovaries of aging *Apc2*$^{-/-}$ mice were abnormal and developed fluid-filled cysts, which were suspected to be epithelial. Stemming from this observation and based on tissue specificity of APC2 functions previously characterized (Daly 2013), we aimed to characterize the effect of deleting APC2 on ovarian homeostasis during early adulthood (in 10-week-old mice). Our objectives were:

1- To explore whether APC2 loss results in WNT signalling activation in the ovaries.

2- To characterize the ovarian phenotype caused by APC2 loss, with special attention to folliculogenesis, ovulation, corpus luteum formation and fertility.

3- To define the possible molecular mechanisms of the observed phenotype.

We hypothesized that APC2 loss in the ovary activates WNT signalling, causing subfertility due to defects in folliculogenesis and/or ovulation/corpus luteum formation. For the first time, roles of APC2 in ovarian homeostasis are characterized. Study findings highlight the importance of functional APC2 for ovarian folliculogenesis and fertility. WNT signalling was activated post-APC2 deletion in ovaries, and this is proposed as one of the mechanisms causing the subfertility observed in *Apc2*$^{-/-}$ mice. The subfertility observed is of ovarian origin, and caused by reduced ovulation due to aberrant folliculogenesis. Possible mechanisms include (1) defects in response to gonadotrophin caused by over-expression of *Lhcgr*, (2) increased granulosa cell apoptosis due to upregulation of *Foxo1* as a result of suppression of PI3K/AKT signalling, (3) defective follicular steroidogenesis, and (4) impaired follicular vascularization.

4.2. Results

4.2.1. APC2 loss in the ovaries activates canonical WNT signalling

In order to determine whether APC2 loss altered canonical WNT signalling in the ovary, expression levels of a subset of Wnt-target genes were quantified. Total RNA was extracted from whole ovaries, collected at diestrus stage from 10-week-old virgin *Apc2*$^{+/+}$ and *Apc2*$^{-/-}$ mice. Gene expression levels were compared using quantitative RT-PCR. Results revealed significant increases in the expression levels of *Apc*, *Axin2*, *Ctnnb1*, *Fgf1*, and *Lgr5* in *Apc2*$^{-/-}$ compared to *Apc2*$^{+/+}$ ovaries (Figure 4.1). However, the expression levels of *Cd44*, *Lef1* and *Wif1* were not significantly changed (Figure 4.1).

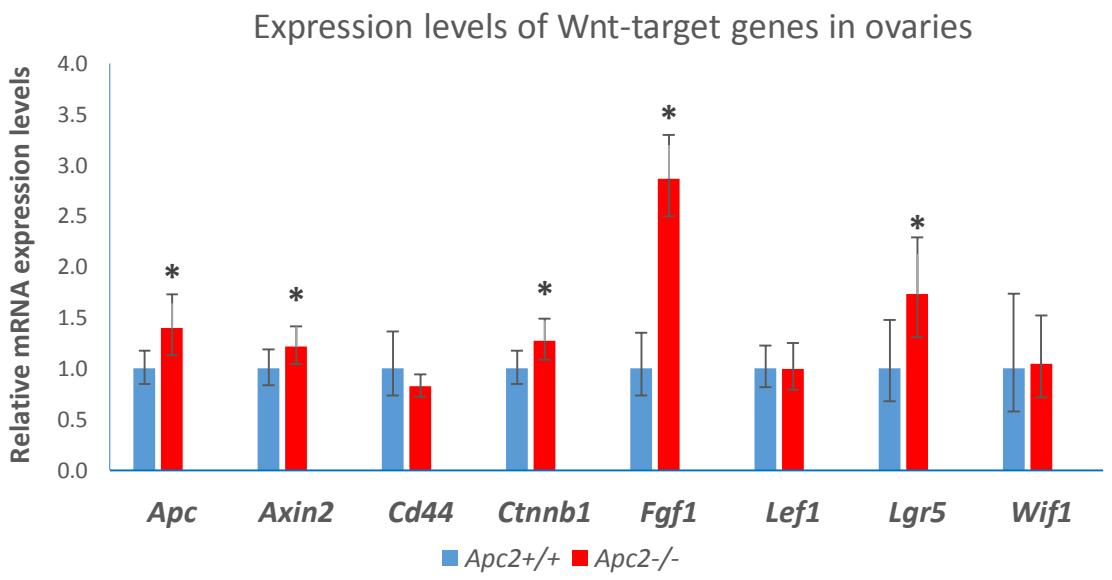

Figure 4.1: APC2 loss causes activation of canonical WNT signalling in the ovary. Expression levels of a subset of Wnt-target genes were compared between *Apc2*$^{+/+}$ and *Apc2*$^{-/-}$ ovarian extracts using qRT-PCR and normalized to *Actb* expression. Expression levels of five out of eight genes analysed were significantly elevated. Data are shown as mean±95% confidence intervals of relative mRNA expression levels, n=3-4. Statistical significance was determined according to Cumming *et al.* (Cumming *et al.* 2007). * denotes significance from *Apc2*$^{+/+}$ at $p<0.05$.

In order to determine the subcellular localization of β-catenin protein in different ovarian compartments, immunohistochemistry (IHC) was performed on ovaries collected from 10-week-old *Apc2*$^{+/+}$ and *Apc2*$^{-/-}$ female mice at diestrus stage. Microscopic examination of stained sections showed that β-catenin was differentially expressed in all ovarian compartments, but the expression pattern was comparable in *Apc2*$^{+/+}$ (Figure 4.2a-g) and *Apc2*$^{-/-}$ (Figure 4.2h-n) ovaries. In the ovarian surface epithelium, β-catenin was mainly membranous and cytoplasmic (Figure 4.2a,c,h). Granulosa cells of growing follicles showed strong membranous, cytoplasmic and nuclear expression of β-catenin, with the strongest expression observed in the primary, secondary and small antral follicles (Figure 4.2a-c,h,i). The nuclear expression was not frequently observed in granulosa cells of large antral (Figure 4.2d,j) and pre-ovulatory follicles (Figure 4.2e,k). The expression levels of β-catenin were weaker in atretic follicles, showing strong membranous but weak cytoplasmic staining in the granulosa cells (Figure 4.2d,g,h,i,k-n), with higher expression observed in atretic follicles from *Apc2*$^{-/-}$ ovaries (Figure 4.2n) as compared to *Apc2*$^{+/+}$ ovaries (Figure 4.2g). Theca cells mainly showed membranous and cytoplasmic β-catenin expression. In corpora lutea, β-catenin expression was mainly membranous, with occasional cytoplasmic staining (Figure 4.2a,d,f,l,m).

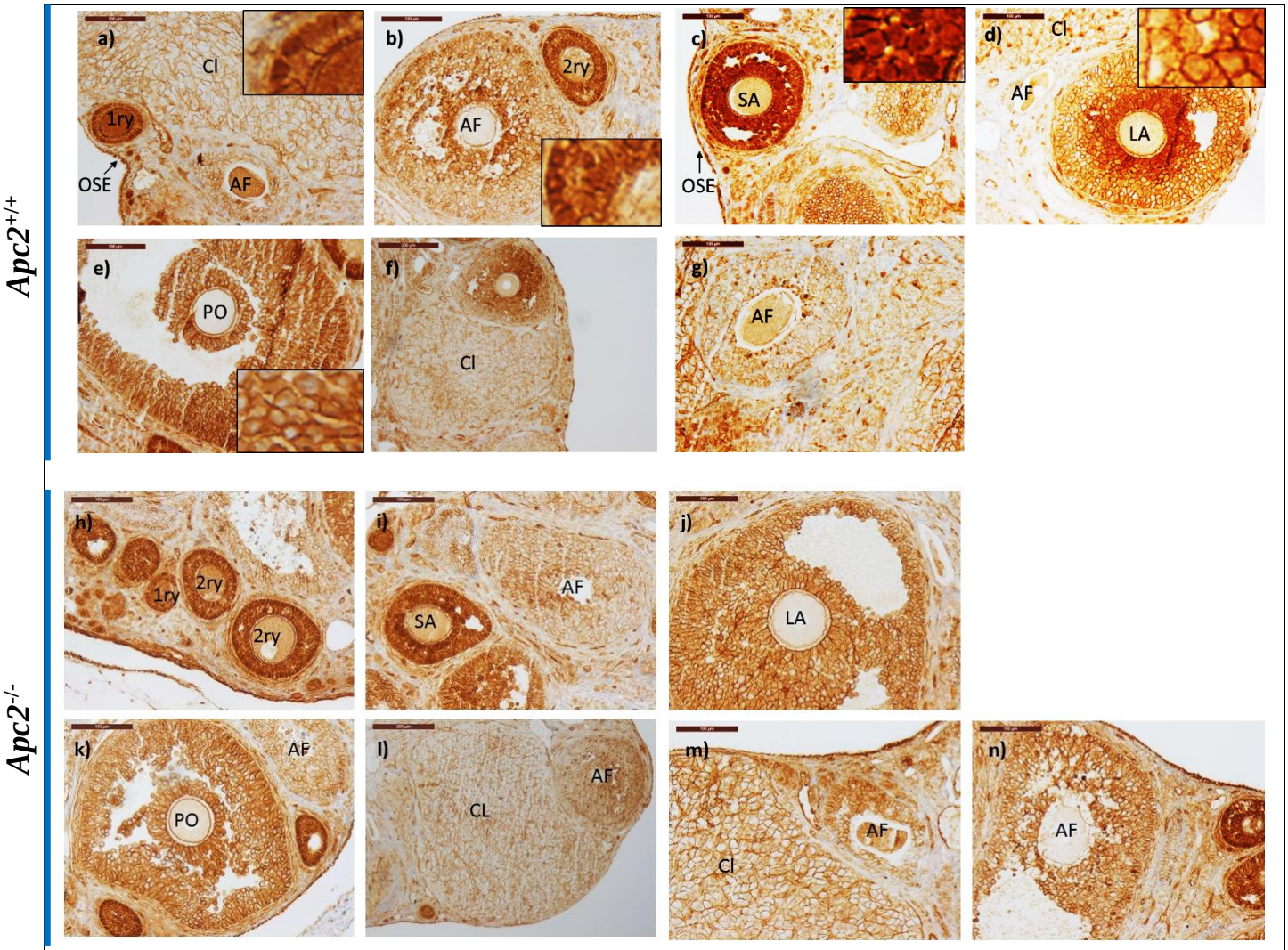

Figure 4.2: Immunohistochemical localization of β-catenin protein in ovaries of (a-g) *Apc2*$^{+/+}$ and (h-n) *Apc2*$^{-/-}$ 10-week-old female mice. OSE: ovarian surface epithelium. 1ry: primary follicle. 2ry: secondary follicle. SA: small (early) antral follicle. LA: large antral follicle. PO: pre-ovulatory follicle. Cl: corpus luteum. AF: atretic follicles. Scale bars: 100 µm, except (f, l) scale bars: 200 µm. Insets shows granulosa cells of growing follicles at 4X original magnification

4.2.2. Constitutive loss of APC2 protein induces subfertility in female mice

In order to evaluate effects of APC2 loss on normal ovarian homeostasis, fertility was first assessed in *Apc2*$^{+/-}$ and *Apc2*$^{-/-}$, as compared to *Apc2*$^{+/+}$ mice, by retrospective analysis of matings set for breeding. Only mice fulfilling the following criteria were included in the

analysis; 7-11 week-old female mice of the experimental genotypes housed with 7-9 week-old males of the corresponding genotype housed as trios (2 females and 1 male) for 3 months. 4 matings were analysed for each genotype. Litter sizes at the time of weaning, 3-4 weeks after birth, were used in the analysis.

Although partial loss of APC2 protein in the *Apc2*$^{+/-}$ mice did not affect the length of time between mating and producing the first litter, as compared to *Apc2*$^{+/+}$ mice (21.25±0.48 days vs. 20.75±0.92 days, mean ± S.E, Figure 4.3a), a reduction in mean cumulative number of weaned pups was observed (18.5±1.32 vs. 31.75±5.68, mean ± S.E., Figure 4.3c). This was coupled with a non-significant decrease in the gestation frequency in the *Apc2*$^{+/-}$ vs. *Apc2*$^{+/+}$ mice (3±0.41 vs. 3.75±0.14, mean ± S.E., Figure 4.3b). However, the complete loss of APC2 protein in *Apc2*$^{-/-}$ mice markedly impaired fertility in 3 of the cages analysed; as reflected by the significant increase in time to first litter (32.38±5 days, $p<0.05$, Figure 4.3a), the significant decrease in gestation frequency (2.13±0.77 rounds, $p<0.05$, Figure 4.3b) and the reduction in mean cumulative numbers of weaned pups (13.5±4.9, $p<0.05$, Figure 4.3c). Mice in one *Apc2*$^{-/-}$ breeding cage were completely infertile and did not show any signs of pregnancy throughout the length of the study.

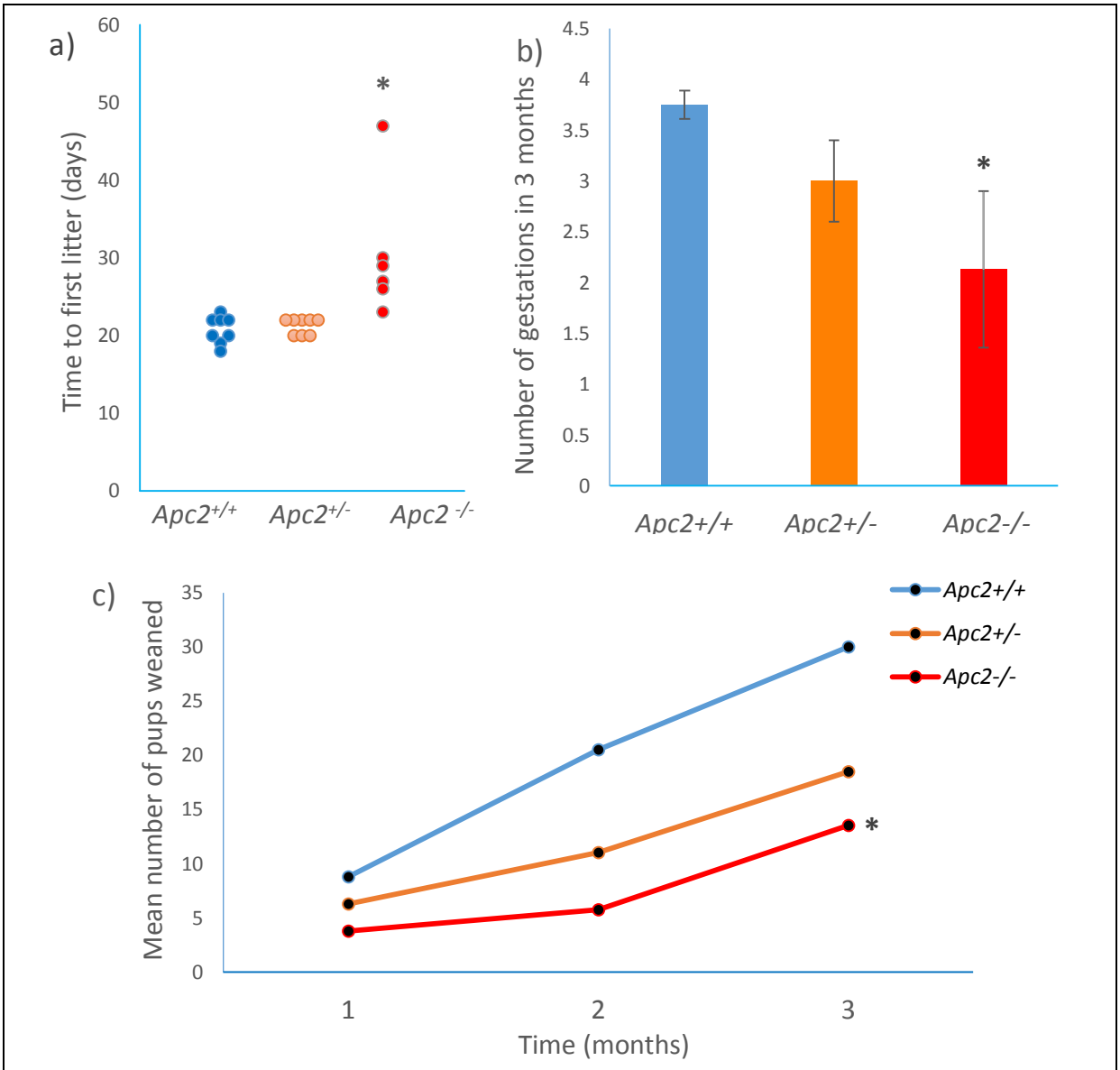

Figure 4.3: APC2 loss causes subfertility in adult mice. (a) Mating efficiency of the different *Apc2* experimental genotypes as a function of time recorded in days between pairing the mice and delivering the first litter. One $Apc2^{+/+}$, $Apc2^{+/-}$ or $Apc2^{-/-}$ male was crossed with 2 $Apc2^{+/+}$, 2 $Apc2^{+/-}$ or 2 $Apc2^{-/-}$ female mice respectively. (b) Breeding efficiency as reflected by number of gestations occurring in 3 months period. Data are shown as mean ± S.E. (c) Cumulative number of pups weaned in 3 months' time. n=4. Statistical significance between groups was determined using ANOVA test followed by Games-Howell post hoc analysis (variances of experimental groups were not homogeneous, tested by Levene's test). * denotes significance from $Apc2^{+/+}$ at $p<0.05$.

Histological analysis of ovaries, oviducts and uteri of 10-week-old virgin *Apc2*$^{+/+}$ and *Apc2*$^{-/-}$ mice were performed to assess the etiological causes of subfertility in *Apc2*$^{-/-}$ mice. For this purpose, fixed ovaries, oviducts and uteri were serially sectioned into 100 sections 5 µm apart, and every 10th section was stained by H&E and analysed. No gross morphological differences were observed in the oviducts and uteri of *Apc2*$^{+/+}$ and *Apc2*$^{-/-}$ mice (results not shown). In addition, no problems were reported during labour in all the experimental groups, suggesting that uterine problems are not contributing to the observed subfertility phenotype in APC2-deficient mice. Volume of ovaries of *Apc2*$^{+/+}$ and *Apc2*$^{-/-}$ mice were not different (Figure 4.4a), although a significant decrease in body weight was recorded in *Apc2*$^{-/-}$ mice as compared to *Apc2*$^{+/+}$ mice (16.88±0.43 vs. 21.5±0.61, $p<0.05$, Figure 4.4b).

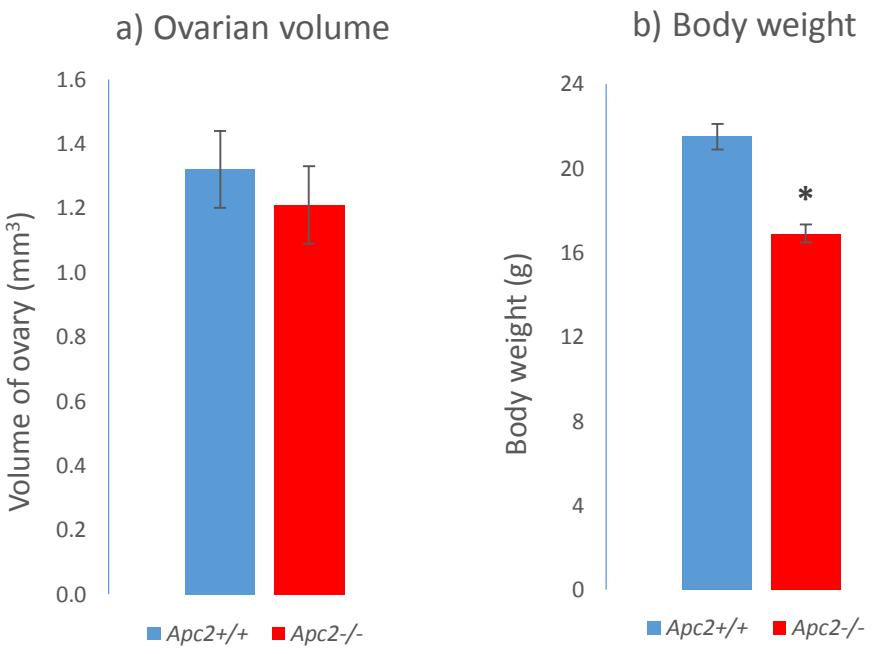

Figure 4.4: Ovarian sizes are not changed post-APC2 deletion. (a) Volume of *Apc2*$^{+/+}$ and *Apc2*$^{-/-}$ ovaries collected at diestrus stage. (b) Body weights of *Apc2*$^{+/+}$ and *Apc2*$^{-/-}$ female mice. n=4. Data are represented as mean±S.E. Statistical significance was determined by t-test. * denotes significance from *Apc2*$^{+/+}$ at $p<0.05$.

Morphometric analysis revealed a significant decrease in the number of corpora lutea formed in *Apc2*$^{-/-}$ vs. *Apc2*$^{+/+}$ ovaries (2.5±0.5 vs. 5±1.08, $p<0.05$, Figure 4.5a and Figure 4.6a,b). However, there was a non-significant increase in the total number of growing follicles in *Apc2*$^{-/-}$ vs. *Apc2*$^{+/+}$ ovaries (81.5±12.67 vs. 66.25±7.19 in *Apc2*$^{+/+}$ ovaries, Figure 4.5b and Figure 4.6a,b). Gene expression analysis was performed on RNA extracted from *Apc2*$^{+/+}$ and *Apc2*$^{-/-}$ ovaries for the germ cell marker *Gdf9*, to confirm growing follicles count results (Figure 4.5c). A non-significant increase in *Gdf9* expression levels was observed in *Apc2*$^{-/-}$ vs. *Apc2*$^{+/+}$ ovaries (Figure 4.5c). Collectively, these findings suggested that the subfertility observed in APC2-deficient mice is of ovarian origin and is caused by reduced ovulation.

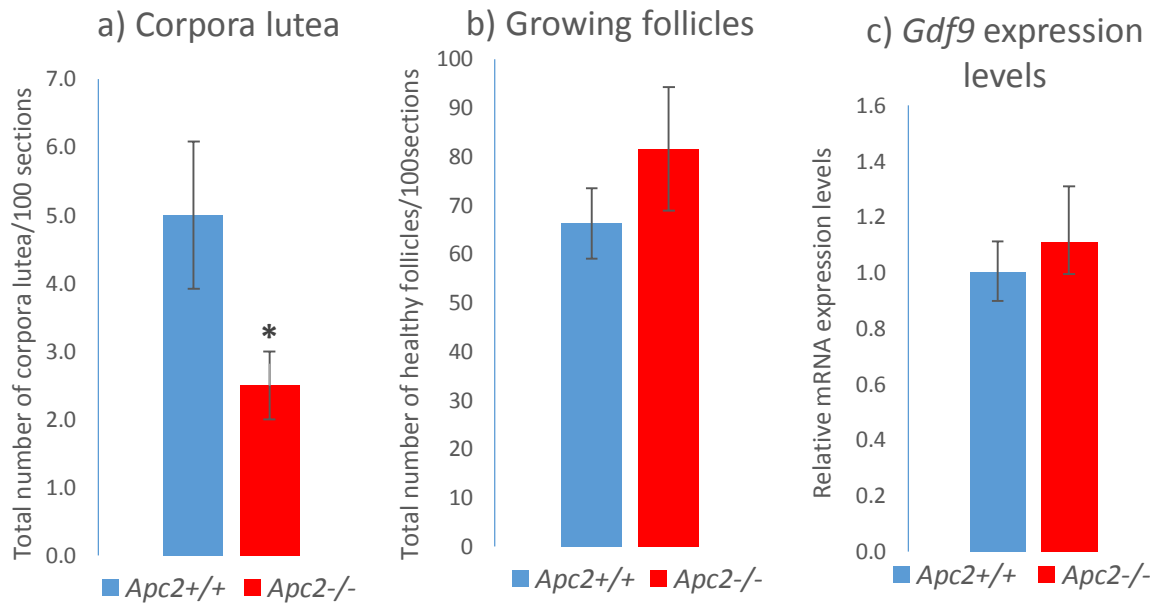

Figure 4.5: Subfertility in 10-week-old *Apc2*$^{-/-}$ mice is caused by reduced ovulation. Total number of (a) corpora lutea, and (b) healthy growing follicles, counted across 100 serial sections of ovaries collected at diestrus stage. (c) Expression levels of *Gdf9* gene in *Apc2*$^{+/+}$ and *Apc2*$^{-/-}$ ovaries. n=4. Data are represented as mean±S.E., except the gene expression levels which are expressed as mean±95% confidence interval. Statistical significance was determined by t-test. * denotes significance from *Apc2*$^{+/+}$ at $p<0.05$.

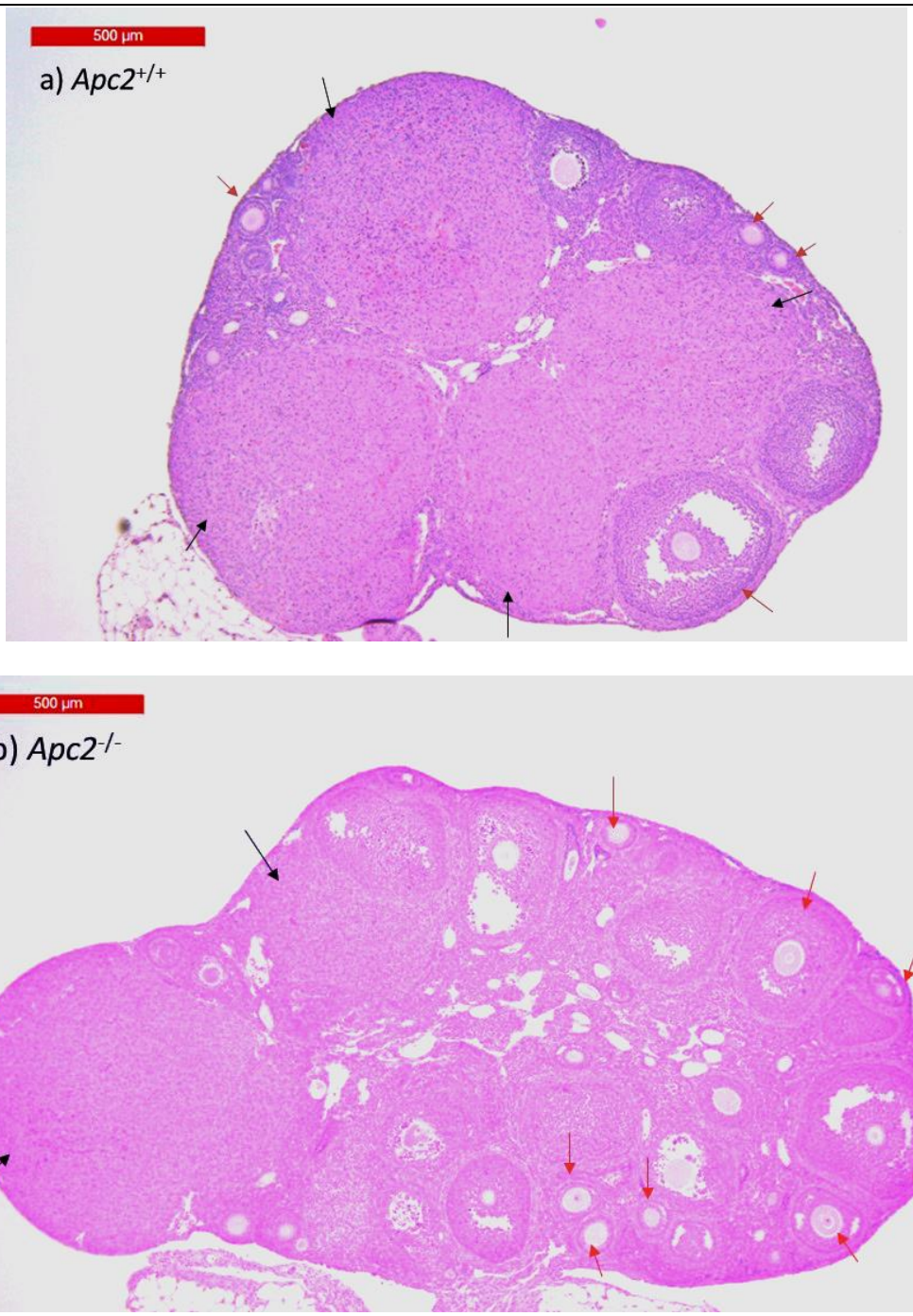

Figure 4.6: Reduced corpus luteum formation in *Apc2*$^{-/-}$ mice. Representative photomicrograph of (a) *Apc2*$^{+/+}$ and (b) *Apc2*$^{-/-}$ ovaries, showing a trend of increase in growing follicles (red arrows) and a significant decrease in corpora lutea (black arrows) in *Apc2*$^{-/-}$ compared to *Apc2*$^{+/+}$ ovarian section. scale bar 500 µm. n=4.

4.2.3. Subfertility of constitutive APC2-deficient female mice is not caused by extra-ovarian defects

As APC2 loss is constitutive in all mouse organs, the genotype dose-dependent subfertility observed in APC2-deficient mice could be due to defects in extra-ovarian regulation of ovarian functions, triggered by hypothalamic/pituitary endocrine signals. To test this hypothesis, the following experiments were conducted.

First, serum samples were collected from 10-week-old virgin *Apc2*$^{+/+}$ and *Apc2*$^{-/-}$ female mice at diestrus stage, and levels of follicle stimulating hormone (FSH) and luteinizing hormones (LH) were measured using ELISA kits. No significant differences were observed in serum levels of either hormones (Figure 4.7).

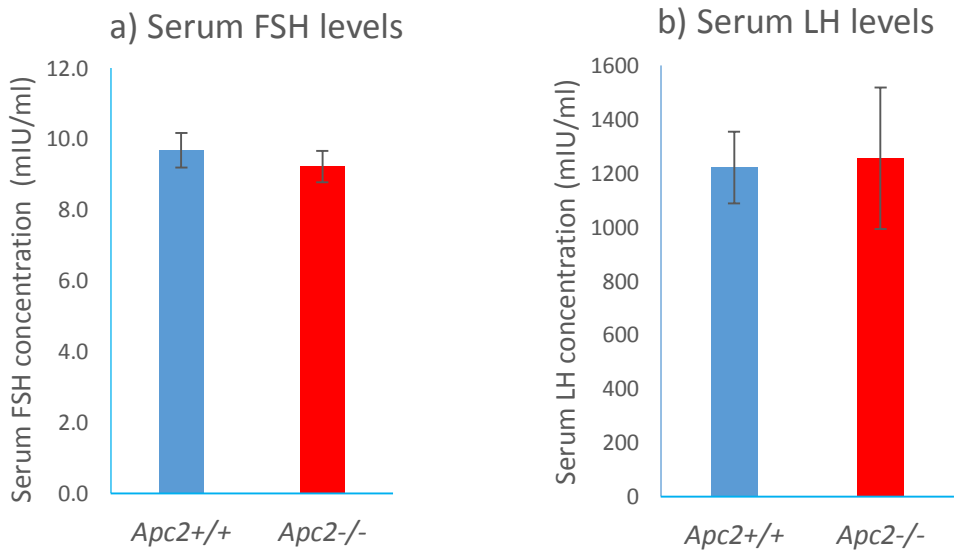

Figure 4.7: Constitutive loss of APC2 has no effect on fertility hormones produced by pituitary gland. Serum levels of (a) FSH and (b) LH measured by ELISA kits. n=4-6. Data represented as mean±S.E.

A second experiment performed to confirm the ovarian origin of the observed subfertility was the administration of exogenous gonadotrophins, following the superovulation protocol (Section 3.3.3), performed on 10-week-old virgin mice from the three experimental genotypes. Mice were euthanized 16-17 hours post-HCG injection, and oviducts were

dissected. Cumulus oocyte complexes (COCs) were collected from the ampulla in 40 µl PBS and counted. Morphology of ovulated COCs was assessed to determine their integrity. All ovulated oocytes were surrounded by cumulus cells of comparable thickness, irrespective of the genotype (Figure 4.8). Quantitative analysis of retrieved COCs showed a gene dose-dependent decrease in the number of COCs retrieved from the oviducts of *Apc2*$^{+/-}$ and *Apc2*$^{-/-}$ mice as compared to *Apc2*$^{+/+}$ mice (3.33±0.95 and 2.25±1.24 vs. 6.83±1.39 respectively, Figure 4.9a). Morphometric analysis of ovulated oocytes, after treating the COCs with collagenase/dispase to remove the cumulus cells, revealed that they were healthy with no signs of fragmentation, and of comparable sizes (Figure 4.8,4.9b). Collectively, these results indicated that the main defect occurring in APC2-deficient mice is a reduction in number of ovulated oocytes while maintaining a normal COCs morphology.

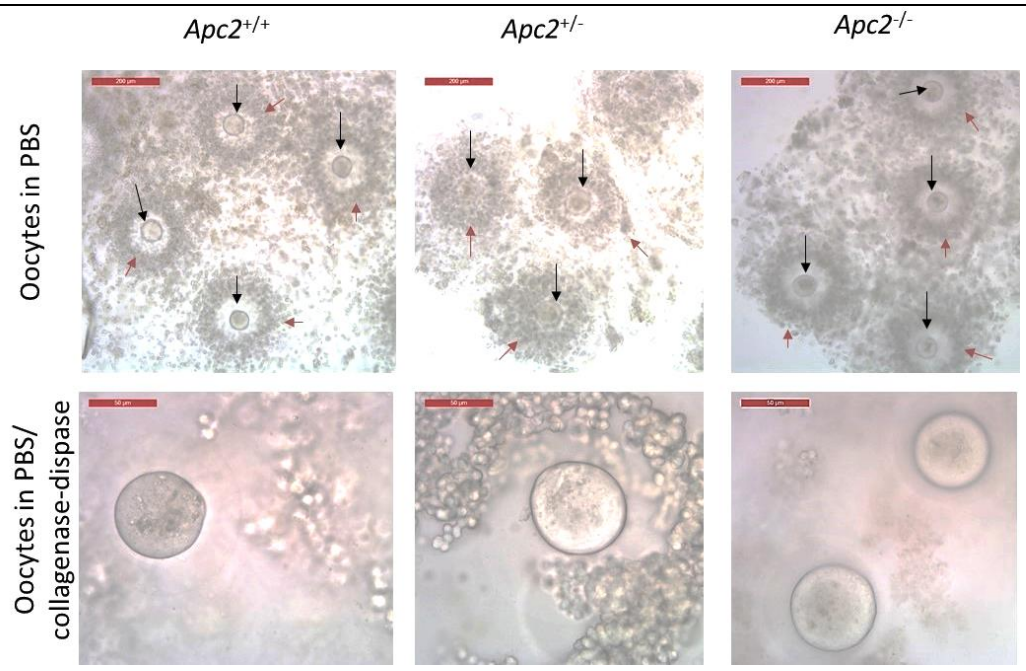

Figure 4.8: Characterizing oocytes ovulated after exogenous gonadotrophin administration. (a) Representative photomicrographs of retrieved COCs showing the presence of oocytes (black arrows) surrounded by cumulus cells (red arrows) in the upper panel. Scale bar 200 µm. In the lower panel, higher magnification was used to examine oocytes after freeing them from cumulus cells, 10 minutes post-collagenase/dispase treatment. Scale bar 50 µm.

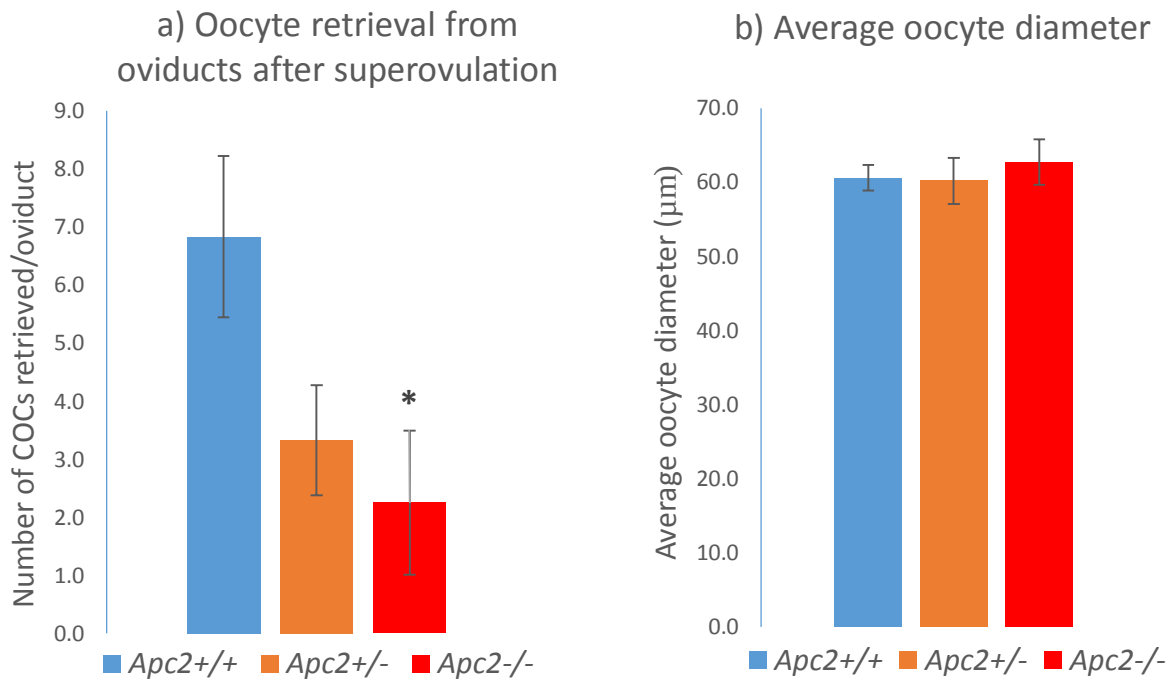

Figure 4.9: APC2-deficiency caused a reduction in ovulated healthy oocytes post-gonadotrophin administration. (a) APC2-deficiency caused a gene dose-dependent decrease in the number of ovulated COCs retrieved from the oviducts post-superovulation. (b) Average oocyte diameter was not different among the experimental groups. n=3-5. Statistical significance between groups was determined using ANOVA test followed by LSD post hoc analysis (variances of experiment groups were homogeneous tested by Levene's test). * denotes significance from *Apc2*$^{+/+}$ at $p<0.05$.

Histologic analysis of ovaries dissected from superovulated *Apc2*$^{+/+}$ and *Apc2*$^{-/-}$ mice, 24 hours post-HCG administration, was conducted to test whether exogenous gonadotrophin administration could normalize the number of corpora lutea formed. Results showed that external gonadotrophin administration could not rescue the previously described ovarian phenotype in APC2-deficient female mice (Figure 4.5 and 4.6). Similar to the non-superovulated ovaries, a significant decrease in the number of corpora lutea was observed in superovulated *Apc2*$^{-/-}$ ovaries as compared to *Apc2*$^{+/+}$ ovaries (4.8±0.97 vs. 8.6±1.03, $p<0.05$, Figure 4.10a and 4.11a,b). This was associated with a non-significant increase in healthy

growing follicles in *Apc2*$^{-/-}$ ovaries in contrast to *Apc2*$^{+/+}$ ovaries (69.2±6.96 vs. 52.4±5.73, Figure 4.10b and 4.11a,b). Taken together, the results from these investigations in which mice were exogenously-administered gonadotrophins, suggest that the subfertility phenotype is not due to extra-ovarian defects in pituitary gonadotrophin secretion, but rather due to intra-ovarian defects in response to gonadotrophins.

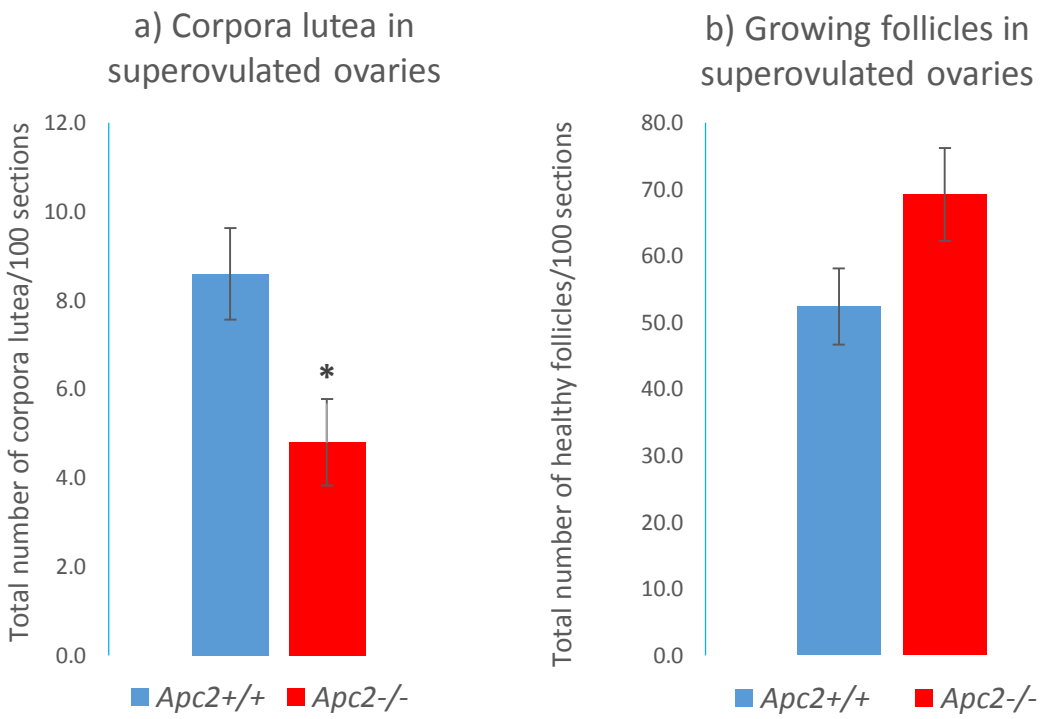

Figure 4.10: External gonadotrophin administration could not rescue reduced ovulation in *Apc2*$^{-/-}$ ovaries. Total number of (a) corpora lutea, and (b) healthy follicles counted across 100 serial sections of superovulated stage-matched ovaries. n=5. Data are represented as mean±S.E. Statistical significance was determined by t-test. * denotes significance from *Apc2*$^{+/+}$ at $p<0.05$.

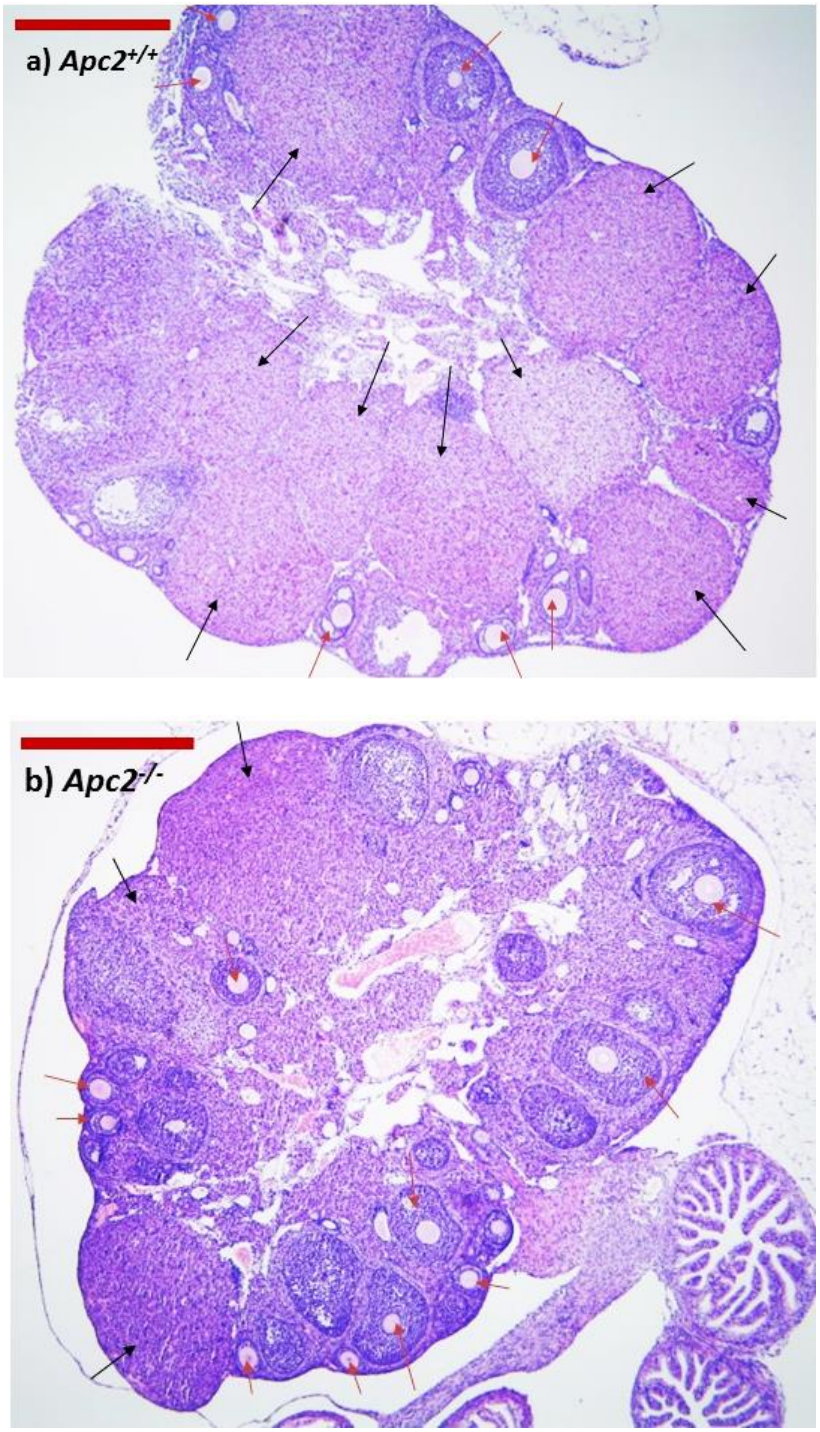

Figure 4.11: Decreased corpus luteum formation in *Apc2*$^{-/-}$ ovaries collected post-gonadotrophin administration. Representative photomicrograph of (a) *Apc2*$^{+/+}$, and (b) *Apc2*$^{-/-}$ superovulated ovarian section, showing a trend of increase in growing follicles (red arrows), and a significant decrease in corpora lutea (black arrows) in *Apc2*$^{-/-}$ compared to *Apc2*$^{+/+}$ ovarian section. scale bar 500 µm. n=5.

4.2.4. Reduced ovulation of *Apc2*$^{-/-}$ mice is not caused by defects in terminal granulosa cell differentiation or ovulation process

In order to identify the cause of reduced ovulation observed in *Apc2*$^{-/-}$ female mice, two different hypotheses were tested. The first was that APC2 loss causes defects in the terminal differentiation of granulosa cells and oocyte ovulation in response to LH surge. The second hypothesis was that APC2 loss impairs follicular growth leading to a decrease in the number of follicles reaching the pre-ovulatory stage (Section 4.2.5).

To test the first hypothesis, serial-sectioned ovaries were examined to identify pre-ovulatory follicles and corpora lutea. As all the ovaries were collected at the diestrus stage of the oestrous cycle, a post-ovulatory stage distant from ovulation, only few follicles were present in late antral to pre-ovulatory stage. Microscopic examination of these follicles did not reveal any morphological differences between *Apc2*$^{+/+}$ and *Apc2*$^{-/-}$ follicles (Figure 4.12a,b). Follicles from both genotypes contained an oocyte of comparable size, surrounded by layers of granulosa cells forming COC. COC expansion was not evident at this stage in any of the follicles examined from both genotypes. However, the main observation was that follicles examined at that stage in *Apc2*$^{-/-}$ ovaries were smaller and fewer as compared to *Apc2*$^{+/+}$ ovaries (Section 4.2.5).

EGF and EGF receptor (EGFR) ligands, Amphiregulin (AREG) and Epiregulin (EREG), are involved in COC expansion in response to LH surge (Park *et al.* 2004). In order to investigate whether defects in ovulation are contributing to the subfertility observed in *Apc2*$^{-/-}$ female mice, gene expression analysis of *Egf*, *Areg*, *Ereg* and *Egfr* were performed by qRT-PCR. A significant increase in *Egf* expression levels was observed in *Apc2*$^{-/-}$ ovaries as compared to *Apc2*$^{+/+}$ (Figure 4.12c). No significant differences were observed in the expression levels of the other genes tested between the two studied genotypes (Figure 4.12c).

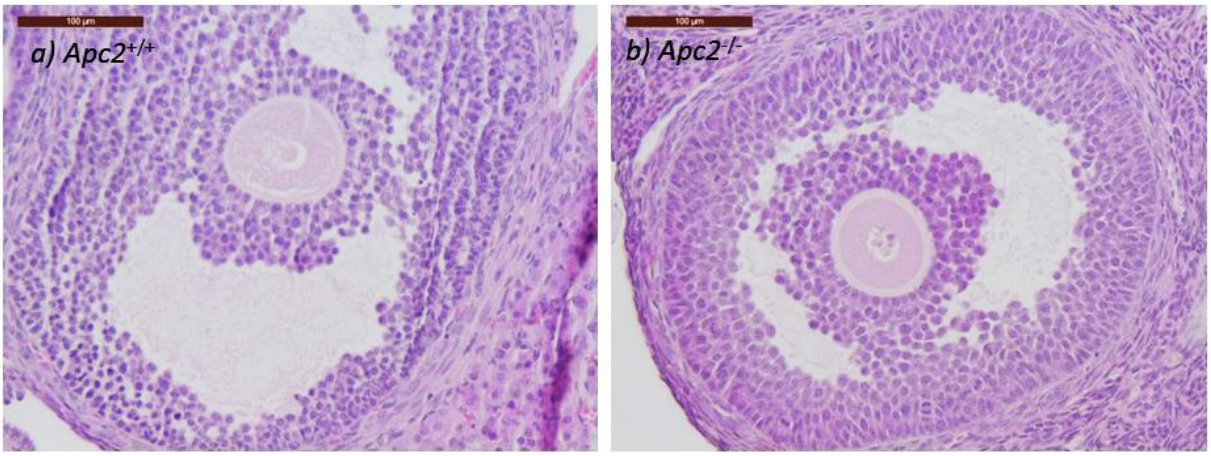

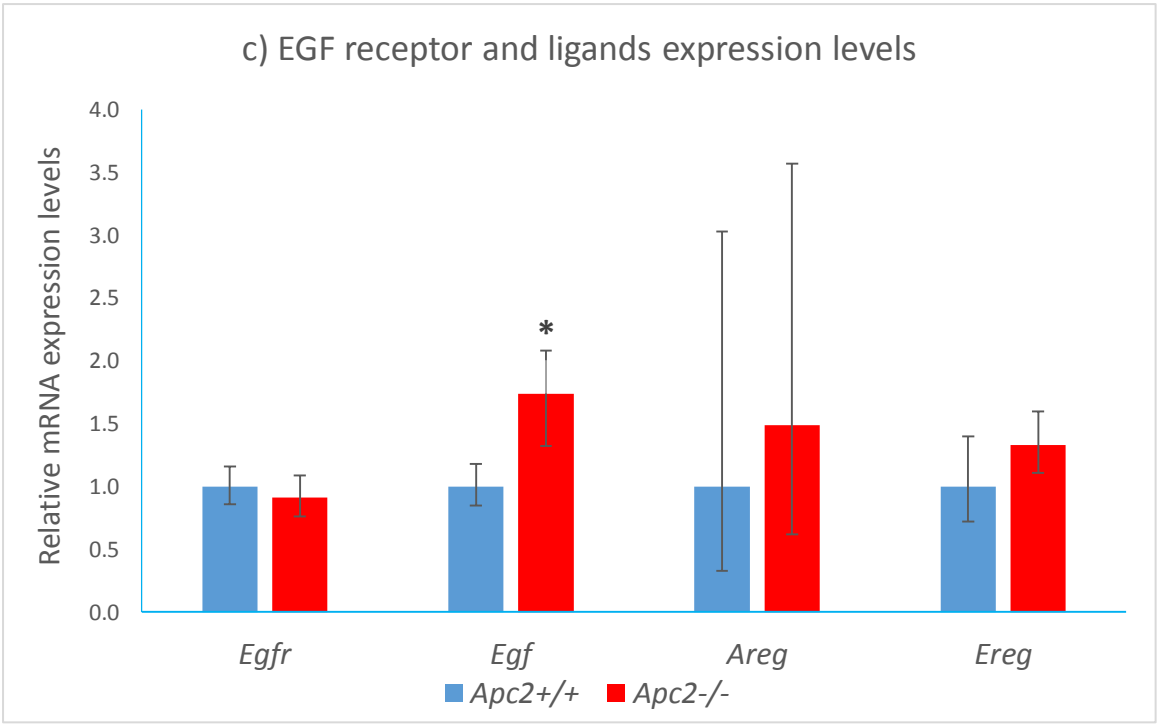

Figure 4.12: APC2-deficiency does not impair the ovulation process. Representative photomicrograph of follicles approaching the pre-ovulatory stage in (a) *Apc2*$^{+/+}$ and (b) *Apc2*$^{-/-}$ ovarian sections. Scale bar 100 µm. (c) Gene expression levels of a subset of *Egf* ligands and receptor, known to regulate COC expansion. Expression levels were compared between *Apc2*$^{+/+}$ and *Apc2*$^{-/-}$ ovarian extracts using qRT-PCR and normalized to *Actb* expression. Data are shown as mean±95% confidence intervals. n=4. Statistical significance was determined according to Cumming *et al.* (Cumming *et al.* 2007). * denotes significance from *Apc2*$^{+/+}$ at $p<0.05$.

Morphometric analysis of corpora lutea did not reveal any histologic differences between *Apc2*$^{+/+}$ and *Apc2*$^{-/-}$ ovaries (Figure 4.13a,b). Apart from the significant decrease in the number of corpora lutea observed in *Apc2*$^{-/-}$ ovaries (Figure 4.5a), the size of formed corpora lutea were comparable in *Apc2*$^{+/+}$ and *Apc2*$^{-/-}$ ovaries (667.1±8.7 µm vs. 693.7±51 µm, Figure 4.13c). In addition, they were equally healthy as reflected by comparable neovascularization capacity (CD34 immunostaining, Figure 4.13d,e). Proliferation (Ki67 immunostaining, Figure 4.14a-c) and apoptosis frequency (cleaved caspase 3 immunostaining, Figure 4.14d,e) were assessed in corpora lutea of both genotypes, by counting positively-staining cells and normalizing to corpus luteum area, and were not different. Overall, therefore, it is unlikely that defects in ovulation process and granulosa cells terminal differentiation are contributing to the observed phenotype.

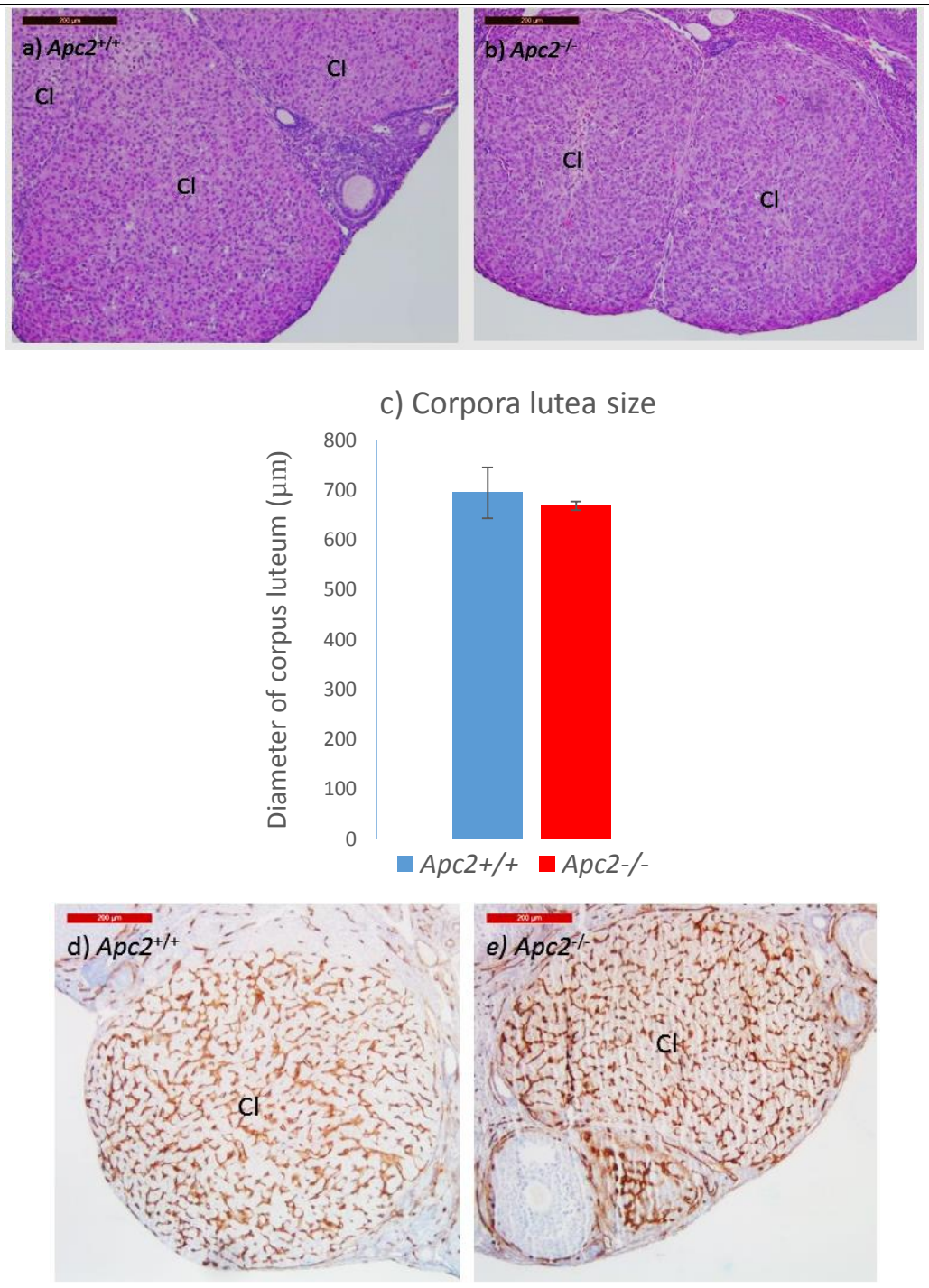

Figure 4.13: Characterizing effects of APC2 deletion on corpora lutea. Representative photomicrographs of corpus luteum in (a) *Apc2*$^{+/+}$, and (b) *Apc2*$^{-/-}$ ovarian sections. (c) Histogram showing comparable corpora lutea size in the two genotypes. Representative photomicrographs of CD34 immunostaining in corpora lutea of (d) *Apc2*$^{+/+}$ and (e) *Apc2*$^{-/-}$ ovarian sections. n=4. Data are represented as mean±S.E. Scale bars 200 µm.

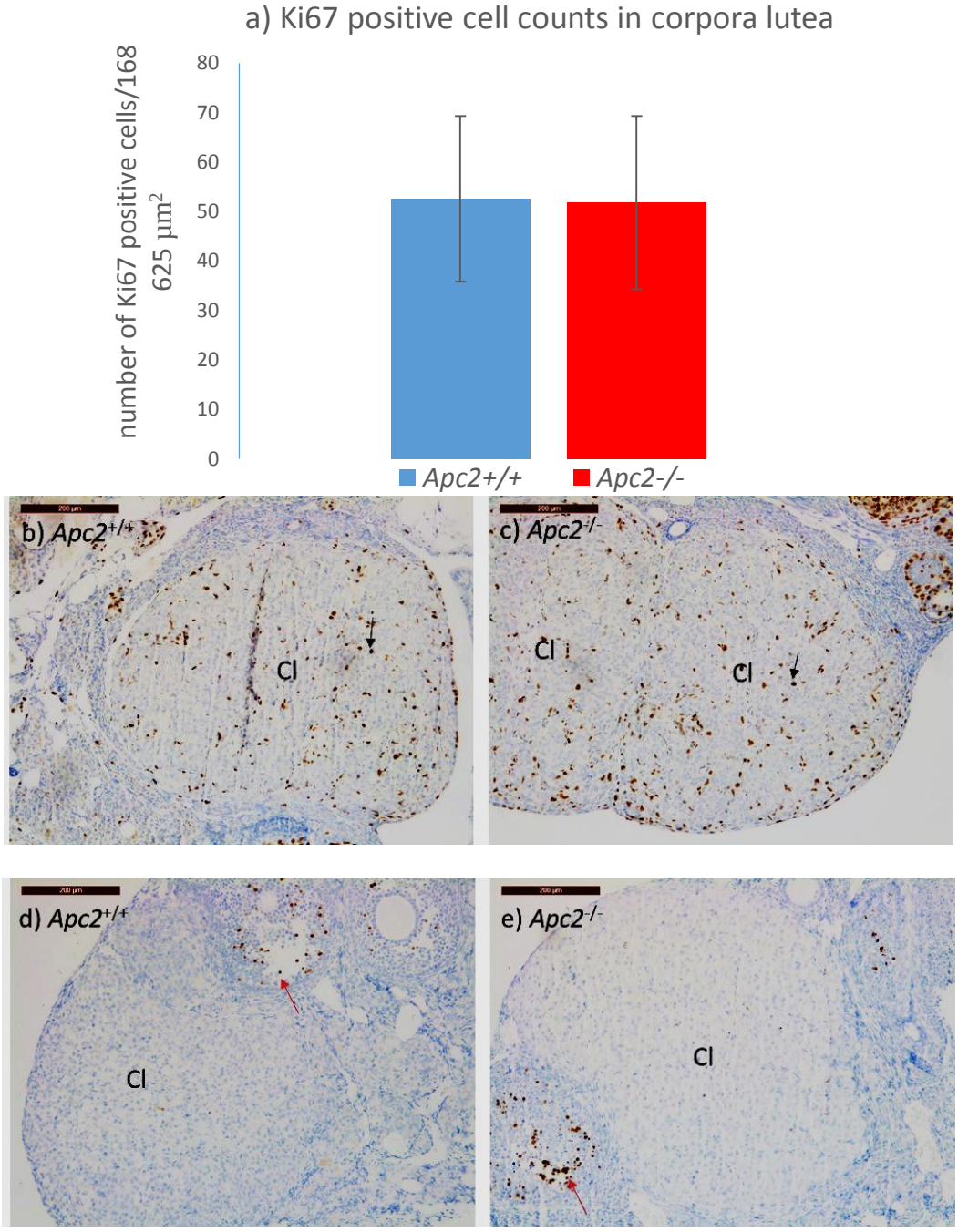

Figure 4.14: Characterizing effects of APC2 deletion on proliferation and apoptosis of corpora lutea. (a) Histogram reflecting equivalent positive Ki67 cell counts in the two genotypes. Representative photomicrographs of Ki67-positive cells (black arrows) in (b) *Apc2*$^{+/+}$, and (c) *Apc2*$^{-/-}$ corpora lutea. Cleaved caspase 3 positive cells (red arrows in atretic follicles) were absent in corpora lutea of (d) *Apc2*$^{+/+}$, and (e) *Apc2*$^{-/-}$ ovarian sections. n=4. Data are represented as mean±S.E. Scale bars 200 µm.

4.2.5. Reduced ovulation of *Apc2*$^{-/-}$ mice is caused by defects in follicular growth

Morphometric analysis was performed on the serial-sectioned *Apc2*$^{+/+}$ and *Apc2*$^{-/-}$ ovaries, collected at the diestrus stage, to evaluate whether the reduced ovulation rate observed in *Apc2*$^{-/-}$ mice is caused by a reduction in number of follicles ready to ovulate. As previously mentioned, there was a non-significant increase in the total number of healthy growing follicles in *Apc2*$^{-/-}$ ovaries (Figure 4.5b). When follicle counts were analysed per follicular stage, a non-significant increase was found in the number of primary and antral follicles in *Apc2*$^{-/-}$ ovaries (34.5±5.6 and 25.75±4.4 vs. 26.25±4.21 and 18.25±2.17 respectively, Figure 4.15a). However, it was observed that most of the antral follicles were small. A non-significant decrease in the number of pre-ovulatory follicles was observed in *Apc2*$^{-/-}$ ovaries (0.75±0.25 vs. 1.5±0.87, Figure 4.15a).

A size distribution analysis for all the healthy antral and pre-ovulatory follicles was performed, and represented as a percentage of total number of antral and pre-ovulatory follicles per serial-sectioned ovary. A significant increase was observed in the percentage of small follicles, having a diameter less than 200 µm, in *Apc2*$^{-/-}$ ovaries (56.29±4.9 vs. 32.8±5.7, $p<0.05$, Figure 4.15b). However, a significant decrease was observed in the percentage of follicles with diameter bigger than 300 µm in *Apc2*$^{-/-}$ (16.15±2.1 vs. 32.04±5.3, $p<0.05$, Figure 4.15b). The reduction in size of follicles was evident in the larger follicles, with no single follicle observed greater than 450 µm in *Apc2*$^{-/-}$ovaries, in contrast to 6 follicles observed in the all the ovaries of the *Apc2*$^{+/+}$ cohort.

An analysis of atretic follicles was performed to determine whether the reduction in number of follicles bigger than 300 µm is due to increased atresia. There was not a significant change in the total number of atretic follicles between *Apc2*$^{+/+}$ and *Apc2*$^{-/-}$ ovaries (195±24.5 vs. 203.5±23.8, Figure 4.16a). Most of the follicles counted were small atretic follicles present in the ovarian medulla (Figure 4.16b,c). Counting atretic follicles present in the antral and pre-

ovulatory stages did not reveal a significant difference between *Apc2*$^{+/+}$ and *Apc2*$^{-/-}$ ovaries (23±5.6 vs. 22.5±4.6, Figure 4.16a). However measuring the size of atretic antral and pre-ovulatory follicles revealed a non-significant increase in the percentage of atretic follicles whose diameter is bigger than 300 µm in *Apc2*$^{-/-}$ ovaries (34.7±7.74 vs. 27.1±7.1 in *Apc2*$^{+/+}$ ovaries, Figure 4.16d). All the aforementioned results suggest that the main defect in *Apc2*$^{-/-}$ ovaries is the reduced ability of healthy follicles to grow beyond a certain size (300 µm), limiting the availability of follicles reaching the pre-ovulatory stage.

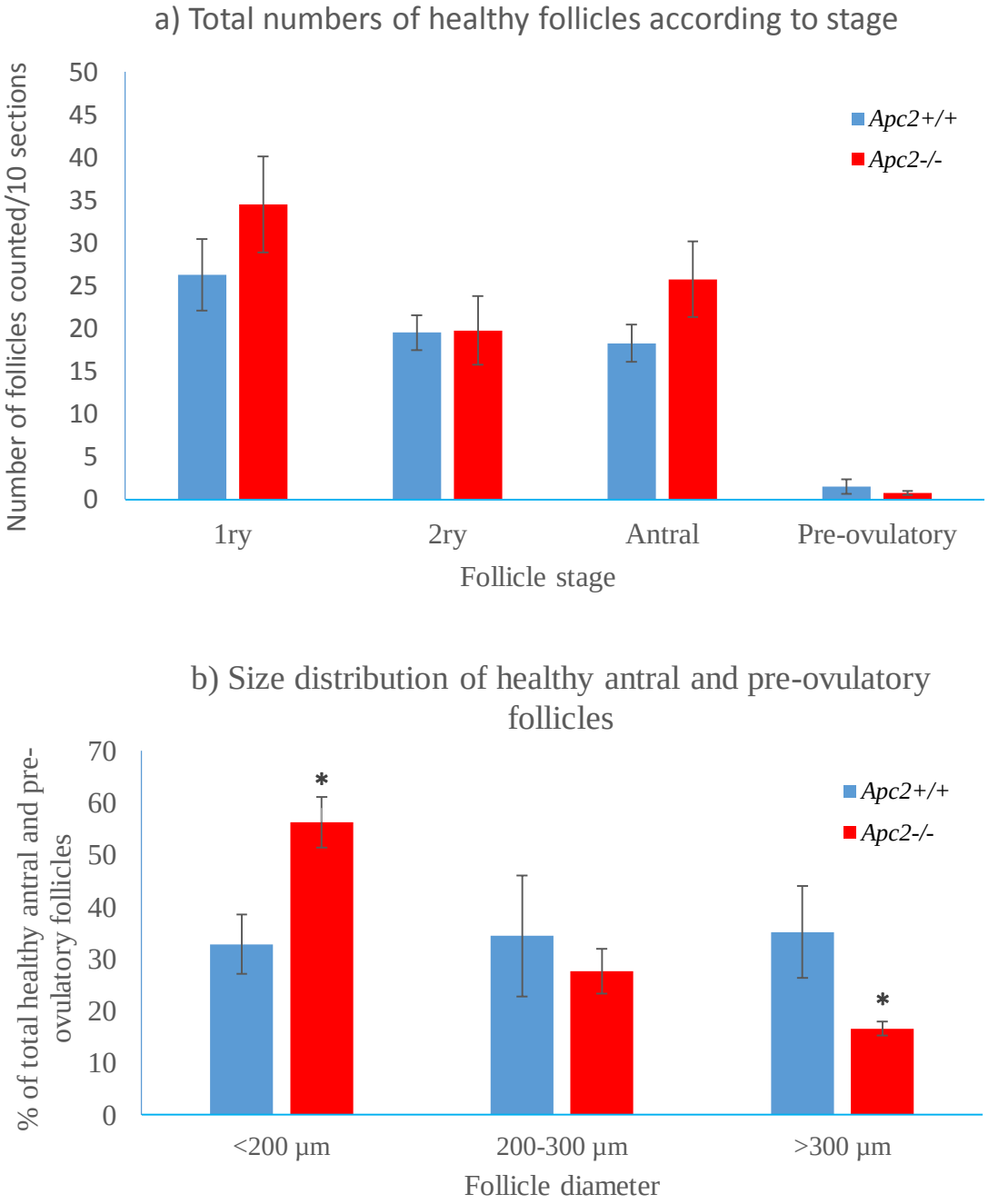

Figure 4.15: APC2-deficiency impairs follicular growth in the ovary. (a) Histogram showing total number of primary (1ry), secondary (2ry), antral and pre-ovulatory follicles in *Apc2*$^{+/+}$ and *Apc2*$^{-/-}$ ovarian sections. (b) Size distribution of healthy antral and pre-ovulatory follicles. n=4. Data are represented as mean±S.E. Statistical significance was determined by t-test. * denotes significance from *Apc2*$^{+/+}$ at $p<0.05$.

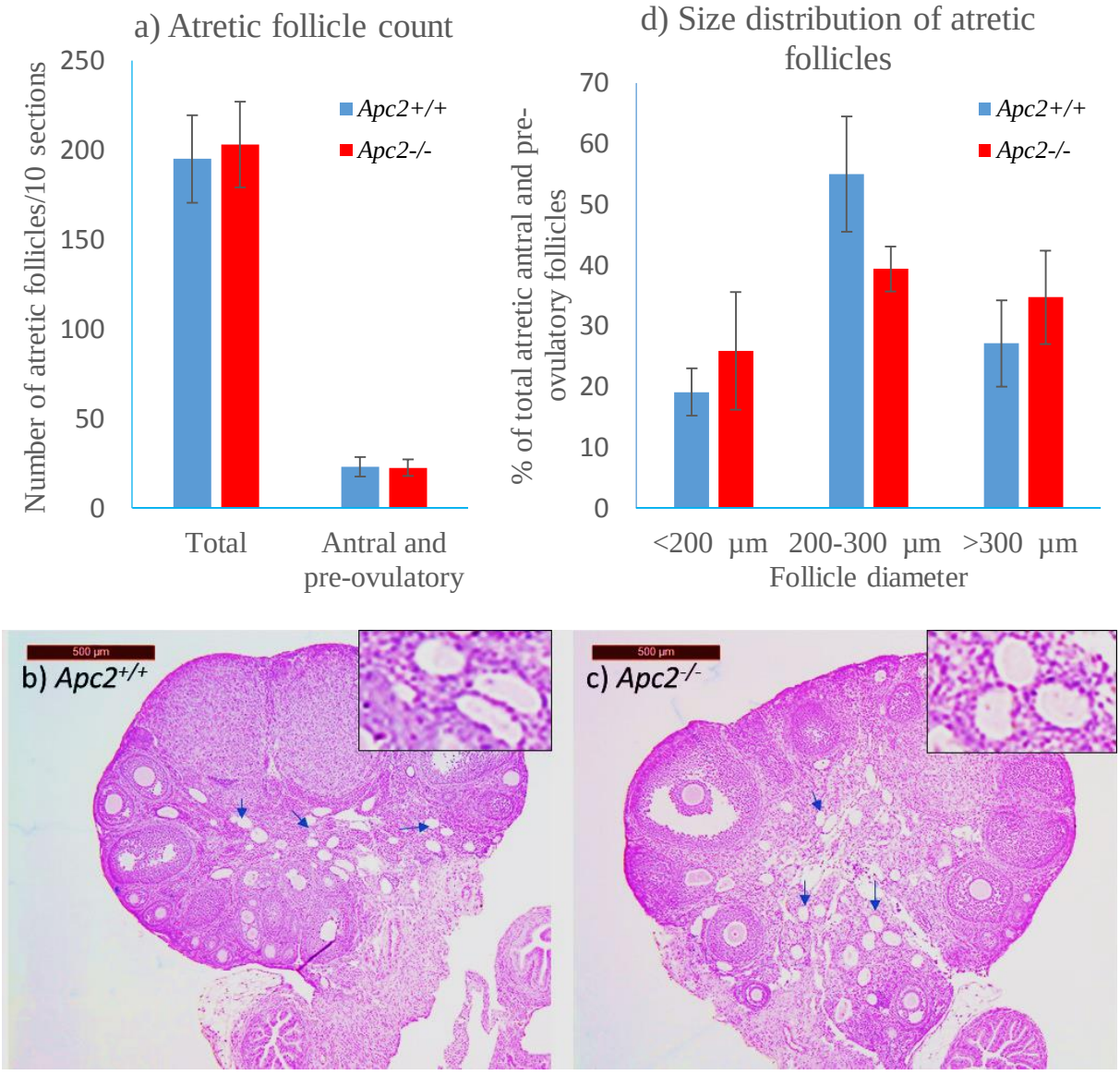

Figure 4.16: Analysis of atretic follicles in the ovaries collected from *Apc2*$^{+/+}$ and *Apc2*$^{-/-}$ mice. (a) Histogram of atretic follicle counts in ovaries of *Apc2*$^{+/+}$ and *Apc2*$^{-/-}$ mice. Representative photomicrographs of (b) *Apc2*$^{+/+}$ and (c) *Apc2*$^{-/-}$ ovarian sections, showing that most of the atretic follicles (arrows) are small, and present in the ovarian medulla. Insets shows 5X original magnification of small atretic follicles (arrows). (d) Size distribution of atretic antral and pre-ovulatory follicles. n=4. Data are represented as mean±S.E. Statistical significance was determined by t-test. * denotes significance from *Apc2*$^{+/+}$ at $p<0.05$. Scale bars 500 µm.

4.2.6. Impaired follicular growth in *Apc2*$^{-/-}$ ovaries is due to increased apoptosis

The impaired follicular growth observed in *Apc2*$^{-/-}$ ovaries could be either due to reduced proliferation or increased apoptosis. In order to unravel which of these mechanisms is causing the observed defects in folliculogenesis, immunohistochemistry for markers of proliferation (Ki67 antigen) and apoptosis (cleaved caspase 3 protein) were used. Follicular cells positively-stained were quantified and normalized to the follicle area. A non-significant increase in the number of granulosa cells with nuclear staining for Ki67 was observed in *Apc2*$^{-/-}$ follicles, as compared to *Apc2*$^{+/+}$ follicles (30.85±3.6 vs. 23.27±4.5, Figure 4.17a,b). There was no significant difference in the number of theca cells staining positively for Ki67 between *Apc2*$^{+/+}$ and *Apc2*$^{-/-}$ follicles (12±0.62 vs. 11.8±0.6, Figure 4.17a). In contrast, a significant increase in granulosa cells positively staining for cleaved caspase 3 was observed in *Apc2*$^{-/-}$ follicles compared to *Apc2*$^{+/+}$ follicles (14.22±1.3 vs. 6.04±1.01, $p<0.05$, Figure 4.17c,d).

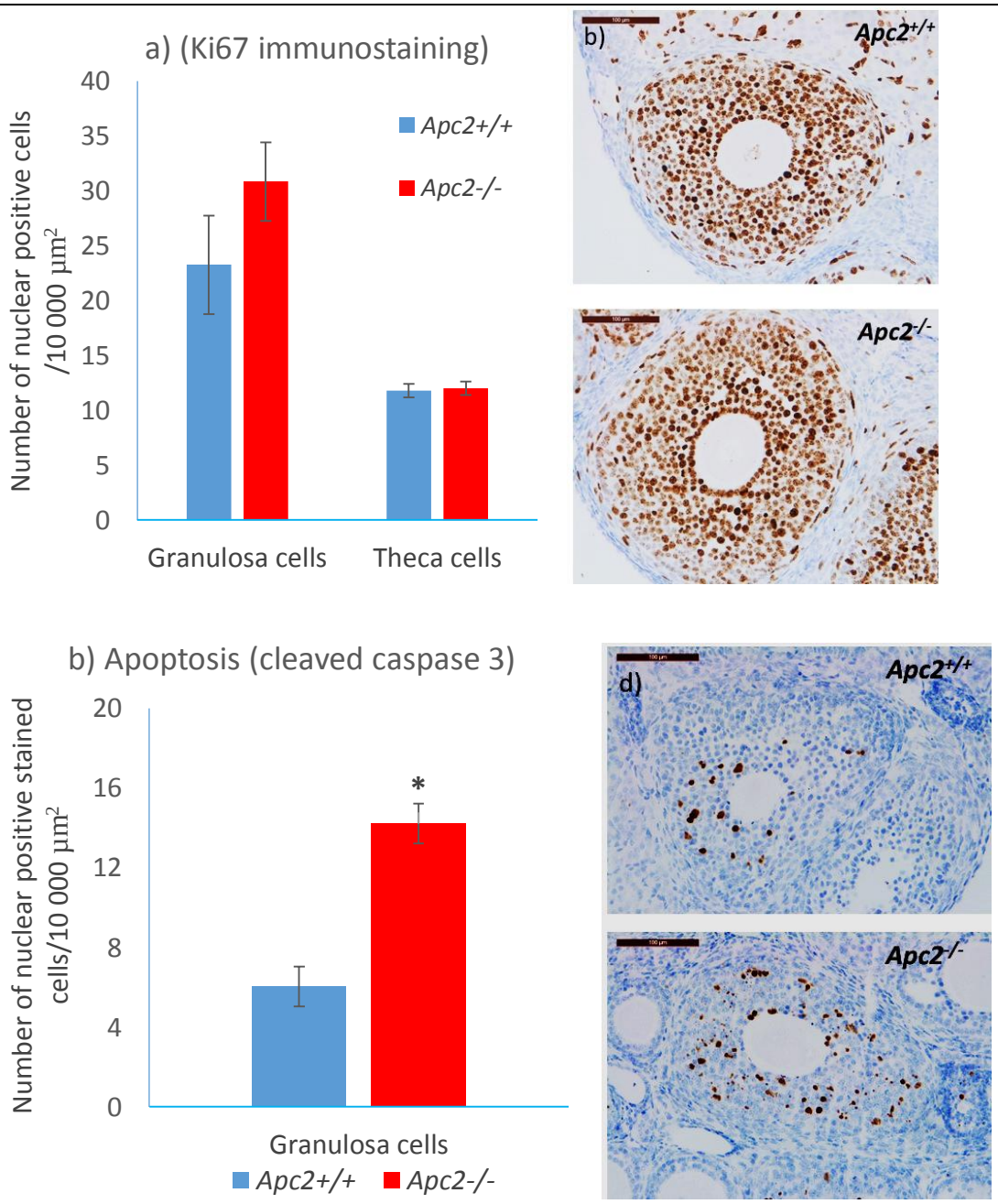

Figure 4.17: Restricted follicular growth in *Apc2*$^{-/-}$ ovaries is caused by increased granulosa cells apoptosis. (a) Histogram showing comparable proliferation of *Apc2*$^{+/+}$ and *Apc2*$^{-/-}$ follicular cells. (b) Representative photomicrographs of Ki67 immunostaining in *Apc2*$^{+/+}$ and *Apc2*$^{-/-}$ ovarian follicles. (c) Histogram showing more than a 2-fold increase of apoptosis in granulosa cells of *Apc2*$^{-/-}$ follicles. (d) Representative photomicrographs for cleaved caspase 3 immunostaining. n=4. Data are represented as mean±S.E. Statistical significance was determined by t-test. * denotes significance from *Apc2*$^{+/+}$ at $p<0.05$. Scale bars 100 µm.

Members of FOX family of transcription factors are well-known regulators of apoptosis. Previous studies have shown that overexpression of FOXO1, FOXO3 or FOXL2 induces granulosa cell apoptosis (Kim *et al.* 2011; Matsuda *et al.* 2011; Shen *et al.* 2012). A gene expression analysis was performed for these *Fox* member genes on RNA extracted from *Apc2*$^{+/+}$ and *Apc2*$^{-/-}$ whole ovaries. A significant increase was observed only in *Foxo1* expression levels in *Apc2*$^{-/-}$ vs. *Apc2*$^{+/+}$ ovaries (Figure 4.18a).

The expression levels of a panel of FOXO target genes involved in cell cycle regulation and apoptosis were investigated. Of the studied genes, *Bcl6* and *Cdkn1b* were significantly upregulated in *Apc2*$^{-/-}$ as compared to *Apc2*$^{+/+}$ ovaries, while *Bcl2l1*, *Fasl* and *Tnfsf10* expression levels were not significantly changed (Figure 4.18d).

PTEN/PI3K/AKT signalling is the most studied regulator of FOXO transcriptional activity and post-translational modification (Tzivion *et al.* 2011). On activation of AKT, FOXO proteins are inactivated by being phosphorylated and translocated out of the nucleus to the cytoplasm. Immunohistochemistry was performed to determine the level and localization of PTEN, p-AKT and p-FOXO 1,3,4 in *Apc2*$^{+/+}$ and *Apc2*$^{-/-}$ follicles. PTEN expression was stronger in theca cells and granulosa cells of *Apc2*$^{-/-}$ follicles (Figure 4.19a). This was associated with a non-significant increase in *Pten* gene expression levels in *Apc2*$^{-/-}$ ovaries (Figure 4.19a). However, p-AKT immunostaining was weaker in granulosa cell of *Apc2*$^{-/-}$ follicles (Figure 4.19b). Consequently, the expression of p-FOXO1,3,4 was very weak in the granulosa cells of *Apc2*$^{-/-}$ ovarian follicles (Figure 4.19c). In summary, the previous results showed that the increased apoptosis seen in *Apc2*$^{-/-}$ follicles is associated with upregulation of *Foxo1* and its downstream effector genes, which may be secondary to decreased activation of PI3K/p-AKT signalling as a result of PTEN upregulation.

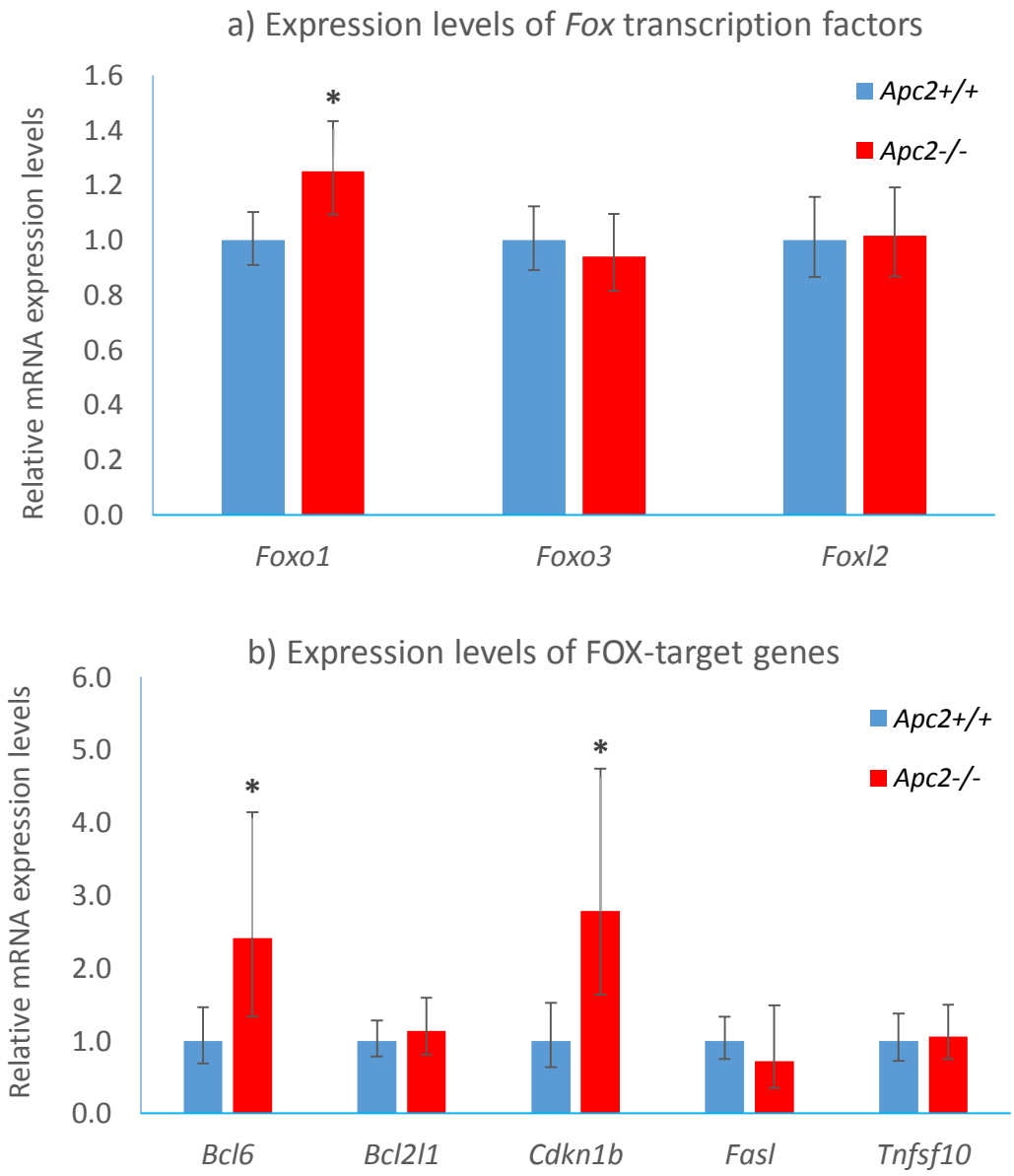

Figure 4.18: Increased apoptosis in *Apc2*$^{-/-}$ ovaries is driven by upregulation of *Foxo1* and downstream targets. Relative expression levels of a panel of (a) *Fox* transcription factors, and (b) FOX downstream target genes performed on RNA extracted from *Apc2*$^{+/+}$ and *Apc2*$^{-/-}$ 10-week-old ovaries, normalized to *Actb* expression. n=3-4. Data are represented as mean±95% confidence interval. Statistical significance was determined using Cumming *et al.* (Cumming *et al.* 2007) method for qRT-PCR data. * denotes significance from *Apc2*$^{+/+}$ at $p<0.05$.

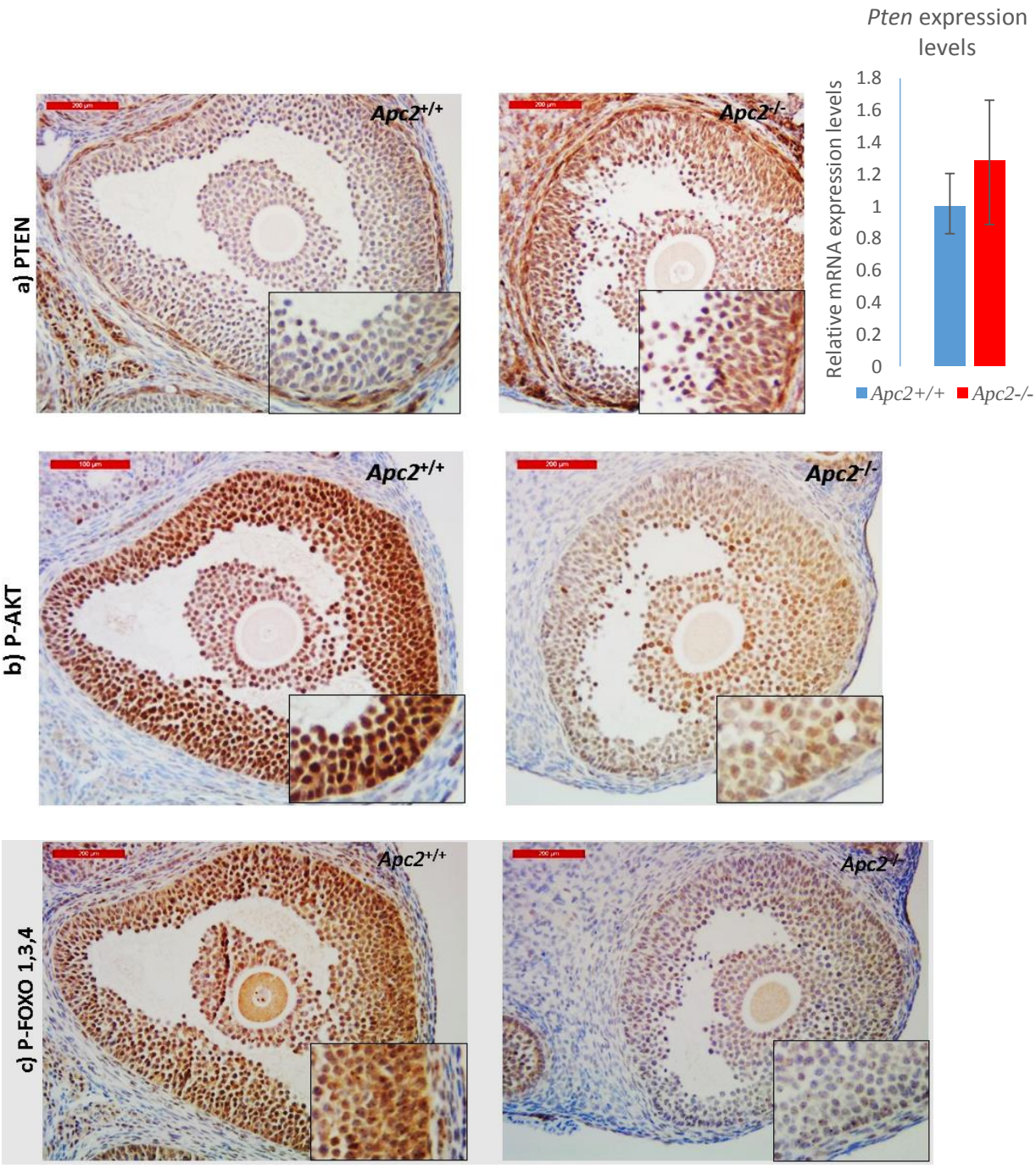

Figure 4.19: Characterizing PTEN/PI3K/AKT signalling in *Apc2*$^{-/-}$ ovaries. Representative photomicrographs of (a) PTEN (together with *Pten* gene expression levels), (b) p-AKT (ser-473), and (c) p-FOXO1,3,4 immunostaining in *Apc2*$^{+/+}$ and *Apc2*$^{-/-}$ ovarian follicles. n=4. Data are represented as mean±95% confidence interval. Scale bars 200 µm. Insets show 2X original magnification.

4.2.7. Defects in response to gonadotrophin is caused by upregulation of *Lhcgr*

As noted in section 4.2.3., the results of exogenous gonadotrophin administration suggested that the subfertility observed in *Apc2*$^{-/-}$ female mice is due to intra-ovarian defects in response to gonadotrophin. To explore this, a gene expression analysis of ovarian gonadotrophin receptors, *Fshr* (follicle stimulating hormone receptor) and *Lhcgr* (Leutinizing hormone chorionic gonadotrophin receptor) was performed, together with the steroid hormone receptors *Pgr* (progesterone receptor), *Esr1*(estrogen receptor α), *Esr2* (estrogen receptor β) and *Ar* (androgen receptor). There were no significant differences in the expression levels of any of the receptors apart from the *Lhcgr*, which was more than 3 times increased in the *Apc2*$^{-/-}$ ovaries as compared to *Apc2*$^{+/+}$ ovaries (Figure 4.20).

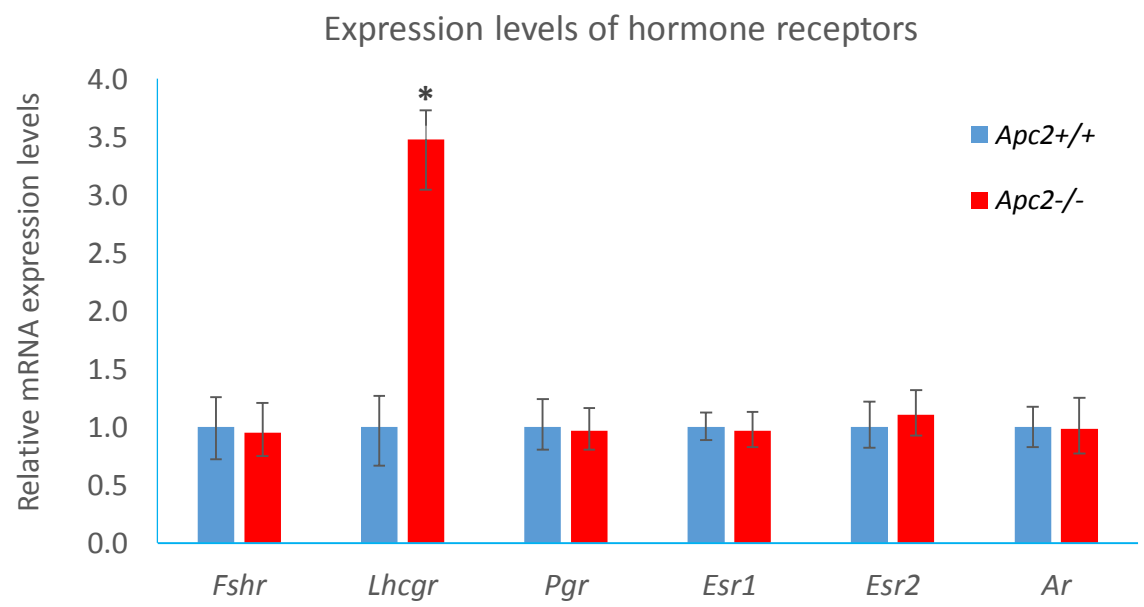

Figure 4.20: Gene expression levels of hormone receptors performed by qRT-PCR on RNA extracted from whole ovaries of *Apc2*$^{+/+}$ and *Apc2*$^{-/-}$ 10-week-old female mice. Relative expression levels are normalized to *Actb* expression. n=3-4. Data are represented as mean±95% confidence interval. Statistical significance was determined according to Cumming *et al.* (Cumming *et al.* 2007). * denotes significance from *Apc2*$^{+/+}$ at $p<0.05$.

4.2.8. APC2 deletion impairs follicle steroidogenesis and vascularization

It has been previously reported that activation of canonical WNT signalling inhibits follicular growth by impairing follicle steroidogenesis in addition to increasing granulosa cell apoptosis (Li *et al.* 2014). To investigate whether WNT signalling activation (as a result of APC2 deletion) impairs follicle steroidogenesis, expression levels of genes involved in estradiol synthesis were performed. Expression levels of *Cyp11a1* (gene coding for cholesterol side chain cleavage enzyme) were comparable in *Apc2*$^{+/+}$ and *Apc2*$^{-/-}$ ovarian extracts (Figure 4.21a). However, the expression levels of *Cyp17a1* (coding for steroid 17-α-hydroxylase/17,20 lyase), and *Cyp19a1* (coding for aromatase) were significantly reduced in *Apc2*$^{-/-}$ as compared to *Apc2*$^{+/+}$ ovaries ($p<0.05$, Figure 4.21a).

The vascular network surrounding the growing follicles is essential for follicular development, by delivering nutrients and oxygen. Disruption of angiogenesis has been previously described to impair follicular growth (Robinson *et al.* 2009). In order to find out whether defects in follicular vascularization contribute to the subfertility phenotype in *Apc2*$^{-/-}$ ovaries, expression levels of *Vegfa* gene and immunostaining for CD34 protein were performed. *Vegfa* expression was significantly decreased in *Apc2*$^{-/-}$ ovaries as compared to *Apc2*$^{+/+}$ (Figure 4.21b). However, it should be taken into consideration that the reduction of *Vegfa* expression levels is-in part- attributable to the reduction in the number of corpora lutea formed in *Apc2*$^{-/-}$ ovaries. CD34 immunostaining enabled the visualization of follicular vascularization. In *Apc2*$^{+/+}$ ovaries, the late antral to pre-ovulatory follicles were surrounded by 2 continuous layers of endothelial cells (Figure 4.21c). In *Apc2*$^{-/-}$ ovaries, however, the endothelial cells surrounding the follicles were discontinuous, reflecting a degree of impairment of follicular vascularization (Figure 4.21c)

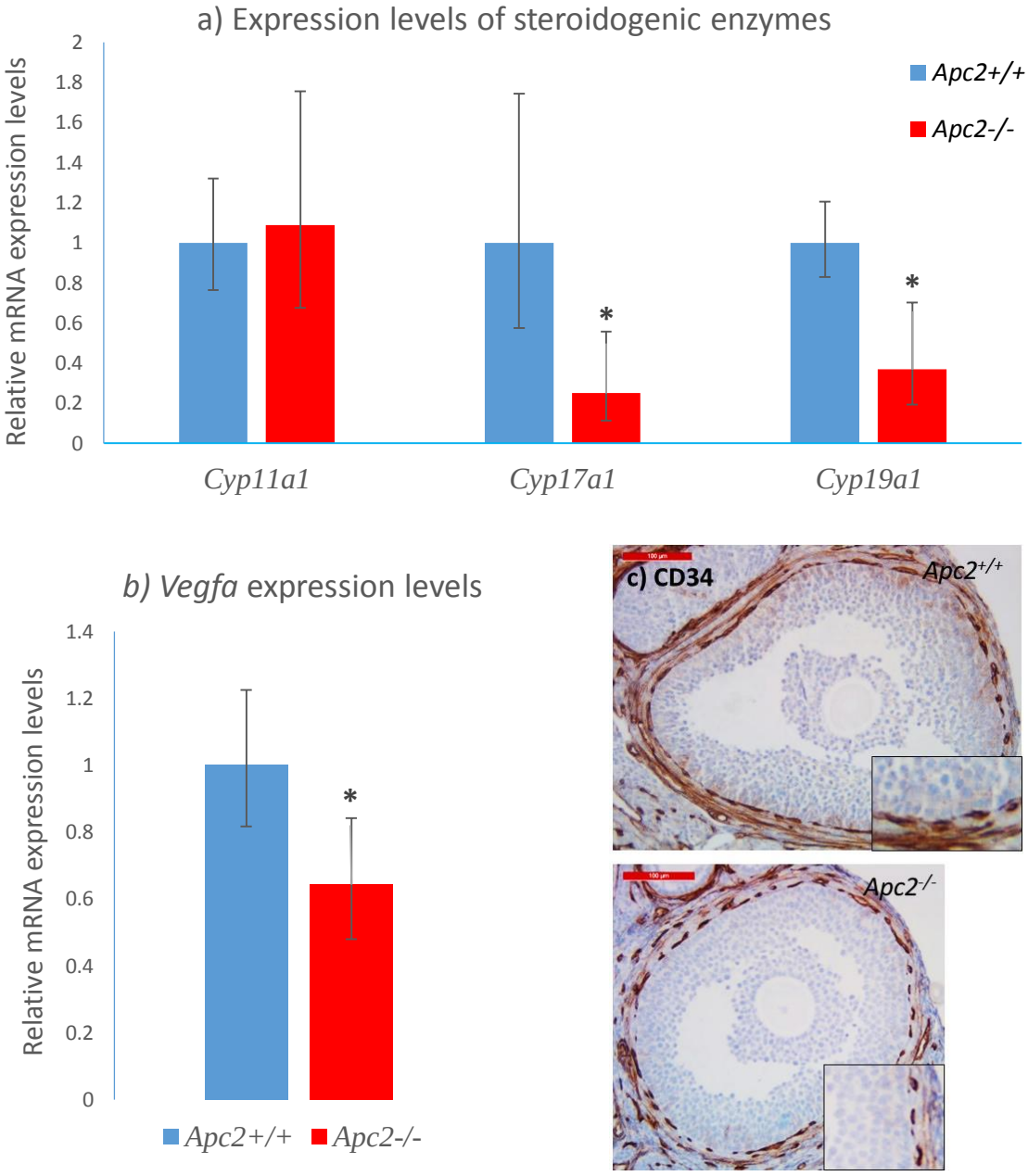

Figure 4.21: APC2 deletion impairs follicle steroidogenesis and vascularization. Gene expression levels of (a) steroidogenic enzymes, and (b) *Vegfa* performed by qRT-PCR on RNA extracted from whole ovaries of 10-week-old *Apc2*$^{+/+}$ and *Apc2*$^{-/-}$ female mice. Relative expression levels are normalized to *Actb* expression. (c) CD34 immunostaining of follicles. n=3-4. Data are represented as mean±95% confidence interval. Statistical significance was determined according to Cumming *et al.* (Cumming *et al.* 2007). * denotes significance from *Apc2*$^{+/+}$ at $p<0.05$. Scale bars 100 µm. Insets show 2X original magnification.

4.3. Discussion

4.3.1. APC2 deletion in the ovary activates WNT signalling

APC deletion is known to activate WNT signalling in some tissues such as the intestine (Sansom *et al.* 2004) and the uterus (Tanwar *et al.* 2011b), but not in the mammary gland (Daly *et al.* 2016). Deleting APC exclusively in the OSE and in ovarian granulosa cells was shown to activate WNT signalling in the ovary (Tanwar *et al.* 2013). However, when it comes to its homologous protein, APC2, the question is more challenging. Although APC2 has been previously shown to downregulate β-catenin in a range of colorectal cancer cell lines (Van Es *et al.* 1999; Schneikert *et al.* 2013), limited data from *in vivo* studies has supported this finding. This could be partly due to the nature of the *in vivo* studies conducted with *Apc2* knockout mouse, which were mostly exploring non-WNT functions of APC2 in the brain and nervous system (Shintani *et al.* 2012; Almuriekhi *et al.* 2015). Even when studies were directed towards investigating APC2 functions in WNT signalling, deletion of APC2 on its own was not enough to activate WNT signalling in mouse mammary glands (Daly *et al.* 2016). On the contrary, APC2 deletion activated WNT signalling in the small intestine and the liver (Daly 2013). It was thus crucial to unravel the effect of APC2 deletion on WNT signalling in the ovary.

Loss of Axin1 and β-catenin-binding domains of APC2 protein in the *Apc2*$^{-/-}$ mouse (Appendix 3) caused the activation of canonical WNT signalling in the ovary, as reflected by the upregulation of *Ctnnb1* and its downstream target genes *Axin2* and *Fgf1* (Figure 4.1). Expression levels of this subset of β-catenin target genes were evaluated because of their relevance to the ovarian tissue. *Axin2* is believed to be a downstream target of WNT/β-catenin/TCF, which functions to regulate the activated WNT signalling through negative feedback loops (Jho *et al.* 2002). *Axin2* mRNA expression levels (Li *et al.* 2014) as well as reporter mice (De Cian *et al.* 2016) have been used extensively as surrogates of WNT signalling activation in the ovary. *Fgf1*, known to be overexpressed in epithelial ovarian cancer (Zaid *et*

al. 2011; Smith *et al.* 2012), has been shown to be a downstream target of Wnt/β-catenin/Tcf signalling in the ovary (King *et al.* 2015). The observed overexpression of *Apc* could be interpreted in terms of functional redundancy between APC and APC2 previously reported in some tissues, where the presence of only one of the 2 APC proteins is sufficient to prevent WNT signalling perturbation and phenotypic changes (Ahmed *et al.* 2002; Daly *et al.* 2016). In the current study, it could be regarded as a compensatory mechanism to regulate the activated pathway. However, at that stage, WNT signalling was not inhibited as reflected by the expression levels of *Wif1*.

4.3.2. APC2 deletion caused subfertility in adult mice

Genetically-engineered mouse models GEMMs provide a valuable tool to dissect functions of canonical WNT signalling in the ovary. Previous attempts to characterize roles of canonical WNT signalling on adult ovarian homeostasis have mainly relied on mutations in genes coding for Wnt secreted glycoproteins (Boyer *et al.* 2010; Abedini *et al.* 2016), positive modulator secreted proteins (De Cian *et al.* 2016), frizzled receptors (Hsieh *et al.* 2005; Lapointe *et al.* 2012), and β-catenin (Boerboom *et al.* 2005; Boerboom *et al.* 2006; Hernandez Gifford *et al.* 2009; Fan *et al.* 2010a). However, equivalent functional studies targeting negative regulators of the pathway are lacking, apart from one study performed on APC (Tanwar *et al.* 2013). It was thus important to characterize the role of APC2 in adult ovaries and to investigate whether these roles could be related to its canonical WNT-regulatory functions.

Using GEMMs, it is clear that tight regulation of WNT signalling is important for adult ovarian functions. Surprisingly, complete silencing of the pathway through deleting its main transducer β-catenin has no effect on adult ovarian functions (Hernandez Gifford *et al.* 2009; Fan *et al.* 2010a). However, it is apparent that over-activation of canonical WNT signalling has deleterious effects on follicle growth (Boerboom *et al.* 2005; Abedini *et al.* 2016), ovulation

process and luteinisation (Fan *et al.* 2010a; De Cian *et al.* 2016). The discrepancies in the phenotype of ovarian subfertility seen in the published mouse models could be, in part, related to the follicular stage when WNT signalling is activated. When this happens early in folliculogenesis, at the secondary follicle stage onward, the subfertility is caused by defects in follicular growth (Boerboom *et al.* 2005; Abedini *et al.* 2016). However, when the activation happens at later stages of folliculogenesis, from the antral follicle stage onward, the subfertility is caused by defects in ovulation process and/or corpus luteum formation (Fan *et al.* 2010a; De Cian *et al.* 2016). Evidence from both GEMMs and *in vitro* studies supports this hypothesis.

Using different *cre* transgenes, which drives recombination of floxed genes at specific cells/follicular stages in GEMMs, has helped in defining roles of WNT signalling in folliculogenesis. For instance, Amhr2-*cre* drives the recombination of floxed genes in the OSE and in granulosa cells of growing follicles starting from pre-antral stages (Baarends *et al.* 1995; Fan *et al.* 2009) . However, Cyp19-*cre* drives the recombination of floxed genes specifically in granulosa cells of antral and pre-ovulatory follicles (Fan *et al.* 2008), where *Cyp19a* starts to be expressed. SF1-*cre* (steroidogenic factor 1) targets different cells; it recombines the floxed genes mainly in theca cells of growing follicles and corpora luteal cells (Bingham *et al.* 2006).

In vitro culture of follicles collected at different stages has proven to be another valuable tool, as it can be used to unravel roles of WNT signalling activation on folliculogenesis. Using secondary follicles isolated from mouse ovaries and treating them in culture with WNT activators (Wnt3a or LiCl) or inhibitors (IWR-1), Li group showed that activation of WNT signalling in this early stage of folliculogenesis impairs follicular growth (Li *et al.* 2014). Using COC isolated from pre-ovulatory follicles of mice with either gain- or loss-of-function mutations in the *Ctnnb1* gene, Fan group demonstrated that at this late follicular stage, WNT signalling activation impairs COC expansion (Fan *et al.* 2010a).

When using constitutive knockout mouse models, such as the APC2 model used in this study, it is important to know at which stage of folliculogenesis APC2 is expressed. However, such information is lacking in the literature. In this study, attempts were performed to visualize APC2 protein expression in different stages of folliculogenesis by immunohistochemistry (Appendix 2). However, we could not source an antibody which can differentially stain *Apc2*$^{+/+}$ and *Apc2*$^{-/-}$ ovaries, after the discontinuation of the Zymed c-terminal antibody previously used by Dr. Carl Daly (Daly 2013; Daly *et al.* 2016), a limitation which necessitated a detailed investigation of all the possible outcomes of WNT signalling activation at the different stages of folliculogenesis.

Activation of canonical WNT signalling, driven by APC2 loss, in this study caused subfertility; as reflected by 33% and 57% reductions in gestation frequency and litter size respectively (Figure 4.3). Various degrees of subfertility have been previously reported with other GEMMs after WNT signalling activation. For example, expression of degradation-resistant β-catenin caused a severe reduction of litter size (ranging from 60-95%) as reported by 2 different groups (Boerboom *et al.* 2005; Fan *et al.* 2010a). Litter size was reduced by 52% after deleting WNT5a, which caused activation of canonical WNT signalling (Abedini *et al.* 2016). In accordance with these findings, amplification of R-spondin1 was reported to cause 83% reduction in litter size (De Cian *et al.* 2016). One of the limitations in the current study was crossing different *Apc2* female genotypes with the corresponding male genotype, rather than crossing them all with *Apc2*$^{+/+}$ males. In order to confirm that the subfertility observed here is caused by defects in female fertility, retrieval of oocytes from oviducts of female mice after exogenous gonadotrophin administration was performed. Results from this experiment reflected a genotype-dependent decrease in the number of ovulated oocytes, which mirrored the decrease in number of pups recorded in the mating and breeding experiments (Figure 4.9).

However, a possible contribution of male APC2-deficient mice cannot be excluded, and need to be considered in future research.

The subfertility reported in the current study is due to restricted follicular growth leading to a decrease in the number of ovulated oocytes and corpora lutea formed post-ovulation (Figure 4.5-4.6, 4.15). This is similar to the phenotype reported by Abedini *et al.* after conditional deletion of *Wnt5a* in the granulosa cells of pre-antral follicles using Amhr2-*cre* (Abedini *et al.* 2016). Alhough WNT5a is a known activator of non-canonical WNT signalling (Oishi *et al.* 2003), it has been shown to inhibit canonical WNT signalling in some contexts (Pourreyron *et al.* 2012; Kwack *et al.* 2013). Abedini *et al.* reported that subfertility was caused by WNT signalling activation (Abedini *et al.* 2016). The phenotype reported here due to APC2 loss in the ovaries is in accordance with a previous subfertility phenotype, caused by expression of degradation-resistant β-catenin in granulosa cells of pre-antral follicles (Boerboom *et al.* 2005). However, the phenotype reported here is different from that reported after deleting *Apc* in the ovaries using Amhr2-*cre* (Tanwar *et al.* 2013). Alhough WNT signalling was activated post-APC loss, ovarian functions were normal in early adulthood without any reported effects on folliculogenesis or ovulation (Tanwar *et al.* 2013). Whether functional compensation between APC and APC2 were sufficient to protect against progressing to subfertility in this model remains unanswered. Contradicting this, an ovarian phenotype characterized by increased atretic follicles and elongated oestrous cycle (You *et al.* 2006), or absence of pre-ovulatory follicles and corpora lutea (Bennett *et al.* 2001), was described in the $Apc^{Min/+}$ mouse (a mouse with germline heterozygous mutation in *Apc* gene). However, fertility of female $Apc^{Min/+}$ mouse has not been characterized.

In the current study, WNT signalling activation secondary to APC2 deletion did not affect ovulation process and luteinisation (Figure 4.12-4.14). This was evident through histological examination of pre-ovulatory follicles and corpora lutea, as well as performing

functional analyses. In order to correctly analyse the histologic and molecular changes in a continuously cycling organ such as the ovary, it is important to collect all samples at a specific stage. This will exclude the variation happening in different stages of the oestrous cycle from the analysis. However, one of the limitations of the current study was choosing the diestrus stage to perform the analysis.

The diestrus stage was selected because the initial aim of the study was to characterize roles of APC2 on OSE homeostasis. Choosing the diestrus stage should help in evaluating this, as it is a post-ovulatory stage, rendering it suitable for studying whether APC2 is important for repairing the tear happening in OSE during ovulation. However, the choice of this stage limited the number of pre-ovulatory follicles available for histological examination. Using estrus stage ovaries would have aided in studying pre-ovulatory follicles in more details. In an attempt to overcome this limitation, COCs were collected from oviducts post-gonadotrophin administration, and their morphology were evaluated. Results from this experiment demonstrated that the morphology of ovulated COCs from *Apc2*$^{-/-}$ were comparable to those from *Apc2*$^{+/+}$ (Figure 4.8). These results, in addition to functional analysis of the signalling pathways controlling ovulation process and analysis of corpora lutea (Figure 4.12-4.14), confirmed that APC2-deficiency did not affect the ovulation process or terminal differentiation of granulosa cells prior to corpora lutea formation. Although it has been previously reported that mutation of E-APC (*Drosophila* APC2) mislocalized oocytes in mutant egg chambers (Hamada and Bienz 2002), this was not evident in the current study for both oocytes investigated in ovarian sections or ovulated oocytes.

Based on the results of this study, and previously published results from GEMMs, it can be concluded that APC2 is present in the ovarian follicles as early as the pre-antral stage and that APC2 presence suppresses canonical WNT signalling. The presence of APC2 is

essential for follicular growth and maturation, and its loss represses follicular growth leading to reduced ovulation and corpus luteum formation.

4.3.3. Subfertility caused by APC2-deficiency is due to ovarian defects

As mentioned previously, the APC2-deficient mouse used in the current study is a constitutive knock out mouse, meaning that APC2 is lost in all mouse tissues. In addition to the autocrine and paracrine control of ovarian functions originating from the ovary, exogenous control through the hypothalamic and pituitary hormones are required for triggering folliculogenesis and ovulation (Plant 2015). Given that APC2 expression is enriched in the hypothalamus and pituitary glands, and that APC2 has a low expression in the ovary (The GTEx Consortium 2013), the subfertility observed in APC2-deficient mice could be caused by extra-ovarian defects in gonadotrophin synthesis/release rather than intra-ovarian defects. To test this hypothesis, we first measured levels of FSH and LH in serum collected from *Apc2*$^{+/+}$ and *Apc2*$^{-/-}$ female mice (Figure 4.7). Results revealed comparable levels of these hormones in both genotypes studied. Our findings for FSH serum levels agreed with the finding of unchanged FSH levels in subfertile female mice with activated canonical WNT signalling as a result of Wnt5a deletion (Abedini *et al.* 2016).

Unfortunately, performing FSH and LH hormonal assays in the diestrus stage does not correlate with their peak levels (during proestrus and estrus respectively), making it impossible to address whether peak concentrations were affected. It is evident from published work that even minimal decreases in FSH peak concentration affect the number of antral follicles reaching the pre-ovulatory stage, and increase the number of atretic follicles (Macklon and Fauser 2001). Due to uncertainties related to determination of serum FSH levels at diestrus, we aimed to confirm our findings using an alternative approach. APC2-deficient mice were administered exogenous gonadotrophin and compared to control APC2-intact mice treated similarly. Results revealed that the ovarian phenotype of APC2-deficient mice, characterized

by 50% reduction in number of corpora lutea, was not reversed after gonadotrophin administration, confirming an intra-ovarian origin for the observed phenotype (Figure 4.10-4.11). These findings are in accordance with previous results, which demonstrated the inability of exogenous gonadotrophin administration to rescue subfertility phenotype driven by WNT signalling activation, resulting from the expression of degradation-resistant β-catenin (Boerboom *et al.* 2005).

Reproducing results after exogenous gonadotrophin administration suggests intra-ovarian defects in response to gonadotrophin. Gonadotrophins (FSH and LH) transduce their signal to the ovary via binding with their receptors to initiate a signalling cascade (Fowler and Huhtaniemi 2002). Thus, a dysregulation in the expression of FSHR or LHCGR could be responsible for the subfertility phenotype. To test this hypothesis, gene expression analyses of *Fshr* and *Lhcgr* were performed (Figure 4.20). Results showed a 3.5 fold increase in *Lhcgr* expression levels in APC2-deficient mice. Although the molecular mechanism of subfertility induced by increased expression of *Lhcgr* is not yet understood, a recent study using a mouse model with a gain-of-function mutation in *Lhcgr* proved that overexpression of this receptor causes infertility in female mice (Hai *et al.* 2015). These mice were completely infertile, and histologic analysis of ovaries revealed failure of follicles to progress beyond the pre-antral stage (Hai *et al.* 2015). Whether this is resulting from disrupted expression of *Lhcgr* in certain follicular stages or to higher expression levels, or both, remains unanswered. Differences in the degree of infertility between this model and the APC2-deficient mouse model could be caused by differences in the intensity of overexpression of *Lhcgr* in the two models.

The upregulation of *Lhcgr* in APC2-deficient mice is caused by activation of canonical WNT signalling. This is evident from the work of Law *et al.* which revealed a 3.5 fold increase in *Lhcgr* expression levels in granulosa cells transduced with constitutively active β-catenin, in the presence of FSH (Law *et al.* 2013). Law group demonstrated that β-catenin

phosphorylated at Ser 552 and 675 binds to and activates TCF3 transcriptional activity, which binds to the *Lhcgr* promoter (Law *et al.* 2013). In addition, phospho-β-catenin binds to SF1 to facilitate its placement on *Lhcgr* promoter (Law *et al.* 2013). Both of these β-catenin-driven functions activate the transcription of *Lhcgr* gene, increasing its expression (Law *et al.* 2013).

In published GEMMs of canonical WNT-driven subfertility, upregulation of *Lhcgr* expression has not been previously proposed as a molecular mechanism of subfertility. Some of the published models quantified *Lhcgr* expression, but discrepancy in their results is evident. For example, Abedini *et al.* found a 2 fold increase in *Lhcgr* gene expression (Abedini *et al.* 2016), while De Cian *et al.* reported a decrease in *Lhcgr* expression (De Cian *et al.* 2016). This could be interpreted by differences in the follicular stage when canonical WNT signalling was activated, as well as to the phenotype produced. As mentioned previously, the subfertility phenotype reported by Abedini *et al.* is caused by defects in follicular development (Abedini *et al.* 2016), similar to subfertility phenotype developing in the current study, while the subfertility in De Cian *et al.* model is caused by defects in the ovulation process (De Cian *et al.* 2016).

4.3.4. Defective follicular growth is caused by increased apoptosis resulting from FOXO1 upregulation

Results of the current study revealed equivalent number of follicles in *Apc2*$^{+/+}$ and *Apc2*$^{-/-}$ mice (Figure 4.5). However, antral follicles from *Apc2*$^{-/-}$ ovaries were significantly smaller, failing to grow beyond a certain size (Figure 4.15). This was caused by increased apoptosis of granulosa cells, secondary to the increase of *Foxo1* expression levels (Figure 4.17-4.18).

It was previously mentioned that WNT signalling activation in early stages of follicular development, in the pre-antral follicles, restricts follicular growth (Li *et al.* 2014; Abedini *et al.* 2016). Previous studies have shown that this is mainly due to increased apoptosis of

granulosa cells; reflected by increases in active caspase 3 expression (Abedini *et al.* 2016) or by using TUNEL assay (Li *et al.* 2014). However, WNT signalling activation later in folliculogenesis, in the antral follicles, reduced apoptosis and increased proliferation of granulosa cells (Fan *et al.* 2010a). The FOXO family members, FOXO1 and to a lesser extent FOXO3, appear to be main regulators of apoptosis in granulosa cells of ovarian follicles (Kajihara *et al.* 2009; Shen *et al.* 2012; Liu *et al.* 2013; Shen *et al.* 2014). However, they were not fully explored in the published GEMMs of ovarian subfertility. In addition, GEMMs studying the effects of overexpressing these factors on follicular growth are lacking.

In the current study, *Foxo1* expression levels increased by 25% in *Apc2*$^{-/-}$ ovaries (Figure 4.18). Similar to this finding, *Foxo1* expression was increased after treating cultured pre-antral granulosa cells with WNT3a (Stapp *et al.* 2014). Granulosa cell apoptosis of secondary follicle cultures treated with WNT activators was caused by the nuclear accumulation of another FOX member, the active FOXO3, secondary to inhibition of FOXO3 phosphorylation (Li *et al.* 2014). When apoptosis was markedly reduced in granulosa cells of antral follicles isolated from degradation-resistant β-catenin GEMM, this was accompanied by decreases in FOXO1 mRNA and protein experssion (Fan *et al.* 2010a).

FOXO1 induces apoptosis via regulating the intrinsic mitochondrial apoptotic pathway and/or the extrinsic apoptotic pathway (Zhang *et al.* 2011b). In the current study, the extrinsic pathway was not affected, as reflected by the expression levels of genes coding for FASL and TRAIL (Figure 4.18). However, the expression level of the gene encoding for the cell cycle regulator p27 was upregulated.

Apart from FOXO1 functions in apoptosis, it has been shown to function as a repressor of *Lhcgr* expression (Law *et al.* 2013). Choromatin immunoprecipitation analysis revealed that FOXO1 protein is localized to the *Lhcgr* promoter and functions to repress *Lhcgr* expression, necissating FOXO1 phosphorylation upon FSH stimulation to relieve that repression (Law *et*

al. 2013). A recent RNA deep sequencing study has shown that FOXO1 regulates the expression of most FSH-responsive genes in rat granulosa cells (Herndon *et al.* 2016). Whether the increase of *Foxo1* expression observed in the current study is a direct consequence of canonical WNT signalling activation, or a negative feedback mechanism to repress the upregulated *Lhcgr* remains unclear.

FOXO1 activity is tightly regulated by PTEN/PI3K/AKT signalling (Zhang *et al.* 2011b). Activation of PI3K signalling phosphorylates FOXO1 which is translocated out of the nucleus and becomes inactivated. In the current study, PI3K/AKT signalling was suppressed in *Apc2*$^{-/-}$ antral follicles, as a result of increased PTEN expression (Figure 4.19). The cross talk between canonical WNT signalling and PTEN/PI3K/AKT signalling is well established. For example, it has been shown that activation of canonical WNT signalling alone causes delayed tumour formation in the ovary due to over expression of PTEN (Boerboom *et al.* 2005; Tanwar *et al.* 2013). However, when PTEN was deleted, tumour formation was accelarated (Wu *et al.* 2007; Lague *et al.* 2008; Richards *et al.* 2012). Few studies have explored PTEN/FOXO1 activation in the context of WNT signalling activation as a possible molecular mechanism of subfertility in canonical WNT signalling GEMMs. One exception is the work done by Abedini *et al.* who addressed *Pten* expression in their study and their findings confirmed the upregulation of *Pten* in their subfertility model caused by WNT signalling activation post-Wnt5a deletion (Abedini *et al.* 2016).

4.3.5. Defective steroidogenesis in *Apc2*$^{-/-}$ follicles

The ovary is responsible for the production of female sex hormones estradiol and progesterone, in addition to its ovulatory function (Jamnongjit and Hammes 2006). Progesterone is produced by luteal cells of corpora lutea formed post-ovulation. However, estradiol production in the antral follicles happens in 2 stages; the first stage occurs in theca

cells producing androgens, while the second stage happens in granulosa cells to produce estradiol (Jamnongjit and Hammes 2006).

In the current study, measuring serum levels of estradiol and progesterone were attempted (results not shown). However, as serum samples were hemolyzed, results were not considered reliable. Instead, quantifying expression levels of enzymes catalyzing the rate limiting steps of steroid synthesis was performed (Figure 4.21). *Cyp11a1* gene encodes for the enzyme cholesterol side chain cleavage (P450scc) which catalyzes the first reaction of steroid synthesis in all mammalian tissues (Miller and Bose 2011). In the current study, *Cyp11a1* expression was not changed after APC2 loss. This indicates that the ability of theca cells, granulosa cells and luteal cells to produce progesterone from cholesterol was not affected. This finding is similar to the findings of Abedini *et al.* who reproted that ovarian *Cyp11a1* expression levels were not changed after WNT signalling activation (Abedini *et al.* 2016). However, this finding was different from other studies which showed a decrease in *Cyp11a1* expression after activation of WNT signalling (Li *et al.* 2014; Stapp *et al.* 2014; De Cian *et al.* 2016). These discrepancies could be -in part- caused by differences in the models used in these studies. In three of them, gene expression levels were performed using cultured granulosa cells (Li *et al.* 2014; Stapp *et al.* 2014; Abedini *et al.* 2016). Only in the study (De Cian *et al.* 2016), *Cyp11a1* expression level was performed on whole ovaries. However, these ovaries were isolated from immature superovulated female mice.

Cyp17a1 encodes the enzyme 17alpha-hydroxylase/c17,20 lyase (P450c17), which is exclusively present in theca cells of growing follicles in the adult ovary (Zhang *et al.* 2001). This enzyme catalyses the conversion of progesterone into androgens (Jamnongjit and Hammes 2006). *Cyp19a1* encodes for the aromatase enzyme, which is exclusively present in granulosa cells of the growing follicle catalysing the conversion of androgens into estradiol (Jamnongjit and Hammes 2006). In the current study, a trend of increase in the number of antral follicles

was observed in ovaries of *Apc2*$^{-/-}$ mice. However, the expression levels of *Cyp17a1* and *Cyp19a1* were markedly reduced in *Apc2*$^{-/-}$ ovaries. This may indicate a defective differentiation of antral follicular cells, which impaired their steroidogenic functions. This defect happened in both theca cells and granulosa cells of antral and pre-ovulatory follicles.

In a model with perturbation of more than one signalling pathway, like the current study, it is difficult to dissect the cause of the observed phenotypes. For instance, canonical WNT signalling was reported to inhibit steroidogenesis via repressing *Cyp19a1* in cultured rat granulosa cells (Li *et al.* 2014; Stapp *et al.* 2014). Additionally, FOXO1 has been recently shown to repress FSH-responsive genes including *Cyp19a1* (Herndon *et al.* 2016). On the other hand, over expression of LHCGR caused a decrease in *Cyp17a1* expression in 6-week-old adult mice while not affecting *Cyp19a1* expression (Hai *et al.* 2015). Thus, it is the combination of, and interplay between, these different signalling pathways that ultimately shapes the observed phenotype, and it is perhaps naive to try and identify an individual factor as causative.

4.3.6. APC2 is essential for normal follicular vascularity

Angiogenesis plays important roles in normal ovarian homeostasis. Being a continuously cycling organ, good vascularity is required during follicle growth, ovulation and corpus luteum formation (Robinson *et al.* 2009). This vascular network surrounding the follicles and ramifying through the corpora lutea supplies the growing follicles and newly formed corpora lutea with nutrients, oxygen and hormones essential for their maturation (Robinson *et al.* 2009). In the current study, the effect of deleting APC2 on angiogenesis was investigated by visualizing new blood vessel formation using the endothelial marker CD34 (Figure 4.21). Results revealed intact vascularization of corpora lutea but reduced vascularity surrounding the growing follicles. This reduced vessel formation around follicles may be one of the mechanisms causing the restricted follicular growth and subfertility described here.

Little attention has been given to the degree of vascularity in previous studies exploring effects of canonical WNT signalling on ovarian homeostasis. Generally, effects of canonical WNT signalling on embryonic vasculature morphogenesis is well established, with canonical WNT signalling being activated in early angiogenesis (Corada *et al.* 2010). Work done with GEMMs showed that canonical WNT signalling should be tightly regulated in endothelial cells, with both loss-of-function (Cattelino *et al.* 2003) or gain-of-function (Corada *et al.* 2010) mutations of β-catenin impairing normal vascularization. Activation of canonical WNT signalling in adult angiogenesis was described in pathological conditions such as tumour formation (Boerboom *et al.* 2005). Other than this, canonical WNT signalling does not appear to be activated in resting adult vasculature (Dejana 2010).

Interaction between β-catenin and FOXO1 has been previously described (Taddei *et al.* 2008) to affect tight junctions in endothelial cells disrupting angiogenesis. FOXO1 represses Claudin 5, an endothelial specific junctional protein. This repression is intensified by β-catenin, by increasing FOXO1 transcriptional activity (Taddei *et al.* 2008). Bearing in mind the increase in expression levels of *Ctnnb1* and *Foxo1* in the current study, a similar synergistic effect could be the cause of reduced vascularity observed in the current study.

Vascular endothelial growth factors (VEGFs) are a group of cytokines, which are essential for neovascularization in many body organs including the ovary (Robinson *et al.* 2009). VEGFA is expressed in granulosa cells and theca cells of antral and pre-ovulatory, and in luteal cells of corpora lutea (Sargent *et al.* 2015). Using GEMMS, it has been reported that deleting *Vegfa* in granulosa cells of ovarian mice, as early as the secondary follicle stage using Amhr2-*cre*, caused subfertility due to restricted follicular growth resulting from increased apoptosis (Sargent *et al.* 2015). In the current study, a significant decrease in the expression of *Vegfa* was observed in $Apc2^{-/-}$ ovaries, which might have contributed to the subfertility phenotype reported, in a manner similar to the previous study (Sargent *et al.* 2015). Bearing in

mind that the qRT-PCR was done on whole ovaries, this reduction in *Vegfa* expression could also mirror the reduction in the number of corpora lutea observed in *Apc2*$^{-/-}$ ovaries.

4.3.7. Conclusion and future work

For the first time, the pleiotropic roles of APC2 protein in ovarian homeostasis have been unravelled; with the overall finding that loss of APC2 causes subfertility with 100% penetrance. Loss of APC2 activated canonical WNT signalling in the ovary. The subfertility phenotype described here is due to restricted follicular growth resulting from increased apoptosis. This phenotype has previously been described when canonical WNT signalling was activated in early stages of follicular development. Thus, we propose that APC2 protein is present in growing follicles as early as the secondary stages, and that its presence is pivotal for suppressing canonical WNT activity to enable follicular maturation.

The molecular mechanisms causing this subfertility are diverse and may be linked to canonical WNT signalling activation on its own, or to its interactions with FOXO1 signalling. One of the molecular mechanisms revealed by the current study is the defect in response to gonadotrophins, and for the first time it is described here to be caused by upregulation of *Lhcgr* expression. A second mechanism is the upregulation of PTEN and its inhibitory effect on PI3K/AKT signalling, coupled with the upregulation of *Foxo1* expression. The upregulated *Ctnnb1*/*Foxo1* expression caused a decrease in aromatase expression and repressed the vascular network surrounding antral/pre-ovulatory follicles, which contributed to the restriction of follicular growth observed.

One limitation of the current study is performing the functional characterization on small groups (n=4). Increasing replicates in the groups used in the current study might help to confirm whether the non-significant changes (increases or decreases) observed are true changes which might be contributing to the reported subfertility phenotype. This might impact on the strength of conclusions which could be drawn from some of the datasets.

To better elucidate the effect of APC2 deletion on various ovarian compartments, inducible knockout systems can be used instead of the constitutive mouse used in the current study. Selectively knocking down APC2 in theca cells, granulosa cells of pre-antral and/or antral follicles as well as in luteal cells will give a clear evidence about APC2 localization and functions in these different cells.

Another question which still remains unanswered is whether a degree of redundancy/compensation is present between APC and APC2 in the ovary. Findings of the current study clearly show that APC2 is required for normal ovarian functioning, and that its loss has detrimental effects even in the presence of intact APC. Whether the same is true with APC is not clear. Based on Tanwar *et al.* work (Tanwar *et al.* 2013), it seems that the presence of intact APC2 in granulosa cells of pre-antral follicles could guard against any deleterious effects on ovarian fertility caused by APC deficiency. Whether this would be true if APC is deleted in other cells/stages is not yet characterized. One of the interesting questions would be to investigate the effect of deleting both genes together in cells of growing follicles at different stages. Based on the previous work done in the Clarke lab (Daly 2013), the outcome would be difficult to predict. When both APC and APC2 were deleted in the mammary gland, tissue homeostasis was disrupted (Daly *et al.* 2016). However, deleting APC2 in the liver of hypomorph $Apc^{fl/fl}$ mouse rescued liver homeostasis and attenuated tumour formation post-APC reduction (Daly 2013).

More experiments need to be directed to investigate whether the molecular mechanisms described in the current studyare common between activated canonical WNT subfertility models. Defining these molecular mechanisms and relating them to activated canonical WNT signalling may direct the use of WNT inhibitors in the treatment of infertility. It is also crucial to investigate whether WNT signalling is misregulated in infertile women and whether this is general or related to specific diseases e.g. endometriosis (Sanchez *et al.* 2014).

5. Characterizing APC2-deficiency in ovaries of aging mice

5.1. Introduction

5.1.1. Granulosa cell tumours (GCTs)

Ovarian tumours are classified into epithelial ovarian cancers (90%), sex cord-stromal tumours (7%) and germ cell tumours (3%). Granulosa cell tumours (GCTs) are the most prevalent sex cord-stromal tumours, accounting for 5% of ovarian cancer cases diagnosed (Colombo *et al.* 2009). They originate from granulosa cells of ovarian follicles and are classified into 2 types; adult GCTs which represent more than 90% of the cases diagnosed, with the remaining classified as juvenile GCTs (Sekkate *et al.* 2013). The gold standard treatment for GCT is complete surgical debulking followed by chemotherapy (Khosla *et al.* 2014). Generally, GCTs have a good prognosis, with the majority of patients being diagnosed in early stages (Khosla *et al.* 2014). However, tumours can recur very late after resection of the primary tumour; the latest recurrence reported was 40 years after initial tumour removal (East *et al.* 2005). This highlights the need for a life-long follow up of GCT cases to avoid complications.

5.1.2. WNT signalling in adult GCTs

Historically, most of the research directed towards identifying the molecular mechanisms behind GCT development studied signalling pathways controlling normal granulosa cell proliferation, focusing on those regulated by FSH (Jamieson and Fuller 2012). This was followed by characterizing roles of oncogenes or tumour suppressor genes known to have roles in carcinogenesis (Jamieson and Fuller 2012). During the last decade, a somatic missense mutation in the *FOXL2* gene (c.402C→G; p.C134W) was detected in 97% of adult GCTs, and was suggested to be oncogenic (Shah *et al.* 2009).

Boerboom *et al.* were the first group to investigate roles of WNT signalling in GCTs (Boerboom *et al.* 2005). Performing immunohistochemistry for β-catenin on equine and human ovarian GCT samples, their results reflected the presence of nuclear β-catenin in 77.8% and 16.7% of equine and human GCT samples analysed, respectively (Boerboom *et al.* 2005). Based on the hypothesis that over-activated WNT signalling can cause adult GCT formation, Boerboom *et al.* generated a GEMM expressing a degradation-resistant β-catenin in granulosa cells of growing follicles and OSE using Amhr2-*cre*, which caused 57% of mice to develop GCTs by 7.5 months of age (Boerboom *et al.* 2005). Tumour formation in this model was accelerated after *Pten* loss or *Kras* activation (Lague *et al.* 2008; Richards *et al.* 2012). Activation of WNT signalling in another GEMM, by introducing a gain-of-function mutation of R-spondin1, caused the formation of adult GCTs in 15.8% of mice aging 12-18 months (De Cian *et al.* 2016). Taken together, these data suggest that WNT signalling upregulation plays a role in GCT pathogenesis. However, additional aberration in other signalling pathways is required to decrease latency/increase progression (Lague *et al.* 2008; Richards *et al.* 2012).

More recent studies of human GCTs have supported the hypothesis that WNT signalling contributes to the pathogenesis of ovarian GCT. Kilnozo *et al.* reported the increase in gene expression and protein levels of β-catenin and LEF1 in human ovarian GCTs (Kilonzo *et al.* 2015). Another study showed the presence of β-catenin immunostaining (membranous and/or cytoplasmic) in all stage I adult GCT samples analysed (Stewart *et al.* 2013). However, β-catenin staining negatively correlated with risk of recurrence (Stewart *et al.* 2013). A recent molecular study conducted on 30 human ovarian GCTs showed epigenetic silencing of *DKK3*, reflected by an 80% increase in hypermethylation of the gene promoter (Xu *et al.* 2016). *DKK3* encodes for Dickkopf (DKK) protein, which antagonizes canonical Wnt/β-catenin signalling (Niehrs 2006), implying a need for WNT signalling activation for GCT development.

5.1.3. Aims, hypothesis and highlights.

The aim of the current study was to characterize effects of constitutive APC2 loss in ovaries of aging mice, with special attention to cyst formation and tumour development. To achieve this, ovaries from APC2-deficient and intact mice (on the background of hypomorph Apc^{fl} allele) were collected at different time points up to a maximum of 18 months. Based on previously published work (Boerboom *et al.* 2005; De Cian *et al.* 2016), we hypothesized that the activation of canonical WNT signalling observed in the 10-week-old ovaries of our APC2-deficient mice (Chapter 4) would drive ovarian GCT formation in a subset of aging mice.

For the first time, it is reported herein that APC2-deficiency increases the risk of ovarian GCT development in aging mice. Previous observations in the Clarke lab noted frequent fluid-filled cyst formation in aging $Apc2^{-/-}$ mice. Here, only one 18-month-old $Apc2^{+/-}$ mouse developed a fluid-filled cyst (3.45%). However, at least 20.7% of APC2-deficient mice developed ovarian GCTs as early as 12 months, compared to just 6.25% seen in one 18-month-old $Apc2^{+/+}$ mouse. Canonical WNT signalling was highly activated in APC2-deficient GCTs. This was associated with a very high expression of PTEN protein. The APC2-deficient GCTs recapitulate the histologic pattern and molecular signature of human adult GCTs.

5.2. Results

5.2.1. APC2-deficient aging mice develop ovarian GCTs

To investigate whether APC2-deficiency promotes cyst and/or tumour formation in aging mice, ovaries were collected from *Apc2*$^{+/+}$, *Apc2*$^{+/-}$ and *Apc2*$^{-/-}$ female mice as early as 6 months of age. Unlike the mice analysed at 10-week time point (Chapter 4), all mice left to age were on a non-induced *Apc*$^{fl/fl}$ background. No tumours were detected in any of these cohorts at the 6-month time point. However, microscopic examination of serial-sectioned *Apc2*$^{+/+}$ and *Apc2*$^{-/-}$ ovaries revealed the presence of a range of cysts (Table 5.1 and Figure 5.1). *Apc2*$^{+/+}$ mice developed haemorrhagic corpus luteum cysts (40%, Figure 5.1a), and blood cysts (40%, Figure 5.1b). *Apc2*$^{-/-}$ mice did not display these types of cysts. Instead, *Apc2*$^{-/-}$ developed follicular cysts (40%, Figure 5.1c,d), and epithelial cysts (20%, Figure 5.1c,d). However, this differential pattern of cyst formation was not significant when tested with Chi-square test of independence.

Table 5.1: Frequency of cysts formed in 6 months old Apc2$^{+/+}$ and Apc2$^{-/-}$ ovaries.

Cyst formed \Genotype	**Corpus luteum cysts**	**Blood cysts**	**Follicular cysts**	**Epithelial cysts**
Apc2$^{+/+}$	2/5 (40%)	2/5 (40%)	0/5 (0%)	0/5 (0%)
Apc2$^{-/-}$	0/5 (0%)	0/5 (0%)	2/5 (40%)	1/5 (20%)

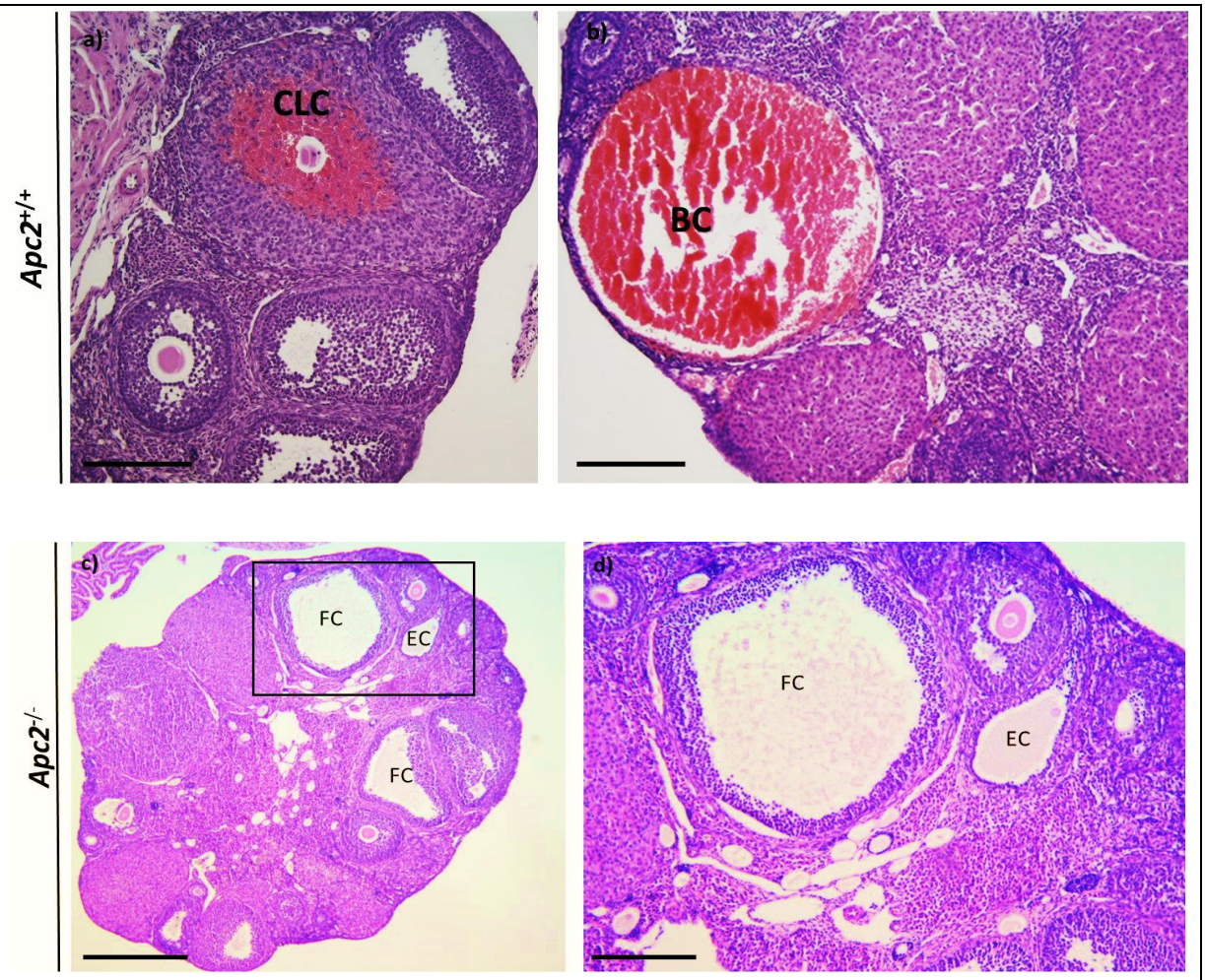

Figure 5.1: Ovarian cysts formed in 6-month-old *Apc2*$^{+/+}$ and *Apc2*$^{-/-}$ mice. Representative photomicrographs of (a) haemorrhagic corpus luteum cyst (CLC), (b) blood cyst (BC), (c) follicular cysts (FC) and epithelial cysts (EC). (d) 2.5X higher magnification of the inset in (c). n=5. Scale bars 200 µm, except (c) 500 µm.

A subset of *Apc2*$^{+/-}$ and *Apc2*$^{-/-}$ mice, accounting for at least 20.7% of the mice (6/29 mouse from both *Apc2*$^{+/-}$ and *Apc2*$^{-/-}$ cohorts at the 12 and 18 month time points), had developed ovarian adult granulosa cell tumours GCTs as early as 12 months of age (Table 5.2). All the mice developed unilateral tumours, apart from one 12-month-old *Apc2*$^{-/-}$ mouse, which developed bilateral tumours. Out of a cohort of nine *Apc2*$^{-/-}$ mice allocated to age to 18 months, only five survived to reach the endpoint. The other four succumbed earlier due to unknown causes, although a unilateral ovarian tumour was detected within one animal dissected at 17

months. Another animal was dissected post-mortem at the age of 12.5 month, but no ovarian tumours were detected. The remaining 2 mice died earlier (before 12 month) and were not dissected.

Table 5.2: Frequency of GCT formation in 12 and 18-month-old Apc2 experimental genotypes.

Ovarian lesion \Genotype	**Ovarian cysts**	**Ovarian granulosa cell tumour**
12-month-old *Apc2*$^{+/+}$	0/10	0/10
12-month-old *Apc2*$^{+/-}$	0/4	0/4
12-month-old *Apc2*$^{-/-}$	0/10	2/10 (20%) (one mouse developed bilateral tumours)
18-month-old *Apc2*$^{+/+}$	0/9	1/9 (11.1%)
18-month-old *Apc2*$^{+/-}$	1/9 (11.1%)	3/9 (33.3%)
18-month-old *Apc2*$^{-/-}$	0/6	1/6 (16.67%)

Tumours ranged in size from small microscopic *in situ* tumours to large macroscopic tumours (Figure 5.2a-e). Morphologically, they recapitulated human ovarian adult GCTs and showed a range of different histologic patterns (Figure 5.2f-l). The tumour cells were highly anaplastic (Figure 5.2m), and mitotic figures were evident (Figure 5.2n). Call-Exner bodies (formed of follicle remnants, Figure5.2j,o) and coffee-bean-shaped nuclei (Figure 5.2o), characteristic of adult GCTs, were occasionally present. Only one 18-month-old *Apc2*$^{+/-}$ mouse developed a large fluid-filled ovarian cyst (Table 5.2 and Figure 5.3a). Microscopic examination revealed it to be epithelial in nature (Figure 5.3b,c). This cyst is similar to the ones previously observed in the Clarke lab in *Apc2*$^{-/-}$ mice as early as 500 days old (Figure 5.3d,e).

Due to the limited tumour material collected in the time available for the study, further histologic analysis were performed on one 12-month-*Apc2*$^{-/-}$ tumour and three 18-month *Apc2*$^{+/-}$ tumours. Only one tumour from both cohorts was used for gene expression analysis. Although results were reproducible and trends of increase/decrease were clear, more samples will need to be gathered in order to test for the significance of variations observed.

Figure 5.2 (on the following page): Aging APC2-deficient mice develop adult GCTs. These tumours ranged in size from (a) small in situ tumours (arrow) to (b) small tumours of normal ovarian size, (c,d) small but macroscopically visible tumours or (E) large macroscopic tumour (arrow). The tumours displayed varying histologic patterns such as (F) follicular, (G) nodular (arrows), (H) insular, (I) luteinized (arrow: leutinized area shown at 4X original magnification in the inset, L:leutinized, NL: non-leutinized), (J) diffuse (arrow: Call-Exner body), and (K) cystic patterns. The tumours were (L) highly vascularized, (M) anaplastic, (N) mitotic (black arrow), and showed (O) Call-Exner body (black arrow) and coffee-bean nuclei (yellow arrow). Scale bars a-d: 500 µm, f-l: 100 µm, m-n: 50 µm, o: 20 µm.

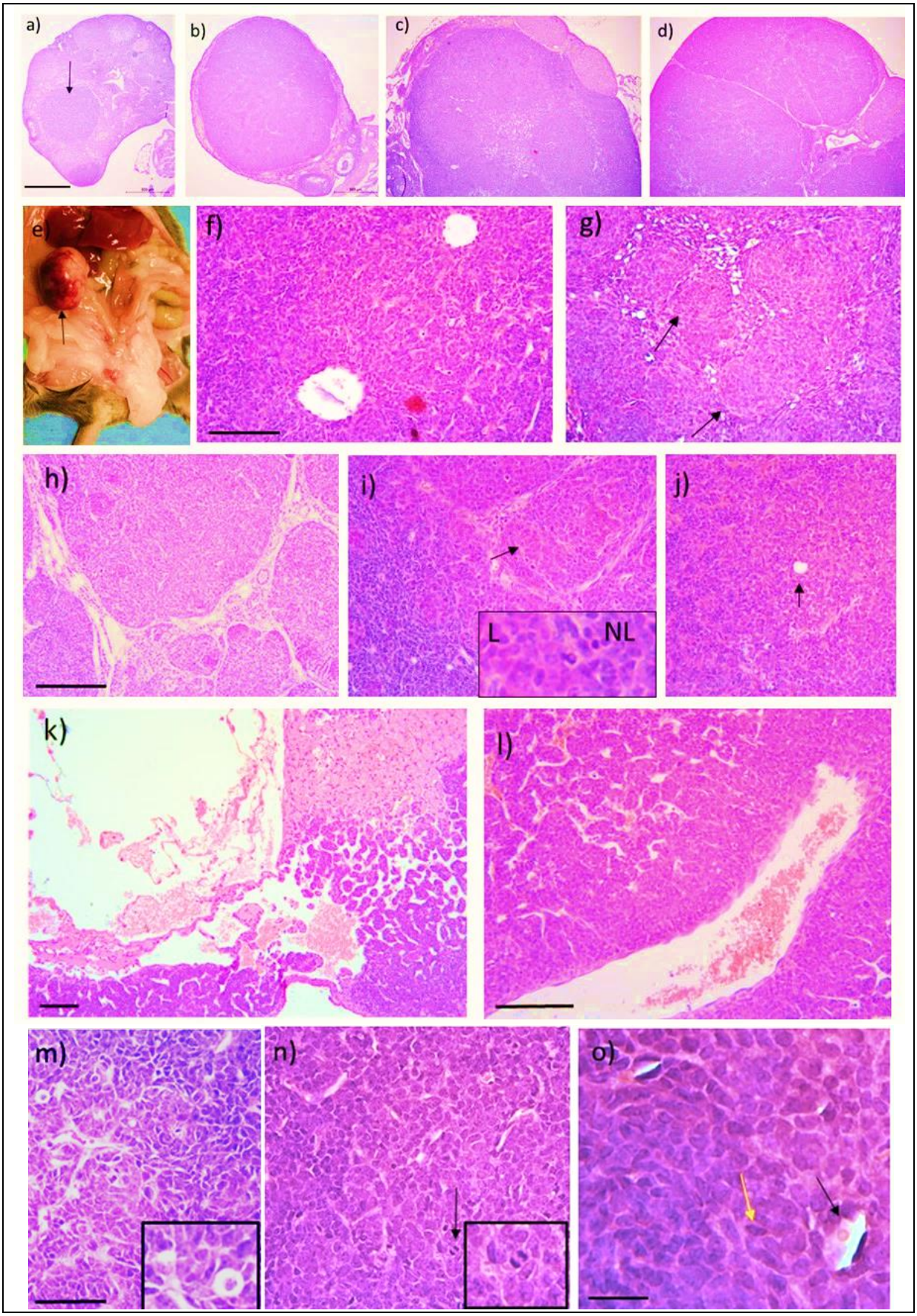
a)
b)
c)
d)
e)
f)
g)
h)
i)
L
NL
j)
k)
l)
m)
n)
o)

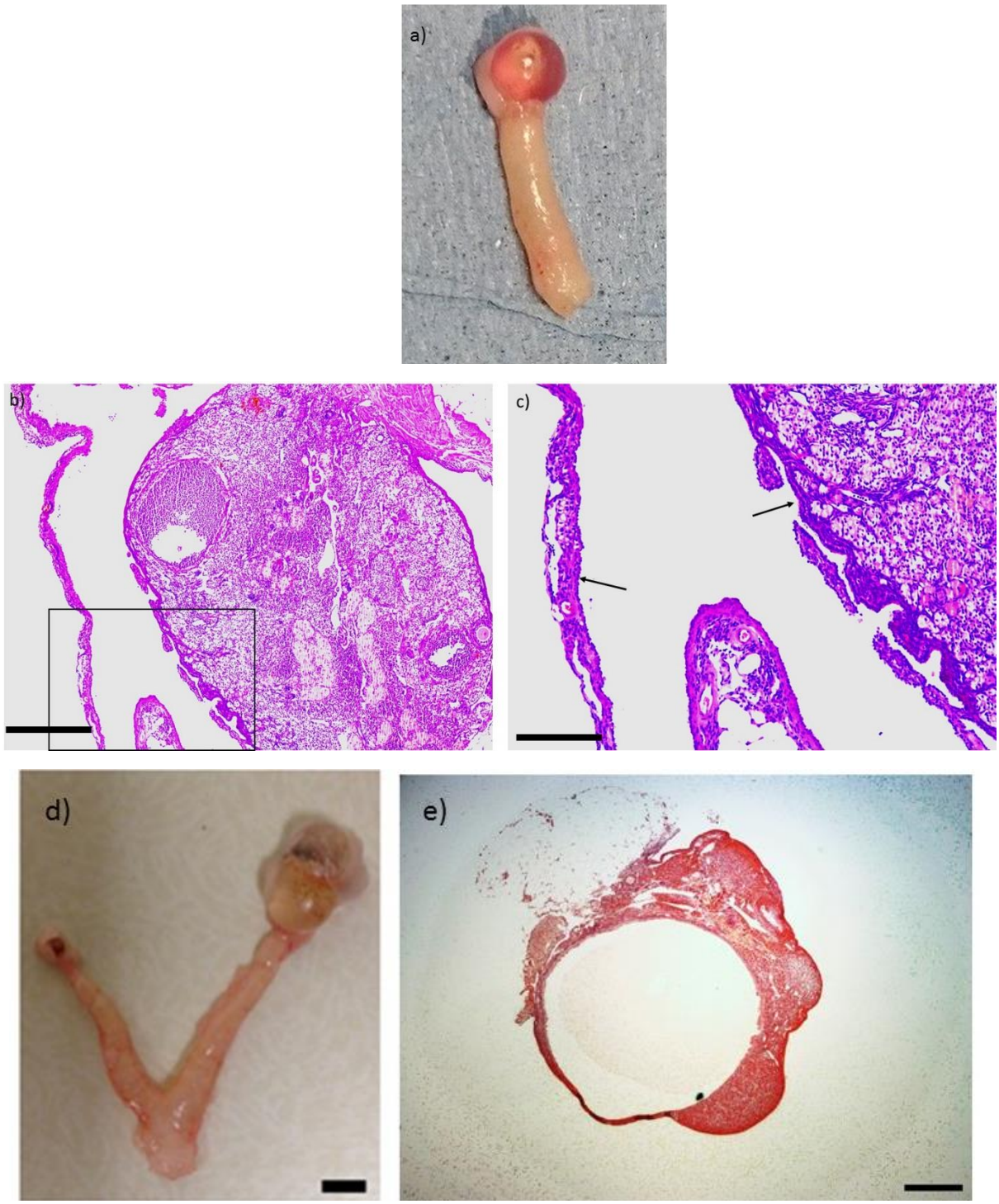

Figure 5.3: Cyst formation in an 18-month-old *Apc2*$^{+/-}$ mouse. Photograph of (a) the macroscopic cyst. (b) Photomicrograph of the cyst. Scale bar 500 µm. (c) 2.5X higher magnification of the inset in (b) (arrows point to epithelial lining of the cyst). Scale bar 200 µm. n=1. (d,e) Representative photographs of cyst developing in *Apc2*$^{-/-}$ ovaries, previously reported in the Clarke group (photos d,e were kindly provided by Dr. Carl Daly).

5.2.2. Activation of canonical WNT signalling drives tumourigenesis in APC2-deficient mice

In order to elucidate whether GCT formation observed in APC2-deficient mice is associated with WNT signalling upregulation, β-catenin IHC was performed on 3 tumours from the 18-month-old *Apc2*$^{+/-}$ cohort (Figure 5.4a), and one tumour from 12-month-old *Apc2*$^{-/-}$ cohort (Figure 5.4b). In all the stained sections, tumour areas (Figure 5.4 black arrows) strongly expressed β-catenin, in contrast to the weak expression encountered in the non-tumour areas (Figure 5.4 red arrows) of the ovary. This high expression was mostly cytoplasmic with frequent nuclear staining.

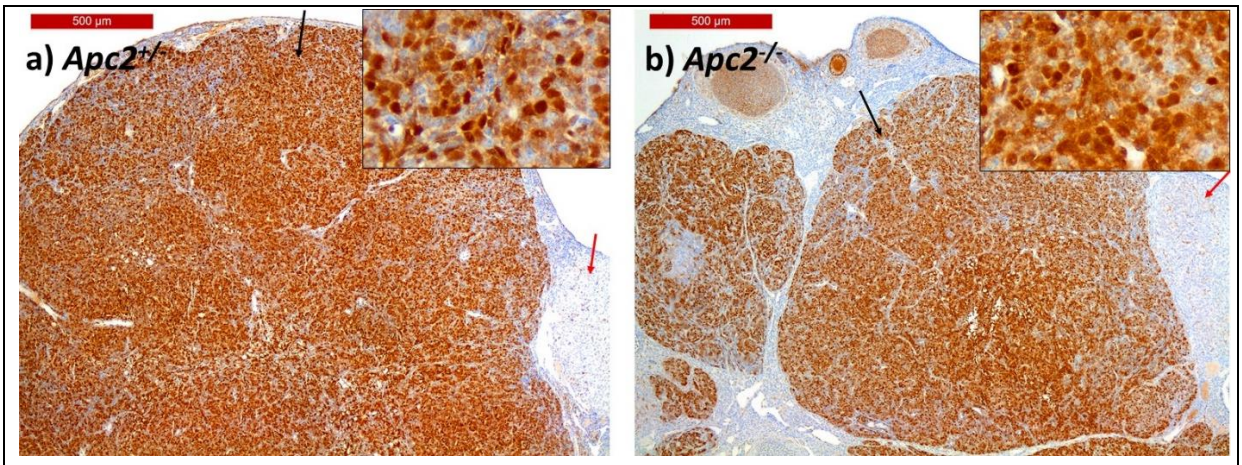

Figure 5.4: Expression of β-catenin protein in APC2-deficient GCTs. Representative photomicrographs of β-catenin immunohistochemistry in (a) 18-month-old *Apc2*$^{+/-}$ (n=3), and (b) 12-month-old *Apc2*$^{-/-}$ ovaries (n=1). Scale bar 500 µm. black arrow: GCT, red arrow: corpus luteum. Insets show GCTs at 5X original magnification.

In addition, gene expression analysis of a subset of Wnt-target genes was performed on one 12-month-old *Apc2*$^{-/-}$ ovarian tumour and one 18-month-old *Apc2*$^{+/-}$ tumour, using quantitative RT-PCR. For each tumour, RNA was extracted from two independent areas of the tumour and subsequently processed both to allow for tumour heterogeneity and to enable technical replicates to partly compensate for the lack of biological replicates. Gene expression

levels of samples from each tumour were compared to the expression levels of three age-matched *Apc2*$^{+/+}$ ovaries. A gene-dose-dependent increase in expression levels was observed for the Wnt-negative regulators *Wif1* (Figure 5.5a) and *Axin2* (Figure 5.5b), which were highly expressed in the tumours. *Apc* (Figure 5.5c) and *Fgf1* (Figure 5.5d) expression levels were only increased in *Apc2*$^{-/-}$ tumour samples. Whether this increase in *Apc* and *Fgf1* expression levels was time-dependent or gene dose-dependent could not be further analysed due to the limited tumour samples present.

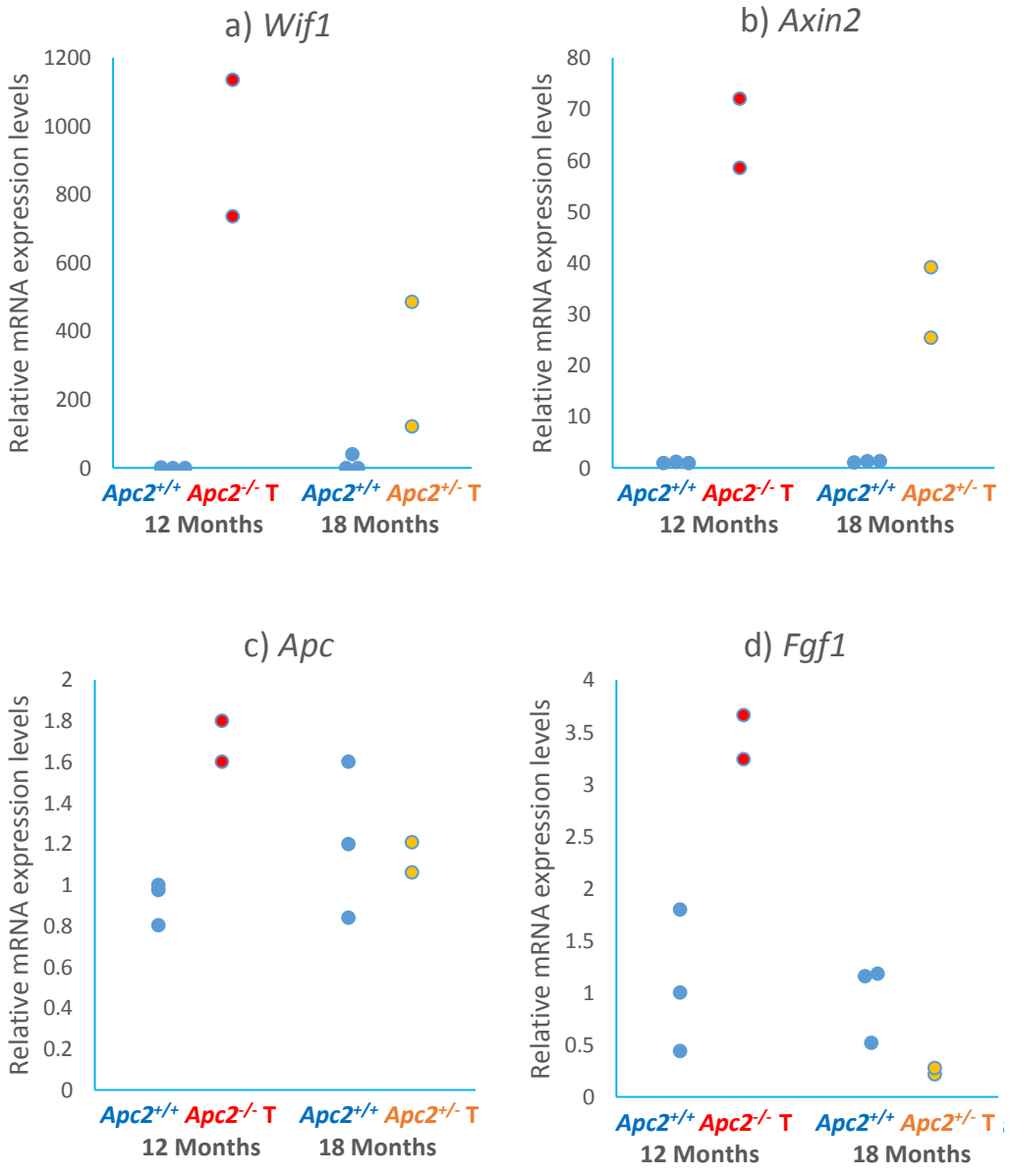

Figure 5.5: Gene expression levels of Wnt-target genes in APC2-deficient GCTs. Expression levels in APC2-deficient tumours (T) were compared to age-matched *Apc2*$^{+/+}$ ovaries using qRT-PCR and normalized to *Actb* expression. Expression levels of negative regulators of WNT signalling (a) *Wif1* and (b) *Axin2* were highly elevated in both tumours. However, expression levels of (c) *Apc* and (d) *Fgf1* were only increased in the 12-month *Apc2*$^{-/-}$ tumour. n=3 for 12-months and 18-months *Apc2*$^{+/+}$ groups. n=1 for 12-months *Apc2*$^{-/-}$ and 18-months *Apc2*$^{+/-}$ tumours, hence statistical analysis not appropriate (results display 2 independent samples from the same tumour). T:tumour.

5.2.3. APC2-deficient tumours are highly proliferative and vascularized

Sustained proliferation is one of the hallmarks of tumour formation (Hanahan and Weinberg 2011). In order to investigate whether this is the case in APC2-deficient GCTs, Ki67 immunohistochemistry was performed on 3 tumours from the 18-month-old *Apc2*$^{+/-}$ cohort (Figure 5.6a), and one tumour from 12-month-old *Apc2*$^{-/-}$ cohort (Figure 5.6b). All tumour areas showed frequent nuclear Ki67 staining, reflecting high proliferative activity.

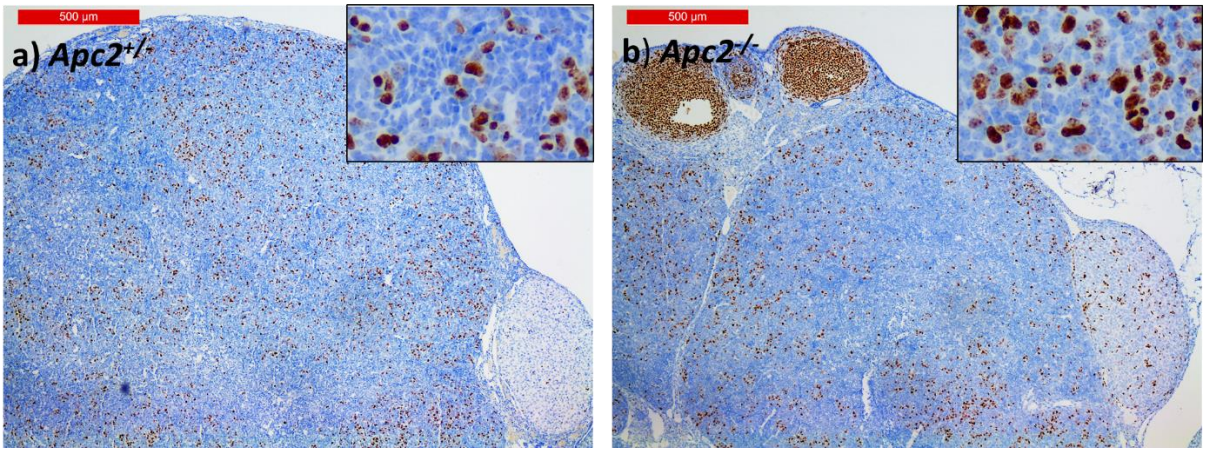

Figure 5.6: APC2-deficient GCTs are highly proliferative. Representative photomicrographs of (a) 18-month-old *Apc2*$^{+/-}$ tumour (n=3) and (b) 12-month-old *Apc2*$^{-/-}$ tumour (n=1). Scale bar 500 µm. Insets show GCTs at 5X original magnification.

Another hallmark of tumour progression is neovascularization (angiogenesis) in order to provide tumour cells with nutrients and oxygen required for growth (Hanahan and Weinberg 2011). Neovascularization was evaluated by CD34 immunostaining (Figure 5.7a,b) and *Vegfa* expression analysis using quantitative RT-PCR (Figure 5.7c). Immunohistochemical staining for CD34 protein revealed high vascularity of all the tumours analysed (Figure 5.7 a,b). *Vegfa* expression levels were elevated in both tumours (Figure 5.7c). However, it was further elevated in the 18-month *Apc2*$^{+/-}$ tumour, which was highly vascular macroscopically (Figure 5.2e) and microscopically (Figure 5.2l). Whether this increase in *Vegfa* expression level was time-

dependent, gene dose-dependent or morphology/size-dependent could not be further analysed due to the limited tumour samples present.

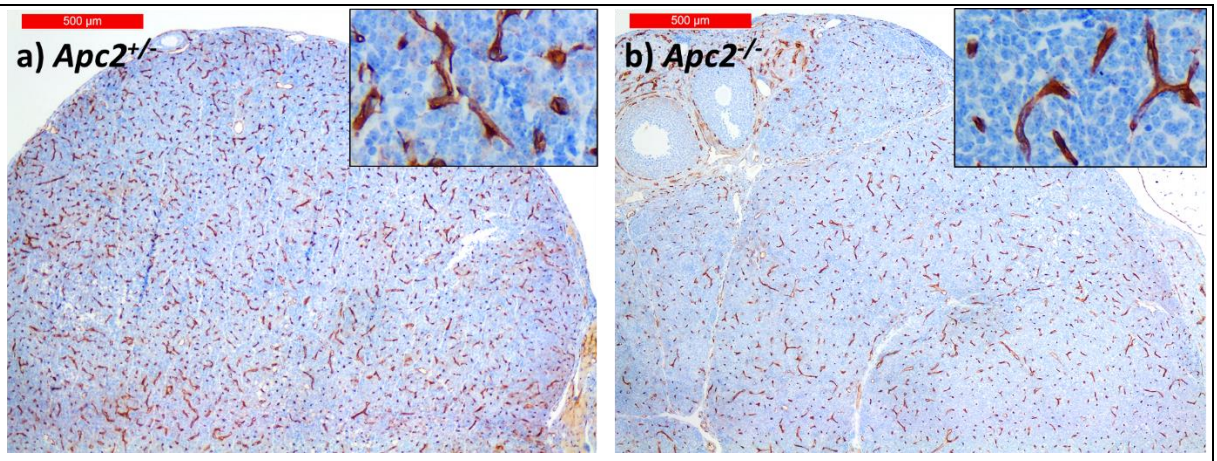

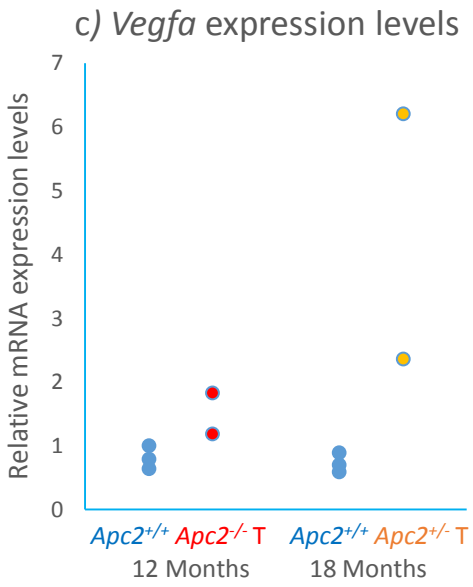

Figure 5.7: Neovascularization in APC2-deficient mice. Representative photomicrographs of CD34 IHC in (a) 18-month-old *Apc2*$^{+/-}$ (n=3), and (b) 12-month-old *Apc2*$^{-/-}$ (n=1) sections. Scale bar 500 µm. Insets show GCTs at 5X original magnification. (c) Gene expression analysis of *Vegfa* in APC2-deficient tumours (T) were performed and compared to age-matched *Apc2*$^{+/+}$ ovaries using qRT-PCR and normalized to *Actb* expression. n=3 for 12-months and 18-months *Apc2*$^{+/+}$ groups. n=1 for 12-months *Apc2*$^{-/-}$ and 18 months *Apc2*$^{+/-}$ tumours (results display 2 independent samples of the same tumour).

5.2.3. APC2-deficient tumour cells resist apoptosis

Resistance to cell death is an important feature of tumourigenesis (Hanahan and Weinberg 2011). Immunohistochemistry for the apoptotic protein cleaved caspase 3 was performed on APC2-deficient tumours. Apoptosis was rarely seen in APC2-deficient tumours (less than 0.5%), as reflected by absence of nuclear cleaved caspase 3 in most of tumour cells, in contrast to cells in non-tumour areas of the ovary (Figure 5.8).

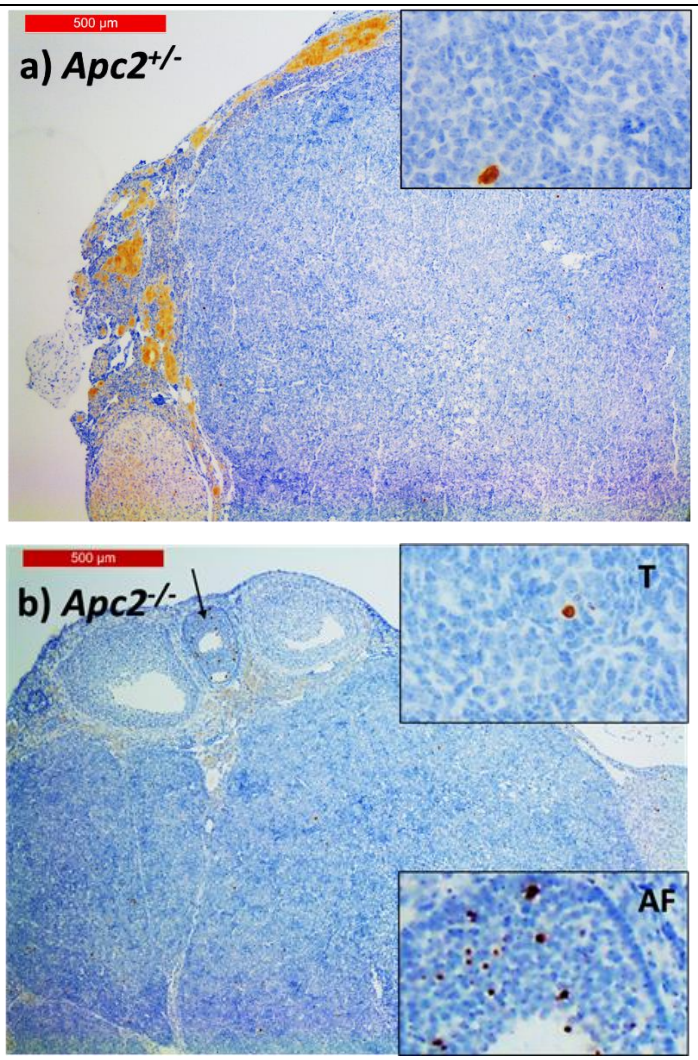

Figure 5.8: Absence of apoptosis in APC2-deficient GCTs. Representative photomicrographs of cleaved caspase 3 immunohistochemistry in (a) 18-month-old *Apc2*$^{+/-}$ (n=3), and (b) 12-month-old *Apc2*$^{-/-}$ (n=1) sections. Scale bar 500 µm. Insets show 5X original magnification. Black arrows denote positively-stained atretic follicle. T: tumour. AF: atretic follicle.

As previously mentioned in section 4.2.6, impaired follicular growth in *Apc2*$^{-/-}$ ovaries was caused by increased apoptosis resulting from increased *Foxo1* expression. However, in APC2-deficient GCTs, apoptosis was absent (Figure 5.8). It was thus crucial to determine *Foxo1* expression levels. IHC for FOXO1 protein showed that nuclear staining was not frequent in tumour cells, as compared to granulosa cells of growing follicles, which showed intense nuclear staining (Figure 5.9a,b). Gene expression analysis of *Foxo1* was performed on one 12-month-old *Apc2*$^{-/-}$ GCT and one 18-month-old *Apc2*$^{+/-}$ GCT. Results showed a downregulation of *Foxo1* expression in both tumours analysed (Figure 5.9c).

Kit ligand *Kitlg*, a pleiotropic factor expressed mainly in granulosa cells, has been shown to play anti-apoptotic roles in the ovary (Abdi *et al.* 2015). In the current study, expression levels of *Kitlg* were increased in both tumours analysed (Figure 5.9d).

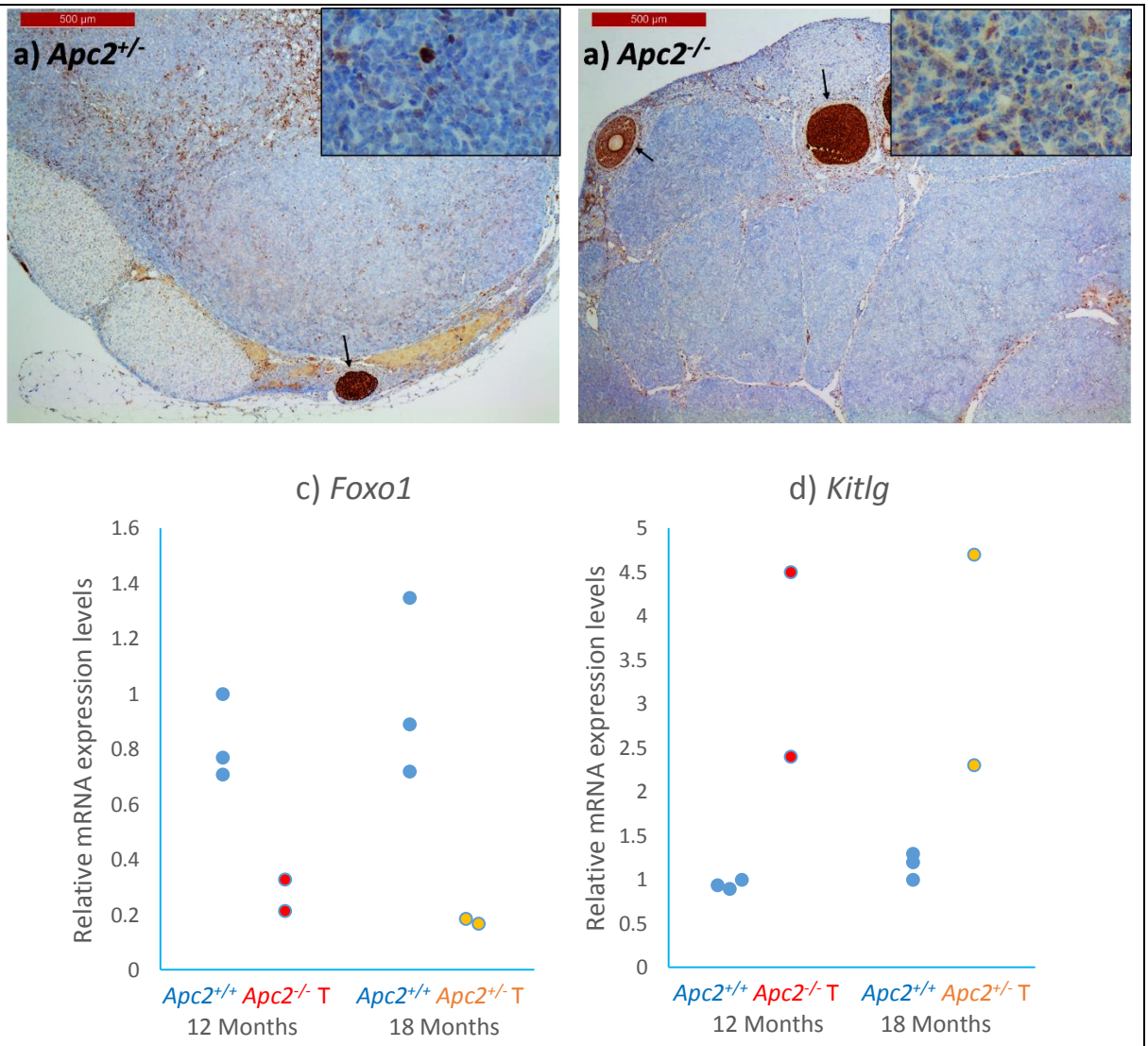

Figure 5.9: Absence of apoptosis observed in APC2-deficient GCTs is associated with downregulation of *Foxo1* and upregulation of *Kitlg*. Representative photomicrographs of FOXO1 immunohistochemistry in (a) 18-month-old *Apc2*$^{+/-}$ (n=3), and (b) 12-month-old *Apc2*$^{-/-}$ (n=1) sections. Scale bar 500 µm. Insets show GCTs at 5X original magnification. Arrows denote positive nuclear staining in growing follicles. Gene expression analysis of (c) *Foxo1*, and (d) *Kitlg* in APC2-deficient tumours (T) were performed and compared to age-matched *Apc2*$^{+/+}$ ovaries using qRT-PCR and normalized to *Actb* expression. n=3 for 12-months and 18-months *Apc2*$^{+/+}$ groups. n=1 for 12-months *Apc2*$^{-/-}$ and 18 months *Apc2*$^{+/-}$ tumours (results display 2 independent samples of the same tumour). T:tumour.

5.2.4. APC2-deficient GCTs recapitulate molecular signature of human adult GCTs

In the last decade, much attention has been given to the role of FOXL2 in adult GCT pathogenesis. It became clear that 97% of adult GCTs carry a somatic missense mutation in the *FOXL2* gene (genomic 402C→G; protein C134W) (Shah *et al.* 2009). Several studies have shown an increase in FOXL2 protein expression in GCTs in human and animal models (D'Angelo *et al.* 2011; Liu *et al.* 2015; Gao *et al.* 2016). In order to investigate whether this is the case in our model, FOXL2 protein and gene expression analysis were performed by immunohistochemistry and quantitative RT-PCR, respectively. Both the protein (Figure 5.10a,b) and gene expression levels (Figure 5.10c) were elevated in APC2-deficient GCTs.

Human adult GCTs of the ovary are characterized by frequent focal immunohistochemical staining for estrogen receptor alpha ERα (Farinola *et al.* 2007). In order to test whether GCTs developing in APC2-deficient mice retain this feature, immunohistochemical staining for ERα was performed. Frequent nuclear ERα staining was evident in all tumours (Figure 5.11a,b). However, the staining in the 12-month-old *Apc2*$^{-/-}$ tumour (Figure 5.11a) was more frequent and more focal as compared to the staining in the 18-month-old *Apc2*$^{+/-}$ tumour (Figure 5.11b). The pattern seen in the immunohistochemical staining correlated with the expression levels of *Esr1* gene (Figure 5.11c), being more expressed in *Apc2*$^{-/-}$ tumour as compared to *Apc2*$^{+/-}$ tumour. Whether this increase is gene-dose dependent or age-dependent could not be further analysed due to limited tumour samples available.

Although estrogen receptor β (ERβ) is known to be highly expressed in ovarian GCTs, poor prognosis is associated with loss of expression of the protein (Staibano *et al.* 2003). In order to identify the status of expression of ERβ in the current study, quantitative RT-PCR was used to determine the gene expression levels of *Esr2*, the gene coding for ERβ protein. *Esr2*

was decreased in both the 12-month-*Apc2*$^{-/-}$ and the 18-month-*Apc2*$^{+/-}$ tumour (Figure 5.11d), however the expression was more variable in the 12-month-*Apc2*$^{-/-}$ tumour.

Inhibin is a secreted glycoprotein formed of 2 subunits (alpha and beta), belongs to the TGFβ family of growth factors, and is known to inhibit FSH secretion from the pituitary glands (Yamashita *et al.* 1997). Previous studies have reported that inhibin levels are elevated in GCTs, where ovarian inhibin secretion is increased resulting in elevated serum levels (Yamashita *et al.* 1997). In order to assess whether inhibin is elevated in APC2-deficient GCT, immunostaining of the inhibin α subunit was performed. Results revealed focal cytoplasmic staining for inhibin α in 18-month-*Apc2*$^{+/-}$ and 12-month-*Apc2*$^{-/-}$ GCTs, with more abundant presence in the 12-month-*Apc2*$^{-/-}$ GCTs (Figure 5.12a,b).

Activin, another TGFβ growth factor, has been previously shown to contribute to GCT development in mice, and is known to bind to activin receptor type II (ACVRII) before signalling through activin receptor type I (ACVRI) (Kim *et al.* 2016). Gene expression analysis was performed for *Acvr1* in 18-month-*Apc2*$^{+/-}$ and 12-month-*Apc2*$^{-/-}$ GCTs, reflecting an increased expression in GCTs from both genotypes (Figure 5.13c). However, *Acvr1* expression was more consistent and elevated in the 12-month-*Apc2*$^{-/-}$ GCT analysed compared to the 18-month-*Apc2*$^{+/-}$ GCT, whose expression reflected a considerable degree of tumour heterogeneity (Figure 5.12c).

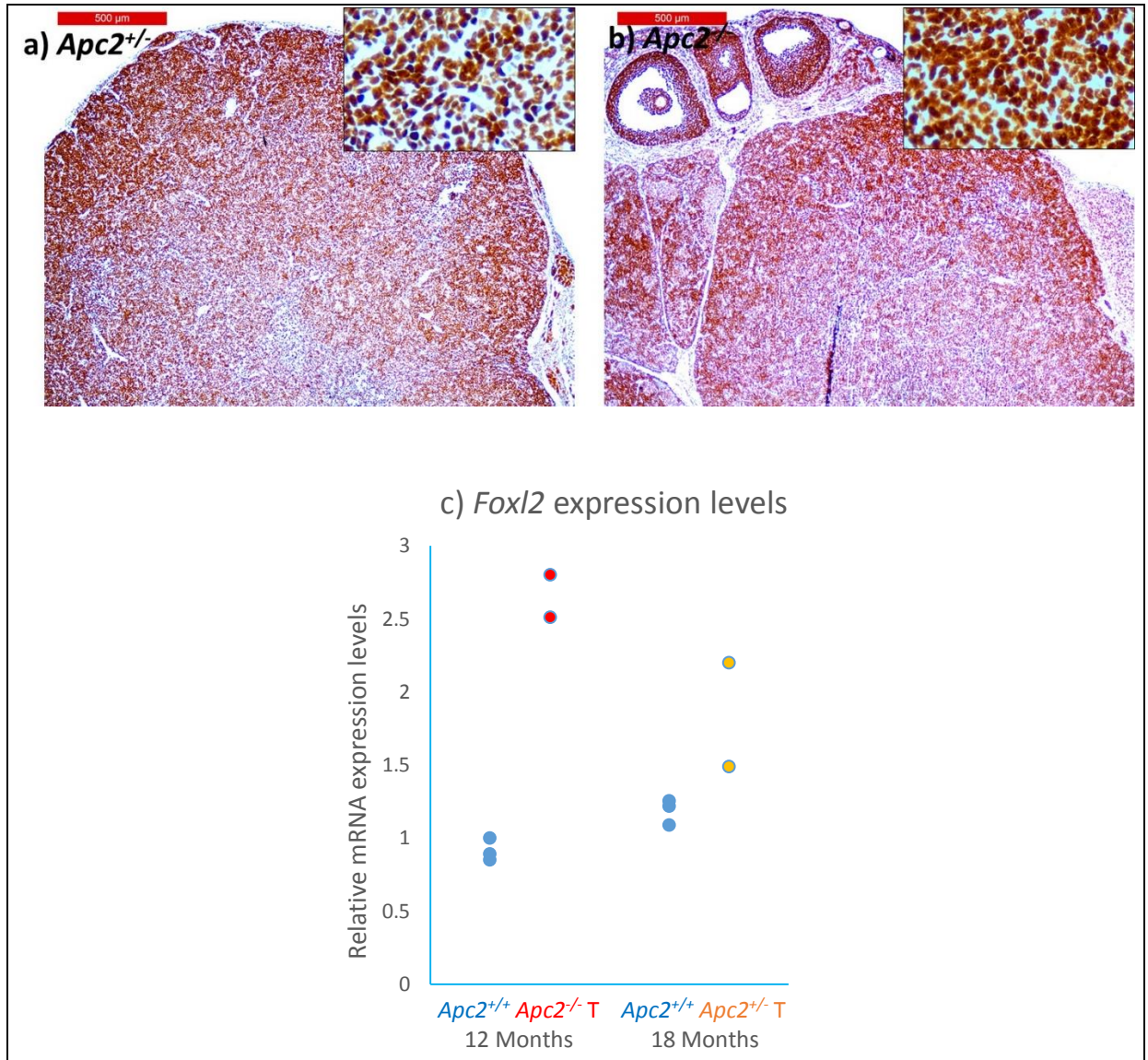

Figure 5.10: Upregulation of FOXL2 in APC2-deficient GCTs. Representative photomicrographs of FOXL2 immunostaining in (a) 18-month-old *Apc2*$^{+/-}$ (n=3), and (b) 12-month-old *Apc2*$^{-/-}$ (n=1) sections. Scale bar 500 µm. Insets show GCT at 5X original magnification. (c) Gene expression analysis of *Foxl2* in APC2-deficient tumours (T) were performed and compared to age-matched *Apc2*$^{+/+}$ ovaries using qRT-PCR and normalized to *Actb* expression. n=3 for 12-months and 18-months *Apc2*$^{+/+}$ groups. n=1 for 12-months *Apc2*$^{-/-}$ and 18 months *Apc2*$^{+/-}$ tumours (results display 2 independent samples of the same tumour). T:tumour.

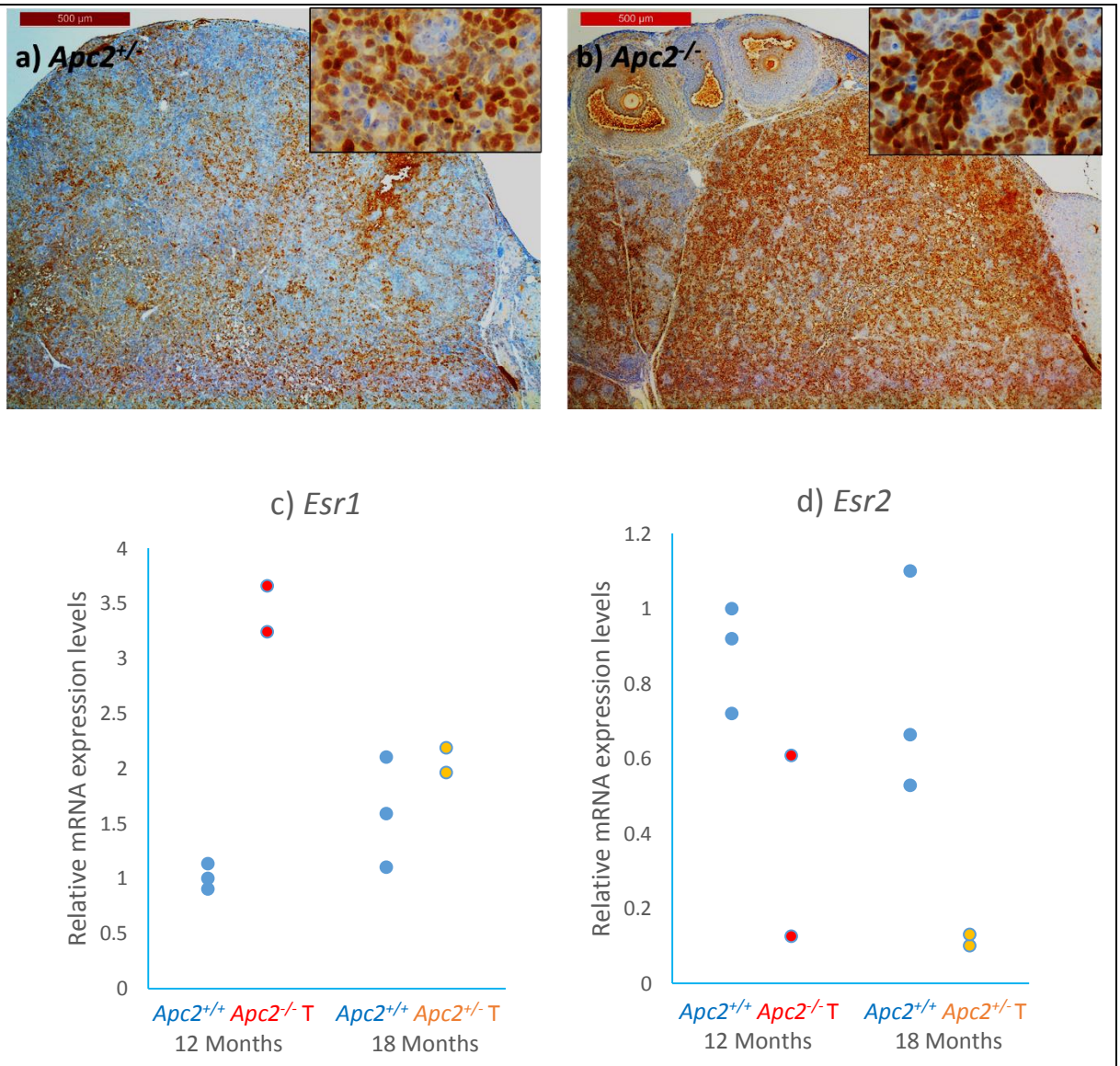

Figure 5.11: Expression of estrogen receptors in APC2-deficient GCTs. Representative photomicrographs of ERα immunohistochemical staining in (a) 18-month-old *Apc2*$^{+/-}$ (n=3), and (b) 12-month-old *Apc2*$^{-/-}$ (n=1) sections. Scale bar 500 µm. Insets show GCT at 5X original magnification. Gene expression analysis of (c) *Esr1*, and (d) *Esr2* in APC2-deficient tumours (T) were performed and compared to age-matched *Apc2*$^{+/+}$ ovaries using qRT-PCR and normalized to *Actb* expression. n=3 for 12-months and 18-months *Apc2*$^{+/+}$ groups. n=1 for 12-months *Apc2*$^{-/-}$ and 18 months *Apc2*$^{+/-}$ tumours (results display 2 independent samples of the same tumour). T:tumour.

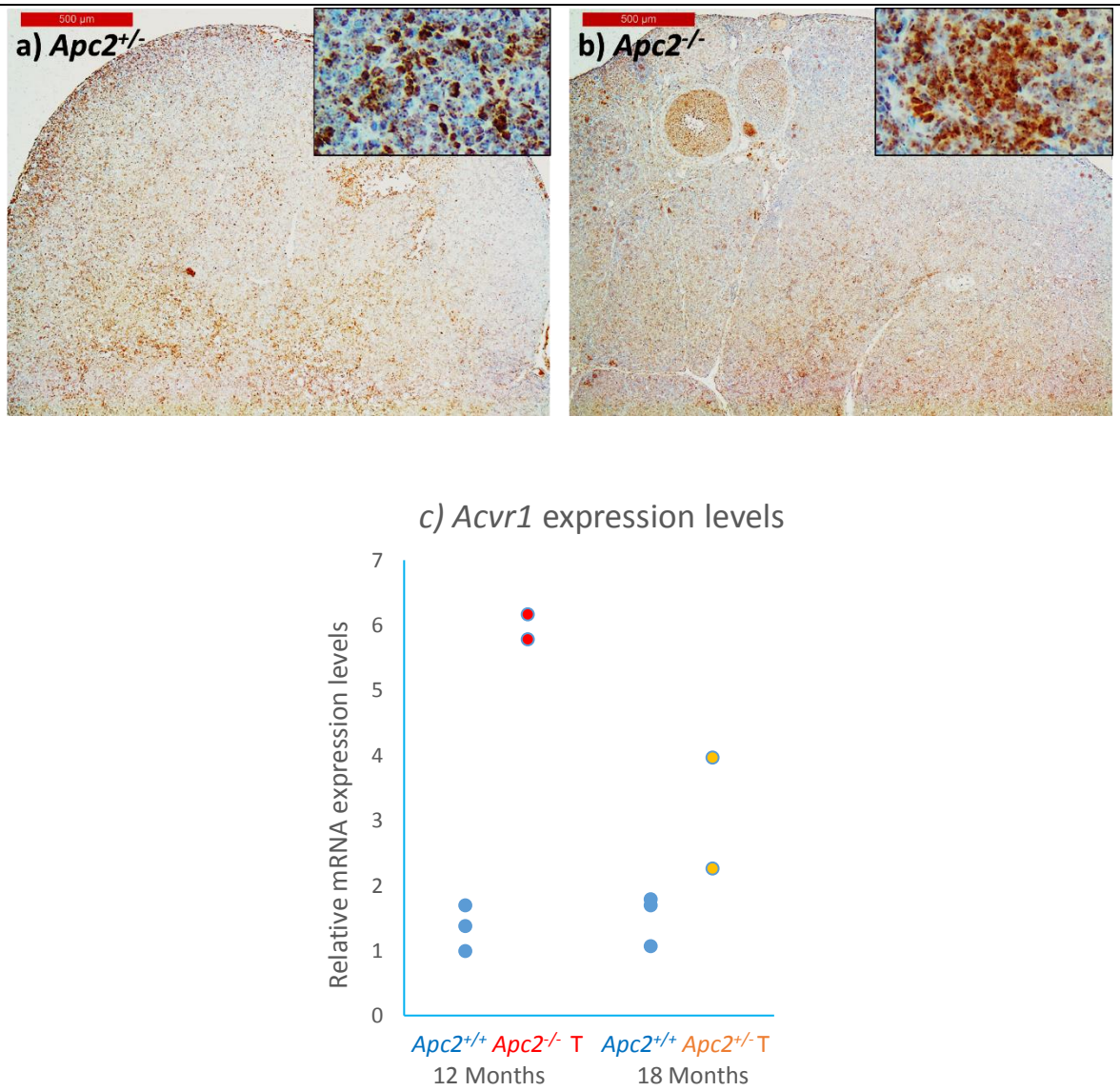

Figure 5.12: Expression analysis of members of TGFβ family of growth factors in APC2-deficient GCTs. Representative photomicrographs of inhibin α immunostaining in (a) 18-month-old *Apc2*$^{+/-}$ (n=3), and (b) 12-month-old *Apc2*$^{-/-}$ (n=1) sections. Scale bar 500 µm. Insets show GCT at 5X original magnification. (c) Gene expression analysis of *Acvr1* in APC2-deficient tumours (T) were performed and compared to age-matched *Apc2*$^{+/+}$ ovaries using qRT-PCR and normalized to *Actb* expression. n=3 for 12-months and 18-months *Apc2*$^{+/+}$ groups. n=1 for 12-months *Apc2*$^{-/-}$ and 18 months *Apc2*$^{+/-}$ tumours (results display 2 independent samples of the same tumour). T:tumour.

5.2.5. PI3K/AKT signalling does not contribute to GCT formation in APC2-deficient mice

In a previously-published adult GCT mouse model driven by WNT signalling activation, it was observed that activation of PI3K/AKT signalling via *Pten* deletion enhances GCT development and progression (Lague *et al.* 2008; Richards *et al.* 2012). Immunohistochemical staining for p-AKT and its downstream target p-FOXO1/3/4 were performed to analyze whether PI3K/AKT signalling contributes to tumour formation in the current study. Both p-AKT (Figure 5.13a,b) and p-FOXO1/3/4 (Figure 5.13c,d) proteins were completely absent in APC2-deficient tumours, in contrast to growing follicles present in the same ovarian section.

PTEN is a tumour suppressor which acts as a negative regulator for PI3K/AKT signalling by converting the active phosphatidyl inositol triphosphate PIP3 to the inactive phosphatidyl inositol biphosphate PIP2 (Georgescu 2010). Immunohistochemical staining and quantitative RT-PCR were performed on APC2-deficient tumours to quantify the expression of PTEN at the protein and gene level, respectively. PTEN protein was strongly expressed in APC2-deficient tumours. In 18-month-old *Apc2*$^{+/-}$ tumours, the protein showed frequent nuclear staining, estimated to range from 50% to 100% of all the tumour cells (Figure 5.14a). However, in the 12-month *Apc2*$^{-/-}$ tumour, the protein was expressed mainly in the cytoplasm with the presence of occasional nuclear staining estimated at 10% of the cells (Figure 5.14b). The mRNA expression level of *Pten* was increased in only one of the two samples analysed from the 12-month-*Apc2*$^{-/-}$ tumour, but was not changed in the 18-month-*Apc2*$^{+/-}$ tumour samples (Figure 5.14c).

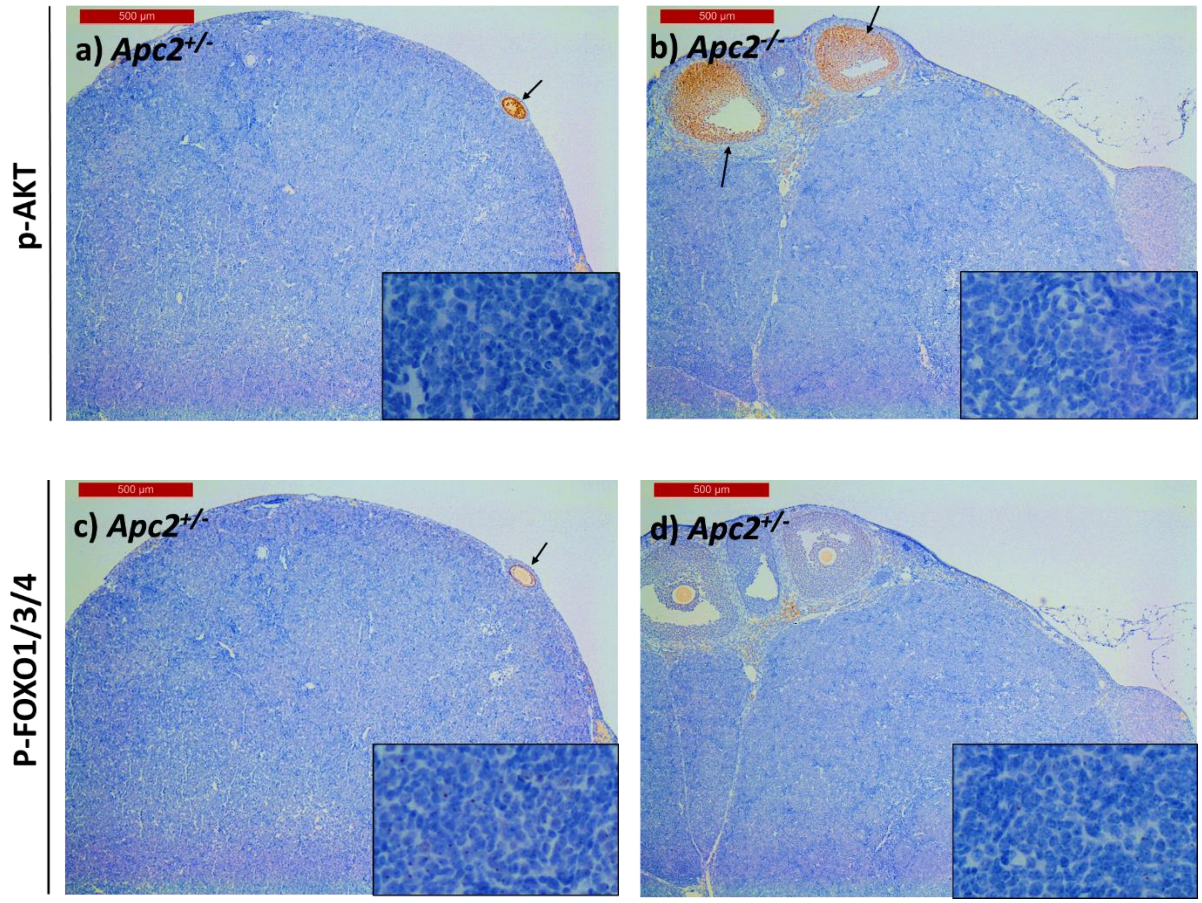

Figure 5.13: PI3K/AKT signalling does not contribute to adult GCT formation in APC2-deficient tumours. Representative photomicrographs of p-AKT immunohistochemical staining in (a) 18-month-old *Apc2*$^{+/-}$ (n=3), and (b) 12-month-old *Apc2*$^{-/-}$ (n=1) sections. Representative photomicrographs of p-FOXO1/3/4 immunohistochemical staining in (c) 18-month-old *Apc2*$^{+/-}$ (n=3), and (d) 12-month-old *Apc2*$^{-/-}$ (n=1) sections. Scale bar 500 µm. Insets show GCTs at 5X original magnification. Black arrows: growing follicles.

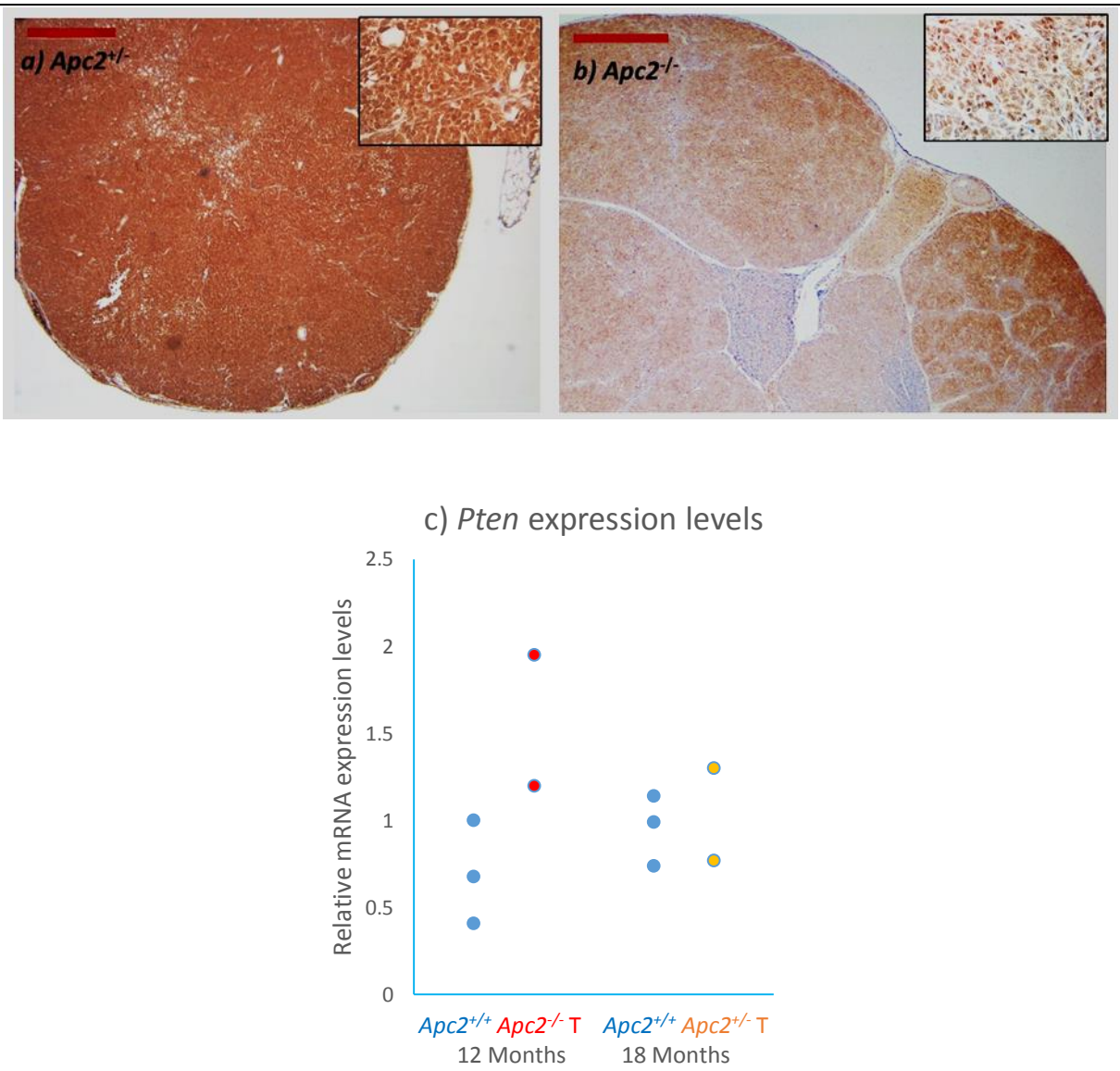

Figure 5.14: Upregulation of PTEN in APC2-deficient GCTs. Representative photomicrographs of PTEN immunohistochemical staining in (a) 18-month-old *Apc2*$^{+/-}$ (n=3), and (b) 12-month-old *Apc2*$^{-/-}$ (n=1) sections. Scale bar 500 µm. Insets show GCTs at 5X original magnification. (c) Gene expression analysis of *Pten* in APC2-deficient tumours (T) were compared to age-matched *Apc2*$^{+/+}$ ovaries using qRT-PCR and normalized to *Actb* expression. n=3 for 12-months and 18-months *Apc2*$^{+/+}$ groups. n=1 for 12-months *Apc2*$^{-/-}$ and 18 months *Apc2*$^{+/-}$ tumours (results display 2 independent samples of the same tumour). T:tumour.

5.2.6. Granulosa cell differentiation is compromised in APC2-deficient GCTs

Functional differentiation of granulosa cells was shown to be impaired in previously published GEMMs of adult GCT (Richards *et al.* 2012; Liu *et al.* 2015; Gao *et al.* 2016). To investigate whether granulosa cell differentiation was disrupted in the current study, quantitative RT-PCR was used to determine the expression level of a subset of genes known to control steroidogenesis (*Cyp11a1* and *Cyp19a1*, Figure 5.15a,b), response to gonadotrophins (*Fshr* and *Lhcgr*, Figure 5.16a,b) and hormone receptors (*Pgr* and *Ar*, Figure 5.16c,b). The expression levels of these six genes were downregulated in both tumours, apart from *Pgr* levels in the 12-month-old *Apc2*$^{-/-}$ tumour, which was highly variable. A degree of variability was present in expression levels of these genes in control mice (*Apc2*$^{+/+}$), which might be interpreted in light of loss of cyclicity due to menopause, causing severe reductions or loss of follicles in ovaries collected at 12 months and 18 months of age, respectively.

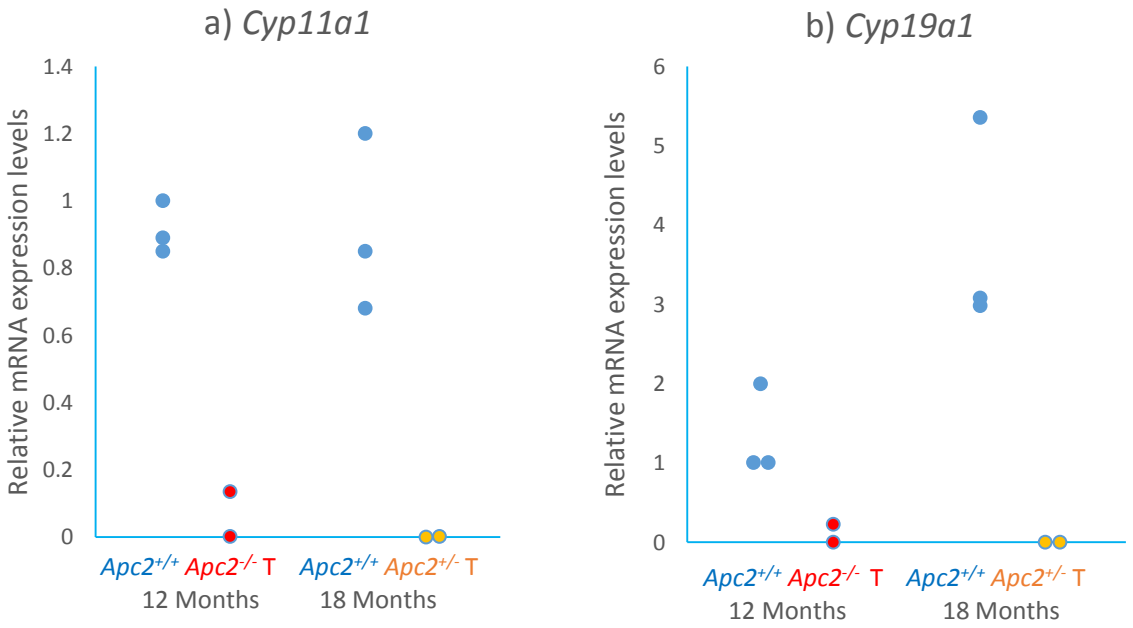

Figure 5.15: Impairment of granulosa cell-steroidogenic machinery in GCTs. Gene expression analysis of (a) *Cyp11a1* and (b) *Cyp19a1* in APC2-deficient tumours (T) were performed and compared to age-matched *Apc2*$^{+/+}$ ovaries using qRT-PCR and normalized to *Actb* expression. n=3 for 12-months and 18-months *Apc2*$^{+/+}$ groups. n=1 for 12-months *Apc2*$^{-/-}$ and 18 months *Apc2*$^{+/-}$ tumours (results display 2 independent samples of the same tumour). T:tumour.

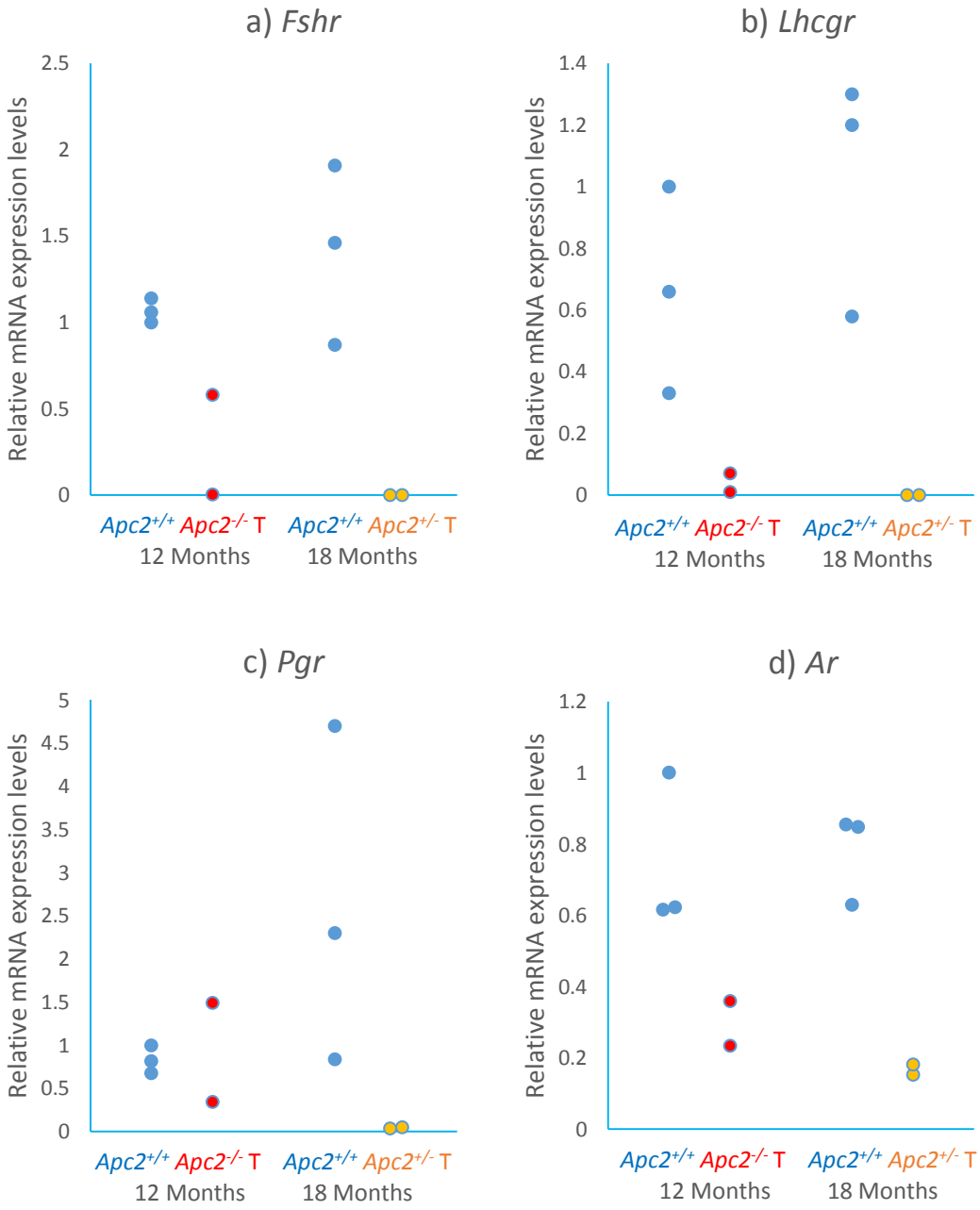

Figure 5.16: Impairment of granulosa cell-hormone response receptors in GCTs. Gene expression analysis of (a) *Fshr*, (b) *Lhcgr*, (c) *Pgr* and (d) *Ar* in APC2-deficient tumours (T) were compared to age-matched *Apc2*$^{+/+}$ ovaries using qRT-PCR and normalized to *Actb* expression. n=3 for 12-months and 18-months *Apc2*$^{+/+}$ groups. n=1 for 12-months *Apc2*$^{-/-}$ and 18 months *Apc2*$^{+/-}$ tumours (results display 2 independent samples of the same tumour). T:tumour.

5.2.7. Ovarian morphology is disrupted after GCT development

Recent reports of adult GCT GEMM revealed the presence of cells expressing epithelial markers within the tumour, in addition to their normal presence in the OSE (Liu *et al.* 2015; De Cian *et al.* 2016; Gao *et al.* 2016). Immunohistochemistry for the epithelial marker E-cadherin (Figure 5.17a,b) was performed to determine the localization of epithelial cells. E-cadherin was present in some parts of the OSE but completely absent elsewhere.

In the current study, apart from one tumour (Figure 5.2a), all tumours analysed caused the disruption of the ovarian architecture (Figure 5.2b-e) and replaced normal ovarian compartments such as follicles and corpora lutea. Molecular markers for some ovarian compartments were assessed using quantitative RT-PCR. The expression levels of *Gdf9* (oocyte marker, Figure 5.18a), *Cyp17a1* (theca cell marker, Figure 5.18b) and *Cdh1* (epithelial marker, Figure 5.18c) were reduced in both GCTs analysed, apart from *Cdh1* in 12-month *Apc2*$^{-/-}$ GCT. Again, a degree of variability was evident among control *Apc2*$^{+/+}$ mice which might be caused by age-related menopause.

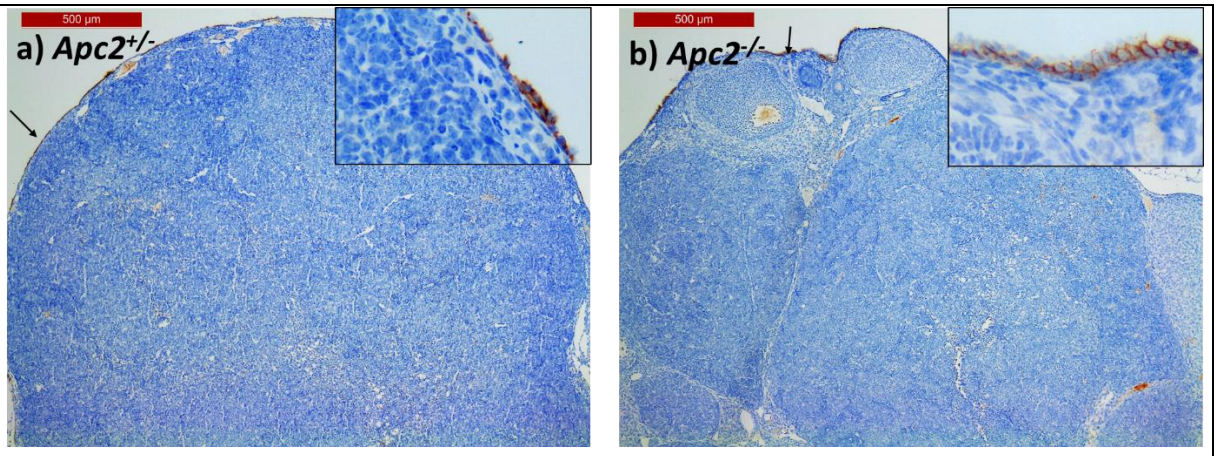

Figure 5.17: Characterizing epithelial traits of APC2-deficient GCTs. Representative photomicrographs of E-cadherin immunohistochemical staining in (a) 18-month-old *Apc2*$^{+/-}$ (n=3), and (b) 12-month-old *Apc2*$^{-/-}$ (n=1) sections. Insets show ovarian surface epithelium at 5X original magnification.. Scale bar: 500 µm. Black arrows: OSE.

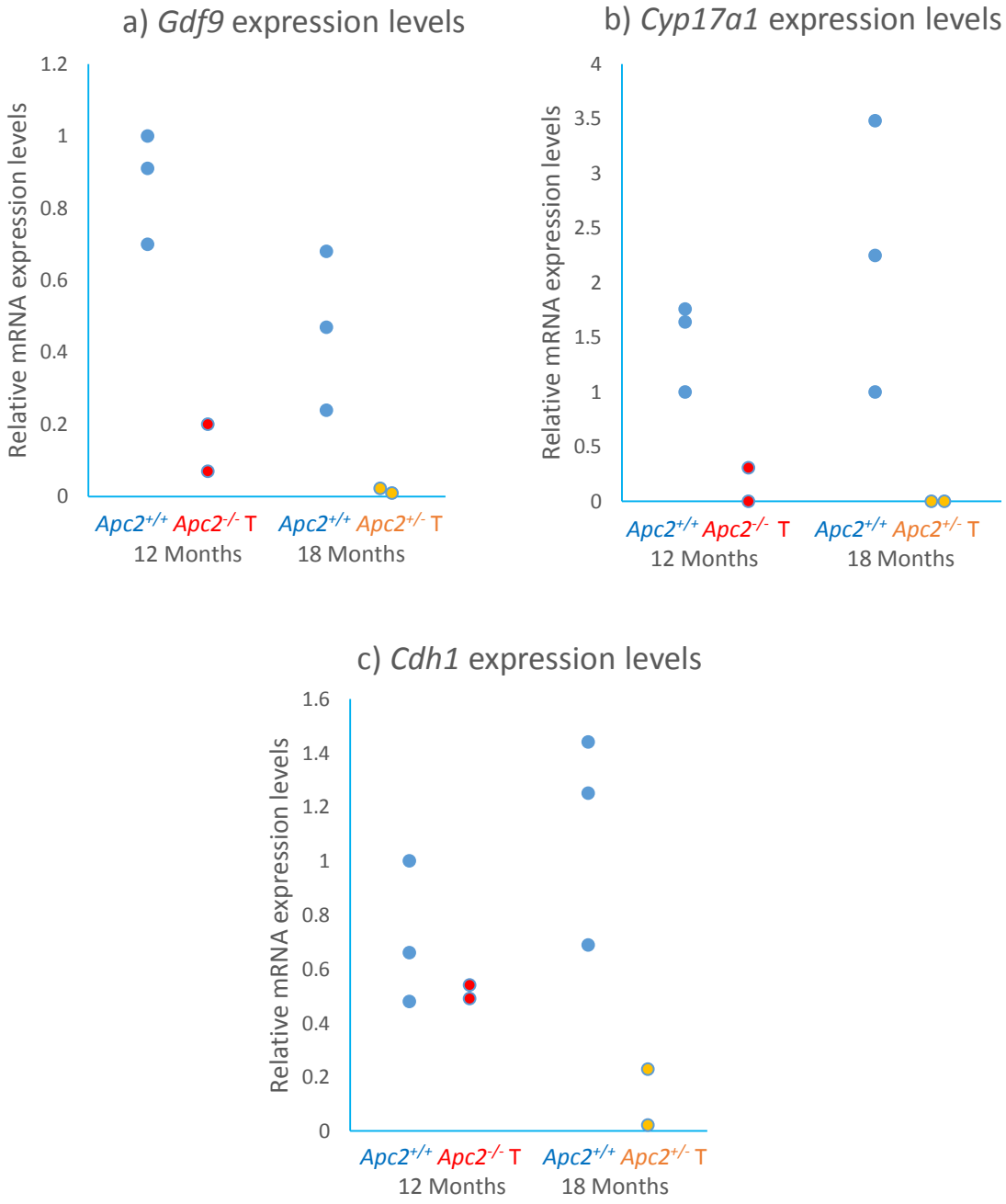

Figure 5.18: Disruption of normal ovarian architecture in APC2-deficient GCTs. Gene expression analysis of (a) *Gdf9*, (b) *Cyp17a1* and (c) *Cdh1* were performed in APC2-deficient tumours (T) and compared to age-matched *Apc2*$^{+/+}$ ovaries using qRT-PCR and normalized to *Actb* expression. n=3 for 12-months and 18-months *Apc2*$^{+/+}$ groups. n=1 for 12-months *Apc2*$^{-/-}$ and 18 months *Apc2*$^{+/-}$ tumours (results display 2 independent samples of the same tumour). T:tumour.

5.2.8. Characterizing the GCT developing in an *Apc*$^{fl/fl}$ mouse with intact APC2

As mentioned earlier, one of the 18-month-*Apc2*$^{+/+}$ mice (on the background of non-induced *Apc*$^{fl/fl}$) developed a small GCT (Table 5.2). The non-induced hypomorphic *Apc*$^{fl/fl}$ allele was previously shown to initiate hepatocellular carcinoma in mice with 100% penetrance by 400 days of age (Daly 2013). In order to investigate whether this tumour was WNT-driven, an immunohistochemical staining for β-catenin was performed, and showed high nuclear β-catenin staining (Figure 5.19). PI3K/AKT did not contribute to tumourigenesis as reflected by immunohistochemical staining for p-AKT and p-FOXO1/3/4 (Figure 5.20). Unlike APC2-deficient tumours, PTEN expression in the *Apc2*$^{+/+}$ tumour was minimal (Figure 5.20). This tumour phenocopied the APC2-deficient GCTs, being highly proliferative (Ki67), vascular (CD34), non-epithelial (E-cadherin), and non-apoptotic (cleaved caspase 3 and FOXO1) (Figure 5.21). Molecular signature of human GCT was retained in the 18-month-*Apc2*$^{+/+}$ tumour as reflected by the high expression of FOXL2 and inhibin α protein, but not the ERα (Figure 5.22).

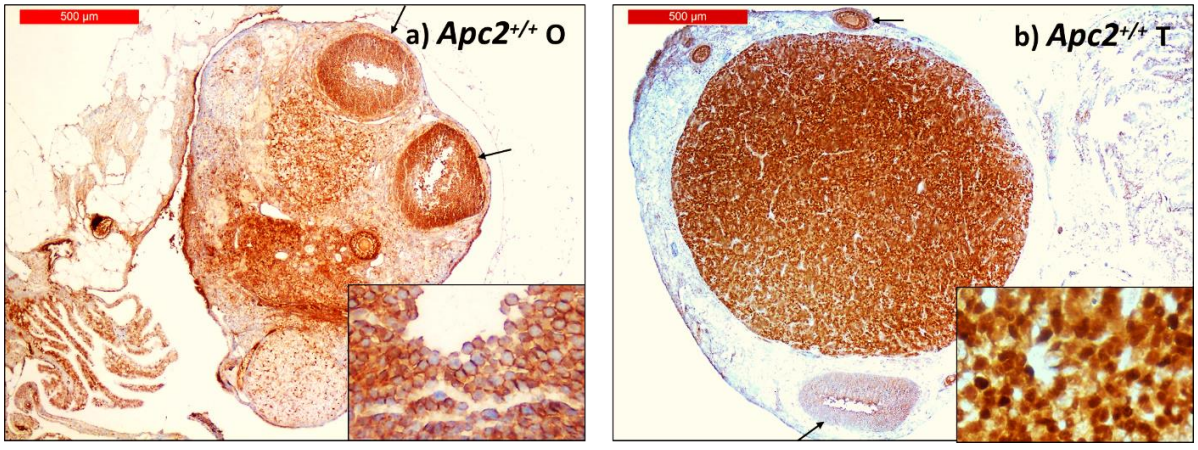

Figure 5.19: Expression of β-catenin protein in 18-month-*Apc*$^{fl/fl}$ ovaries. Representative photomicrographs of β-catenin immunohistochemistry in (a) normal ovary (inset showing membraneous staining for β-catenin in granulosa cells of follicles), and (b) GCT (inset showing nuclear staining for β-catenin in granulosa cells of the tumour). Scale bar 500 µm. Black arrow: ovarian follicles. Insets show 5X original magnification. O:ovary, T: tumour.

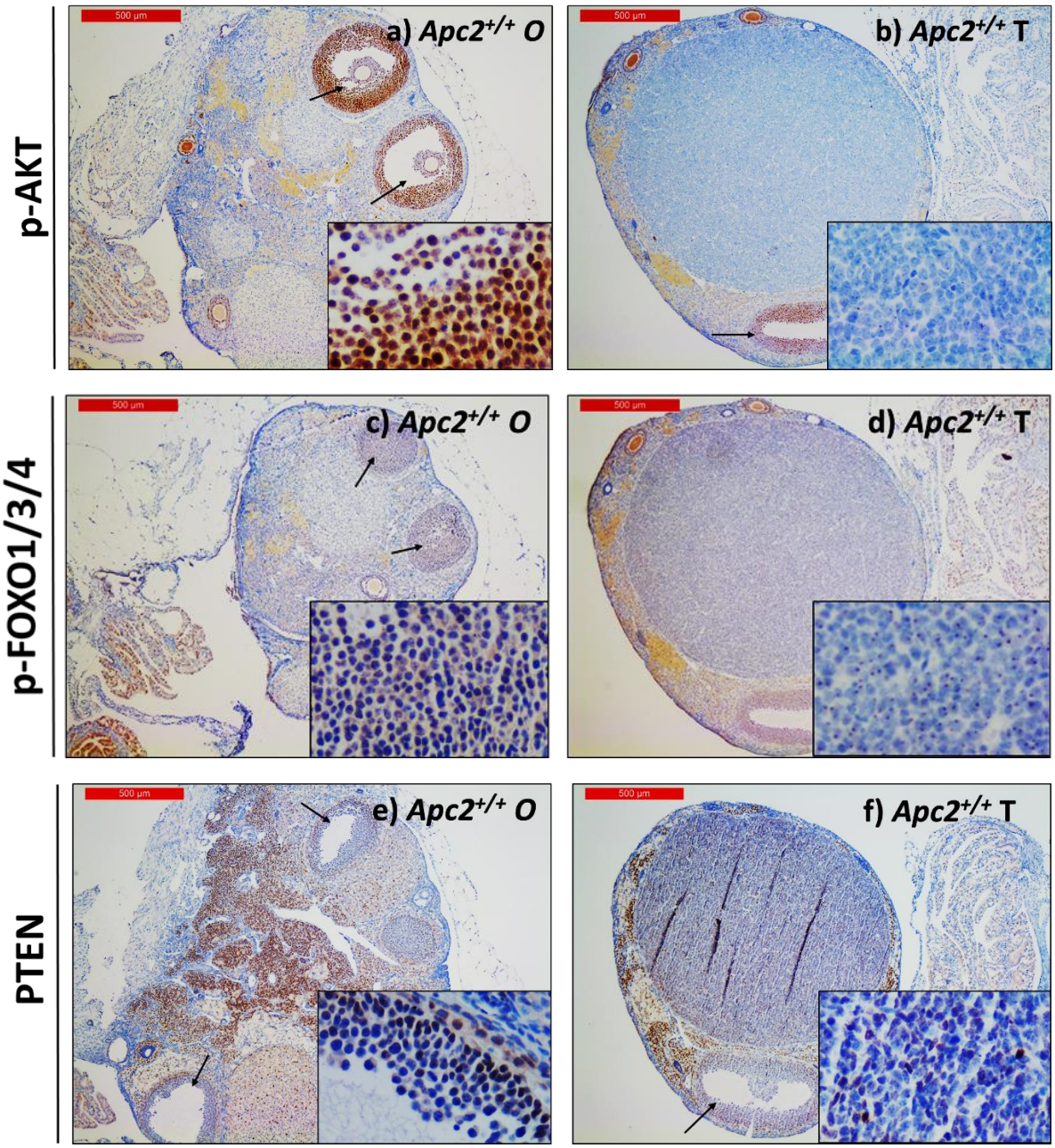

Figure 5.20: PI3K/AKT signalling does not contribute to tumourigenesis in 18-month-*Apc*$^{fl/fl}$ GCT. Representative photomicrographs of (a,b) p-AKT, (c,d) p-FOXO1/3/4, and (e,f) PTEN immunohistochemistry in 18-month-*Apc*$^{fl/fl}$/*Apc2*$^{+/+}$ (a,c,e) normal ovary (insets show staining in granulosa cells of follicles, 5X original magnification), and (b,d,f) GCT (insets show staining in tumour cells, 5X original magnification). Scale bar 500 µm. Black arrow: ovarian follicles. O:ovary, T: tumour.

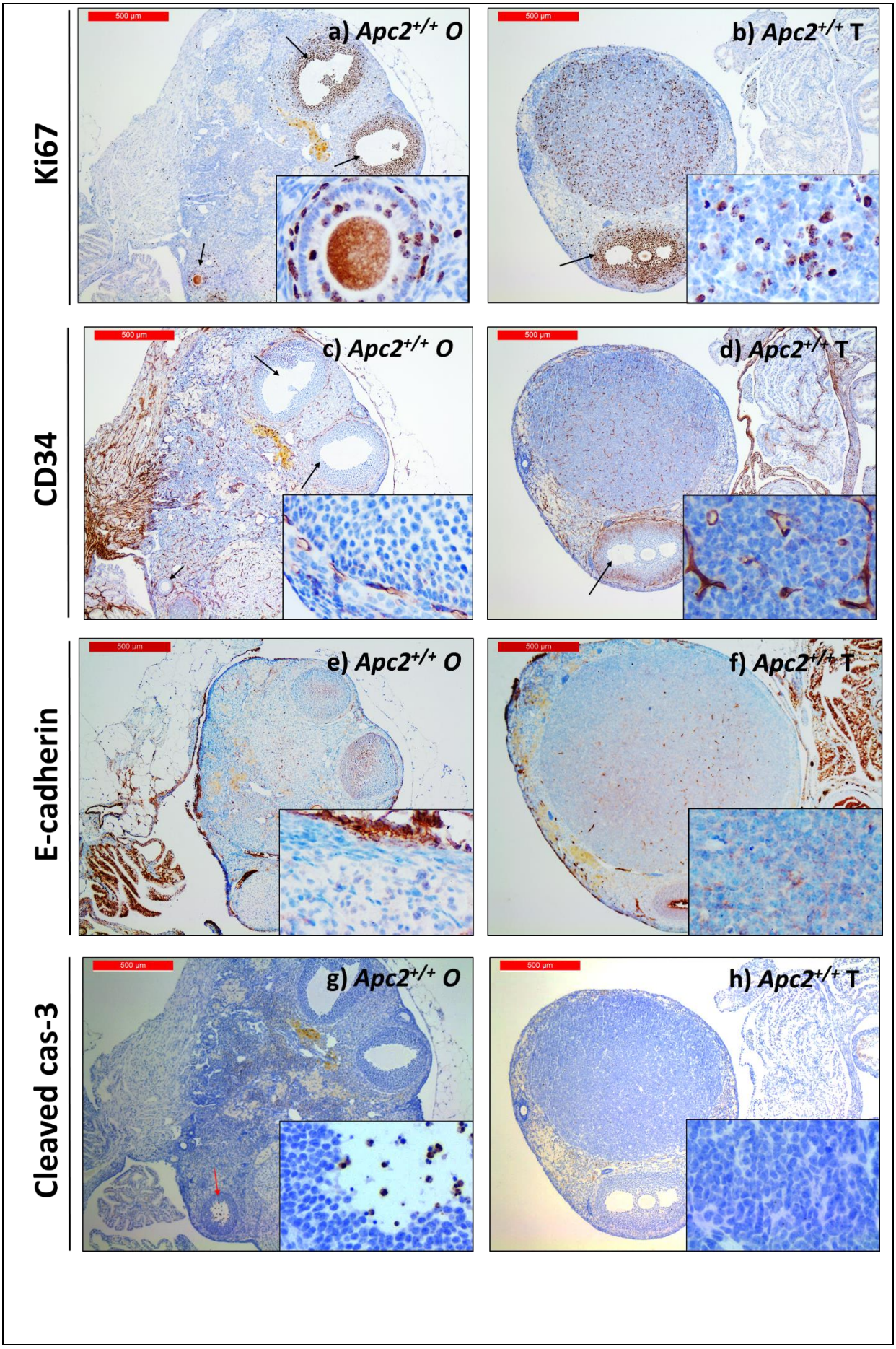
Ki67
CD34
E-cadherin
Cleaved cas-3
500 µm
a) Apc2+/+ O
b) Apc2+/+ T
c) Apc2+/+ O
d) Apc2+/+ T
e) Apc2+/+ O
f) Apc2+/+ T
g) Apc2+/+ O
h) Apc2+/+ T

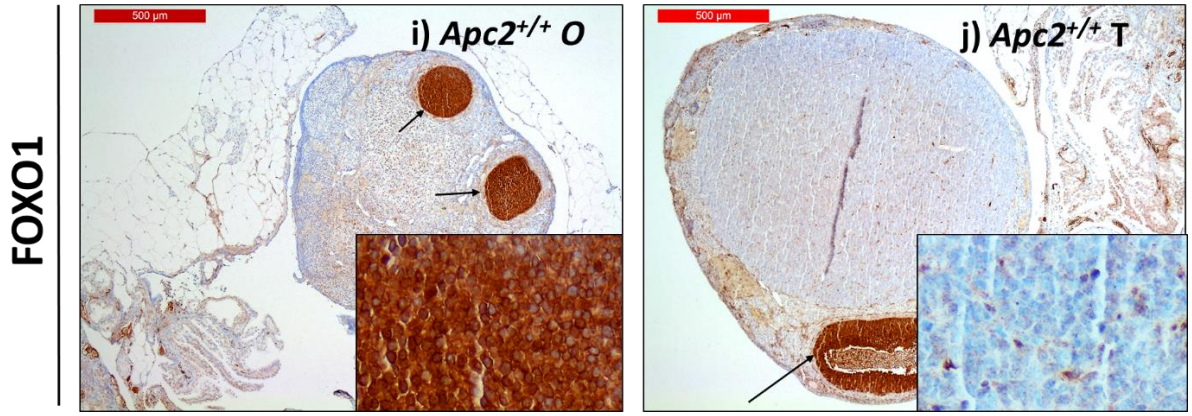

Figure 5.21: The 18-month-*Apc*$^{fl/fl}$/*Apc2*$^{+/+}$ tumour phenocopied APC2-deficient GCTs. Representative photomicrographs of (a,b) Ki67, (c,d) CD34, (e,f) e-cadherin, (g,h) cleaved caspase 3 and (i,j) FOXO1 immunohistochemistry in 18-month-*Apc*$^{fl/fl}$/*Apc2*$^{+/+}$ (a,c,e,g,i) normal ovary (insets show staining in granulosa cells of follicles, 5X original magnification, apart from e where inset shows OSE) and (b,d,f,h,j) GCT (insets show staining in tumour cells, 5X original magnification). Scale bar 500 µm. Black arrow: ovarian follicles. Red arrow: atretic follicle. O:ovary, T: tumour.

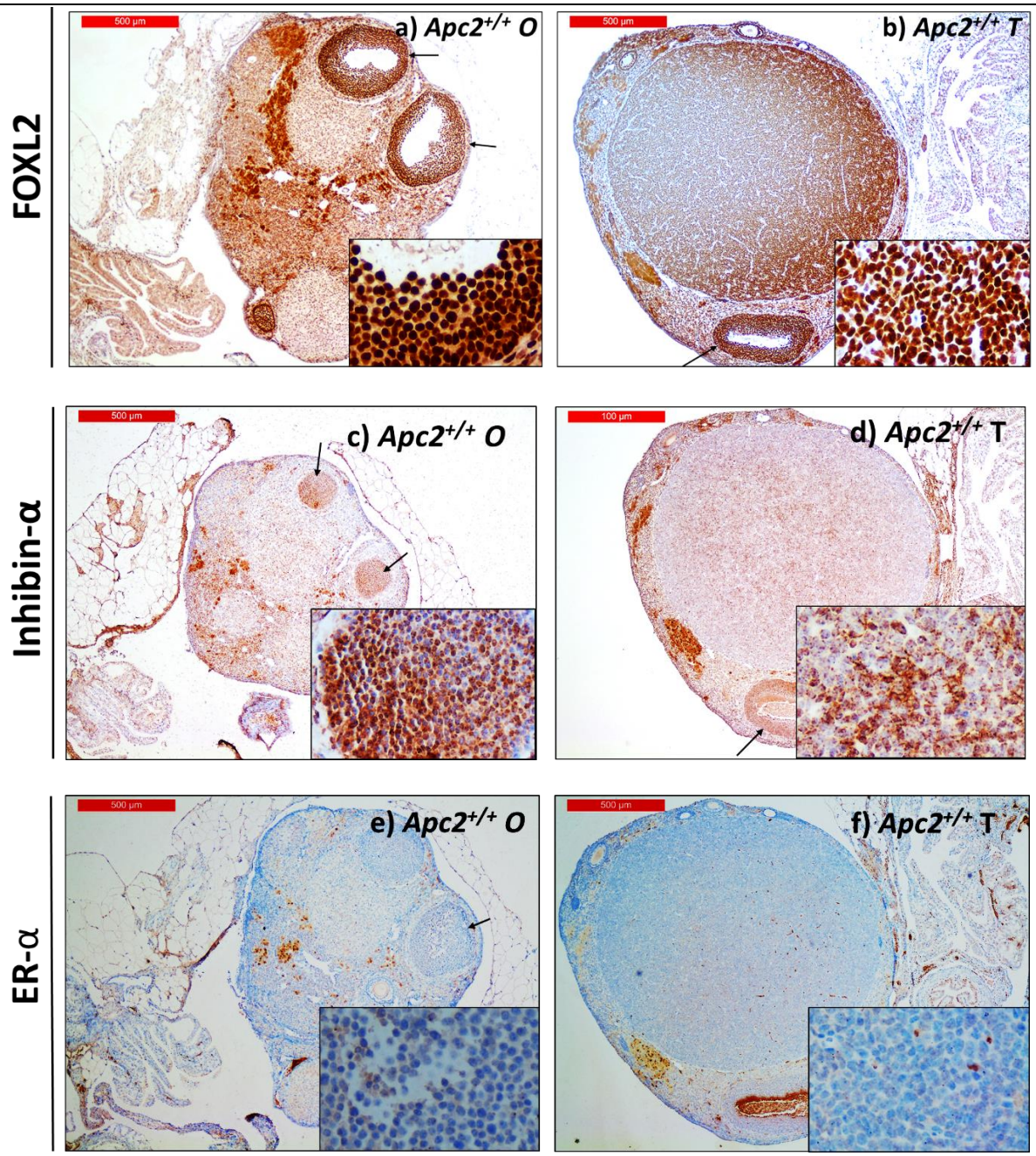

Figure 5.22: Molecular signature of 18-month-*Apc*$^{fl/fl}$/*Apc2*$^{+/+}$ tumour. Representative photomicrographs of (a,b) FOXL2, (c,d) Inhibin-α and (e,f) ERα immunohistochemistry in 18-month-*Apc*$^{fl/fl}$/*Apc2*$^{+/+}$ (a,c,e) normal ovary (insets show staining in granulosa cells of follicles, 5X original magnification) and (b,d,f) GCT (insets show staining in tumour cells, 5X original magnification). Scale bar 500 µm. Black arrow: ovarian follicles. O:ovary, T: tumour.

5.3 Discussion

5.3.1. Reduction or loss of APC2 protein drives ovarian granulosa cell tumour formation in aging mice.

Activation of canonical WNT signalling has been previously shown to drive ovarian GCT formation in two genetically-engineered mouse models; the degradation-resistant β-catenin model (Boerboom *et al.* 2005), and the R-spondin1 gain-of-function model (De Cian *et al.* 2016). In both models, WNT signalling activation was evident and resulted in early-onset subfertility with 100% penetrance (Boerboom *et al.* 2005; De Cian *et al.* 2016). However, tumour formation was delayed and was only evident in a subset of mice. Pre-tumour lesions were identified in both models (Boerboom *et al.* 2005; De Cian *et al.* 2016).

WNT signalling was highly activated in GCT of APC2-deficient mice, as reflected by the strong nuclear expression of β-catenin protein in the tumour areas (Figure 5.4). This high level of WNT signalling activation caused the elevation of Wnt target genes *Axin1* and *Wif1* (Figure 5.5), which function to downregulate the pathway. This expression profile is similar to that described by Richards *et al*. in the ovarian GCTs developing in mice expressing degradation-resistant β-catenin along with *Pten* deletion or *Kras* activation (Richards *et al.* 2012). Although this pattern of expression was retained in both $Apc2^{-/-}$ and $Apc2^{+/-}$ tumours, a dose-dependent increase in the expression of these WNT signalling pathway members was observed in $Apc2^{-/-}$ tumours. However, the main limitation of the current study is the number of samples used to perform the analysis. These gene expression data represent only one tumour collected at 2 different time points and from 2 different genotypes. Whether the changes observed are merely due to the genotype dosage or whether the age is playing a role remains unclear. More samples will be needed to unravel these ambiguities.

In the current study, APC2 deletion caused subfertility with 100% penetrance (Discussed in Chapter 4). Tumour formation was evident in at least 20% of the mice starting at the age of 12 months (Table 5.2, Figure 5.2). Although all the aging mice in the different *Apc2* cohorts carried the hypomorphic Apc^{fl} allele, only one 18-month-old $Apc^{fl/fl}$ mouse with intact APC2 developed an ovarian tumour. It was previously shown that mRNA levels of *Apc* were reduced in non-recombined $Apc^{fl/fl}$ brain and intestines, but APC protein levels were not affected (Shibata *et al.* 1997). However, mRNA and protein levels of *Apc* in $Apc^{fl/fl}$ ovary were not previously characterized and remain unknown. No ovarian GCT formation was reported in previous studies aging the hypomorphic $Apc^{fl/fl}$ mouse after inducing recombination exclusively in the OSE (Wu *et al.* 2011; Tanwar *et al.* 2013). GCT formation is not common in mice although incidence increases with age and has been shown to be strain-specific (Mahler *et al.* 1996; Dixon *et al.* 2014).

This percentage of GCT formation in APC2-deficient mice is lower than the frequency resulting from expression of degradation-resistant β-catenin (57%, (Boerboom *et al.* 2005)), but higher than that reported after activating R-spondin1 (12.5%, (De Cian *et al.* 2016)). Tumour formation was evident in 44% of 6-month-old mice in the β-catenin model (Boerboom *et al.* 2005). However, tumour formation was delayed to 12 months in the R-spondin1 model (De Cian *et al.* 2016), similar to the APC2-deficient model. These discrepancies in frequency and onset of tumour formation could be related to the different functions of these three proteins in WNT signalling. It is expected that over-expression of β-catenin, the main effector of the WNT signalling pathway (Sakanaka *et al.* 2000), would result in the highest frequency and earliest onset of tumour formation. Both APC2 and R-spondin1 differentially regulate WNT signalling, the first through downregulating β-catenin (Van Es *et al.* 1999; Ahmed *et al.* 2002) and the other by positively modulating the pathway via preventing the internalization of the Wnt coreceptor LPR6 (Binnerts *et al.* 2007). Whether the higher prevalence of tumour

formation in APC2-deficient mice compared to R-spondin1 activation is caused by differences in the intensity of WNT signalling activation remains unclear.

In the current study, pre-tumour lesions in the form of solid nests of follicle-like structures with disorganized granulosa cells, previously described in the other models (Boerboom *et al.* 2005; De Cian *et al.* 2016), were not evident. The use of serial sections within the current study to characterize ovaries enabled the discrimination between real cystic lesions and growing follicles. Both *Apc2*$^{+/+}$ and *Apc2*$^{-/-}$ ovaries developed cysts at 6 months, but the type of cysts formed were different between both genotypes (Table 5.1, Figure 5.1). Exclusively in the 6-month-old *Apc2*$^{-/-}$ cohort, mice developed follicular cysts with 40% penetrance, and small epithelial cysts with 20% penetrance. We propose that a proportion of these follicular cysts progressed to form GCTs later on, while the epithelial cysts progressed to form the large fluid-filled cysts only present in one 18-month-old *Apc2*$^{+/-}$ mouse in the current study, but occasionally observed in previous aging APC2-deficient mice in the Clarke lab (Figure 5.3).

5.3.2. Other signalling pathways contributing to GCT formation in APC2-deficient mice.

It was previously shown in section 4.2.6. that in 10-week-old *Apc2*$^{-/-}$ ovaries, granulosa cells had higher apoptotic rates as compared to those of *Apc2*$^{+/+}$ ovaries. However, in the GCTs, complete absence of apoptosis was evident in APC2-deficient tumours. In the 10-week-old *Apc2*$^{-/-}$ ovaries, higher levels of *Foxo1* and downstream targets were found as compared to *Apc2*$^{+/+}$ mice. However, in the GCTs, gene and protein expression levels of *Foxo1* were markedly reduced (Figure 5.9). This may indicate the need for silencing *Foxo1* to switch from apoptosis to tumour formation. This conclusion is in agreement with the results reported by Liu *et al.* using a *Foxo1*/*Foxo3* double knockout mouse model, where 20% of the mice developed granulosa cell tumours starting at 6 months of age (Liu *et al.* 2015).

As discussed in section 4.2.7, *Lhcgr* was highly expressed in 10-week-old *Apc2*$^{-/-}$ ovaries. Overexpression of *Lhcgr* expression at this early stage might have contributed to GCT formation. This hypothesis could be supported by the development of ovarian GCTs in 50% of 24-week-old mice bearing a gain-of-function mutation in *Lhcgr* (Hai *et al.* 2015). Although the expression levels were almost absent in APC2-deficient GCTs (Figure 5.16), this may reflect the impaired differentiation of granulosa cells in the formed tumours.

The molecular pathogenesis of adult GCTs of the ovary has been linked to a somatic missense mutation in *FOXL2* gene detected in 97% of human cases (Shah *et al.* 2009). This missense mutation results in the production of a mutant protein, where a cysteine amino acid at position 134 is replaced by tryptophan. The mechanism by which this mutation drives GCT development has been recently described as a sensitization to phosphorylation of the mutant protein at the S33 phosphorylation site, leading to hyperphosphorylation and subsequent degradation of FOXL2 protein (Kim *et al.* 2014a). In the current study, APC2-deficient GCTs highly expressed FOXL2 protein (Figure 5.10), similar to the finding previously reported in other GEMMs of ovarian adult GCTs (Hai *et al.* 2015; Gao *et al.* 2016). However, due to the unavailability of a commercial antibody targeting phospho-S33 FOXL2 protein, the phosphorylation status of FOXL2 protein detected in the current study, as well as other studies, cannot be confirmed. It remains unclear whether the high FOXL2 protein level detected in the GCTs of our APC2-deficient mice is contributing to tumourigenesis, or is a nascent marker of granulosa cell differentiation which is retained by the tumour cells.

When the expression of a dominant-stable β-catenin or the deletion of *Foxo1*/3 was accompanied by *Pten* deletion, GCT formation was accelerated (Lague *et al.* 2008; Richards *et al.* 2012; Liu *et al.* 2015). In the current study, expression of PTEN protein was highly elevated, although the *Pten* mRNA levels were only slightly altered (Figure 5.14). The protein level was higher in 18-month-*Apc2*$^{+/-}$ GCTs as compared to the 12-month-*Apc2*$^{-/-}$ GCT. PTEN

has been previously identified as a downstream target of WNT signalling (Ahmad *et al.* 2011) in bladder cancer. Ahmad *et al.* have shown that PTEN expression is markedly increased post-WNT signalling activation via APC deletion, GSK3 deletion or β-catenin activation (Ahmad *et al.* 2011), and proposed this as a mechanism for delaying tumour progression in their model. In the APC2-deficient GCTs, the elevated PTEN protein together with the complete absence of p-AKT protein (Figure 5.13) could reflect a part of a defensive/negative feedback mechanism by which the cells try to counteract the activated WNT signalling by silencing PI3K/AKT to prevent tumour progression. This is similar to the blocking effect of PTEN protein on bladder cancer progression (Ahmad *et al.* 2011) and mammary tumour formation (Zhao *et al.* 2005) post-WNT signalling activation reported previously.

In conclusion, although WNT signalling is the main driver of GCT formation in APC2-deficient ovaries, the contribution of other signalling pathways cannot be excluded. Whether perturbation of these signalling pathways are consequences of tumour formation rather than contributing factors cannot be ignored either. More research is required to clarify these complex mechanisms.

5.3.3. Ovarian GCTs of APC2-deficient mice recapitulates human adult GCT histological features and molecular signature

For GEMMs to be useful as a tool in preclinical studies, genotypic and phenotypic similarity between the animal model and the corresponding human tumour need to be present. Although somatic mutation of the *FOXL2* gene remains the main molecular genetic alteration found in adult GCTs in human, a mouse model carrying an equivalent mutation in the mouse *Foxl2* gene has not yet been developed. Thus it is crucial to validate the available mouse models as tools to study tumour pathogenesis and as preclinical models for drug testing.

WNT signalling activation, defined by increased β-catenin expression, has been previously described in a subset of human GCTs of the ovary (Boerboom *et al.* 2005; Stewart *et al.* 2013; Kilonzo *et al.* 2015). In the current study, WNT signalling activation resulting from APC2-deficiency caused the formation of adult GCTs of the ovary, which recapitulate many histologic features of human adults GCTs. A range of histologic patterns described previously in human adult GCTs (Stenwig *et al.* 1979; Kanthan *et al.* 2012; Vani *et al.* 2014) were present in the GCTs formed in APC2-deficient mice (Figure 5.2). However, more than one histological pattern was present in the same tumour, and histological patterns varied among tumours. The cause of this variability is unclear, but is similar to previous reports describing more than one histological pattern in a single adult human GCT (Stenwig *et al.* 1979; Vani *et al.* 2014). Other histologic features which are diagnostic markers for adult GCTs in human ovaries were also retained in our APC2-deficient GCTs, such as the presence of Call-Exner bodies, mitotic figures and coffee-bean-shaped nuclei (Schumer and Cannistra 2003). The recapitulation of these features is similar to those seen in the degradation-resistant β-catenin model (Boerboom *et al.* 2005) as well as in the non-WNT signalling GEMMs such as the *Foxo1/Foxo3* double knockout model (Liu *et al.* 2015) and the constitutively-active TGF β receptor-1 model (Gao *et al.* 2016).

Other features described in human GCTs were retained in APC2-deficient GCTs. For example, high proliferation was evident as reflected by Ki67 immunostaining (Figure 5.6). Increased proliferation is one of the hallmarks of tumour progression (Hanahan and Weinberg 2011). The increased proliferation of granulosa cells could be partly caused by the downregulation of *Esr2* (Figure 5.11), a tumour suppressor gene in the granulosa cells whose expression needs to be suppressed in order to enhance granulosa cell proliferation (Wang *et al.* 2015c). Again, whether this is a consequence of tumourigenesis or contributing to it is not clear. Ovarian GCT development was reported in 2-year-old constitutive *Esr2* knockout mice

(Fan *et al.* 2010b). The same group reported the absence of tumour formation in *Esr1* or *Esr1*/*Esr2* double knockout mice (Fan *et al.* 2010b), suggesting the contribution of estrogen receptor alpha in GCT development. This is in line with the findings of the current study; GCTs developing in APC2-deficient mice showed downregulation of *Esr2* but upregulation of *Esr1* and the presence of nuclear ERα in tumour cells (Figure 5.11).

Increased angiogenesis is another hallmark of tumour formation, which was retained in GCTs formed in APC2-deficient mice (Figure 5.7). New blood vessel formation, visualized in the current study by CD34 immunostaining, is similar to those reported in other GEMMs of ovarian GCTs (Gao *et al.* 2016) as well as in human adult GCTs (Kusamura *et al.* 2003; Färkkilä *et al.* 2011). The interaction between activated canonical WNT signalling, elevated *Fgf1* expression (evident only in *Apc2*$^{-/-}$ tumours) and *Vegfa* expression may account for the prevalent microvessel formation present in APC2-deficient tumours (Carmeliet and Jain 2011).

In conclusion, GCTs in our APC2-deficient mouse model human ovarian adult GCTs, retaining the histologic features as well as the molecular signature (FOXL2, inhibin and ERα expression).

5.3.4. Differentiation is impaired in APC2-deficient GCTs

In the setting of tumour development, where the tumour replaces the normal ovarian tissue, it is expected that most of the ovarian compartment will be lost. This was evident in the microscopic examination of the tissue, where the presence of corpora lutea and follicles was much reduced (Figure 5.2). Although loss of these functional ovarian elements is expected in aging mice, even their remnants were absent due to replacement by tumour tissue. In order to confirm this finding, expression analyses of *Gdf9*, *Cyp17a1* and *Cdh1* (along with E-cadherin immunostaining) were chosen as molecular markers of oocytes, theca cells and epithelial cells respectively (Figure 5.17-5.18). The expression levels of these markers were all reduced in

GCTs of APC2-deficient mice. Of note in GCTs developing in APC2-deficient mice that the expression of E-cadherin was limited to the ovarian surface epithelium (Figure 5.17). Recent GEMMs of GCTs have described the presence of epithelial markers within the tumours, which was explained by dedifferentiation of tumour cells to progenitor epithelial cells (the only cell type harbouring stem cells in the ovary) (Liu *et al.* 2015; De Cian *et al.* 2016), or migration of epithelial cells into the tumour (initiating the tumour)(Gao *et al*. 2016). APC2-deficient GCTs are not reproducing this epithelial phenotype. It is worth mentioning that the cell of origin of ovarian granulosa cells is still not clearly defined, as it is still controversial whether they originate from coelomic epithelium or mesenchymal precursors (Kottarathil *et al.* 2013).

Gdf9 was previously shown to downregulate *Kitlg* in both cumulus cells and KGN, a granulosa cell tumour cell line (Tuck *et al.* 2015). The downregulation of *Gdf9* observed in the current study (Figure 5.18) might explain the upregulation of *Kitlg* (Figure 5.9), which in turn might account for the inhibition of apoptosis (Figure 5.8) observed in GCTs (Abdi *et al.* 2015).

Differentiation of granulosa cells in the tumours was impaired as well. Although tumour cells retained the expression of some early granulosa cell markers such as FOXL2 (Figure 5.10), the expression of granulosa cell functional marker (*Cyp19a1*, *Fshr*, *Ar*, *Esr2*) as well as markers of terminal differentiation (*Lhcgr*, *Pgr*, *Cyp11a1*) were compromised (Figure 5.11, 5.15-5.16). The limited capability of full differentiation of granulosa cells in the tumours has been reported in other GEMMs of adult GCT (Richards *et al.* 2012; Liu *et al.* 2015; Gao *et al.* 2016).

Throughout the study, a degree of heterogeneity was observed in the expression levels of genes from the 12-month-*Apc2*$^{-/-}$ tumour compared to the 18-month-*Apc2*$^{+/-}$ tumour. The reason of this heterogeneity is not clear, owing to the limited number of samples processed. However, one explanation might be the size of the tumour. The tumour collected from the 12-

month-*Apc2*$^{-/-}$ was a small one, and if compared to tumours of similar size, which were examined microscopically, it cannot be excluded that a part of the normal ovarian tissue is present. As the sampling was done blindly, one of the samples could represent the tumour bulk while the other represent the tumour periphery or tumour/normal tissue interphase. On the other hand, the 18-month-*Apc2*$^{+/-}$ tumour was the largest one collected in the current study. As it was divided into 2 parts, one for histological assessment and the other for gene expression analysis, it is apparent from the microscopic examination that all the tissue was replaced by the tumour.

5.3.5. Conclusion and future work

For the first time, roles of the APC2 protein in aging ovaries have been established. It has been shown that APC2 is an important tumour suppressor protein in ovarian granulosa cells. APC2-deficient mice developed GCTs due to activation of WNT signalling, however, the contribution of other signalling pathways cannot be excluded. We propose that the late formation of the tumours as well as the low incidence is caused by upregulation of PTEN. We hypothesize that deleting PTEN simultaneously with APC2 will accelerate tumour formation and progression. The GCTs formed in APC2-deficient mice recapitulate human adult GCT histology and molecular signature, and thus can be successfully used as a model to study tumour biology and in preclinical drug testing.

Some questions remain to be answered. The APC2-deficient mouse used in the current study is a constitutive knockout mouse. Whether ovarian cells, other than granulosa cells, are contributing to tumour development is not clear. In order to dissect the cell of origin of the tumour, conditional deletion of APC2 in granulosa cells as well as in other cellular compartments (e.g. oocytes, theca cells) using a c*re* recombining exclusively in each of these cells would be useful. To the best of our knowledge, a conditional APC2 mouse strain is currently not available and would need to be developed and characterized first before this question could be answered.

Another important question is the interaction between APC and APC2 proteins in GCT development and progression. In the previous work performed in the Clarke lab, APC2 loss caused tumour formation in APC-deficient mice in the mammary glands (Daly *et al.* 2016), but attenuated tumour formation in the liver (Daly 2013). Whether complete silencing of both APC proteins in the granulosa cells would have a synergistic or antagonistic effect on tumour formation remains unanswered.

6. Roles of APC2 in epithelial ovarian tumourigenesis

6.1. Introduction

6.1.1. OSE as an origin for EOC

As discussed in section 1.2.3.1., the cell of origin of EOC is still unclear, and many theories have been postulated based on clinical evidence or mouse models. Historically, it was believed that EOC originates from OSE, the only epithelial cells in the ovary. This theory has been questioned because of the differences in histology and embryonic origin between OSE (single layer of squamous to cuboidal mesothelial cells) and EOC (resembles müllerian duct-derived epithelium). Although no clinical data support this hypothesis, mouse models have been developed driven by deletion of a number of genes exclusively in the OSE, modelling the 4 main histotypes of EOC (serous, endometrioid, mucinous and clear cell) (Wu *et al.* 2007; Szabova *et al.* 2012; Chandler *et al.* 2015; Ren *et al.* 2016), thus providing some support for this theory.

According to the theory, epithelial cells at the site of continuous rupture and repair, are highly susceptible to mutations, and if trapped inside the ovary during ovulation, may form inclusion cysts. Supported by paracrine signals coming from the surrounding niche (inflammatory mediators and steroidal hormones), as well as autocrine signals from inside cells, they accumulate mutations and undergo metaplastic transformation into müllerian epithelium, a pre-requisite for neoplasia. Genes mutated, as well as factors present in the surrounding niche, determine the histotype of EOC (Dubeau 2008; Kurman and Shih Ie 2010).

With the recent isolation and characterization of stem cells from the OSE, this theory has been refined, with the differentiating abilities of stem cells explaining the differences in histology between the originating OSE and the developing EOC (Ng and Barker 2015).

6.1.2. *APC* genes in human epithelial ovarian cancer

Mutations and copy number alterations of *APC* and *APC2* have been previously characterized in human EOC. Inactivating mutations of *APC* were present in just 1.4% (1/72) human OEA (Wu *et al.* 2007). However, using the COSMIC database, 10.94% (7/64) human OEA showed inactivating mutations in *APC*, of which 3 were homozygous (Forbes *et al.* 2016). In contrast, only 1.88% (13/693) of human serous carcinoma cases had mutations in *APC*, which were mostly heterozygous (Forbes *et al.* 2016). No *APC* mutations were detected in mucinous or clear cell carcinoma, however, the datasets were small (10 cases/histotype). In the cBioPortal database, only 2 EOC datasets were available, both for serous ovarian carcinoma cases. In one cBioPortal dataset, *APC* mutations were evident in 1.3% (4/310) and copy number alterations (deletions) in 3.2% (10/310) of cases, while in the other dataset mutations were evident in 1.9% (6/316) and deletions in 0.6% (2/316) cases (CGARN 2011). These findings could support the notion that WNT signalling plays a role in OEA pathogenesis, as well as being implicated in the pathogenesis of ovarian serous adenocarcinoma.

Shortly after its discovery, *APC2* allelic imbalance was reported in 19/20 human ovarian cancer samples, but histotypes of these tumours were not reported (Jarrett *et al.* 2001). Data extracted from cBioPortal showed that *APC2* was deleted in 5.1% (16/311) cases in a human serous ovarian carcinoma dataset, while being deleted in 1.3% (4/316) of cases in the second dataset of the same histotype (CGARN 2011). In the COSMIC database, APC2 copy number alteration was present in one dataset representing human serous ovarian carcinoma, in which 1.56% (9/576) of samples had deletions (Forbes *et al.* 2016).

Data extracted from the COSMIC database did not reveal any epigenetic alteration (hypo or hypermethylation) of either *APC* or *APC2* in the different datasets assessed. Interestingly, in one serous carcinoma dataset of cBioPortal, 0.96% (3/311) of cases showed

homozygous deletion of both genes, while 0.32% (1/311) showed homozygous deletion of *APC2* in addition to a missense mutation in *APC*.

6.1.3. Aims, hypothesis and highlights

The aims of this chapter were to characterize the role of APC2 in OSE homeostasis and whether loss of APC2 contributes to epithelial tumourigenesis, either alone or in combination with other tumour suppressors (APC and/or PTEN). The hypothesis was that APC2 is a tumour suppressor for epithelial tumourigenesis, and that loss of APC2 would disrupt the OSE, leading to formation of epithelial cysts and predisposing to epithelial tumours. However, the findings did not support this hypothesis and revealed that APC2 is dispensable for OSE homeostasis. Unlike the previous observation in the Clarke lab, $Apc2^{-/-}$ female mice did not develop ovarian cysts. Combined loss of APC2 with APC or PTEN in the OSE failed to initiate epithelial tumour formation. Surprisingly, the presence of intact APC2 protein delayed the initiation of OEA development in adenovirus-*cre*-induced $Pten^{fl/fl/}Apc^{fl/fl}$ ovaries, but enhanced tumour growth. This suggests a dualistic role of APC2 protein in WNT-driven OEA, where it acts as a tumour suppressor for tumour initiation but an oncoprotein for tumour progression. APC2 presence does not inhibit OEA tumourigenesis, and its loss might be considered a passive event happening to suppress tumour growth.

6.2. Results

6.2.1. APC2 loss is not disruptive to the ovarian surface epithelium

The OSE is a single layer of squamous to cuboidal epithelium that covers the ovary and is subjected to tear and subsequent repair after ovulation (Auersperg *et al.* 2001). In order to investigate whether APC2-deficiency affects OSE integrity and functionality, a series of histologic, immunohistochemical and *ex-vivo* assays were performed. Histologic examination of H&E-stained 10-week-old *Apc2*$^{+/+}$ and *Apc2*$^{-/-}$ ovarian sections collected at diestrus stage showed no signs of unrepaired tears, epithelial cysts, clefts, hyperplasia or metaplastic changes (shifting to columnar epithelium) in either genotype (Figure 6.1).

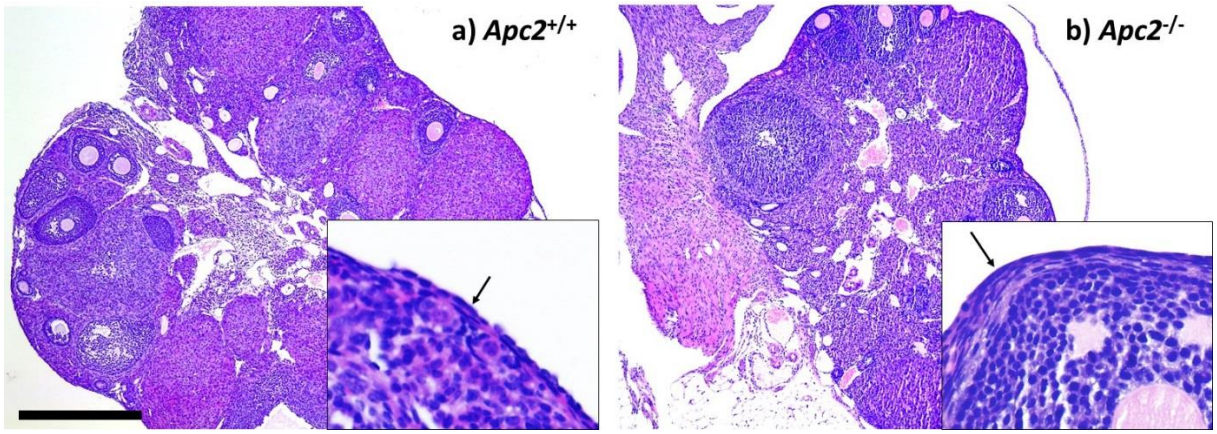

Figure 6.1: OSE integrity is not affected by APC2-deficiency. Photomicrographs of ovaries collected from 10-week-old (a) *Apc2*$^{+/+}$ and (b) *Apc2*$^{-/-}$ mice, showing smooth OSE (black arrows) formed of squamous epithelial cells. n=4. Scale bars 500 µm. Insets show OSE at 5X original magnification.

Being a primitive mesothelium, OSE displays both epithelial and mesenchymal features (Auersperg *et al.* 2001). To test whether these features were affected by APC2-deficiency, immunohistochemistry for epithelial markers (CK18 and E-cadherin) and a mesenchymal marker (vimentin) were performed, but no differences were observed in their intensity or localization between the 2 experimental genotypes (Figure 6.2).

As previously mentioned in section 4.2.4., APC2 deletion caused a trend of increase in proliferation and significantly increased apoptosis in follicle granulosa cells. To investigate whether APC2-deficiency affects proliferation and apoptosis of OSE, immunohistochemistry was performed using Ki67 and cleaved caspase 3 antibodies, respectively. No apoptotic cells were evident in the OSE from either genotype (Figure 6.3a,b), and there was a non significant decrease in proliferation in *Apc2*$^{-/-}$ vs. *Apc2*$^{+/+}$ OSE (23.25±13.1 *Apc2*$^{+/+}$ vs. 14.25±4.6 *Apc2*$^{-/-}$, Figure 6.3c-e).

In order to study effects of APC2-deficiency on proliferation, migration and stemness in more depth, *ex-vivo* assays were performed on OSE isolated from 10-week-old *Apc2*$^{+/+}$ and *Apc2*$^{-/-}$ ovaries. Cell Titer-Glo® viability assay revealed no significant differences in the number of viable cells in the cultured OSE from *Apc2*$^{-/-}$ mice compared to those from *Apc2*$^{+/+}$ mice (Figure 6.4). A scratch assay was used to assess the migratory capabilities of OSE cells. No significant differences in migration were observed between cells isolated from the two genotypes (Figure 6.5). A non-adherent sphere formation (anoikis resistance) assay was used to quantify stem cells (Wang *et al.* 2015a) and showed no significant difference between the 2 genotypes in the number of spheres >50 µm in diameter, although sphere formation was highly variable in *Apc2*$^{+/+}$ OSE cells (Figure 6.6).

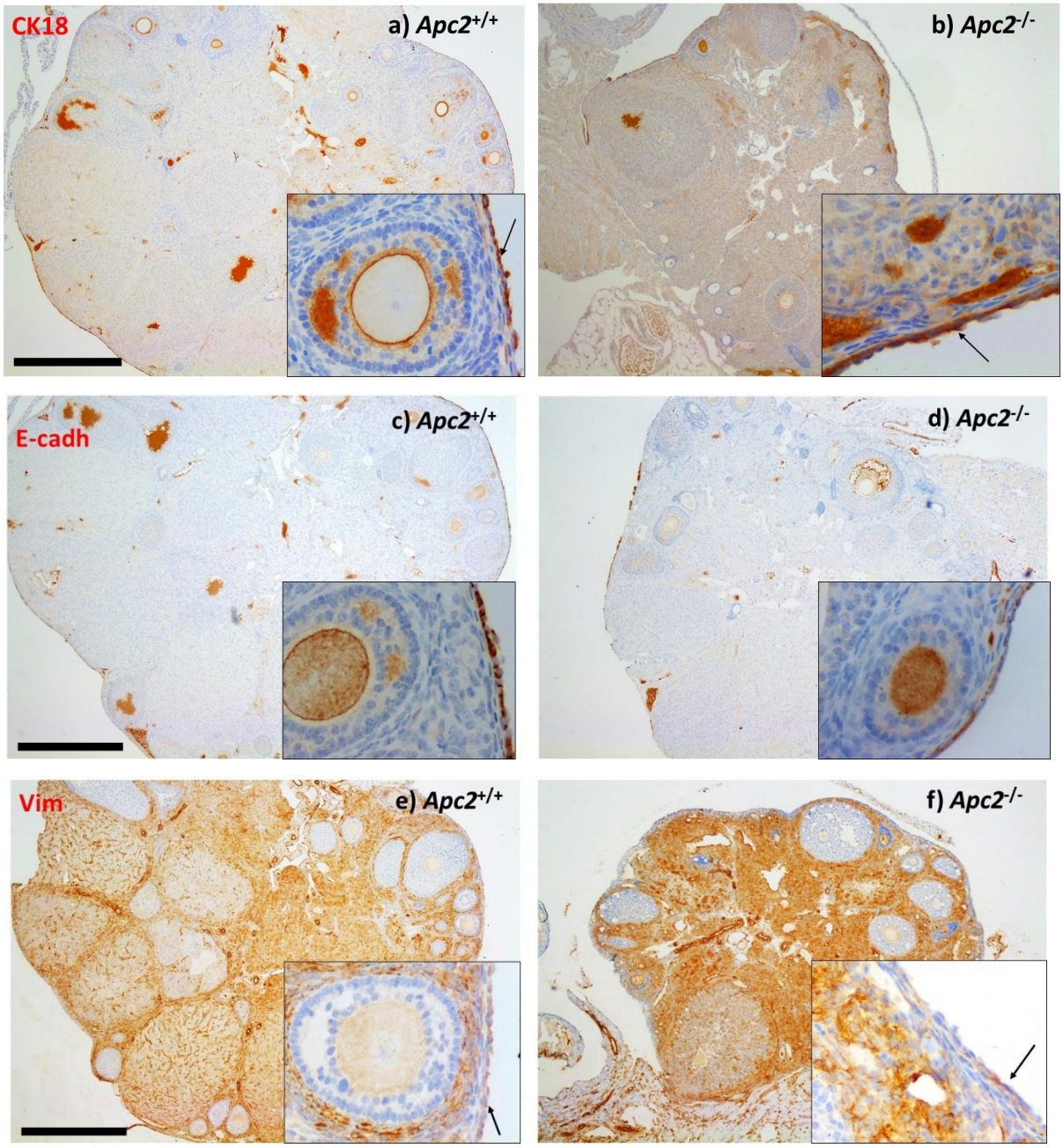

Figure 6.2: APC2-deficiency did not affect epithelial/mesenchymal features of OSE. Photomicrographs of ovaries collected from 10-week-old mice, for immunohistochemistry of CK18 in (a) *Apc2*$^{+/+}$ and (b) *Apc2*$^{-/-}$ ovaries (black arrows: staining in OSE), E-cadherin in (c) *Apc2*$^{+/+}$ and (d) *Apc2*$^{-/-}$ ovaries (staining is present exclusively in OSE), and vimentin in (e) *Apc2*$^{+/+}$ and (f) *Apc2*$^{-/-}$ ovaries (black arrows: OSE, note that vimentin is present in all ovarian compartments apart from growing follicles). n=4. Scale bars 500µm. Insets show OSE at 5X original magnification. CK18: cytokeratin 18. E-cadh: E-cadherin. Vim: vimentin.

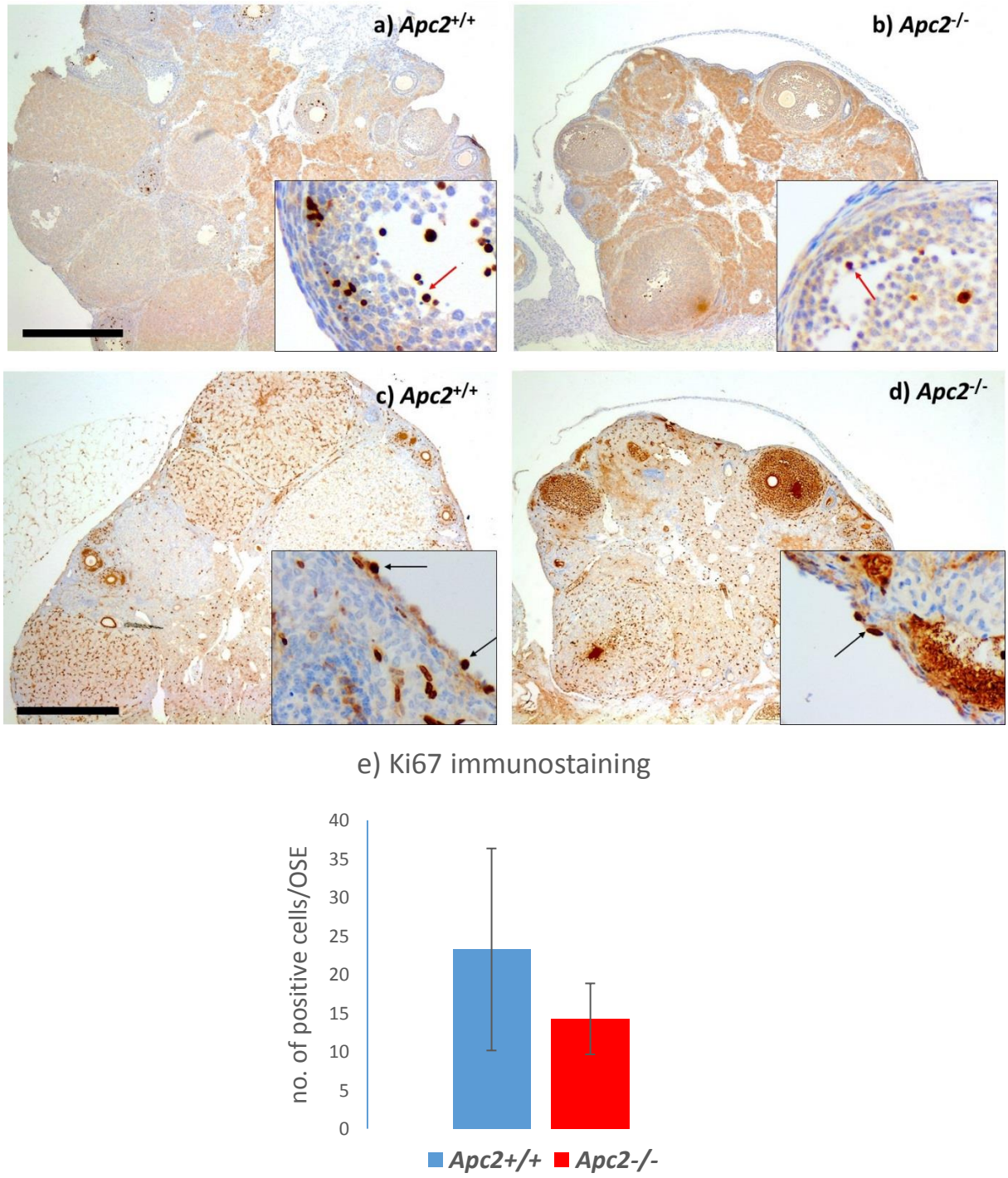

Figure 6.3: Proliferation and apoptosis are not altered in *Apc2*$^{-/-}$ ovaries. Photomicrographs of ovaries collected from 10-week-old mice, showing immunohistochenical staining for cleaved caspase-3 in (a) *Apc2*$^{+/+}$ and (b) *Apc2*$^{-/-}$ mice (red arrows show positively-stained granulosa cells in atretic follicles), and Ki67 in (c) *Apc2*$^{+/+}$ and (d) *Apc2*$^{-/-}$ mice (black arrows show positively stained-cells in the OSE). (e) Histogram for Ki67 immunostaining in OSE. n=4. Scale bars 500µm. Insets show OSE at 5X original magnification.

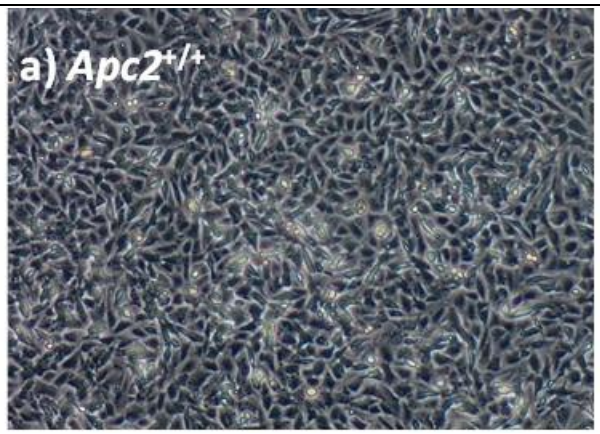

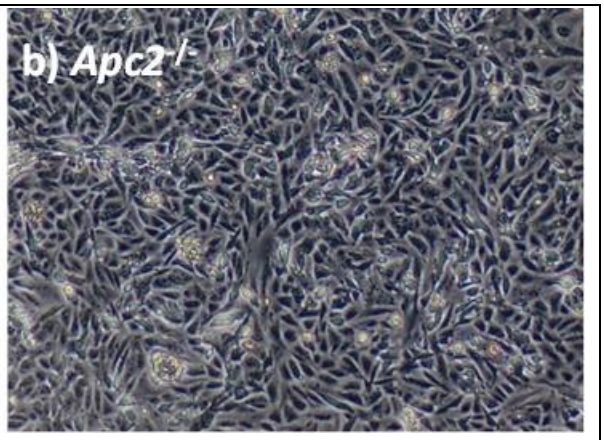

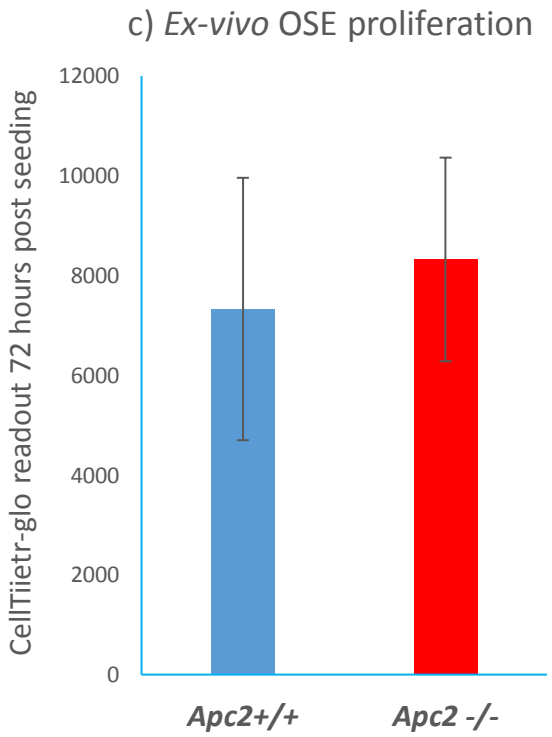

Figure 6.4: APC2-deficiency did not affect proliferation of cultured OSE. Photomicrographs of OSE in culture at confluency, isolated from (a) *Apc2*$^{+/+}$ and (b) *Apc2*$^{-/-}$ ovaries. (c) Proliferation of OSE cells measured as luminescent signal from viable cells by Cell Titer-Glo®. n=3. Results are displayed as mean±S.E.

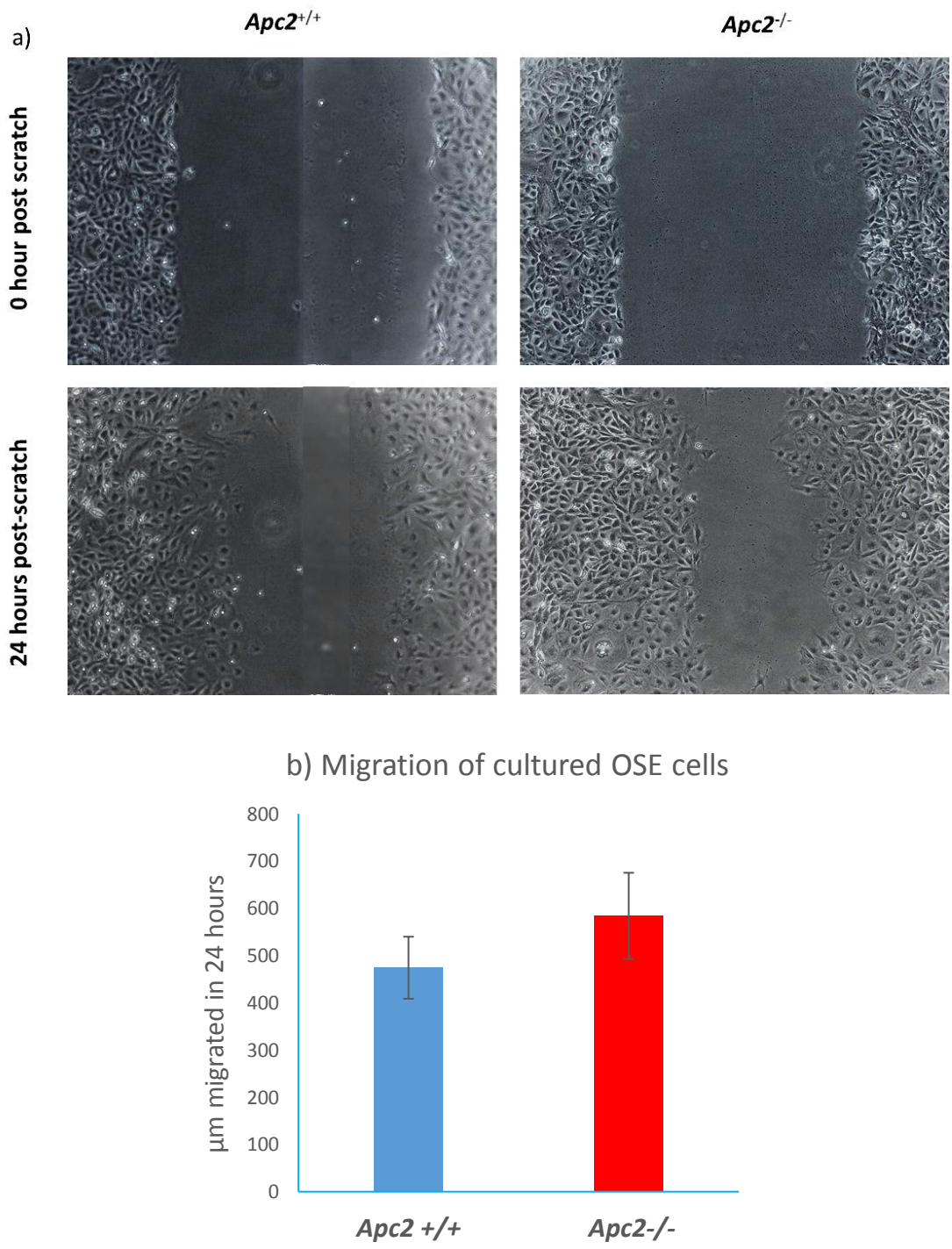

Figure 6.5: Migration of OSE cells in APC2-deficient ovaries. (a) Photomicrographs showing nearly confluent OSE from *Apc2*$^{+/+}$ (left panel) and *Apc2*$^{-/-}$ (right panel) ovaries taken just after the scratch (0 hour, upper panel) and 24 hours later (lower panel). (b) Histogram showing migration rates measured from the differences in scratch width at time of scratch and 24 hours later. n=3. Results are displayed as mean±S.E.

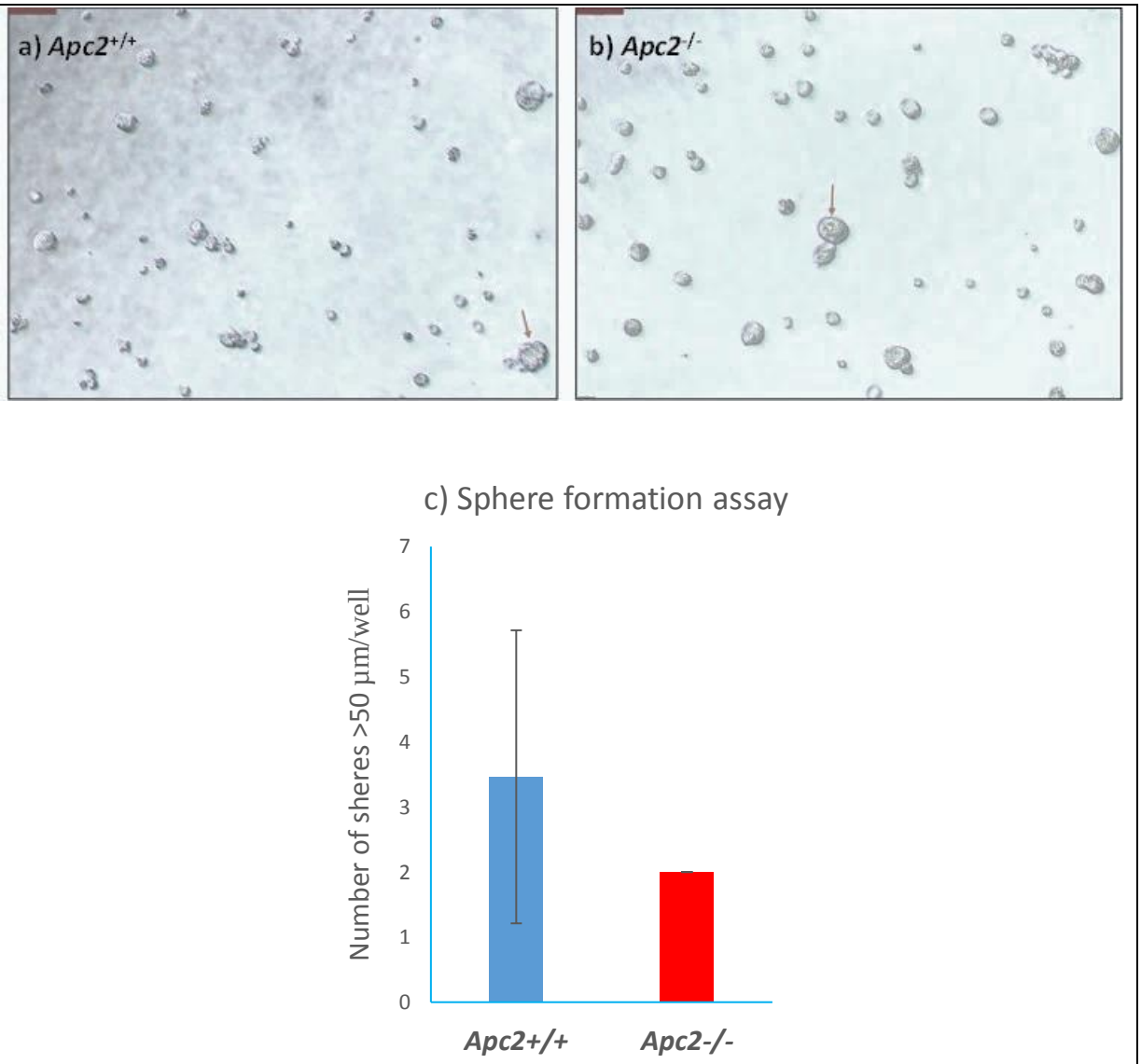

Figure 6.6: OSE cells separated from *Apc2*$^{+/+}$ and *Apc2*$^{-/-}$ form small spheres in suspension cell cultures. Photomicrographs of spheres formed in (a) *Apc2*$^{+/+}$ and (b) *Apc2*$^{-/-}$ OSE suspension cultures. Orange arrows: large spheres. Scale bar 50µm. (c) Histogram showing number of large spheres (>50 µm) formed per well, and reflecting high degree of variability in *Apc2*$^{+/+}$ cultures. n=3. Results are displayed as mean±S.E.

6.2.2. Conditional deletion of APC in the OSE of APC2-deficient mice did not initiate epithelial tumour formation

As shown in section 6.2.1., loss of APC2 protein does not disrupt OSE homeostasis. Whether compensation between APC2 and its homologue APC is protecting the OSE is not

clear. In order to address this, constitutive APC2-deficiency was combined with conditional APC deficiency, by recombining a floxed *Apc* allele exclusively in the OSE using intrabursal injection of adenovirus-*cre*, performed in 10-week-old mice. Ovaries were either collected 8-weeks post-induction (early time point), or when mice were 12-months old (late time point) (Table 6.1). Histopathological examination was performed, along with immunohistochemical characterization of proliferation, WNT signalling activation and epithelial integrity.

Table 6.1.: Numbers of mice analysed in experimental cohorts injected intrabursally by adenovirus-cre for studying compensation between APC proteins.

Genotype/ Time of dissection	**WT**	***Apc*$^{fl/fl}$**	***Apc2*$^{-/-}$**	***Apc*$^{fl/fl}$ *Apc2*$^{-/-}$**
Early time point (8-weeks post-induction)	n=4	n=4	n=3	n=3
Late time point (age of 12 months)	n=7	n=7	n=0	n=3

Preliminary experiments performed by Dr. Carl Daly in the Clarke lab, have shown that adenovirus-*cre* injection causes recombination of floxed genes exclusively in the OSE (Appendix 5). The experimental cohorts outlined in Table 6.1 were induced by intrabursal adenovirus-*cre* injections of both ovaries, in order to minimize the number of mice needed in the study. From each mouse, one ovary was fixed and used for histopathology/immunohistochemical characterization while the other was snap frozen. Wild type mice (WT, with intact APC and APC2 proteins) were injected to determine whether the procedure itself might affect OSE homeostasis. Ovarian sections were stained with H&E and histopathological analysis was performed to determine any abnormalities in the OSE in the experimental cohorts.

In the wild type cohort ($Apc^{+/+}$/$Apc2^{+/+}$), no signs of OSE lesions were observed 8-weeks post-induction (early point). However, age-related OSE irregularities were observed in 6/7 of induced wild type mice aged to 12 months (late point). Invagination was seen in 1/7 ovary (together with slight stromal infiltration and minimal shedding), hyperplasia and multi-layering in 1/7 ovary, slight stromal infiltration in 2/7 ovaries and minimal shedding in 2/7 ovaries (Figure 6.7, Table 6.2).

However, in the induced $Apc^{fl/fl}$ cohort, OSE irregularities appeared in 50% of mice (2/4) as early as 8-weeks post-induction. In a cohort of 4 ovaries examined microscopically, 1/4 had a deep invagination, with shedding and stromal infiltration (Figure 6.8a). Micro-papillary formation was noted in 1/4 ovary. In the 12-month-old mice, a range of ovarian abnormalities were observed in 6/7 ovaries. A large cyst which distorted the overall ovarian structure was present in 1/7 ovary (Figure 6.8b). In addition, micro-papillary growth was evident in 1/7 ovary (Figure 6.8c), shedding in 1/7 ovary (Figure 6.8d), multi-layering in 1/7 ovaries (Figure 6.8e). In addition, 1/7 ovary developed micro-papillary growth, OSE shedding and slight invagination. Another 1/7 ovary displayed micro-papillary growth, and multi-layering (Table 6.2a,b).

Due to the subfertility phenotype discussed in details in Chapter 4, we had difficulty generating sufficient mouse numbers for the $Apc2^{-/-}$ genotype cohorts. For this analysis, 3 $Apc2^{-/-}$ mice were induced and ovaries collected 8-weeks post-induction, but we were unable to generate a cohort of this genotype for the late time point. At 8-weeks post-induction, no signs of OSE irregularities were observed (Figure 6.9), similar to wild type mice collected at the same time point (Figure 6.7a), and to the non-induced $Apc2^{-/-}$ cohorts analysed at 10 weeks (Figure 6.1).

In contrast to induced *Apc*$^{fl/fl}$ cohorts, no OSE abnormalities were recorded in *Apc*$^{fl/fl}$/*Apc2*$^{-/-}$ cohort 8-weeks post-induction (Figure 6.10a), and slight stromal invasion was recorded in only 1/3 of the late time point cohort (Figure 6.10b, Table 6.2).

These results are collectively summarized in table 6.2 and indicate that loss of APC protein in the epithelium disrupts OSE homeostasis, but that this is insufficient to initiate tumourigenesis. Importantly, additional APC2 loss rescues the OSE from disruption. However, this interpretation should be treated with caution due to the limited number of ovaries that were available for the analysis.

Table 6.2: (a) OSE disruptions in 12-month-old induced APC/APC2 experimental cohorts. (b) Individual phenotypic characterization of epithelial lesions in ovaries of Apc$^{fl/fl}$ *cohort.*

(a) Genotype /histologic feature	**WT**	***Apc*$^{fl/fl}$**	***Apc*$^{fl/fl}$ *Apc2*$^{-/-}$**
Number of ovaries with OSE disruptions	6/7	6/7	1/3
Invagination	1/7	1/7 (slight)	0/3
Multi-layering	1/7	2/7	0/3
Stromal infiltration	3/7 (slight)	0/7	1/3 (slight)
OSE shedding	3/7	2/7	0/3
Cyst	0/7	1/7	0/3
Micro-papillary growth	0/7	3/7	0/3

b) *Apc*$^{fl/fl}$ mouse	Invagination	Multi-layering	OSE shedding	Cyst	Micro-papillary growth
1st	No	No	No	Yes	No
2nd	No	No	No	No	Yes
3rd	No	No	Yes	No	No
4th	No	Yes	No	No	No
5th	Yes	No	Yes	No	Yes
6th	No	Yes	No	No	Yes
7th	No	No	No	No	No

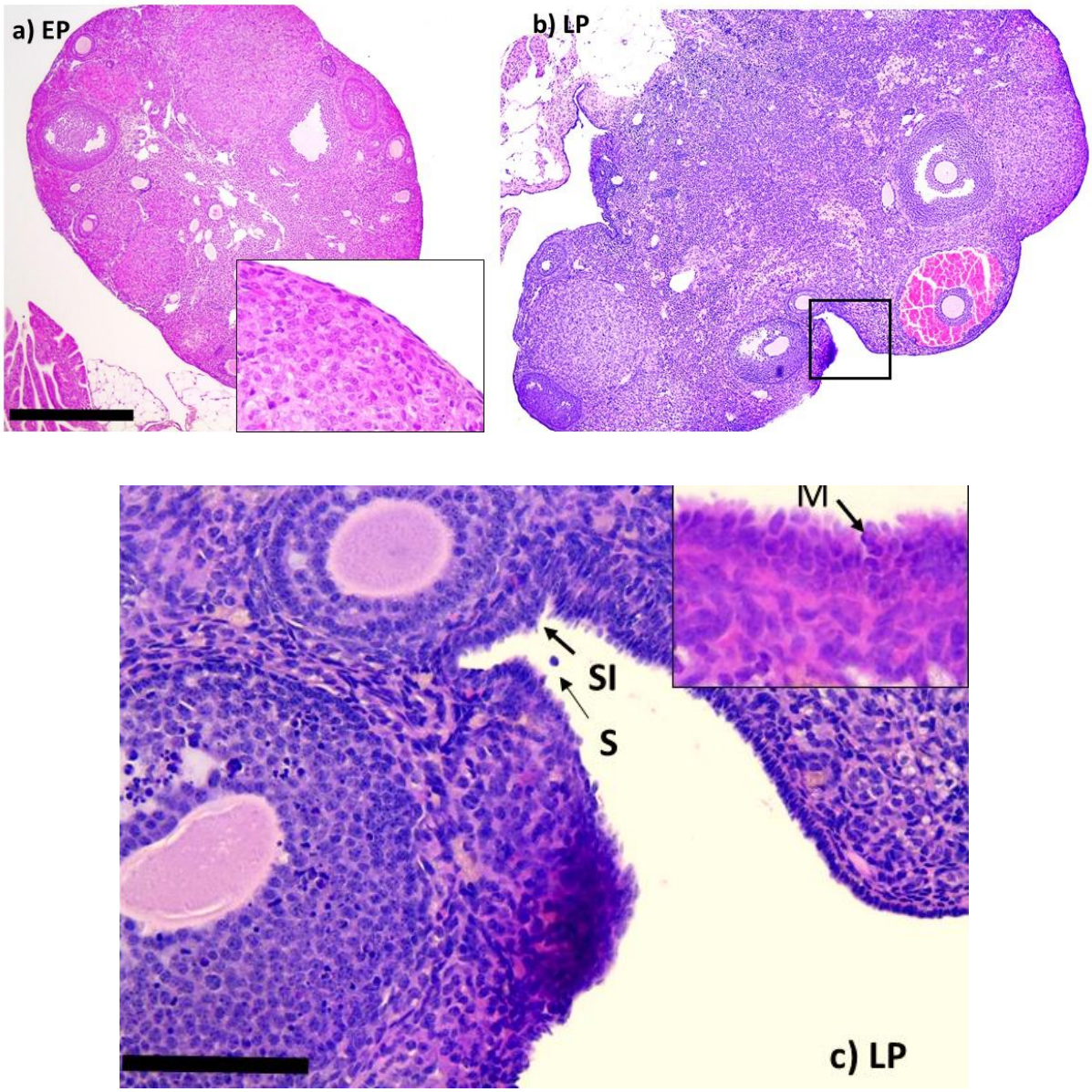

Figure 6.7: OSE homeostasis is disrupted in aging mice. Photomicrographs of H&E-stained ovarian sections at (a) 8-weeks post-induction/early point (EP, inset 5X original magnification), and (b) 12 months of age (9.5 months post-induction/Late point (LP)). Scale bar 500 µm. (c) 5X original magnification of squared area in (b). Inset 2X original magnification. SI: infiltration. M: multi-layering. S: shedding. Scale bar 100 µm. n=4 for EP cohort. n=7 for LP cohort.

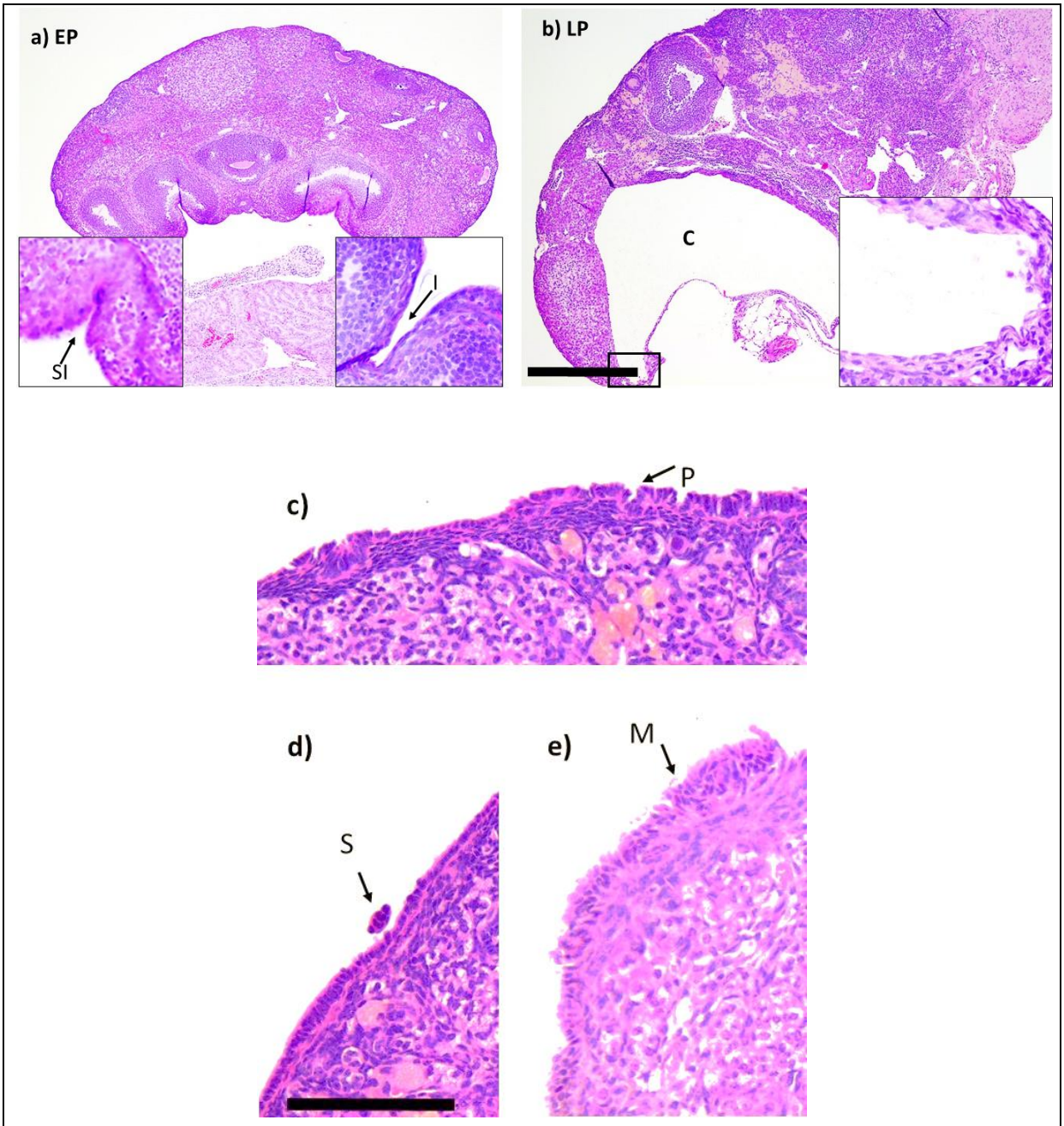

Figure 6.8: OSE abnormalities seen in *Apc*$^{fl/fl}$ ovaries post-induction. Photomicrographs of H&E staining for ovarian sections (a) 8-weeks post-induction/early point (EP, n=4), showing the presence of deep invagination and stromal infiltration, and (b) 12 months of age/late point (LP), showing an ovarian cyst. Scale bar 500 µm. Insets show 5X original magnification. Other OSE irregularities observed in LP (n=7) included (c) micro-papillary formation, (d) epithelial shedding, and (e) epithelial multi-layering. Scale bar in (c-e) 100 µm. I: invagination. SI: stromal infiltration. C: cyst. P: micro-papillary epithelium. S: shedding. M: multi-layering.

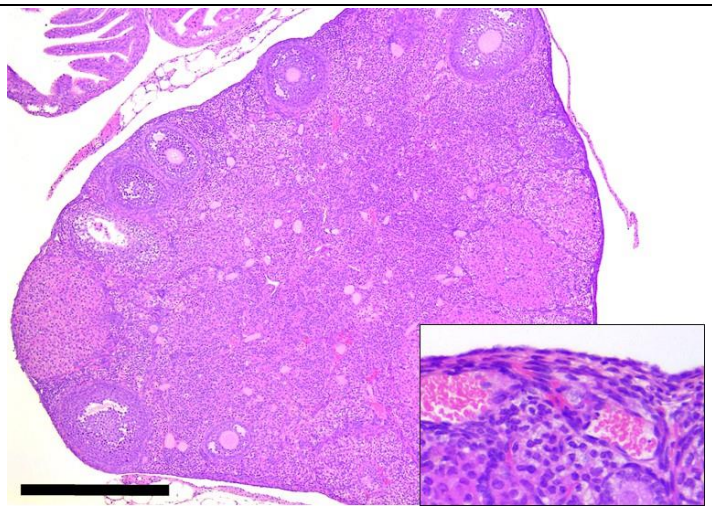

Figure 6.9: OSE irregularities are not evident in *Apc2*$^{-/-}$ mice 8-weeks post-induction. Photomicrograph showing smooth OSE covering the whole ovary. Inset show OSE at 5X original magnification. Scale bar 500 µm. n=3.

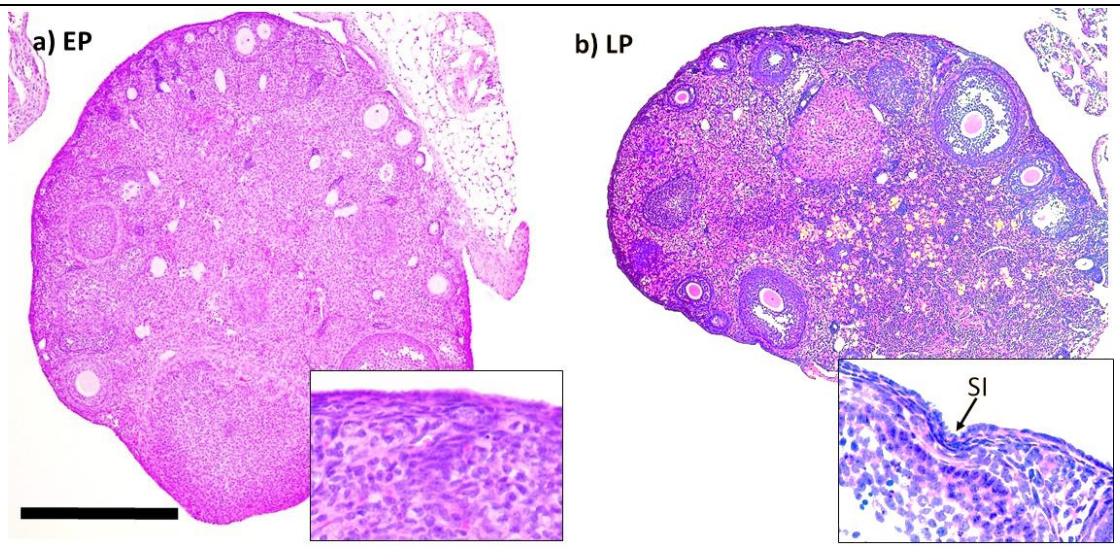

Figure 6.10: Minimal OSE disruption caused after loss of both APC proteins. Photomicrographs of H&E staining for ovarian sections (a) 8-weeks post-induction/early point (EP), with no OSE irregularities observed, and (b) at 12-months of age/late point (LP), with a small stromal infiltration (SI) observed. Scale bar 500 µm. Insets show 5X original magnification. n=3.

In any cellular system, the balance between proliferation and death is an important determinant in homeostasis. In order to assess whether this balance was disrupted after combined loss of APC and APC2 proteins in the epithelium, IHC analysis was performed using cleaved caspase-3 (apoptosis) and Ki67 (proliferation) antibodies respectively, and the number of positive nuclei were counted. It is known that the OSE resists apoptosis, and it is only ever evident in the post-ovulatory site during estrus stage (Slot *et al.* 2006). No apoptotic cells were present in the OSE in any of the experimental cohorts studied at either time point. Ki67 staining was not significantly altered in $Apc^{fl/fl}$ ovaries at both time points (Figure 6.11-12). Additional loss of APC2 did not alter the proliferation observed in the OSE of $Apc^{fl/fl}$ ovaries (Figure 6.11-12). It was noted that OSE proliferation decreased with age in all the cohorts, and was absent in the multi-layering lesions previously recorded (Figure 6.7-6.10).

In order to determine the level of WNT signalling activation in the OSE of mice in these cohorts, β-catenin IHC was performed and cells expressing nuclear β-catenin were counted (Figure 6.13-14). At 8-weeks post-induction, nuclear β-catenin was not evident in the OSE of wild type or $Apc2^{-/-}$ ovaries. However, when *Apc* was deleted, either alone or in combination with *Apc2*, nuclear β-catenin was present in cells of the OSE. Although the same pattern was found in aged mice, nuclear β-catenin levels were much reduced in OSE of $Apc^{fl/fl}$ ovaries, but remained high in double null ovaries. In multi-layering events, nuclear β-catenin was absent.

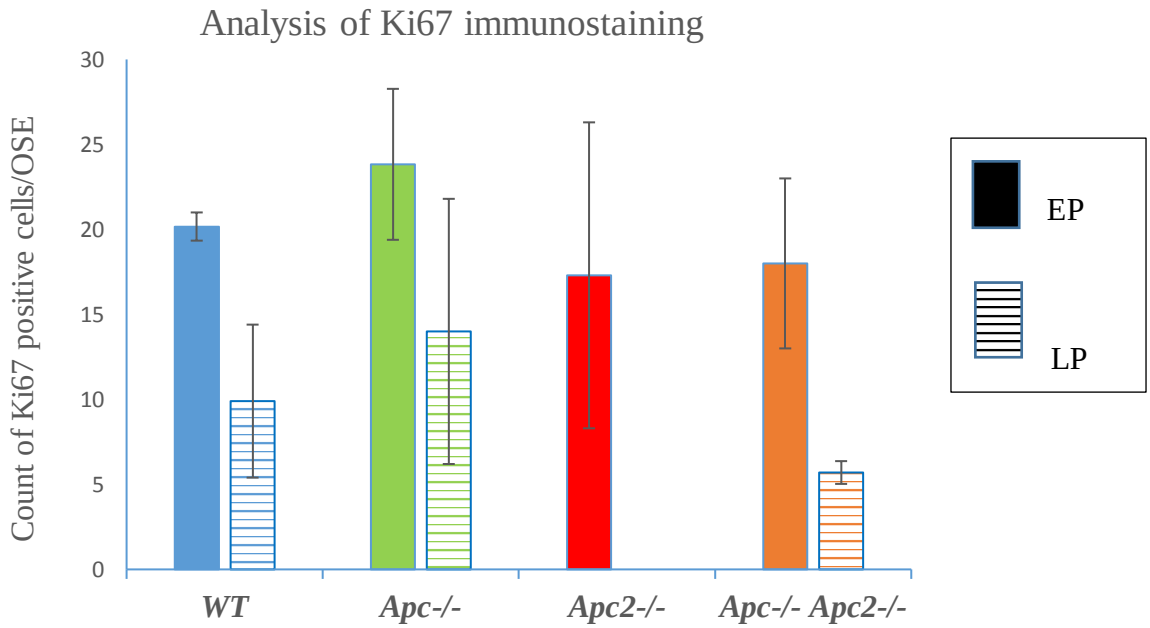

Figure 6.11: Proliferation is not significantly altered after combined loss of APC and APC2 proteins in the OSE. Histogram showing the number of Ki67-positive cells in the OSE. Data are presented as mean±S.E. n=3-4. EP: early point. LP: late point. *Apc*$^{-/-}$: *Apc*$^{fl/fl}$

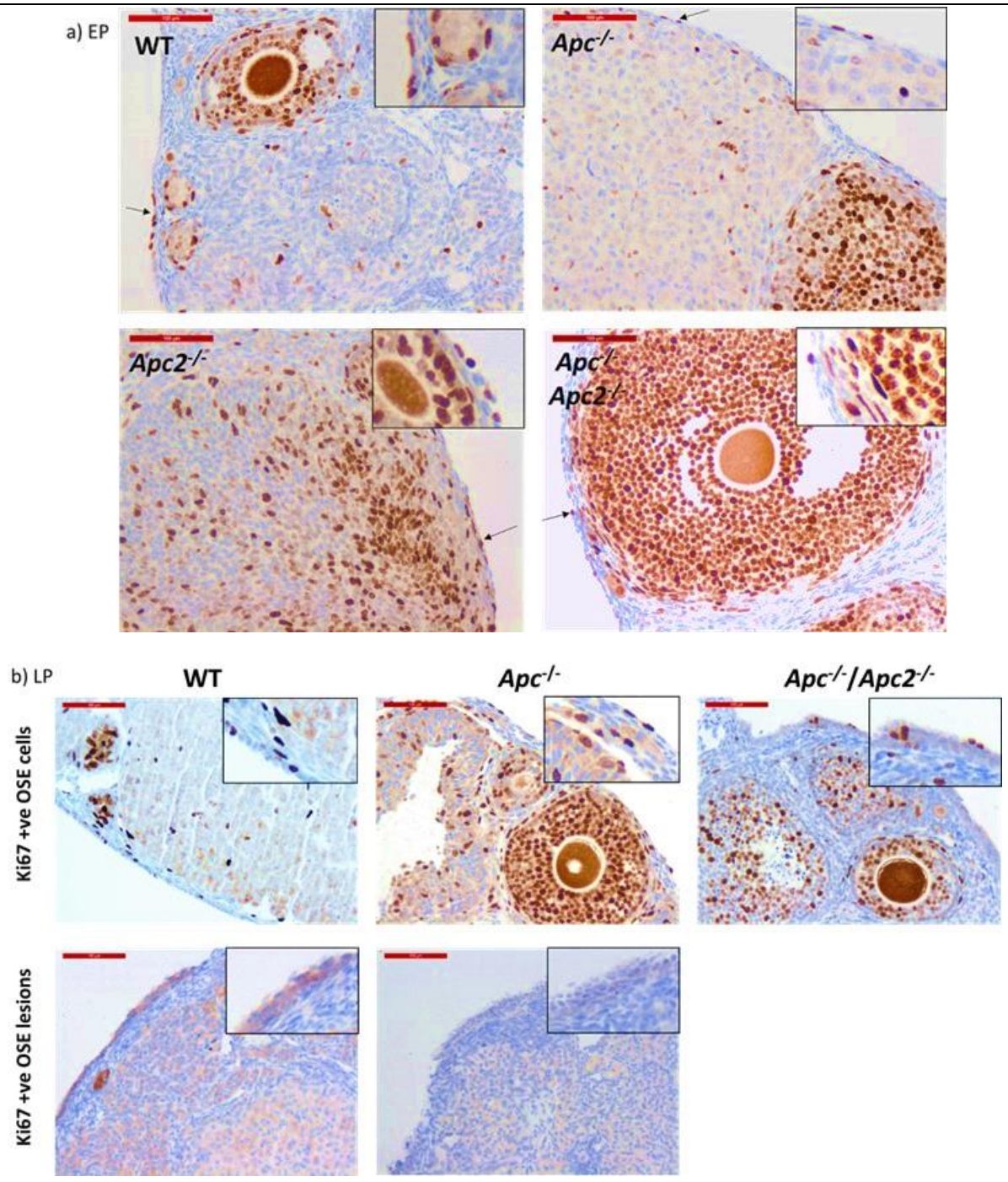

Figure 6.12: Proliferation after combined loss of APC and APC2 proteins in the OSE. Photomicrographs of Ki67 immunostaining in experimental cohorts (a) 8-weeks post-induction, and (b) at 12-months of age; upper panel showing positive cells in the OSE, and lower panel showing absence of positive cells in multi-layering events. Black arrows: Ki67-positive cells in the OSE. Scale bar 100 µm. Insets show OSE at 2X original magnification. n=3-4. EP: early point. LP: late point. $Apc^{-/-}$: $Apc^{fl/fl}$

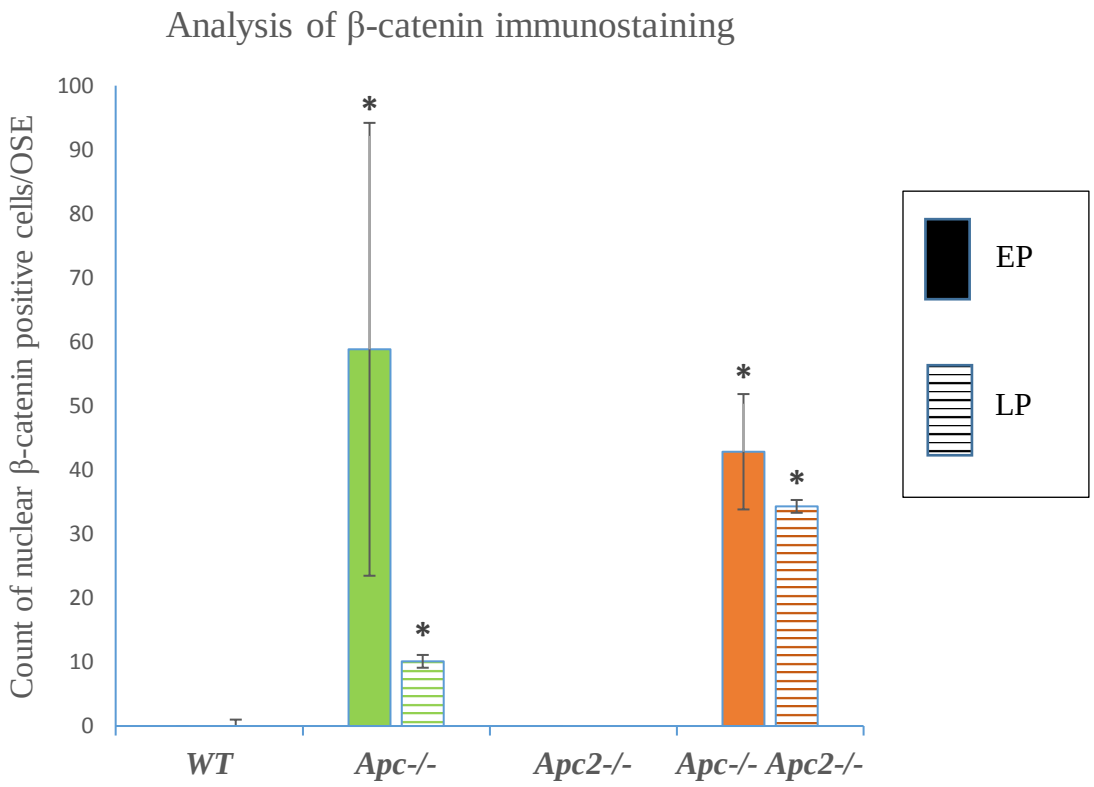

Figure 6.13: β-catenin nuclear staining is evident only after APC loss. Histogram showing the number of nuclear β-catenin positive cells in the OSE. Data are presented as mean±S.E. EP: early point. LP: late point. n=3-4. * denotes significance from age-matched $Apc2^{+/+}$ at $p<0.05$. $Apc^{-/-}$: $Apc^{fl/fl}$

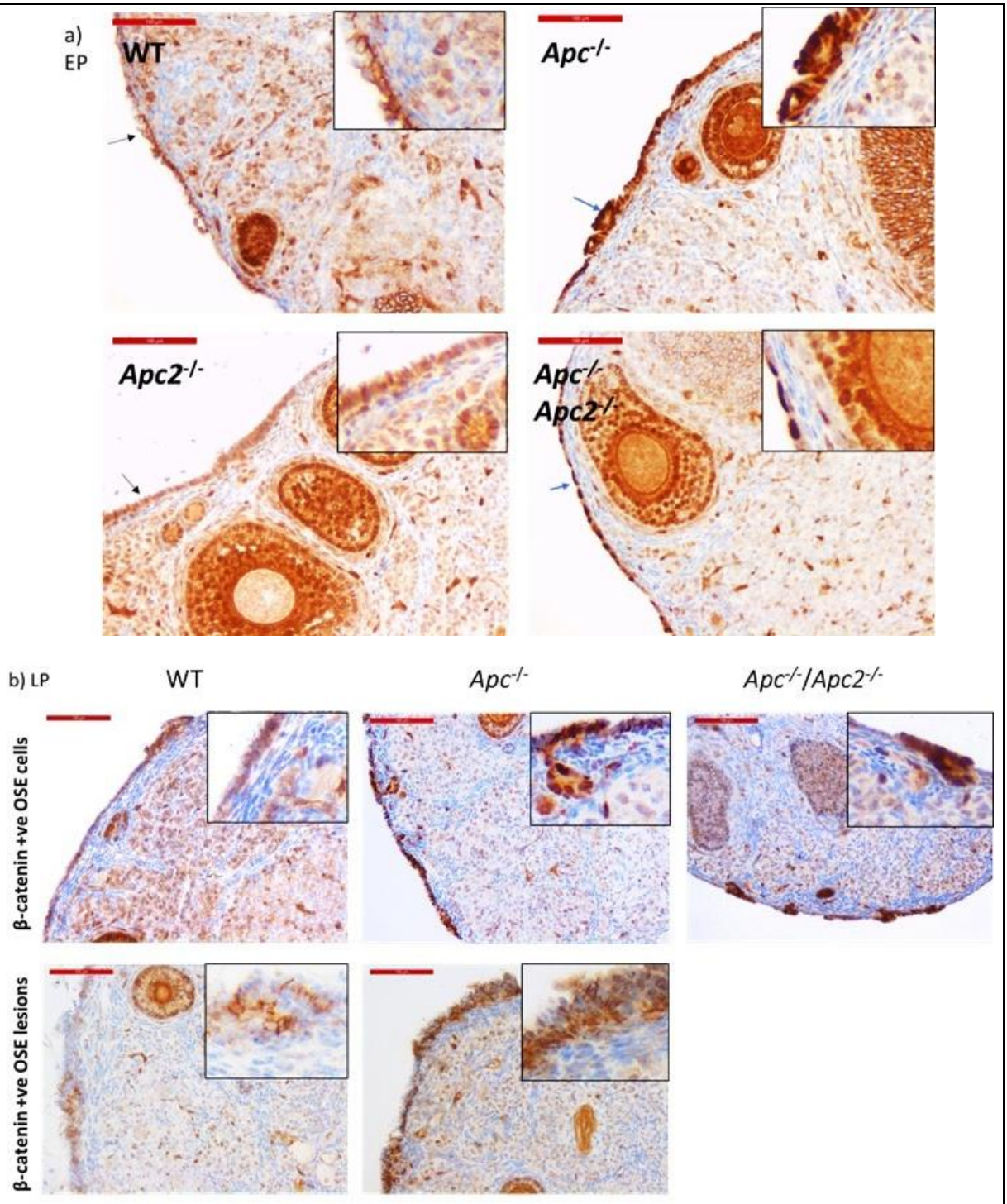

Figure 6.14: Activation of WNT signalling post-APC loss in the OSE. Photomicrographs of β-catenin immunostaining in experimental cohorts at (a) 8-weeks post-induction, and (b) 12-months of age; upper panel shows positive cells in the OSE, and lower panel shows absence of positive cells in multi-layering events. Scale bar 100 µm. Insets show OSE at 2X original magnification. EP: early point. LP: late point. $Apc^{-/-}$: $Apc^{fl/fl}$. n=3-4.

It has been previously reported that E-cadherin is differentially expressed in OSE cells according to their morphology, being absent in squamous cells and present in cuboidal and columnar cells, and was linked to metaplasia preceding tumour formation (Maines-Bandiera and Auersperg 1997). To examine the effectof loss of APC proteins on E-cadherin expression, IHC was performed and the percentage of E-cadherin positive OSE was quantified (Figure 6.15-16). No significant differences were observed between the experimental cohorts at 8-weeks post-induction; however, levels were significantly increased in the double mutant mice at the late time point compared to all other groups ($p<0.05$). This was accompanied by stromal infiltration of E-cadherin positive cells (Figure 6.16).

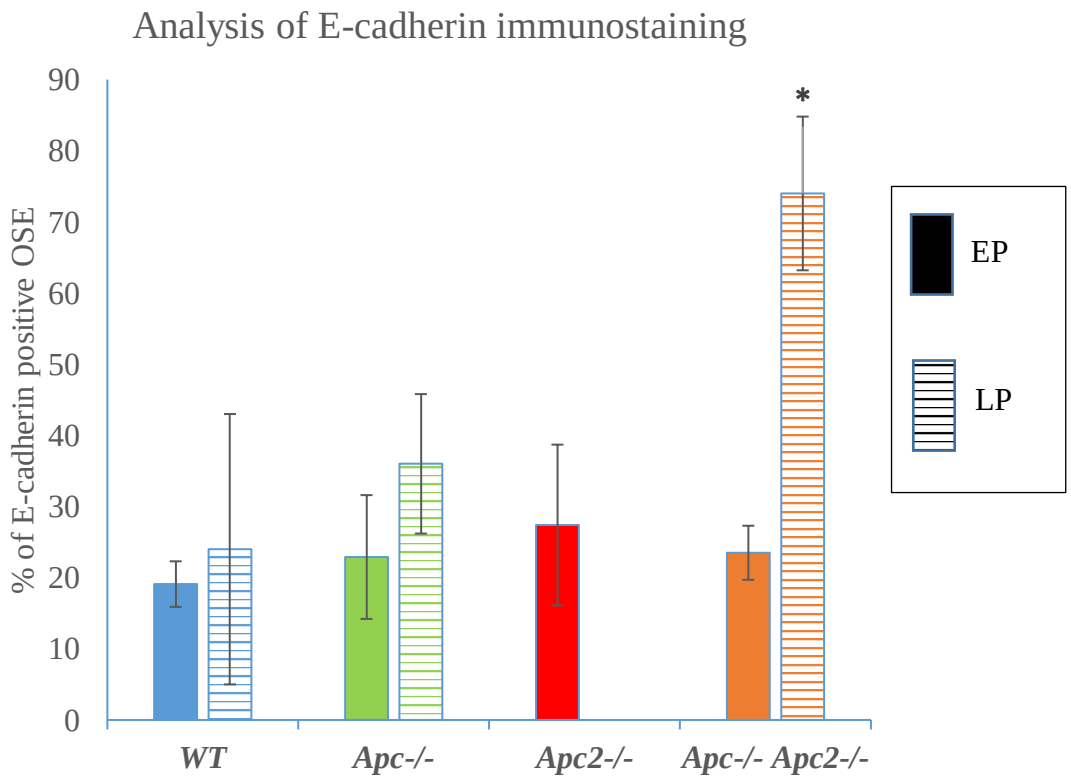

Figure 6.15. E-cadherin staining is elevated in OSE of aged mice after combined loss of both APC and APC2 proteins. Histogram showing the percentage of E-cadherin positive OSE. Data are presented as mean±S.E. EP: early point. LP: late point. $Apc^{-/-}$: $Apc^{fl/fl}$. n=3-4. * denotes significance from all other groups at $p<0.05$.

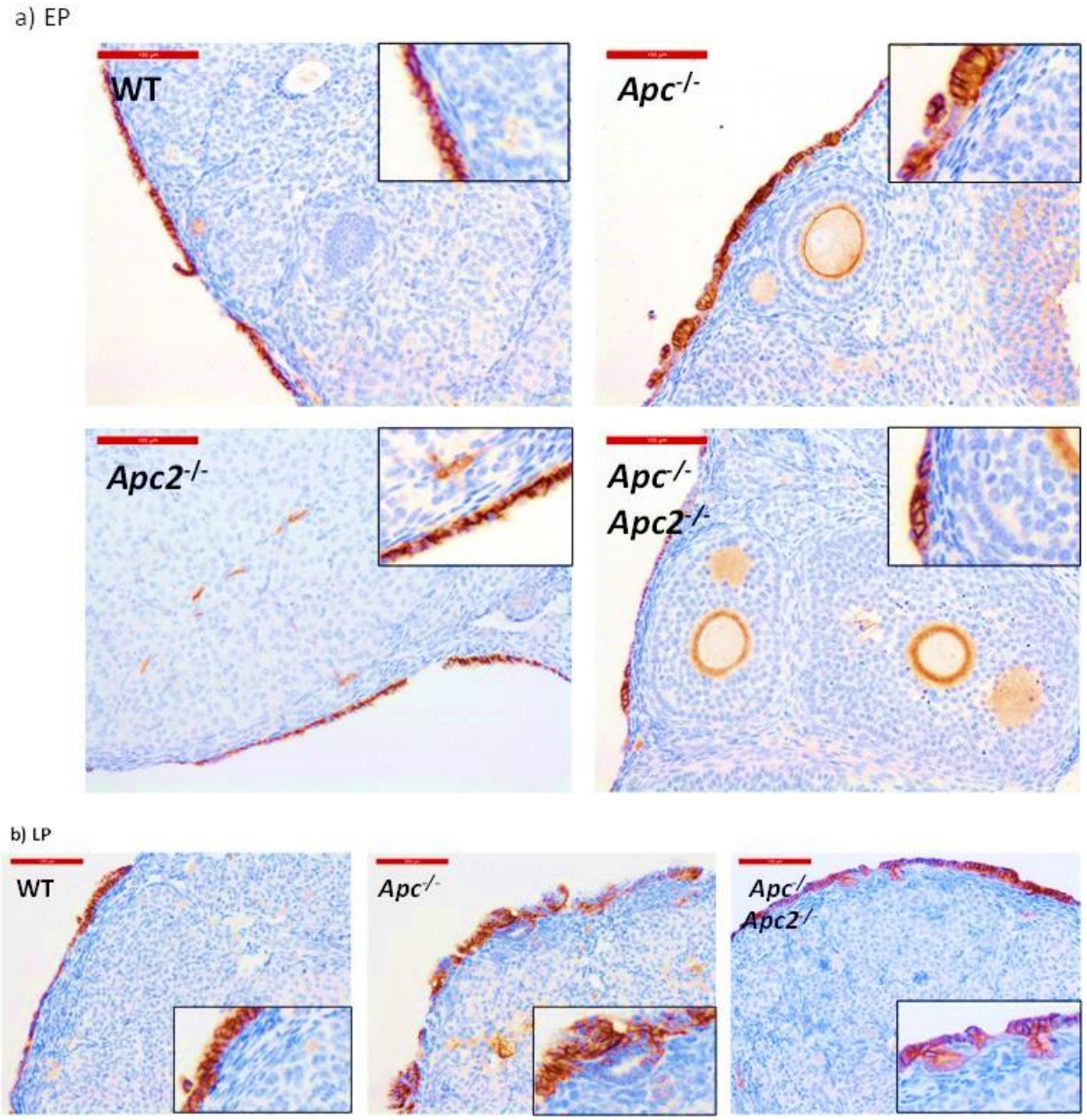

Figure 6.16: E-cadherin immunohistochemical staining in Ad-*cre* induced $Apc^{fl/fl}$ ovaries. Photomicrographs of E-cadherin immunostaining in experimental cohorts (a) 8-weeks post-induction, and (b) at 12-months of age. Staining exclusively present in the OSE, except in LP $Apc^{-/-}/Apc2^{-/-}$, where E-cadherin positive cells infiltrated the stroma under the OSE. Scale bar 100 µm. Insets show OSE at 2X original magnification. EP: early point. LP: late point. $Apc^{-/-}$: $Apc^{fl/fl}$. n=3-4.

In conclusion, deleting APC in the OSE, either alone or in combination with APC2, did not cause tumour development in the ovaries.

6.2.3. Conditional deletion of PTEN in the OSE of APC2-deficient mice is not enough to initiate tumourigenesis.

It has been shown, both in growing follicles and in GCTs, that PTEN protein expression is elevated in APC2-deficient ovaries (Sections 4.2.6 and 5.2.5). In addition, it has been previously reported that combined deletion of PTEN and APC in the OSE by intrabursal adenovirus-*cre* induction, initiates OEAs with 100% penetrance as early as 6-weeks post-induction (Wu *et al.* 2007). In order to test whether the same is true with APC2 deletion rather than APC, *Apc2*$^{-/-}$ mice were crossed with *Pten*$^{fl/fl}$ mice, and intrabursal injection of adenovirus-*cre* was used to induce recombination of the floxed *Pten* gene exclusively in the surface epithelium of ovaries in 10-week-old mice. Ovaries were collected 8 weeks later and subjected to histopathological and IHC analysis. An outline of experimental groups induced by adenovirus-*cre* in this experiment is shown in Table 6.3.

Table 6.3: Experimental cohorts injected intrabursally with adenovirus-cre to characterize effects of combined deletion of APC2 and PTEN in the OSE.

Genotype/ Time of dissection	***Pten*$^{fl/fl}$**	***Pten*$^{fl/fl}$ /*Apc2*$^{-/-}$**
Early time point (8-weeks post-induction)	n=5	n=3
Late time point (age of 12 months)	n=6	n=4 (not analysed, still alive)

When *Pten*$^{fl/fl}$ ovaries were induced and collected 8 weeks later, a range of OSE pathologies were observed in 4/5 mice (Table 6.4, Figure 6.17). Multi-layering together with invagination was evident in 1/5 ovary, stromal infiltration together with glandular formation and micro-papillary growth in 1/5 ovary, OSE shedding in 1/5, and invagination in 1/5 of ovaries analysed (Table 6.4, Figure 6.17). When induced *Pten*$^{fl/fl}$ mice were left to age and

ovaries collected at 12-month, 5/6 showed severe disruption of the epithelium with 2/6 (33.3%) developing OEA, 1/6 (16.7%) developing pre-tumour lesions (serous papillary hyperplasia) and 1/6 (16.7%) displaying a large bursal cyst (accompanied with oviductal tumour), which enclosed the ovary (Table 6.4, Figure 6.17). Stromal infiltration, which ranged from slight to deep, was observed in all the ovaries analysed (100%). Shedding, multi-layering, micro-papillary growth and small glands were observed in 5/6 ovaries (83.3%). Out of 3 ovaries examined 8-weeks post-combined loss of PTEN and APC2 in OSE, one did not show any pathologic alterations. Of the other 2 ovaries, one displayed shedding, and the other one displayed shedding in addition to multi-layering and deep invagination (Table 6.4, Figure 6.18). Due to the subfertility of *Apc2*$^{-/-}$ mice, generating *Pten*$^{fl/fl}$ /*Apc2*$^{-/-}$ female mice took longer than anticipated. This caused delays in the induction of this cohort assigned to age until 12 months, making it unavailable for analysis at the time of writing.

Table 6.4: OSE disruptions observed in PTEN/APC2 experimental cohorts. EP: early point, 8-weeks post-induction. LP: late point, at 12 months of age.

Experimental group /histologic feature	***Pten*$^{fl/fl}$ EP**	***Pten*$^{fl/fl}$*/Apc2*$^{-/-}$ EP**	***Pten*$^{fl/fl}$ LP**
Total OSE disruptions	4/5	2/3	5/6
Invagination	2/5	1/3	0/6
Multi-layering	1/5	1/3	5/6
Stromal infiltration	1/5	0/3	6/6
OSE shedding	1/5	2/3	5/6
Gland formation	1/5	0/3	5/6
Micro-papillary growth	1/5	0/3	5/6
Poorly differentiated OEA	0/5	0/3	2/6
Pre-tumour lesions	0/5	0/3	1/6
Cyst	0/5	0/3	1/6

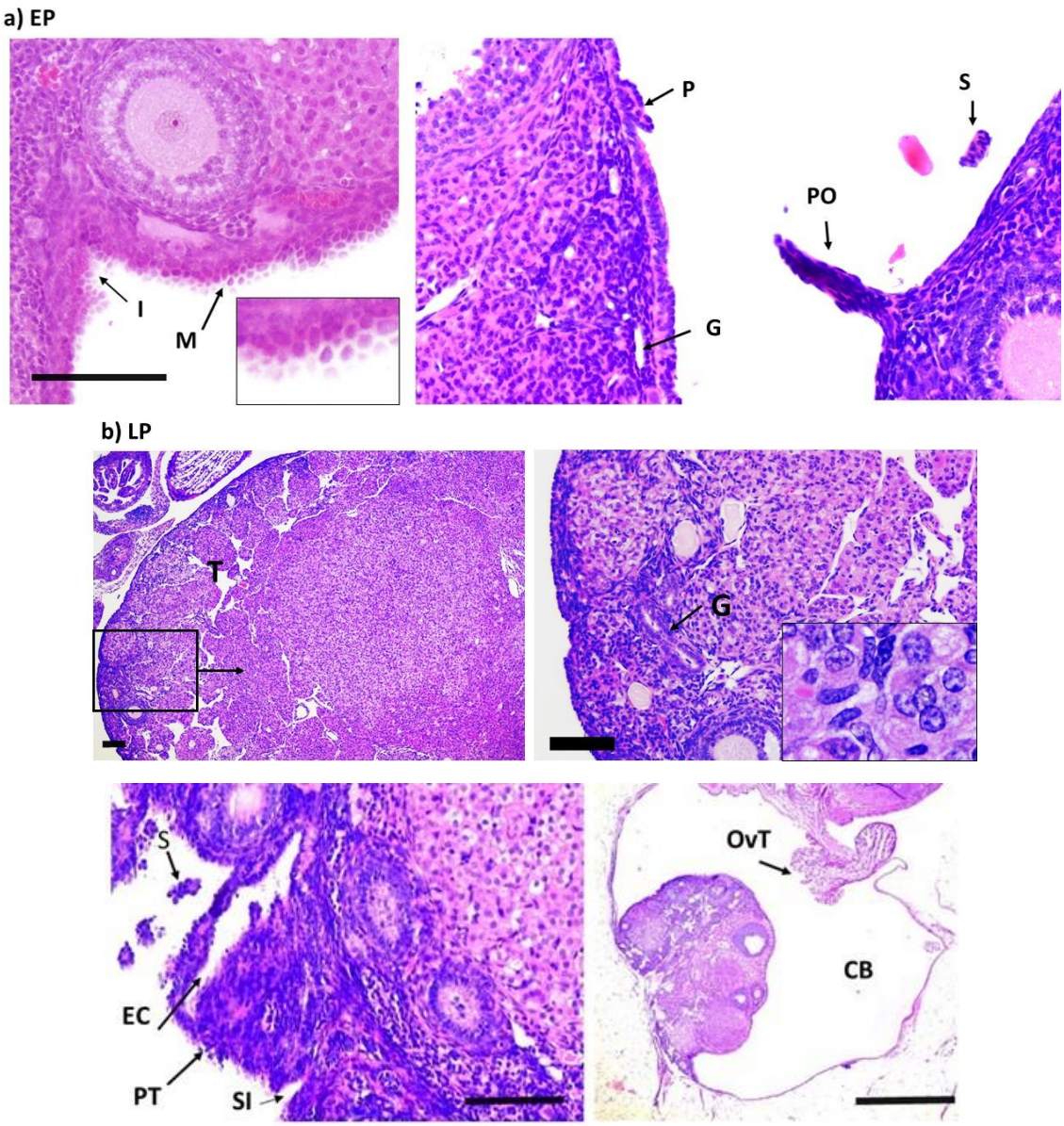

Figure 6.17: A subset of induced *Pten*$^{fl/fl}$ ovaries display tumourigenesis upon aging. Photomicrographs displaying abnormalities observed in *Pten*$^{fl/fl}$ OSE at (a) 8-weeks post-induction (Scale bar 100 µm, n=5) and (b) 12 months of age (n=6). In (b), the upper panel shows an OEA, Left panel is 5X original magnification. Inset shows highly metaplastic cells at 10X original magnification, scale bar 100 µm. Lower left panel shows serous papillary hyperplasia, scale bar 100 µm, right panel shows a bursal cyst and oviductal tumour, scale bar 1 mm. EP: early point, LP: late point. I: invagination, M: multi-layering, P: micro-papillary formation, PO: papillary outgrowth, S: shedding, T:tumour, G: gland, EC: epithelial cyst, PT: pre-tumour lesion, SI: stromal infiltration, CB: bursal cyst, OvT: oviductal tumour.

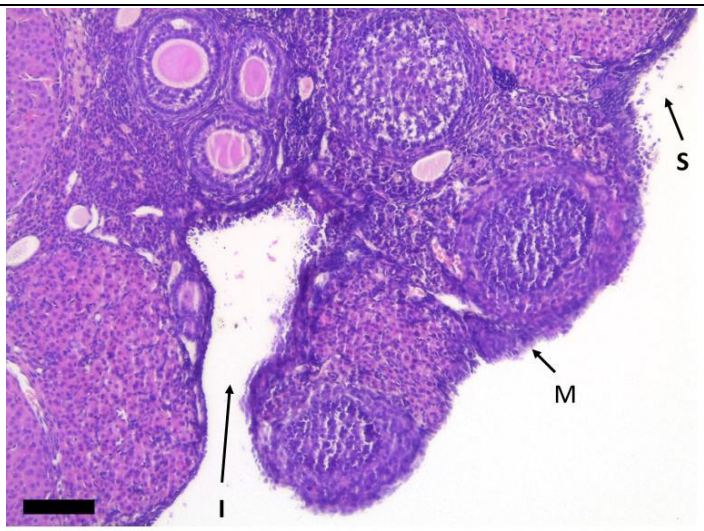

Figure 6.18: OSE is disrupted following combined APC2 and PTEN loss in the epithelium. Photomicrograph displaying a range of abnormalities observed in *Pten*$^{fl/fl}$/*Apc2*$^{-/-}$ OSE 8-weeks post-induction (Scale bar 100 µm, n=3) I: invagination, M: multi-layering, S: shedding.

In order to assess the level of activation of PI3K/AKT signalling post-PTEN deletion, IHC for p-AKT (Ser473) was performed. In the *Pten*$^{fl/fl}$ ovaries collected 8-weeks post-induction, p-AKT levels were variable and ranged from weak (2/3) to moderate (1/3) staining in the OSE without involvement of the underlying stroma (Figure 6.19). However, in the aged cohort, p-AKT immunostaining was high in the OSE and in the lesions previously described, apart from the oviductal tumour (Figure 6.19). In the *Pten*$^{fl/fl}$/*Apc2*$^{-/-}$ ovaries collected 8-weeks post-induction, p-AKT staining ranged from weak (2/3) to strong (1/3) staining in the OSE (Figure 6.19).

Ki67 immunohistochemistry was used to quantify differences in OSE proliferation between *Pten*$^{fl/fl}$/*Apc2*$^{-/-}$ and *Pten*$^{fl/fl}$ ovaries, 8-weeks post-induction, and there was a non-significant increase in proliferation in *Pten*$^{fl/fl}$/*Apc2*$^{-/-}$ ovaries (Figure 6.20). When Ki67 immunostaining was assessed in the *Pten*$^{fl/fl}$ aged ovaries, the tumour and pre-tumour lesions were not highly proliferative (Figure 6.20).

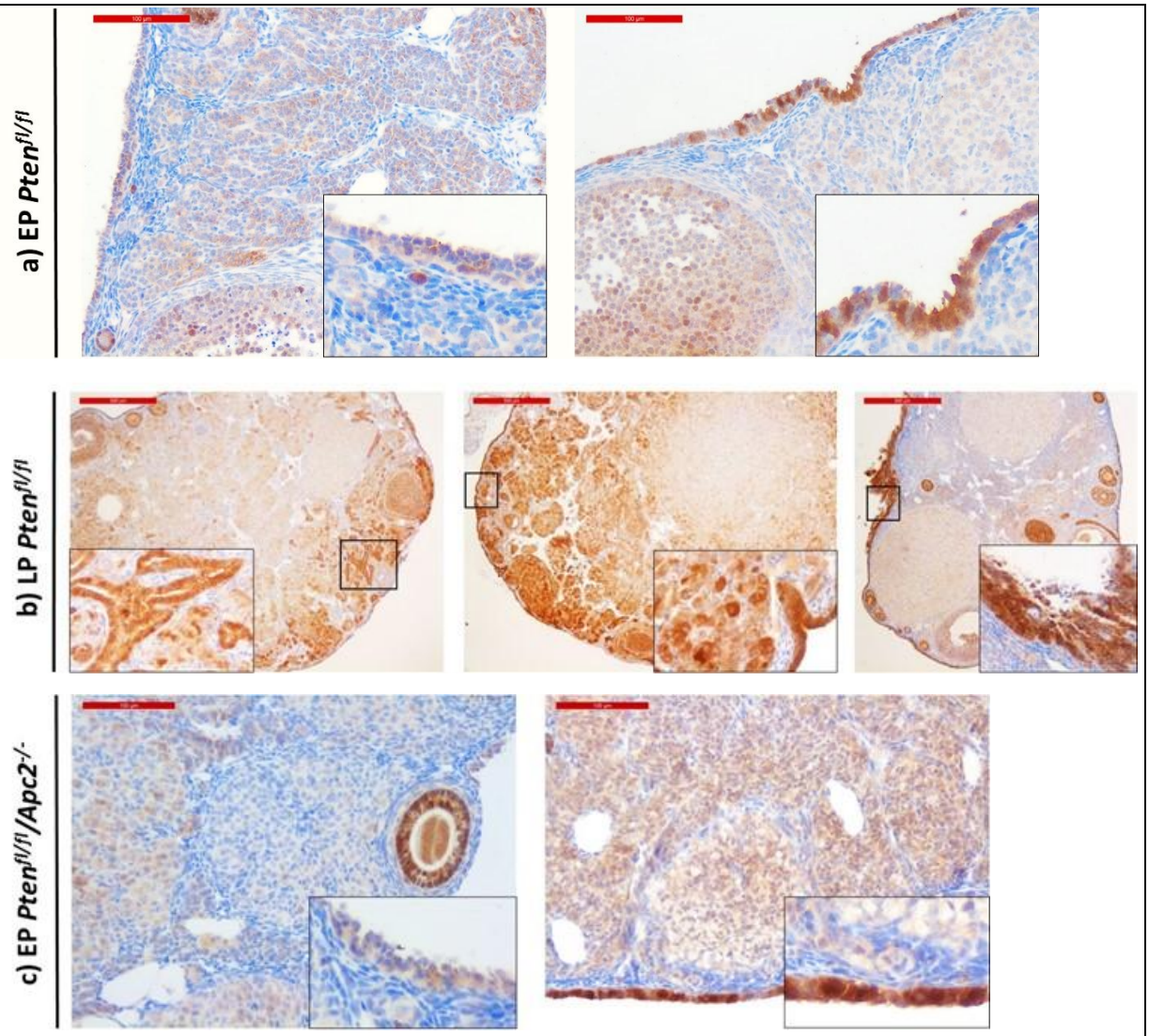

Figure 6.19: p-AKT is differentially expressed post PTEN-loss in *Apc2*$^{+/+}$ and *Apc2*$^{-/-}$ ovaries. Representative photomicrographs of p-AKT (Ser473) immunostaining in the OSE/lesions in (a) *Pten*$^{fl/fl}$ ovaries 8-weeks post-induction; scale bar 100 µm; insets show OSE at 2X original magnification, (b) induced *Pten*$^{fl/fl}$ ovaries aged to 12 months, scale bar 500 µm, insets show black squares at 5X original magnification, and (c) *Pten*$^{fl/fl}$ /*Apc2*$^{-/-}$ ovaries 8-weeks post-induction, scale bar 100 µm, insets show OSE at 2X original magnification EP: early point. LP: late point.

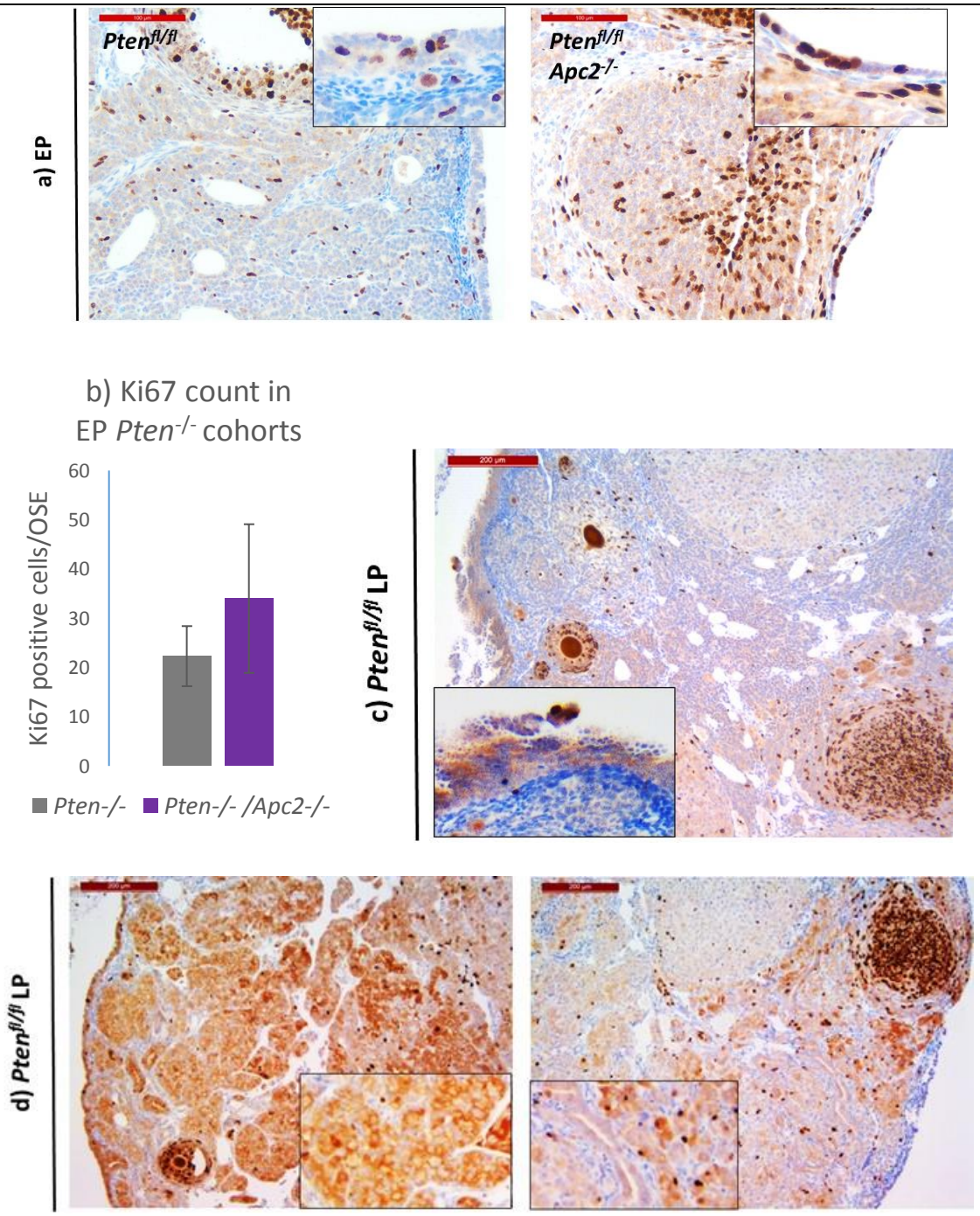

Figure 6.20: Lesions in *Pten*$^{fl/fl}$-aged ovaries are not highly proliferative. (a) Photomicrographs of Ki67 immunohistochemistry in *Pten*$^{fl/fl}$ and *Pten*$^{fl/fl}$/*Apc2*$^{-/-}$ ovaries 8-weeks post-induction (Scale bar 100 µm, n=3). (b) Histogram of Ki67-positive cells in the OSE at early time point (mean±S.E). Photomicrographs of Ki67 immunohistochemistry in (c) a pre-tumour lesion and (d) OEA tumours of aged *Pten*$^{fl/fl}$ ovaries. Scale bars 200 µm. Insets 2X original magnification. *Pten*$^{-/-}$: *Pten*$^{fl/fl}$

E-cadherin immunostaining was performed and the percentage of positively stained OSE quantified in *Pten*$^{fl/fl}$/*Apc2*$^{-/-}$ and *Pten*$^{fl/fl}$ ovaries, at 8-weeks post-induction. Similar to Ki67 immunostaining, a non-significant increase of E-cadherin expression was observed in *Pten*$^{fl/fl}$/*Apc2*$^{-/-}$ (Figure 6.21). In both groups, the expression of E-cadherin was confined to the OSE, with no apparent stromal infiltration. However, in aged *Pten*$^{fl/fl}$ ovaries, E-cadherin expression was present in the OSE as well as the pre-tumour lesions, tumours and the lining of the bursal cyst described previously (Figure 6.22).

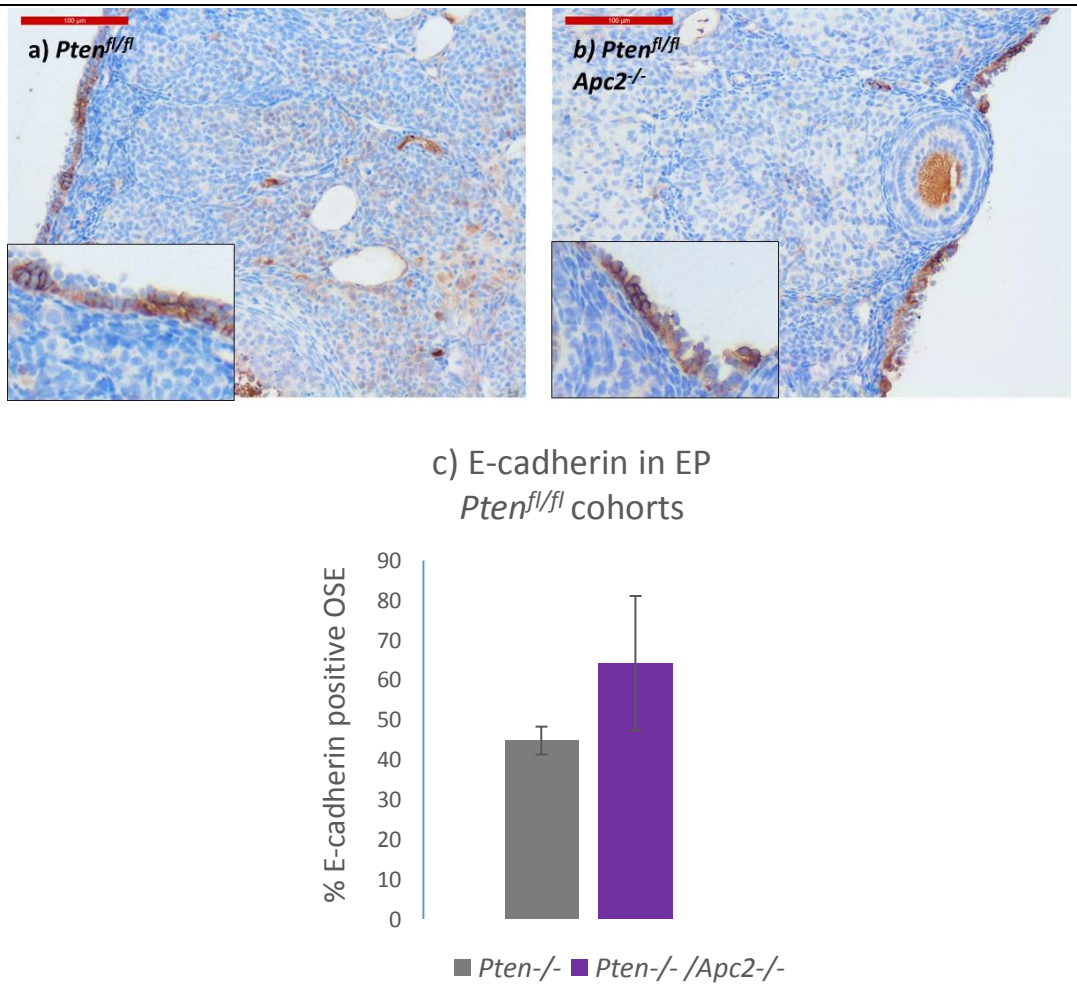

Figure 6.21: E-cadherin expression in *Apc2*$^{+/+}$ and *Apc2*$^{-/-}$ ovaries 8-weeks after PTEN-loss. Photomicrographs of E-cadherin immunohistochemistry in (a) *Pten*$^{fl/fl}$ and (b) *Pten*$^{fl/fl}$/*Apc2*$^{-/-}$ ovaries 8-weeks post-induction. Scale bar 100 µm. Insets are 2X original magnification. (c) Histogram of % of E-cadherin-positive OSE (mean±S.E.). n=3. *Pten*$^{-/-}$: *Pten*$^{fl/fl}$

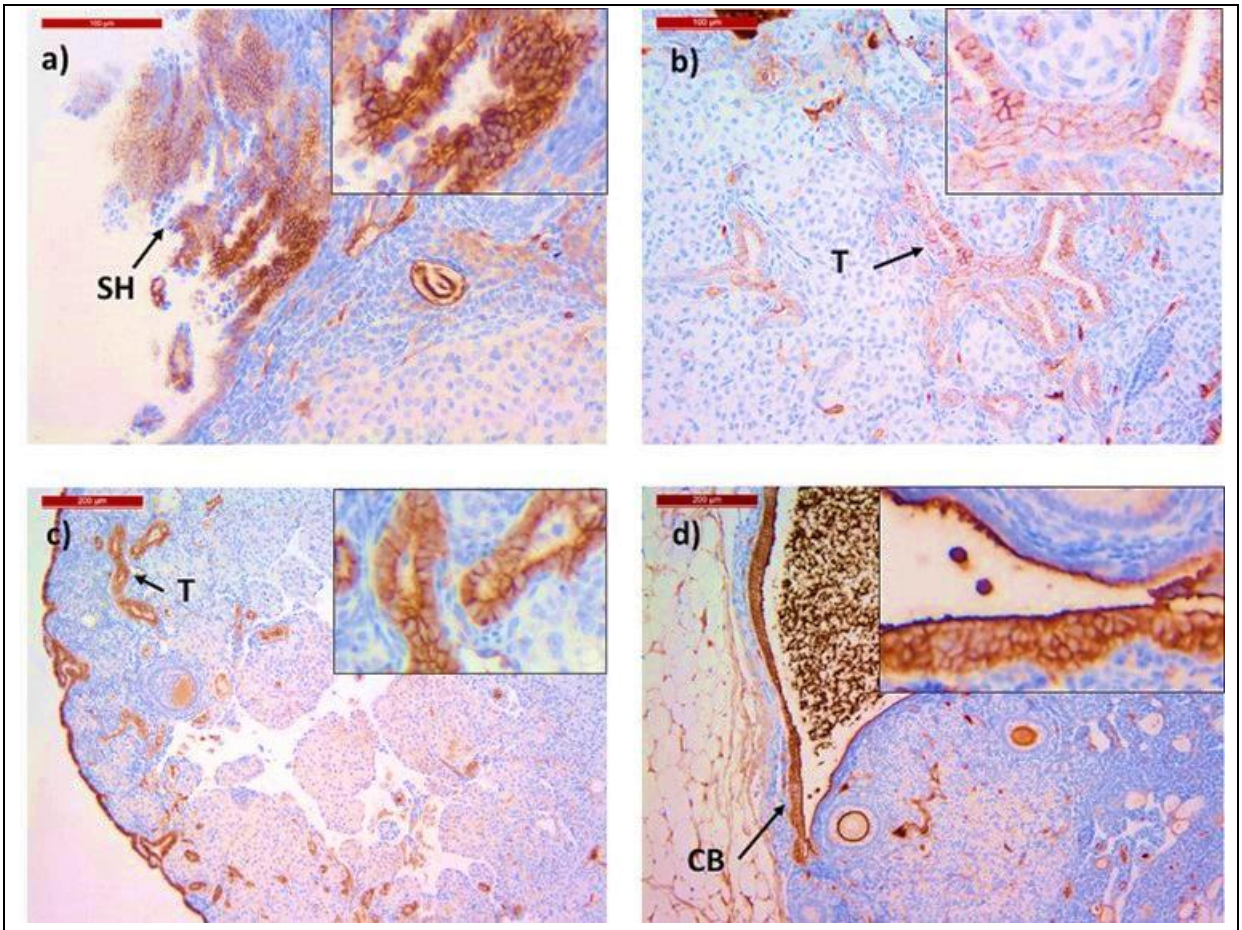

Figure 6.22: E-cadherin expression in *Pten*$^{fl/fl}$ - aged ovarian lesions. Photomicrographs of E-cadherin IHC in (a) pre-tumour lesion (serous hyperplasia of the OSE), (b,c) OEA tumours, and (d) bursal cyst. Scale bars: 100 µm (a,b), 200 µm (c,d). Black arrows: areas of E-cadherin-positivity in the lesions. Insets show higher magnification for the black arrow area (2X for a,b, 4X for c,d). SH: serous hyperplasia. T: tumour. CB: Bursal cyst.

In conclusion, unlike with APC (Wu *et al.* 2007), the combined loss of PTEN with APC2 in the OSE was insufficient to initiate tumour formation 8-weeks post-adenovirus-*cre* induction.

6.2.4. Loss of APC2 promotes initiation of OEA

As previously mentioned, deep deletions in *APC2* sequence were detected in 5.1% cases in one dataset of human serous ovarian carcinoma (TCGA). In addition, copy number alterations (deletions) have been shown in 19/20 ovarian tumour samples analysed (Jarrett *et*

al. 2001). It has been proposed that APC2 could be a potential epithelial tumour suppressor in the ovary (Jarrett *et al.* 2001), although it is not known whether APC2 loss contributes to tumourigenesis or results from it. In order to shed some light on this unexplored field, tumour initiation was assessed in adenovirus-*cre*-induced $Pten^{fl/fl}/Apc^{fl/fl}$ mice, which were either wild type, heterozygous or homozygous for the *Apc2* gene ($Apc2^{+/+}$, $Apc2^{+/-}$ or $Apc2^{-/-}$ respectively). Ovaries were collected 15-days post-induction (n=3), and examined microscopically for the presence of pre-tumour lesions (tumourlets), which have previously been described at 3 weeks post-induction in the $Pten^{fl/fl}/Apc^{fl/fl}$ model (Wu *et al.* 2011). In the $Apc2^{+/+}$ cohort, no tumourlets developed (Figure 6.23). However, in both the $Apc2^{+/-}$ and $Apc2^{-/-}$ cohorts, 2/3 ovaries (66.67%) developed tumourlets (mean number = 9 tumourlets in both cohorts), which were mostly small/medium surface/sub-surface lesions, apart from one ovary in the $Apc2^{-/-}$ cohort which developed a larger stromal tumourlet as well as regional metastasis of tumour tissue to outside the ovary (Figure 6.23). IHC showed high levels of expression of β-catenin in these structures (Figure 6.23). Collectively, these results indicate that loss of APC2 accelerates tumour formation in the adenovirus-*cre*-induced $Pten^{fl/fl}/Apc^{fl/fl}$ OEA model.

To further characterize this phenotype, IHC for Ki67, E-cadherin, and p-AKT were also carried out. Proliferation (Ki67 staining) was counted in OSE as well as in tumourlets when present, as it was very difficult to distinguish OSE in these pre-tumour lesions post-neoplastic transformation (Figure 6.24a,b). As a result of the high variability among data of the 3 groups, the increase in proliferation seen in APC2-deficient cohorts was not significant. All the tumourlets observed in APC2-deficient cohorts were highly proliferative (Figure 6.24a). A non-significant increase in E-cadherin immunostaining was observed in OSE from APC2-deficient mice (Figure 6.24a,b). It is noteworthy that not all cells in the tumourlets were expressing E-cadherin (Figure 6.24a).

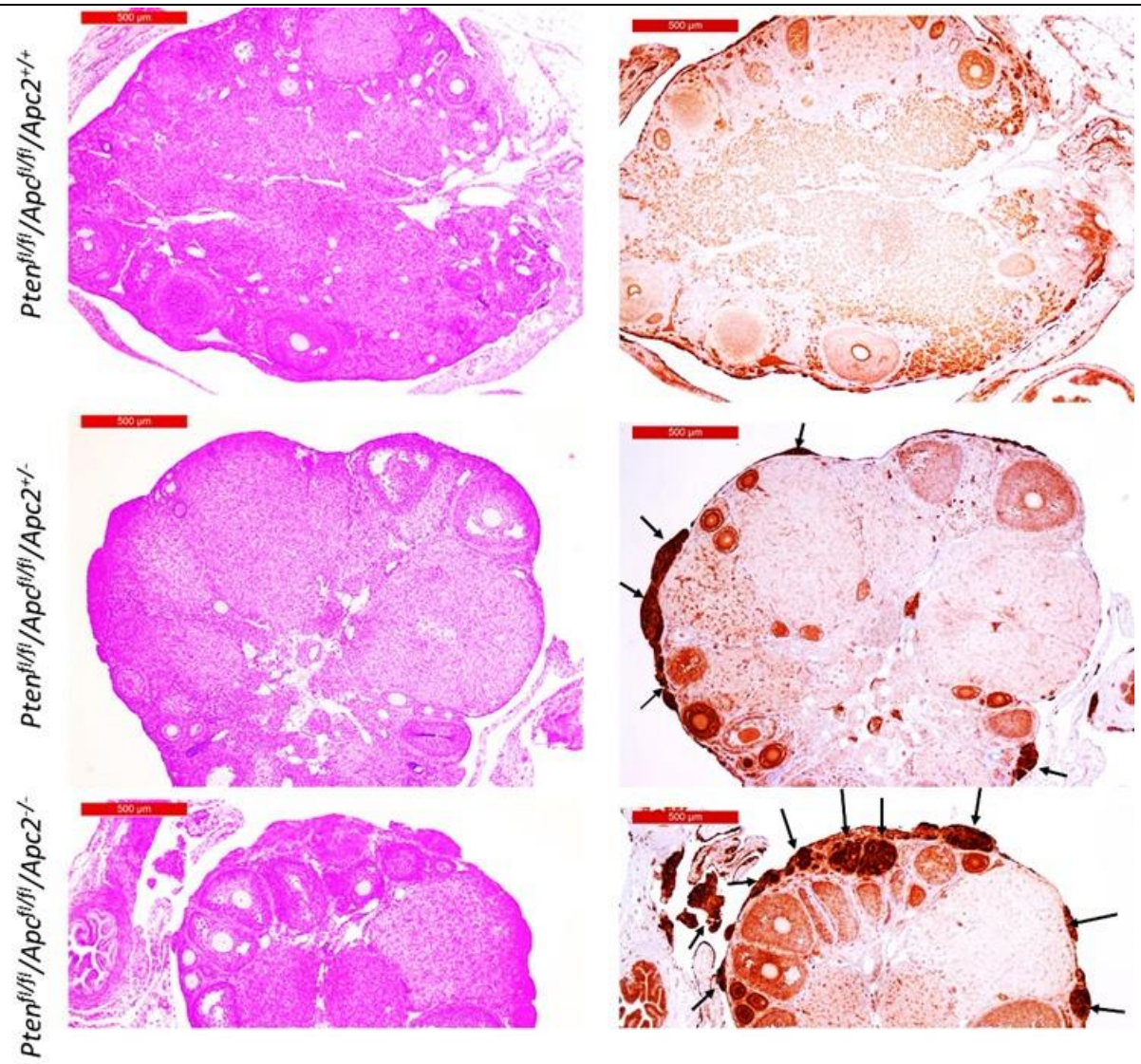

Figure 6.23: APC2 delays tumour initiation in adenovirus-*cre*-induced *Pten*$^{fl/fl}$/*Apc*$^{fl/fl}$ OEA model. Photomicrographs of H&E staining (left panel) and β-catenin staining (right panel) of ovaries dissected from the 3 experimental groups, 15-days post-induction. n=3. Black arrows indicate tumourlets. Scale bars 500 µm.

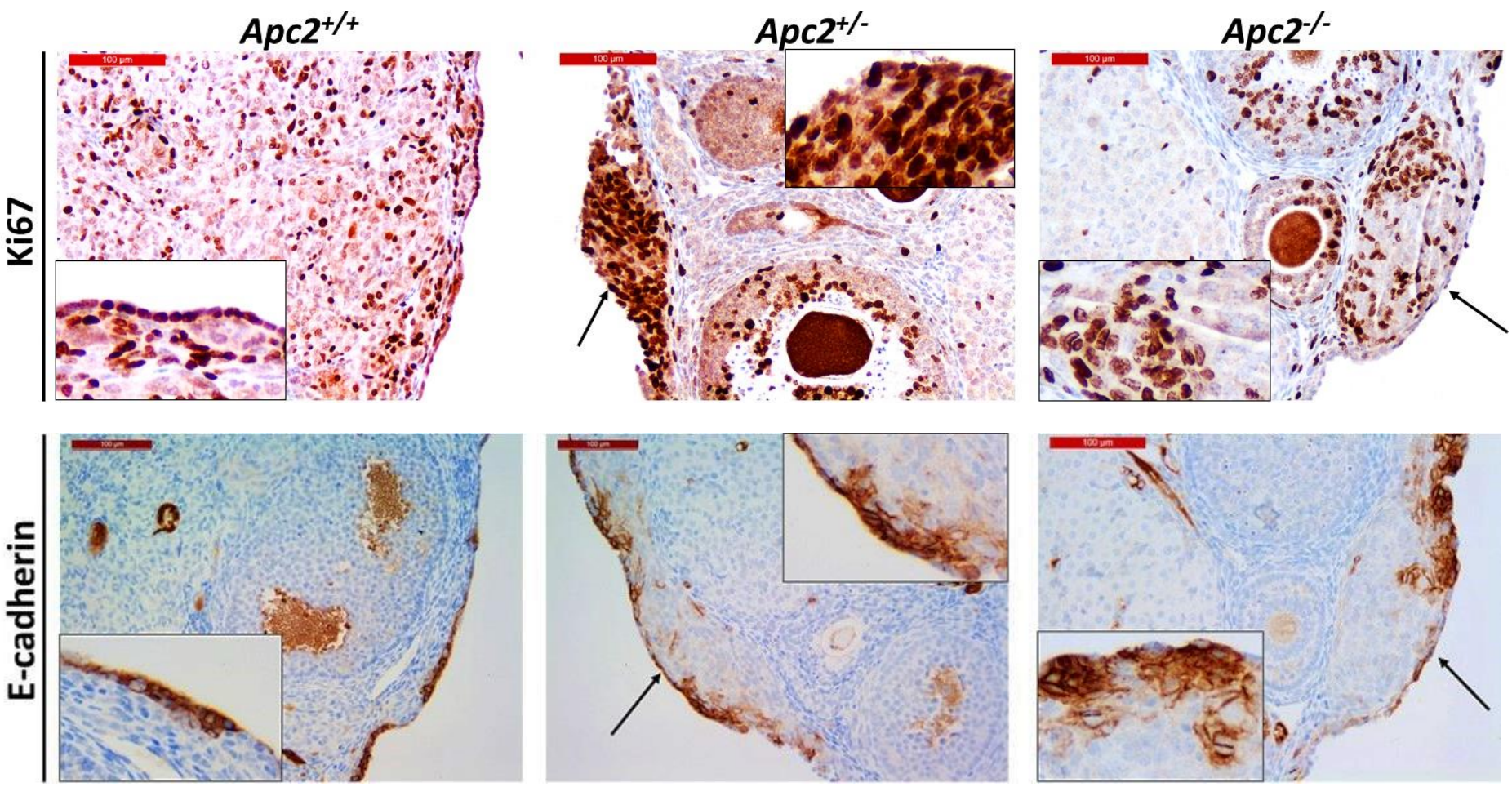

Figure 6.24a: Effect of APC2-deficiency on proliferation and epithelial differentiation in *Pten*$^{fl/fl}$/*Apc*$^{fl/fl}$ ovaries collected 15-days post-induction. Photomicrographs of Ki67 (upper panel), and E-cadherin (lower panel) in *Apc2*$^{+/+}$ (left panel), *Apc2*$^{+/-}$ (middle panel) and *Apc2*$^{-/-}$ (right panel) Ad-*cre Pten*$^{fl/fl}$/*Apc*$^{fl/fl}$ ovaries. Black arrows: tumourlets. n=3. Scale bar 100 µm. Insets show OSE/tumourlet at 2X original magnification.

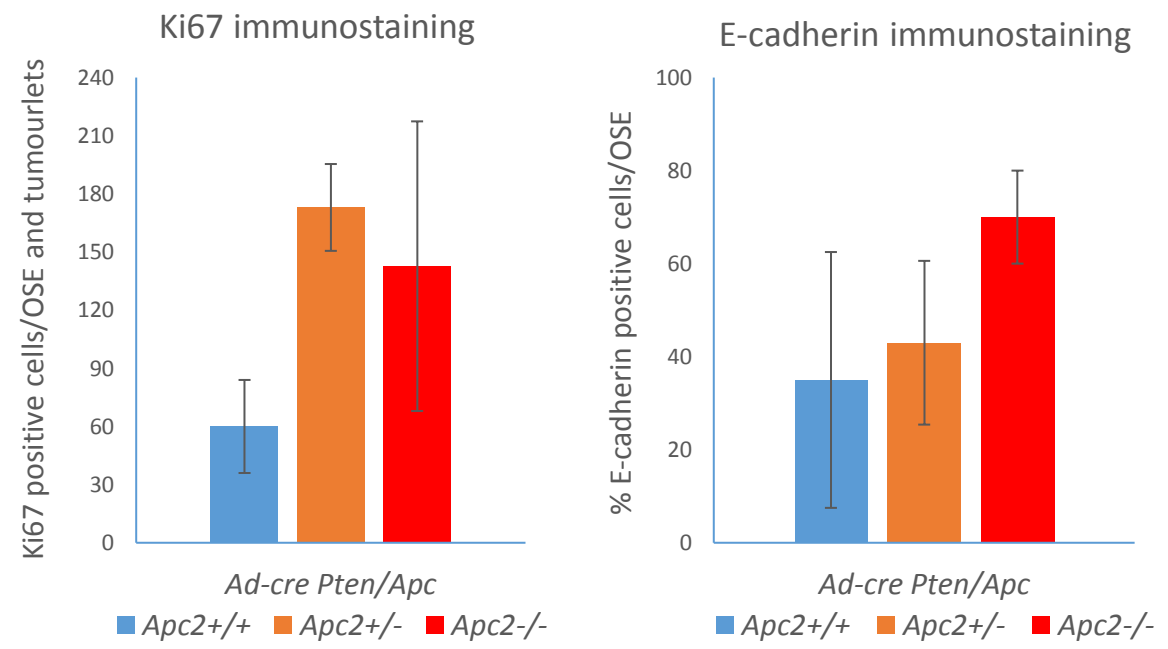

Figure 6.24b: Quantitative analysis of proliferation and OSE epithelial differentiation in APC2-deficient *Pten*$^{fl/fl}$/*Apc*$^{fl/fl}$ ovaries 15 days post-induction. Histograms of Ki67 positive cells in the OSE (left panel) and % of E-cadherin positive OSE (right panel). Data are shown as mean±S.E. n=3. *Ad-cre Pten/Apc*: Ad-*cre Pten*$^{fl/fl}$/*Apc*$^{fl/fl}$.

Nuclear β-catenin and p-AKT IHC were used to assess activation of WNT signalling and PI3K/AKT signalling, respectively, in the 3 cohorts (Figure 6.25). 1/3 (33.3%) ovaries/cohort did not show nuclear β-catenin immunostaining, but intense cytoplasmic staining was present in some parts of the OSE. In the *Apc2*$^{+/+}$ cohort, nuclear β-catenin staining was variable in the 2 mice which did show positivity (40% of OSE cells in one and 100% in the other). In the APC2-deficient cohorts, nuclear staining was also evident in the OSE, and much more strongly in the tumourlets (Figure 6.25). p-AKT expression was variable in the OSE of all the studied cohorts, but was highly expressed in the tumourlets of APC2-deficient mice (Figure 6.25).

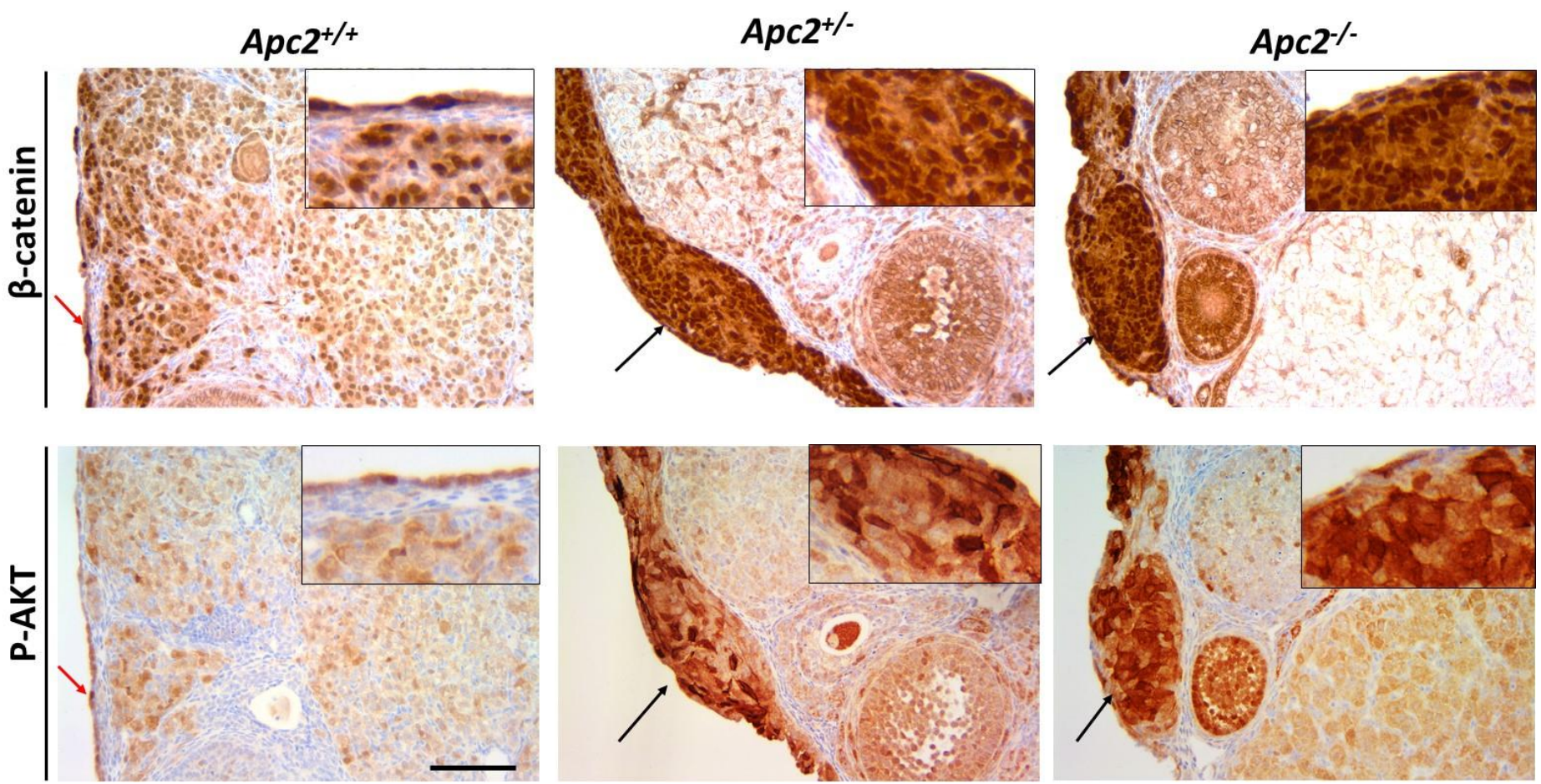

Figure 6.25: WNT signalling and PI3K/AKT signalling are activated in APC2-deficient OSE and tumourlets of *Pten*$^{fl/fl}$/*Apc*$^{fl/fl}$ ovaries 15-days post-induction. Photomicrographs of β-catenin (upper panel), and p-AKT (lower panel) in *Apc2*$^{+/+}$ (left panel), *Apc2*$^{+/-}$ (middle panel) and *Apc2*$^{-/-}$ (right panel) cohorts. Black arrows: tumourlets. Red arrows: OSE. Scale bar 100 µm. Insets show OSE/tumourlet at 2X original magnification.

6.2.5. Loss of APC2 attenuates OEA growth

In order to further define roles of APC2 in OEA, tumour burden was assessed in the same cohorts of mice, but ovaries were collected at a later time point of 8-weeks post-induction (n=3 for *Apc2*$^{+/+}$ and *Apc2*$^{-/-}$, n=6 for *Apc2*$^{+/-}$). At the time of dissection, ovarian dimensions were measured by callipers, and used to calculate ovarian volume (Section 3.4.2). In the *Apc2*$^{+/+}$ tumour cohort, dissected ovaries were significantly larger than those collected from either *Apc2*$^{+/-}$ or *Apc2*$^{-/-}$ cohorts ($p<0.05$, Figure 6.26). Although ovaries collected from *Apc2*$^{-/-}$ tumour cohort were smaller than those from the *Apc2*$^{+/-}$ tumour cohort, this difference was not statistically significant by ANOVA/LSD test (Figure 6.26).

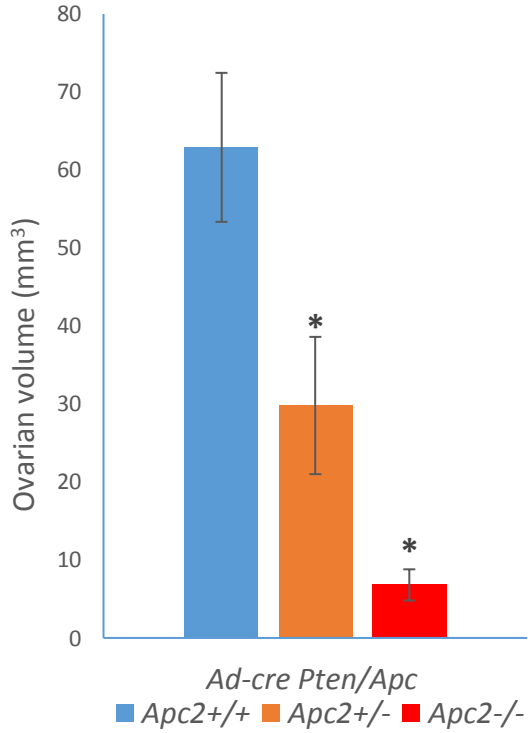

Figure 6.26: Volume of ovaries collected from *Apc2*$^{+/+}$ (n=3), *Apc2*$^{+/-}$ (n=6) and *Apc2*$^{-/-}$ (n=3) *Pten*$^{fl/fl}$/*Apc*$^{fl/fl}$ mice at 8-weeks post-induction. Data are presented as mean±S.E. Statistical significance between groups was determined using ANOVA test followed by LSD test (variance between experimental groups was homogenous, tested by Levene's test). * denotes significance from *Apc2*$^{+/+}$ at $p<0.05$. *Ad-cre Pten/Apc*: Ad-*cre Pten*$^{fl/fl}$/*Apc*$^{fl/fl}$.

Ovaries were examined microscopically for the presence of OEA, as previously described at 6-weeks post-induction in the *Pten*$^{fl/fl}$/*Apc*$^{fl/fl}$ model (Wu *et al.* 2007). OEA with 100% penetrance was evident in both the *Apc2*$^{+/+}$and *Apc2*$^{+/-}$ tumour cohorts. However, in the *Apc2*$^{-/-}$ cohort, only 2/3 (66.67%) of ovaries showed OEA formation, with 1/3 (33.33%) showing just pre-tumour lesions (tumourlets), similar to the ones described at 15-days post-induction. OEA completely replaced the ovarian tissue in 2/3 (66.67%) of *Apc2*$^{+/+}$ ovaries and 1/6 (16.67%) of *Apc2*$^{+/-}$ ovaries, but failed to do so in any of the *Apc2*$^{-/-}$ (0/3) ovaries (Figure 6.27a-c). Large blood cysts were evident in 2/3 (66.67%) of *Apc2*$^{+/+}$ and 2/6 (33.33%) of *Apc2*$^{+/-}$, but were absent in *Apc2*$^{-/-}$ (0/3) (Figure 6.27d). 66.67% of *Apc2*$^{+/+}$ and *Apc2*$^{+/-}$ tumours were formed of many separate tumour lobules (6.27e), which were not evident in any of the *Apc2*$^{-/-}$ tumours. Squamous differentiation and focal keratinization were minimal in *Apc*$^{+/+}$ tumours (forming 7% of the whole section), but were more evident in *Apc2*$^{+/-}$ and *Apc2*$^{-/-}$ tumours, forming 20% and 40% of the whole sections analysed respectively (Figures 6.27f, 6.30b). Gland formation (frequently filled with mucin) was evident in all tumours analysed, apart from the *Apc2*$^{-/-}$ ovary with tumourlets. However, glands were more abundant, present in groups and packed closely together in *Apc2*$^{+/+}$ tumours (Figure 6.27g). Glandular stromal invasion was evident in all *Apc2*$^{+/+}$ and *Apc2*$^{+/-}$ tumours, but was only seen in 1/3 *Apc2*$^{-/-}$ tumours (Figure 6.27h). Cancer-associated fibroblasts were evident in all tumour cohorts, but were present at higher levels in the *Apc2*$^{+/+}$ tumours, surrounding tumour lobules (Figure 6.27i). Tumour-infiltrating immune cells were present in all *Apc*$^{+/+}$ tumours, but were absent in both *Apc2*$^{+/-}$ and *Apc2*$^{-/-}$ tumours (Figure 6.27j). Large undifferentiated tumour areas, staining negatively for E-cadherin, were observed in 1/3 (33.33%) of *Apc2*$^{+/+}$ tumours and 2/3 (66.67%) of *Apc2*$^{-/-}$ tumours respectively (Figure 6.27k-l). A summary of this histologic characterization of tumours is outlined in table 6.5.

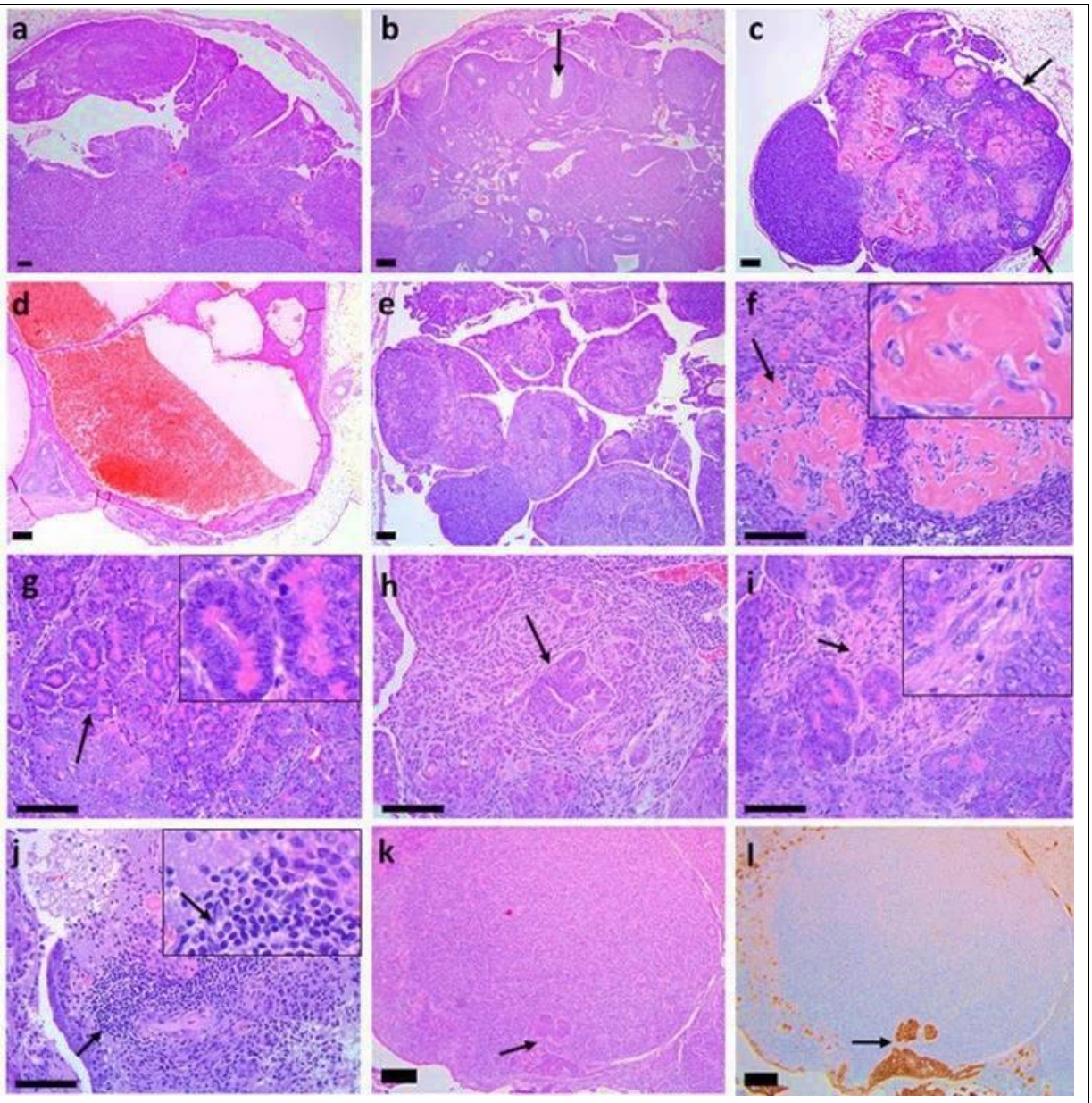

Figure 6.27: Histologic characterization of OEA formed in *Apc2* experimental cohorts of $Pten^{fl/fl}/Apc^{fl/fl}$ ovaries 8-weeks post-induction. Representative photomicrographs of H&E staining showing (a) $Apc2^{+/+}$ tumour replacing normal ovarian structures, (b) $Apc2^{+/-}$, and (c) $Apc2^{-/-}$ tumours where ovarian structures are still present (black arrow: follicle), (d) blood cyst, (e) tumour lobules, (f) squamous differentiation and focal keratinization, (g) packed mucin-filled glands (black arrow), (h) epithelial glands invading stroma (black arrow), (i) cancer-associated fibroblasts (black arrow), and (j) immune cell infiltration (black arrow: immune cells). (k,l) non-epithelial differentiated tumour (black arrow: epithelial differentiation) stained with H&E (h) and E-cadherin antibody (i). Scale bar 100 µm. Insets show 2.5X original magnification.

Table 6.5: Summary of histologic features characterized in OEA developing in ovaries of Apc2 experimental cohorts of Ad-cre Pten$^{fl/fl}$/Apc$^{fl/fl}$ female mice at 8-weeks post-induction.

***Apc2* Genotype /histologic feature**	***Apc2*$^{+/+}$**	***Apc2*$^{+/-}$**	***Apc2*$^{-/-}$**
Tumour penetrance	100% (3/3)	100% (6/6)	66.67 (2/3)
Fully replace normal ovarian tissue	66.67% (2/3)	16.67% (1/6)	0% (0/3)
Blood cysts	66.67% (2/3)	33.33% (2/6)	0% (0/3)
Tumour lobules	66.67% (2/3)	66.67% (4/6)	0% (0/3)
Squamous differentiation & focal keratinization (% tumour/tumourlet area)	7%	21%	36.67%
Gland stromal invasion	100% (3/3)	100% (6/6)	33.33% (1/3)
Tumour-infiltrating immune cells	100% (3/3)	0% (0/6)	0% (0/3)
Large epithelial-undifferentiated areas	33.33% (1/3)	0% (0/6)	66.67% (2/3)

Unlike the early time point (15-days post-induction), when APC2 presence delayed tumour formation in adenovirus-*cre* induced *Pten*$^{fl/fl}$/*Apc*$^{fl/fl}$ ovaries, the presence of APC2 promoted tumour growth in ovaries collected 8-weeks post-induction. This difference may be caused by a disruption in the balance between proliferation and apoptosis. In order to investigate these mechanisms, immunohistochemistry for Ki67 and cleaved caspase 3 were performed. Quantification in 3 different tumour areas/ovary (whenever possible) revealed no significant differences in proliferation or apoptosis between the 3 cohorts (Figure 6.28). It was observed that cleaved caspase 3 was higher in larger tumours compared to smaller ones, irrespective of genotype.

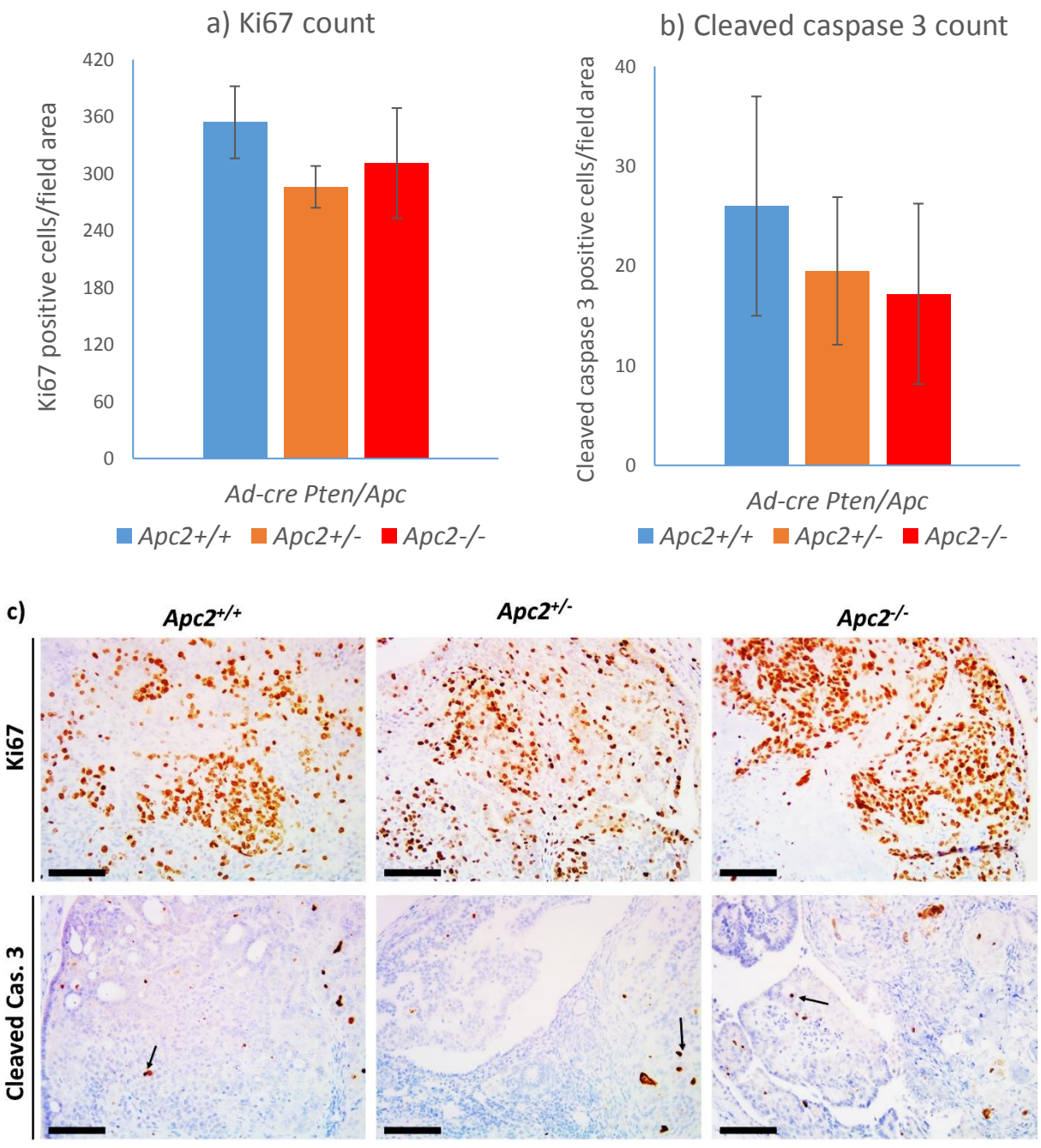

Figure 6.28: Proliferation and apoptosis are not significantly-changed in APC2-deficient tumours of Ad-*cre* *Pten*$^{fl/fl}$/*Apc*$^{fl/fl}$ ovaries 8-weeks post-induction. Histograms showing the number of positively-stained cells for (a) Ki67, and (b) cleaved caspase 3 in tumour cohorts. n=3 for *Apc2*$^{+/+}$ and *Apc2*$^{-/-}$ groups. n=5 for *Apc2*$^{+/-}$ group. Data are presented as mean±S.E. (c) Representative photomicrographs of Ki67 (upper panel), and cleaved caspase3 (lower panel) in experimental cohorts. Black arrow: positively-stained cells. Scale bar 100 µm.

Upon histologic examination of tumours, the presence of blood-filled cysts was observed only in the *Apc2*$^{+/+}$ and *Apc2*$^{+/-}$ cohorts. As shown previously, *Apc2*$^{+/+}$ tumours developed the largest tumours in all experimental cohorts, which was not caused by increased proliferation or decreased apoptosis. However, it might be caused by increased new blood vessels formation (angiogenesis), providing the tumour with nutrients and oxygen required for tumour growth (Nishida *et al.* 2006). In order to investigate whether this was the mechanism causing enhanced tumour growth in *Apc2*$^{+/+}$ cohort, CD34 immunostaining was performed. Analysis of the CD34 immunostaining revealed enhanced vascularity in all tumours and tumourlets, which was comparable among all experimental cohorts (Figure 6.29).

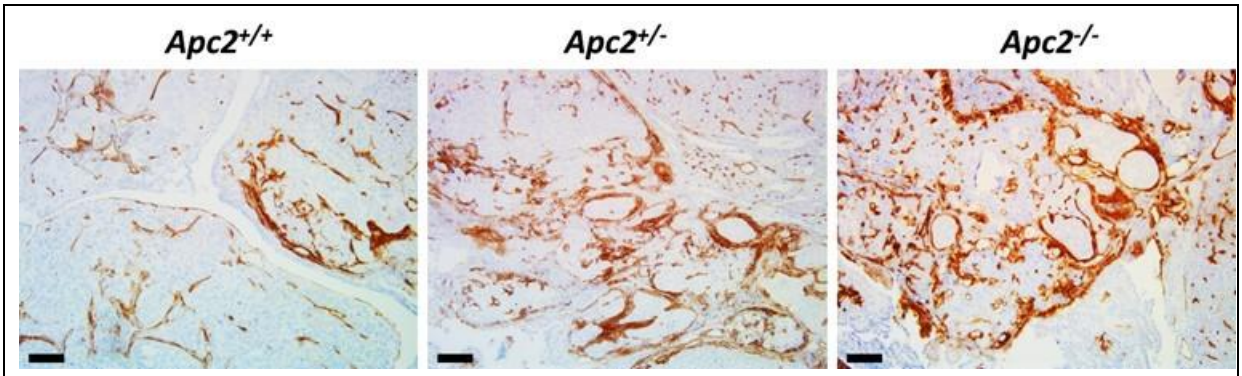

Figure 6.29: Representative photomicrographs of CD34 immunohistochemical staining performed on sections from different *Apc2* experimental cohorts of Ad-*cre* *Pten*$^{fl/fl}$/*Apc*$^{fl/fl}$ ovaries 8-weeks post-induction. Scale bar 100 µm.

It was observed that tumours developing in *Apc2*$^{+/+}$ Ad-*cre* *Pten*$^{fl/fl}$/*Apc*$^{fl/fl}$ more frequently form epithelial glands, which were more packed together and invading the stroma, compared to the other cohorts. In order to investigate whether APC2 presence enhances epithelial differentiation, E-cadherin immunostaining was performed and the percentage of area staining positively for E-cadherin was calculated. The analysis revealed that *Apc2*$^{+/+}$ tumours were expressing significantly higher levels of E-cadherin compared to *Apc2*$^{-/-}$ tumours (Figure 6.30), as larger areas of the *Apc2*$^{-/-}$ tumours had keratinized areas with minimal

squamous differentiation (Figure 6.30). Epithelial differentiation was slightly lower in *Apc2*$^{+/-}$ tumours compared to *Apc2*$^{+/+}$ tumours, but not significantly (Figure 6.30).

Simultaneous activation of WNT signalling and PI3K/AKT signalling pathways drives OEA development in adenovirus-*cre*-induced *Pten*$^{fl/fl}$/*Apc*$^{fl/fl}$ ovaries (Wu *et al*. 2007). Whether APC2 loss altered the level of activation of these pathways, thus impacting on tumour progression in the *Apc2*$^{-/-}$ tumour cohort, was evaluated by IHC for β-catenin and p-AKT, the main effectors of WNT and PI3K signalling pathways, respectively. All tumours, irrespective of genotype, showed intense staining for β-catenin, which was mostly cytoplasmic but frequently nuclear (Figure 6.31). p-AKT staining was focal, ranging from membranous to cytoplasmic, and was comparable across tumours of all cohorts (Figure 6.31).

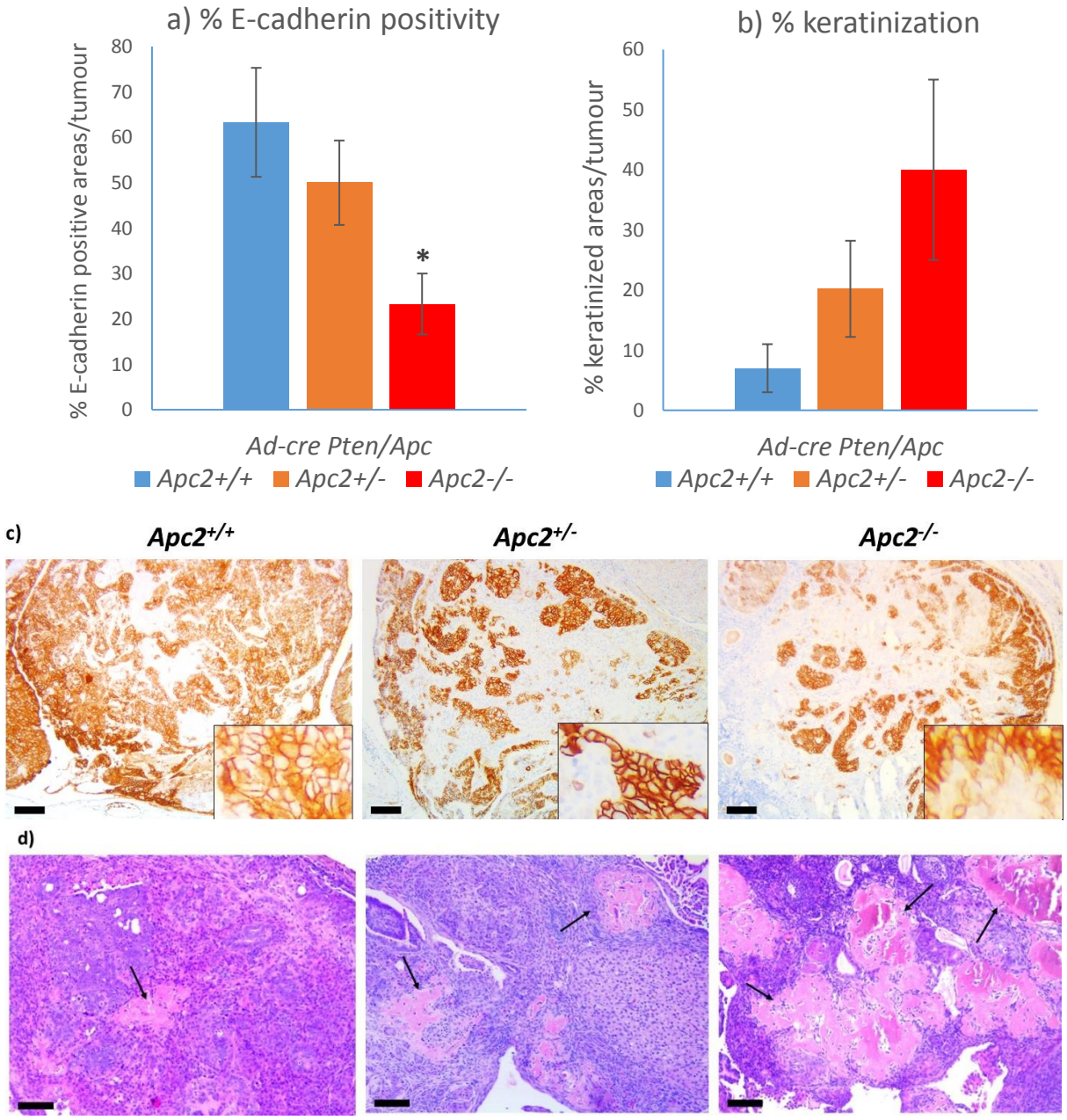

Figure 6.30: APC2 presence enhances epithelial differentiation of OEA developing in Ad-*cre* *Pten*$^{fl/fl}$/*Apc*$^{fl/fl}$ ovaries at 8-weeks post-induction. Histogram showing % tumour area (a) positively-staining for E-cadherin, and (b) keratinized with squamous differentiation. n=3 for *Apc2*$^{+/+}$ and *Apc2*$^{-/-}$ groups. n=6 for *Apc2*$^{+/-}$ group. Data are presented as mean±S.E. Representative photomicrographs of (c) E-cadherin immunostaining, and (d) areas of focal keratinization/squamous differentiation in experimental cohorts. Scale bar 100 µm. Insets show tumour areas at 4X original magnification.

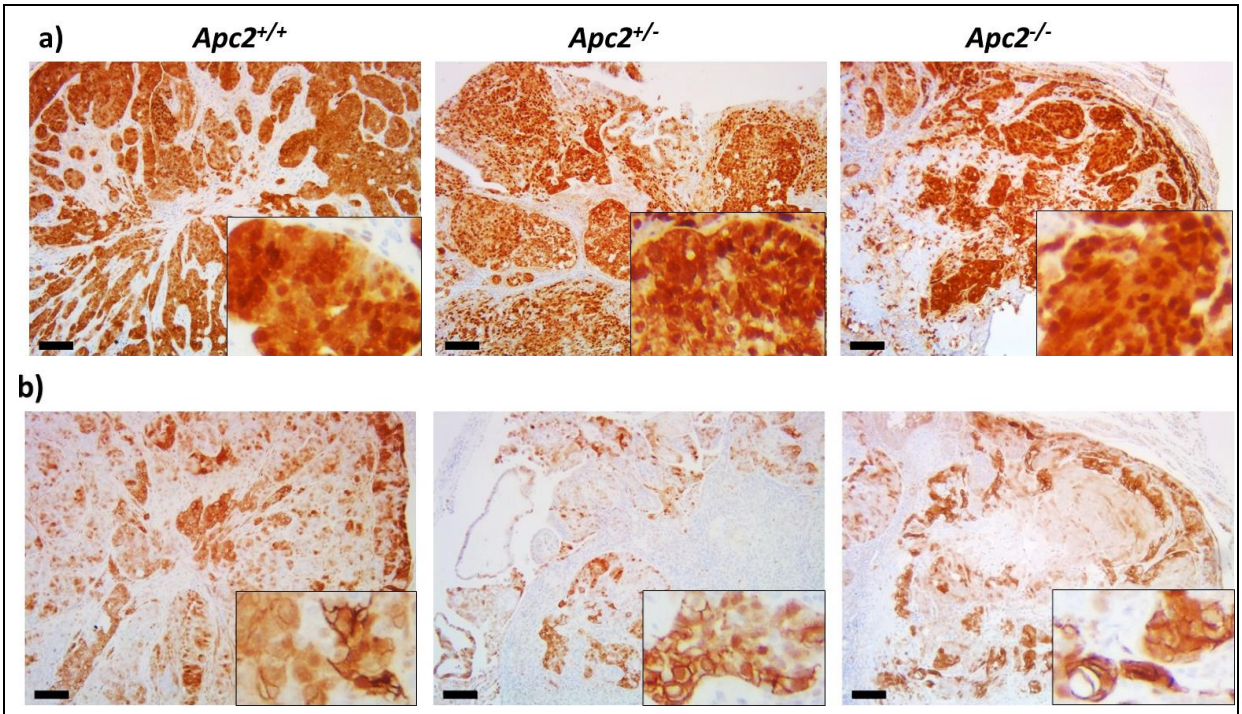

Figure 6.31: WNT signalling and PI3K signalling pathways are activated in OEA formed in Ad-*cre* *Pten*$^{fl/fl}$/*Apc*$^{fl/fl}$ ovaries at 8-weeks post-induction irrespective of *Apc2* genotype. Representative photomicrographs of IHC for (a) β-catenin, and (b) p-AKT (ser473) in different tumour cohorts. n=3 for *Apc2*$^{+/+}$ and *Apc2*$^{-/-}$ groups, n=4 for *Apc2*$^{+/-}$ group. Scale bar 100 µm. Insets show tumour at 4X original magnification.

6.2.6. Transcriptome analysis of *Apc2*$^{+/+}$ *and Apc2*$^{-/-}$ *Ad-cre Pten*$^{fl/fl}$/*Apc*$^{fl/fl}$ ovaries

In order to explore in more depth how APC2 loss acts as a suppressor of OEA tumour progression, RNA sequencing was performed on RNA extracted from ovaries collected at 8-weeks post-induction from *Pten*$^{fl/fl}$/*Apc*$^{fl/fl}$/*Apc2*$^{+/+}$ and *Pten*$^{fl/fl}$/*Apc*$^{fl/fl}$/*Apc2*$^{-/-}$ mice (3 mice/cohort). From 35,156 transcripts analysed, 289 with false discovery rate (FDR) <0.05 were differentially-expressed in *Apc2*$^{+/+}$ tumours, as compared to *Apc2*$^{-/-}$ tumours (Table 6.6). 36 were significantly upregulated in *Apc2*$^{+/+}$ tumours (Table 6.7), while 253 were significantly downregulated in *Apc2*$^{+/+}$ tumours (and therefor upregulated in *Apc2*$^{-/-}$ tumours) (Table 6.8). It is of note that many of the *Apc2*$^{+/+}$ downregulated (*Apc2*$^{-/-}$ upregulated) transcripts are involved in normal ovarian functions, which might be due to the presence of more normal

ovarian tissue in *Apc2*$^{-/-}$ tumours compared to the large tumours in *Apc*$^{+/+}$ ovaries, which replace most or all of the normal tissue. Protein-protein interactions between the most differentially regulated genes (FDR<0.05) in *Apc2*$^{+/+}$ vs. *Apc2*$^{-/-}$ Ad-*cre Pten*$^{fl/fl}$/*Apc*$^{fl/fl}$ tumours were analysed using the STRING v.10.5 online tool (Szklarczyk *et al.* 2017). Only known interactions extracted from curated experiments or databases were used to analyse the data. Few interactions were found in the *Apc*$^{+/+}$ upregulated gene list, with only one important hub identified (LRGUK, Figure 6.32a). Proteins identified from the *Apc2*$^{+/+}$ downregulated (*Apc2*$^{-/-}$ upregulated) gene list, however, were more closely connected, with many hubs identified (Figure 6.32b). The largest hubs were ESR2, BMPR1b, TRIB2, CCNO, ASZ1 and FBXW family, with most of them being known as regulators of normal ovarian functions. A network showing all interactive proteins was prepared using Cytoscape v.3.4.0. Software (Lopes *et al.* 2010)(Figure 6.32c). This revealed the additional presence of interactions between *Apc2*$^{+/+}$ upregulated and downregulated proteins, with new hubs identified (e.g. Hunk).

Table 6.6: Global differential expression analysis of Ad-cre Pten$^{fl/fl}$/Apc$^{fl/fl}$/Apc2$^{+/+}$ (n=3) vs. Pten$^{fl/fl}$/Apc$^{fl/fl}$/Apc2$^{-/-}$ (n=3) ovaries 8-weeks post-induction

Global differential expression analysis						
Total number of transcripts	**Significantly differentially expressed transcripts (FDR <0.05)**		**Significantly downregulated transcripts in *Apc2*$^{+/+}$ vs. *Apc2*$^{-/-}$ (FDR <0.05)**		**Significantly upregulated transcripts in *Apc2*$^{+/+}$ vs. *Apc2*$^{-/-}$ (FDR <0.05)**	
	Number	Percentage	Number	Percentage	Number	Percentage
35 156	289	0.82%	253	0.72%	36	0.102%

Table 6.7: List of upregulated gene transcripts in Apc2$^{+/+}$ (n=3) vs. Apc2$^{-/-}$ (n=3) Ad-cre Pten$^{fl/fl}$/Apc$^{fl/fl}$ ovaries 8-weeks post-induction

Gene ID	Target gene	Log2 fold change *Apc2*$^{+/+}$ ovaries vs. *Apc2*$^{-/-}$ ovaries	Fold change *Apc2*$^{+/+}$ ovaries vs. *Apc2*$^{-/-}$ ovaries	P-value	FDR
NM_010401	Histidine ammonia lyase (*Hal*)	3.69	**12.86**	7.27E-23	1.99E-18
NM_007969	WAP four-disulfide core domain 18 (*Wfdc18*)	2.19	**4.58**	3.24E-07	2.79E-04
NM_010743, NM_001294171	Interleukin 1 receptor-like 1 (*Il1rl1*)	1.84	**3.58**	1.55E-05	3.8E-03
NM_009160	Surfactant associated protein D (*Sftpd*)	1.83	**3.57**	2.02E-05	4.4E-03
NM_178924	Uroplakin 1B (*Upk1b*)	1.81	**3.5**	6.81E-07	4.3E-04
NM_026323	WAP four-disulfide core domain 2 (*Wfdc2*)	1.78	**3.43**	1.69E-06	8.5E-04
NM_021382	Tachykinin receptor 3 (*Tacr3*)	1.78	**3.43**	1.25E-06	6.58E-04
NM_009474	Urate oxidase (*Uox*)	1.76	**3.38**	4.27E-05	8.1E-03
NM_021443	Chemokine (C-C motif) ligand 8 (*Ccl8*)	1.73	**3.32**	5.88E-05	9.94E-03
NM_001112702, NM_021467	Troponin I, skeletal, slow 1 (*Tnni1*)	1.68	**3.22**	5.58E-05	9.8E-03
NM_009778	Complement component 3 (*C3*)	1.67	**3.21**	5.95E-05	9.94E-03
NM_008522	Lactotransferrin (*Ltf*)	1.62	**3.18**	1.85E-04	2.3E-02
NR_073011	Spermatogenesis associated glutamate (E)-rich protein pseudogene (*4930572O03Rik*)	1.58	**3.07**	1.41E-04	1.91E-02
NM_001308501, NM_010340	G-protein-coupled receptor 50 (*Gpr50*)	1.56	**2.95**	3.25E-04	3.5E-02
NR_028262	Rhabdomyosarcoma 2 associated transcript (non-coding RNA)(*Rmst*)	1.56	**2.94**	2.47E-04	2.8E-02

NM_001165965, NM_177091	Fibronectin type III domain containing 7 (*Fndc7*)	1.54	**2.92**	2.67E-04	3.02E-02
NM_001109751, NM_173004, NM_001109749	Contactin 4 (Cntn4)	1.54	**2.89**	4.01E-04	4.11E-02
NM_001002898	Signal-regulatory protein beta 1A (*Sirpb1a*)	1.49	**2.81**	5.14E-04	4.7E-02
NM_001167828, NM_199146	Tripartite motif-containing 30D (*Trim30d*)	1.46	**2.74**	1.19E-08	2.96E-05
NM_018857	Mesothelin (*Msln*)	1.45	**2.68**	4.67E-05	8.6E-03
NM_001271809, NR_073451, NR_073452, NM_001271810	Protocadherin 11 X-linked (*Pcdh11x*)	1.38	**2.6**	2.23E-04	2.6E-02
NM_001081957	WAP four-disulfide core domain 17 (*Wfdc17*)	1.25	**2.38**	2.21E-06	9.5E-04
NM_028886	Leucine-rich repeats and guanylate kinase domain containing (*Lrguk*)	1.22	**2.33**	4.2E-04	4.2E-02
NM_010197	Fibroblast growth factor 1 (*Fgf1*)	1.21	**2.32**	1.5E-04	1.96E-02
NR_002897	Small nucleolar RNA, H/ACA box 64 (*Snora64*)	1.2	**2.3**	1.16E-04	1.6E-02
NM_015755	Hormonally upregulated Neu-associated kinase (*Hunk*)	0.914	**1.88**	2.34E-04	2.71E-02

Table 6.8: List of downregulated gene transcripts in $Apc2^{+/+}$ (n=3) vs. $Apc2^{-/-}$ (n=3) Ad-cre $Pten^{fl/fl}/Apc^{fl/fl}$ ovaries 8-weeks post-induction.

Gene ID	Target gene	Log_2 fold change $Apc2^{+/+}$ ovaries vs. $Apc2^{-/-}$ ovaries	Fold change $Apc2^{+/+}$ ovaries vs. $Apc2^{-/-}$ ovaries	P-value	FDR
NM_001005371	Predicted gene 13084 (*Gm13084*)	-2.41	**0.188**	1.66E-08	3.76E-05

NM_145708	Oocyte specific homeobox 2 (*Obox2*)	-2.38	**0.193**	3.09E-09	1.06E-05
NM_010564	Inhibin alpha (*Inha*)	-2.32	**0.200**	6.82E-09	1.87E-05
NM_175290	NLR family, pyrin domain containing 14 (*Nlrp14*)	-2.32	**0.201**	4.15E-08	6.29E-05
NM_172479	Solute carrier family 38, member 5 (*Slc38a5*)	-2.31	**0.201**	3.05E-09	1.06E-05
NM_172953	Serine (or cysteine) peptidase inhibitor, clade A, member 5 (*Serpina5*)	-2.30	**0.203**	1.15E-09	5.24E-06
NM_001033214	RIKEN cDNA E330034G19 gene (*E330034G19Rik*)	-2.29	**0.205**	1.78E-08	3.76E-05
NM_019977	Myo-inositol oxygenase (*Miox*)	-2.27	**0.207**	3.00E-08	5.47E-05
NM_001243837	Complement component 7 (*C7*)	-2.23	**0.213**	1.11E-11	7.60E-08
NR_121593, NR_121595, NR_121596, NR_121594	Predicted gene 1965 (*Gm1965*)	-2.18	**0.221**	4.34E-07	3.20E-04
NR_131241, NM_001039143, NR_131242, NM_001305857, NM_011860	NLR family, pyrin domain containing 5 (*Nlrp5*)	-2.18	**0.221**	4.07E-08	6.29E-05
NM_001014395	F-box and WD-40 domain protein 22 (*Fbxw22*)	-2.17	**0.222**	5.10E-07	3.41E-04
NM_153106	Peptidyl arginine deaminase, type VI (*Padi6*)	-2.17	**0.223**	1.81E-07	1.91E-04
NR_015609	Expressed sequence C86187 (*C86187*)	-2.16	**0.223**	4.74E-07	3.25E-04
NM_001166065	Glucosaminyl (N-acetyl) transferase 4, core 2 (beta-1,6-N-acetylglucosaminyltransferase) (*Gcnt4*)	-2.12	**0.230**	1.58E-07	1.81E-04
NM_010933	Natriuretic peptide type C (*Nppc*)	-2.12	**0.230**	6.67E-07	4.34E-04
NM_138311	H1 histone family, member O, oocyte-specific (*H1foo*)	-2.12	**0.231**	4.17E-07	3.20E-04
NM_001201390	RIKEN cDNA E330021D16 gene (*E330021D16Rik*)	-2.12	**0.231**	3.65E-07	3.03E-04
NM_001270792	Predicted gene 2042 (*Gm2042*)	-2.11	**0.232**	1.76E-07	1.91E-04
NM_178657	Oogenesin 1 (*Oog1*)	-2.08	**0.236**	1.95E-07	1.91E-04
NM_001122678, NM_001167793_3	Predicted gene 3286 (*Gm3286*)	-2.08	**0.236**	8.84E-07	5.14E-04
NM_001122668	RIKEN cDNA E330014E10 gene (*E330014E10Rik*)	-2.07	**0.239**	1.17E-06	6.39E-04
NM_011776	Zona pellucida glycoprotein 3 (*Zp3*)	-2.07	**0.239**	1.30E-06	6.72E-04
NM_001122678, NM_001167793, NM_001167792	Predicted gene 3286 (*Gm3286*)	-2.06	**0.239**	1.42E-06	6.84E-04
NM_177069	F-box and WD-40 domain protein 21 (*Fbxw21*)	-2.06	**0.239**	1.63E-06	7.34E-04

NM_001105254	Predicted gene 10436 (*Gm10436*)	-2.06	**0.240**	3.05E-07	2.79E-04
NM_001164523, NM_001111286	Oocyte maturation, alpha (*Omt2a*)	-2.03	**0.244**	2.60E-06	1.08E-03
NM_027802	Oocyte specific homeobox 1 (*Obox1*)	-2.03	**0.244**	1.06E-06	5.94E-04
NM_008181	Glutathione S-transferase, alpha 1 (*Ya*)(*Gsta1*)	-2.02	**0.247**	2.69E-06	1.10E-03
NM_201258	Oogenesin 3 (*Oog3*)	-2.01	**0.248**	1.62E-06	7.34E-04
NM_001002894	NLR family, pyrin domain containing 14 (*Nlrp14*)	-2.01	**0.248**	8.53E-07	5.14E-04
NM_001309485, NM_001289468, NM_001309484, NR_110339, NM_009337	T cell lymphoma breakpoint 1 (*Tcl1*)	-2.01	**0.249**	2.88E-06	1.15E-03
NM_177070	F-box and WD-40 domain protein 16 (*Fbxw16*)	-2.00	**0.249**	3.47E-06	1.26E-03
NM_001113187	KH domain containing 1B (*Khdc1b*)	-1.99	**0.252**	1.40E-06	6.84E-04
NM_019493	B cell translocation gene 4 (*Btg4*)	-1.99	**0.252**	1.53E-06	7.11E-04
NM_008458	Serine (or cysteine) peptidase inhibitor, clade A, member 3C (*Serpina3c*)	-1.97	**0.256**	4.88E-09	1.49E-05
NM_001098799	TOX high mobility group box family member 2 (*Tox2*)	-1.96	**0.257**	6.37E-06	1.92E-03
NM_008032	AF4/FMR2 family, member 2 (*Aff2*)	-1.96	**0.258**	9.01E-07	5.14E-04
NM_008182	Glutathione S-transferase, alpha 2 (*Yc2*) (*Gsta2*)	-1.94	**0.260**	6.59E-06	1.96E-03
NM_172896, NM_175290	NLR family, pyrin domain containing 4A (*Nlrp4a*)	-1.94	**0.261**	6.33E-06	1.92E-03
NR_003564	Transcription elongation factor B (SIII), polypeptide 2 pseudogene (*Gm15698*)	-1.93	**0.262**	6.07E-06	1.91E-03
NM_007996, NM_001301728	Ferredoxin 1 (*Fdx1*)	-1.92	**0.265**	1.21E-06	6.51E-04
NM_010701	Leukocyte cell derived chemotaxin 1 (*Lect1*)	-1.92	**0.265**	4.47E-06	1.53E-03
NM_145947	Solute carrier family 26, member 7 (*Slc26a7*)	-1.91	**0.267**	1.51E-06	7.11E-04
NM_001033404	Predicted gene 813 (*Gm813*)	-1.90	**0.268**	1.13E-05	2.99E-03
NM_172925	Kelch-like 31 (*Klhl31*)	-1.90	**0.268**	1.13E-05	2.99E-03
NM_009580	Zona pellucida glycoprotein 1 (*Zp1*)	-1.89	**0.269**	8.37E-06	2.39E-03
NM_013479	Bcl2-like 10 (*Bcl2l10*)	-1.88	**0.271**	1.01E-05	2.76E-03
NM_010720	Lipase, endothelial (*Lipg*)	-1.87	**0.274**	5.73E-06	1.84E-03
NM_130869	NOBOX oogenesis homeobox (*Nobox*)	-1.86	**0.275**	1.33E-05	3.44E-03
NM_145210	2'-5' oligoadenylate synthetase 1E (*Oas1e*)	-1.86	**0.275**	1.54E-05	3.80E-03

NM_001033269, NM_001039683, NR_104407, NM_001286180, NM_001286178, NM_001286179	Eukaryotic translation initiation factor 4E family member 1B (*Eif4e1b*)	-1.86	**0.276**	1.80E-05	4.15E-03
NM_172673	FERM domain containing 5 (*Frmd5*)	-1.85	**0.278**	3.08E-06	1.17E-03
NM_175011	RIKEN cDNA E330017A01 gene (*E330017A01Rik*)	-1.84	**0.280**	2.21E-05	4.76E-03
NM_027664	Ribosomal modification protein rimK-like family member B (*Rimklb*)	-1.84	**0.280**	4.52E-06	1.53E-03
NM_013523	Follicle stimulating hormone receptor (*Fshr*)	-1.83	**0.282**	2.47E-05	5.24E-03
NM_019779	Cytochrome P450, family 11, subfamily a, polypeptide 1 (*Cyp11a1*)	-1.83	**0.282**	1.71E-05	4.01E-03
NM_027582	Aldo-keto reductase family 1, member C-like (*Akr1cl*)	-1.83	**0.282**	3.40E-06	1.26E-03
NM_011077	Phosphate regulating endopeptidase homolog, X-linked (*Phex*)	-1.82	**0.283**	2.79E-08	5.46E-05
NM_011169, NM_001253782, NM_001253781	Prolactin receptor (*Prlr*)	-1.82	**0.283**	3.53E-06	1.26E-03
NM_133893	2'-5' oligoadenylate synthetase 1D (*Oas1d*)	-1.81	**0.285**	2.22E-05	4.76E-03
NM_133353	Oocyte secreted protein 1 (*Oosp1*)	-1.79	**0.289**	1.54E-05	3.80E-03
NM_146879	Olfactory receptor 330 (*Olfr330*)	-1.79	**0.290**	3.18E-05	6.45E-03
NM_007468	Apolipoprotein A-IV(*Apoa4*)	-1.78	**0.291**	1.02E-05	2.76E-03
NM_001199218, NM_023805, NM_001199217	Solute carrier family 38, member 3 (*Slc38a3*)	-1.78	**0.292**	1.68E-05	4.01E-03
NM_177571	Predicted gene 13103 (*Gm13103*)	-1.78	**0.292**	4.06E-05	7.90E-03
NM_001042612	NLR family, pyrin domain containing 9C (*Nlrp9c*)	-1.77	**0.292**	4.24E-05	8.13E-03
NM_001267625, NM_058212, NM_001267626	D4, zinc and double PH.D. fingers, family 3 (*Dpf3*)	-1.77	**0.293**	1.99E-05	4.39E-03
NM_009757	Bone morphogenetic protein 15 (*Bmp15*)	-1.77	**0.294**	6.34E-06	1.92E-03
NM_015793	F-box and WD-40 domain protein 14 (*Fbxw14*)	-1.75	**0.297**	5.29E-05	9.47E-03
NM_198661	Oogenesin 2 (*Oog2*)	-1.75	**0.298**	5.65E-05	9.80E-03
NM_207707, NR_104386, NM_010157	Estrogen receptor 2 (beta) (*Esr2*)	-1.74	**0.299**	6.31E-06	1.92E-03
NM_001122660	Predicted gene 10639 (*Gm10639*)	-1.74	**0.299**	5.78E-05	9.87E-03

NM_153110, NM_001177551	Tripartite motif-containing 61 (*Trim61*)	-1.73	**0.301**	3.41E-05	6.82E-03
NM_153529	Neuritin 1 (*Nrn1*)	-1.73	**0.301**	1.69E-05	4.01E-03
NM_001159627, NM_001159628, NM_010417, NM_181273	Hephaestin (*Heph*)	-1.73	**0.301**	1.26E-07	1.51E-04
NM_173773	Oogenesin 4 (*Oog4*)	-1.73	**0.302**	6.87E-05	1.09E-02
NM_001007077	Predicted gene 13023 (*Gm13023*)	-1.72	**0.303**	6.05E-05	9.99E-03
NM_001004145	NLR family, pyrin domain containing 4G (*Nlrp4g*)	-1.72	**0.303**	7.05E-05	1.12E-02
NM_011775	Zona pellucida glycoprotein 2 (*Zp2*)	-1.70	**0.307**	1.93E-05	4.29E-03
NM_001271798, NM_001271800, NM_001081377, NM_001081377	Protocadherin 9 (*Pcdh9*)	-1.69	**0.309**	8.00E-06	2.33E-03
NM_027741, NM_001305882	Maestro (*Mro*)	-1.69	**0.311**	9.70E-06	2.71E-03
NM_199036	F-box and WD-40 domain protein 15 (*Fbxw15*)	-1.68	**0.312**	1.02E-04	1.46E-02
NM_001177542	Expressed sequence C87977 (*C87977*)	-1.68	**0.312**	9.69E-05	1.41E-02
NM_031387, NM_001002241, NM_001002238, NM_001002240	Tudor domain containing 1 (Tdrd1)	-1.68	**0.312**	8.98E-05	1.34E-02
NM_029948	PRAME family member 12 (*Pramef12*)	-1.68	**0.313**	9.39E-05	1.38E-02
NM_194058	NLR family, pyrin domain containing 9B (*Nlrp9b*)	-1.66	**0.316**	1.26E-04	1.75E-02
NM_001267625, NM_058212, NM_001267626	D4, zinc and double PH.D. fingers, family 3 (*Dpf3*)	-1.66	**0.317**	5.62E-05	9.80E-03
NM_001143683	Metallophosphoesterase domain containing 2 (*Mpped2*)	-1.66	**0.317**	1.33E-04	1.82E-02
NM_001164284	Expressed sequence C87414 (*C87414*)	-1.65	**0.319**	1.30E-04	1.79E-02
NM_001177419, NM_001177420	F-box and WD-40 domain protein 28 (*Fbxw28*)	-1.65	**0.320**	1.48E-04	1.97E-02
NM_001008428	F-box and WD-40 domain protein 20 (*Fbxw20*)	-1.64	**0.322**	1.60E-04	2.06E-02
NM_053171	CUB and Sushi multiple domains 1 (*Csmd1*)	-1.63	**0.323**	1.42E-06	6.84E-04
NM_001166433, NM_001033211	expressed sequence AU022751(*AU022751*)	-1.62	**0.324**	1.79E-04	2.25E-02
NM_177598	F-box and WD-40 domain protein 13 (*Fbxw13*)	-1.62	**0.325**	1.58E-04	2.06E-02
NM_027022	CKLF-like MARVEL transmembrane domain containing 2A (*Cmtm2a*)	-1.62	**0.325**	1.41E-04	1.91E-02

NM_001277218, NM_001277216, NM_001277220, NM_007560	Bone morphogenetic protein receptor, type 1B (*Bmpr1b*)	-1.61	**0.327**	4.69E-05	8.62E-03
NM_053242, NM_001286607, NM_212435	Forkhead box P2 (*Foxp2*)	-1.61	**0.327**	1.45E-05	3.70E-03
NM_145981	Phytanoyl-CoA hydroxylase interacting protein (*Phyhip*)	-1.61	**0.327**	1.86E-04	2.31E-02
NM_026436	Transmembrane protein 86A (*Tmem86a*)	-1.61	**0.328**	1.73E-05	4.03E-03
NR_015524	Centrosomal protein 83, opposite strand (*Cep83os*)	-1.61	**0.328**	5.01E-06	1.67E-03
NM_139218	Developmental pluripotency-associated 3 (*Dppa3*)	-1.61	**0.329**	1.51E-04	2.00E-02
NM_153409, NM_001290665, NM_178634, NM_178634	Cysteine-serine-rich nuclear protein 3 (*Csrnp3*)	-1.60	**0.329**	5.54E-05	9.80E-03
NM_026480	Oocyte expressed protein (*Ooep*)	-1.60	**0.331**	9.82E-05	1.42E-02
NM_201370	WEE1 homolog 2 (S. pombe) (*Wee2*)	-1.59	**0.331**	1.66E-04	2.13E-02
NR_027385, NM_198663	Expressed sequence C87499 (*C87499*)	-1.59	**0.333**	2.35E-04	2.71E-02
NM_009692	Apolipoprotein A-I (Apoa1)	-1.59	**0.333**	8.52E-05	1.29E-02
NM_001271704, NM_181317	K+ voltage-gated channel, subfamily S, 2 (*Kcns2*)	-1.58	**0.334**	1.67E-04	2.13E-02
NR_037571	Predicted gene 7056 (*Gm7056*)	-1.58	**0.334**	2.54E-04	2.89E-02
NM_029837	Metallophosphoesterase domain containing 2 (*Mpped2*)	-1.58	**0.334**	1.49E-04	1.98E-02
NM_001033794	F-box and WD-40 domain protein 18 (*Fbxw18*)	-1.58	**0.335**	2.35E-04	2.71E-02
NM_008807, NM_001290998, NM_001290996, NM_001290999, NM_001045555	Tubby-like protein 2 (*Tulp2*)	-1.58	**0.336**	4.15E-05	8.00E-03
NM_011824	Gremlin 1, DAN family BMP antagonist (*Grem1*)	-1.57	**0.337**	1.89E-05	4.28E-03
NR_033577	Apolipoprotein L 7c pseudogene (*Gm8221*)	-1.57	**0.338**	3.07E-04	3.35E-02
NM_001167938, NM_001167937	DNA segment, Chr 6, ERATO Doi 527, expressed (*D6Ertd527e*)	-1.55	**0.342**	3.37E-04	3.59E-02
NM_029416	Kruppel-like factor 17 (*Klf17*)	-1.55	**0.342**	2.15E-04	2.57E-02
NM_001168589	Vertebrae development associated (*Vrtn*)	-1.54	**0.343**	3.75E-04	3.95E-02
NM_172815	R-spondin 2 (*Rspo2*)	-1.54	**0.344**	3.84E-04	4.00E-02
NM_007445	Anti-Mullerian hormone (*Amh*)	-1.54	**0.344**	3.80E-04	3.99E-02
NM_145144	Allograft inflammatory factor 1-like (*Aif1l*)	-1.54	**0.344**	2.75E-04	3.08E-02
NM_001081062	Cyclin O (*Ccno*)	-1.54	**0.345**	3.93E-04	4.08E-02

NM_144551	Tribbles pseudokinase 2 (*Trib2*)	-1.54	**0.345**	4.29E-06	1.49E-03
NM_026763	Collagen, type VI, alpha 4 (*Col6a4*)	-1.52	**0.348**	9.62E-05	1.41E-02
NM_001164284	Expressed sequence C87414 (*C87414*)	-1.52	**0.348**	4.09E-04	4.16E-02
NM_007762	Corticotropin releasing hormone receptor 1 (*Crhr1*)	-1.52	**0.348**	4.30E-04	4.22E-02
NM_053123, NM_001290708	SWI/SNF related, matrix associated, actin dependent regulator of chromatin, subfamily a, member 1 (*Smarca1*)	-1.52	**0.349**	7.40E-05	1.16E-02
NM_010934	Neuropeptide Y receptor Y1 (*Npy1r*)	-1.52	**0.350**	1.14E-04	1.62E-02
NM_011158	Protein kinase, cAMP dependent regulatory, type II beta (*Prkar2b*)	-1.51	**0.351**	1.67E-04	2.13E-02
NM_015764, NM_001252071	Gene regulated by estrogen in breast cancer protein (*Greb1*)	-1.51	**0.352**	1.15E-04	1.62E-02
NM_010582	Inter-alpha trypsin inhibitor, heavy chain 2 (*Itih2*)	-1.50	**0.354**	5.08E-04	4.70E-02
NR_044992	Predicted gene 6367 (*Gm6367*)	-1.50	**0.354**	4.13E-04	4.16E-02
NM_001013774	Karyopherin alpha 7 (importin alpha 8) (*Kpna7*)	-1.50	**0.354**	4.92E-04	4.65E-02
NR_040604	RIKEN cDNA 4930590L20 gene (*4930590L20Rik*)	-1.48	**0.359**	3.19E-04	3.47E-02
NM_023729	Ankyrin repeat, SAM and basic leucine zipper domain containing 1 (*Asz1*)	-1.47	**0.361**	5.25E-04	4.81E-02
NM_001195048, NM_001195046, NM_001195049, NM_001195047, NM_008778	p21 protein (Cdc42/Rac)-activated kinase 3 (*Pak3*)	-1.46	**0.364**	4.16E-04	4.16E-02
NM_001113399, NM_001113400, NM_178723	Zinc finger protein 385B (*Zfp385b*)	-1.45	**0.365**	2.41E-04	2.76E-02
NM_001080781	RIKEN cDNA 1700029H14 gene (*1700029H14Rik*)	-1.45	**0.367**	5.30E-04	4.83E-02
NM_178678	Leucine rich repeat transmembrane neuronal 3 (*Lrrtm3*)	-1.44	**0.369**	4.22E-04	4.16E-02
NM_001033220	Expressed sequence AU021092 (*AU021092*)	-1.42	**0.373**	2.14E-04	2.57E-02
NM_007741	Collagen, type IX, alpha 2 (*Col9a2*)	-1.42	**0.374**	2.78E-04	3.10E-02
NM_001083628	Growth regulation by estrogen in breast cancer-like (*Greb1l*)	-1.42	**0.375**	2.37E-06	1.00E-03
NR_038184, NR_038185	RIKEN cDNA C430049B03 gene (*C430049B03Rik*)	-1.41	**0.375**	2.23E-04	2.63E-02
NM_011485	Steroidogenic acute regulatory protein (*Star*)	-1.41	**0.376**	2.07E-04	2.51E-02

NM_001146045, NM_001100458	Family with sequence similarity 169, member A (*Fam169a*)	-1.38	**0.384**	9.85E-05	1.42E-02
NM_134072	Aldo-keto reductase family 1, member C14 (*Akr1c14*)	-1.38	**0.385**	4.05E-04	4.14E-02
NM_011825	Gremlin 2, DAN family BMP antagonist (*Grem2*)	-1.38	**0.385**	2.98E-04	3.29E-02
NM_011516	Synaptonemal complex protein 1 (*Sycp1*)	-1.36	**0.391**	7.18E-11	3.94E-07
NM_001285841	Syntabulin (syntaxin-interacting) (*Sybu*)	-1.35	**0.394**	3.30E-04	3.56E-02
NM_001005510	Spectrin repeat containing, nuclear envelope 2 (*Syne2*)	-1.32	**0.402**	1.27E-04	1.75E-02
NM_153574	Family with sequence similarity 13, member A (*Fam13a*)	-1.31	**0.402**	4.47E-04	4.33E-02
NM_026247, NR_037145	Asparagine-linked glycosylation 13 (*Alg13*)	-1.26	**0.418**	1.79E-12	2.46E-08
NM_008149	Glycerol-3-phosphate acyltransferase, mitochondrial (*Gpam*)	-1.26	**0.419**	5.27E-04	4.81E-02
NM_001277730, NM_001134741	Tudor domain containing 5 (*Tdrd5*)	-1.24	**0.423**	2.76E-04	3.08E-02
NM_207663, NM_183312, NM_201639	Synemin, intermediate filament protein (*Synm*)	-1.24	**0.423**	3.32E-04	3.57E-02
NM_175526	C-type lectin domain family 1, member a (*Clec1a*)	-1.19	**0.438**	3.53E-04	3.74E-02
NM_019699	Fatty acid desaturase 2 (*Fads2*)	-1.18	**0.441**	3.84E-04	4.00E-02
NM_010295	Glutamate-cysteine ligase, catalytic subunit (*Gclc*)	-1.14	**0.455**	4.86E-04	4.62E-02
NM_008256	3-hydroxy-3-methylglutaryl-Coenzyme A synthase 2 (*Hmgcs2*)	-1.12	**0.460**	4.40E-04	4.29E-02
NM_001291184	Proprotein convertase subtilisin/kexin type 6 (*Pcsk6*)	-1.10	**0.468**	5.13E-04	4.72E-02
NR_073123, NM_172960	AarF domain containing kinase 5 (*Adck5*)	-1.09	**0.470**	7.55E-05	1.18E-02
NM_001286062, NM_009640	Angiopoietin 1 (*Angpt1*)	-1.07	**0.477**	5.07E-04	4.70E-02
NM_012026	Rho guanine nucleotide exchange factor (GEF) 28 (*Arhgef28*)	-1.06	**0.481**	3.07E-05	6.28E-03
NM_177595	Mohawk homeobox (*Mkx*)	-1.05	**0.483**	4.87E-04	4.62E-02
NM_001252489, NM_001252490, NR_045524, NM_207530	Oxysterol binding protein-like 1A (*Osbpl1a*)	-1.03	**0.489**	3.98E-04	4.10E-02
NM_001253751	Farnesyl diphosphate synthetase (*Fdps*)	-1.02	**0.494**	1.59E-04	2.06E-02
NM_146006	Lanosterol synthase (*Lss*)	-0.99	**0.505**	6.21E-05	1.01E-02
NR_037964	RIKEN cDNA 2610507I01 gene (*2610507I01Rik*)	-0.97	**0.509**	2.55E-04	2.89E-02
NM_011183, NM_001128605	Presenilin 2 (*Psen2*)	-0.94	**0.522**	5.92E-05	9.94E-03

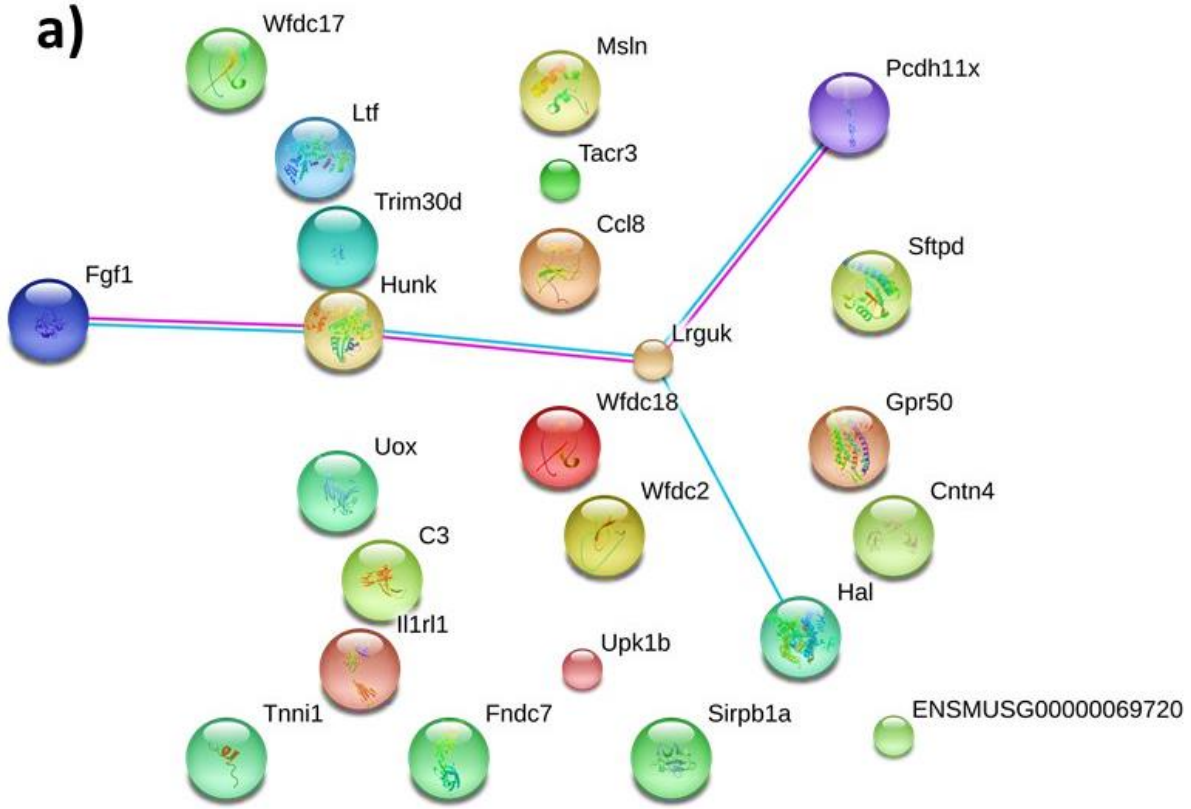

Figure 6.32: Protein-protein interaction networks of (a-b) differentially-expressed genes, with FDR<0.05 generated by STRING (a) upregulated genes, (b) downregulated genes (on next page) in *Apc2*$^{+/+}$ vs. *Apc2*$^{-/-}$ Ad-*cre Pten*$^{fl/fl}$/*Apc*$^{fl/fl}$ ovaries 8-weeks post-induction. Small nodes (circles): proteins of unknown 3D structures. Large nodes (circles): some 3D protein structure is known or predicted. Turquoise lines: known interactions from curated databases. Purple lines: experimentally-determined interactions. Red arrows: highly-connected hubs. (c) Network of interactive proteins of most differentially-expressed genes (on the following page) generated by Cytoscape. Yellow nodes: upregulated, blue nodes: downregulated.

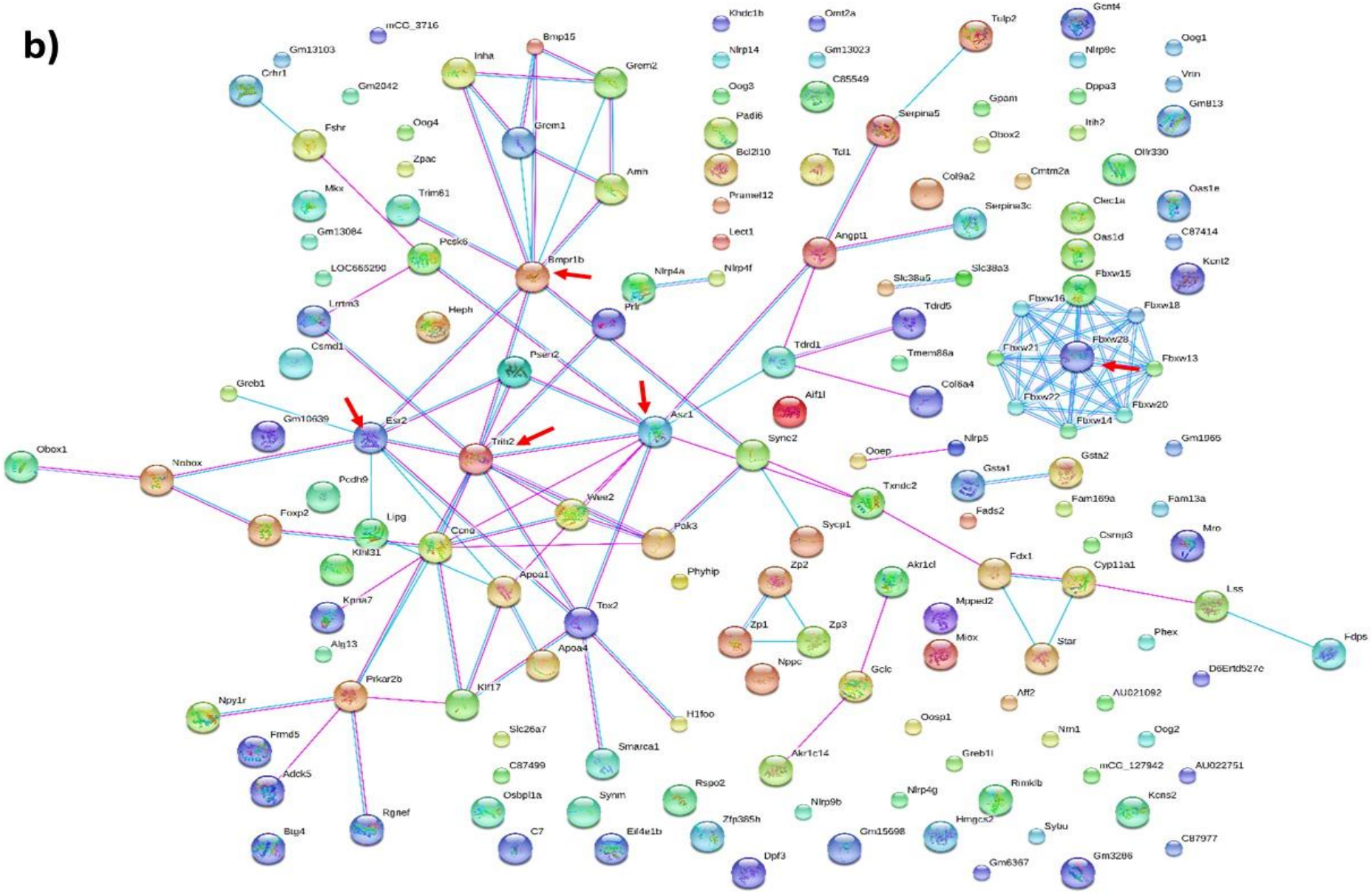
b)
mCC_3716
Gm13103
Crhr1
Gm2042
Fshr
Oog4
Zpac
Mkx
Trim61
Gm13084
Pcsk6
LOC665290
Lrrtm3
Csmd1
Heph
Bmp15
Inha
Grem2
Grem1
Amh
Bmpr1b
Nlrp4a
Nlrp4f
Prlr
Psen2
Greb1
Gm10639
Esr2
Obox1
Nnhox
Pcdh9
Foxp2
Lipg
Klhl31
Ccnb
Trib2
Asz1
Wee2
Pak3
Apoa1
Tox2
Apoa4
Kpna7
Alg13
Prkar2b
Klf17
Npy1r
Frmd5
Adck5
Rgnef
Btg4
Slc26a7
C87499
Osbpl1a
C7
Smarca1
Eif4e1b
H1foo
Rspo2
Synm
Zfp385b
Dpf3
Khdc1b
Nlrp14
Oog3
Padi6
Bcl2l10
Prame12
Lect1
Omt2a
Gm13023
C85549
Tcl1
Angpt1
Tulp2
Serpina5
Gpam
Obox2
Col9a2
Cmtm2a
Serpina3c
Slc38a5
Slc38a3
Tdrd5
Tdrd1
Tmem88a
Col8a4
Aif1l
Sync2
Ooep
Nlrp5
Txndc2
Fads2
Sycp1
Phyhip
Zp2
Zp1
Zp3
Nppc
Akr1cl
Mpped2
Miox
Gclc
Akr1c14
Fbxw15
Fbxw16
Fbxw18
Fbxw21
Fbxw28
Fbxw13
Fbxw22
Fbxw20
Fbxw14
Gsta1
Gsta2
Fam169a
Fam13a
Csrnp3
Mro
Fdx1
Cyp11a1
Lss
Star
Fdps
Phex
D6Ertd527e
Aff2
Oosp1
Nlrp9b
Nlrp4g
Hmgcs2
Gm15698
Gm6367
Rimklb
Sytl1
Nlrp9c
Dppa3
Itih2
Olfr330
Clec1a
Oas1d
Oas1e
C87414
Kcnt2
Gcnt4
Oog1
Vrtn
Gm813
Gm1965
Oog2
Nm1
Greb1l
mCC_127942
AU022751
Kcns2
C87977
Gm3286
AU021092

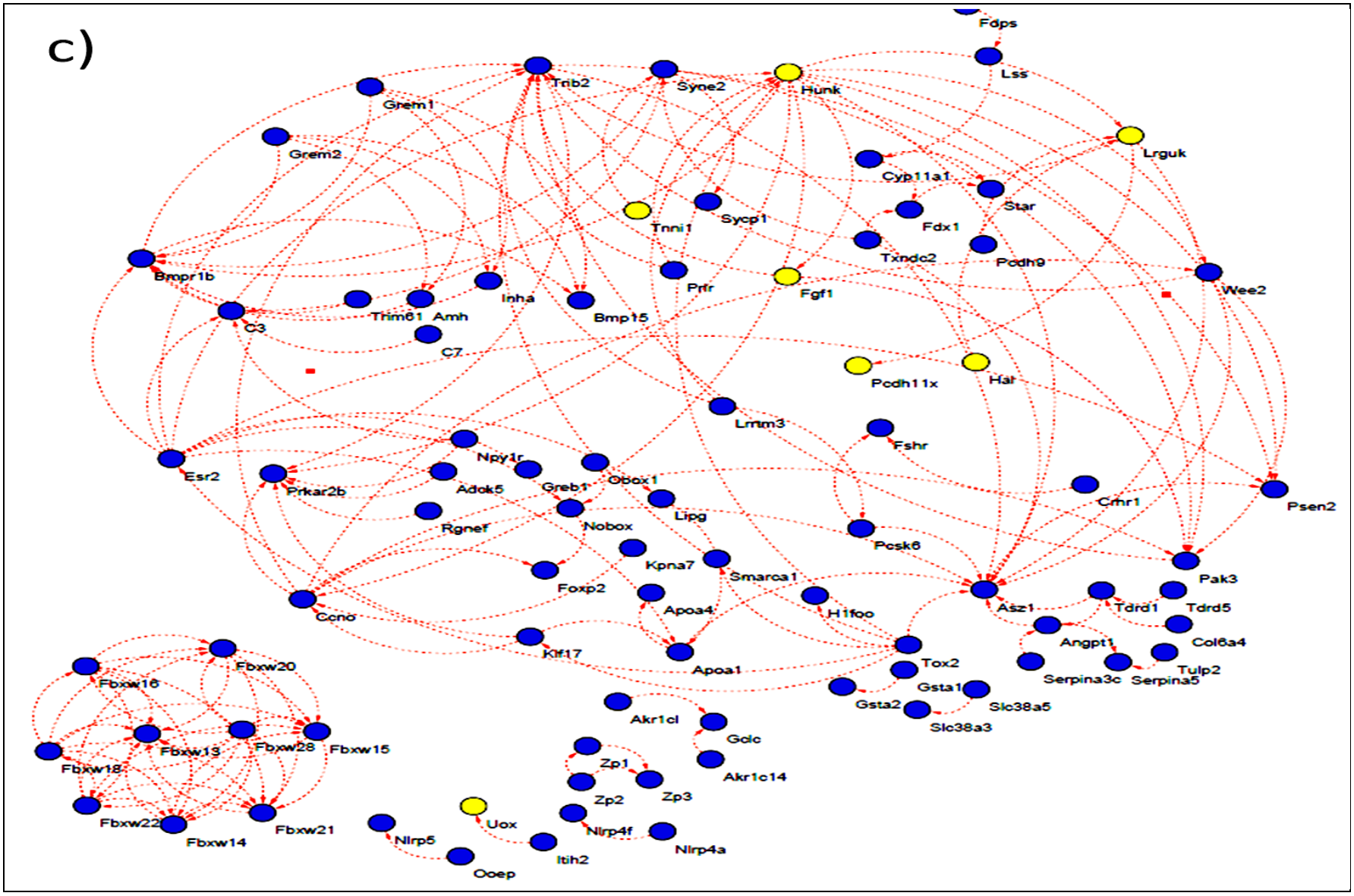
c)
Fdps
Lss
Trib2
Syne2
Hunk
Grem1
Grem2
Lrguk
Cyp11a1
Star
Tnni1
Sycp1
Fdx1
Txndc2
Pcdh9
Bmpr1b
Prlr
Fgf1
Wee2
Inha
Trim61
Amh
Bmp15
C3
C7
Pcdh11x
Hal
Lrrtm3
Fshr
Esr2
Npy1r
Prkar2b
Adok5
Greb1
Obox1
Crhr1
Psen2
Rgnef
Nobox
Lipg
Pcsk6
Kpna7
Smarca1
Pak3
Foxp2
Apoa4
H1foo
Asz1
Tdrd1
Tdrd5
Ccno
Angpt1
Col6a4
Klf17
Apoa1
Tox2
Serpina3c
Serpina5
Tulp2
Gsta1
Gsta2
Slc38a5
Slc38a3
Akr1cl
Gclc
Akr1c14
Fbxw20
Fbxw16
Fbxw13
Fbxw28
Fbxw15
Fbxw18
Zp1
Zp2
Zp3
Fbxw22
Fbxw14
Fbxw21
Uox
Nlrp4f
Nlrp4a
Nlrp5
Itih2
Ooep

A heat map was generated for the genes with FDR<0.05. It is of note that the 3 ovaries collected from each of the 2 experimental cohorts, clustered together (Figure 6.33).

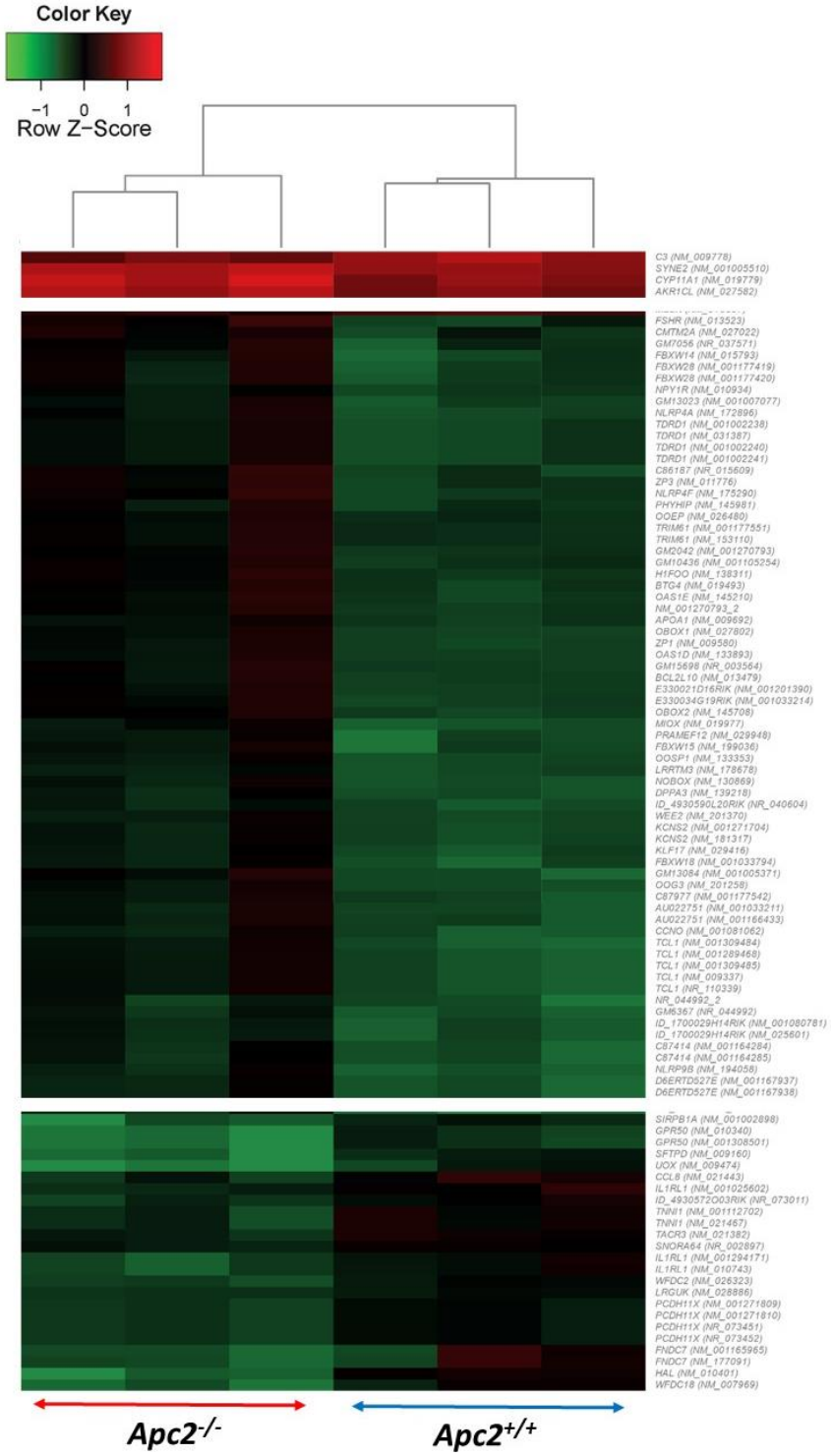

Figure 6.33: Partial heat maps of differentially-expressed genes, showing the clustering of *Apc2*$^{+/+}$ and *Apc2*$^{-/-}$ Ad-*cre* *Pten*$^{fl/fl}$/*Apc*$^{fl/fl}$ ovaries into 2 distinct clusters. Red indicates high expression, green indicates low expression. n=3.

Gene ontology analysis was performed for all upregulated genes in *Apc2*$^{+/+}$ tumours with FDR<0.1 and biological processes regulated were identified using DAVID Bioinformatics Resources 6.8 (Huang da *et al.* 2009) and selecting for GOTERM BP DIRECT database for functional annotation (Table 6.9). It can be seen that upregulated genes are mostly those involved in processes such as inflammation, chemotaxis, immune response, proteolysis, ERK and other signalling events.

Table 6.9: Identifying biological processes enriched in Apc2$^{+/+}$ (n=3) vs. Apc2$^{-/-}$ (n=3) Ad-cre Pten$^{fl/fl}$/Apc$^{fl/fl}$ ovaries 8-weeks post-induction.

Biological process	P-Value	Genes
Positive regulation of inflammatory response	2.04E-04	NM_009139, NM_021443, NM_001294171, NM_011338, NM_010743
Lymphocyte chemotaxis	0.00165	NM_009139, NM_021443, NM_011338
Monocyte chemotaxis	0.0024	NM_009139, NM_021443, NM_011338
Positive regulation of phagocytosis	0.0035	NM_001002898, NM_009160, NM_009778
Chemokine-mediated signalling pathway	0.0045	NM_009139, NM_021443, NM_011338
Positive regulation of ERK1 and ERK2 cascade	0.0048	NM_009139, NM_021443, NM_011338, NM_009778
Regulation of angiotensin levels in blood	0.0055	NM_010779, NM_007753
Cellular response to interferon-gamma	0.0068	NM_009139, NM_021443, NM_011338
Neutrophil chemotaxis	0.007	NM_009139, NM_021443, NM_011338
Cell chemotaxis	0.0089	NM_009139, NM_021443, NM_011338
Cellular response to interleukin-1	0.0093	NM_009139, NM_021443, NM_011338
Immune response	0.013	NM_009139, NM_021443, NM_010779, NM_011338
Cellular response to tumour necrosis factor	0.017	NM_009139, NM_021443, NM_011338
Complement activation, alternative pathway	0.018	NM_001142706, NM_009778, NM_008198
Chemotaxis	0.0195	NM_009139, NM_021443, NM_011338
Inflammatory response	0.024	NM_009139, NM_021443, NM_011338, NM_009778
Complement activation	0.027	NM_001142706, NM_009778, NM_008198
Positive regulation of GTPase activity	0.029	NM_009139, NM_021443, NM_011338
Immune system process	0.032	NM_001142706, NM_008522, NM_009160, NM_009778, NM_008198
Positive regulation of protein phosphorylation	0.044	NM_009778, NM_198111, NM_010197

Cell surface receptor signalling pathway	0.06	NM_001308501, NM_001080815, NM_178924, NM_010340
GO:0006508~proteolysis	0.08887667	NM_001142706, NM_008522, NM_010779, NM_007753, NM_008198

A similar analysis was performed for the downregulated genes in *Apc2*$^{+/+}$ *vs. Apc2*$^{-/-}$ *Ad-cre Pten*$^{fl/fl}$/*Apc*$^{fl/fl}$ ovaries with FDR<0.1. As expected, most of the cellular pathways identified regulate normal ovarian homeostasis e.g. folliculogenesis and steroidogenesis (Table 6.10).

Table 6.10: Identifying biological processes downregulated in Apc2$^{+/+}$ *(n=3) vs. Apc2*$^{-/-}$ *(n=3) Ad-cre* Pten$^{fl/fl}$/*Apc*$^{fl/fl}$ *ovaries 8-weeks post-induction.*

Term	P-Value	Genes
Negative regulation of cell differentiation	7.29E-13	NM_198661, NM_001007077, NM_029948, NM_198663, NM_001270792, NM_001167793, NM_001270793, NR_027385, NM_178657, NM_001005371, NM_201258, NM_001177542, NM_001164285, NM_173773, NM_001164284, NM_001122678, NM_001105254, NM_001122668, NM_177571, NM_001167792
Negative regulation of apoptotic process	6.02E-08	NM_198661, NM_001007077, NM_010295, NM_029948, NM_198663, NM_001270792, NM_001167793, NM_001270793, NR_027385, NM_009640, NM_019739, NM_011824, NM_178657, NM_001005371, NM_011562, NM_201258, NM_001177542, NM_001164285, NM_173773, NM_001164284, NM_001122678, NM_001105254, NM_001122668, NM_001286062, NM_177571, NM_001167792, NM_013479
Negative regulation of transcription, DNA-templated	4.12E-07	NM_198661, NM_001007077, NM_010295, NM_029948, NM_001270792, NM_212435, NM_198663, NM_001167793, NM_001270793, NM_001286607, NR_027385, NM_011824, NM_001005371, NM_178657, NM_011776, NM_201258, NM_001177542, NM_001164285, NM_173773, NM_001164284, NM_001122678, NM_001105254, NM_001122668, NM_177571, NM_053242, NM_001167792, NM_027022
Ovarian follicle development	8.14E-06	NM_010157, NM_133893, NM_130869, NM_009757, NM_009640, NM_013523, NM_207707, NR_104386, NM_001286062, NM_010564
Steroid biosynthetic process	1.33E-05	NM_008256, NM_001012306, NM_019779, NM_001253751, NM_146006, NM_007996, NM_001301728, NM_134469, NM_011485
Positive regulation of cell proliferation	1.36E-05	NM_198661, NM_001007077, NM_029948, NM_198663, NM_001270792, NM_001167793, NM_001270793, NR_027385, NM_011824, NM_178657, NM_001005371, NM_011562, NM_201258, NM_001177542, NM_001164285,

		NM_173773, NM_001164284, NM_001122678, NM_001105254, NM_001122668, NM_177571, NM_001167792
Cholesterol metabolic process	1.05E-04	NM_009692, NM_008256, NM_019779, NM_001253751, NM_007468, NM_007996, NM_001301728, NM_134469, NM_011485
Cholesterol biosynthetic process	1.44E-04	NM_009692, NM_008256, NM_001253751, NM_007468, NM_146006, NM_134469
Meiotic cell cycle	1.50E-04	NM_011516, NM_001002240, NM_001145885, NM_001002241, NM_183015, NM_031387, NM_023729, NM_010029, NM_201370, NM_001002238, NM_138311
DNA methylation involved in gamete generation	4.33E-04	NM_001002240, NM_001145885, NM_001002241, NM_001277730, NM_031387, NM_023729, NM_010029, NM_001002238, NM_001134741
Phospholipid homeostasis	0.003	NM_009692, NM_008149, NM_010720
Response to nutrient	0.0033	NM_010295, NM_009692, NM_170778, NM_010720, NM_011485
Reverse cholesterol transport	0.0052	NM_009692, NM_007468, NM_010720
Steroid metabolic process	0.0055	NM_009692, NM_008256, NM_019779, NM_001253751, NM_007996, NM_001301728, NM_134469
Cell differentiation	0.0145	NM_001002240, NM_001002241, NM_001277730, NM_031387, NM_023729, NM_130869, NM_009640, NM_019739, NM_012026, NM_001134741, NM_007560, NM_011562, NM_001145885, NM_007445, NM_001277216, NM_153519, NM_010029, NM_001277220, NM_001002238, NM_001286062, NM_001146002, NM_001277218, NM_001002894, NM_010701
Lipid metabolic process	0.0157	NM_009692, NM_008256, NM_019779, NM_019699, NM_001253751, NM_146006, NM_007996, NM_001301728, NM_134469, NM_008149, NM_010720, NM_053178
Iron ion transport	0.0172	NM_001159627, NM_010417, NM_181273, NM_175011, NM_001033404, NM_001159628
Positive regulation of proteasomal ubiquitin-dependent protein catabolic process	0.0174	NM_010295, NM_001033214, NM_144551, NM_001128605, NM_011183
Response to stilbenoid	0.0186	NM_008181, NM_008182, NM_007468
Spermatogenesis	0.0219	NM_001002240, NM_001277730, NM_001002241, NM_031387, NM_023729, NM_001134741, NM_011516, NM_001145885, NM_153519, NM_010029, NM_013523, NM_001002238, NM_001146002, NM_172953, NM_001002894
piRNA metabolic process	0.0246	NM_001002240, NM_001145885, NM_001002241, NM_031387, NM_023729, NM_010029, NM_001002238
Cellular response to fibroblast growth factor stimulus	0.0262	NM_010295, NM_011562, NM_011485

Cellular response to insulin stimulus	0.0381	NM_010295, NM_019739, NM_008149, NM_011485
Negative regulation of cytokine secretion involved in immune response	0.0413	NM_009692, NM_009640, NM_001286062
Activation of transmembrane receptor protein tyrosine kinase activity	0.0413	NM_001253781, NM_001253782, NM_009640, NM_011169, NM_001286062
Negative regulation of oocyte maturation	0.0413	NM_201370, NM_010933
Regulation of intestinal cholesterol absorption	0.0413	NM_009692, NM_007468
Metabolic process	0.0421	NM_001195049, NM_001195048, NM_008256, NM_008778, NM_023913, NM_053178, NM_001195047, NM_001195046, NM_008182, NM_001122660, NM_001012306, NR_037145, NM_008149, NM_026247
Glucocorticoid metabolic process	0.0493	NM_009692, NM_011485
Sperm chromatin condensation	0.0493	NM_011516, NM_013523
Determination of dorsal identity	0.0493	NM_011825, NM_011824

As positive regulation of the ERK signalling was enriched in *Apc2*$^{+/+}$ *vs. Apc2*$^{-/-}$ *Ad-cre Pten*$^{fl/fl}$*/Apc*$^{fl/fl}$ ovaries in this analysis, IHC was used to determine the levels of phospho-ERK1/2 protein in *Apc2*$^{+/+}$ and *Apc2*$^{-/-}$ *Ad-cre Pten*$^{fl/fl}$*/Apc*$^{fl/fl}$ ovaries. High cytoplasmic/nuclear focal staining was frequently observed in *Apc2*$^{+/+}$ *Ad-cre Pten*$^{fl/fl}$*/Apc*$^{fl/fl}$ tumour-bearing ovaries, at both the periphery as well as within tumours (Figure 6.34). However, staining was only evident in 1/3 *Apc2*$^{-/-}$ *Ad-cre Pten*$^{fl/fl}$*/Apc*$^{fl/fl}$ tumours and was confined to the tumour periphery. In the *Apc2*$^{-/-}$ *Ad-cre Pten*$^{fl/fl}$*/Apc*$^{fl/fl}$ ovary with tumourlets, high expression was observed exclusively in the OSE (Figure 6.34).

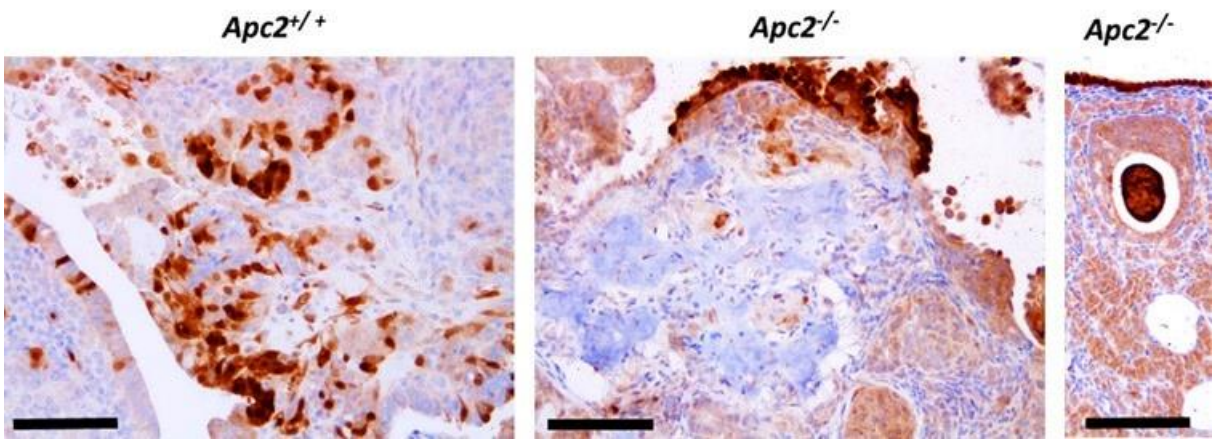

Figure 6.34: p-ERK1/2 is upregulated in *Apc2*$^{+/+}$ Ad-*cre* induced *Pten*$^{fl/fl}$/*Apc*$^{fl/fl}$ tumours. Photomicrographs of p-ERK1/2 immunostaining in *Apc2*$^{+/+}$ (left) and *Apc2*$^{-/-}$ (middle) tumours, as well as OSE of *Apc2*$^{-/-}$ non-tumour ovary (right) (on background of Ad-*cre* *Pten*$^{fl/fl}$/*Apc*$^{fl/fl}$ and collected 8-weeks post-induction). Scale bar 100µm. n=3.

Detailed analysis of genes with FDR<1X10^{-4} (Table 6.11) showed that the most differentially regulated gene was histidine ammonia lyase (HAL), which was nearly 13-fold over-expressed in *Apc2*$^{+/+}$ *Ad-cre Pten*$^{fl/fl}$/*Apc*$^{fl/fl}$ tumours. It catalyses the degradation of L-histidine to L-glutamine, an important nutrient for ovarian cancer cells (Yuan *et al.* 2015). Apart from the *Trim30d* gene, which was upregulated in *Apc2*$^{+/+}$ tumours, all other genes were downregulated in *Apc2*$^{+/+}$ tumours (upregulated in *Apc2*$^{-/-}$ tumours, Table 6.11). Most of these genes are exclusively expressed in normal ovarian tissue or regulate ovarian homeostasis. However, the list also includes *C7*,which represses important genes such as *MYC*, and 2 serine/cysteine peptidase inhibitors, which prevent inhibition of peptidases with important roles during tumour progression (Mason and Joyce 2011) (Table 6.11). Function categories were extracted from SP Comment tool of the DAVID Bioinformatics Resources 6.8.

Table 6.11: Functions of genes most differentially regulated (FDR<1X10^{-4}) in Apc2$^{+/+}$ (n=3) vs. Apc2$^{-/-}$ (n=3) Ad-cre Pten$^{fl/fl}$/Apc$^{fl/fl}$ ovaries. Red denotes upregulated genes.

Gene	P value	FDR p	Fold change	Function
Histidine ammonia lyase *(Hal)*	7.27E-23	1.99E-18	12.86	L-histidine degradation into L-glutamate
Asparagine-linked glycosylation 13 *(Alg13)*	1.79E-12	2.46E-08	0.4179	Involved in protein N-glycosylation. Essential for the second step of the dolichol-linked oligosaccharide pathway
Complement component 7 (*C7*)	1.11E-11	7.6E-08	0.2135	Component of heterochromatin. Recognizes and binds histone H3 tails methylated at 'Lys-9', leading to epigenetic repression. Probably involved in the repression of many genes located in euchromatin, such as E2F1, MYC and CDC25A.
Synaptonemal complex protein 1 (*Sycp1*)	7.18E-11	3.94E-07	0.3907	Major component of the transverse filaments of synaptonemal complexes (SCS), formed between homologous chromosomes during meiotic prophase.
Serine (or cysteine) peptidase inhibitor, clade A, member 5 (*Serpina5*)	1.15E-09	5.24E-06	0.2027	Inhibits activated protein C as well as plasminogen activators.
Solute carrier family 38, member 5 (*Slc38a5*)	3.05E-09	1.06E-05	0.2013	Functions as a sodium-dependent amino acid transporter which counter transport protons. Mediates the saturable, pH-sensitive, and electrogenic cotransport of several neutral amino acids including glycine, asparagine, alanine, serine, glutamine and histidine with sodium.
Oocyte specific homeobox 2 (*Obox2*)	3.09E-09	1.06E-05	0.1927	Regulation of oocyte transcription
Serine (or cysteine) peptidase inhibitor, clade A, member 3C (*Serpina3c*)	4.88E-09	1.49E-05	0.2557	The reactive center loop (RCL) extends out from the body of the protein and directs binding to the target protease. The protease cleaves the serpin at the reactive site within the RCL,

				establishing a covalent linkage between the serpin reactive site and the protease. The resulting inactive serpin-protease complex is highly stable
Inhibin alpha (*Inha*)	6.82E-09	1.87E-05	0.2003	Inhibins and activins inhibit and activate, respectively, the secretion of follitropin by the pituitary gland. Inhibins/activins are involved in regulating a number of diverse functions such as hypothalamic and pituitary hormone secretion, gonadal hormone secretion, germ cell development and maturation, erythroid differentiation, insulin secretion, nerve cell survival, embryonic axial development or bone growth, depending on their subunit composition. Inhibins appear to oppose the functions of activins. Belongs to the TGF-beta family.
Tripartite motif-containing 30D (*Trim30d*)	1.19E-08	2.96E-05	2.7440	
RIKEN cDNA E330034G19 gene (*E330034G19Rik*)	1.78E-08	3.76E-05	0.2051	Positive regulation of proteasomal ubiquitin-dependent protein catabolic processes.
Predicted gene 13084 (*Gm13084*)	1.66E-08	3.76E-05	0.1883	Present in the ovary
Phosphate regulating endopeptidase homolog, X-linked (*Phex*)	2.79E-08	5.46E-05	0.2826	Binds 1 zinc ion per subunit. Probably involved in bone and dentin mineralization and renal phosphate reabsorption.
Myo-inositol oxygenase (*Miox*)	3E-08	5.47E-05	0.2066	Polyol metabolism; myo-inositol degradation into D-glucuronic acid; D-glucuronic acid from myo-inositol.
NLR family, pyrin domain containing 5 (*Nlrp5*)	4.36E-08	6.29E-05	0.2237	Expression is first detected in oocytes of type 3A primary follicles. Transcripts accumulate during oogenesis. During meiotic maturation, the vast majority of the transcripts are degraded and virtually none is detected by 2-cell stage embryogenesis.
NLR family, pyrin domain containing 4F (*Nlrp4f*)	4.15E-08	6.29E-05	0.2008	May be involved in inflammation. Highly expressed in the ovaries.

6.3. Discussion

6.3.1. APC2 is dispensable for OSE homeostasis

The aim of the current study was to characterize roles of the APC2 protein in the OSE using the constitutive *Apc2*$^{-/-}$ mouse, which was achieved by performing *in vivo* and *ex vivo* assays. The results described here clearly show that APC2 is dispensable for OSE homeostasis in early adulthood; APC2 loss did not impair the wound repairing capabilities of the OSE, affect proliferation or differentiation, or initiate metaplastic changes (Figures 6.1-6.6). WNT signalling was not activated in the OSE following APC2 loss, as reflected by comparable membranous β-catenin staining in both *Apc2*$^{+/+}$ and *Apc2*$^{-/-}$ ovaries (Figure 4.2), and similar expression levels of genes of the WNT signalling cascade in cultured OSE (Appendix 4). β-catenin has been previously shown to localize to the cell membrane within the OSE of mouse adult ovary (Usongo *et al.* 2013). Here, APC2 deletion failed to activate WNT signalling and re-locate β-catenin to the nucleus. This is different form the effect of canonical WNT signalling activators LiCl and Wnt3a, which did cause nuclear localization in OSE cultures, but failed to activate downstream TCF/LEF complexes (Usongo *et al.* 2013). *Ex-vivo* assays of OSE isolated from *Apc2*$^{+/+}$ and *Apc2*$^{-/-}$ ovaries did not reveal any changes in epithelial morphology, proliferation, migration or sphere forming abilities (Figure 6.4-6.6). Again, this differs from the phenotype seen post-LiCl or Wnt3a treatment of OSE, where increased proliferation (measured by Brdu), and impaired differentiation (seen as morphological changes of cells to an elongated shape, together with decreased E-cadherin expression) were evident (Usongo *et al.* 2013).

Genetic alterations in oncogenes or tumour suppressor genes in the WNT signalling pathway have been previously shown to cause OSE-related pathologies. Mutation of APC caused different phenotypes depending on the method utilized to induce recombination of the floxed *Apc* allele. When adenovirus-*cre* was used, 18% of *Apc*$^{fl/fl}$ mice developed endometriosis

by the age of 12 months (Wu *et al.* 2011). However, when Amhr2-*cre* was used, 35% of mice developed OEAs by the age of 11 months (Tanwar *et al.* 2013). Tumour formation was more pronounced when degradation-resistant β-catenin was expressed in the OSE, causing the formation of tumours, mostly OEAs, in 50% of mice aged 8-12 months (Tanwar *et al.* 2011a). In the current study, when $Apc2^{+/+}$, $Apc2^{+/-}$ and $Apc2^{-/-}$ female mice (on the background of non-induced hypomorph Apc^{fl} allele) were aged to 18 months, only one $Apc2^{+/-}$ mouse developed a cyst. Other than this, no OSE pathologies were observed in APC2-deficient mice and epithelial tumour formation was not evident.

In conclusion, loss of APC2 is not disruptive to the OSE. Importantly, as no phenotypic changes were observed in the OSE of 10-week-old ovaries, this time point could be used to explore the effect of combining APC2 loss with deletion of APC or PTEN in the OSE.

6.3.2. Combining APC2 loss with APC loss is not sufficient to initiate tumourigenesis

Functional redundancy/compensation between APC and APC2 proteins has been previously described in the mammary gland, where tumour formation was only evident after deleting both APC proteins in the epithelium (Daly *et al.* 2016). A similar approach was performed here to see whether deletion of both proteins would drive EOC formation. We used intrabursal injection of adenovirus-*cre* to recombine the *Apc* gene, as it has been successfully used by other groups, and because it only recombines genes in the OSE (Flesken-Nikitin *et al.* 2003; Wu *et al.* 2007; Tirodkar *et al.* 2014), unlike Amhr2-*cre*, which causes recombination in granulosa cells as well as in the OSE (Connolly *et al.* 2003; Tanwar *et al.* 2013). It has been previously reported that 90% of OSE cells were infected post-adenovirus *cre*, and that the recombination rate (detected using LacZ reporter mice) ranged from 60-80% of OSE cells (Flesken-Nikitin *et al.* 2003). When this technique was applied in the current study, neither APC deletion on its own, nor combined APC/APC2 deletion, were enough to initiate epithelial tumourigenesis. Indeed, additional loss of APC2 in Ad-*cre* $Apc^{fl/fl}$ ovaries protected the

epithelium from age-related and/or APC-loss-related OSE disruption in aging mice (Figures 6.8-6.10).

The decrease in nuclear β-catenin in aging Ad-*cre* $Apc^{fl/fl}$ mice compared to 8-weeks post-induction (Figure 6.13) was not expected, especially with the higher incidence of OSE disruptions and pathologies seen in the older group. However, using a β-catenin-responsive reporter construct (Mohamed *et al.* 2004), it was previously reported that the number of OSE cells showing β-catenin/TCF signalling does decrease with age (Usongo and Farookhi 2012). One possible explanation for the higher levels at 8-weeks post-induction, is that the loss of APC, which would be driving activation of WNT signalling, had only recently happened, in contrast to the late time point. As such, cells expressing nuclear β-catenin were lost as previously described (Usongo and Farookhi 2012). It is not known why the β-catenin active cells are lost with age, but one possible explanation may be that these cells are lost during ovulation and are replaced by neighboring cells, with lower/normal β-catenin expression levels. As such cells have been described as potential stem cells in the OSE (Usongo and Farookhi 2012), another explanation might be that they are differentiating into non β-catenin-active cells, which might explain why the multi-layering, seen in aging $Apc^{fl/fl}$ ovaries, are not expressing nuclear β-catenin.

However, in the Ad-*cre* $Apc^{fl/fl}$/$Apc2^{-/-}$ aging cohort, higher levels of nuclear β-catenin were observed, when compared to the Ad-*cre* $Apc^{fl/fl}$ aging group, but this was not accompanied by OSE disruptions (Figure 6.13). As APC2-deficiency is due to constitutive gene knockout in these mice, this might suggest an essential interaction between β-catenin-positive epithelial clones and the surrounding stroma, which might be disrupted post-APC2 deletion. The role of APC2 in the stroma is not yet explored, but we have shown that APC2 loss affects ovarian angiogenesis, folliculogenesis and steroidogenesis. It has been previously proposed that ovarian epithelial metaplasia requires inflammatory mediators and steroidogenic hormones

(Wei *et al.* 2011). With the finding that both *Cyp17a1* and *Cyp19a1* were downregulated in *Apc2*$^{-/-}$ ovaries (Figure 4.21), it might be expected that intra-ovarian levels of estradiol would be lower in Ad-*cre Apc*$^{fl/fl}$/*Apc2*$^{-/-}$ ovaries as compared to Ad-*cre Apc*$^{fl/fl}$ or wild type ovaries, thus protecting the OSE from metaplastic changes resulting from the interaction between mutational hits and hormones. If these β-catenin positive cells in the OSE are stem cells, as previously proposed (Usongo and Farookhi 2012), then signals from the surrounding microenvironment would dictate whether they remain quiescent, self-renew or differentiate (Jones and Wagers 2008). It is known that ovarian steroids are required for normal functioning of mammary stem cells and that estrogen deprivation decreases their repopulating frequency and outgrowth potential post-transplantation into fat pads (Asselin-Labat *et al.* 2010). Whether the same is true for ovarian stem cells remains to be explored.

6.3.3. Combining APC2 loss with PTEN loss is not sufficient to initiate tumourigenesis

Combining APC and PTEN loss in the OSE of the mouse leads to the development of OEA with 100% penetrance by 6-weeks post-genes deletion (Wu *et al.* 2007). Based on the structural similarity between APC and APC2 proteins, a similar outcome might be expected when both PTEN and APC2 are deleted in the OSE. However, we have shown that in mice with a constitutive *Apc2* knockout, deletion of PTEN in the OSE is not sufficient to initiate OEA by 8-weeks post-induction. This might be explained by functional differences between APC and APC2 in the regulation of WNT signalling. As discussed previously (Section 1.3.1.3), *in vivo* WNT signalling activation post-APC deletion is reproducible in many organs, including the ovaries. However, *in vivo* WNT signalling activation post-APC2 deletion is tissue and context-specific (Section 4.3.1). In the current study, constitutive loss of APC2 did not cause WNT signalling activation in the OSE (Appendix 4). In addition, due to the constitutive nature of APC2 deletion, signals coming from the stroma are dissimilar in the 2 models, which may

affect the metaplastic potential of the OSE post-APC2 deletion, in a similar way to that discussed in section 6.3.2.

It is not unusual that bimutational hits in the OSE are not enough to initiate epithelial ovarian tumourigenesis. For instance, combining ARID1A loss and PIK3CA activation in the OSE failed to induce tumourigenesis in mice followed until the age of 12 months (Zhai *et al.* 2016). In another study, however, the same genetic alterations led to the development of ovarian clear cell carcinoma (Chandler *et al.* 2015), and this was attributed to the difference in the mutant *Pik3ca* alleles used (Zhai *et al.* 2016). Similarly, combined deletion of PTEN and activation of PIK3CA in the OSE failed to initiate epithelial tumourigenesis, but caused the development of non-epithelial tumours and micropapillary OSE proliferation in 82% and 100% of mice respectively (Wu *et al.* 2013). However, in another study, the same mutational alterations lead to the development of ovarian tumours, of which 67% were serous adenocarcinoma (Kinross *et al.* 2012).

Here, $Pten^{fl/fl}$ ovaries collected at 12 months of age showed a range of OSE abnormalities and pathologies (Table 6.4). Pre-tumour lesions, in the form of serous hyperplasia or epithelial cysts, were evident in 33% (2/6) of the mice, and poorly-differentiated small OEA were also evident in 33% (2/6) of the mice. These pathologies, although of higher percentage of tumour development in the current study, have been previously reported; firstly, where 62% of mice developed endometrial glandular lesions and 7.5% ovarian tumours (Dinulescu *et al.* 2005), and secondly, where 83.3% developed serous papillary hyperplasia (Kinross *et al.* 2012). However, our results are different from a previous report in which only 2% (1/47) of mice, of a similar age, showed endometriosis (Wu *et al.* 2011). In all of these studies, adenovirus-*cre* injection was the method used to induce recombination of the floxed *Pten* allele; however, the dose that was used varied between studies, ranging from as high as $2.4x10^8$ pfu in our study and $2x10^8$ pfu (Kinross *et al.* 2012), to $5x10^7$ pfu (Wu *et al.* 2011) and

as low as $2.5x10^7$ pfu (Dinulescu *et al.* 2005). In our study, the loxP sites flank exons 4 and 5 of *Pten*, which is similar to the allele used by the Wu group, but different from the one used by Dinulescu and Kinross groups, which flanked only exon 5. Comparing and contrasting these studies suggest that the higher percentage of tumourigenesis observed in the current study may be caused by the combination of a high viral dose used in the induction and a bigger deletion in the *Pten* gene (floxing both exons 4 and 5). Characterization of *PTEN* exon 4 deletion in humans revealed a 37% reduction of PTEN protein, and marked increase in p-AKT, suggestive of a lipid phosphatase activity for exon 4 (Agrawal *et al.* 2005), which might in our case, synergize with the attenuated phosphatase activity arising from exon 5 deletion (Suzuki *et al.* 2001)

One of the induced $Pten^{fl/fl}$ mice of the aged cohort developed an oviductal tumour (Figure 6.17). This might be explained in terms of the limitation of the intrabursal viral injection technique discussed earlier (Section 1.4.4.1). In the current study, we chose to inject the adenovirus-*cre* directly into the ovarian bursa rather than performing the trans-infundibular intra-oviductal injection used by others (Dinulescu *et al.* 2005; Wu *et al.* 2007) to try to avoid any possible recombination in the oviduct. However, owing to the anatomical location of the infundibulum, which directly opens into the bursa, recombination within the oviduct cannot be excluded. As p-AKT levels were surprisingly low in this lesion, there is the possibility that another-spontaneous- mutation had arisen and was driving this oviductal tumour; however, this possibility has not been explored.

6.3.4. APC2 loss promotes OEA initiation in $Pten^{fl/fl}/Apc^{fl/fl}$ mice

A previous study reported that ovarian tumour initiation, as indicated by the development of tumourlets, was not evident in the first 2 weeks following *Ad-cre* induction of $Pten^{fl/fl}/Apc^{fl/fl}$ mice, but was present in 6/10 of mice 3-weeks post-induction (Wu *et al.* 2011). In the current study, the choice of 15 days post-induction as an early time point was made based

on these reported data, to characterize the early events preceding tumour formation. Our results reproduced what has been published before, as no tumourlets were evident 2-weeks post-induction in *Apc2*$^{+/+}$ adenovirus-*cre*-induced *Pten*$^{fl/fl}$/*Apc*$^{fl/fl}$ ovaries. However, when APC2 protein was reduced or lost, in *Apc2*$^{+/-}$ or *Apc2*$^{-/-}$ cohorts, respectively, tumourlet formation was evident in 66.7% of the mice at this timepoint (Figure 6.23). Both clonal expansion (in the form of tumourlets) and invasion of basement membrane were observed, reflecting an earlier initiation of tumour development in APC2-deficient Ad-*cre Pten*$^{fl/fl}$/*Apc*$^{fl/fl}$ mice. As the *Apc2*$^{-}$ allele is constitutive in nature, it is difficult to know whether this effect is due to loss of APC2 in transformed epithelial cells, the surrounding microenvironment or even cells outside the ovary.

One explanation for the early initiation of tumourigenesis following APC2 loss in Ad-*cre Pten*$^{fl/fl}$/*Apc*$^{fl/fl}$ mice could be a disruption in immunoediting of transformed epithelial cells. According to the immunoediting hypothesis, innate immune cells recognize proliferative neoplastic cells and an adaptive tumour immunity develops, leading to their elimination (Dunn *et al.* 2004). If the elimination is not complete, it is followed by an 'equilibrium' phase, where more immune-resistant tumour cells are produced and an equilibrium exists between immune cells and tumour cells, resulting in reduced-immunogenic tumour clones which stay dormant for long periods before they can completely 'escape' immune defence mechanisms and grow (Dunn *et al.* 2004). Both innate and adaptive immune responses are required for initiating this tumour-specific immunity, and T-cells have been shown to play important roles during the 'elimination' phase (Dunn *et al.* 2004). WNT signalling activation, by inhibiting GSK3 or using Wnt3a, has been previously shown to reduce T-cell expansion and disrupt T-cell functions, by preventing the differentiation of naïve T-cells into mature effector T-cells (Muralidharan *et al.* 2011). Whether APC2 loss activates WNT signalling in T-cells in a similar manner, thus disrupting tumour cell immunoediting, is unknown and remains to be explored.

The early invasion seen post-APC2 loss could be explained, at least in part, by the basal epithelial cell extrusion hypothesis (Slattum and Rosenblatt 2014). The normal extrusion direction of the cells is apical, and in the ovaries would result in shedding of transformed cells outside the ovary. However, when the extrusion is basally-shifted, the transformed cells would breach the basement membrane and invade the ovary (Slattum and Rosenblatt 2014). It has been shown that apical extrusion needs coupling between microtubules and actin filaments, and that a shift to basal extrusion happens post-APC truncating mutations due to disruption of microtubule dynamics (Slattum and Rosenblatt 2014). A previous study has shown defective neuronal migration post-APC2 deletion in the brain, caused by defects in actin and microtubule dynamics (Shintani *et al.* 2012). APC2 was shown to be distributed along microtubules, causing their stability when overexpressed in cultured chick retina, and APC2 knockdown impaired microtubule stability (Shintani *et al.* 2009). It is possible that a similar disruption of microtubule dynamics may have been affected in the absence of APC2 in the transformed cells of Ad-*cre* $Apc^{fl/fl}$/$Pten^{fl/fl}$ ovaries, thus facilitating the basal extrusion of cells and enabling tumourlet invasion to take place.

6.3.5. APC2 is required for OEA progression

Before starting this project, we hypothesized that APC2 acts as a tumour suppressor for epithelial ovarian tumourigenesis, and that APC2-deficiency would cause the development of larger tumours in the Ad-*cre* $Apc^{fl/fl}$/$Pten^{fl/fl}$ ovarian model. This was based on assumptions from previous studies, which demonstrated *APC2* allelic imbalance in human ovarian tumours (Jarrett *et al.* 2001), as well as copy number alterations (deletions) in human and murine high grade serous ovarian carcinoma (Perets *et al.* 2013). However, we unexpectedly found that, following the initial rapid development of tumourlets when APC2 was absent in Ad-*cre* $Pten^{fl/fl}$/$Apc^{fl/fl}$ ovaries, confirming that it is a tumour suppressor for tumour initiation, tumour progression at 8-weeks post-induction was actually hampered by APC2 loss (Figure 6.26),

suggesting it was acting as an oncoprotein. This is similar to the attenuation of hepatocellular carcinoma found when APC2 was deleted in *Apc*$^{fl/fl}$ mice; only micro-adenomas were present in the livers of *Apc*$^{fl/fl}$/*Apc2*$^{-/-}$ mice in contrast to hepatocellular carcinoma developing in *Apc*$^{fl/fl}$ at 400 days of age (Daly 2013). This has been seen in the ovarian setting as well, when *Arid1a,* another gene believed to be a tumour suppressor for ovarian epithelial tumourigenesis, was deleted using the same OEA model used in the current study (Zhai *et al.* 2016). *Arid1a* silencing prolonged survival and enhanced glandular epithelial differentiation of tumours (Zhai *et al.* 2016). Although different from our findings, that smaller tumours develop post APC2-loss, ARID1A-deficiency caused larger tumour formation, which was unexpectedly associated with prolonged survival (Zhai *et al.* 2016). In the current study, survival was not evaluated; however, a recent study analysing data for high grade serous ovarian cancer cases from The Cancer Genome Atlas, showed that elevated *APC2* levels are associated with decreased overall, as well as, progression-free survival following chemotherapy (Seagle *et al.* 2016).

In the current study, APC2-deficiency in Ad-*cre Apc*$^{fl/fl}$/*Pten*$^{fl/fl}$ ovaries collected 8-weeks post-induction did not enhance glandular epithelial differentiation, in fact, it was reduced, and differentiation into keratinizing squamous cell carcinoma was observed (Figure 6.30). The presence of discrete areas of focal squamous differentiation and keratinization has previously been described in tumours developing in Ad-*cre Pten*$^{fl/fl}$/*Apc*$^{fl/fl}$ ovaries 6-weeks post-induction (Wu *et al.* 2007). However, the large keratinized areas, resembling ovarian squamous cell carcinoma seen in our APC2-deficient tumours, have not been previously described. Although ovarian squamous cell carcinoma is rare, and originates from teratoma or endometriosis, a recent case report presented an ovarian squamous cell carcinoma arising from OEA (Shoji *et al.* 2016), although the molecular driver of this differentiation was not characterized. WNT signalling activation has been shown to play important roles in the pathogenesis of squamous cell carcinoma in a number of organs (Aminuddin and Ng 2016;

Sherwood and Leigh 2016; Shiah *et al.* 2016). Extracting data from the Cancer Genome Atlas revealed that *APC2* is mutated (missense mutations) in 2.24%, 1.73% and 1.57% of squamous cell carcinomas of lung, cervix and head and neck respectively. In addition, downregulation of *Apc2* was recently shown in a rat model of oral squamous cell carcinoma (Peng *et al.* 2015). Whether a higher level of WNT signalling disruption is required for ovarian squamous cell metaplasia is unknown, but it could be hypothesized that partial compensation between APC and APC2 protects ovarian epithelial cells from squamous metaplasia and keratinization when only APC (as well as PTEN) is deficient, and that simultaneous loss of both APC proteins facilitates the squamous metaplasia. This hypothesis might be supported by results of *Axin2* RNAscope analysis (performed shortly before thesis submission), which revealed lower expression of *Axin2* RNA in areas where abundant packed epithelial gland formation was evident in $Apc2^{+/+}$ Ad-*cre* $Apc^{fl/fl}/Pten^{fl/fl}$ tumours, as compared to other areas of the tumour as well as to $Apc2^{-/-}$ Ad-*cre* $Apc^{fl/fl}/Pten^{fl/fl}$ tumours (Appendix 7).

No significant differences were observed between $Apc2^{+/+}$ and $Apc2^{-/-}$ Ad-*cre* $Apc^{fl/fl}/Pten^{fl/fl}$ tumours in terms of proliferation or apoptosis (Figure 6.28). This was unexpected, as the presence of APC2 resulted in the formation of larger tumours, suggesting an imbalance between the two processes. It is known that Ki67 marks proliferative cells in all stages of the cell cycle (Scholzen and Gerdes 2000), meaning that it is marking all cycling cells whether or not they will finally reach the mitotic phase. However, if the cells enter the cell cycle and become arrested later on, or if mitosis fails, this cannot be visualized using Ki67 immunostaining. IHC for phospho-histone 3 protein, which marks the fraction of proliferating cells undergoing mitosis (Pérez-Cadahía *et al.* 2009), revealed a significant decrease in mitotic cells in $Apc2^{-/-}$ tumours compared to $Apc2^{+/+}$ tumours (24.1±2.2 vs. 48.5±1.99, mean±S.E., $p<0.05$), which may explain the decreased size of tumours in which APC2 levels were reduced or absent. Previous work with *Drosophila* embryos identified a small yet significant increase

in mitotic defects post-APC2 loss caused by chromosome segregation errors (Poulton *et al.* 2013). An interesting finding was that although all the squamous-differentiated cells present in keratin pools were Ki67 positive, they were not mitotic (phospho-histone 3 negative, Appendix 6). This may indicate that differentiation of tumour cells into the squamous morphology post-APC2-deficiency is one of the mechanisms by which tumour growth is arrested following rapid initiation.

6.3.6. Identifying possible molecular mechanisms of APC2-dependent tumour progression

RNA sequencing was performed to compare the transcriptome of tumours developing in Ad-*cre* $Pten^{fl/fl}/Apc^{fl/fl}$ ovaries at 8-weeks post-induction, either when APC2 protein was present ($Apc2^{+/+}$) or absent ($Apc2^{-/-}$). One of the main limitations of this study was that the RNA used for sequencing was extracted from whole ovaries. Histological analysis of the other ovary from each mouse showed that normal ovarian tissue was always present in tumours lacking APC2, due to the decreased tumour progression in animals of this genotype (Table 6.5). These facts need to be taken into consideration when interpreting the data, especially for genes which are downregulated in $Apc2^{+/+}$ as compared to $Apc2^{-/-}$ tumours.

The most significantly differentially-regulated gene, when comparing $Apc2^{+/+}$ with $Apc2^{-/-}$ Ad-*cre* $Apc^{fl/fl}/Pten^{fl/fl}$ tumours, was Histidine ammonia lyase (*Hal*), also known as histidase, which was 13-fold upregulated (Table 6.7,6.11), and catalyses the first step in histidine catabolism (Kawai *et al.* 2005). While its deficiency is known to cause histidinemia or histidinurea, which are characterized by mental impairment (Kawai *et al.* 2005), the pathogenesis of HAL overexpression is not yet fully characterized. A recent study in amphibian metamorphosis reported that HAL expression is increased during intestinal stem cell development, especially in proliferating stem cells (Luu *et al.* 2017), suggesting a role for HAL in regulating intestinal stem cell proliferation and function. Whether HAL plays similar roles

in adult stem cells in other organs, or in cancer stem cells, remains to be investigated. Normally, HAL is not expressed in the ovaries, but is highly expressed in EOC, including OEAs (data extracted from The Human Protein Atlas database, (Uhlen *et al.* 2015)). The end product of histidine catabolism is glutamine, which has been previously shown to promote ovarian cancer cell proliferation when used as a nutrient by cultured cells (Yuan *et al.* 2015). In addition, glutamine-dependent ovarian cancer cells have been reported as highly invasive, when compared to glucose-dependent cancer cells (Yang *et al.* 2014). It would be interesting to further explore the role of HAL in EOC, particularly whether its upregulation contributes to tumourigenesis and whether it may be a potential therapeutic target.

Of the most significantly downregulated genes in *Apc2*$^{+/+}$ vs. *Apc2*$^{-/-}$ Ad-*cre* *Pten*$^{fl/fl}$/*Apc*$^{fl/fl}$ ovaries, *Serpina5*, *Serpina3c* and *C7* could all potentially be linked to tumourigenesis (Table 6.8, 6.11). *Serpina5* (serine protease inhibitor, clade A, member 5) encodes a protein which inhibits peptidase activity and has been shown to suppress serous ovarian tumour formation (Sieben *et al.* 2005), probably by inhibiting MAPK signalling (Lee *et al.* 2013). *Serpina3c*, another serine protease inhibitor, has been shown to be downregulated in human colorectal cancer tissue, and localizes to epithelial tumour cells, as well as surrounding stroma (Dimberg *et al.* 2011). *C7*, which codes for complement component 7 protein, is a potential tumour suppressor whose expression is decreased in ovarian cancer (Ying *et al.* 2016), as well as in other cancers such as oesophageal, kidney and colorectal (Oka *et al.* 2001).

Protein-protein interaction were visualized with STRING and Cytoscape tools in order to identify the highly connected/most interacting proteins, named protein hubs, which are proposed to play more central roles in developing the phenotype (Vallabhajosyula *et al.* 2009), tumour progression in our case, compared to other less-essential proteins. When protein-protein interactions were plotted from the list of genes significantly upregulated (FDR<0.05) in *Apc2*$^{+/+}$

vs. *Apc2*$^{-/-}$ Ad-*cre Apc*$^{fl/fl}$/*Pten*$^{fl/fl}$ ovaries, only one hub (LRGUK) was identified (Figure 6.32a). Cytoscape plotting (Figure 6.32c) revealed that it regulates PCDH11x and is regulated by HUNK and HAL. Little is known about the LRGUK (leucine rich repeats and guanylate kinase domain containing) protein, but according to The Human Protein Atlas, it is not expressed in normal ovaries but is expressed in ovarian cancers, including OEAs (Uhlen *et al.* 2015). GUK (guanylate kinase), a paralogue of LRGUK, has been shown to be a target for 6-thioguanine and 8-azaguanine cancer chemotherapeutic agents (Stolworthy and Black 2001).

Many hubs were identified when protein-protein interactions of genes significantly downregulated (FDR<0.05) in *Apc2*$^{+/+}$ vs. *Apc2*$^{-/-}$ Ad-*cre Apc*$^{fl/fl}$/*Pten*$^{fl/fl}$ ovaries were plotted (Figure 6.32b). The most connected hubs were BMPR1b, ASZ1, TRIB2, ESR2 and members of FBXW family. BMPR1b (bone morphogenetic protein receptor 1b) expression is decreased in EOC, which correlates with poor survival (Ma *et al.* 2010). ASZ1 (ankyrin repeat, SAM and basic leucine zipper domain containing 1, also known as GASZ) is a germ cell-specific protein (Yan *et al.* 2002), whose reduction would be expected when oocytes are absent. Whether it has other roles, or whether its expression is disrupted in cancer, is not yet known. TRIB2 (Tribbles 2) is a pseudokinase whose expression is decreased in platinum-resistant EOC and is associated with poor survival (Kritsch *et al.* 2017). ESR2 (estrogen receptor beta) is known to have tumour suppressor roles for EOC both *in vitro* and *in vivo* (Bossard *et al.* 2012), and ESR2 agonists were successfully proven to inhibit the proliferation of EOC cells *in vitro* (Liu *et al.* 2017; Schuler-Toprak *et al.* 2017). FBXW (F-box and WD-40 domain) proteins, shown to be downregulated in the current study, are highly expressed in normal mouse ovaries (Yue *et al.* 2014); however, they clustered separately when protein-protein interactions were plotted (Figure 6.32b,c), meaning that they are only predicted to interact with each other, and their function is unknown. Whether their reduced expression is caused by the absence of normal ovarian tissue in *Apc2*$^{+/+}$ tumours, or whether they play a role in tumourigenesis, is not known.

FBXW7, another family member, which was not significantly decreased in the current study, is a tumour suppressor in EOC and is downregulated in the 4 main histotypes (Kitade *et al.* 2016).

Plotting the protein-protein interactions of differentially expressed interacting genes (extracted from the protein-protein interaction analysis performed for upregulated (Figure 6.32a) and downregulated (Figure 6.32b) genes), to visualize protein-protein interactions between upregulated and downregulated protein-coding genes (Figure 6.35c), lead to the identification of an important new hub in the network, the HUNK (Hormonally Up-regulated Neu-associated Kinase) protein, which was significantly upregulated in $Apc2^{+/+}$ Ad-*cre* $Apc^{fl/fl}/Pten^{fl/fl}$ tumours. Extracting data from the Human Protein Atlas revealed that it is moderately expressed in EOC, including OEAs, in a pattern similar to that seen in breast cancer (Uhlen *et al.* 2015). HUNK function has not been characterized in EOC, but in breast cancer it plays pivotal roles in tumourigenesis, and is involved in resistance to inhibitors in $HER2^{+}$ ($ERBB2^{+}$) breast cancer through regulation of autophagy (Zambrano *et al.* 2017).

When biological pathway analysis was performed for the most downregulated genes in $Apc2^{+/+}$ vs. $Apc2^{-/-}$ Ad-*cre* $Apc^{fl/fl}/Pten^{fl/fl}$ tumours, pathways most represented were those regulating normal ovarian homeostasis (Table 6.10). However, analysis of biological pathways of upregulated genes revealed an enrichment in pathways regulating inflammatory responses, immune responses, cellular responses to interferon gamma, interleukin 1 and tumour necrosis factor (Table 6.9). In addition, immune infiltration was only evident in $Apc2^{+/+}$ Ad-*cre* $Apc^{fl/fl}/Pten^{fl/fl}$ tumours (Table 6.5). Historically, EOC has been hypothesized to originate from the OSE, which undergoes metaplastic changes caused by inflammation taking place during ovulation at the site of rupture (Ness and Cottreau 1999). EOC progression has been shown to be governed by the interaction between tumour cells and the surrounding microenvironment, mainly immune cells and inflammatory cytokines and chemokines (Maccio and Madeddu

2012). Chemokines (e.g. *Ccl8*), which encode for small proteins secreted by tumour and stromal cells (Balkwill 2004), as well as growth factors (e.g. *Fgf1*) and cytokine receptors (e.g. *Il1rl1*), were upregulated in *Apc2*$^{+/+}$ Ad-*cre Apc*$^{fl/fl}$/*Pten*$^{fl/fl}$ tumours. Although little effort has been made previously to unravel the inflammatory cytokine/immune status in OEA mouse models and their contribution to tumour initiation and progression, these roles have been characterized in an ovarian clear cell carcinoma mouse model arising from the deletion of *Arid1a* and activation of *Pik3ca* in the OSE (Chandler *et al.* 2015). In this model, tumour progression was mediated by high IL-6 levels, which activated pro-tumourigenic cytokine signalling (Chandler *et al.* 2015). Because of the time constraint, further characterization of immune/inflammatory status and tumour microenvironment were not performed in the current study, but are highly recommended for future investigation.

One of the limitations of the current study was that results of RNA sequencing analysis were not confirmed by qRT-PCR because of the limited tumour samples collected. However, positive regulation of ERK1/2 signalling one of the upregulated biological pathways in *Apc2*$^{+/+}$ vs. *Apc2*$^{-/-}$ Ad-*cre Apc*$^{fl/fl}$/*Pten*$^{fl/fl}$ tumours (Table 6.9), was confirmed by immunohistochemical analysis of p-ERK1/2 (Figure 6.34). *ERK* (extracellular signal–regulated kinase, also known as *MAPK*) is downstream of *KRAS*, which is mutated in 10.65% (44/413) OEA human cases, as extracted from COSMIC database. Interestingly, the first OEA mouse model was based on deleting *Pten* and expression of an active mutant of *Kras* in the OSE (Dinulescu *et al.* 2005). KRAS/BRAF/MEK/ERK canonical signalling is activated in many cancers, including EOC (Samatar and Poulikakos 2014), with accumulating evidence that activation of the pathway is needed for EOC progression (Wilhelm *et al.* 2004; Bourguignon *et al.* 2005). The presence of p-ERK1/2 positive cells inside the tumours in *Apc2*$^{+/+}$ Ad-*cre Apc*$^{fl/fl}$/*Pten*$^{fl/fl}$ tumours compared to their peripheral localization, if any, in the *Apc2*$^{-/-}$ Ad-*cre Apc*$^{fl/fl}$/*Pten*$^{fl/fl}$ tumours (Figure 6.34)

might indicate that the presence of ERK1/2-positive clones is needed for tumour invasion and progression in the *Pten*$^{fl/fl}$/*Apc*$^{fl/fl}$ model.

6.3.7. Conclusion and future directions

Results of the current study have shown that APC2 is dispensable for OSE homeostasis. APC2 loss on its own, or in combination with APC or PTEN loss in the OSE, failed to initiate EOC. When APC2 loss was introduced to the Ad-*cre* *Pten*$^{fl/fl}$/*Apc*$^{fl/fl}$ tumour model, early initiation of tumourigenesis was observed, but reduced progression was evident, as reflected by ovarian volumes 8-weeks post-induction. Several mechanisms were shown to be responsible for this tumour growth restriction, including differentiation to squamous phenotype with hyperkeratinisation, decreased mitosis, decreased p-ERK1/2 expression and disrupted immune/inflammatory signalling. Owing to the constitutive nature of the *Apc2*$^{-}$ allele, both tumour cell autonomous and non-autonomous (from stromal cells) mechanisms could be contributing to the observed phenotype. In conclusion, the assumption that APC2 protein is a tumour suppressor for growth of OEA histotype of EOC is not supported by the findings of the current study. Instead, APC2 played a dualistic function in Wnt-driven OEA, a tumour suppressor for initiation but an oncoprotein for progression. However, although this is true in the current study, it needs to be tested in a non-Wnt ovarian tumour model, and in a model representing serous adenocarcinoma histotype before it could be extended, generalized or used to determine its relevance to human data.

Dissecting autonomous and/or non-autonomous contributions of APC2 to phenotypes observed in the current study, could be tested by intrabursal injection of adenovirus-*cre* together with short hairpin RNA vector targeting *Apc2* to the OSE of *Pten*$^{fl/fl}$/*Apc*$^{fl/fl}$ ovary. Comparing and contrasting tumours developing in this model with tumours generated in the current study might help to clearly unravel roles of APC2 in neoplastic OSE.

To understand the clinical significance of the current data, it would be crucial to define APC2 loss in terms of tumour size, stage, sensitivity/resistance to chemotherapy, whether it happens in association with certain mutations, in certain histotypes and whether it is present in the tumour cells and/or stromal cells. With the recent report that increased APC2 expression in HGSOC is correlated with poor survival (Seagle *et al.* 2016), and stemming from results of the current study, more work should be directed to unravel contributions of APC2 protein in EOC before deciding whether targeting APC2 could be considered as a therapeutic intervention.

Out of the functional analysis performed in the current study, 2 targets appear very attractive to be considered for future projects, namely HAL and HUNK. With the data present in the Human Protein Atlas showing that they are overexpressed in epithelial ovarian tumours, irrespective of histotype, and with lack of information in literature regarding their roles in EOC, proposed future work would be phenotypically characterizing them first *in vitro*, through knockdown and overexpression in EOC cell lines, before phenotypic characterization of the produced cells *in vivo* using transplantation models. These targets could then be judged for usefulness as therapeutic interventions for treating EOC.

7. General discussion

The work presented in this thesis set out to determine roles for APC2 in ovarian WNT signalling activation, homeostasis, fertility and tumourigenesis. This study has revealed, for the first time, that APC2-deficiency activates WNT signalling in the ovary during early adulthood, which subsequently disrupts ovarian homeostasis and causes subfertility originating from an ovarian defect. Follicle growth was perturbed in APC2-deficient mice secondary to defective response to gonadotrophins, reduced follicular vascularity, downregulation of genes coding for steroidogenic enzymes and upregulation of *Foxo1* expression, which contributed to increased apoptosis of granulosa cells in APC2-deficient follicles. The second major finding of the current study was the development of WNT-driven adult GCT in at least 20% of APC2-deficient female mice (on the background of non-induced $Apc^{fl/fl}$) as early as 12 months. These tumours recapitulated human adult GCT histology and molecular signature. One of the significant findings that emerged from this study is that APC2 loss does not contribute to ovarian epithelial tumourigenesis (as distinct from sex cord-originating GCTs); epithelial tumour formation was not evident when APC2 was lost on its own, or combined with APC or PTEN loss. On the contrary, OSE disruption caused by age and/or APC loss in the epithelium was attenuated post-APC2 loss. APC2-deficiency in Ad-*cre* $Pten^{fl/fl}/Apc^{fl/fl}$ OEA model attenuated tumour growth, although this attenuation was preceded by earlier initiation. Taken together, these results suggest that APC2 is an important regulator of ovarian WNT signalling and plays essential roles in ovarian homeostasis and fertility. In addition, it is a tumour suppressor for GCT development, but plays a dualistic role in WNT-driven OEA: a tumour suppressor for initiation and an oncoprotein for progression.

The findings from this study make several distinct contributions of fundamental new knowledge to the current literature, being the first to highlight the role of APC2 as an important regulator of WNT signalling in the ovary. Initial studies performed in *Drosophila* and on cell

lines to functionally-characterize APC2 demonstrated the presence of β-catenin and Axin1 binding sites in APC2, which enable it to regulate WNT signalling (Hamada *et al.* 1999; Van Es *et al.* 1999; Ahmed *et al.* 2002; Akong *et al.* 2002; McCartney *et al.* 2006; Roberts *et al.* 2012). However, in an *in vivo* setting, APC2 regulation of WNT signalling is tissue specific, with WNT signalling activation post-APC2 loss only evident in the small intestine and liver but not the mammary glands (Daly 2013; Daly *et al.* 2016).

The current findings also extend our knowledge of deleterious effects of WNT signalling activation on ovarian homeostasis and fertility, which had previously been suggested from studies investigating WNT signalling activation and ovarian subfertility in mice (Boerboom *et al.* 2005; Fan *et al.* 2010a; Abedini *et al.* 2016; De Cian *et al.* 2016). Results presented here have clearly shown that reduced ovulation observed in APC2-deficient mice is not caused by defects in ovulation and terminal differentiation of granulosa cells (which happen when WNT signalling is activated in antral follicles), but rather caused by restricted follicular growth and failure to reach the pre-ovulatory stage. This phenotype is similar to previous phenotypes published when WNT signalling was activated in pre-antral follicles (Boerboom *et al.* 2005; Abedini *et al.* 2016), implying that APC2 is expressed in growing follicles as early as the pre-antral stage.

In addition, this research provides additional evidence with respect to roles of WNT signalling activation in the pathogenesis of ovarian GCT. Accumulating evidence from clinical data has pointed to this role of WNT signalling (Boerboom *et al.* 2005; Stewart *et al.* 2013; Kilonzo *et al.* 2015; Xu *et al.* 2016), and GEMMs proved that WNT signalling activation on its own is sufficient to initiate ovarian GCTs (Boerboom *et al.* 2005; De Cian *et al.* 2016).

The findings in this study provide a new understanding of roles of APC2 in ovarian epithelial tumourigenesis. Reports from previous work (Jarrett *et al.* 2001; Perets *et al.* 2013),

as well as data extracted from cBioPortal database have shown loss of *APC2* (allelic imbalance or mutational deletions) in human ovarian carcinoma. In addition, the role of WNT signalling in human OEA pathogenesis (Wu *et al.* 2001; Tanwar *et al.* 2013), and in different GEMMs developing OEAs post-WNT signalling activation alone (Tanwar *et al.* 2011a; Tanwar *et al.* 2013; van der Horst *et al.* 2014), or in combination with PTEN-loss (Wu *et al.* 2007; Tanwar *et al.* 2011a; Wu *et al.* 2011; Zhai *et al.* 2016), led to the hypothesis that APC2 was a tumour suppressor for ovarian epithelial tumourigenesis. However, findings of the current study do not support this hypothesis. Instead, they suggest that APC2 is an oncoprotein for WNT-driven OEA progression, similar to its role in WNT-driven hepatocellular carcinoma (Daly 2013). This new hypothesis is supported by a recent finding that increased APC2 levels in human HGSOC are associated with decreased overall survival as well as progression-free survival post-chemotherapy (Seagle *et al.* 2016).

One important feature of tumours developing in APC2-deficient $Pten^{fl/fl}/Apc^{fl/fl}$-induced ovaries, as compared to $Apc^{+/+}$ tumours, was squamous metaplasia and keratinization with reduced mitotic capacities. This could be explained in terms of the 'just right' hypothesis of WNT signalling activation According to the hypothesis, a 'moderate' dose of WNT signalling activation is required for tumourigenesis. However, if this dose is exceeded, tumourigenesis is attenuated as tumour cells undergo abnormal differentiation rather than proliferation. This was evident in intestinal tumours (Bordonaro *et al.* 2008), and in mammary gland organoids (Jardé *et al.* 2016), where hyper-induction of WNT signalling caused increased apoptosis or squamous metaplasia, respectively. Using the 'just right' hypothesis to explain the findings of the current study (Figure 6.1), one can postulate that WNT signalling activation post APC2-loss was 'counteracted' by other signalling pathways in granulosa cells of ovaries during early adulthood so as to reach a 'just right' level to cause GCT formation only in a subset of aging mice. However, it never reached the 'just right' level needed to induce epithelial ovarian

tumourigenesis even when the dose was ‘increased’ post APC-loss. In contrast, in the *Pten*$^{fl/fl}$/*Apc*$^{fl/fl}$ tumour model, APC/APC2 loss combined with PI3K pathway activation enabled the ‘just right’ level to be reached earlier causing early initiation but was followed by ‘hyperinduction’, which delayed/prevented tumour growth probably by inducing differentiation into non-mitotic squamous keratinized cells (Appendix 6-7).

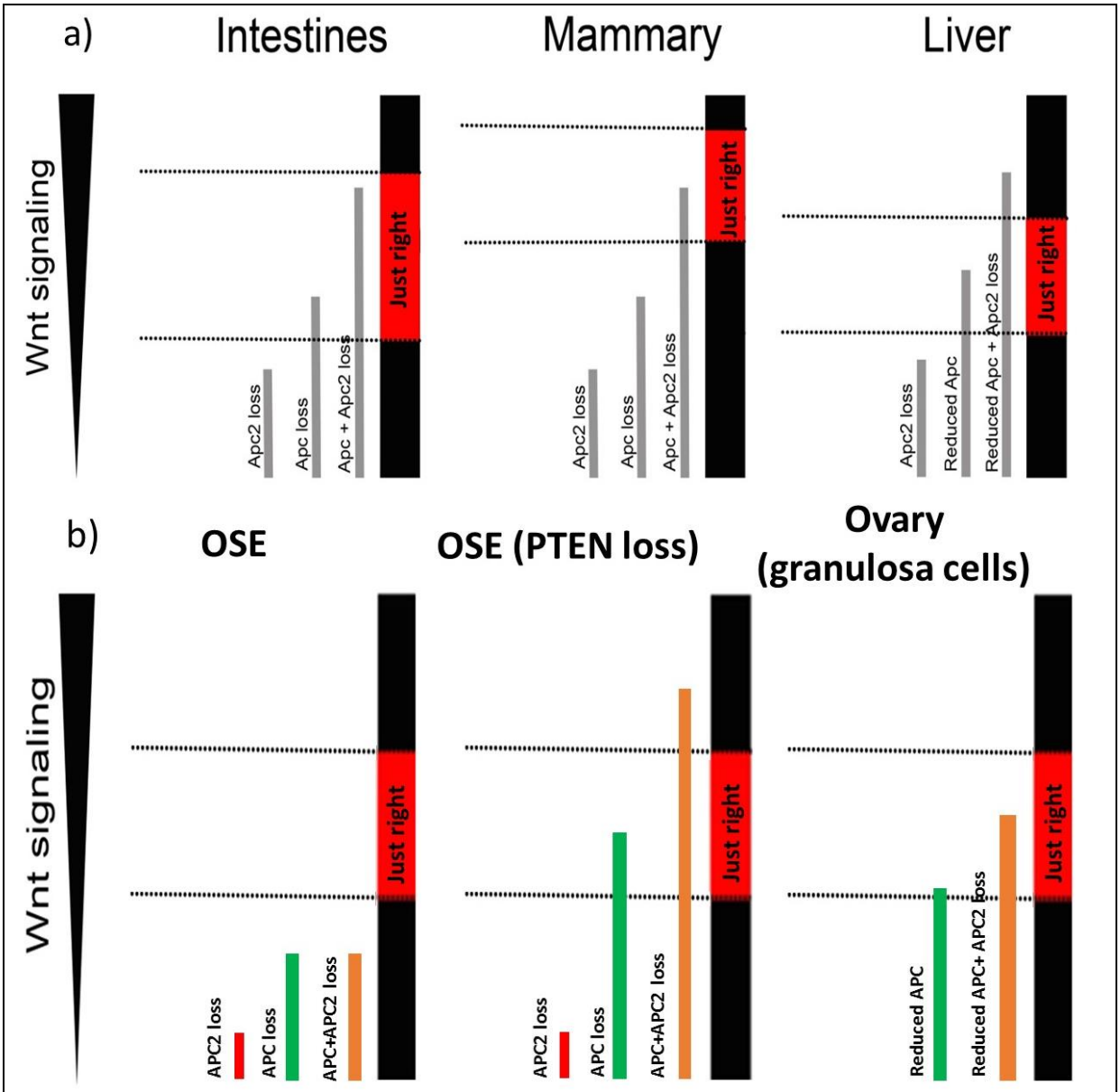

Figure 6.1: Using the 'just right' hypothesis of WNT signalling to explain interactions between APC and APC2 in tumourigenesis. (a) APC2 loss does not modulate WNT-driven tumourigenesis post-APC loss in the intestines, synergize with APC loss to reach the 'just right' level of WNT activation to drive mammary gland tumourigenesis, but exceeds the 'just right' level required for hepatocellular carcinoma in non-induced $Apc^{fl/fl}$ mice (reduced APC level) (Daly 2013). (b) In the ovary, loss of APC or APC2 alone or in combination in the OSE fails to activate WNT signalling to reach the 'just right' level for tumourigenesis. However, in PTEN-deficient OSE, APC loss is enough to activate WNT signalling to the 'just right' level, but combined APC/APC2 loss causes hyper-activation of WNT signalling exceeding the 'just

right' level and attenuating tumour progression. In granulosa cells, reduced APC (non-induced $Apc^{fl/fl}$) was enough to reach the 'just right' level of WNT signalling activation to drive tumourigenesis in 1/19 mice. However, combined APC2 deficiency with APC reduction caused the 'just right' level to be reached in 20% of mice, causing GCT formation.

Given the constitutive nature of the *Apc2*$^{-}$ allele, both autonomous and non-autonomous mechanisms are expected to contribute to the described phenotypes. Results of the current study have clearly shown the intra-ovarian origin of the subfertility phenotype described in APC2-deficient mice, and that hypothalamic-pituitary regulation of ovarian functions is not contributing to the subfertility phenotype. Although the subfertility is caused by increased apoptosis of granulosa cells, a contribution of endothelial cells to the phenotype was evident. Whether the same phenotype could be reproduced if APC2-deletion was targeted exclusively in granulosa cells (using Amhr2 or Cyp19a-*cre*) remains unknown, due to the unavailability of an *Apc2*$^{-}$ conditional allele. The same applies to GCTs developing in APC2-deficient mice, which – in contrast – displayed enhanced angiogenesis. In the case of epithelial tumours developing in APC/PTEN-deficient mice, findings of the current study suggest that non-epithelial cells are contributing to enhanced tumour formation seen when APC2 was intact. This was evident by the presence of immune cell infiltrates in tumours, and enrichment of immune and inflammatory pathways, which were absent when *Apc2* was deleted. This would imply that APC2-deficiency in immune cells is disruptive, and may be preventing a positive contribution to tumour growth. In addition, the constitutive nature of *Apc2*$^{-}$ allele might be contributing to the early initiation of tumourigenesis observed in APC2-deficient tumours, by modulating T-cell 'immunoediting' suppression of tumourigenesis. Furthermore, although the current study focused on WNT signalling-regulatory functions of APC2, contributions of non-WNT functions of APC2 cannot be ignored. Previous studies have pointed to APC2 in regulating cytoskeleton and microtubule association (McCartney *et al.* 1999; Nakagawa *et al.*

2000b; Jarrett *et al.* 2001; Shintani *et al.* 2009; Shintani *et al.* 2012), spindle anchoring during mitosis (McCartney *et al.* 2001), and a possible modulating role of cell cycle progression and apoptosis via translocating p53-binding protein 2 (also known as apoptosis-stimulating protein 2 of p53 ASPP2) to the perinucleus (Nakagawa *et al.* 2000a). Disruption of these roles, although not explored in the current study, might have contributed to GCT formation in APC2-deficient mice, and to early initiation of tumourigenesis happening in APC2-deficient $Pten^{fl/fl}/Apc^{fl/fl}$ adenovirus-*cre* induced ovaries.

Also, it is naïve to think that WNT signalling activation is the sole driver of the reported phenotypes, or to ignore the cross talk between WNT signalling and other signalling pathways. For example, unlike early adulthood, FOXO1 expression was absent in APC2-deficient GCT, implying a need to silence FOXO1 and to stop FOXO1-driven granulosa cell apoptosis as a prerequisite for tumourigenesis. However, the cause of the 'switch' from present FOXO1/granulosa cell apoptosis to absent FOXO1/granulosa cell proliferation and tumourigenesis was not identified and needs to be characterized. This question needs to be extended to WNT-driven tumourigenesis in other organs to determine whether it is associated with silencing FOXO1. Answering this question might help in identifying new targets for cancer treatment. It is noteworthy to mention here that PTEN levels remained elevated in granulosa cells at early adulthood and in granulosa cell tumours, which means that the control of FOXO1 expression is not solely happening through PTEN/p-AKT axis, which is typically thought to regulate FOXO1 nuclear localisation. The high levels of PTEN in granulosa cells of growing follicles might have contributed to increased apoptosis by inhibiting the translocation of FOXO1 outside the nucleus and thus ensuring FOXO1 activates pro-apoptotic target genes. In addition, high PTEN expression levels found in GCT of APC2-deficient ovaries might be responsible for the late development of tumourigenesis, as previously described in other models (Lague *et al.* 2008; Richards *et al.* 2012; Liu *et al.* 2015). It is thus possible to hypothesize that,

similar to previously published models, deleting *Pten* in granulosa cells of APC2-deficient ovaries would lead to rapid tumour development. The upregulation of ERK signalling in large tumours developing in *Pten*$^{fl/fl}$/*Apc*$^{fl/fl}$/*Apc2*$^{+/+}$- induced ovaries is another example of contribution of different signalling pathways to tumourigenesis, which was not explored in detail in the current work due to time constraints.

Given the very low expression of APC2 in the ovary, an important role in regulating ovarian homeostasis is perhaps unexpected. However, in the mouse mammary gland, where the expression of APC2 is lower than that of the ovary, combined loss of APC2 and APC initiated tumourigenesis, in contrast to failure of APC loss on its own to do so (Daly *et al.* 2016). In contrast, loss of APC2 on a background of floxed APC attenuated hepatocellular carcinoma developing in *Apc*$^{fl/fl}$ aging mouse liver (Daly 2013). This raises the question about defining the functional interaction between both APC proteins in the ovary. There are clear discrepancies between the subfertility phenotype described post-APC2 deletion in the current study and the absence of ovarian defects in APC-deficient mice, despite WNT signalling activation (Tanwar *et al.* 2013). Similarly, it is noteworthy that aged *Apc*$^{fl/fl}$ mice have not been previously reported to develop GCTs (Buchert *et al.* 2010; Wu *et al.* 2011), as confirmed in the cohorts collected at 12 months in the current study (both non-induced and adenovirus-*cre*-induced *Apc*$^{fl/fl}$ cohorts did not develop GCTs). Even when Amhr2-*cre* was used to induce recombination of *Apc*$^{fl/fl}$ in the OSE and granulosa cells, female mice developed OEA by 11 months of age, but none developed GCTs (Tanwar *et al.* 2013). Taking into account that 20% of *Apc2*$^{-/-}$ mice (on a non-induced *Apc*$^{fl/fl}$ background) developed GCT at the age of 12 months, and none developed OEA by the age of 18 months, and that APC2 loss attenuates OEA growth in Ad-*cre* *Pten*$^{fl/fl}$/*Apc*$^{fl/fl}$ ovaries, it could be proposed that APC and APC2 play distinct and antagonistic roles in the OSE and in granulosa cells of growing follicles (similar to their functional antagonism in the liver, but different from their functional compensation in the

mammary gland). It is to be noted that one of the non-induced *Apc*$^{fl/fl}$ mice developed a small GCT at the age of 18 months driven by WNT signalling activation. Given the hypomorph nature of floxed *Apc* allele, previously shown in other organs e.g. the liver (Buchert *et al.* 2010), this raises the question of whether loss of APC2 on a wild type *Apc* background is sufficient to drive GCT formation, similar to those developing when floxed *Apc* background was present. This question however remains unanswered and needs to be explored.

A key aspect of this study was the establishment of consistent methodologies and interventions. When characterizing ovarian homeostasis, it is crucial to collect all ovaries at the same stage of the oestrous cycle in order to eliminate the cycle stage as a variable. Choosing which stage to work with in this study was an important point to be considered. As the main goal of the study, initially, was to characterize roles of APC2 in the OSE, ovaries were collected at the diestrus stage (which is post-ovulatory), to determine whether APC2 regulates wound repair after ovulation. However, the choice of this stage limited the number of pre-ovulatory follicles present, which were needed to characterize subfertility. Two methods were used for collecting ovaries at a synchronized stage, exogenous gonadotrophin administration and manual staging. Gonadotrophin administration partially synchronized female mice, with only 70% of mice present in the diestrus stage 22-24 hours post-HCG administration. In addition, this method interferes with normal ovarian homeostasis, causing unrepairable tears in the OSE of all mice, irrespective of the genotype, due to forcing many follicles to ovulate at the same time. Although more time-consuming, manually-staging mice using the vaginal cytology method (Byers *et al.* 2012), proved to be more accurate.

Initial characterisation of ovarian homeostasis by counting follicles and corpora lutea in one section/ovary, was found to be unreliable. For example, a pre-ovulatory follicle missing an ovum in a section could be mis-regarded as a cyst. In addition, because different follicular stages are distributed in the cortex of the whole ovary, counting one section is not enough to

represent the number of follicles in the ovary. Characterization of serially-sectioned ovaries, by sectioning the ovary into 100 sections 5 µm apart, and staining the 10th section by H&E to be examined microscopically, although time consuming, must be carried out for correct analysis. However, because most of the organ is then sectioned at one time, preserving antigens present in the cut sections placed on poly-l-lysine (PLL) -coated slides for an extended period should be considered. In the current study, re-dipping the PLL sections in wax proved to be effective in preserving both cytoplasmic and nuclear antigens for years, and is recommended for future studies.

The 3Rs (reduction, replacement, refinement) principles for animal research were considered while designing all experiments presented in the thesis. For example, to assess fertility, a retrospective analysis of breeders rather than setting mating experiments was the chosen method. One limitation here was that the extracted data available for different genotypes of female *Apc2* mice (*Apc2*$^{+/+}$, *Apc2*$^{+/-}$, *Apc2*$^{-/-}$) represented crossings to males of the corresponding genotype, rather than to wild type males. Effects of *Apc2*-gene dosage on male fertility are not yet characterized, with the caveat that male fertility might be affected in APC2-deficient male mice, and could contribute to the delayed pregnancy and reduced litter size observed in APC2-deficient crosses. In order to address this issue, another experiment was designed using female mice from the 3 different *Apc2* genotypes, where ovulated oocytes post-gonadotrophin administration were retrieved and counted. This experiment confirmed that APC2-deficient mice ovulate less and would be expected to give smaller litter size. Another example of considering the 3Rs principles was viral induction of both ovaries to minimize the number of animals used in the experiments, in contrast to previous publications which induced only one ovary leaving the other ovary to serve as control (Flesken-Nikitin *et al.* 2003; Wu *et al.* 2007), wherein the current study, external controls (induced wild type mice) were used instead. A method refinement was performed, as well, by changing the injection site, through

injecting the adenovirus-*cre* directly into the bursal space via the bursal membrane rather than using the trans-infundibular intra-oviductal route (Flesken-Nikitin *et al.* 2003; Wu *et al.* 2007). This refinement was employed to avoid recombination of floxed genes in the oviducts, by avoiding direct injection into their infundibular ends. Despite this, one of the aged $Pten^{fl/fl}$-induced mice displayed an oviductal tumour, which might be explained in terms of the anatomical location of the oviduct, which directly opens into the bursa, and the leakage of virus from bursa to oviduct.

In order to dissect contributions of APC2 in EOC development, APC2 loss was introduced to an established mouse model of OEA and a comparative study between tumours formed with/without APC2 were performed. The $Pten^{fl/fl}/Apc^{fl/fl}$ adenovirus-*cre* induced OEA model (Wu *et al.* 2007) was chosen because it is based on WNT signalling activation through APC loss, and was successfully used previously to elucidate contributions of oncogenes (Wu *et al.* 2013), or tumour suppressors (Zhai *et al.* 2016) to ovarian epithelial tumourigenesis. However, the OEA histotype is different from the serous adenocarcinoma histotype where APC2 loss has been reported (Perets *et al.* 2013). Whether the phenotypes reported here would be reproducible if APC2 loss was introduced to a serous carcinoma tumour model [e.g. Pax8-driven deletions of *Brca*/*Tp53*/*Pten* model (Perets *et al.* 2013)], or to a non-WNT driven OEA model [e.g. Mucin1-expressing/*Kras* activated/ *Pten* deleted model (Tirodkar *et al.* 2014)] needs to be unravelled before oncogenic roles of *Apc2* could be generalized to all ovarian epithelial tumours.

An important limitation in the current study was the absence of an APC2 antibody which could be used for immunohistochemistry to differentiate between $Apc2^{+/+}$ and $Apc2^{-/-}$ tissues. The antibody previously used by Dr Carl Daly was discontinued by the manufacturer. For this study, 3 different antibodies were tested, but none were reliable for use in immunohistochemistry (although an Abcam antibody could differentiate between APC2 levels

in western blot of protein extract from brains), with similar staining patterns observed in *Apc2*$^{+/+}$ and *Apc2*$^{-/-}$ ovaries (Appendix 2). This meant the inability to define, for instance, at which follicular stage APC2 is expressed. In order to bypass this limitation, all possible phenotypes previously published in the setting of WNT signalling activation and ovarian subfertility in mice were analysed in the APC2 null mice (Boerboom *et al.* 2005; Fan *et al.* 2010a; Abedini *et al.* 2016; De Cian *et al.* 2016). An alternative approach was to design RNAscope probes by which *Apc2* mRNA could be hybridized and visualized *in situ*. However, this was hampered by the lack of information regarding the genetic engineering of the *Apc2*$^{-}$ allele. Many attempts were made over the course of this work, using a number of different approaches, to sequence the engineered allele. Only a partial sequence was obtained in-house. To confirm the partial results and, potentially, to unravel the full sequence, a walking primer project was performed by Eurofins Genomics and results have become available shortly before submission of this thesis (Appendix 3). The difficulties in obtaining a full sequence of the allele are due to secondary structures and the formation of multiple hairpins, which Eurofins also had difficulties with. However, the sequencing did reveal 60 bases were deleted in exon 14 of *Apc2* mutant gene, resulting in a frameshift mutation and a pre-mature stop codon, translated into a truncated non-functional protein (Appendix 3). The western blot showed a loss of the 240 kDa APC2 band in *Apc2*$^{-/-}$ mice, and did not detect a smaller truncated fragment in *Apc2*$^{-/-}$ when an antibody binding to the truncated region was used (Appendix 2). However, this small difference in the nucleotide sequence makes designing RNAscope probes impossible, at least 300 bases need to be unique in order to design probes which can faithfully show differences between *Apc2*$^{+/+}$ and *Apc2*$^{-/-}$ genotypes. The newly-developed BaseScope assay, which can detect short RNA targets down to 50 bases, could be considered instead.

Delays in inducing cohorts needed in Chapter 6 as a result of technical/administrative reasons (amending project licence to allow for intrabursal injections, preparing a surgical suite

with class II biological safety cabinet to perform inductions, health and safety approvals for viral injections, practicing intrabursal injection by the technician), as well as the sad death of Professor Alan Clarke resulted in most of this work happening late in the project, which limited the time available for the analysis. For instance, the non-autonomous contributions of the constitutive *Apc2*$^{-}$ allele in modulating inflammatory and immune responses, impacting on tumour initiation and progression, were not fully characterized. Another important limitation is the small cohort sizes used in here to characterize roles of APC2 in OEA tumourigenesis. More mice have been induced in the *Apc2*$^{+/+}$ and *Apc2*$^{-/-}$ tumour cohorts to be collected 8 weeks post-induction (which will be after thesis submission). Tumours collected from these mice will add more weight to the data presented here, and will enable the confirmation of the RNAseq data by performing qRT-PCR on independent samples.

In conclusion, the findings of the current study provide fundamental new knowledge on the role of APC2 in regulating ovarian WNT signalling, homeostasis and tumourigenesis. The finding that WNT signalling activation in growing follicles impairs ovulation raises the importance of the assessment of WNT signalling activation in the setting of human female subfertility/infertility. This could provide new insights into the molecular pathogenesis of this condition, and may help in designing new treatment interventions for these patients. In addition, the clinical relevance of data gathered from the GEMMs in this study needs to be investigated. As shown here, and as previously reported (Boerboom *et al.* 2005; Hai *et al.* 2015; Liu *et al.* 2015; De Cian *et al.* 2016), mutations which cause female subfertility or infertility in early adulthood in mice are followed by development of GCT upon aging. Is this the case in human females?

In addition, the study has led to a potential paradigm shift in our understanding of APC2 roles in epithelial ovarian tumourigenesis. The findings have shown that *Apc2* can be either an oncogene or a tumour suppressor gene depending on context. Furthermore, the RNA seq

analysis performed in the current study on *Apc2*$^{+/+}$ and *Apc2*$^{-/-}$ *Pten*$^{fl/fl}$/*Apc*$^{fl/fl}$–induced ovaries, together with literature searching enabled the identification of genes/proteins which are upregulated in epithelial ovarian tumours such as HAL and HUNK. Roles of these proteins in epithelial ovarian cancer have not yet been characterized and are highly recommended for future work. Downregulation of *Esr2* was evident in GCT developing in APC2-deficient female mice, as well as in large OEAs developing in *Apc2*$^{+/+}$ vs. *Apc2*$^{-/-}$ *Pten*$^{fl/fl}$/*Apc*$^{fl/fl}$–induced ovaries. This raises the question of whether downregulation of *Esr2* is required for ovarian tumourigenesis, irrespective of tumour type. Recent work exploring treatment interventions to make use of *ESR2* as a possible ovarian tumour suppressor, by using estrogen receptor β-agonist (synthetic agonists or phytoestrogens) has proven its efficacy in decreasing OC cell growth (Schuler-Toprak *et al.* 2017), and in sensitizing resistant OC cells to chemotherapy (Liu *et al.* 2017).

With OC standing as the most lethal gynaecological malignancy accounting for 4128 deaths in UK in 2014, equivalent to 56% of cases diagnosed in that year (CancerResearchUK 2017), the current study provided important contributions to our fundamental understanding of the pathogenesis of this highly-heterogeneous ill-defined group of tumours.

8. References

Abdi, S., Salehnia, M. and Hosseinkhani, S. (2015). Kit ligand decreases the incidence of apoptosis in cultured vitrified whole mouse ovaries. *Reproductive biomedicine online* **30:**493-503.

Abedini, A., Zamberlam, G., Lapointe, E., Tourigny, C., Boyer, A., Paquet, M., Hayashi, K. *et al.* (2016). WNT5a is required for normal ovarian follicle development and antagonizes gonadotropin responsiveness in granulosa cells by suppressing canonical WNT signaling. *The FASEB Journal* **30:**1534-1547.

Abubaker, K., Luwor, R. B., Escalona, R., McNally, O., Quinn, M. A., Thompson, E. W., Findlay, J. K. *et al.* (2014). Targeted Disruption of the JAK2/STAT3 Pathway in Combination with Systemic Administration of Paclitaxel Inhibits the Priming of Ovarian Cancer Stem Cells Leading to a Reduced Tumor Burden. *Frontiers in oncology* **4:75.**

Adhikari, D. and Liu, K. (2013). Regulation of Quiescence and Activation of Oocyte Growth in Primordial Follicles.*Oogenesis*. Springer, pp. 49-62.

Agrawal, S., Pilarski, R. and Eng, C. (2005). Different splicing defects lead to differential effects downstream of the lipid and protein phosphatase activities of PTEN. *Human Molecular Genetics* **14:**2459-2468.

Ahmad, I., Morton, J. P., Singh, L. B., Radulescu, S. M., Ridgway, R. A., Patel, S., Woodgett, J. *et al.* (2011). beta-Catenin activation synergizes with PTEN loss to cause bladder cancer formation. *Oncogene* **30:**178-189.

Ahmed, N., Abubaker, K., Findlay, J. and Quinn, M. (2013). Cancerous ovarian stem cells: obscure targets for therapy but relevant to chemoresistance. *Journal of cellular biochemistry* **114:**21-34. .

Ahmed, N., Thompson, E. W. and Quinn, M. A. (2007). Epithelial–mesenchymal interconversions in normal ovarian surface epithelium and ovarian carcinomas: an exception to the norm. *Journal of cellular physiology* **213:**581-588.

Ahmed, Y., Nouri, A. and Wieschaus, E. (2002). Drosophila Apc1 and Apc2 regulate Wingless transduction throughout development. *Development* **129:**1751-1762.

Akong, K., Grevengoed, E. E., Price, M. H., McCartney, B. M., Hayden, M. A., DeNofrio, J. C. and Peifer, M. (2002). Drosophila APC2 and APC1 play overlapping roles in wingless signaling in the embryo and imaginal discs. *Developmental biology* **250:**91-100.

Almuriekhi, M., Shintani, T., Fahiminiya, S., Fujikawa, A., Kuboyama, K., Takeuchi, Y., Nawaz, Z. *et al.* (2015). Loss-of-Function Mutation in APC2 Causes Sotos Syndrome Features. *Cell Reports* **10:**1585-1598.

Altuntas, C. Z., Jaini, R., Kesaraju, P., Jane-wit, D., Johnson, J. M., Covey, K., Flask, C. A. *et al.* (2012). Autoimmune mediated regulation of ovarian tumor growth. *Gynecologic oncology* **124:**98-104.

Aminuddin, A. and Ng, P. Y. (2016). Promising Druggable Target in Head and Neck Squamous Cell Carcinoma: Wnt Signaling. *Frontiers in Pharmacology* **7:**244.

Anastas, J. N. and Moon, R. T. (2013). WNT signalling pathways as therapeutic targets in cancer. *Nature reviews. Cancer* **13:**11-26.

Anglesio, M. S., Kommoss, S., Tolcher, M. C., Clarke, B., Galletta, L., Porter, H., Damaraju, S. *et al.* (2013). Molecular characterization of mucinous ovarian tumours supports a stratified treatment approach with HER2 targeting in 19% of carcinomas. *The Journal of pathology* **229:**111-120.

Aoki, K. and Taketo, M. M. (2007). Adenomatous polyposis coli (APC): a multi-functional tumor suppressor gene. *Journal of Cell Science* **120:**3327-3335.

Arend, R. C., Londono-Joshi, A. I., Straughn, J. M., Jr. and Buchsbaum, D. J. (2013). The Wnt/beta-catenin pathway in ovarian cancer: a review. *Gynecologic Oncology* **131:**772-779. .

Asselin-Labat, M.-L., Vaillant, F., Sheridan, J. M., Pal, B., Wu, D., Simpson, E. R., Yasuda, H. *et al.* (2010). Control of mammary stem cell function by steroid hormone signalling. *Nature* **465:**798-802.

Auersperg, N., Wong, A. S., Choi, K. C., Kang, S. K. and Leung, P. C. (2001). Ovarian surface epithelium: biology, endocrinology, and pathology. *Endocrine reviews* **22:**255-288.

Baarends, W. M., Uilenbroek, J. T., Kramer, P., Hoogerbrugge, J. W., van Leeuwen, E. C., Themmen, A. P. and Grootegoed, J. A. (1995). Anti-mullerian hormone and anti-mullerian hormone type II receptor messenger ribonucleic acid expression in rat ovaries during postnatal development, the estrous cycle, and gonadotropin-induced follicle growth. *Endocrinology* **136:**4951-4962.

Bajwa, P., Nagendra, P. B., Nielsen, S., Sahoo, S. S., Bielanowicz, A., Lombard, J. M., Wilkinson, J. E. *et al.* (2016). Age related increase in mTOR activity contributes to the pathological changes in ovarian surface epithelium. *Oncotarget* **7:**19214-19227.

Bakker, S. T., van de Vrugt, H. J., Visser, J. A., Delzenne-Goette, E., van der Wal, A., Berns, M. A., van de Ven, M. *et al.* (2012). Fancf-deficient mice are prone to develop ovarian tumours. *The journal of pathology* **226:**28-39.

Balkwill, F. (2004). Cancer and the chemokine network. *Nature reviews. Cancer* **4:**540-550.

Balla, A., Danilovich, N., Yang, Y. and Sairam, M. R. (2003). Dynamics of ovarian development in the FORKO immature mouse: structural and functional implications for ovarian reserve. *Biology of reproduction* **69:**1281-1293.

Bapat, S. A., Mali, A. M., Koppikar, C. B. and Kurrey, N. K. (2005). Stem and progenitor-like cells contribute to the aggressive behavior of human epithelial ovarian cancer. *Cancer research* **65:**3025-3029.

Beamer, W. G., Hoppe, P. C. and Whitten, W. K. (1985). Spontaneous malignant granulosa cell tumors in ovaries of young SWR mice. *Cancer research* **45:**5575-5581.

Beamer, W. G., Shultz, K. L. and Tennent, B. J. (1988). Induction of ovarian granulosa cell tumors in SWXJ-9 mice with dehydroepiandrosterone. *Cancer research* **48:**2788-2792.

Beamer, W. G., Shultz, K. L., Tennent, B. J. and Shultz, L. D. (1993). Granulosa cell tumorigenesis in genetically hypogonadal-immunodeficient mice grafted with ovaries from tumor-susceptible donors. *Cancer research* **53:**3741-3746.

Bell, S. M., Lam, W. K., Carr, I. M., Cartwright, E. J., Pinchin, K., Wedgwood, S., Markham, A. F. *et al.* (1999). Assignment of the murine adenomatous polyposis coli 2 (Apc2) gene to mouse chromosome band 10B5-C2 by in situ hybridisation. *Cytogenetics and cell genetics* **86:**81-82.

Benchabane, H. and Ahmed, Y. (2009). The Adenomatous Polyposis Coli Tumor Suppressor and Wnt signaling in the Regulation of Apoptosis. *Advances in experimental medicine and biology* **656:**75-84.

Bennett, L. M., McAllister, K. A., Ward, T., Malphurs, J., Collins, N. K., Seely, J. C., Davis, B. J. *et al.* (2001). Mammary tumor induction and premature ovarian failure in ApcMin mice are not enhanced by Brca2 deficiency. *Toxicologic pathology* **29:**117-125.

Biason-Lauber, A. and Chaboissier, M. C. (2015). Ovarian development and disease: The known and the unexpected. *Seminars in cell & developmental biology* **45:**59-67.

Bidus, M. A., Elkas, J. C., Rose, G. S., Di Saia, P. and Creasman, W. (2012). Germ cell, stromal, and other ovarian tumors. *Clinical gynecologic oncology. 8th ed. Philadelphia, Pa: Elsevier/Saunders* 329-356.

Bingham, N. C., Verma-Kurvari, S., Parada, L. F. and Parker, K. L. (2006). Development of a steroidogenic factor 1/Cre transgenic mouse line. *Genesis* **44:**419-424.

Binnerts, M. E., Kim, K. A., Bright, J. M., Patel, S. M., Tran, K., Zhou, M., Leung, J. M. *et al.* (2007). R-Spondin1 regulates Wnt signaling by inhibiting internalization of LRP6. *Proceedings of the National Academy of Sciences of the United States of America* **104:**14700-14705.

Bodek, G., Vierre, S., Rivero-Muller, A., Huhtaniemi, I., Ziecik, A. J. and Rahman, N. A. (2005). A novel targeted therapy of Leydig and granulosa cell tumors through the luteinizing hormone receptor using a hecate-chorionic gonadotropin beta conjugate in transgenic mice. *Neoplasia* **7:**497-508.

Boerboom, D., Paquet, M., Hsieh, M., Liu, J., Jamin, S. P., Behringer, R. R., Sirois, J. *et al.* (2005). Misregulated Wnt/beta-catenin signaling leads to ovarian granulosa cell tumor development. *Cancer Research* **65:**9206-9215.

Boerboom, D., White, L. D., Dalle, S., Courty, J. and Richards, J. S. (2006). Dominant-stable beta-catenin expression causes cell fate alterations and Wnt signaling antagonist expression in a murine granulosa cell tumor model. *Cancer Research* **66:**1964-1973.

Bonome, T., Levine, D. A., Shih, J., Randonovich, M., Pise-Masison, C. A., Bogomolniy, F., Ozbun, L. *et al.* (2008). A gene signature predicting for survival in suboptimally debulked patients with ovarian cancer. *Cancer research* **68:**5478-5486.

Bordonaro, M., Lazarova, D. L. and Sartorelli, A. C. (2008). Hyperinduction of Wnt activity: a new paradigm for the treatment of colorectal cancer? *Oncology research* **17:**1-9.

Bossard, C., Busson, M., Vindrieux, D., Gaudin, F., Machelon, V., Brigitte, M., Jacquard, C. *et al.* (2012). Potential role of estrogen receptor beta as a tumor suppressor of epithelial ovarian cancer. *PLoS One* **7:**e44787.

Bouabe, H. and Okkenhaug, K. (2013). Gene Targeting in Mice: a Review. *Methods in molecular biology* **1064:**315-336.

Bounin, A., Charbotel, B., Fervers, B. and Bergeret, A. (2014). [Professional risk factors associated with the cancer of the ovary. Literature review]. *Bulletin du cancer* **101:**1089-1108.

Bourguignon, L. Y., Gilad, E., Rothman, K. and Peyrollier, K. (2005). Hyaluronan-CD44 interaction with IQGAP1 promotes Cdc42 and ERK signaling, leading to actin binding, Elk-

1/estrogen receptor transcriptional activation, and ovarian cancer progression. *Journal of Biological Chemistry* **280:**11961-11972.

Boyer, A., Lapointe, É., Zheng, X., Cowan, R. G., Li, H., Quirk, S. M., DeMayo, F. J. *et al.* (2010). WNT4 is required for normal ovarian follicle development and female fertility. *The FASEB Journal* **24:**3010-3025.

Brown, C., LaRocca, J., Pietruska, J., Ota, M., Anderson, L., Smith, S. D., Weston, P. *et al.* (2010). Subfertility caused by altered follicular development and oocyte growth in female mice lacking PKB alpha/Akt1. *Biology of reproduction* **82:**246-256.

Buamah, P. (2000). Benign conditions associated with raised serum CA-125 concentration. *Journal of surgical oncology* **75:**264-265.

Buchert, M., Athineos, D., Abud, H. E., Burke, Z. D., Faux, M. C., Samuel, M. S., Jarnicki, A. G. *et al.* (2010). Genetic Dissection of Differential Signaling Threshold Requirements for the Wnt/β-Catenin Pathway In Vivo. *PLoS Genetics* **6:**e1000816.

Budiu, R. A., Elishaev, E., Brozick, J., Lee, M., Edwards, R. P., Kalinski, P. and Vlad, A. M. (2013). Immunobiology of human mucin 1 in a preclinical ovarian tumor model. *Oncogene* **32:**3664-3675.

Byers, S. L., Wiles, M. V., Dunn, S. L. and Taft, R. A. (2012). Mouse estrous cycle identification tool and images. *PLoS One* **7:**e35538.

Caburet, S., Georges, A., L'Hote, D., Todeschini, A. L., Benayoun, B. A. and Veitia, R. A. (2012). The transcription factor FOXL2: at the crossroads of ovarian physiology and pathology. *Molecular and cellular endocrinology*
356:55-64.

Caillaud, M., Duchamp, G. and Gerard, N. (2005). In vivo effect of interleukin-1beta and interleukin-1RA on oocyte cytoplasmic maturation, ovulation, and early embryonic development in the mare. *Reproductive biology and endocrinology* **3:**26.

Caillaud, M. and Gerard, N. (2009). In vivo and in vitro effects of interleukin-1beta on equine oocyte maturation and on steroidogenesis and prostaglandin synthesis in granulosa and cumulus cells. *Reproduction, fertility, and development* **21:**265-273.

CancerResearchUK. (2017). Cancer Research UK. Ovarian cancer statistics. [Online]. Available at: http://www.cancerresearchuk.org/health-professional/cancer-statistics/statistics-by-cancer-type/ovarian-cancer [Accessed: 10 July].

Canipari, R., Cellini, V. and Cecconi, S. (2012). The ovary feels fine when paracrine and autocrine networks cooperate with gonadotropins in the regulation of folliculogenesis. *Current pharmaceutical design* **18:**245-255.

Carmeliet, P. and Jain, R. K. (2011). Molecular mechanisms and clinical applications of angiogenesis. *Nature* **473:**298-307.

Castiblanco, G. A., Pires, N. Y., Wistuba, O. I., Riquelme, S. E., Andrade, M. L. and Corvalan, R. A. (2006). [Pathogenic role of PTEN tumor suppressor gene in ovarian cancer associated to endometriosis]. *Revista medica de Chile* **134:**271-278.

Cattelino, A., Liebner, S., Gallini, R., Zanetti, A., Balconi, G., Corsi, A., Bianco, P. *et al.* (2003). The conditional inactivation of the β-catenin gene in endothelial cells causes a defective vascular pattern and increased vascular fragility. *The Journal of cell biology* **162:**1111-1122.

Center for Animal Resources and Development, K. U., Japan. (2016). In Vitro Fertilization (IVF) using Ultra-Superovulation Reagent [Online]. Japan: Kumamoto University. Available at: http://card.medic.kumamoto-u.ac.jp/card/english/sigen/manual/onlinemanual.html [Accessed: 2/3/2017].

CGARN. (2011). Cancer Genome Atlas Research Network. Integrated genomic analyses of ovarian carcinoma. *Nature* **474:**609-615.

Cha, S. W., Tadjuidje, E., Tao, Q., Wylie, C. and Heasman, J. (2008). Wnt5a and Wnt11 interact in a maternal Dkk1-regulated fashion to activate both canonical and non-canonical signaling in Xenopus axis formation. *Development* **135:**3719-3729.

Chamberlain, G., Steer 3rd, P., Cartwright, J., Duncan, W. and Critchley, H. (2013). Johnson MH (2008) Essential Reproduction, 6th edn. John Wiley, Chichester Moore K (1988) The Developing Human: Clinically Oriented Embryology. WB Saunders, London Philipp EE, Setchell M (ed)(1991) Scientific Foundations of. *Essential Obstetrics and Gynaecology E-Book* **331:**409.

Chandler, R. L., Damrauer, J. S., Raab, J. R., Schisler, J. C., Wilkerson, M. D., Didion, J. P., Starmer, J. *et al.* (2015). Coexistent ARID1A-PIK3CA mutations promote ovarian clear-cell tumorigenesis through pro-tumorigenic inflammatory cytokine signalling. *Nature communications* **6:**6118.

Chang, H.-M., Qiao, J. and Leung, P. C. K. (2017). Oocyte–somatic cell interactions in the human ovary—novel role of bone morphogenetic proteins and growth differentiation factors. *Human Reproduction Update* **23:**1-18.

Chassot, A.-A., Ranc, F., Gregoire, E. P., Roepers-Gajadien, H. L., Taketo, M. M., Camerino, G., De Rooij, D. G. *et al.* (2008). Activation of β-catenin signaling by Rspo1 controls differentiation of the mammalian ovary. *Human molecular genetics* **17:**1264-1277.

Cheaib, B., Auguste, A. and Leary, A. (2015). The PI3K/Akt/mTOR pathway in ovarian cancer: therapeutic opportunities and challenges. *Chinese Journal of Cancer* **34:**4-16.

Checura, C. M., Beg, M. A., Parrish, J. J. and Ginther, O. J. (2010). Functional relationships among intrafollicular insulin-like growth factor 1, circulatory gonadotropins, and development of the dominant follicle in mares. *Animal reproduction science* **118:**270-278.

Childs, G. V., Miller, B. T. and Miller, W. L. (1997). Differential effects of inhibin on gonadotropin stores and gonadotropin-releasing hormone binding to pituitary cells from cycling female rats. *Endocrinology* **138:**1577-1584.

Cipriano, S. C., Chen, L., Burns, K. H., Koff, A. and Matzuk, M. M. (2001). Inhibin and p27 interact to regulate gonadal tumorigenesis. *Molecular endocrinology* **15:**985-996.

Clevers, H. (2006). Wnt/b-Catenin Signaling in Development and Disease. *Cell* **127:**469-480.

Cliffton, E. E. and Wolstenholme, J. T. (1949). Hypervolemia and associated changes in mice bearing a transplanted granulosa cell tumor. *Cancer research* **9:**331-335.

Colombo, N., Peiretti, M. and Castiglione, M. (2009). Non-epithelial ovarian cancer: ESMO clinical recommendations for diagnosis, treatment and follow-up. *Annals of oncology* **20 Suppl 4:**24-26.

Connolly, D. C., Bao, R., Nikitin, A. Y., Stephens, K. C., Poole, T. W., Hua, X., Harris, S. S. *et al.* (2003). Female mice chimeric for expression of the simian virus 40 TAg under control of the MISIIR promoter develop epithelial ovarian cancer. *Cancer Research* **63:**1389-1397.

Connolly, D. C. and Hensley, H. H. (2009). Xenograft and Transgenic Mouse Models of Epithelial Ovarian Cancer and Non Invasive Imaging Modalities to Monitor Ovarian Tumor Growth In situ -Applications in Evaluating Novel Therapeutic Agents. *Current protocols in pharmacology* **45:**14.12.11-14.12.26.

Corada, M., Nyqvist, D., Orsenigo, F., Caprini, A., Giampietro, C., Taketo, M. M., Iruela-Arispe, M. L. *et al.* (2010). The Wnt/β-Catenin Pathway Modulates Vascular Remodeling and Specification by Upregulating Dll4/Notch Signaling. *Developmental Cell* **18:**938-949.

Cordero, A. B., Kwon, Y., Hua, X. and Godwin, A. K. (2010). In vivo Imaging and Therapeutic Treatments in an Orthotopic Mouse Model of Ovarian Cancer. *Journal of visualized experiments JoVE* **42:**e2125.

Cormio, G., Rossi, C., Cazzolla, A., Resta, L., Loverro, G., Greco, P. and Selvaggi, L. (2003). Distant metastases in ovarian carcinoma. *International journal of gynecological cancer* **13:**125-129.

Coward, J. I. G., Middleton, K. and Murphy, F. (2015). New perspectives on targeted therapy in ovarian cancer. *International Journal of Women's Health* **7:**189-203.

Crist, R. C., Roth, J. J., Baran, A. A., McEntee, B. J., Siracusa, L. D. and Buchberg, A. M. (2010). The armadillo repeat domain of Apc suppresses intestinal tumorigenesis. *Mammalian genome* **21:**450-457.

Cumming, G., Fidler, F. and Vaux, D. L. (2007). Error bars in experimental biology. *The Journal of cell biology* **177:**7-11.

Cunnea, P. and Stronach, E. A. (2014). Modeling platinum sensitive and resistant high-grade serous ovarian cancer: development and applications of experimental systems. *Frontiers in Oncology* **4:81.**

D'Angelo, E., Mozos, A., Nakayama, D., Espinosa, I., Catasus, L., Munoz, J. and Prat, J. (2011). Prognostic significance of FOXL2 mutation and mRNA expression in adult and juvenile granulosa cell tumors of the ovary. *Modern Pathology* **24:**1360-1367.

Daly, C. (2013). The roles of the Apc proteins in homeostasis and tumourigenesis. Thesis PhD, Cardiff University.

Daly, C. S., Shaw, P., Ordonez, L. D., Williams, G. T., Quist, J., Grigoriadis, A., Van Es, J. H. *et al.* (2016). Functional redundancy between Apc and Apc2 regulates tissue homeostasis and prevents tumorigenesis in murine mammary epithelium. *Oncogene* **36:**1793-1803.

De Cian, M. C., Pauper, E., Bandiera, R., Vidal, V. P., Sacco, S., Gregoire, E. P., Chassot, A. A. *et al.* (2016). Amplification of R-spondin1 signaling induces granulosa cell fate defects and cancers in mouse adult ovary. *Oncogene* **36:**208-218.

Dejana, E. (2010). The Role of Wnt Signaling in Physiological and Pathological Angiogenesis. *Circulation Research* **107:**943-952.

Deligdisch, L., Einstein, A. J., Guera, D. and Gil, J. (1995). Ovarian dysplasia in epithelial inclusion cysts. A morphometric approach using neural networks. *Cancer* **76:**1027-1034.

Dimberg, J. A. N., StrÖM, K., LÖFgren, S., Zar, N., Hugander, A. and Matussek, A. (2011). Expression of the serine protease inhibitor serpinA3 in human colorectal adenocarcinomas. *Oncology Letters* **2:**413-418.

Dinulescu, D. M., Ince, T. A., Quade, B. J., Shafer, S. A., Crowley, D. and Jacks, T. (2005). Role of K-ras and Pten in the development of mouse models of endometriosis and endometrioid ovarian cancer. *Nature medicine* **11:**63-70.

Dixon, D., Alison, R., Bach, U., Colman, K., Foley, G. L., Harleman, J. H., Haworth, R. *et al.* (2014). Nonproliferative and Proliferative Lesions of the Rat and Mouse Female Reproductive System. *Journal of Toxicologic Pathology* **27:**1S-107S.

Domenice, S., Correa, R. V., Costa, E. M., Nishi, M. Y., Vilain, E., Arnhold, I. J. and Mendonca, B. B. (2004). Mutations in the SRY, DAX1, SF1 and WNT4 genes in Brazilian sex-reversed patients. *Brazilian journal of medical and biological research* **37:**145-150.

Doufekas, K. and Olaitan, A. (2014). Clinical epidemiology of epithelial ovarian cancer in the UK. *International journal of women's health* **6:537-45.**

du Bois, A., Kristensen, G., Ray-Coquard, I., Reuss, A., Pignata, S., Colombo, N., Denison, U. *et al.* (2016). Standard first-line chemotherapy with or without nintedanib for advanced ovarian cancer (AGO-OVAR 12): a randomised, double-blind, placebo-controlled phase 3 trial. *The Lancet Oncology* **17:**78-89.

Du, S. J., Purcell, S. M., Christian, J. L., McGrew, L. L. and Moon, R. T. (1995). Identification of distinct classes and functional domains of Wnts through expression of wild-type and chimeric proteins in Xenopus embryos. *Molecular and cellular biology* **15:**2625-2634.

Dubeau, L. (1999). The cell of origin of ovarian epithelial tumors and the ovarian surface epithelium dogma: does the emperor have no clothes? *Gynecologic oncology* **72:**437-442.

Dubeau, L. (2008). The cell of origin of ovarian epithelial tumours. *The Lancet. Oncology* **9:**1191-1197.

Dunlop, C. E. and Anderson, R. A. (2014). The regulation and assessment of follicular growth. *Scandinavian journal of clinical and laboratory investigation.* **74:**13-17.

Dunn, G. P., Old, L. J. and Schreiber, R. D. (2004). The Three Es of Cancer Immunoediting. *Annual Review of Immunology* **22:**329-360.

Durlinger, A. L., Kramer, P., Karels, B., de Jong, F. H., Uilenbroek, J. T., Grootegoed, J. A. and Themmen, A. P. (1999). Control of Primordial Follicle Recruitment by Anti-Mullerian Hormone in the Mouse Ovary1. *Endocrinology* **140:**5789-5796.

East, N., Alobaid, A., Goffin, F., Ouallouche, K. and Gauthier, P. (2005). Granulosa cell tumour: a recurrence 40 years after initial diagnosis. *Journal of obstetrics and gynaecology Canada : JOGC* **27:**363-364.

Edson, M. A., Nagaraja, A. K. and Matzuk, M. M. (2009). The Mammalian Ovary from Genesis to Revelation. *Endocrine Reviews* **30:**624-712.

Edson, M. A., Nalam, R. L., Clementi, C., Franco, H. L., Demayo, F. J., Lyons, K. M., Pangas, S. A. *et al.* (2010). Granulosa cell-expressed BMPR1A and BMPR1B have unique functions in regulating fertility but act redundantly to suppress ovarian tumor development. *Molecular endocrinology* **24:**1251-1266.

Emmen, J. M. and Korach, K. S. (2003). Estrogen receptor knockout mice: phenotypes in the female reproductive tract. *Gynecological endocrinology* **17:**169-176.

Fan, H.-Y., Liu, Z., Cahill, N. and Richards, J. S. (2008). Targeted Disruption of Pten in Ovarian Granulosa Cells Enhances Ovulation and Extends the Life Span of Luteal Cells. *Molecular Endocrinology* **22:**2128-2140.

Fan, H.-Y., O'Connor, A., Shitanaka, M., Shimada, M., Liu, Z. and Richards, J. S. (2010a). β-Catenin (CTNNB1) Promotes Preovulatory Follicular Development but Represses LH-Mediated Ovulation and Luteinization. *Molecular Endocrinology* **24:**1529-1542.

Fan, H. Y., Liu, Z., Paquet, M., Wang, J., Lydon, J. P., DeMayo, F. J. and Richards, J. S. (2009). Cell type-specific targeted mutations of Kras and Pten document proliferation arrest in granulosa cells versus oncogenic insult to ovarian surface epithelial cells. *Cancer research* **69:**6463-6472.

Fan, X., Gabbi, C., Kim, H. J., Cheng, G., Andersson, L. C., Warner, M. and Gustafsson, J. A. (2010b). Gonadotropin-positive pituitary tumors accompanied by ovarian tumors in aging female ERbeta-/- mice. *Proceedings of the National Academy of Sciences of the United States of America*
107:6453-6458.

Farinola, M. A., Gown, A. M., Judson, K., Ronnett, B. M., Barry, T. S., Movahedi-Lankarani, S. and Vang, R. (2007). Estrogen receptor alpha and progesterone receptor expression in ovarian adult granulosa cell tumors and Sertoli-Leydig cell tumors. *International journal of gynecological pathology* **26:**375-382.

Färkkilä, A., Anttonen, M., Pociuviene, J., Leminen, A., Butzow, R., Heikinheimo, M. and Unkila-Kallio, L. (2011). Vascular endothelial growth factor (VEGF) and its receptor VEGFR-2 are highly expressed in ovarian granulosa cell tumors. *European Journal of Endocrinology* **164:**115-122.

Ferlay, J., Soerjomataram, I., Dikshit, R., Eser, S., Mathers, C., Rebelo, M., Parkin, D. M. *et al.* (2015). Cancer incidence and mortality worldwide: sources, methods and major patterns in GLOBOCAN 2012. *International journal of cancer*
136:E359-386.

Fleming, J. S., Beaugié, C. R., Haviv, I., Chenevix-Trench, G. and Tan, O. L. (2006). Incessant ovulation, inflammation and epithelial ovarian carcinogenesis: revisiting old hypotheses. *Molecular and Cellular Endocrinology* **247:**4-21.

Flesken-Nikitin, A., Choi, K. C., Eng, J. P., Shmidt, E. N. and Nikitin, A. Y. (2003). Induction of carcinogenesis by concurrent inactivation of p53 and Rb1 in the mouse ovarian surface epithelium. *Cancer research* **63:**3459-3463.

Flesken-Nikitin, A., Hwang, C. I., Cheng, C. Y., Michurina, T. V., Enikolopov, G. and Nikitin, A. Y. (2013). Ovarian surface epithelium at the junction area contains a cancer-prone stem cell niche. *Nature.* **495:**241-245. .

Forbes, S. A., Beare, D., Boutselakis, H., Bamford, S., Bindal, N., Tate, J., Cole, C. G. *et al.* (2016). COSMIC: somatic cancer genetics at high-resolution. *Nucleic acids research* **45:**D777-D783.

Ford, C. E., Punnia-Moorthy, G., Henry, C. E., Llamosas, E., Nixdorf, S., Olivier, J., Caduff, R. *et al.* (2014). The non-canonical Wnt ligand, Wnt5a, is upregulated and associated with epithelial to mesenchymal transition in epithelial ovarian cancer. *Gynecologic oncology* **134:**338-345.

Fowler, P. A. and Huhtaniemi, I. T. (2002). The ovarian gonadotropin receptors in health and disease. *Gynecologic Oncology Research and Practice* **3:**55-63.

Fraser, M., Leung, B., Jahani-Asl, A., Yan, X., Thompson, W. E. and Tsang, B. K. (2003). Chemoresistance in human ovarian cancer: the role of apoptotic regulators. *Reproductive Biology and Endocrinology* **1:**66-79.

Fujiwara, K., Kurosaki, A. and Hasegawa, K. (2013). Clinical trials of neoadjuvant chemotherapy for ovarian cancer: what do we gain after an EORTC trial and after two additional ongoing trials are completed? *Current oncology reports* **15:**197-200.

Fujiwara, K., Shintani, D. and Nishikawa, T. (2016). Clear-cell carcinoma of the ovary. *Annals of oncology* **27 Suppl 1:**i50-i52.

Furth, J. (1946). Transplantability of induced granulosa cell tumors and of luteoma in mice; secondary effects of these growths. *Proceedings of the Society for Experimental Biology and Medicine.* **61:**212-214.

Furth, J. and Moshman, J. (1951). On the specificity of hypervolaemia and congestive changes in tumor-bearing mice. *Cancer research* **11:**543-551.

Furth, J. and Sobel, H. (1947). Hypervolemia in Mice Bearing Transplantable Granulosa Cell Tumors. *Science* **105:**41.

Gao, Y., Vincent, D. F., Davis, A. J., Sansom, O. J., Bartholin, L. and Li, Q. (2016). Constitutively active transforming growth factor beta receptor 1 in the mouse ovary promotes tumorigenesis. *Oncotarget* **7:**40904-40918.

Garson, K., Macdonald, E., Dube, M., Bao, R., Hamilton, T. C. and Vanderhyden, B. C. (2003). Generation of tumors in transgenic mice expressing the SV40 T antigen under the control of ovarian-specific promoter 1. *Journal of the Society for Gynecologic Investigation* **10:**244-250.

Gava, N., Clarke, C. L., Bye, C. and Byth, K. (2008). Global gene expression profiles of ovarian surface epithelial cells in vivo. *Journal of molecular endocrinology* **40:**281-296.

Geng, L. Y., Fang, M., Yi, J. M., Jiang, F., Moeen-ud-Din, M. and Yang, L. G. (2008). Effect of overexpression of inhibin alpha (1-32) fragment on bovine granulosa cell proliferation, apoptosis, steroidogenesis, and development of co-cultured oocytes. *Theriogenology* **70:**35-43.

Georgescu, M.-M. (2010). PTEN Tumor Suppressor Network in PI3K-Akt Pathway Control. *Genes & Cancer* **1:**1170-1177.

Gerard, N., Caillaud, M., Martoriati, A., Goudet, G. and Lalmanach, A. C. (2004). The interleukin-1 system and female reproduction. *The Journal of endocrinology* **180:**203-212.

Ginther, O., Beg, M., Bergfelt, D., Donadeu, F. and Kot, K. (2001). Follicle selection in monovular species. *Biology of Reproduction* **65:**638-647.

Gold, E., Marino, F. E., Harrison, C., Makanji, Y. and Risbridger, G. (2013). Activin-beta(c) reduces reproductive tumour progression and abolishes cancer-associated cachexia in inhibin-deficient mice. *The Journal of pathology* **229:**599-607.

Goto, M., Iwase, A., Harata, T., Takigawa, S., Suzuki, K., Manabe, S. and Kikkawa, F. (2009). IGF1-induced AKT phosphorylation and cell proliferation are suppressed with the increase in PTEN during luteinization in human granulosa cells. *Reproduction* **137:**835-842.

Gray, S. H. (2013). Menstrual Disorders. *Pediatrics in Review* **34:**6.

Griffin, J. E. and Ojeda, S. R. (1992). Textbook of endocrine physiology. Oxford University Press.

Guan, B., Rahmanto, Y. S., Wu, R. C., Wang, Y., Wang, Z., Wang, T. L. and Shih Ie, M. (2014). Roles of deletion of Arid1a, a tumor suppressor, in mouse ovarian tumorigenesis. *JNCI: Journal of the National Cancer Institute* **106:**dju 146.

Hai, L., McGee, S. R., Rabideau, A. C., Paquet, M. and Narayan, P. (2015). Infertility in Female Mice with a Gain-of-Function Mutation in the Luteinizing Hormone Receptor Is Due to Irregular Estrous Cyclicity, Anovulation, Hormonal Alterations, and Polycystic Ovaries. *Biology of Reproduction* **93:**16.

Hamada, F. and Bienz, M. (2002). A Drosophila APC tumour suppressor homologue functions in cellular adhesion. *Nature cell biology* **4:**208-213.

Hamada, F., Murata, Y., Nishida, A., Fujita, F., Tomoyasu, Y., Nakamura, M., Toyoshima, K. *et al.* (1999). Identification and characterization of E-APC, a novel Drosophila homologue of the tumour suppressor APC. *Genes to cells* **4:**465-474.

Hanahan, D. and Weinberg, Robert A. (2011). Hallmarks of Cancer: The Next Generation. *Cell* **144:**646-674.

Hansen, J. M., Coleman, R. L. and Sood, A. K. (2016). Targeting the tumour microenvironment in ovarian cancer. *European Journal of Cancer* **56:**131-143.

Hasan, N., Ohman, A. W. and Dinulescu, D. M. (2015). The promise and challenge of ovarian cancer models. *Translational cancer research* **4:**14-28.

Hashiguchi, Y., Tsuda, H., Inoue, T., Berkowitz, R. S. and Mok, S. C. (2006). PTEN expression in clear cell adenocarcinoma of the ovary. *Gynecologic Oncology Research and Practice* **101:**71-75.

Hatanaka, S., Sawada, S. and Midorikawa, O. (1981). Effect of hormonal milieu on the growth of transplantable granulosa cell tumors in mice. *Gan* **72:**151-155.

Hernandez Gifford, J. A. (2015). The role of WNT signaling in adult ovarian folliculogenesis. *Reproduction* **150:**R137-148.

Hernandez Gifford, J. A., Hunzicker-Dunn, M. E. and Nilson, J. H. (2009). Conditional Deletion of Beta-Catenin Mediated by Amhr2cre in Mice Causes Female Infertility. *Biology of Reproduction* **80:**1282-1292.

Herndon, M. K., Law, N. C., Donaubauer, E. M., Kyriss, B. and Hunzicker-Dunn, M. (2016). Forkhead box O member FOXO1 regulates the majority of follicle-stimulating hormone responsive genes in ovarian granulosa cells. *Molecular and cellular endocrinology* **434:**116-126.

Holland, J. D., Klaus, A., Garratt, A. N. and Birchmeier, W. (2013). Wnt signaling in stem and cancer stem cells. *Current opinion in cell biology* **25:**254-264. .

Hollander, M. C., Blumenthal, G. M. and Dennis, P. A. (2011). PTEN loss in the continuum of common cancers, rare syndromes and mouse models. *Nature reviews. Cancer* **11:**289-301.

Horta, M. and Cunha, T. M. (2015). Sex cord-stromal tumors of the ovary: a comprehensive review and update for radiologists. *Diagnostic and Interventional Radiology* **21:**277-286.

Hosaka, T., Biggs, W. H., 3rd, Tieu, D., Boyer, A. D., Varki, N. M., Cavenee, W. K. and Arden, K. C. (2004). Disruption of forkhead transcription factor (FOXO) family members in mice reveals their functional diversification. *Proceedings of the National Academy of Sciences of the United States of America*
101:2975-2980.

House, C. D., Hernandez, L. and Annunziata, C. M. (2014). Recent Technological Advances in Using Mouse Models to Study Ovarian Cancer. *Frontiers in Oncology* **4:**26.

Howell, J. S., Marchant, J. and Orr, J. W. (1954). The induction of ovarian tumours in mice with 9:10-dimethyl-1:2-benzanthracene. *British journal of cancer* **8:**635-646.

Hrabovszky, E., Kallo, I., Szlavik, N., Keller, E., Merchenthaler, I. and Liposits, Z. (2007). Gonadotropin-releasing hormone neurons express estrogen receptor-beta. *The Journal of clinical endocrinology and metabolism*
92:2827-2830.

Hsieh, M., Boerboom, D., Shimada, M., Lo, Y., Parlow, A. F., Luhmann, U. F., Berger, W. *et al.* (2005). Mice null for Frizzled4 (Fzd4−/−) are infertile and exhibit impaired corpora lutea formation and function. *Biology of reproduction* **73:**1135-1146.

Huang da, W., Sherman, B. T. and Lempicki, R. A. (2009). Systematic and integrative analysis of large gene lists using DAVID bioinformatics resources. *Nature protocols* **4:**44-57.

Huncharek, M. and Muscat, J. (2011). Perineal talc use and ovarian cancer risk: a case study of scientific standards in environmental epidemiology. *European journal of cancer prevention* **20:**501-507.

Inestrosa, N. C. and Varela-Nallar, L. (2015). Wnt signalling in neuronal differentiation and development. *Cell and Tissue Research* **359:**215-223.

Jameson, S. A., Lin, Y. T. and Capel, B. (2012). Testis development requires the repression of Wnt4 by Fgf signaling. *Developmental biology* **370:**24-32.

Jamieson, S. and Fuller, P. J. (2012). Molecular Pathogenesis of Granulosa Cell Tumors of the Ovary. *Endocrine Reviews* **33:**109-144.

Jamnongjit, M. and Hammes, S. R. (2006). Ovarian Steroids: The Good, the Bad, and the Signals that Raise Them. *Cell cycle* **5:**1178-1183.

Jardé, T., Lloyd-Lewis, B., Thomas, M., Kendrick, H., Melchor, L., Bougaret, L., Watson, P. D. *et al.* (2016). Wnt and Neuregulin1/ErbB signalling extends 3D culture of hormone responsive mammary organoids. *Nature communications* **7:**13207.

Jarrett, C. R., Blancato, J., Cao, T., Bressette, D. S., Cepeda, M., Young, P. E., King, C. R. *et al.* (2001). Human APC2 localization and allelic imbalance. *Cancer research* **61:**7978-7984.

Jelovac, D. and Armstrong, D. K. (2011). Recent Progress in the Diagnosis and Treatment of Ovarian Cancer. *CA: a cancer journal for clinicians* **61:**183-203.

Jho, E. H., Zhang, T., Domon, C., Joo, C. K., Freund, J. N. and Costantini, F. (2002). Wnt/beta-catenin/Tcf signaling induces the transcription of Axin2, a negative regulator of the signaling pathway. *Molecular and cellular biology* **22:**1172-1183.

Jiang, H., Li, Q., He, C., Li, F., Sheng, H., Shen, X., Zhang, X. *et al.* (2014). Activation of the Wnt pathway through Wnt2 promotes metastasis in pancreatic cancer. *American journal of cancer research* **4:**537-544.

Jones, D. L. and Wagers, A. J. (2008). No place like home: anatomy and function of the stem cell niche. *Nature reviews Molecular cell biology* **9:**11-21.

Jull, J. W., Streeter, D. J. and Sutherland, L. (1966). The mechanism of induction of ovarian tumors in the mouse by 7,12-dimethylbenz-[alpha]anthracene. I. Effect of steroid hormones and carcinogen concentration in vivo. *Journal of the National Cancer Institute* **37:**409-420.

Kajihara, T., Uchino, S., Suzuki, M., Itakura, A., Brosens, J. J. and Ishihara, O. (2009). Increased ovarian follicle atresia in obese Zucker rats is associated with enhanced expression of the forkhead transcription factor FOXO1. *Medical molecular morphology* **42:**216-221.

Kalfa, N., Veitia, R. A., Benayoun, B. A., Boizet-Bonhoure, B. and Sultan, C. (2009). The new molecular biology of granulosa cell tumors of the ovary. *Genome medicine* **1:**81.

Kananen, K., Markkula, M., Rainio, E., Su, J. G., Hsueh, A. J. and Huhtaniemi, I. T. (1995). Gonadal tumorigenesis in transgenic mice bearing the mouse inhibin alpha-subunit promoter/simian virus T-antigen fusion gene: characterization of ovarian tumors and establishment of gonadotropin-responsive granulosa cell lines. *Molecular endocrinology* **9:**616-627.

Kananen, K., Rilianawati, Paukku, T., Markkula, M., Rainio, E. M. and Huhtaniemi, I. (1997). Suppression of gonadotropins inhibits gonadal tumorigenesis in mice transgenic for the mouse inhibin alpha-subunit promoter/simian virus 40 T-antigen fusion gene. *Endocrinology* **138:**3521-3531.

Kandel, E. S. and Hay, N. (1999). The Regulation and Activities of the Multifunctional Serine/Threonine Kinase Akt/PKB. *Experimental Cell Research* **253:**210-229.

Kanthan, R., Senger, J.-L. and Kanthan, S. (2012). The Multifaceted Granulosa Cell Tumours-Myths and Realities: A Review. *ISRN obstetrics and gynecology* **2012:**12.

Katayama, T., Kyan, H., Nakashima, M., Rahayu, E. Y., Murakami, N. and Kuroda, H. (2000). Involvement of distinct signaling pathways in activin-induced increases in FSH secretion and enlargement of FSH cell population in the rat pituitary. *Endocrine journal* **47:**239-247.

Kawai, Y., Moriyama, A., Asai, K., Coleman-Campbell, C. M., Sumi, S., Morishita, H. and Suchi, M. (2005). Molecular characterization of histidinemia: identification of four missense mutations in the histidase gene. *Human genetics* **116:**340-346.

Khosla, D., Dimri, K., Pandey, A. K., Mahajan, R. and Trehan, R. (2014). Ovarian Granulosa Cell Tumor: Clinical Features, Treatment, Outcome, and Prognostic Factors. *North American Journal of Medical Sciences* **6:**133-138.

Kilonzo, B. M., Neff, T., Samuelson, M. I. and Goodheart, M. J. (2015). Wnt signaling in granulosa cell tumors of the ovary. *Proceedings in Obstetrics and Gynecology* **4:**1-1.

Kim, A., Ueda, Y., Naka, T. and Enomoto, T. (2012). Therapeutic strategies in epithelial ovarian cancer. *Journal of experimental & clinical cancer research* **31:**14.

Kim, J. H., Kim, Y. H., Kim, H. M., Park, H. O., Ha, N. C., Kim, T. H., Park, M. *et al.* (2014a). FOXL2 posttranslational modifications mediated by GSK3beta determine the growth of granulosa cell tumours. *Nature communications* **5:**2936.

Kim, J. H., Yoon, S., Park, M., Park, H. O., Ko, J. J., Lee, K. and Bae, J. (2011). Differential apoptotic activities of wild-type FOXL2 and the adult-type granulosa cell tumor-associated mutant FOXL2 (C134W). *Oncogene* **30:**1653-1663.

Kim, S. Y., Ebbert, K., Cordeiro, M. H., Romero, M. M., Whelan, K. A., Suarez, A. A., Woodruff, T. K. *et al.* (2016). Constitutive Activation of PI3K in Oocyte Induces Ovarian Granulosa Cell Tumors. *Cancer research* **76:**3851-3861.

Kim, T. H., Suh, D. H., Kim, M.-K. and Song, Y. S. (2014b). Metformin against cancer stem cells through the modulation of energy metabolism: special considerations on ovarian cancer. *BioMed research international* **2014:**132702.

King, C. M., Barbara, C., Prentice, A., Brenton, J. D. and Charnock-Jones, D. S. (2016). Models of endometriosis and their utility in studying progression to ovarian clear cell carcinoma. *The Journal of Pathology* **238:**185-196.

King, M. L., Lindberg, M. E., Stodden, G. R., Okuda, H., Ebers, S. D., Johnson, A., Montag, A. *et al.* (2015). WNT7A/beta-catenin signaling induces FGF1 and influences sensitivity to niclosamide in ovarian cancer. *Oncogene* **34:**3452-3462.

Kinross, K. M., Brown, D. V., Kleinschmidt, M., Jackson, S., Christensen, J., Cullinane, C., Hicks, R. J. *et al.* (2011). In vivo activity of combined PI3K/mTOR and MEK inhibition in a Kras(G12D);Pten deletion mouse model of ovarian cancer. *Molecular cancer therapeutics* **10:**1440-1449.

Kinross, K. M., Montgomery, K. G., Kleinschmidt, M., Waring, P., Ivetac, I., Tikoo, A., Saad, M. *et al.* (2012). An activating Pik3ca mutation coupled with Pten loss is sufficient to initiate ovarian tumorigenesis in mice. *The Journal of clinical investigation* **122:**553-557.

Kitade, S., Onoyama, I., Kobayashi, H., Yagi, H., Yoshida, S., Kato, M., Tsunematsu, R. *et al.* (2016). FBXW7 is involved in the acquisition of the malignant phenotype in epithelial ovarian tumors. *Cancer science* **107:**1399-1405.

Kiyosu, C., Tsuji, T., Yamada, K., Kajita, S. and Kunieda, T. (2012). NPPC/NPR2 signaling is essential for oocyte meiotic arrest and cumulus oophorus formation during follicular development in the mouse ovary. *Reproduction* **144:**187-193.

Knight, P. G. and Glister, C. (2006). TGF-β superfamily members and ovarian follicle development. *Reproduction* **132:**191-206.

Knutson, K. L., Karyampudi, L., Lamichhane, P. and Preston, C. (2015). Targeted Immune Therapy of Ovarian Cancer. *Cancer metastasis reviews* **34:**53-74.

Kottarathil, V. D., Antony, M. A., Nair, I. R. and Pavithran, K. (2013). Recent Advances in Granulosa Cell Tumor Ovary: A Review. *Indian Journal of Surgical Oncology* **4:**37-47.

Krarup, T. (1969). Oocyte destruction and ovarian tumorigenesis after direct application of a chemical carcinogen (9:0-dimethyl-1:2-benzanthrene) to the mouse ovary. *International journal of cancer* **4:**61-75.

Kritsch, D., Hoffmann, F., Steinbach, D., Jansen, L., Photini, S. M., Gajda, M., Mosig, A. S. *et al.* (2017). Tribbles 2 mediates cisplatin sensitivity and DNA damage response in epithelial ovarian cancer. *International journal of cancer* **doi:10.1002/ijc.30860**.

Kuang, H., Zhang, L., Peng, J. and Chen, Q. (2009). Premature ovarian failure, menopause and ovarian cancer, three nodes on the same string: Pten and other potential genes on the go. *Medical hypotheses* **73:**961-962.

Kulkarni, A. A., Roy, B., Rao, P. S., Wyant, G. A., Mahmoud, A., Ramachandran, M., Sengupta, P. *et al.* (2013). Supramolecular nanoparticles that target phosphoinositide-3-kinase overcome insulin resistance and exert pronounced antitumor efficacy. *Cancer Research* **73:**6987-6997.

Kurman, R. J. and Shih, I.-M. (2016). The Dualistic Model of Ovarian Carcinogenesis: Revisited, Revised, and Expanded. *The American Journal of Pathology* **186:**733-747.

Kurman, R. J. and Shih Ie, M. (2010). The origin and pathogenesis of epithelial ovarian cancer: a proposed unifying theory. *The American journal of surgical pathology* **34:**433.

Kusamura, S., Derchain, S., Alvarenga, M., Gomes, C. P., Syrjanen, K. J. and Andrade, L. A. (2003). Expression of p53, c-erbB-2, Ki-67, and CD34 in granulosa cell tumor of the ovary. *International journal of gynecological cancer* **13:**450-457.

Kwack, M. H., Kim, M. K., Kim, J. C. and Sung, Y. K. (2013). Wnt5a attenuates Wnt/beta-catenin signalling in human dermal papilla cells. *Experimental dermatology* **22:**229-231.

Kwon, M. J. and Shin, Y. K. (2013). Regulation of ovarian cancer stem cells or tumor-initiating cells. *International journal of molecular sciences* **14:**6624-6648. .

Lague, M. N., Paquet, M., Fan, H. Y., Kaartinen, M. J., Chu, S., Jamin, S. P., Behringer, R. R. *et al.* (2008). Synergistic effects of Pten loss and WNT/CTNNB1 signaling pathway activation in ovarian granulosa cell tumor development and progression. *Carcinogenesis* **29:**2062-2072.

Lan, Z. J., Krause, M. S., Redding, S. D., Li, X., Wu, G. Z., Zhou, H. X., Bohler, H. C. *et al.* (2017). Selective deletion of Pten in theca-interstitial cells leads to androgen excess and ovarian dysfunction in mice. *Molecular and cellular endocrinology* **444:**26-37.

Lapointe, E. and Boerboom, D. (2011). WNT signaling and the regulation of ovarian steroidogenesis. *Frontiers in bioscience (Scholar edition)* **3:**276-285.

Lapointe, E., Boyer, A., Rico, C., Paquet, M., Franco, H. L., Gossen, J., DeMayo, F. J. *et al.* (2012). FZD1 Regulates Cumulus Expansion Genes and Is Required for Normal Female Fertility in Mice. *Biology of Reproduction* **87:**104.

Law, N. C., Weck, J., Kyriss, B., Nilson, J. H. and Hunzicker-Dunn, M. (2013). Lhcgr expression in granulosa cells: roles for PKA-phosphorylated β-catenin, TCF3, and FOXO1. *Molecular endocrinology* **27:**1295-1310.

Le, P. N., McDermott, J. D. and Jimeno, A. (2014). Targeting the Wnt pathway in human cancers: Therapeutic targeting with a focus on OMP-54F28. *Pharmacology & therapeutics* **146:**1-11.

Lee, E. K., Chung, K. W., Yang, S. K., Park, M. J., Min, H. S., Kim, S. W. and Kang, H. S. (2013). DNA methylation of MAPK signal-inhibiting genes in papillary thyroid carcinoma. *Anticancer research* **33:**4833-4839.

Lee, K. R. and Nucci, M. R. (2003). Ovarian mucinous and mixed epithelial carcinomas of mullerian (endocervical-like) type: a clinicopathologic analysis of four cases of an uncommon variant associated with endometriosis. *International journal of gynecological pathology* **22:**42-51.

Lee, S. J., Ghosh, S. C., Han, H. D., Stone, R. L., Bottsford-Miller, J., Shen de, Y., Auzenne, E. J. *et al.* (2012). Metronomic activity of CD44-targeted hyaluronic acid-paclitaxel in ovarian carcinoma. *Clinical Cancer Research* **18:**4114-4121. .

Li, J., Yen, C., Liaw, D., Podsypanina, K., Bose, S., Wang, S. I., Puc, J. *et al.* (1997). PTEN, a putative protein tyrosine phosphatase gene mutated in human brain, breast, and prostate cancer. *Science* **275:**1943-1947.

Li, L., Ji, S. Y., Yang, J. L., Li, X. X., Zhang, J., Zhang, Y., Hu, Z. Y. *et al.* (2014). Wnt/beta-catenin signaling regulates follicular development by modulating the expression of Foxo3a signaling components. *Molecular and cellular endocrinology* **382:**915-925.

Li, S. D. and Howell, S. B. (2010). CD44-targeted microparticles for delivery of cisplatin to peritoneal metastases. *Molecular pharmaceutics* **7:**280-290. .

Liang, C.-C., Park, A. Y. and Guan, J.-L. (2007). In vitro scratch assay: a convenient and inexpensive method for analysis of cell migration in vitro. *Nature Protocols* **2:**329-333.

Lili, L. N., Matyunina, L. V., Walker, L. D., Wells, S. L., Benigno, B. B. and McDonald, J. F. (2013). Molecular profiling supports the role of epithelial-to-mesenchymal transition (EMT) in ovarian cancer metastasis. *Journal of Ovarian Research* **6:**49-56.

Lin, S., Long, H. X., Xiang, T., Zhu, B. and Xie, R. K. (2011). [Isolation and identification of cancer stem cells from primary human ovarian cancer tissues]. *Chinese journal of oncology* **33:**896-899.

Lipschutz, A., Iglesias, R., Panasevich, V. I. and Salinas, S. (1967). Granulosa-cell tumours induced in mice by progesterone. *British journal of cancer* **21:**144-152.

Lipschutz, A., Panasevich, V. I. and Cerisola, H. (1964). Comaparative tumorigenesis in intrasplenic, intrarenal and intrahepatic ovarian grafts. *British journal of cancer* **18:**655-666.

Liu, J., Viswanadhapalli, S., Garcia, L., Zhou, M., Nair, B. C., Kost, E., Rao Tekmal, R. *et al.* (2017). Therapeutic utility of natural estrogen receptor beta agonists on ovarian cancer. *Oncotarget* **8:**50002-50014.

Liu, K., Rajareddy, S., Liu, L., Jagarlamudi, K., Boman, K., Selstam, G. and Reddy, P. (2006). Control of mammalian oocyte growth and early follicular development by the oocyte PI3 kinase pathway: New roles for an old timer. *Developmental Biology* **299:**1-11.

Liu, Z., Castrillon, D. H., Zhou, W. and Richards, J. S. (2013). FOXO1/3 depletion in granulosa cells alters follicle growth, death and regulation of pituitary FSH. *Molecular endocrinology* **27:**238-252.

Liu, Z., Ren, Y. A., Pangas, S. A., Adams, J., Zhou, W., Castrillon, D. H., Wilhelm, D. *et al.* (2015). FOXO1/3 and PTEN Depletion in Granulosa Cells Promotes Ovarian Granulosa Cell Tumor Development. *Molecular endocrinology* **29:**1006-1024.

Liu, Z., Rudd, M. D., Hernandez-Gonzalez, I., Gonzalez-Robayna, I., Fan, H. Y., Zeleznik, A. J. and Richards, J. S. (2009). FSH and FOXO1 regulate genes in the sterol/steroid and lipid biosynthetic pathways in granulosa cells. *Molecular endocrinology* **23:**649-661.

Livak, K. J. and Schmittgen, T. D. (2001). Analysis of relative gene expression data using real-time quantitative PCR and the 2(-Delta Delta C(T)) Method. *Methods* **25:**402-408.

Livingstone, C. and Borai, A. (2014). Insulin-like growth factor-II: its role in metabolic and endocrine disease. *Clinical endocrinology* **80:**773-781.

Lokadasan, R., James, F. V., Narayanan, G. and Prabhakaran, P. K. (2016). Targeted agents in epithelial ovarian cancer: review on emerging therapies and future developments. *ecancermedicalscience* **10:**626.

Looyenga, B. D. and Hammer, G. D. (2007). Genetic removal of Smad3 from inhibin-null mice attenuates tumor progression by uncoupling extracellular mitogenic signals from the cell cycle machinery. *Molecular endocrinology* **21:**2440-2457.

Lopes, C. T., Franz, M., Kazi, F., Donaldson, S. L., Morris, Q. and Bader, G. D. (2010). Cytoscape Web: an interactive web-based network browser. *Bioinformatics* **26:**2347-2348.

Luo, C., Zuñiga, J., Edison, E., Palla, S., Dong, W. and Parker-Thornburg, J. (2011). Superovulation Strategies for 6 Commonly Used Mouse Strains. *Journal of the American Association for Laboratory Animal Science : JAALAS* **50:**471-478.

Luu, N., Fu, L., Fujimoto, K. and Shi, Y. B. (2017). Direct regulation of histidine ammonia-lyase 2 gene by thyroid hormone in the developing adult intestinal stem cells. *Endocrinology* **158:**1022-1033.

Luvero, D., Milani, A. and Ledermann, J. A. (2014). Treatment options in recurrent ovarian cancer: latest evidence and clinical potential. *Therapeutic advances in medical oncology* **6:**229-239. .

Ma, Y., Ma, L., Guo, Q. and Zhang, S. (2010). Expression of bone morphogenetic protein-2 and its receptors in epithelial ovarian cancer and their influence on the prognosis of ovarian cancer patients. *Journal of Experimental & Clinical Cancer Research* **29:**85.

Maatouk, D. M., DiNapoli, L., Alvers, A., Parker, K. L., Taketo, M. M. and Capel, B. (2008). Stabilization of beta-catenin in XY gonads causes male-to-female sex-reversal. *Human molecular genetics* **17:**2949-2955.

Maccio, A. and Madeddu, C. (2012). Inflammation and ovarian cancer. *Cytokine* **58:**133-147.

Macklon, N. S. and Fauser, B. C. (2001). Follicle-stimulating hormone and advanced follicle development in the human. *Archives of medical research* **32:**595-600.

Maehama, T. and Dixon, J. E. (1998). The tumor suppressor, PTEN/MMAC1, dephosphorylates the lipid second messenger, phosphatidylinositol 3,4,5-trisphosphate. *The Journal of biological chemistry* **273:**13375-13378.

Mahler, J. F., Stokes, W., Mann, P. C., Takaoka, M. and Maronpot, R. R. (1996). Spontaneous lesions in aging FVB/N mice. *Toxicologic pathology* **24:**710-716.

Maines-Bandiera, S. L. and Auersperg, N. (1997). Increased E-cadherin expression in ovarian surface epithelium: an early step in metaplasia and dysplasia? *International journal of gynecological pathology* **16:**250-255.

Mangili, G., Ottolina, J., Gadducci, A., Giorda, G., Breda, E., Savarese, A., Candiani, M. *et al.* (2013). Long-term follow-up is crucial after treatment for granulosa cell tumours of the ovary. *British journal of cancer* **109:**29-34.

Mani, A. M., Fenwick, M. A., Cheng, Z., Sharma, M. K., Singh, D. and Wathes, D. C. (2010). IGF1 induces up-regulation of steroidogenic and apoptotic regulatory genes via activation of phosphatidylinositol-dependent kinase/AKT in bovine granulosa cells. *Reproduction* **139:**139-151.

Marchler-Bauer, A., Bo, Y., Han, L., He, J., Lanczycki, C. J., Lu, S., Chitsaz, F. *et al.* (2017). CDD/SPARCLE: functional classification of proteins via subfamily domain architectures. *Nucleic Acids Research* **45:**D200-d203.

Marcus, C. S., Maxwell, G. L., Darcy, K. M., Hamilton, C. A. and McGuire, W. P. (2014). Current approaches and challenges in managing and monitoring treatment response in ovarian cancer. *Journal of Cancer* **5:**25-30. .

Maria, V. B. and Rebecca, J. B. (2011). Diverse mechanisms for activation of Wnt signalling in the ovarian tumour microenvironment. *Biochemical Journal* **437:**1-12.

Mason, S. D. and Joyce, J. A. (2011). Proteolytic Networks in Cancer. *Trends in cell biology* **21:**228-237.

Masuda, M., Sawa, M. and Yamada, T. (2015). Therapeutic targets in the Wnt signaling pathway: Feasibility of targeting TNIK in colorectal cancer. *Pharmacology & Therapeutics* **156:**1-9.

Matsuda, F., Inoue, N., Maeda, A., Cheng, Y., Sai, T., Gonda, H., Goto, Y. *et al.* (2011). Expression and function of apoptosis initiator FOXO3 in granulosa cells during follicular atresia in pig ovaries. *The Journal of reproduction and development* **57:**151-158.

Matzuk, M. M., Finegold, M. J., Su, J. G., Hsueh, A. J. and Bradley, A. (1992). Alpha-inhibin is a tumour-suppressor gene with gonadal specificity in mice. *Nature* **360:**313-319.

Mayani, H. (2003). A glance into somatic stem cell biology: basic principles, new concepts, and clinical relevance. *Archives of medical research* **34:**3-15.

McCartney, B. M., Dierick, H. A., Kirkpatrick, C., Moline, M. M., Baas, A., Peifer, M. and Bejsovec, A. (1999). Drosophila APC2 is a cytoskeletally-associated protein that regulates wingless signaling in the embryonic epidermis. *The Journal of cell biology* **146:**1303-1318.

McCartney, B. M., McEwen, D. G., Grevengoed, E., Maddox, P., Bejsovec, A. and Peifer, M. (2001). Drosophila APC2 and Armadillo participate in tethering mitotic spindles to cortical actin. *Nature cell biology* **3:**933-938.

McCartney, B. M., Price, M. H., Webb, R. L., Hayden, M. A., Holot, L. M., Zhou, M., Bejsovec, A. *et al.* (2006). Testing hypotheses for the functions of APC family proteins using null and truncation alleles in Drosophila. *Development* **133:**2407-2418.

McGee, E. A. and Hsueh, A. J. W. (2000). Initial and Cyclic Recruitment of Ovarian Follicles*. *Endocrine Reviews* **21:**200-214.

McGee, S. R. and Narayan, P. (2013). Precocious Puberty and Leydig Cell Hyperplasia in Male Mice With a Gain of Function Mutation in the LH Receptor Gene. *Endocrinology* **154:**3900-3913.

McLaughlin, E. A. and McIver, S. C. (2009). Awakening the oocyte: controlling primordial follicle development. *Reproduction* **137:**1-11.

McLean, A. C., Valenzuela, N., Fai, S. and Bennett, S. A. L. (2012). Performing Vaginal Lavage, Crystal Violet Staining, and Vaginal Cytological Evaluation for Mouse Estrous Cycle Staging Identification. *Journal of Visualized Experiments : JoVE* 4389.

Meehan, R. S. and Chen, A. P. (2016). New treatment option for ovarian cancer: PARP inhibitors. *Gynecologic Oncology Research and Practice* **3:**1-8.

Menczer, J., Komarov, H., Shenboum, M., Insler, V. and Czernobilsky, B. (1977). Attempted induction of granulosa cell tumor in Balb-C mice by gonadotropin administration. *Gynecologic investigation* **8:**314-322.

Mikaeili, S., Rashidi, B. H., Safa, M., Najafi, A., Sobhani, A., Asadi, E. and Abbasi, M. (2016). Altered FoxO3 expression and apoptosis in granulosa cells of women with polycystic ovary syndrome. *Archives of gynecology and obstetrics* **294:**185-192.

Miller, W. L. and Bose, H. S. (2011). Early steps in steroidogenesis: intracellular cholesterol trafficking: Thematic Review Series: Genetics of Human Lipid Diseases. *Journal of Lipid Research* **52:**2111-2135.

Mohamed, O. A., Clarke, H. J. and Dufort, D. (2004). β-catenin signaling marks the prospective site of primitive streak formation in the mouse embryo. *Developmental Dynamics* **231:**416-424.

Moore, R. G., McMeekin, D. S., Brown, A. K., DiSilvestro, P., Miller, M. C., Allard, W. J., Gajewski, W. *et al.* (2009). A novel multiple marker bioassay utilizing HE4 and CA125 for the

prediction of ovarian cancer in patients with a pelvic mass. *Gynecologic Oncology Research and Practice* **112:**40-46.

Mullany, L. K., Fan, H. Y., Liu, Z., White, L. D., Marshall, A., Gunaratne, P., Anderson, M. L. *et al.* (2011). Molecular and functional characteristics of ovarian surface epithelial cells transformed by KrasG12D and loss of Pten in a mouse model in vivo. *Oncogene.* **30:**3522-3536. .

Munksgaard, P. S. and Blaakaer, J. (2011). The association between endometriosis and gynecological cancers and breast cancer: a review of epidemiological data. *Gynecologic oncology* **123:**157-163.

Muralidharan, S., Hanley, P., Liu, E., Chakraborty, R., Bollard, C., Shpall, E., Rooney, C. *et al.* (2011). Activation of Wnt signaling arrests effector differentiation in human peripheral and cord blood-derived T lymphocytes(). *Journal of immunology* **187:**5221-5232.

Murdoch, W. J. and McDonnel, A. C. (2002). Roles of the ovarian surface epithelium in ovulation and carcinogenesis. *Reproduction* **123:**743-750.

Nagaraj, A. B., Joseph, P., Kovalenko, O., Singh, S., Armstrong, A., Redline, R., Resnick, K. *et al.* (2015). Critical role of Wnt/beta-catenin signaling in driving epithelial ovarian cancer platinum resistance. *Oncotarget* **6:**23720-23734.

Nakagawa, H., Koyama, K., Murata, Y., Morito, M., Akiyama, T. and Nakamura, Y. (2000a). APCL, a central nervous system-specific homologue of adenomatous polyposis coli tumor suppressor, binds to p53-binding protein 2 and translocates it to the perinucleus. *Cancer research* **60:**101-105.

Nakagawa, H., Koyama, K., Murata, Y., Morito, M., Akiyama, T. and Nakamura, Y. (2000b). EB3, a novel member of the EB1 family preferentially expressed in the central nervous system, binds to a CNS-specific APC homologue. *Oncogene* **19:**210-216.

Ness, R. B. and Cottreau, C. (1999). Possible Role of Ovarian Epithelial Inflammation in Ovarian Cancer. *JNCI: Journal of the National Cancer Institute* **91:**1459-1467.

Ng, A. and Barker, N. (2015). Ovary and fimbrial stem cells: biology, niche and cancer origins. *Nature reviews. Molecular cell biology* **16:**625-638.

Ng, A., Tan, S., Singh, G., Rizk, P., Swathi, Y., Tan, T. Z., Huang, R. Y. *et al.* (2014). Lgr5 marks stem/progenitor cells in ovary and tubal epithelia. *Nature cell biology* **16:**745-757.

NICE. (2011). NICE guidelines [CG122]. Ovarian cancer: recognition and initial management. April 2011. Available at https://www.nice.org.uk/guidance/cg122/chapter/1-Guidance [Online]. Available at: [Accessed: 14 April].

Niehrs, C. (2006). Function and biological roles of the Dickkopf family of Wnt modulators. *Oncogene* **25:**7469-7481.

Nishida, N., Yano, H., Nishida, T., Kamura, T. and Kojiro, M. (2006). Angiogenesis in Cancer. *Vascular Health and Risk Management* **2:**213-219.

Nomura, M., Sakamoto, R., Morinaga, H., Wang, L., Mukasa, C. and Takayanagi, R. (2013). Activin stimulates CYP19A gene expression in human ovarian granulosa cell-like KGN cells via the Smad2 signaling pathway. *Biochemical and biophysical research communications* **436:**443-448.

Nossov, V., Amneus, M., Su, F., Lang, J., Janco, J. M. T., Reddy, S. T. and Farias-Eisner, R. (2008). The early detection of ovarian cancer: from traditional methods to proteomics. Can we really do better than serum CA-125? *American journal of obstetrics and gynecology* **199:**215-223.

Obata, K., Morland, S. J., Watson, R. H., Hitchcock, A., Chenevix-Trench, G., Thomas, E. J. and Campbell, I. G. (1998). Frequent PTEN/MMAC mutations in endometrioid but not serous or mucinous epithelial ovarian tumors. *Cancer research* **58:**2095-2097.

Oishi, I., Suzuki, H., Onishi, N., Takada, R., Kani, S., Ohkawara, B., Koshida, I. *et al.* (2003). The receptor tyrosine kinase Ror2 is involved in non-canonical Wnt5a/JNK signalling pathway. *Genes to cells* **8:**645-654.

Oka, R., Sasagawa, T., Ninomiya, I., Miwa, K., Tanii, H. and Saijoh, K. (2001). Reduction in the local expression of complement component 6 (C6) and 7 (C7) mRNAs in oesophageal carcinoma. *European journal of cancer* **37:**1158-1165.

Okamoto, S., Okamoto, A., Nikaido, T., Saito, M., Takao, M., Yanaihara, N., Takakura, S. *et al.* (2009). Mesenchymal to epithelial transition in the human ovarian surface epithelium focusing on inclusion cysts. *Oncology reports* **21:**1209-1214.

Oliver, S. and McCartney, B. (2014). The Wnt signaling and cytoskeletal regulator APC2 controls stem cell niche size, architecture, and stem cell number in the Drosophila ovary. . *55th annual Drosophila research conference.* . MOLECULAR BIOLOGY OF THE CELL (Vol. 25)

Orsi, N. M., Baskind, N. E. and Cummings, M. (2014). Anatomy, Development, Histology, and Normal Function of the Ovary.*Pathology of the Ovary, Fallopian Tube and Peritoneum*. Springer, pp. 1-32.

Ottolenghi, C., Pelosi, E., Tran, J., Colombino, M., Douglass, E., Nedorezov, T., Cao, A. *et al.* (2007). Loss of Wnt4 and Foxl2 leads to female-to-male sex reversal extending to germ cells. *Human molecular genetics* **16:**2795-2804.

Ouyang, J. X., Luo, T., Sun, H. Y., Huang, J., Tang, D. F., Wu, L., Zheng, Y. H. *et al.* (2013). RNA interference mediated pten knock-down inhibit the formation of polycystic ovary. *Molecular and cellular biochemistry* **380:**195-202.

Pal, M. K., Jaiswar, S. P., Dwivedi, V. N., Tripathi, A. K., Dwivedi, A. and Sankhwar, P. (2015). MicroRNA: a new and promising potential biomarker for diagnosis and prognosis of ovarian cancer. *Cancer Biology & Medicine* **12:**328-341.

Palacios, J. and Gamallo, C. (1998). Mutations in the beta-catenin gene (CTNNB1) in endometrioid ovarian carcinomas. *Cancer research* **58:**1344-1347.

Pan, H., Cui, H., Liu, S., Qian, Y., Wu, H., Li, L., Guan, Y. *et al.* (2014). Lgr4 gene regulates corpus luteum maturation through modulation of the WNT-mediated EGFR-ERK signaling pathway. *Endocrinology* **155:**3624-3637.

Pan, Z., Sun, M., Liang, X., Li, J., Zhou, F., Zhong, Z. and Zheng, Y. (2016). The Controversy, Challenges, and Potential Benefits of Putative Female Germline Stem Cells Research in Mammals. *Stem cells international* **2016:**1728278.

Pangas, S. A., Li, X., Umans, L., Zwijsen, A., Huylebroeck, D., Gutierrez, C., Wang, D. *et al.* (2008). Conditional deletion of Smad1 and Smad5 in somatic cells of male and female gonads leads to metastatic tumor development in mice. *Molecular and cellular biology* **28:**248-257.

Parakh, T. N., Hernandez, J. A., Grammer, J. C., Weck, J., Hunzicker-Dunn, M., Zeleznik, A. J. and Nilson, J. H. (2006). Follicle-stimulating hormone/cAMP regulation of aromatase gene expression requires beta-catenin. *Proceedings of the National Academy of Sciences of the United States of America*
103:12435-12440.

Park, J.-Y., Su, Y.-Q., Ariga, M., Law, E., Jin, S.-L. C. and Conti, M. (2004). EGF-like growth factors as mediators of LH action in the ovulatory follicle. *Science* **303:**682-684.

Pavlik, E. J., DePriest, P. D., Gallion, H. H., Ueland, F. R., Reedy, M. B., Kryscio, R. J. and van Nagell, J. R., Jr. (2000). Ovarian volume related to age. *Gynecologic Oncology* **77:**410-412.

Pellegrino, M., Maiorino, R. and Schonauer, S. (2010). WNT4 signaling in female gonadal development. *Endocrine, metabolic & immune disorders drug targets* **10:**168-174.

Pelosi, E., Omari, S., Michel, M., Ding, J., Amano, T., Forabosco, A., Schlessinger, D. *et al.* (2013). Constitutively active Foxo3 in oocytes preserves ovarian reserve in mice. *Nature communications* **4:**1843.

Peng, X., Li, W., Johnson, W. D., Torres, K. E. and McCormick, D. L. (2015). Overexpression of lipocalins and pro-inflammatory chemokines and altered methylation of PTGS2 and APC2

in oral squamous cell carcinomas induced in rats by 4-nitroquinoline-1-oxide. *PLoS One* **10:**e0116285.

Perets, R., Wyant, Gregory A., Muto, Katherine W., Bijron, Jonathan G., Poole, Barish B., Chin, Kenneth T., Chen, Jin Yun H. *et al.* (2013). Transformation of the Fallopian Tube Secretory Epithelium Leads to High-Grade Serous Ovarian Cancer in Brca;Tp53;Pten Models. *Cancer Cell* **24:**751-765.

Pérez-Cadahía, B., Drobic, B. and Davie, J. R. (2009). H3 phosphorylation: dual role in mitosis and interphaseThis paper is one of a selection of papers published in this Special Issue entitled 30th Annual International Asilomar Chromatin and Chromosomes Conference and has undergone the Journal's usual peer review process. *Biochemistry and Cell Biology* **87:**695-709.

Plant, T. M. (2015). 60 YEARS OF NEUROENDOCRINOLOGY: The hypothalamo-pituitary–gonadal axis. *Journal of Endocrinology* **226:**T41-T54.

Poulton, J. S., Mu, F. W., Roberts, D. M. and Peifer, M. (2013). APC2 and Axin promote mitotic fidelity by facilitating centrosome separation and cytoskeletal regulation. *Development.* **140:**4226-4236. .

Pourreyron, C., Reilly, L., Proby, C., Panteleyev, A., Fleming, C., McLean, K., South, A. P. *et al.* (2012). Wnt5a is strongly expressed at the leading edge in non-melanoma skin cancer, forming active gradients, while canonical Wnt signalling is repressed. *PLoS One* **7:**e31827.

Prat, J. (2013). Staging classification for cancer of the ovary, fallopian tube, and peritoneum. *International Journal of Gynecology and Obstetrics* **124:**1-5.

Przybycin, C. G. and Soslow, R. A. (2011). Typing of ovarian carcinomas: an update. *Diagnostic Histopathology* **17:**165-177.

Rahman, N. A., Bennink, H. J., Chrusciel, M., Sharp, V., Zimmerman, Y., Dina, R., Li, X. *et al.* (2012). A novel treatment strategy for ovarian cancer based on immunization against zona pellucida protein (ZP) 3. *The Faseb journal* **26:**324-333.

Rajanahally, S., Agno, J. E., Nalam, R. L., Weinstein, M. B., Loveland, K. L., Matzuk, M. M. and Li, Q. (2010). Genetic evidence that SMAD2 is not required for gonadal tumor development in inhibin-deficient mice. *Reproductive Biology and Endocrinology* **8:**69.

Randall, L. M. and Pothuri, B. (2016). The genetic prediction of risk for gynecologic cancers. *Gynecologic Oncology Research and Practice* **141:**10-16.

Rao, A. R. (1981). Effects of carcinogen and/or mutagen on normal and gonatotropin-primed ovaries of mice. *International journal of cancer* **28:**105-110.

Reddy, P., Liu, L., Adhikari, D., Jagarlamudi, K., Rajareddy, S., Shen, Y., Du, C. *et al.* (2008). Oocyte-specific deletion of Pten causes premature activation of the primordial follicle pool. *Science* **319:**611-613.

Ren, Y. A., Mullany, L. K., Liu, Z., Herron, A. J., Wong, K. K. and Richards, J. S. (2016). Mutant p53 Promotes Epithelial Ovarian Cancer by Regulating Tumor Differentiation, Metastasis, and Responsiveness to Steroid Hormones. *Cancer research* **76:**2206-2218.

Richards, J. S., Fan, H. Y., Liu, Z., Tsoi, M., Lague, M. N., Boyer, A. and Boerboom, D. (2012). Either Kras activation or Pten loss similarly enhance the dominant-stable CTNNB1-induced genetic program to promote granulosa cell tumor development in the ovary and testis. *Oncogene* **31:**1504-1520.

Richards, J. S. and Pangas, S. A. (2010). The ovary: basic biology and clinical implications. *The Journal of clinical investigation* **120:**963-972.

Rico, C., Lague, M. N., Lefevre, P., Tsoi, M., Dodelet-Devillers, A., Kumar, V., Lapointe, E. *et al.* (2012). Pharmacological targeting of mammalian target of rapamycin inhibits ovarian granulosa cell tumor growth. *Carcinogenesis* **33:**2283-2292.

Rilianawati, Kero, J., Paukku, T. and Huhtaniemi, I. (2000). Long-term testosterone treatment prevents gonadal and adrenal tumorigenesis of mice transgenic for the mouse inhibin-alpha subunit promoter/simian virus 40 T-antigen fusion gene. *The Journal of endocrinology* **166:**77-85.

Risma, K. A., Clay, C. M., Nett, T. M., Wagner, T., Yun, J. and Nilson, J. H. (1995). Targeted overexpression of luteinizing hormone in transgenic mice leads to infertility, polycystic ovaries, and ovarian tumors. *Proceedings of the National Academy of Sciences of the United States of America*
92:1322-1326.

Roberts, D. M., Pronobis, M. I., Poulton, J. S., Kane, E. G. and Peifer, M. (2012). Regulation of Wnt signaling by the tumor suppressor adenomatous polyposis coli does not require the ability to enter the nucleus or a particular cytoplasmic localization. *Molecular biology of the cell* **23:**2041-2056.

Robinson, R. S., Woad, K. J., Hammond, A. J., Laird, M., Hunter, M. G. and Mann, G. E. (2009). Angiogenesis and vascular function in the ovary. *Reproduction* **138:**869-881.

Roby, K. F., Taylor, C. C., Sweetwood, J. P., Cheng, Y., Pace, J. L., Tawfik, O., Persons, D. L. *et al.* (2000). Development of a syngeneic mouse model for events related to ovarian cancer. *Carcinogenesis.* **21:**585-591.

Rodriguez, A. and Pangas, S. A. (2016). Regulation of germ cell function by SUMOylation. *Cell and tissue research* **363:**47-55.

Romero, I. L., Gordon, I. O., Jagadeeswaran, S., Mui, K. L., Lee, W. S., Dinulescu, D. M., Krausz, T. N. *et al.* (2009). Effects of Oral Contraceptives or a Gonadotropin-releasing Hormone Agonist on Ovarian Carcinogenesis in Genetically Engineered Mice. *Cancer prevention research* **2:**792-799.

Rosen, D. G., Yang, G., Liu, G., Mercado-Uribe, I., Chang, B., Xiao, X., Zheng, J. *et al.* (2009). Ovarian cancer: pathology, biology, and disease models. *Frontiers in bioscience : a journal and virtual library* **14:**2089-2102.

Ryland, G. L., Hunter, S. M., Doyle, M. A., Rowley, S. M., Christie, M., Allan, P. E., Bowtell, D. D. *et al.* (2013). RNF43 is a tumour suppressor gene mutated in mucinous tumours of the ovary. *The Journal of pathology* **229:**469-476.

Saito, M., Okamoto, A., Kohno, T., Takakura, S., Shinozaki, H., Isonishi, S., Yasuhara, T. *et al.* (2000). Allelic imbalance and mutations of the PTEN gene in ovarian cancer. *International Journal of Cancer* **85:**160-165.

Sakanaka, C., Sun, T. Q. and Williams, L. T. (2000). New steps in the Wnt/beta-catenin signal transduction pathway. *Recent progress in hormone research* **55:**225-236.

Samatar, A. A. and Poulikakos, P. I. (2014). Targeting RAS-ERK signalling in cancer: promises and challenges. *Nature reviews. Drug discovery* **13:**928-942.

Sanchez, A. M., Vigano, P., Quattrone, F., Pagliardini, L., Papaleo, E., Candiani, M. and Panina-Bordignon, P. (2014). The WNT/beta-catenin signaling pathway and expression of survival promoting genes in luteinized granulosa cells: endometriosis as a paradigm for a dysregulated apoptosis pathway. *Fertility and sterility* **101:**1688-1696.

Sánchez, F. and Smitz, J. (2012). Molecular control of oogenesis. *Biochimica et Biophysica Acta (BBA) - Molecular Basis of Disease* **1822:**1896-1912.

Sansom, O. J., Reed, K. R., Hayes, A. J., Ireland, H., Brinkmann, H., Newton, I. P., Batlle, E. *et al.* (2004). Loss of Apc in vivo immediately perturbs Wnt signaling, differentiation, and migration. *Genes & development* **18:**1385-1390.

Sar, M. and Welsch, F. (1999). Differential expression of estrogen receptor-beta and estrogen receptor-alpha in the rat ovary. *Endocrinology* **140:**963-971.

Sargent, K. M., Lu, N., Clopton, D. T., Pohlmeier, W. E., Brauer, V. M., Ferrara, N., Silversides, D. W. *et al.* (2015). Loss of Vascular Endothelial Growth Factor A (VEGFA) Isoforms in Granulosa Cells Using pDmrt-1-Cre or Amhr2-Cre Reduces Fertility by Arresting Follicular Development and by Reducing Litter Size in Female Mice. *PLoS ONE* **10:**e0116332.

Sauer, B. (1998). Inducible Gene Targeting in Mice Using the Cre/loxSystem. *Methods* **14:**381-392.

Schmidt, D., Ovitt, C. E., Anlag, K., Fehsenfeld, S., Gredsted, L., Treier, A. C. and Treier, M. (2004). The murine winged-helix transcription factor Foxl2 is required for granulosa cell differentiation and ovary maintenance. *Development* **131:**933-942.

Schmit, F., Utermark, T., Zhang, S., Wang, Q., Von, T., Roberts, T. M. and Zhao, J. J. (2014). PI3K isoform dependence of PTEN-deficient tumors can be altered by the genetic context. *Proceedings of the National Academy of Sciences of the United States of America* **111:**6395-6400.

Schneikert, J., Vijaya Chandra, S. H., Ruppert, J. G., Ray, S., Wenzel, E. M. and Behrens, J. (2013). Functional Comparison of Human Adenomatous Polyposis Coli (APC) and APC-Like in Targeting Beta-Catenin for Degradation. *PLoS ONE* **8:**e68072.

Scholzen, T. and Gerdes, J. (2000). The Ki-67 protein: from the known and the unknown. *Journal of cellular physiology* **182:**311-322.

Schuler-Toprak, S., Moehle, C., Skrzypczak, M., Ortmann, O. and Treeck, O. (2017). Effect of estrogen receptor beta agonists on proliferation and gene expression of ovarian cancer cells. *BMC Cancer* **17:**319.

Schumer, S. T. and Cannistra, S. A. (2003). Granulosa cell tumor of the ovary. *Journal of clinical oncology* **21:**1180-1189.

Seagle, B. L., Dandapani, M., Yeh, J. Y. and Shahabi, S. (2016). Wnt Signaling and Survival of Women With High-Grade Serous Ovarian Cancer: A Brief Report. *International journal of gynecological cancer* **26:**1078-1080.

Seidman, J. D., Zhao, P. and Yemelyanova, A. (2011). "Primary peritoneal" high-grade serous carcinoma is very likely metastatic from serous tubal intraepithelial carcinoma: assessing the new paradigm of ovarian and pelvic serous carcinogenesis and its implications for screening for ovarian cancer. *Gynecologic oncology* **120:**470-473.

Sekkate, S., Kairouani, M., Serji, B., Tazi, A., Mrabti, H., Boutayeb, S. and Errihani, H. (2013). Ovarian granulosa cell tumors: a retrospective study of 27 cases and a review of the literature. *World Journal of Surgical Oncology* **11:**142.

Shaaban, A. M., Rezvani, M., Elsayes, K. M., Baskin, H., Jr., Mourad, A., Foster, B. R., Jarboe, E. A. *et al.* (2014). Ovarian malignant germ cell tumors: cellular classification and clinical and imaging features. *Radiographics* **34:**777-801.

Shah, S. P., Kobel, M., Senz, J., Morin, R. D., Clarke, B. A., Wiegand, K. C., Leung, G. *et al.* (2009). Mutation of FOXL2 in granulosa-cell tumors of the ovary. *The New England journal of medicine* **360:**2719-2729.

Sharpless, N. E. and Depinho, R. A. (2006). The mighty mouse: genetically engineered mouse models in cancer drug development. *Nature reviews. Drug discovery* **5:**741-754. .

Shen, C., Sheng, Q., Zhang, X., Fu, Y. and Zhu, K. (2016). Hypermethylated APC in serous carcinoma based on a meta-analysis of ovarian cancer. *Journal of Ovarian Research* **9:**60.

Shen, M., Lin, F., Zhang, J., Tang, Y., Chen, W. K. and Liu, H. (2012). Involvement of the up-regulated FoxO1 expression in follicular granulosa cell apoptosis induced by oxidative stress. *The Journal of biological chemistry* **287:**25727-25740.

Shen, M., Liu, Z., Li, B., Teng, Y., Zhang, J., Tang, Y., Sun, S. C. *et al.* (2014). Involvement of FoxO1 in the effects of follicle-stimulating hormone on inhibition of apoptosis in mouse granulosa cells. *Cell death & disease* **5:**e1475.

Sherwood, V. and Leigh, I. M. (2016). WNT Signaling in Cutaneous Squamous Cell Carcinoma: A Future Treatment Strategy? *The Journal of investigative dermatology* **136:**1760-1767.

Shiah, S. G., Shieh, Y. S. and Chang, J. Y. (2016). The Role of Wnt Signaling in Squamous Cell Carcinoma. *Journal of dental research* **95:**129-134.

Shibata, H., Toyama, K., Shioya, H., Ito, M., Hirota, M., Hasegawa, S., Matsumoto, H. *et al.* (1997). Rapid colorectal adenoma formation initiated by conditional targeting of the Apc gene. *Science* **278:**120-123.

Shintani, T., Ihara, M., Tani, S., Sakuraba, J., Sakuta, H. and Noda, M. (2009). APC2 plays an essential role in axonal projections through the regulation of microtubule stability. *The Journal of neuroscience* **29:**11628-11640.

Shintani, T., Takeuchi, Y., Fujikawa, A. and Noda, M. (2012). Directional neuronal migration is impaired in mice lacking adenomatous polyposis coli 2. *The Journal of neuroscience* **32:**6468-6484.

Shiomi-Sugaya, N., Komatsu, K., Wang, J., Yamashita, M., Kikkawa, F. and Iwase, A. (2015). Regulation of secondary follicle growth by theca cells and insulin-like growth factor 1. *The Journal of Reproduction and Development* **61:**161-168.

Shoji, T., Takatori, E., Murakami, K., Kaido, Y., Takeuchi, S., Kikuchi, A. and Sugiyama, T. (2016). A case of ovarian adenosquamous carcinoma arising from endometrioid adenocarcinoma: a case report and systematic review. *Journal of ovarian research* **9:**48.

Sieben, N. L. G., Oosting, J., Flanagan, A. M., Prat, J., Roemen, G. M. J. M., Kolkman-Uljee, S. M., van Eijk, R. *et al.* (2005). Differential Gene Expression in Ovarian Tumors Reveals Dusp 4 and Serpina 5 As Key Regulators for Benign Behavior of Serous Borderline Tumors. *Journal of Clinical Oncology* **23:**7257-7264.

Siegel, R. L., Miller, K. D. and Jemal, A. (2015). Cancer statistics, 2015. *CA: a cancer journal for clinicians* **65:**5-29.

Silva, J. R., Figueiredo, J. R. and van den Hurk, R. (2009). Involvement of growth hormone (GH) and insulin-like growth factor (IGF) system in ovarian folliculogenesis. *Theriogenology* **71:**1193-1208.

Simmons, A. R., Baggerly, K. and Bast, R. C., Jr. (2013). The emerging role of HE4 in the evaluation of epithelial ovarian and endometrial carcinomas. *Oncology* **27:**548-556.

Singer, G., Oldt, R., Cohen, Y., Wang, B. G., Sidransky, D., Kurman, R. J. and Shih, I.-M. (2003). Mutations in BRAF and KRAS characterize the development of low-grade ovarian serous carcinoma. *Journal of the National Cancer Institute* **95:**484-486.

Slattum, G. M. and Rosenblatt, J. (2014). Tumour cell invasion: an emerging role for basal epithelial cell extrusion. *Nature reviews. Cancer* **14:**495-501.

Slot, K. A., Voorendt, M., de Boer-Brouwer, M., van Vugt, H. H. and Teerds, K. J. (2006). Estrous cycle dependent changes in expression and distribution of Fas, Fas ligand, Bcl-2, Bax, and pro-and active caspase-3 in the rat ovary. *Journal of endocrinology* **188:**179-192.

Smalley, M. J. and Dale, T. C. (1999). Wnt Signalling in Mammalian Development and Cancer. *Cancer and Metastasis Reviews* **18:**215-230.

Smith, G., Ng, M. T., Shepherd, L., Herrington, C. S., Gourley, C., Ferguson, M. J. and Wolf, C. R. (2012). Individuality in FGF1 expression significantly influences platinum resistance and progression-free survival in ovarian cancer. *British journal of cancer* **107:**1327-1336.

Smith, P. K., Krohn, R. I., Hermanson, G. T., Mallia, A. K., Gartner, F. H., Provenzano, M. D., Fujimoto, E. K. *et al.* (1985). Measurement of protein using bicinchoninic acid. *Analytical Biochemistry* **150:**76-85.

Smolikova, K., Mlynarcikova, A. and Scsukova, S. (2012). Role of interleukins in the regulation of ovarian functions. *Endocrine regulations* **46:**237-253.

Soriano, P. (1999). Generalized lacZ expression with the ROSA26 Cre reporter strain. *Nature genetics* **21:**70-71.

Staibano, S., Franco, R., Mezza, E., Chieffi, P., Sinisi, A., Pasquali, D., Errico, M. E. *et al.* (2003). Loss of oestrogen receptor beta, high PCNA and p53 expression and aneuploidy as markers of worse prognosis in ovarian granulosa cell tumours. *Histopathology* **43:**254-262.

Stapp, A. D., Gomez, B. I., Gifford, C. A., Hallford, D. M. and Hernandez Gifford, J. A. (2014). Canonical WNT signaling inhibits follicle stimulating hormone mediated steroidogenesis in primary cultures of rat granulosa cells. *PLoS One* **9:**e86432.

Stenwig, J. T., Hazekamp, J. T. and Beecham, J. B. (1979). Granulosa cell tumors of the ovary. A clinicopathological study of 118 cases with long-term follow-up. *Gynecologic oncology* **7:**136-152.

Stewart, C. J., Doherty, D., Guppy, R., Louwen, K. and Leung, Y. C. (2013). β-Catenin and E-cadherin expression in stage I adult-type granulosa cell tumour of the ovary: correlation with tumour morphology and clinical outcome. *Histopathology* **62:**257-266.

Stocco, C., Telleria, C. and Gibori, G. (2007). The Molecular Control of Corpus Luteum Formation, Function, and Regression. *Endocrine Reviews* **28:**117-149.

Stolworthy, T. S. and Black, M. E. (2001). The mouse guanylate kinase double mutant E72Q/D103N is a functional adenylate kinase. *Protein engineering* **14:**903-909.

Su, G., Morris, J. H., Demchak, B. and Bader, G. D. (2014). Biological network exploration with Cytoscape 3. *Current protocols in bioinformatics* **47:**8.13.11-18.13.24.

Suh, D. H., Kim, H. S., Kim, B. and Song, Y. S. (2014). Metabolic orchestration between cancer cells and tumor microenvironment as a co-evolutionary source of chemoresistance in ovarian cancer: A therapeutic implication. *Biochemical pharmacology* **92:**00484-00485.

Sun, J., Zhang, Q., Wang, Z. and Yan, B. (2013). Effects of Nanotoxicity on Female Reproductivity and Fetal Development in Animal Models. *International Journal of Molecular Sciences* **14:**9319-9337.

Suzuki, A., Yamaguchi, M. T., Ohteki, T., Sasaki, T., Kaisho, T., Kimura, Y., Yoshida, R. *et al.* (2001). T Cell-Specific Loss of Pten Leads to Defects in Central and Peripheral Tolerance. *Immunity* **14:**523-534.

Szabova, L., Yin, C., Bupp, S., Guerin, T. M., Schlomer, J. J., Householder, D. B., Baran, M. L. *et al.* (2012). Perturbation of Rb, p53, and Brca1 or Brca2 cooperate in inducing metastatic serous epithelial ovarian cancer. *Cancer research* **72:**4141-4153.

Szklarczyk, D., Franceschini, A., Wyder, S., Forslund, K., Heller, D., Huerta-Cepas, J., Simonovic, M. *et al.* (2015). STRING v10: protein–protein interaction networks, integrated over the tree of life. *Nucleic Acids Research* **43:**D447-D452.

Szklarczyk, D., Morris, J. H., Cook, H., Kuhn, M., Wyder, S., Simonovic, M., Santos, A. *et al.* (2017). The STRING database in 2017: quality-controlled protein-protein association networks, made broadly accessible. *Nucleic Acids Research* **45:**D362-d368.

Taddei, A., Giampietro, C., Conti, A., Orsenigo, F., Breviario, F., Pirazzoli, V., Potente, M. *et al.* (2008). Endothelial adherens junctions control tight junctions by VE-cadherin-mediated upregulation of claudin-5. *Nature cell biology* **10:**923-934.

Takeda, T., Banno, K., Okawa, R., Yanokura, M., Iijima, M., Irie-Kunitomi, H., Nakamura, K. *et al.* (2016). ARID1A gene mutation in ovarian and endometrial cancers (Review). *Oncology reports* **35:**607-613.

Tanwar, P. S., Kaneko-Tarui, T., Lee, H.-J., Zhang, L. and Teixeira, J. M. (2013). PTEN loss and HOXA10 expression are associated with ovarian endometrioid adenocarcinoma differentiation and progression. *Carcinogenesis* **34:**893-901.

Tanwar, P. S., Zhang, L., Kaneko-Tarui, T., Curley, M. D., Taketo, M. M., Rani, P., Roberts, D. J. *et al.* (2011a). Mammalian target of rapamycin is a therapeutic target for murine ovarian endometrioid adenocarcinomas with dysregulated Wnt/beta-catenin and PTEN. *PLoS One* **6:**e20715.

Tanwar, P. S., Zhang, L., Roberts, D. J. and Teixeira, J. M. (2011b). Stromal deletion of the APC tumor suppressor in mice triggers development of endometrial cancer. *Cancer research* **71:**1584-1596.

TCGA. (2012). Comprehensive molecular characterization of human colon and rectal cancer. *Nature* **487:**330-337.

Tennent, B. J., Beamer, W. G., Shultz, L. D. and Adamson, E. D. (1989). Epidermal growth factor receptors in spontaneous ovarian granulosa cell tumors of SWR-derived mice. *International journal of cancer* **44:**477-482.

Testa, J. R., Getts, L. A., Salazar, H., Liu, Z., Handel, L. M., Godwin, A. K. and Hamilton, T. C. (1994). Spontaneous transformation of rat ovarian surface epithelial cells results in well to poorly differentiated tumors with a parallel range of cytogenetic complexity. *Cancer Research* **54:**2778-2784.

The GTEx Consortium. (2013). The Genotype-Tissue Expression (GTEx) project. *Nature genetics* **45:**580-585.

Tirodkar, T. S., Budiu, R. A., Elishaev, E., Zhang, L., Mony, J. T., Brozick, J., Edwards, R. P. *et al.* (2014). MUC1 Positive, Kras and Pten Driven Mouse Gynecologic Tumors Replicate Human Tumors and Vary in Survival and Nuclear Grade Based on Anatomical Location. *PloS one* **9:**e102409.

Tomao, F., Papa, A., Strudel, M., Rossi, L., Lo Russo, G., Benedetti Panici, P., Ciabatta, F. R. *et al.* (2014). Investigating molecular profiles of ovarian cancer: an update on cancer stem cells. *Journal of Cancer* **5:**301-310. .

Tomaselli, S., Megiorni, F., De Bernardo, C., Felici, A., Marrocco, G., Maggiulli, G., Grammatico, B. *et al.* (2008). Syndromic true hermaphroditism due to an R-spondin1 (RSPO1) homozygous mutation. *Human mutation* **29:**220-226.

Tomizuka, K., Horikoshi, K., Kitada, R., Sugawara, Y., Iba, Y., Kojima, A., Yoshitome, A. *et al.* (2008). R-spondin1 plays an essential role in ovarian development through positively regulating Wnt-4 signaling. *Human molecular genetics* **17:**1278-1291.

Treuting, P. M. and Dintzis, S. M. (2011). Comparative Anatomy and Histology: A Mouse and Human Atlas (Expert Consult). Academic Press.

Tsoi, M., Lague, M. N., Boyer, A., Paquet, M., Nadeau, M. E. and Boerboom, D. (2013). Anti-VEGFA Therapy Reduces Tumor Growth and Extends Survival in a Murine Model of Ovarian Granulosa Cell Tumor. *Translational oncology* **6:**226-233.

Tuck, A. R., Mottershead, D. G., Fernandes, H. A., Norman, R. J., Tilley, W. D., Robker, R. L. and Hickey, T. E. (2015). Mouse GDF9 decreases KITL gene expression in human granulosa cells. *Endocrine* **48:**686-695.

Tzivion, G., Dobson, M. and Ramakrishnan, G. (2011). FoxO transcription factors; Regulation by AKT and 14-3-3 proteins. *Biochimica et Biophysica Acta (BBA) - Molecular Cell Research* **1813:**1938-1945.

Uematsu, K. and Huggins, C. (1968). Induction of leukemia and ovarian tumors in mice by pulse-doses of polycyclic aromatic hydrocarbons. *Molecular pharmacology* **4:**427-434.

Uhlen, M., Fagerberg, L., Hallstrom, B. M., Lindskog, C., Oksvold, P., Mardinoglu, A., Sivertsson, A. *et al.* (2015). Proteomics. Tissue-based map of the human proteome. *Science* **347:**1260419.

Uhlenhaut, N. H. and Treier, M. (2011). Forkhead transcription factors in ovarian function. *Reproduction* **142:**489-495.

Usongo, M. (2013). Canonical Wnt signalling in mouse ovarian surface epithelium. *OA Biology* **1:**3-8.

Usongo, M. and Farookhi, R. (2012). β-catenin/Tcf-signaling appears to establish the murine ovarian surface epithelium (OSE) and remains active in selected postnatal OSE cells. *BMC Developmental Biology* **12:**17.

Usongo, M., Li, X. and Farookhi, R. (2013). Activation of the Canonical WNT Signaling Pathway Promotes Ovarian Surface Epithelial Proliferation Without Inducing β-Catenin/Tcf-Mediated Reporter Expression. *Developmental Dynamics* **242:**291-300.

Usset, J. L., Raghavan, R., Tyrer, J. P., McGuire, V., Sieh, W., Webb, P., Chang-Claude, J. *et al.* (2016). Assessment of multifactor gene-environment interactions and ovarian cancer risk: candidate genes, obesity, and hormone-related risk factors. *Cancer epidemiology & prevention biomarkers* **25:**780-790.

Vallabhajosyula, R. R., Chakravarti, D., Lutfeali, S., Ray, A. and Raval, A. (2009). Identifying Hubs in Protein Interaction Networks. *PLoS ONE* **4:**e5344.

van Amerongen, R., Fuerer, C., Mizutani, M. and Nusse, R. (2012). Wnt5a can both activate and repress Wnt/β-catenin signaling during mouse embryonic development. *Developmental biology* **369:**101-114.

van der Horst, P. H., van der Zee, M., Heijmans-Antonissen, C., Jia, Y., DeMayo, F. J., Lydon, J. P., van Deurzen, C. H. *et al.* (2014). A mouse model for endometrioid ovarian cancer arising from the distal oviduct. *International journal of cancer* **135:**1028-1037.

Van Es, J., Kirkpatrick, C., Van de Wetering, M., Molenaar, M., Miles, A., Kuipers, J., Destree, O. *et al.* (1999). Identification of APC2, a homologue of the adenomatous polyposis coli tumour suppressor. *Current biology* **9:**105-S102.

Van Nie, R. (1957). Hormone dependence and hormone production of isografted granulosa-cell tumours in mice. *Acta physiologica et pharmacologica Neerlandica* **5:**495-496.

Vani, B. R., Geethamala, K., Geetha, R. L. and Srinivasa, M. V. (2014). Granulosa cell tumor of ovary: A clinicopathological study of four cases with brief review of literature. *Journal of Mid-Life Health* **5:**135-138.

Visser, J. A., Durlinger, A. L., Peters, I. J., van den Heuvel, E. R., Rose, U. M., Kramer, P., de Jong, F. H. *et al.* (2007). Increased oocyte degeneration and follicular atresia during the estrous cycle in anti-Mullerian hormone null mice. *Endocrinology* **148:**2301-2308.

Vivanco, I. and Sawyers, C. L. (2002). The phosphatidylinositol 3-Kinase AKT pathway in human cancer. *Nature reviews. Cancer* **2:**489-501.

Voloshanenko, O., Erdmann, G., Dubash, T. D., Augustin, I., Metzig, M., Moffa, G., Hundsrucker, C. *et al.* (2013). Wnt secretion is required to maintain high levels of Wnt activity in colon cancer cells. *Nature Communications* **4:2610.**

Walters Haygood, C. L., Arend, R. C., Straughn, J. M. and Buchsbaum, D. J. (2014). Ovarian cancer stem cells: Can targeted therapy lead to improved progression-free survival? *World journal of stem cells* **6:**441-447. .

Wang, H., Galbán, S., Wu, R., Bowman, B., Witte, A., Vetter, K., Galbán, C. J. *et al.* (2013). Molecular Imaging Reveals a Role for AKT in Resistance to Cisplatin for Ovarian Endometrioid Adenocarcinoma. *Clinical cancer research* **19:**158-169.

Wang, H., Paczulla, A. and Lengerke, C. (2015a). Evaluation of stem cell properties in human ovarian carcinoma cells using multi and single cell-based spheres assays. *Journal of visualized experiments : JoVE* e52259.

Wang, L., Mezencev, R., Bowen, N. J., Matyunina, L. V. and McDonald, J. F. (2012). Isolation and characterization of stem-like cells from a human ovarian cancer cell line. *Molecular and cellular biochemistry* **363:**257-268. .

Wang, Y., Chen, J., Yang, W., Mo, F., Senz, J., Yap, D., Anglesio, M. S. *et al.* (2015b). The oncogenic roles of DICER1 RNase IIIb domain mutations in ovarian Sertoli-Leydig cell tumors. *Neoplasia* **17:**650-660.

Wang, Y., Liu, W., Du, J., Yu, Y., Liang, N., Liang, M., Yao, G. *et al.* (2015c). NGF promotes mouse granulosa cell proliferation by inhibiting ESR2 mediated down-regulation of CDKN1A. *Molecular and cellular endocrinology* **406:**68-77.

Wang, Y., Zhang, Z., Lu, Y., Yao, R., Jia, D., Wen, W., LaRegina, M. *et al.* (2008). Enhanced susceptibility to chemical induction of ovarian tumors in mice with a germ line p53 mutation. *Molecular Cancer Research* **6:**99-109.

Waters, H. G. and Green, J. A. (1959). The vascular system of two transplantable mouse granulosa-cell tumors. *Cancer Research* **19:**326-329.

Wei, J.-J., William, J. and Bulun, S. (2011). Endometriosis and Ovarian Cancer: A Review of Clinical, Pathologic, and Molecular Aspects. *International journal of gynecological pathology* **30:**553-568.

Wicha, M. S., Liu, S. and Dontu, G. (2006). Cancer stem cells: an old idea—a paradigm shift. *Cancer research* **66:**1883-1890.

Wilhelm, S. M., Carter, C., Tang, L., Wilkie, D., McNabola, A., Rong, H., Chen, C. *et al.* (2004). BAY 43-9006 exhibits broad spectrum oral antitumor activity and targets the RAF/MEK/ERK pathway and receptor tyrosine kinases involved in tumor progression and angiogenesis. *Cancer research* **64:**7099-7109.

Wu, R., Baker, S. J., Hu, T. C., Norman, K. M., Fearon, E. R. and Cho, K. R. (2013). Type I to type II ovarian carcinoma progression: mutant Trp53 or Pik3ca confers a more aggressive tumor phenotype in a mouse model of ovarian cancer. *The American journal of pathology* **182:**1391-1399.

Wu, R., Hendrix-Lucas, N., Kuick, R., Zhai, Y., Schwartz, D. R., Akyol, A., Hanash, S. *et al.* (2007). Mouse Model of Human Ovarian Endometrioid Adenocarcinoma Based on Somatic Defects in the Wnt/β-Catenin and PI3K/Pten Signaling Pathways. *Cancer Cell* **11:**321-333.

Wu, R., Hu, T. C., Rehemtulla, A., Fearon, E. R. and Cho, K. R. (2011). Preclinical testing of PI3K/AKT/mTOR signaling inhibitors in a mouse model of ovarian endometrioid adenocarcinoma. *Clinical Cancer Research* **17:**7359-7372.

Wu, R., Zhai, Y., Fearon, E. R. and Cho, K. R. (2001). Diverse mechanisms of beta-catenin deregulation in ovarian endometrioid adenocarcinomas. *Cancer Research* **61:**8247-8255.

Wu, R., Zhai, Y., Kuick, R., Karnezis, A. N., Garcia, P., Naseem, A., Hu, T. C. *et al.* (2016). Impact of oviductal versus ovarian epithelial cell of origin on ovarian endometrioid carcinoma phenotype in the mouse. *J Pathol* **240:**341-351.

Wullschleger, S., Loewith, R. and Hall, M. N. (2006). TOR signaling in growth and metabolism. *Cell* **124:**471-484.

Xu, B., Nie, Y., Liu, X., Feng, S., Yang, Z., Wang, Z., Zheng, Q. I. *et al.* (2014). Quantitative analysis of APC promoter methylation in hepatocellular carcinoma and its prognostic implications. *Oncology Letters* **7:**1683-1688.

Xu, Y., Li, X., Wang, H., Xie, P., Yan, X., Bai, Y. and Zhang, T. (2016). Hypermethylation of CDH13, DKK3 and FOXL2 promoters and the expression of EZH2 in ovary granulosa cell tumors. *Molecular Medicine Reports* **14:**2739-2745.

Yamaguchi, K., Huang, Z., Matsumura, N., Mandai, M., Okamoto, T., Baba, T., Konishi, I. *et al.* (2014). Epigenetic determinants of ovarian clear cell carcinoma biology. *International journal of cancer.* **135:**585-597.

Yamashita, K., Yamoto, M., Shikone, T., Minami, S., Imai, M., Nishimori, K. and Nakano, R. (1997). Production of inhibin A and inhibin B in human ovarian sex cord stromal tumors. *American journal of obstetrics and gynecology* **177:**1450-1457.

Yan, W., Rajkovic, A., Viveiros, M. M., Burns, K. H., Eppig, J. J. and Matzuk, M. M. (2002). Identification of Gasz, an evolutionarily conserved gene expressed exclusively in germ cells and encoding a protein with four ankyrin repeats, a sterile-alpha motif, and a basic leucine zipper. *Molecular endocrinology* **16:**1168-1184.

Yang, L., Moss, T., Mangala, L. S., Marini, J., Zhao, H., Wahlig, S., Armaiz-Pena, G. *et al.* (2014). Metabolic shifts toward glutamine regulate tumor growth, invasion and bioenergetics in ovarian cancer. *Molecular Systems Biology* **10:**728.

Ying, L., Zhang, F., Pan, X., Chen, K., Zhang, N., Jin, J., Wu, J. *et al.* (2016). Complement component 7 (C7), a potential tumor suppressor, is correlated with tumor progression and prognosis. *Oncotarget* **7:**86536-86546.

Ying, X., Li-Ya, Q., Feng, Z., Yin, W. and Ji-Hong, L. (2015). MiR-939 promotes the proliferation of human ovarian cancer cells by repressing APC2 expression. *Biomedicine & pharmacotherapy* **71:**64-69.

You, S., Ohmori, M., Peña, M. M. O., Nassri, B., Quiton, J., Al-Assad, Z. A., Liu, L. *et al.* (2006). Developmental abnormalities in multiple proliferative tissues of Apc(Min/+) mice. *International Journal of Experimental Pathology* **87:**227-236.

Yuan, L., Sheng, X., Willson, A. K., Roque, D. R., Stine, J. E., Guo, H., Jones, H. M. *et al.* (2015). Glutamine promotes ovarian cancer cell proliferation through the mTOR/S6 pathway. *Endocrine-related cancer* **22:**577-591.

Yue, F., Cheng, Y., Breschi, A., Vierstra, J., Wu, W., Ryba, T., Sandstrom, R. *et al.* (2014). A comparative encyclopedia of DNA elements in the mouse genome. *Nature* **515:**355-364.

Zaid, T., Thompson, M., Wong, K., Yeung, T., Yeung, Z., Kwan, S., Co, C. *et al.* (2011). Overexpression of fibroblast growth factor 1 and fibroblast growth factor receptor 4 in high-grade serous ovarian carcinoma: Correlation with survival and implications for therapeutic targeting. *Gynecologic Oncology* **120:**S52.

Zambrano, J. N., Neely, B. A. and Yeh, E. S. (2017). Hormonally up-regulated neu-associated kinase: A novel target for breast cancer progression. *Pharmacological research* **119:**188-194.

Zhai, Y., Kuick, R., Tipton, C., Wu, R., Sessine, M., Wang, Z., Baker, S. J. *et al.* (2016). Arid1a inactivation in an Apc- and Pten-defective mouse ovarian cancer model enhances epithelial differentiation and prolongs survival. *The Journal of pathology* **238:**21-30.

Zhang, B., Cai, F. F. and Zhong, X. Y. (2011a). An overview of biomarkers for the ovarian cancer diagnosis. *European Journal of Obstetrics & Gynecology and Reproductive Biology* **158:**119-123.

Zhang, J. Q., Gao, B. W., Wang, J., Ren, Q. L., Chen, J. F., Ma, Q., Zhang, Z. J. *et al.* (2016). Critical Role of FoxO1 in Granulosa Cell Apoptosis Caused by Oxidative Stress and Protective

Effects of Grape Seed Procyanidin B2. *Oxidative medicine and cellular longevity* **2016:**6147345.

Zhang, P., Compagnone, N. A., Fiore, C., Vigne, J. L., Culp, P., Musci, T. J. and Mellon, S. H. (2001). Developmental gonadal expression of the transcription factor SET and its target gene, P450c17 (17alpha-hydroxylase/c17,20 lyase). *DNA and cell biology* **20:**613-624.

Zhang, X. and Hao, J. (2015). Development of anticancer agents targeting the Wnt/β-catenin signaling. *American Journal of Cancer Research* **5:**2344-2360.

Zhang, X., Tang, N., Hadden, T. J. and Rishi, A. K. (2011b). Akt, FoxO and regulation of apoptosis. *Biochimica et Biophysica Acta (BBA) - Molecular Cell Research* **1813:**1978-1986.

Zhao, H., Cui, Y., Dupont, J., Sun, H., Hennighausen, L. and Yakar, S. (2005). Overexpression of the tumor suppressor gene phosphatase and tensin homologue partially inhibits wnt-1-induced mammary tumorigenesis. *Cancer Research* **65:**6864-6873.

Zudova, D., Wyrobek, A. J., Bishop, J. and Marchetti, F. (2004). Impaired fertility in T-stock female mice after superovulation. *Reproduction* **128:**573-581.

9. Appendices

Appendix 1: List of preparations used in the Material and Methods section

1X Tris Borate EDTA (TBE) buffer

10.8 gram Tris base (Fisher Bioreagents, USA) + 5.5 gram Boric acid (Riedel-de Haen, Germany) + 0.585 gram EDTA (Sigma-Aldrich, USA) in 1000 ml ultrapure water (Sigma, USA), pH: 8

Sterile saline solution

0.9 g of sodium chloride (Sigma, USA) dissolved in 100 ml distilled water and autoclaved

1X Citrate buffer

2.94 g Sodium citrate tribasic dihydrate (Sigma, USA) in 1000 ml distilled water, pH: 6

1X TBST buffer

6.05 gram of tris base (Fisher Bio reagents, USA) + 8.76 gram of sodium chloride (Sigma, USA) in 1000 ml distilled water+ 1 ml of Tween 20 (Sigma, USA) , pH: 7.4

0.1% sterile gelatine solution

100 mg gelatine (Sigma, USA) dissolved in 100 ml of sterile 1X PBS (Gibco, Life Technologies, USA), sterilized by autoclaving

Appendix 2: Expression levels of APC2 in *Apc2*$^{+/+}$ and *Apc2*$^{-/-}$ mice

Upon starting this project, knowing that the only antibody previously used by Dr. Carl Daly to differentiate between *Apc2* different genotypes by immunohistochemistry was discontinued by the manufacturer, many techniques were attempted. The *Apc2*$^{-/-}$ mouse was a gift from the Clevers lab who did not reveal the exact genetic structure of the *Apc2*$^{-}$ construct inserted into the mouse embryonic cells. Dr. Karen Reed personal communication with the Clevers group revealed uncertainty about the method and the site of the genetic alteration in the *Apc2* gene. However, they suggested that the genetic alteration they had performed was in *Apc2* exon 13, a 215 bp exon present before the large terminal exon 14 (4990 bp).

Gene expression analysis of *Apc2* was first attempted. RNA was extracted from ovaries and cDNA was used for qRT-PCR assay. The first gene expression analysis performed was a Taqman gene expression assay using an *Apc2* mouse Taqman probe which spans exon junction between exons 13 and 14. This assay confirmed the presence of *Apc2* mRNA in the whole ovarian tissue. There was a significant change in *Apc2* expression between *Apc2*$^{+/+}$ and *Apc2*$^{-/-}$ mice, surprisingly a 16-fold increase of *Apc2* expression in *Apc2*$^{-/-}$ mice as compared to *Apc2*$^{+/+}$ mice. Subsequent gene expression analysis was performed using the SYBR Green gene expression assay, which enables the design of primers to target the amplification of specified sequences. Gene expression analysis using primers specific for exon 13 (one designed to amplify the beginning of the exon, the other one to amplify the end of the exon) of the *Apc2* mRNA resulted in a 10±1 folds increase of *Apc2* expression levels in *Apc2*$^{-/-}$ mice as compared to *Apc2*$^{-/-}$ mice. However, when performing the expression analysis using primers specific for exon 14, a comparable expression was observed in the 2 genotypes (Figure A2.1).

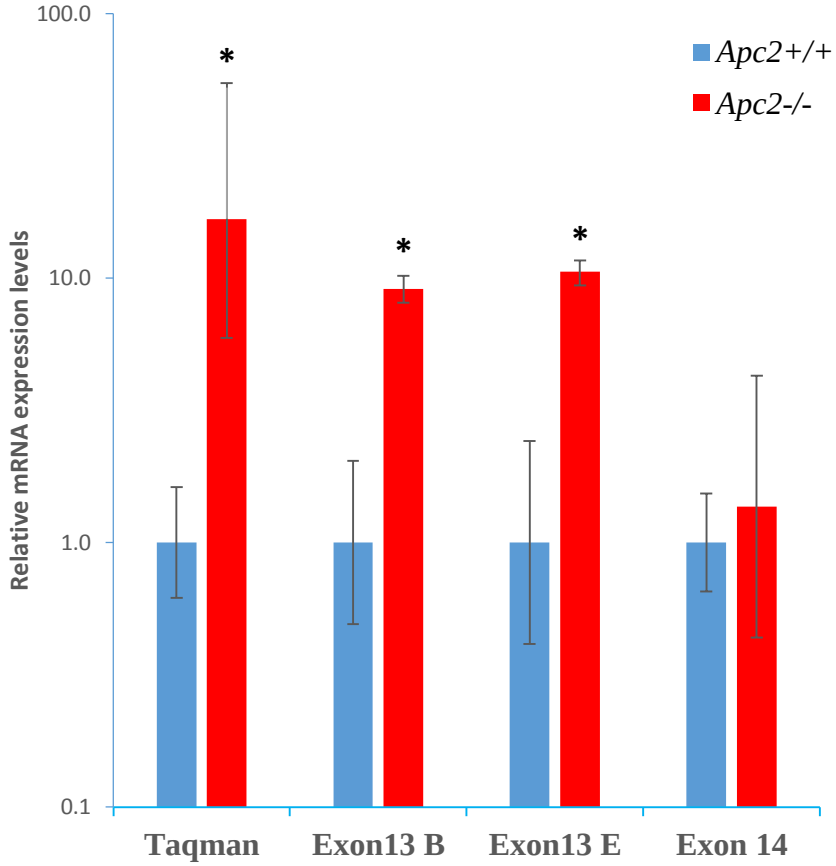

Figure A2.1: Gene expression levels of *Apc2* in $Apc2^{-/-}$ vs. $Apc2^{+/+}$ ovaries was performed by qRT-PCR and normalized to *Actb* expression using Taqman probe, or primers designed specifically for exon 13 (B: beginning, E: end) or exon 14. Data are shown as mean±95% confidence intervals of relative mRNA expression levels, n=3-4. Statistical significance was determined according to Cumming *et al.* (Cumming *et al.* 2007). * denotes significance from $Apc2^{+/+}$ at $p<0.05$.

In order to visualize APC2 expression pattern in the ovary, immunohistochemistry was attempted using 3 different antibodies (A2.2a). But, because there were no difference in the protein expression staining patterns between $Apc2^{+/+}$ and $Apc2^{-/-}$ ovaries, these antibodies were not considered reliable for use in immunohistochemistry, and could not be used to describe expression patterns of APC2 in the ovary. These antibodies were then tried for western blotting using Hela cells as a positive control. The Abcam APC2 antibody (ab113370) was the only

antibody which gave a protein band of the expected size (240 kDa). Protein samples were then prepared from *Apc2*$^{+/+}$ and *Apc2*$^{-/-}$ ovaries and used for APC2 protein detection by western blotting. However, owing to the very low expression levels of APC2 in the ovaries, no bands were detected. Because *Apc2*$^{-}$ allele is constitutive, brain protein extracts were used to confirm differences in APC2 protein levels between *Apc2*$^{+/+}$ and *Apc2*$^{-/-}$, as APC2 is highly expressed in the brain. A band of size equivalent to APC2 protein was detected in *Apc2*$^{+/+}$ brain, but not in *Apc2*$^{-/-}$ brain (Figure A2.2b).

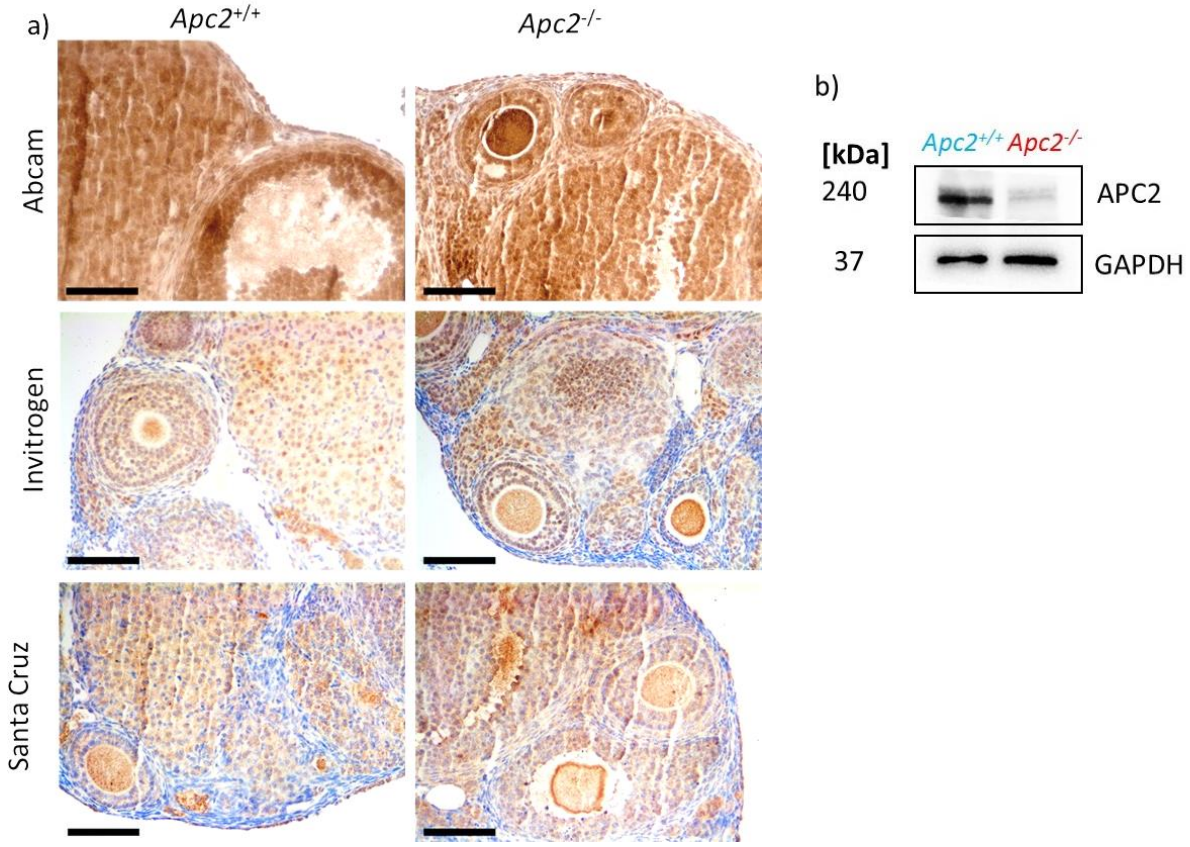

Figure A2.2: Protein expression of APC2 in *Apc2*$^{+/+}$ and *Apc2*$^{-/-}$ mice by (a) immunohistochemistry of ovaries using 3 different antibodies from Abcam, Invitrogen and Santa Cruz. Scale bars: 100 µm. (b) western blotting of brain tissue using Abcam APC2 antibody. GAPDH was used as a loading control protein.

Appendix3: *Apc2*$^{-}$ allele sequencing

To characterize the site of genetic manipulation in *Apc2*$^{-}$ allele, the genotyping primer pair provided by the Clevers lab (primer pair 1, Table 3.10) was first blasted using Primer-Blast program to detect the target template, but no templates were detected, implying that the primer is designed specifically to target *Apc2*$^{-}$ genetic construct. Following this, the primer pair was used to amplify genomic DNA extracted from *Apc2*$^{-/-}$ mouse, and the amplified DNA was sent to Eurofins genomic services for sequencing (Figure A3.1a). Blasting sequencing results revealed that the sequence was mostly aligned to exon 14 (starting at base 265 and ending at base 762) of mouse *Apc2*, apart from the first 15 bp which were not aligned to exon 14. Instead, this short fragment showed 100% alignment with a range of cloning vectors, suggesting that the cloning vector insert is present in exon 14.

To determine the sequence of the insert used for cloning to define its effect on *Apc2* gene and protein production in the '*Apc2*$^{-/-}$' mouse, another forward primer complementary to exon 13 was designed and used together with the same reverse primer (designed by Clevers lab) to amplify genomic DNA from *Apc2*$^{-/-}$ mouse (primer pair 2, Table 3.10). Gel electrophoresis revealed that the size of this region was approximately 4500 bp, 1800 bp larger than the *Apc2*$^{+/+}$ amplicon (Figure A3.1b). The amplified DNA was sent to Eurofins genomic services for sequencing, and sequence results revealed that the first half of intron 13-14 is intact and completely aligned to the published mouse *Apc2* gene sequence. Forward primers complementary to the intron were designed and used together with the same reverse primer to further amplify and sequence this region. However, either multiple bands or no bands were detected. As a result, a primer-walking project was performed by Eurofins genomic sequencing, and the full length of the amplified region (starting at exon 13 and ending by base 762 of exon 14) was sequenced (Figure A3.2). Sequencing results revealed that the full length of exon 13, intron 13-14 and first 204 bases of exon 14 were intact. However, a targeting vector

(containing a neomycin cassette and 2 loxP sites) was inserted following base 204 of exon 14. 60 bases of exon 14 were deleted in the *Apc2*$^{-}$ allele (base 205-264), after which the remaining sequence aligned again with *Apc2* exon 14 mouse sequence (base 265-762) (Figure A3.3). Gene targeting caused a frame shift mutation resulting in pre-mature stop codon in the mRNA, consequently translated to a truncated protein (formed of the first 671 (of 2274) amino acids of mouse APC2 protein) (Figure A3.4). This truncated protein lacked important functional conserved domains such as one of the six armadillo repeats (mediate interaction between APC2 and β-catenin), SAMP motif (binds to Axin), and APC basic domain (interacts with microtubules), as extracted from conserved domain database (Marchler-Bauer *et al.* 2017) (Figure A3.5).

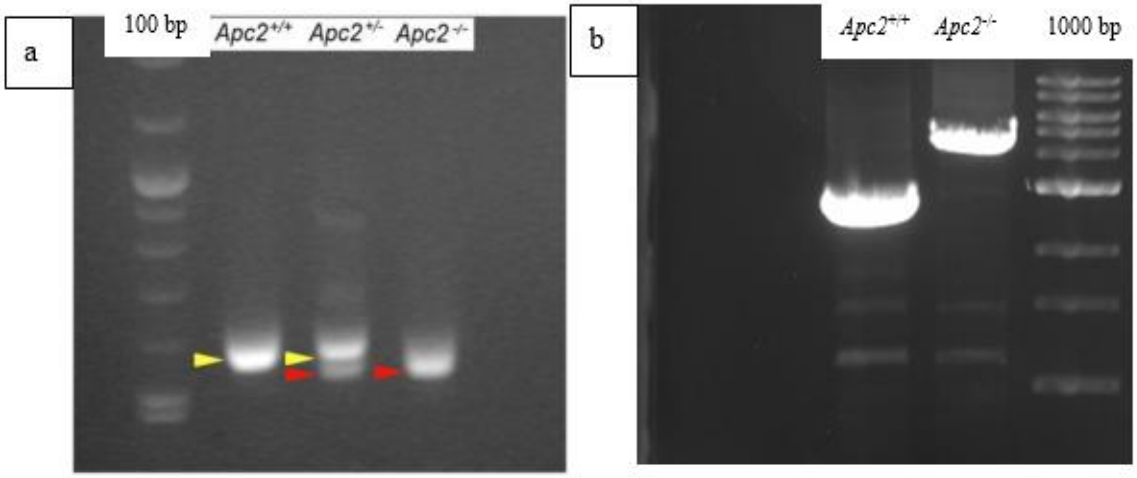

Figure A3.1: Gel electrophoresis of *Apc2* DNA amplified using (a) the genotyping primers (Primer pair 1, Table 3.10), and (b) primers designed to amplify the sequence beginning from exon 13 to exon 14 (primer pair 2, Table 3.10).Yellow arrowhead: *Apc*$^{+}$ PCR fragment (size: 580 bp). Red arrowhead: *Apc*$^{-}$ PCR fragment (size 495: bp). Picture (a) was produced by Dr. Carl Daly

ctgtcagcacacagcacagagaacaaggcagccatctgccaggtagatggtgcactgggtttcctggtgagcaccctcacataccgtt
gccaagggaactccctggcagtcatcgagagtggcggtgggatcctgcgcaacgtgtcaagcctcattgccacacgggaggactac
aggtcagctcccatcacgatccacccaaatcacagaggccgggaatgggagatggtgggggagcagtggctgctcttgcagagaa
cctgggtttggttgtcagcactgcatggtgacacacaaacacccttaactccagttccacgggatcctgtgccctcttcttacatccgtgg
gcaccaggcacacatgtggcacacagacaaacatccaggcataacaaccatacacagagtataacataaaccacattactagataat
gttcataataaggcagacgtggcagggcgtgatccccatcccagcacccgggaagcagagagaggatgccctacaagtctaaggc
cagcctggtttctagcaagttctaggccagtcaggactgtcaaatgagatctttcctcaaggccaggtatggtgtgtgtctcagtaactgt
ccatatgtgccactttgttcccagcactcgggggtgggcggctcaccacatgtgacttcagttccagggccctgccactcccttctgctg
ctggtgggcacttcacacatggtgcacagacagacacacacccgtacacatgaaataaaatgacaggaattttaaagttgggctgaag
agatggctcagtggttaagagcactgactgctcttccaaaggtcctgagttcagttcccagcaaccacatggtgtctcacaaccatctgt
aatgggatctgatgtcctcttctggtgcatcttatacataaaatcataaaataaataaataatttttttttggtttttgagacccctagctgtctt
ggaactcattctgtagaccaggcttgcctcaaactcagaaatctgcctgtctctgcctcccaagtgctgggattaaaggtgtgcgacacc
actgcccagaaaataaatctttttaaaaaaatacttttaaaattaagtcttaaaaacaaatgagccgggcgtggtggcacacacctttaatc
ccagcacttgggaggcagagacaggcggattttggagtccgaggccatcctggtctatagagtgagtttcaggacagcgagggctac
acagagaaaccttgtctcgaaaaacaaaaaagtcttaaaaacaaaccaaatatataacccagatatggaggtacaggacacacaccta
taaacctggcacaggaaagccaccttcagctagctatggagtttaaagttagcctcggcttgctcagacccttcctcaaaacaaaacaa
acccaaacagctgcggggaatcacgcagcgcggctgggaaagcttacggtatagctattttatttttttctcaaattcacacctaaaggat
ggacattttaatctgctatagaggttctagtcttgtgtggtgggcggggcgtgtaggggcatggctaagccttgctagcaagctggggtc
gttcagctagtgggggtaaagtggaggtgggcatggttgagcacaggcttgacaggtcggtatggaccgggcggggcggggcgg
ggcggggcaagccaaggggcatagcgaggcagtgttgtgattggctgagcggggtcatcacaggcaggggtgaacctgatttactt
ggttggctaagagttcagcaaggtagaggtgagtatagcggagatggggatatgggtgggcatgactgaacaaagggcatagctag
gctagaggagtggctgagtcaggcaagcatggctgggctggggctgctgggctggggaccttgggagaggagctctcatgtagggt
gtggcaggaatggcagtgtgatgtggatggtgagcactgcaggactggagtaaagcccacctttttttcctctgggtttccccaggcag
gtgctccgtgaccacaactgcctgcagacactgctgcagcacctcacatcacacagtttgaccatcgtgagcaatgcctgtggcaccct
ctggaacctgtctgcccgcagcccccgcgatcaggaactgttgtgggacctgggggccgtgggcatgctacgcaacctcgtccactc
caaacacaagatgatcgccatgggccgctctagctagaactagtggatccggaacccttaatataacttcgtataatgtatgctatacga
agttattaggtccctcgacctgcagcccaagctgatcctctagtcgagccccagctggttctttccgcctcagaagccatagagcccac
cgcatccccagcatgcctgctattgtcttcccaatcctccccctttgctgtcctgccccacccccacccccccagaatagaatgacacctact
cagacaatgcgatgcaatttcctcattttattaggaaaggacagtgggagtggcaccttccagggtcaaggaaggcacgggggaggg
gcaaacaacagatggctggcaactagaaggcacagtcgaggctgatcagcgagctctagctagagaattgatcccctcagaagaact
cgtcaagaaggcgatagaaggcgatgcgctgcgaatcgggagcggcgataccgtaaagcacgaggaagcggtcagcccattcgc
cgccaagctcttcagcaatatcacgggtagccaacgctatgtcctgatagcggtccgccacacccagccggccacagtcgatgaatc
cagaaaagcggccattttccaccatgatattcggcaagcaggcatcgccatgggtcacgacgagatcatcgccgtcgggcatgcgcg
ccttgagcctggcgaacagttcggctggcgcgagcccctgatgctcttcgtccagatcatcctgatcgacaagaccggcttccatccg
agtacgtgctcgctcgatgcgatgtttcgcttggtggtcgaatgggcaggtagccggatcaagcgtatgcagccgccgcattgcatca
gccatgatggatactttctcggcaggagcaaggtgagatgacaggagatcctgccccggcacttcgcccaatagcagccagtcccttc
ccgcttcagtgacaacgtcgagcacagctgcgcaaggaacgcccgtcgtggccagccacgatagccgcgctgcctcgtcctgcagt
tcattcagggcaccggacaggtcggtcttgacaaaaagaaccgggcgcccctgcgctgacagccggaacacggcggcatcagagc
agccgattgtctgttgtgcccagtcatagccgaatagcctctccacccaagcggccggagaacctgcgtgcaatccatcttgttcaatg
gccgatcccatattggctgcaggtcgaaaggcccggagatgaggaagaggagaacagcgcggcagacgtgcgcttttgaagcgtg
cagaatgccgggcctccggaggaccttcgggcgcccgccccgcccctgagcccgcccctgagcccgccccccggacccaccccctt
cccagcctctgagcccagaaagcgaaggagcaaagctgctattggccgctgccccaaaggcctacccgcttccattgctcagcggtg
ctgtccatctgcacgagactagtgagacgtgctacttccatttgtcacgtcctgcacgacgcgagctgcggggcgggggggaacttcc
tgactaggggaggagtagaaggtggcgcgaaggggccaccaaagaacggagccggttggcgcctaccggtggatgtggaatgtg
tgcgaggccagaggccacttgtgtagcgccaagtgcccagcggggctgctaaagcgcatgctccagactgccttgggaaaagcgc
ctcccctacccggtagaattccgatcatattcaataacccttaatataacttcgtataatgtatgctatacgaagttattaggtctgaagagg
agtttacgtccagccaagcttatcgataccgtcgacctcgacatggctgtctccccaggcacctgcgtgcccagtctttacgtccgcaag
cagagggctctggaagctgagttggacactcggcacctggtgcatgcactcggtcacttagagaagcagagtctgcctgaggcaga
gaccacttcaaagaagcccctgccacccctccgccacctggacgggctggtgcaggactatgcctctgattctggctgctttgacgat
gatgatgcaccatccctggctgctgctgccaccacagctgagcccgccagcccagcagtgatgtctatgttccttggcggtcccttcctt
cagggccaggcactggcccgcaccccacctgcccgccagggtggcctagaagccgagaaggaggctggtggggaggcagctgt
ggctgccaaggccaaggccaagctggcgttggctgtggctcggatcgacagattggtggaggacatctctgccctgcacacctcatc

Figure A3.2: Sequence of *Apc2*$^{-}$ region amplified using primer pair 2 (See Table 3.10)

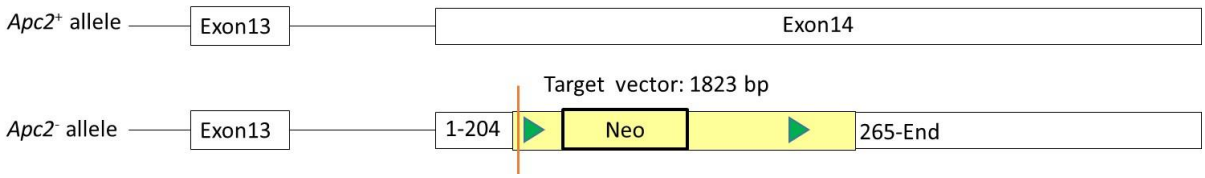

Figure A3.3: Schematic diagram of the structure of *Apc2* wild type (*Apc2*$^{+}$) and mutant (*Apc2*$^{-}$) alleles. Orange line: place of stop codon. Green triangles: loxP sites. Yellow: Target vector construct. Neo: Neomycin.

MTSSMASYEQLVRQVEALKAENTHLRQELRDNSSHLSKLETETSGMKEVLKHLQGK
LEQEARVLVSSGQTEVLEQLKALQTDISSLYNLKFHAPALGPEPAARTPEGSPVHGSG
PSKDSFGELSRATIRLLEELDQERCFLLSEIEKEEKEKLWYYSQLQGLSKRLDELPHV
DTFSMQMDLIRQQLEFEAQHIRSLMEERFGTSDEMVQRAQIRASRLEQIDKELLEAQ
DRVQQTEPQALLAVKPVAVEEEQEAEVPTHPEDGTPQPGNSKVEVVFWLLSMLATR
DQEDTARTLLAMSSSPESCVAMRRSGCLPLLLQILHGTEAGSVGRAGIPGAPGAKDA
RMRANAALHNIVFSQPDQGLARKEMRVLHVLEQIRAYCETCWDWLQARDSGTETP
VPIEPQICQATCAVMKLSFDEEYRRAMNELGGLQAVAELLQVDYEMHKMTRDPLNL
ALRRYAGMTLTNLTFGDVANKATLCARRGCMEAIVAQLGSESEELHQVVSSILRNLS
WRADINSKKVLREVGSMTALMECVLRASKESTLKSVLSALWNLSAHSTENKAAICQ
VDGALGFLVSTLTYRCQGNSLAVIESGGGILRNVSSLIATREDYSLQTLLQHLTSHSL
TIVSNACGTLWNLSARSPRDQELLWDLGAVGMLRNLVHSKHKMIAMGRSS*

Figure A3.4: Amino acid sequence of truncated APC2 protein formed in *Apc2*$^{-/-}$ mice. Amino acids in red are those translated because of the frame shift mutation.* denotes end of protein (equivalent to stop codon)

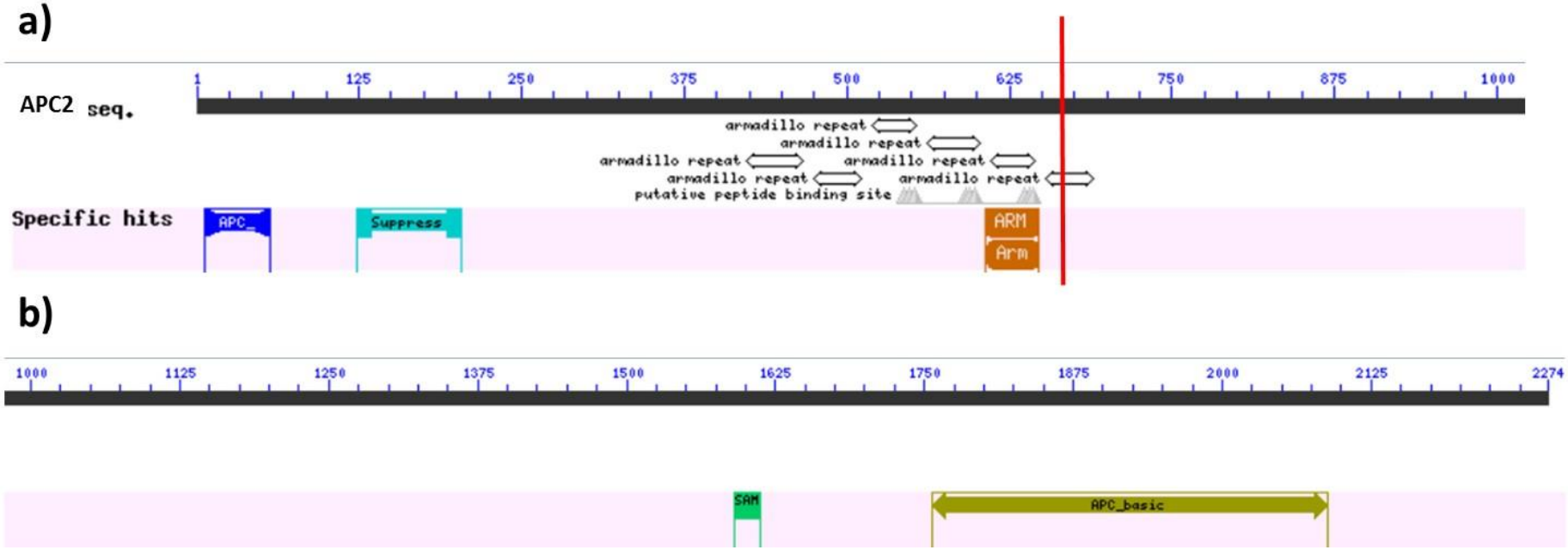

Figure A3.5: Conserved domains of mouse APC2 protein in (a) first 1000 amino acid sequence of the APC2 protein. Red line: Place of truncation in APC2 protein produced by *Apc2*$^{-/-}$ mouse, and (b) remaining amino acid sequence of the APC2 protein. APC-: coiled-coil N-terminus of APC. Suppress: APC suppressor protein. ARM/Arm: armadillo/β-catenin-like repeats. SAM: SAMP motif. APC basic: APC basic domain.(Marchler-Bauer *et al.* 2017)

Appendix 4: Expression levels of Wnt-target genes in the OSE

In order to determine whether APC2 loss activates WNT signalling in the OSE, expression levels of a subset of Wnt target genes were identified. OSE was isolated from *Apc2*$^{+/+}$ and *Apc2*$^{-/-}$ ovaries (Section 3.4.8), and cultured for 3-4 days until reaching confluency (Section 3.9.1). Cells were trypsinized, washed (Section 3.9.2) and collected in Eppendorf tubes. RNA was extracted from these cells using RNeasy plus micro kit (Qiagen, USA). The extracted RNA was used to prepare cDNA prior to performing gene expression analysis (Section 3.6). No significant differences were observed in the expression levels of all genes analysed (Figure A4.1)

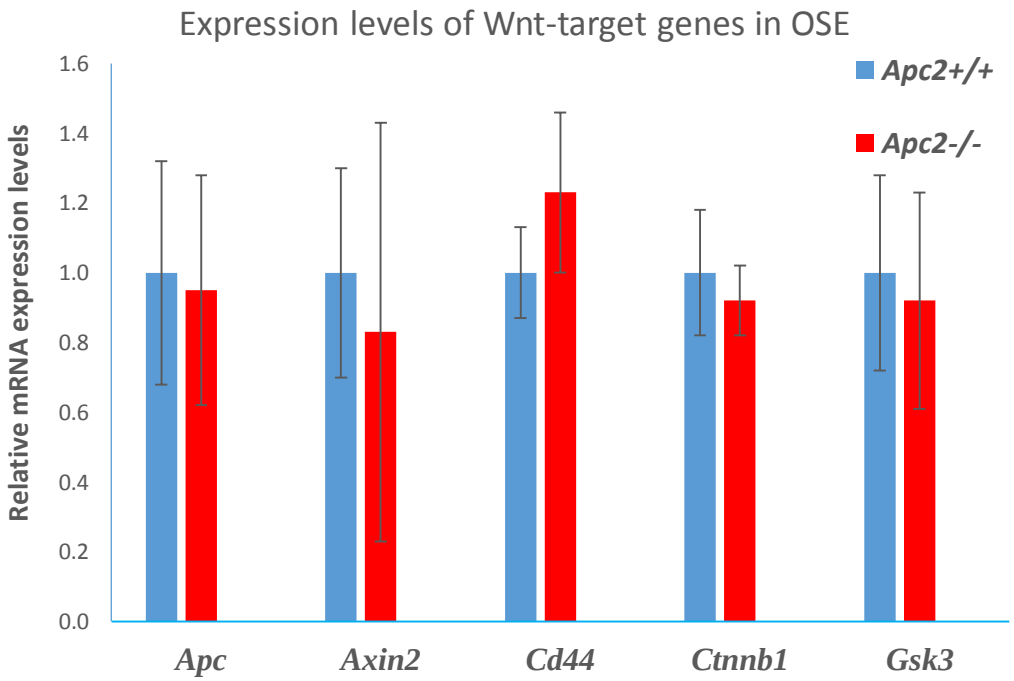

Figure A4.1: APC2 loss does not activate canonical WNT signalling in the OSE. Expression levels of a subset of Wnt-target genes were compared between *Apc2*$^{+/+}$ and *Apc2*$^{-/-}$ OSE extracts using qRT-PCR and normalized to *Actb* expression. Data are shown as mean±S.E. n=3. Statistical significance was determined by t-test.

Appendix 5: Recombination of floxed genes in the OSE post-adenovirus-*cre* injection (Previous work performed by Dr. Carl Daly)

Preliminary experiments were performed by Dr. Carl Daly to confirm that recombination of floxed genes post adenovirus-*cre* intrabursal injections are confined to the OSE. First, a ROSA26 *cre* reporter strain (Soriano 1999) was induced by intrabursal adenovirus-*cre* injection to check *cre*-mediated recombination in the OSE, which induces the expression of a *lacZ (β-galactosidase)* gene. Whole ovaries were dissected and incubated with X-gal to check for lacZ activity. LacZ positivity (blue staining) indicated that recombination events had occurred in the ovarian surface post-induction (Figure A5.1 left panel). Fluorescent immunohistochemistry with a β-galactosidase antibody revealed recombination had occurred exclusively in the OSE (Figure A5.2 right panel). Following this, an $Apc^{fl/fl}$ mouse was induced by intrabursal injection of adenovirus-*cre* to check recombination of floxed *Apc*. Fluorescent immunohistochemistry against APC on sections from $Apc^{fl/fl}$ ovaries post-adenovirus *cre* induction reflected the loss of APC protein exclusively in cells of the OSE (Figure A5.2).

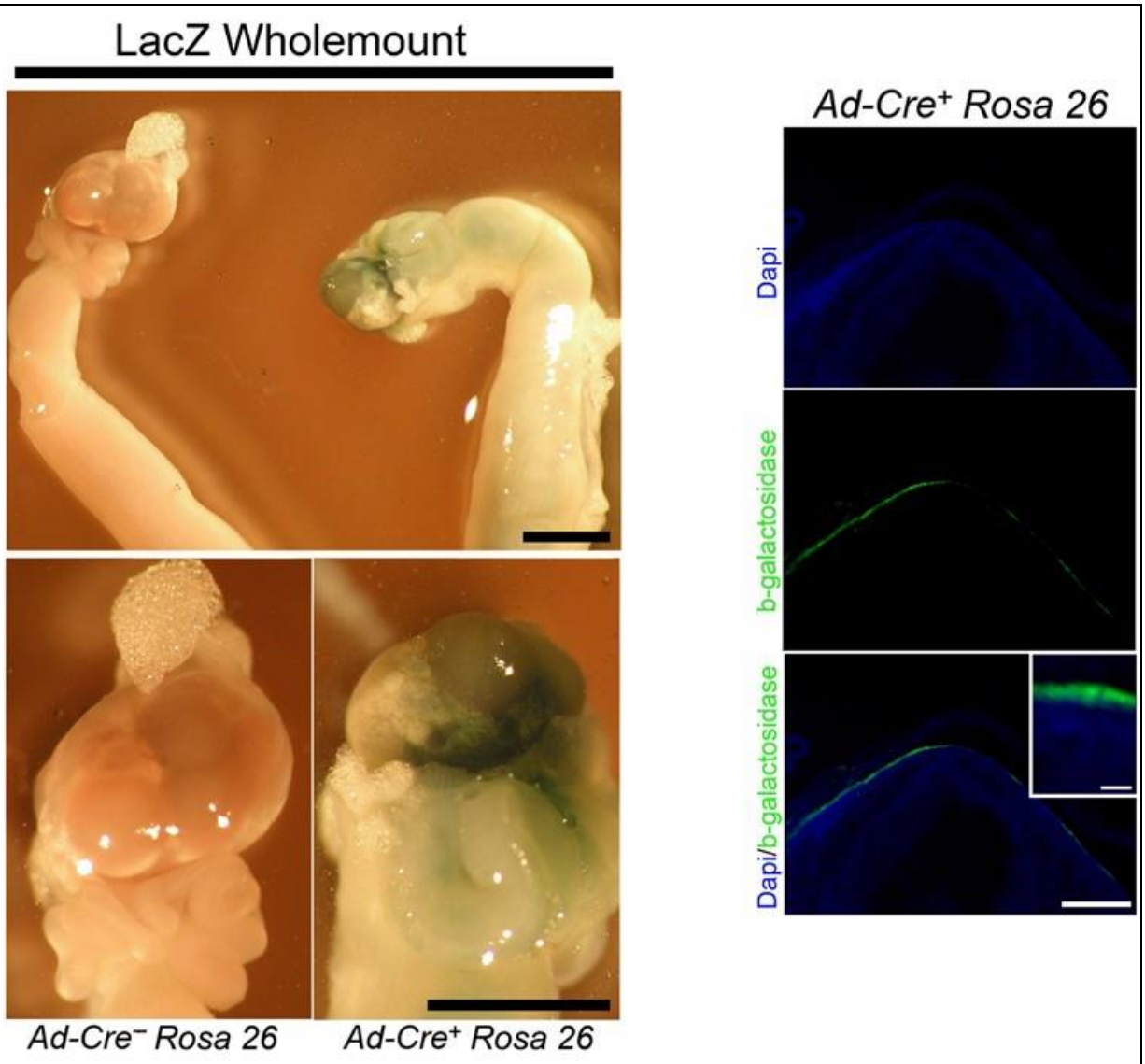

Figure A5.1: Intrabursal injection of adenovirus-*cre* successfully induced the recombination of floxed β-galactosidase gene in Rosa26 reporter mice. Whole mount ovaries (left panel) showing blue staining with post X-gal incubation only in adenovirus-*cre* injected ovary. Scale bar 2 mm. Fluorescent immunohistochemistry (right panel) post-adenovirus *cre* injection revealed that β-galactosidase staining was only present in the OSE compartment of the ovary. Scale bar 200µm. All pictures were produced by Dr. Carl Daly.

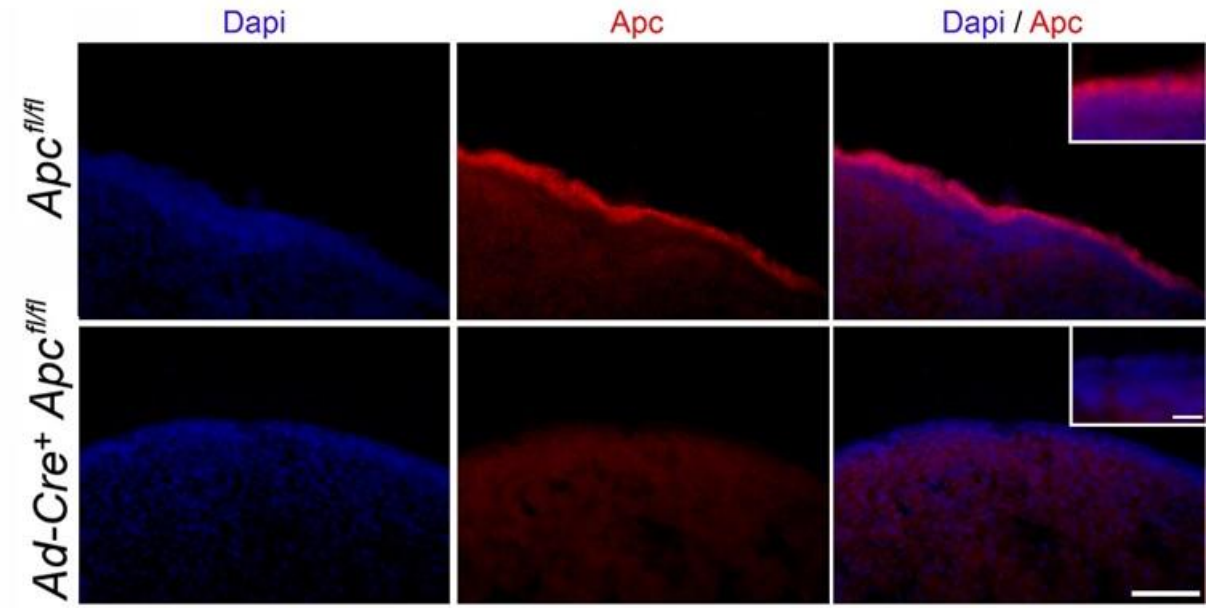

Figure A5.2: APC protein is absent from the OSE post-adenovirus *cre* injection. APC protein is present in the OSE of non-induced $Apc^{fl/fl}$ ovaries (middle upper panel). However, it is lost post-adenovirus *cre* injection (middle lower panel). Scale bar 100 µm. All pictures were produced by Dr. Carl Daly.

Appendix 6: phospho-histone 3 protein expression analysis in Ad-*cre* *Pten*$^{fl/fl}$/*Apc*$^{fl/fl}$ OEA post-APC2 loss

As illustrated in Figure 6.28, there were no significant differences in proliferation between *Apc2*$^{+/+}$ and *Apc2*$^{-/-}$ Ad-*cre* *Pten*$^{fl/fl}$/*Apc*$^{fl/fl}$ tumours when assessed by Ki67 immunohistochemistry. It is known that Ki67 marks cells at any stage of the cell cycle, which does not necessarily mean that these cells are mitotic (Scholzen and Gerdes 2000). In order to visualize and quantify mitotic cells, phospho-histone 3 (pH3) immunohistochemistry was performed. A 2-fold change was observed in the number of mitotic cells in *Apc2*$^{+/+}$ vs. *Apc2*$^{-/-}$ Ad-*cre* *Pten*$^{fl/fl}$/*Apc*$^{fl/fl}$ tumours (48.5±1.99 vs. 24.1±2.2, mean±S.E., n=3, $p<0.05$, Figure A6.1). It was observed that cells with squamous differentiation present in keratinized areas of *Apc2*$^{-/-}$ Ad-*cre* *Pten*$^{fl/fl}$/*Apc*$^{fl/fl}$ tumours, although positively staining for Ki67, are not mitotic (negatively staining for pH3) (Figure A6.2). This might indicate that squamous metaplasia of OEA cells post-APC2 loss is one of the mechanisms causing reduced tumour growth, by inhibiting mitosis.

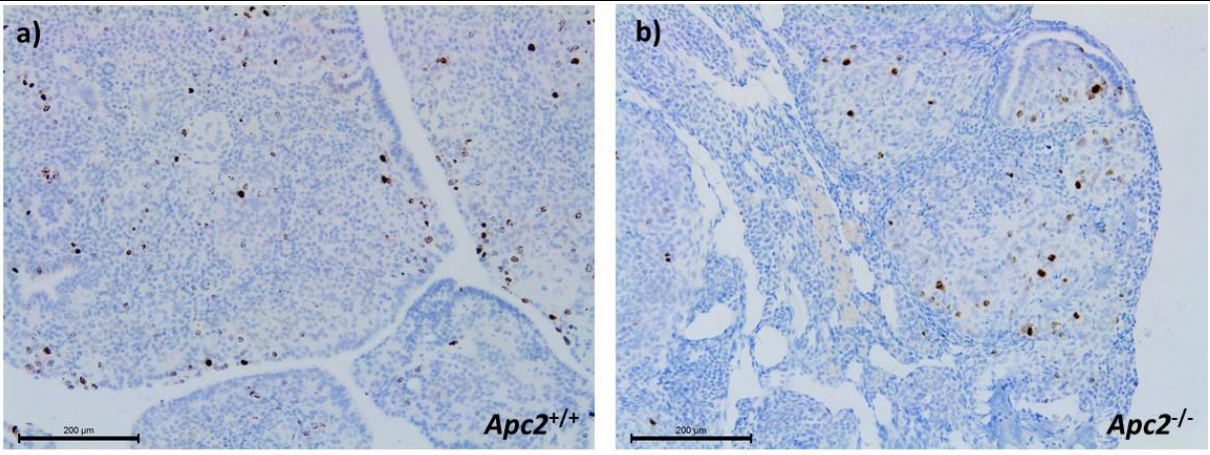

Figure A6.1: phospho-histone 3 expression is reduced in Ad-*cre* *Pten*$^{fl/fl}$/*Apc*$^{fl/fl}$ tumours post-APC2 loss. Representative photomicrographs of phospho-histone 3 in (a) *Apc2*$^{+/+}$, and (b) *Apc2*$^{-/-}$ Ad-*cre* *Pten*$^{fl/fl}$/*Apc*$^{fl/fl}$ tumours collected 8-weeks post-induction. n=3. Scale bar 200 µm.

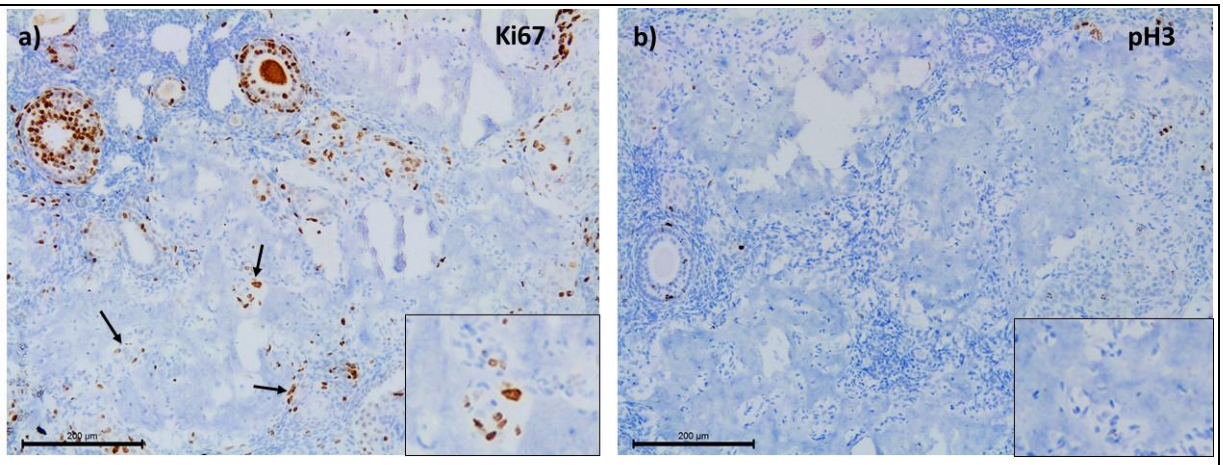

Figure A6.2: Squamous differentiated cells in keratinized areas in APC2-deficient Ad-*cre* *Pten*$^{fl/fl}$/*Apc*$^{fl/fl}$ tumours are not mitotic. Representative photomicrographs of (a) Ki67, and (b) pH3 immunohistochemistry in *Apc2*$^{-/-}$ Ad-*cre* *Pten*$^{fl/fl}$/*Apc*$^{fl/fl}$ tumours. Black arrows: Ki67 positive cells. Insets show 2X original magnification. n=3. Scale bars 200 µm.

Appendix 7: *Axin2* RNAscope in Ad-*cre* $Pten^{fl/fl}/Apc^{fl/fl}$ OEA.

As illustrated in Figure 6.31, β-catenin immunostaining was very intense in all tumours irrespective of genotype. Another way of visualizing WNT signalling activation in tumours was attempted, by visualizing *Axin2* RNA expression patterns using the novel *in situ* hybridization technology RNA scope (ACD Biotechne, Canada). $Apc2^{+/+}$ and $Apc2^{-/-}$ Ad-*cre* $Pten^{fl/fl}/Apc^{fl/fl}$ tumour tissue sections were hybridized to mouse *Axin2* RNAscope probe (ACD biotechne, catalogue number 400331). Expression analysis revealed comparable expression of *Axin2* in $Apc2^{+/+}$ and $Apc2^{-/-}$ tumours, which was intense and patchy, irrespective of genotype (Figure A7.1). As mentioned previously (Section 6.2.5), epithelial glands were more abundant and packed together in areas of $Apc2^{+/+}$ Ad-*cre* $Pten^{fl/fl}/Apc^{fl/fl}$ tumours, in contrast to $Apc2^{-/-}$ Ad-*cre* $Pten^{fl/fl}/Apc^{fl/fl}$ tumours which mostly displayed reduced discrete glands. It was observed that areas of glandular differentiation in $Apc2^{+/+}$ Ad-*cre* $Pten^{fl/fl}/Apc^{fl/fl}$ tumours display reduced *Axin2* expression, as compared to $Apc2^{-/-}$ Ad-*cre* $Pten^{fl/fl}/Apc^{fl/fl}$ tumours (Figure A7.1). This might indicate that sustained levels of activated WNT signalling in $Apc2^{-/-}$ Ad-*cre* $Pten^{fl/fl}/Apc^{fl/fl}$ tumours attenuates epithelial glandular differentiation.

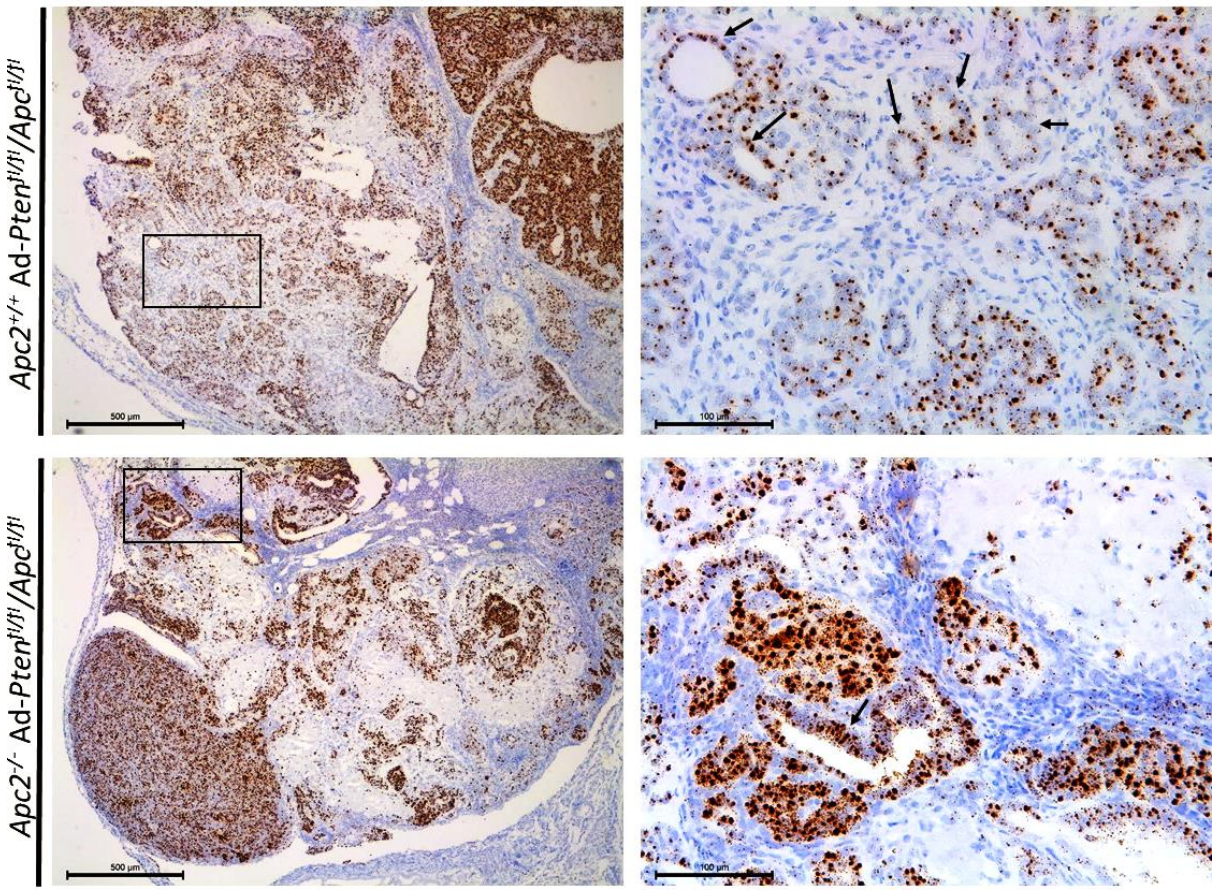

Figure A7.1: *Axin2* RNAscope of Ad-*cre* $Pten^{fl/fl}/Apc^{fl/fl}$ tumours. Representative photomicrographs of *Axin2* RNAscope in $Apc2^{+/+}$ (upper panels), and $Apc2^{-/-}$ Ad-*cre* $Pten^{fl/fl}/Apc^{fl/fl}$ tumours (lower panels). Right panels represent 5X magnification of black rectangles in left panels. Black arrows: *Axin2* positive staining in glands. n=3. Scale bars 500 µm left panel, 100 µm right panel.